2019

Are proteostasis defects responsible for amyotrophic lateral sclerosis?

Isabella Lambert-Smith
University of Wollongong

UNIVERSITY OF WOLLONGONG AUSTRALIA

Are proteostasis defects responsible for amyotrophic lateral sclerosis?

Isabella Lambert-Smith

Professor Justin Yerbury
Associate Professor Darren Saunders
Professor Heath Ecroyd

A thesis submitted in fulfilment of the requirements for the award of the degree

Doctor of Philosophy

from the

School of Chemistry and Molecular Bioscience and the Illawarra Health and Medical Research Institute
University of Wollongong

August 2019

This research has been conducted with the support of the Australian Government Research Training Program Scholarship

Abstract

The pathological hallmark of Amyotrophic lateral sclerosis (ALS) is the presence of ubiquitylated protein inclusions in affected motor neurons, which is indicative of disruption in the mechanisms that maintain proteome homeostasis (proteostasis) in these cells. Moreover, many of the genes in which mutations are associated with ALS encode proteins that have important roles in the maintenance of proteostasis. It is thus hypothesised that dysfunction in the proteostasis network underlies motor neuron degeneration in ALS. Whilst proteostasis dysfunction in ALS has been a major focus of research in the past two decades, there is an urgent need to identify the precise molecular mechanisms that lead to this dysfunction. Addressing this gap in knowledge is a necessary step towards understanding what causes neurodegeneration in ALS, and to the identification of novel therapeutic targets to prevent this.

In work presented in Chapter III, yeast were used as a model biological system for high-throughput screening to identify alterations in the proteostasis network caused by expression of pathological isoforms of TDP-43, FUS and SOD1. Whilst the expression of $SOD1^{A4V}$ in yeast was not toxic, it was associated with up-regulation of proteins involved in mRNA metabolism (DCP2 and ASC1), the ubiquitin-proteasome system (UPS) and the endoplasmic reticulum-associated degradation pathway (ERAD) (UBA1, PRE2 and UFD1). The expression of FUS^{WT} was moderately toxic to yeast, while TDP-43^{WT} expression markedly reduced yeast viability. Up-regulation of UFD1, a key protein in maintaining ER proteostasis, correlated with suppression of $SOD1^{A4V}$ toxicity and increased cellular capacity to manage pathological FUS. Moreover, changes in abundance of HAC1 (involved in the unfolded protein response), DSK2 (ubiquitin-dependent protein degradation in the ERAD pathway and the UPS) and PBP1 (involved in diverse RNA processing pathways that control gene expression) were key differences between expression of TDP-43^{WT} versus FUS^{WT}, with these proteins being down-

regulated in TDP-43^{WT}-expressing yeast and up-regulated in FUS^{WT}-expressing yeast. The increased abundance of these proteins in FUS^{WT}-expressing yeast may have augmented the cellular capacity to restore ER proteostasis and UPS activity. Moreover, the decreased abundance of these proteins in TDP-43^{WT}-expressing yeast, which correlated with higher toxicity, suggests that disruptions in ubiquitin-dependent protein degradation and ER proteostasis may be associated with TDP-43 associated pathology. Hence, disruptions in gene expression regulation, ER proteostasis and UPS activity could underlie different genetic forms of ALS.

Through work presented in Chapter IV, a key hit from the SOD1^{A4V} yeast screen (the E1 ubiquitin-activating enzyme, UBA1) was validated, demonstrating that increased UBA1 expression suppresses mutant SOD1 toxicity in neuronal cells (NSC-34). The expression of SOD1^{A4V} in NSC-34 cells caused disruption to UPS activity, and this correlated with cellular toxicity. SOD1^{A4V} aggregation into large inclusions was a prominent feature in these cells. Remarkably, increased expression of catalytically-active UBA1, but not a catalytically-inactive mutant, improved cell viability. Interestingly, the protective mechanism by which increased UBA1 expression prevented toxicity in these cells did not involve suppression of SOD1^{A4V} aggregation. It has been previously reported that aggregates formed by SOD1 promote cellular toxicity by sequestering ubiquitin, causing ubiquitin dyshomeostasis. Hence, increasing the levels of UBA1 in NSC-34 cells expressing SOD1^{A4V} may have improved cell viability through amelioration of SOD1^{A4V}-mediated deficiency in the cellular pool of activated ubiquitin.

The work presented in Chapter V involved the use of conformationally-destabilised mutants of firefly luciferase (Fluc) to develop a high content screening (HCS) assay to examine protein folding/re-folding capacity in NSC-34 cells expressing SOD1^{A4V} and CCNF^{S621G}. It was demonstrated that these Fluc isoforms can be used in high-throughput format to report on

reductions in the activity of the chaperone network that result from the expression of $SOD1^{A4V}$, providing multiplexed information at single-cell resolution. In addition to $SOD1^{A4V}$ and $CCNF^{S621G}$, NSC-34 cell models of ALS-associated mutants of TDP-43, FUS, VAPB, VCP, OPTN and UBQLN2 were generated that, in future work, can be screened using this assay. For ALS-associated mutant proteins that do cause reductions in the protein quality control capacity of neuronal cells, as is the case for $SOD1^{A4V}$, this assay has potential to be applied in drug screening studies to identify candidate compounds that are able to ameliorate this deficiency.

In summary, this PhD thesis describes the development and use of two novel high-throughput methodologies to investigate proteostasis disturbances caused by mutations in ALS-associated genes. The common alterations identified in the proteostasis network caused by pathological TDP-43, FUS and SOD1 expression lay the groundwork for further research in this area. In the future both methodologies can be exploited for drug screening applications. Continued development of HCS assays capable of measuring deficiencies in the proteostasis network will be valuable in the search for therapeutic targets and development of drugs to treat ALS. Overall, the work achieved in this PhD provides substantial foundation for further investigation into the specific proteostasis components that could be potent targets for therapeutic intervention in ALS.

Acknowledgments

This PhD journey has been challenging, but above all utterly brilliant and rewarding, and there are many people that I am extremely grateful to for helping me along the way. First of all, Mum. You are an inspiration. Through everything that comes up in life you remain so loving, kind, generous and caring, and have taught me so much about resilience. You sparked my initial interest in biology (and, really, all things science), and I would never have dreamed of undertaking a PhD if it wasn't for your encouragement, your love and belief in me. Dad, I am so grateful to you for always encouraging me to pursue my interests, and for opening my eyes to what is possible through hard work and determination. Your insatiable wanderlust has nurtured my own curiosity for this wonderful world.

I would like to say a massive thank you to my primary supervisor, Professor Justin Yerbury. The seed that led to me pursuing this PhD was planted in my undergraduate studies, with the fantastic lecture you presented on amyotrophic lateral sclerosis. You sparked my interest in finding out more about ALS, and generously took me on for a summer research project, which led to an Honours project and then onto this PhD. I feel extremely privileged to have been able to be one of your students – I am certain that your past, present and future students share that same sentiment. I'm yet to meet a more resilient, determined, brilliant, kind and generous individual. I have learnt so much from you over these years, and I am very grateful for the truly awesome opportunities you have provided for me throughout my PhD.

I have so much gratitude for my co-supervisors, Associate Professor Darren Saunders and Professor Heath Ecroyd. Darren, from the very early days of my PhD your amazing energy and passion have been inspirational. There have been many ups and downs throughout this PhD journey, but yours and Justin's kindness and guidance have helped me to traverse it all and to learn from every experience. I am also very grateful to you for welcoming me into your lab and

research team at the Kinghorn Cancer Centre, and for guiding me through the work we conducted there and at the Garvan Institute. Thank you to my friend and desk buddy at the Kinghorn, Jessie Mckenna, and the other members of the Saunders research team.

Heath, I am very grateful to you for taking on the role as a co-supervisor and helping to support and guide me in the last more than year and a half of my PhD. Your insight, guidance and encouragement have been invaluable.

I would like to thank Professor Stephen Oliver and Dr Giorgio Favrin for welcoming me into the SGO yeast biology lab on the other side of the world and for taking me under your wing(s) to undertake a significant part of my PhD project at the University of Cambridge. I learnt a great deal during my time there, personally and academically, and feel very fortunate to have been able to work with the brilliant scientists of the SGO lab (in particular, Bessie, Dan, Trevor, Marta and Lu). A special thank you to my friends in Cambridge, Leonor, Kate, and Maya, for making my time over there so memorable.

I am so grateful to all my wonderful friends and fellow IHMRI inhabitants who have helped to create some pretty awesome memories throughout my PhD; Nat, Luke, Rafaa, Clare, Di, Elahe, Liyu, Claudia, Heema, Ili, Emma, Amy, Sandeep, Mauricio, Jen, Sam W., Sam A., Dan Whiten, Bec Dabbs, Bec San Gil, BJ, Anthea, Dez, Jeremy, Dzung, Mon, Rachelle.

Finally, a very big thank you to my loving, fun, quirky family. In particular: my big brother, Ben, for being a constant source of encouragement, laughter, optimism and inspiration; my Nanna, for being a kickass strong independent woman, and being an inspiration through all the good you do in this world; my Grandma and Grandpa, for providing so much love and encouragement to all of us in the Keohan family, and helping me believe in myself.

Certification

I, Isabella Ann Lambert-Smith, declare that this thesis submitted in fulfilment of the requirements for the conferral of the degree Doctor of Philosophy, from the University of Wollongong, is wholly my own work unless otherwise referenced or acknowledged. This document has not been submitted for qualifications at any other academic institution.

_____

Isabella Ann Lambert-Smith

25th August 2019

Table of Contents

List of figures

List of tables

List of abbreviations

Aβ	Amyloid beta
AD	Alzheimer's disease
ADP	Adenosine diphosphate
ALS	Amyotrophic lateral sclerosis
ANOVA	Analysis of variance
APC	Anaphase-promoting complex
ARF	Adenosine diphosphate (ADP) ribosylation factor
ATP	Adenosine triphosphate
ATXN2	Ataxin-2
BCA	Bicinchoninic acid
C9ORF72	Chromosome 9 open reading frame 72
CCNF	Cyclin F
CFP	Cyan fluorescent protein
CJD	Creutzfeldt-Jakob disease
CYLD	CYLD lysine 63 deubiquitinase
DBP	DNA-binding protein
DDR	DNA damage response
DENN	Differentially Expressed in Normal and Neoplasia (protein domain)
DMEM/F-12	Dulbecco's modified eagle medium/Nutrient mixture F12
DMSO	Dimethyl sulfoxide
DNA	Deoxyribonucleic acid
DPR	Dipeptide-repeat protein
DsRed	Red fluorescent protein from *Discosoma* species
DUB	De-ubiquitylating enzyme
ECFP	Enhanced cyan fluorescent protein
EDTA	Ethylenediaminetetraacetic acid
EGFP	Enhanced green fluorescent protein

ER	Endoplasmic reticulum
ERAD	Endoplasmic reticulum-associated degradation
ERGIC	ER-Golgi intermediate compartment
EWSR1	Ewing sarcoma breakpoint region 1
fALS	Familial amyotrophic lateral sclerosis
FBS	Foetal bovine serum
FI	Fluorescence intensity
Fluc	Firefly luciferase
$Fluc^{DM}$	'Double mutant' firefly luciferase (containing two mutations)
$Fluc^{SM}$	'Single mutant' firefly luciferase (containing a single mutation)
$Fluc^{WT}$	Wild-type firefly luciferase
FTD	Frontotemporal dementia
FUS	Fused in sarcoma
$^{GAL}DsRed^{empty}$	pAG416GAL-ccdB-DsRed vector control
GDP	Guanosine diphosphate
GEF	GDP/GTP exchange factor
GO	Gene ontology
GRR	Glycine-rich region
GTP	Guanosine triphosphate
HCS	High content screening
HD	Huntington's disease
hnRNP	Heterogeneous nuclear ribonucleoprotein
hnRNPA1	Heterogeneous nuclear ribonucleoprotein A1
HRP	Horseradish peroxidase
HSE	Heat shock element
HSP	Heat shock protein
HSR	Heat shock response
Htt	Huntingtin

IBMPFD	Inclusion body myopathy with Paget's disease of bone and frontotemporal dementia
IC_{50}	The half maximal inhibitory concentration
ICC	Immunocytochemistry
IgG	Immunoglobulin G
IPOD	Insoluble protein deposit
IPSC	Induced pluripotent stem cell
JUNQ	Juxtanuclear quality control compartment
LTP	Long-term potentiation
MATR3	Matrin-3
mCherry	Monomeric cherry fluorescent protein
MJD	Machado-Joseph disease
mRNA	Messenger RNA
MW	Molecular weight
N_2	Molecular nitrogen
NF-κB	Nuclear factor kappa B
NLS	Nuclear localisation sequence
NSC-34	Murine motor neuron-like neuroblastoma × spinal cord hybrid cell line
OD	Optical density
OPTN	Optineurin
ORF	Open reading frame
P-body	Processing body
PBS	Phosphate-buffered saline
PCR	Polymerase chain reaction
PD	Parkinson's disease
PEG	Polyethylene glycol
PEST	Proline-, glutamic acid-, serine-, threonine-enriched (protein domain)
PFA	Paraformaldehyde
PFN1	Profilin-1

PMN	Piecemeal microautophagy of the nucleus
POAG	Primary open angle glaucoma
RAC	19S proteasome regulatory particle assembly-chaperones
RAD	Ribosome-associated degradation
RAN	Repeat-associated non-ATG-initiated (translation)
RBP	RNA-binding protein
RIPA	Radioimmunoprecipitation assay buffer
RNA	Ribonucleic acid
RNP	Ribonucleoprotein
RQC	Ribosome quality control
RRM	RNA recognition motif
RSC	Remodel the Structure of Chromatin (chromatin-remodelling complex)
sALS	Sporadic amyotrophic lateral sclerosis
SCF	SKP1-cullin-F-Box protein ubiquitin ligase complex
SD	Synthetic medium supplemented with glucose
SDS	Sodium dodecyl sulphate
SG	Stress granule
SGA	Synthetic genetic array
SGal	Synthetic medium supplemented with galactose
SGD	*Saccharomyces* Genome Database
SHRED	Stress-induced homeostatically-regulated protein degradation
SMA	Spinal muscular atrophy
SMN	Survival motor neuron
SOC	Super optimal broth with catabolite repression
SOD1	Copper/zinc superoxide dismutase
SQSTM1	Sequestosome-1/p62
SRaf	Synthetic medium supplemented with raffinose
STUbL	SUMO-targeted ubiquitin ligase
SUMO	Small ubiquitin-like modifier

TAF15	TATA box-binding protein-associated factor 15
TBK1	TANK-binding kinase 1
TBS	Tris-buffered saline
TBS-T	Tris-buffered saline Tween-20
TDP-43	TAR DNA-binding protein 43
tdTomato	Tandem tomato fluorescent protein
tGFP	Turbo green fluorescent protein
UBA	Ubiquitin-associated domain
UBA1	Ubiquitin-activating enzyme E1
UBL	Ubiquitin-like domain
UBQLN2	Ubiquilin-2
UPR	Unfolded protein response
UPS	Ubiquitin-proteasome system
VAPB	VAMP (vesicle-associated membrane protein)-associated protein B
VC	Vector control
VCP	Transitional endoplasmic reticulum ATPase/p97
v/v	Volume per volume
WT	Wild-type
w/v	Weight for volume
XL-SMA	X-linked spinal muscular atrophy
YNB	Yeast nitrogen base
YPD	Yeast extract-peptone-dextrose

List of publications and presentations

Publications

Published

Farrawell, N. E., **Lambert-Smith, I. A.**, Mitchell, K., McKenna, J., McAlary, L., Ciryam, P., Vine, K. L., Saunders, D. N., Yerbury, J. J. (2018) 'SOD1^{A4V} aggregation alters ubiquitin homeostasis in a cell model of ALS', *Journal of Cell Science*; doi: 10.1242/jcs.209122.

Zeineddine, R., Farrawell, N. E., **Lambert-Smith, I. A.**, Yerbury, J. J. (2017) 'Addition of exogenous SOD1 aggregates causes TDP-43 mislocalisation and aggregation', *Cell Stress and Chaperones*; doi:10.1007/s12192-017-0804-y.

Ciryam, P., **Lambert-Smith, I. A.**, Bean, D. M., Freer, R., Cid, F., Tartaglia, G. G., Saunders, D. N., Wilson, M. R.,Oliver, S. G., Morimoto, R. I., Dobson, C. M., Vendruscolo, M., Favrin, G., Yerbury, J. J. (2017) 'Spinal motor neuron protein supersaturation patterns are associated with inclusion body formation in ALS', *PNAS*; 114 (20): E3935-E3943.

Farrawell, N. E., **Lambert-Smith, I. A.**, Warraich, S. T., Blair, I. P., Saunders, D., Hatter, D. M.,Yerbury, J. J. (2015) 'Distinct Partitioning of ALS associated TDP-43, FUS and SOD1 mutants into cellular inclusions', *Scientific Reports*; 5: 13416-1 – 13416-14.

Manuscripts in preparation

Lambert-Smith, I. A., Farrawell, N. E., Bloomfield, M., Bean, D., Cao, L., Vine, K. L., Favrin, G., Saunders, D. N., Oliver, S. G., Yerbury, J. J. 'Increased levels of UBA1 protect against SOD1 and TDP-43 toxicity in amyotrophic lateral sclerosis models'.

Conference presentations

Lambert-Smith, I. A., Saunders, D. N., Oliver, S., Yerbury, J. J., Favrin, G. (2017) 'Augmenting ubiquitin-proteasome system capacity rescues NSC-34 motor neurones from mutant SOD1 toxicity'. Poster presentation at the 28th International Symposium on ALS/MND; 8-10 December 2017; The Westin Boston Waterfront, Boston, USA.

Lambert-Smith, I. A., Saunders, D. N., Oliver, S., Yerbury, J. J., Favrin, G. (2016) 'A GFP-fusion yeast library reveals responses in the proteostasis network to SOD1, TDP-43 and FUS'. Poster presentation at the 27th International Symposium on ALS/MND; 7-9 December 2016; The Conference Centre Dublin, Ireland.

Lambert-Smith, I. A., Cao, L., Bean, D., Saunders, D. N., Oliver, S., Yerbury, J. J., Favrin, G. (2015) 'A collection of GFP fusion proteins reveals responses in the proteostasis network to TDP-43, FUS and SOD1 in a yeast model of ALS'. Poster presentation at the MND Australia Research Meeting; 22-23 November 2015; The University of Sydney, NSW Australia.

Lambert-Smith, I. A., Saunders, D., Yerbury, J. J. (2014) 'fALS-associated mutants disrupt proteostasis in neuronal cell culture'. Poster presentation at the 25th International Symposium on ALS/MND; 5-7 December 2014; The Square conference centre, Brussels, Belgium.

Lambert-Smith, I. A., Farrawell, N. E., Yerbury, J. J. (2014) 'fALS-associated proteins form aggregates via distinct pathways in cells'. Poster presentation at the 39th Lorne Conference on Protein Structure and Function; 9-13 February 2014; Mantra Lorne, Lorne, VIC Australia.

Chapter 1: Introduction

1.1 Introduction

Amyotrophic lateral sclerosis (ALS) is one of the most prevalent forms of motor neuron disease worldwide (Dormann *et al.* 2010). Now considered to be a heterogeneous disorder (Robberecht and Philips 2013), it is typified by the progressive loss of motor neurons of the motor cortex, brainstem and spinal cord. The muscles served by these motor neurons consequently atrophy, weaken and become vulnerable to spasticity and fasciculations. Typically, death results within 3-5 years of symptom onset as degeneration progresses to the motor neurons serving the respiratory muscles and diaphragm, resulting in respiratory failure (Boillee *et al.* 2006). However, in some cases disease duration can be quite variable (Strong *et al.* 2005, Wang *et al.* 2008).

A significant proportion of patients also suffer cognitive and behavioural impairment. In fact, ALS and frontotemporal dementia (FTD) are increasingly recognised as being part of a pathological spectrum (Basso *et al.* 2009, Robberecht and Philips 2013, van der Zee *et al.* 2013). ALS itself is classified as either familial (fALS) or sporadic (sALS). fALS comprises ~10% of all reported cases, with the remaining ~90% of sALS patients having no apparent family history of disease (Ilieva *et al.* 2009). Genetic studies of fALS patients have led to the identification of a growing list of causative genetic mutations that segregate with disease. The first of these were discovered in *SOD1* (copper/zinc superoxide dismutase) (Rosen *et al.* 1993), and this list has grown to include *TARDBP* (TAR DNA-binding protein 43; TDP-43) (Neumann *et al.* 2006), *FUS* (Fused in Sarcoma) (Kwiatkowski *et al.* 2009, Vance *et al.* 2009), *C9ORF72* (chromosome 9 open reading frame 72) (DeJesus-Hernandez *et al.* 2011), *VAPB* (VAMP (vesicle-associated membrane protein)-associated protein B) (Nishimura *et al.* 2004, Nishimura *et al.* 2004), *OPTN* (optineurin) (Maruyama *et al.* 2010), *ANG* (angiogenin) (Greenway *et al.* 2006), *SETX* (senataxin) (Chen *et al.* 2004), *VCP* (transitional endoplasmic reticulum ATPase/p97) (Johnson *et al.* 2010), *UBQLN2* (ubiquilin-2) (Deng *et al.* 2011), *hnRNPA1* (heterogeneous nuclear

ribonucleoprotein A1) (Kim *et al.* 2013), *MATR3* (matrin-3) (Johnson *et al.* 2014), *CCNF* (cyclin F) (Williams *et al.* 2016), *PFN1* (profilin-1) (Wu *et al.* 2012), *SQSTM1* (p62) (Fecto *et al.* 2011), *TBK1* (TANK-binding kinase 1) (Cirulli *et al.* 2015), *CYLD* (CYLD lysine 63 deubiquitinase) (Dobson-Stone *et al.* 2013), *EWSR1* (Ewing sarcoma breakpoint region 1) (Couthouis *et al.* 2012) and *TAF15* (TATA box-binding protein-associated factor 15) (Ticozzi *et al.* 2011), among others. This list is not exhaustive, with more than 50 potential ALS genes now published. Establishing the causality of many of these mutations, however, has remained challenging for geneticists.

Mutations in many of the genes associated with fALS have also been detected in sALS patients, including *C9ORF72* (Shatunov *et al.* 2010), *TARDBP* (Sreedharan *et al.* 2008), *FUS* (Belzil *et al.* 2009, Corrado *et al.* 2010, DeJesus-Hernandez *et al.* 2010, Lai *et al.* 2011), *ANG* (Greenway *et al.* 2006), *MATR3* (Lin *et al.* 2015, Leblond *et al.* 2016), *EWSR1* (Couthouis *et al.* 2012), *OPTN* (van Blitterswijk *et al.* 2012), *VCP* (Koppers *et al.* 2012) and *SQSTM1* (Fecto *et al.* 2011, Teyssou *et al.* 2013). The genetic contribution to sALS is estimated to be ~65% (Al-Chalabi *et al*. 2010, Al-Chalabi and Visscher 2014), but current methodologies for genetic analysis have fallen short in identifying genetic variants in the majority of sALS cases (Andersen and Al-Chalabi, 2011, Renton *et al.* 2014, Dharmadasa *et al.* 2017, Nguyen *et al.* 2018). In terms of clinical presentation and pathological features, sALS and fALS are largely indistinguishable. Rather, fALS and sALS are distinguished based on the presence of a recorded family history of ALS. However, advances in genetic analysis techniques are paving the way towards the identification of previously unknown familial relatedness between individuals with sALS carrying identical ALS-associated gene variants (Twine *et al.* 2019). The hallmark pathology of ubiquitylated TDP-43-positive inclusions in affected motor neurons is observed in post-mortem tissue from both individuals with sALS and those with fALS (Leigh *et al.* 1991, Neumann *et al.* 2006). Moreover, while clinical presentation is heterogeneous overall amongst

individuals with ALS, there is no definitive delineation between those with fALS and those with sALS. Thus, continued efforts to identify relatedness amongst individuals with sALS and to identify genetic variants that contribute to sALS risk are warranted to aid diagnosis and prognosis of individuals with fALS and sALS, improve patient outcomes and provide insight into the genetic mechanisms that contribute to ALS pathogenesis.

The currently identified ALS-associated genes cover a diverse range of molecular functions and thus it is becoming increasingly apparent that motor neuron dysfunction and death is unlikely to be caused by one mechanism alone. The key to understanding ALS will be to discern how the ALS-associated genes and their respective molecular pathways interconnect. As a starting point, it is well established that inclusion bodies (inclusions) containing aggregated proteins are a characteristic feature of the affected motor neurons in post-mortem spinal cord tissue from ALS patients. The universal presence of inclusions in ALS indicates that there is disruption of the cellular mechanisms that maintain proteome homeostasis (proteostasis) in motor neurons. The objective of this introductory chapter is to summarise current evidence for, and understanding of, the potential roles of ALS-associated mutant proteins in proteostasis dysfunction in motor neurons and how they contribute to disease.

1.2 Proteostasis involves the co-ordination of interacting molecular processes

The primary function of motor neurons is to respond to the binding of neurotransmitters to cell surface receptors and to generate, propagate and transmit action potentials for rapid information transfer from the motor areas of the brain to the muscles. This is dependent on homeostasis of the intra- and extracellular environment (Kanning *et al.* 2010). Proteostasis is defined as the maintenance of all proteins in the cellular proteome in a conformation, concentration and location that is required for their correct function (Balch *et al.* 2008). It involves stringent regulation of the processes of transcription, RNA processing and transport, translation, protein folding, protein trafficking and transport, and protein degradation (Hartl *et al.* 2011, Yerbury *et*

al. 2016) (Figure 1.1). This requires readaptation of the innate biology of the cell in response to constant intrinsic and extrinsic changes. These processes are intricately connected to each other, creating a dynamic system in equilibrium, such that disturbances in one component lead to significant changes in other components.

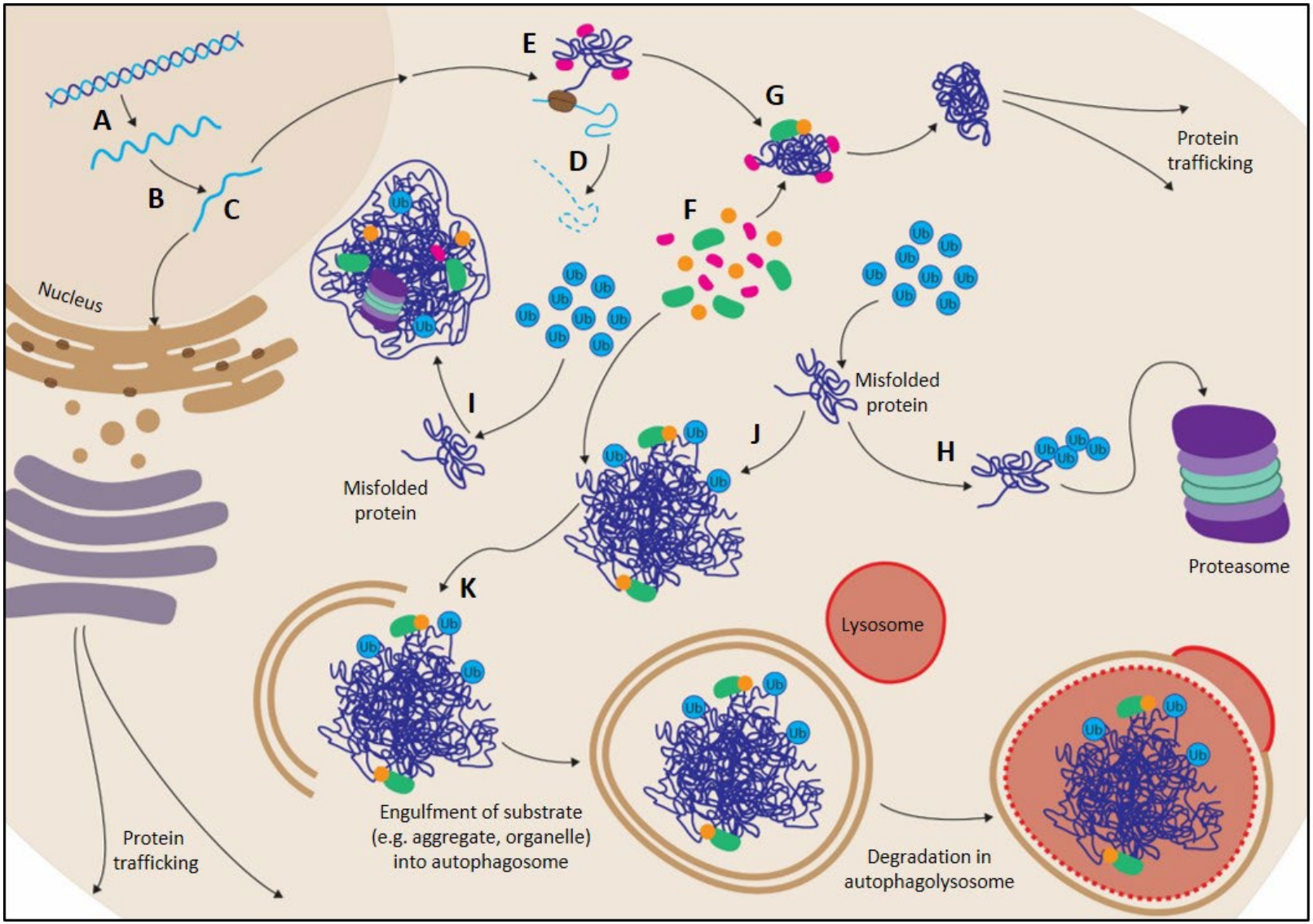
A
B
C
D
E
F
G
Nucleus
Protein trafficking
Misfolded protein
I
J
H
Misfolded protein
Proteasome
K
Lysosome
Engulfment of substrate (e.g. aggregate, organelle) into autophagosome
Degradation in autophagolysosome
Protein trafficking

Figure 1.1. Summary of the interacting molecular processes that maintain proteome homeostasis (proteostasis). The maintenance of cellular proteostasis requires stringent regulation of the processes constituting RNA metabolism and protein quality control. RNA metabolic processes include (A) transcription, (B) mRNA splicing and processing, (C) mRNA transport into the cytosol or the rough endoplasmic reticulum (rER) and (D) mRNA decay. From the moment (E) a nascent protein has been translated, it enters the realm of the protein quality control network. (F) Molecular chaperones (G) mediate folding of nascent proteins into their native conformation. When molecular chaperones are unable to fold aberrant misfolded proteins into their native conformation, (H) ubiquitylation can direct the misfolded proteins for proteasomal degradation. The ubiquitin-proteasome system is also responsible for the regulated degradation of many proteins with key roles in signalling pathways. Alternatively, (I) ubiquitylation can assist in the active segregation of misfolded proteins from the cytosol into distinct types of inclusions that function as protein quality control compartments, e.g. aggresomes. (J) In some instances, misfolded proteins that escape these mechanisms can aggregate. (K) Molecular chaperones can assist in directing aggregates for proteolytic degradation through the selective macroautophagy pathway, which is also the primary degradative pathway for the clearance of long-lived proteins, macromolecular structures and old or damaged organelles.

1.2.1 RNA metabolism

Fundamentally, the appropriate levels of proteins in the cell are maintained through the correct regulation of transcription, mRNA splicing and processing, transport from the nucleus to distinct locations in the cytoplasm, and translation into nascent polypeptides. A multitude of DNA- and RNA-binding proteins (D/RBPs) exist that interact with nascent and mature mRNA molecules to ensure their proper functioning (Baltz *et al.* 2012, Castello *et al.* 2012). Together, these DBPs and RBPs form an elaborate network crucial to maintaining the appropriate levels of mRNAs and their encoded proteins (Janssens and Van Broeckhoven 2013). The regulation of RNA metabolism is crucial in the preservation of a functional cellular environment, and multiple neurodegenerative diseases have now been linked to dysfunctional RNA metabolism (Cooper *et al.* 2009, Todd and Paulson 2010, Belzil *et al.* 2013). For example, the survival motor neuron (SMN) protein, genetically linked to the motor neuron disease spinal muscular atrophy (SMA), is critical for efficient splicing activity (Liu *et al.* 1997, Pellizzoni *et al.* 1998). SMN assists in assembly of the spliceosome, a molecular complex responsible for splicing pre-mRNA transcripts (Liu *et al.* 1997, Pellizzoni *et al.* 1998). Loss of SMN function due to SMA-causing mutations leads to impaired spliceosomal activity (Wan *et al.* 2005). Moreover, knockdown of SMN in zebrafish and mouse models causes splicing defects and motor neuron degeneration (Winkler *et al.* 2005, Zhang *et al.* 2008). Beyond SMA, mutations causing SMN

deficiency have also been implicated as a risk factor for sALS (Veldink *et al.* 2005, Corcia *et al.* 2006). Although SMN has multiple functions in cells beyond splicing activity (Rossoll *et al.* 2003, Zhang *et al.* 2003, Carrel *et al.* 2006, Zhang *et al.* 2006), these data nevertheless suggest that there is a crucial role for efficient mRNA splicing in the maintenance of motor neuron health. Furthermore, dysregulation of proper splicing activity is prevalent in ALS caused by mutations in *TARDBP* and *FUS* (Hoell *et al.* 2011, Polymenidou *et al.* 2011, Lagier-Tourenne *et al.* 2012, Arnold *et al.* 2013).

Once an mRNA has been translated into a nascent polypeptide, regulation of the fate of the mRNA is crucial for proper control of gene expression and cellular protein levels (Wang *et al.* 2002, Yang *et al.* 2003). Integral in mRNA regulation are mechanisms of mRNA decay, which are intricately controlled by highly conserved networks of enzymes in eukaryotes (Parker and Song 2004). Typically, mRNA decay is deadenylation-dependent, initiating through the removal of the mRNA poly(A) tail by any of several different poly(A)-specific exoribonucleases (Boeck *et al.* 1996, Körner *et al.* 1998, Tucker *et al.* 2001). Following this, the deadenylated mRNA is degraded through either a 5' to 3' directed pathway or a 3' to 5' directed pathway. The 5' to 3' pathway proceeds through the action of decapping enzymes, DCP1 and DCP2, that remove the 5' cap of the mRNA (Steiger *et al.* 2003). This then facilitates completion of the decay pathway by the XRN1 exonuclease (Larimer *et al.* 1992). Alternatively, structures comprised of a network of exonucleases, termed exosome complexes, degrade their mRNA substrates through the 3' to 5' direction (Anderson and Parker 1998, Mukherjee *et al.* 2002, Wang *et al.* 2002). As for the nascent polypeptide, it enters the realm of the protein quality control network. This network encompasses the proteins and pathways that regulate protein folding and re-folding, trafficking of proteins to their correct cellular location, and that monitor the efficient compartmentalisation and clearance of misfolded proteins and those at the end of their functional life cycle in the cell.

1.2.2 Protein quality control

Mechanisms of protein folding, re-folding and the prevention of protein aggregation are managed by networks of molecular chaperones and co-chaperones (Balch *et al.* 2008, Yerbury and Kumita 2010). These include several systems of 'heat-shock proteins' (HSPs); the small HSP (sHSP), HSP40, HSP60 (chaperonin), HSP70, HSP90 and HSP100 systems. Hartl *et al.* (2011) provides an expansive review of the molecular chaperone networks and so this will not be covered here. The full repertoire of chaperones, co-chaperones, folding enzymes and adaptors that make up these systems in human cells, the chaperone network (chaperome), has been quantified to comprise 332 proteins (Brehme *et al.* 2014). Many proteins of the chaperome are abundantly expressed in cells and encompass a considerable proportion of the cellular machinery (Bukau *et al.* 2006, Ron and Walter 2007). Under normal physiological conditions, the various proteins of the chaperome have diverse roles in regulating correct protein folding, preventing protein folding intermediates and aberrant proteins from misfolding, and targeting stressed or aberrant proteins for degradation (Sherman and Goldberg 2001, Gidalevitz *et al.* 2006, Douglas and Dillin 2010, Yerbury and Kumita 2010, Gidalevitz *et al.* 2011, Yerbury *et al.* 2013). Extensive evidence indicates that they do this by recognising and binding to exposed hydrophobic stretches of the target protein's amino acid sequence, thereby preventing unfavourable interactions between non-native protein species (Voisine *et al.* 2010, Hartl *et al.* 2011, Wyatt *et al.* 2013).

Abnormal physiological demands on the proteostasis network, such as the overexpression of proteins above normal concentrations, can alter the chaperone-substrate balance. Mutations that increase the propensity of a protein to aggregate can also tip this balance to disfavour proteostasis by exceeding the cellular chaperome capacity (Gidalevitz *et al.* 2006, Yerbury *et al.* 2013). Age itself leads to a decline in the capacity of the chaperome. Gene expression analysis of human brain tissue has revealed that, during normal brain aging, almost a third of

chaperone-encoding genes are down-regulated (Brehme *et al.* 2014). A considerable proportion of this chaperome deterioration was also detected in post-mortem brain tissue from patients with Alzheimer's (AD), Parkinson's (PD) and Huntington's disease (HD). Moreover, a subset of these repressed chaperones was identified to comprise an intricate subnetwork that is critical in buffering against proteotoxic stress during cellular aging. As with ALS, AD, PD and HD are age-correlated diseases and are each primarily associated with genetic mutations that introduce increased proteostatic burden through the production of aggregation-prone proteins. It stands to reason that a declining capacity of the protective chaperone subnetwork (Brehme *et al.* 2014) with increased age may make this system highly vulnerable to genetic mutations that lead to accumulation of mutant, aggregation-prone proteins.

1.2.2.1 Ubiquitin-dependent protein degradation

When molecular chaperones are unable to fold aberrant proteins into their native conformation, regulatory components and co-factors of the HSP40, HSP70 and HSP90 systems help to prepare and direct the substrate proteins for proteolytic degradation through the ubiquitin-proteasome system (UPS) or through selective macroautophagy (Arndt *et al.* 2007, Ding and Yin 2008, Gamerdinger *et al.* 2009, Arndt *et al.* 2010, Kampinga and Craig 2010, Jin *et al.* 2013). Ubiquitylation of substrate proteins, i.e. the conjugation of ubiquitin molecules to substrate proteins, is critically important for directing proteins through these proteolytic systems (Tan *et al.* 2008, Kraft *et al.* 2010). The UPS is the main proteolytic system for the degradation of regulatory proteins and damaged, misfolded proteins. Substrate proteins are ubiquitylated through the co-ordinated action of E1 ubiquitin-activating, E2 ubiquitin-conjugating and E3 ubiquitin-ligase enzymes in a multistep cascade of enzymatic reactions, and subsequently targeted to the 19S regulatory particle of the 26S proteasome (Hershko and Ciechanover 1998, Crews 2003, Kleiger and Mayor 2014). Inside the 20S core particle of the proteasome, substrate proteins are cleaved into small peptides (Bhattacharyya *et al.* 2014). Selective macroautophagy

(referred to as autophagy from hereon) is primarily responsible for the clearance of long-lived proteins, macromolecular complexes, organelles and aggregates formed by misfolded proteins, and is a highly conserved pathway among eukaryotes (Hughes and Rusten 2007, Jin *et al.* 2013).

Ubiquitylation also plays a role in alternative routes of protein quality control, assisting in the active segregation of misfolded proteins from the cytosol into distinct types of inclusions (Kawaguchi *et al.* 2003, Tan *et al.* 2008, Zhang and Qian 2011). These structures have been reported to contain high concentrations of quality control machinery. For instance, aggresomes and the related juxtanuclear quality control compartment (JUNQ) contain ubiquitylated proteins targeted for proteasomal degradation, active proteasomes, HSP70 and other chaperones (Johnston *et al.* 1998, Kopito 2000, Arrasate *et al.* 2004, Kaganovich *et al.* 2008, Treusch *et al.* 2009, Zhang and Qian 2011, Weisberg *et al.* 2012, Polling *et al.* 2014). However, in a cell that has been exposed to excessive protein-folding stress, the capacity of these quality control mechanisms can be exceeded, enabling misfolded proteins to escape compartmentalisation or degradation. Critically, rogue misfolded proteins are then able to amplify this initial deficiency in the proteostasis network. Through their abnormal conformations they can interact aberrantly with other proteins, including components of the proteostasis network, impairing their normal functions and further disrupting mechanisms of proteostasis (Matsumoto *et al.* 2005, Gidalevitz *et al.* 2006, Weisberg *et al.* 2012).

1.2.2.2 Diverse cellular processes are governed by the ubiquitin-proteasome system

The UPS is not only crucial for the clearance of damaged, aberrant proteins that escape the chaperone network in the cell, but it is also responsible for the turnover of short-lived proteins and numerous other cellular functions, including cell cycle progression and DNA repair pathways (Ciechanover 1998, Ciechanover 2006). The UPS plays a key role in cellular responses to stimuli, including stress, which require the concentrations and localisation of certain key proteins to be tightly regulated and rapidly increased or decreased (reviewed in

Ciechanover and Stanhill (2014)). For instance, the UPS is involved in spatiotemporal regulation of the levels of different transcriptional activators, coactivators and repressors that are required for the coordination of cellular responses to diverse stimuli. Its role in transcription regulation extends beyond degradative control of transcriptional activators and repressor concentrations (Muratani and Tansey 2003) to controlling their localisation (Hoppe *et al.* 2000) and proteolytically modulating their structure to convert them into functional states (Palombella *et al.* 1994).

At least 38 E2 and > 600 E3 genes have now been identified in the human genome, along with 2 E1 ubiquitin-activating enzymes, UBA1 and UBA6 (Deshaies and Joazeiro 2009, Schulman and Harper 2009, Ye and Rape 2009, Kaneko *et al.* 2016). These E1, E2 and E3 enzymes work in highly organised sequential enzymatic reactions to conjugate ubiquitin to specific protein substrates and direct their fate. The full repertoire of E1, E2 and E3 enzymes, de-ubiquitylating enzymes (DUBs), and the total population of ubiquitin molecules at any one time in a human cell is estimated to account for ~1.3% of the total cellular proteome (Kulak *et al.* 2014).

Ubiquitin itself is a highly conserved, small 76-amino acid protein that is encoded by four genes at different loci in the genome; two polyubiquitin precursor genes, *UBB, UBC,* and two ribosomal fusion genes, *UBA52* and *RPS27A* (Wiborg *et al.* 1985). *UBB* is comprised of head-to-tail repeats of three ubiquitin units, *UBC* of nine ubiquitin units, while *UBA52* and *RPS27A/UBA80* encode ribosomal subunits that are each fused to the C terminus of a single ubiquitin unit. Following translation, various DUBs process the ubiquitin repeats to generate free ubiquitin (Monia *et al.* 1989, Wilkinson *et al.* 1995).

Ubiquitylation serves functions beyond protein degradation via the UPS, and does so by circulating in different cellular 'pools' (Dantuma *et al.* 2006, Groothuis *et al.* 2006) at levels estimated to be ~8×10^7 copies, or 85 μM, in a human cell (Kaiser *et al.* 2011). In one of these pools, ubiquitin is conjugated to substrate proteins by an isopeptide bond either as a single

monomeric entity, monoubiquitin, or as polyubiquitin chains of various topologies (comprehensively reviewed in Komander and Rape (2012)). 'Activated' ubiquitin comprises another pool, thioester-linked via its carboxyl terminus to a catalytic cysteine residue of an E1 ubiquitin-activating enzyme (Haas and Rose 1982). This forms the initial step of the E1-E2-E3 multistep enzymatic cascade that leads to the conjugation of ubiquitin to substrate proteins. 'Free' ubiquitin makes up a third pool. The distribution of ubiquitin in these pools is in a constant state of flux as competing ubiquitin-dependent processes extract free ubiquitin, decreasing its availability while replenishment occurs through combinations of *de novo* ubiquitin synthesis and the actions of diverse DUBs that release conjugated ubiquitin (Monia *et al.* 1989, Wilkinson *et al.* 1995, Verma *et al.* 2002, Yao and Cohen 2002, Nijman *et al.* 2005).

1.2.2.3 Ubiquitin conjugation comprises a versatile cellular signalling system

A huge diversity of molecular processes depend on the signalling specificity provided by the conjugation of ubiquitin in defined linkage arrangements (Figure 1.2). In human cells, monoubiquitin-conjugates (Figure 1.2) account for more than 60% of the total cellular ubiquitin pool, with a majority of this comprised of monoubiquitylated histone H2A (Joo *et al.* 2007, Kaiser *et al.* 2011). Monoubiquitylation of histone H2A is required for gene silencing (de Napoles *et al.* 2004, Wang *et al.* 2004, Baarends *et al.* 2005) and changes in the ubiquitylation status of histone H2A are involved in cellular responses to various stressors by modulating expression of key genes (Carlson *et al.* 1987, Mimnaugh *et al.* 1997). Monoubiquitylation can mediate internalisation of cell surface receptors and regulation of their levels, and further regulates the activity of proteins involved in different stages of endocytosis (Terrell *et al.* 1998, Lucero *et al.* 2000, Nakatsu *et al.* 2000, Roth and Davis 2000, Katzmann *et al.* 2001). In addition, monoubiquitylation is involved in the process of enveloped viruses budding from the plasma membrane of infected cells (Ott *et al.* 1998, Harty *et al.* 2000, Patnaik *et al.* 2000, Strack *et al.* 2000).

As well as monoubiquitylation, additional ubiquitin molecules can be progressively added to the first conjugated ubiquitin of substrate proteins to form an extensive number of defined polyubiquitin chains. The diversity of polyubiquitin chains that exist are possible due to the seven internal lysine residues of ubiquitin (Lys6, Lys11, Lys27, Lys29, Lys33, Lys48, Lys63), and in some cases the Met1 at its amino-terminus, which serve as sites for the carboxyl-terminus glycine residue of an additional ubiquitin to link to (Chau *et al.* 1989, Thrower *et al.* 2000, Dammer *et al.* 2011, Walczak *et al.* 2012). About 11% of the total ubiquitin pool is used for polyubiquitylation of a vast range of protein substrates (Kaiser *et al.* 2011). Polyubiquitin chains can have varying lengths, and linkages that are either homogenous throughout the chain, or heterogenous with changes in the Lys or Met1 residue used for each successive ubiquitin. The fates of proteins tagged with homogenous Lys11, Lys48 and Lys63 polyubiquitin linkages have been studied extensively, whereas Lys6, Lys27, Lys29 and Lys33 are less well understood and account for less than 1% of total cellular ubiquitin (Figure 1.2) (Peng *et al.* 2003, Xu *et al.* 2009, Kaiser *et al.* 2011). Homogenous Lys48-linked chains are widely understood to be the main signal for proteasomal degradation, while Lys11-, Lys29- and Lys63- linkages have also been implicated as proteasome-targeting signals for a lower proportion of protein substrates (Johnson *et al.* 1995, Baboshina and Haas 1996, Thrower *et al.* 2000, Ravid and Hochstrasser 2008, Xu *et al.* 2009, Kaiser *et al.* 2011, Kim *et al.* 2011). As for the targeting of substrates for lysosomal degradation via the autophagy pathway, both monoubiquitylation and polyubiquitylation with Lys63-linkages can serve as signals to adaptor proteins that link substrates to the autophagy machinery (Figure 1.2) (reviewed in Kirkin *et al.* (2009) and Korolchuk *et al.* (2010)).

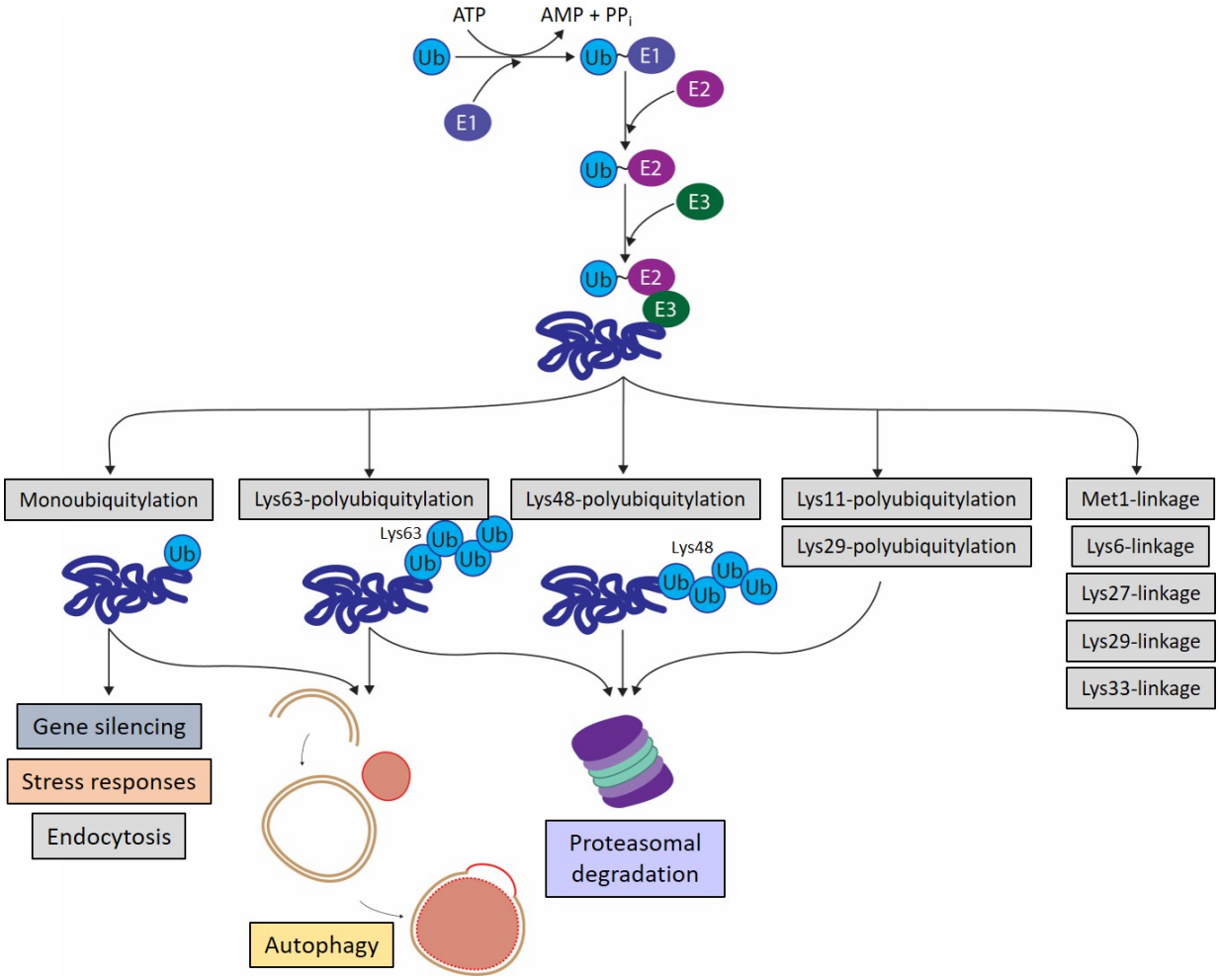

Figure 1.2. Schematic representation of the diversity of ubiquitin signals in cells. The conjugation of ubiquitin in defined linkage arrangements to various substrates in the cell provides unparalleled signalling specificity for diverse molecular processes. Ubiquitylation is an ATP-dependent process and occurs through the co-ordinated action of E1, E2 and E3 enzymes. Monoubiquitylation is involved in the regulation of gene silencing and the expression of genes involved in cellular stress responses. Monoubiquitylation also mediates endocytosis, and can additionally serve as a signal for selective autophagy. Beyond monoubiquitylation, additional ubiquitin molecules can be progressively added to form an extensive number of defined polyubiquitin chains. The diversity of polyubiquitin chains that exist are possible due to the seven internal lysine residues of ubiquitin (Lys6, Lys11, Lys27, Lys29, Lys33, Lys48, Lys63), and in some cases the Met1 at its amino-terminus. Specificity of polyubiquitin chain linkages is enabled through the activity of the specific E2 and E3 enzymes involved. At least 38 E2 and > 600 E3 genes have now been identified in the human genome, along with 2 E1 ubiquitin-activating enzymes, UBA1 and UBA6 (Deshaies and Joazeiro 2009, Schulman and Harper 2009, Ye and Rape 2009, Kaneko *et al*. 2016). Lys48-polyubiquitin chains constitute the main signal for proteasomal degradation. Lys11-, Lys29- and Lys63-linkages have also been implicated as proteasome-targeting signals for a lower proportion of protein substrates. Lys63-polyubiquitin chains serve as a major signal to adaptor proteins that link substrates to the autophagy machinery. Lys6, Lys27, Lys29 and Lys33 are less well understood and account for less than 1% of total cellular ubiquitin (Peng *et al.* 2003, Xu *et al.* 2009, Kaiser *et al.* 2011).

The stunning diversity of polyubiquitin chain linkages are generated through the coordinated action of E1, E2 and E3 enzymes in a multistep cascade of enzymatic reactions, with specificity enabled through the activity of the specific E2 and E3 enzymes involved (Deshaies and Joazeiro

2009, Rotin and Kumar 2009, Schulman and Harper 2009, Ye and Rape 2009, Zimmerman *et al.* 2010, Budhidarmo *et al.* 2012, Primorac and Musacchio 2013, Berndsen and Wolberger 2014, Spratt *et al.* 2014, Vittal *et al.* 2015). The conjugation process begins when the active site cysteine of an E1 ubiquitin-activating enzyme forms a thioester linkage with the carboxyl terminus of ubiquitin, activating the ubiquitin molecule (Haas *et al.* 1982) (Figure 1.2). The next step involves an E2 ubiquitin-conjugating enzyme with high affinity for the activated ubiquitin (Hershko *et al.* 1983, Pickart and Rose 1985). The activated ubiquitin is transferred to the active site cysteine of the E2 enzyme via *trans*-thioesterification, in coordination with relinquishment of the E1 enzyme (Eletr *et al.* 2005). Finally, linking the activated ubiquitin to the target substrate protein depends on the specificity provided by the E2 enzyme and its cognate E3 ubiquitin-ligase. E3 enzymes of the Really Interesting New Gene (RING)/U-box families (comprising > 600 human genes) link their associated E2 enzyme, charged with ubiquitin, to their specific substrate protein (Figure 1.3, a) (Deshaies and Joazeiro 2009, Budhidarmo *et al.* 2012). In contrast, ubiquitin can be transferred from the E2 enzyme to an active site cysteine of an E3 enzyme of the Homologous to E6-AP Carboxyl Terminus (HECT) family (~30 human genes) or of the RING between RING (RBR) family (~12 human genes) (Figure 1.3, b) (Rotin and Kumar 2009, Smit and Sixma 2014, Spratt *et al.* 2014).

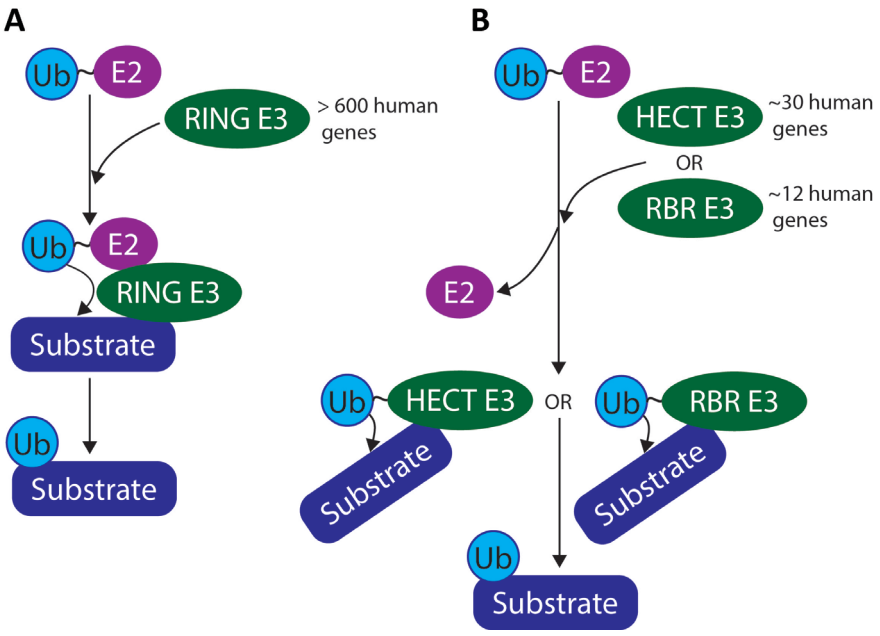

Figure 1.3. E3 ubiquitin-ligase enzymes of the RING, HECT and RBR families link ubiquitin to substrate proteins through different mechanisms. The conjugation of activated ubiquitin to its target substrate depends on the specificity provided by the E2 ubiquitin-conjugating enzyme and its cognate E3 ubiquitin-ligase enzyme. (A) E3 enzymes of the Really Interesting New Gene (RING)/U-box families (comprising > 600 human genes) link their associated E2 enzyme, charged with ubiquitin, to the specific substrate. (B) In contrast, ubiquitin can be transferred from the E2 enzyme to an active site cysteine of an E3 enzyme of the Homologous to E6-AP Carboxyl Terminus (HECT) family (~30 human genes) or of the RING between RING (RBR) family (~12 human genes).

1.3 Ubiquitin homeostasis and proteostasis in motor neurons: a challenging cellular environment

As structurally and functionally complex post-mitotic cells, the specialised environments within different neuron sub-types of the central nervous system (CNS) have uniquely high demands for efficient ubiquitin homeostasis and overall proteostasis (Yerbury *et al.* 2016). While exit from the cell cycle is necessary for the differentiation of neurons (Herrup 2013, Anda *et al.* 2016), an inherent disadvantage of the post-mitotic state is that damage caused to DNA, proteins and organelles that is not ameliorated through cellular repair processes accumulates throughout the aging process, as cells are unable to dilute damaged proteins and organelles through cell division (Evans *et al.* 2004, Akbari and Krokan 2008, Barzilai *et al.* 2008, Martin 2008, McKinnon 2009, Yerbury *et al.* 2016). Moreover, there have been several studies demonstrating that extracellular factors (e.g. chondroitin sulphate proteoglycans (CSPGs) in

the perineuronal net, a specialised extracellular matrix structure in the CNS) and intrinsic molecular programs within most neurons largely inhibit any capacity for axon regeneration following injury and damage accumulation (Dou and Levine 1994, Di Giovanni 2009, Liu *et al.* 2011, Schwab and Strittmatter 2014, Carulli *et al.* 2016, Tedeschi and Bradke 2017).

With their specialised structures and functions, neurons have exceptionally high ATP requirements (Hall *et al.* 2012). However, dysfunction of the organelle that drives energy production, the mitochondria, has been found to increase with age (Kujoth *et al.* 2005). In particular, somatic mutations in mitochondrial DNA have been extensively reported to occur in neurons and contribute to the pathogenesis of several neurodegenerative diseases (Linnane *et al.* 1989, Corral-Debrinski *et al.* 1992, Corral-Debrinski *et al.* 1992, Corral-Debrinski *et al.* 1994, Brierley *et al.* 1998, Michikawa *et al.* 1999, Lin *et al.* 2002, Coskun *et al.* 2004, Kraytsberg *et al.* 2006). ATP is crucial for the maintenance of proteostasis and ubiquitin homeostasis (Yerbury *et al.* 2016). It is required for protein synthesis, for the activity of most chaperones in the human chaperome, and for ubiquitylation, thus for all downstream ubiquitin-dependent molecular processes (Hershko *et al.* 1980, Haas *et al.* 1982, Brehme *et al.* 2014). These requirements for ATP are higher in motor neurons as these processes need to be carried out efficiently in the far-reaching locales of the motor neuron, from the soma, along axons through to synaptic terminals. Hence, an age-related decline in mitochondrial function and subsequent disruptions in energy metabolism increase the vulnerability of motor neurons to proteostasis dysfunction with increasing age (Yerbury *et al.* 2016).

Recently it was discovered that the proteome of spinal motor neurons is supersaturated (i.e. the concentration of individual proteins is high relative to their solubility) in comparison to oculomotor neurons, which are resistant to degeneration in ALS (Ciryam *et al.* 2015, Yerbury *et al.* 2019). This suggests that the metastability of the spinal motor neuron proteome may contribute to a distinct susceptibility to proteostasis dysfunction. As discussed in section 1.2.2,

the expression of a sub-network of chaperones in the human chaperome, including many ATP-dependent chaperones, has been reported to decline with age (Brehme *et al.* 2014). As cells age their ability to activate appropriate responses to proteotoxic stress deteriorates (Ben-Zvi *et al.* 2009). Together, these age-related changes are potently problematic in motor neurons harbouring genetic mutations, as the proteostasis network is compromised in its ability to manage any aberrant mutant RNA or protein species that result. Mutant RNA and protein species are then able to further aggravate dysfunction in the proteostasis network by overloading key components and disrupting their functions (Matsumoto *et al.* 2005, Gidalevitz *et al.* 2006, Weisberg *et al.* 2012). For instance, it has been postulated that genetic mutations that increase protein aggregation-propensity may decrease the ability of the chaperone network to correctly fold other proteins or direct them to degradative machinery, leading to accumulation of misfolded proteins (Bruijn *et al.* 2004).

Deterioration of the proteostasis network in aging neurons is evident in the fact that pathological protein inclusions are a common feature of several different age-associated neurodegenerative diseases. Critically, disruption of the functioning of the UPS and of molecular chaperones (e.g. HSP40, HSP70) is well documented to occur in these diseases, and in some cases increasing the levels of components of these systems has been reported to suppress pathological protein aggregation (Bence *et al.* 2001, Cleveland and Rothstein 2001, Watanabe *et al.* 2001, Kim *et al.* 2002, Takeuchi *et al.* 2002, Urushitani *et al.* 2002, Bruijn *et al.* 2004, Holmberg *et al.* 2004, Kabashi *et al.* 2004, Bennett *et al.* 2005, Yerbury *et al.* 2013). Indeed, the affected motor neurons in post-mortem spinal cord tissue from individuals with sALS and fALS universally contain ubiquitin-positive inclusions, providing strong evidence that the proteostasis network is dysfunctional in ALS; in particular, the UPS and ubiquitin homeostasis (Leigh *et al.* 1991). As will be discussed in the following section, extensive evidence indicates that many of the genetic mutations that segregate with ALS disrupt the proteostasis network.

1.4 A growing list of genes are associated with ALS

Many of the ALS-associated genes encode proteins with functional roles in the maintenance of proteostasis in cells, or that are aggregation-prone, or that, in their mutant form, cause dysfunction of components of proteostasis machinery (Table 1.1). Hence, proteostasis dysfunction in motor neurons may be an underlying pathogenic link between the different ALS-associated genetic mutations.

Table 1.1. List of some of the ALS-associated genetic mutations and the potential mechanisms by which they lead to disruptions in cellular proteome homeostasis (proteostasis).

Gene; Protein	Disease phenotype	Function	Chromosomal locus	Examples of ALS-associated mutations	Potential mechanisms of proteostasis disruption	References
***SOD1;* Cu/Zn superoxide dismutase (SOD1)**	ALS ALS/FTD	Catalyses the conversion of superoxide radicals to molecular oxygen and hydrogen peroxide.	21q22.11	> 180 mutations. Most common: G93A; D90A; A4V; I113T; L144F	Impaired molecular chaperone activity and UPS activity.	Shibata *et al.* (1996), Bruijn *et al*. (1997), Bruening *et al*. (1999), Johnston *et al*. (2000), Kato *et al.* (2000), Watanabe *et al.* (2001), Takeuchi *et al*. (2002), Urushitani *et al.* (2002), Wang *et al*. (2002), Cheroni *et al*. (2005), Matsumoto *et al*. (2005), Cheroni *et al*. (2009), Crippa *et al.* (2010), Onesto *et al.* (2011).
***TARDBP;* TAR DNA binding protein 43 kDa (TDP-43)**	ALS ALS/FTD FTD	Predominantly localised to nucleus; binds DNA and RNA, regulates transcription, mRNA splicing and transport. Assembly and regulation of stress granules.	1p36.22	G287S; G290A; S292N; G294A; G298; A315T; E331K; R361S; D169G; M337V; G348C; A382T; N390D; N390S	Cytoplasmic accumulation; disrupted stress granule dynamics; disruptions in transcription, mRNA processing; disruptions in expression of TDP-43 and FUS mRNA targets.	Neumann *et al.* (2006), Sreedharan *et al.* (2008), Ayala *et al.* (2008), Belzil *et al.* (2009), Johnson *et al.* (2009), Kwiatkowski *et al.* (2009), Ticozzi *et al*. (2009), Vance *et al.* (2009), Blair *et al*. (2010), Corrado *et al*. (2010), DeJesus-Hernandez *et al*. (2010), Deng *et al*. (2010), Van Langenhove *et al*. (2010), Dewey *et al.* (2011), Lai *et al*. (2011), Polymenidou *et al*. (2011), Sephton *et al*. (2011), Tollervey *et al*. (2011), Colombrita *et al*. (2012), Dichmann and Harland (2012), Ishigaki *et al*. (2012), Keller *et al.* (2012), Lagier-Tourenne *et al*. (2012), Rogelj *et al*. (2012), Nakaya *et al*. (2013).
***FUS;* Fused in sarcoma (FUS)**	ALS ALS/FTD FTD	Predominantly localised to nucleus; binds DNA and RNA, regulates transcription, mRNA splicing and transport. Assembly and regulation of stress granules.	16p11.2	H517Q; R521G; insGG; delGG; R244C; R514S; G515C; R518K; R521C; R521G; R521H; R522G; R524T; R524S; P525L		
***UBQLN2;* Ubiquilin-2 (UBQLN2)**	ALS ALS/FTD	Member of the ubiquilin protein family; ubiquitin-like proteins involved in the UPS and autophagy.	Xp11.21	P497H; P497S; P506T; P509S; P525S	Impaired UPS activity and autophagy.	Deng *et al.* (2011), Fecto *et al.* (2012), Teyssou *et al.* (2017).
***OPTN;* Optineurin (OPTN)**	ALS ALS/FTD	Maintenance of the Golgi complex; membrane trafficking; post-Golgi trafficking to lysosomes; exocytosis.	10p13	Deletion of exon 5; R96L; E478G; A481V; Q398X; Q165X	Golgi dysfunction and impaired post-Golgi trafficking; impaired autophagy; aberrant accumulation of OPTN.	Sahlender *et al.* (2005), del Toro *et al.* (2009), Maruyama *et al.* (2010), Ito *et al.* (2011), Keller *et al.* (2012).

***VAPB*; Vesicle-associated membrane protein [VAMP]-associated protein B (VAPB)**	ALS SMA	Localised to ER membrane & pre-Golgi intermediates; regulates ER-organelle & ER-cytoskeleton interactions; recruits lipid-binding proteins to cytosolic surface of ER membranes; homeostatic and signalling functions at neuromuscular synapse.	20q13.3	P56S	ER dysfunction; oligomerisation and aggregation; dominant-negative inhibition of wild-type VAPB.	Skehel *et al.* (2000), Nishimura *et al.* (2004a), Nishimura *et al.* (2004b), Kaiser *et al.* (2005), Loewen and Levine (2005), Teuling *et al.* (2007), Ratnaparkhi *et al*. (2008), Suzuki *et al*. (2009), Forrest *et al*. (2013), Kuijpers *et al*. (2013), Qin *et al.* (2013).
***VCP*; Transitional endoplasmic reticulum ATPase/p97 (VCP)**	ALS ALS/FTD FTD	AAA+-ATPase; regulates a variety of cellular functions: cell signalling, cell cycling, organelle biogenesis, protein degradation via autophagy, UPS & ER-associated degradation (ERAD).	9p13	R191Q; R159G; D592N; R155H; I151V; I114P	Impaired ERAD, UPS and autophagy.	Ye *et al.* (2001), Watts *et al.* (2004), Weihl *et al.* (2007), Ju *et al.* (2009), Gitcho *et al.* (2009), Johnson *et al.* (2010), Meyer *et al.* (2012).
***SQSTM1;* Sequestosome-1 (p62)**	ALS ALS/FTD	Multifunctional; roles in UPS and autophagy.	5q35	P392L; A33V; V153I; S370P; K238E; K344E; P348L	Impaired UPS activity and autophagy; aberrant accumulation and aggregation of p62.	Fecto *et al.* (2011), Teyssou *et al.* (2013), Rubino *et al.* (2012).
***C9ORF72;* Chromosome 9 open reading frame 72 (C9ORF72)**	ALS ALS/FTD FTD	Membrane trafficking and autophagy.	9p21.2	$(GGGGCC)_n$ hexanucleotide repeat expansion	Loss of function in autophagy; proteotoxicity through production and aberrant activity of dipeptide-repeat (DPR) proteins; disruption of RNA metabolism through production and activity of RNA foci.	Todd and Paulson (2010), Hernandez *et al.* (2011), Renton *et al.* (2011), Mori *et al.* (2013), May *et al.* (2014), Peters *et al.* (2015), Haeusler *et al.* (2016), Webster *et al.* (2016), Chitiprolu *et al.* (2018).
***TAF15*; TATA-binding protein associated factor 15 (TAF15)**	ALS	Predominantly localised to nucleus; binds DNA and RNA, regulates transcription, mRNA splicing and transport. Stress granule dynamics.	17q11.1-q11.2	G391E; R408C; G473E; M368T; D386N; R388H; R395Q	Disrupted stress granule dynamics; disruptions in transcription, mRNA processing.	Couthouis *et al.* (2011), Ticozzi *et al.* (2011).

1.4.1 SOD1 and C9ORF72; the major genetic players?

Mutations in the gene encoding SOD1 are among the most well studied in fALS, accounting for a significant proportion (20-25%) of all fALS cases (Bosco *et al.* 2010, Chen *et al.* 2013) and 2% of sALS cases (Pasinelli and Brown 2006). The first reports of an association between mutant SOD1 and ALS were published in 1993 (Deng *et al*., 1993; Rosen *et al*., 1993), and since then at least 180 different mutations that are associated with ALS have been identified in this gene, located at chromosomal locus 21q22.11 (Abel *et al.* 2013). Disease onset and progression is variable among individuals with different *SOD1* mutations, and even between people with the same *SOD1* mutation (Picher-Martel *et al.* 2016). The propensity of SOD1 mutants to unfold and aggregate correlates with cellular toxicity, and it has been proposed that this may contribute to variation in disease severity associated with different *SOD1* mutations (McAlary *et al.* 2016). The Ala4Val mutation in *SOD1* (*SOD1*^{A4V}) has been documented to present as one of the more severe forms of ALS with rapid disease progression (Cudkowicz *et al.* 1997, Juneja *et al.* 1997). In zebrafish ALS models, it has been found that the disease phenotype is most aggressive in animals injected with *SOD1*^{A4V} mRNA compared to *SOD1*^{G93A} or *SOD1*^{G37R} mRNA (Lemmens *et al.* 2007).

In its wild-type form (SOD1^{WT}), SOD1 is a 32 kDa soluble cytosolic homodimeric protein, with one copper- and one zinc-binding site per monomer (Crapo *et al.* 1992, Strong *et al.* 2005). It is a highly conserved antioxidant that catalyses the conversion of superoxide radicals to molecular oxygen and hydrogen peroxide, protecting cells from uncontrolled reactions with harmful oxygen free radicals (McCord and Fridovich 1969). Of all cell types in the body it is found in its highest concentration within motor neurons (Bergeron *et al.* 1996).

Most *SOD1* mutations are dominant, and it is now widely recognised that mutations contribute to neurodegeneration via a toxic gain-of-function mechanism as opposed to a loss of antioxidant activity (Gurney *et al.* 1994, Ripps *et al.* 1995, Wong *et al.* 1995, Reaume *et al.* 1996, Bruijn

et al. 1997, Nagai *et al.* 2001, Howland *et al.* 2002, Wang *et al.* 2003, Jonsson *et al.* 2004). Supporting this is the finding that transgenic *SOD1* knockout mice do not develop ALS symptoms (Reaume *et al.* 1996). Moreover, increased expression of $SOD1^{WT}$ accelerates disease progression (Jaarsma *et al.* 2000, Deng *et al.* 2006). Studies using conformation-specific antibodies that are selective for misfolded $SOD1^{WT}$ with altered post-translational modifications have detected misfolded $SOD1^{WT}$ in sALS patients, demonstrating that $SOD1^{WT}$ is able to adopt abnormal conformations (Bosco *et al.* 2010, Pokrishevsky *et al.* 2012). Ubiquitylated intracellular inclusions containing detergent-insoluble protein aggregates immunoreactive to SOD1 are a characteristic pathological feature observed in post-mortem spinal cord tissue samples from *SOD1*-fALS patients (Shibata *et al.* 1996, Kato *et al.* 2000) as well as in mutant *SOD1* transgenic mouse models (Bruijn *et al.* 1997, Johnston 2000, Watanabe *et al.* 2001, Wang *et al.* 2003). Interestingly, Keller *et al.* (2012) found that *SOD1*-fALS patients possess a unique immunohistochemical signature, including the presence of C9ORF72-positive inclusions. In fact, the TDP-43-positive inclusions that are a hallmark of most genetic variants of fALS and sALS are not found in *SOD1*-fALS patients or transgenic mouse models (Mackenzie *et al.* 2007).

Beyond the presence of ubiquitin in SOD1 inclusions, there is extensive evidence indicating that aberrant interactions occur between mutant SOD1 and other proteostasis components. The first report of an effect of mutant SOD1 in modulating the activity of different molecular chaperones was published ~20 years ago (Bruening *et al.* 1999). Numerous studies have since documented correlations between mutant SOD1 aggregation, modulation of the activity of chaperones and decreases in UPS activity in neuronal cell culture and in spinal cord motor neurons in mouse models of *SOD1*-fALS (Watanabe *et al.* 2001, Takeuchi *et al.* 2002, Cheroni *et al.* 2005, Matsumoto *et al.* 2005, Cheroni *et al.* 2009, Crippa *et al.* 2010). Critically, the activity of the UPS is significantly more compromised by mutant SOD1 in spinal cord motor

neurons of *SOD1*^{G93A} mice than in non-motor neurons (Urushitani *et al.* 2002). Corroborating this evidence that motor neurons have a distinct vulnerability to UPS dysfunction, Onesto *et al.* (2011) observed that mutant SOD1 aggregation and UPS dysfunction occurred exclusively in motor neuron-like NSC-34 cells, and not in C2C12 muscle cells. Given that molecular chaperones and the UPS are essential for the maintenance of proteostasis and for the regulation of normal cellular activities, these data indicate that a potential mechanism of mutant SOD1 neurotoxicity is through decreasing the capacity of the UPS and the chaperone network (Figure 1.4). The increased burden on proteostasis machinery likely impairs the ability of the cell to correctly fold or degrade other proteins, leading to drastic disruptions in diverse molecular processes, cellular dysfunction and loss of viability.

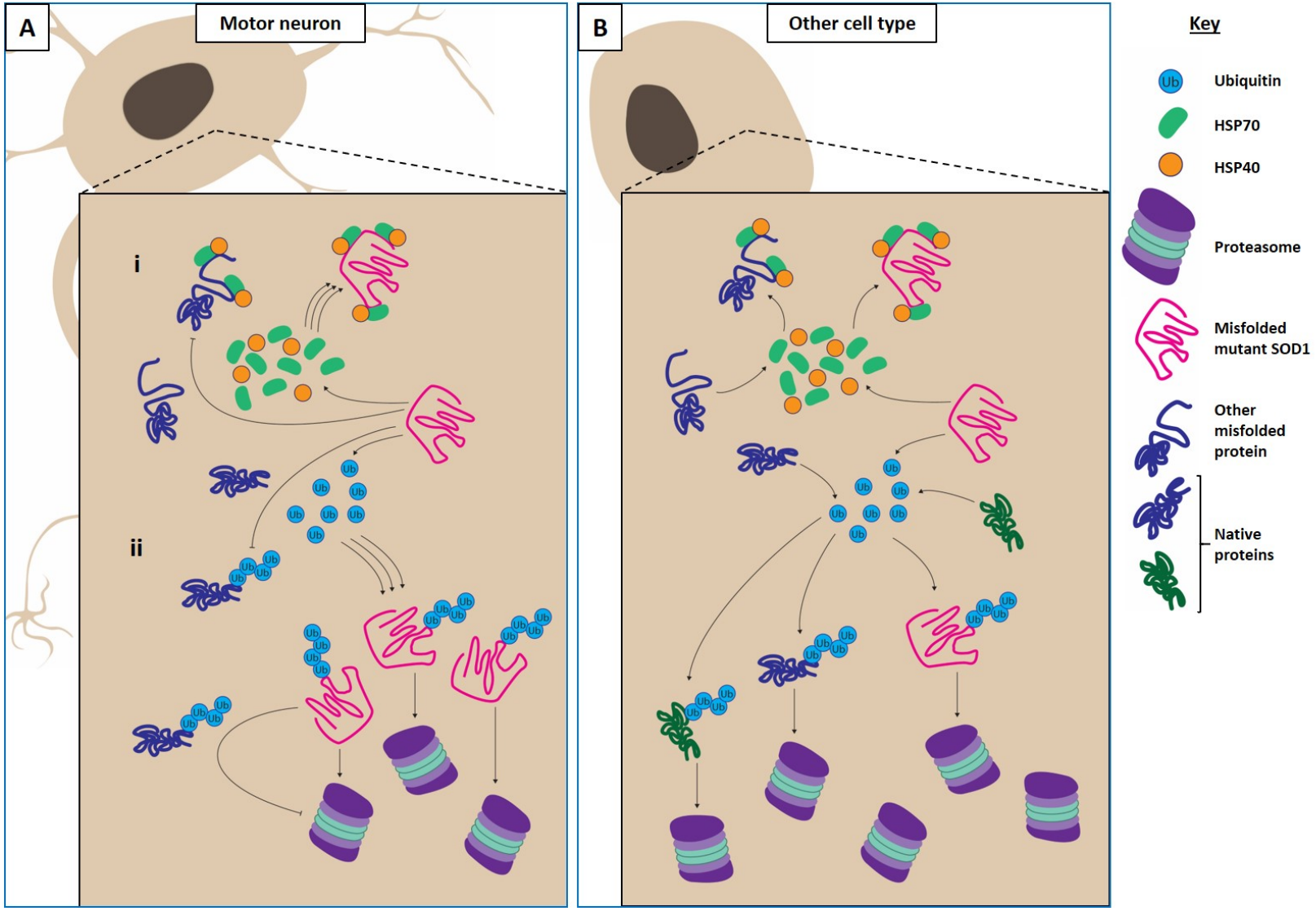
A
Motor neuron
B
Other cell type
i
ii
Key
Ub
Ubiquitin
HSP70
HSP40
Proteasome
Misfolded mutant SOD1
Other misfolded protein
Native proteins

Figure 1.4. Potential pathogenic mechanisms of mutant SOD1 on the UPS and chaperone activity in motor neurons. Compared to other cell types, motor neurons have a distinct vulnerability to mutant SOD1-mediated UPS dysfunction and disruptions in the activity of molecular chaperones. (A) In motor neurons, (i) misfolded mutant SOD1 may overload the capacity of molecular chaperone systems, e.g. the HSP70/HSP40 system, thereby decreasing the capacity of these chaperone systems to fold other proteins in the cell, leading to accumulation of aberrant protein species. (ii) Evidence indicates that mutant SOD1 may be preferentially targeted for proteasomal degradation, however, this conversely may cause overloading of the UPS in motor neurons, disrupting the proteasomal degradation of other substrate proteins in the cell. (B) In other cell types (e.g. muscle cells, non-motor neurons) the expression of mutant SOD1 does not lead to disruptions in the capacity of the molecular chaperone systems or of the UPS.

The most common genetic cause of ALS currently identified is a $(GGGGCC)_n$ repeat expansion that occurs either in the first intron or the promoter of the *C9ORF72* gene on chromosome 9, varying depending on the transcript isoform (Beck *et al.* 2013). In normal, healthy individuals the GGGGCC hexanucleotide sequence is repeated no more than 33 times, compared to up to hundreds and even thousands of repeats in patients with ALS, FTD and ALS/FTD (DeJesus-Hernandez *et al.* 2011, Beck *et al.* 2013, van der Zee *et al.* 2013). Hernandez *et al.* (2011) first identified this hexanucleotide expansion in a large cohort of fALS patients also exhibiting a FTD phenotype, as well as in a smaller percentage of sALS patients. Mutant *C9ORF72* accounts for about 40% of fALS and 7% of sALS (Majounie *et al.* 2012).

The function of C9ORF72 was elucidated over several studies in the past decade. Initially, two independent groups identified homology of full-length C9ORF72 with DENN (Differentially Expressed in Normal and Neoplasia)-domain proteins (Zhang *et al.* 2012, Levine *et al.* 2013). DENN-domain proteins are highly conserved GDP/GTP exchange factors (GEFs) for Rab-GTPases, which regulate many aspects of membrane trafficking. This implicated a very important role for C9ORF72 in key cellular processes, including the autophagic protein degradation pathway. It was through the work of Webster *et al.* (2016) that the role of C9ORF72 in regulating the first steps of autophagy was demonstrated. One of the major theories regarding the pathological role of the *C9ORF72* mutation in FTD and ALS is that it leads to haploinsufficiency and thus a loss-of-function mechanism (DeJesus-Hernandez *et al.* 2011).

Pathogenicity of *C9ORF72* mutation is also believed to result from accumulation of the non-coding repeat expansion mRNA in the cytoplasm and nucleus, forming toxic RNA foci that sequester RBPs (Todd and Paulson 2010, DeJesus-Hernandez *et al.* 2011, Renton *et al.* 2011). RNA foci are characteristic molecular hallmarks of pathogenesis in myotonic dystrophy and several other neurological disorders (Wojciechowska and Krzyzosiak 2011). Additionally, ALS patients with the *C9ORF72* mutation exhibit the characteristic intracellular inclusions of misfolded proteins, particularly phosphorylated TDP-43 aggregates (DeJesus-Hernandez *et al.* 2011). Cytoplasmic inclusions that are unique to *C9ORF72*-ALS, *C9ORF72*-ALS/FTD and *C9ORF72*-FTD have also been reported; characteristically TDP-43-negative, p62-, ubiquitin- and UBQLN2-positive inclusions that contain poly-(Gly-Ala), -(Gly-Pro) and –(Gly-Arg) dipeptide-repeat (DPR) proteins (Mori *et al.* 2013, May *et al.* 2014).

DPR pathology is a direct consequence of the GGGGCC hexanucleotide repeat expansion, through repeat-associated non-ATG-initiated (RAN) translation of this intronic repeat from both the sense and antisense transcripts (Ash *et al.* 2013, Gendron *et al.* 2013, Mann *et al.* 2013, Mori *et al.* 2013, Zu *et al.* 2013, May *et al.* 2014). Poly-(Gly-Ala) DPRs are the most abundant DPR species in post-mortem brain tissue from individuals with repeat expansions in *C9ORF72* (Mori *et al.* 2013). Proteomic analysis of poly-(Gly-Ala) aggregates has detected strong enrichment for p62, the proteasome subunits PSMB4, PSMB5, PSMB6, PSMC6, and PSMD13, several ubiquitin-related proteins, including UBQLN1 and UBQLN2, and the multifunctional protein UNC119 (May *et al.* 2014). UNC119 is required for axon development and maintenance and has key roles in synaptic functions (Maduro and Pilgrim 1995). *UNC119* mutation in *Caenorhabditis elegans* leads to motor dysfunction (Knobel *et al.* 2001). It is thus possible that DPR aggregates contribute to neuronal dysfunction and degeneration in individuals with *C9ORF72* repeat expansions through sequestering proteins, such as UNC119, with important functions in neuronal health. Accumulating evidence suggests that it is a combination of

C9ORF72 haploinsufficiency and the toxic gain-of-function mechanisms of aberrant RNA foci and DPRs that cause the full spectrum of pathology observed in individuals with *C9ORF72* repeat expansions (Peters *et al.* 2015, Haeusler *et al.* 2016, Chitiprolu *et al.* 2018).

1.4.2 Mutations in genes involved in protein degradation pathways

1.4.2.1 *UBQLN2* mutations

Several ALS-associated genes function in protein degradation pathways. Mutations in the *UBQLN2* gene (chromosomal locus Xp11.21) cause X-linked fALS and ALS/FTD (Deng *et al.* 2011). UBQLN2 is a member of the ubiquilin protein family, ubiquitin-like proteins that are involved in delivering ubiquitylated proteins to the proteasome and have roles in autophagy (Ko *et al.* 2004, Rothenberg *et al.* 2010). UBQLN2 has an N-terminal ubiquitin-like (UBL) domain that binds to the proteasome and a C-terminal ubiquitin-associated (UBA) domain that binds to substrate proteins. Interestingly, Deng *et al.* (2011) found that all the *UBQLN2* mutations (P497H, P497S, P506T, P509S and P525S) detected in patients affect proline residues in a unique PXX repeat region, indicating that these mutations could confer a common pathogenic property on the UBQLN2 protein. Through work using cell culture models, these researchers investigated the functional consequence of mutant UBQLN2 on ubiquitin-mediated protein degradation and found that protein degradation via the UPS was impaired. Moreover, mutations in *UBQLN2* have been found to cause impaired autophagy (Fecto *et al.* 2012, Teyssou *et al.* 2017). Such disruptions to degradative pathways, which are crucial for proteostasis, could contribute significantly to further proteostasis disruptions and the accumulation and aggregation of aberrant proteins in the cell.

Examining post-mortem spinal cord sections from two fALS patients with a P497H or P506T mutation, Deng *et al*. (2011) observed skein-like inclusions that were immunoreactive to two types of UBQLN2 antibodies. These same inclusions were also immunoreactive for p62, TDP-43, FUS and OPTN, proteins that, as discussed in other sections of this chapter, are found in

inclusions in other types of ALS. Of note, these inclusions were not found to contain SOD1. UBQLN2 was also detected in the skein-like inclusions observed in a broad spectrum of ALS cases; sporadic and familial forms of ALS, including those caused by either *SOD1* or *TARDBP* mutations, and ALS/FTD (Deng *et al.* 2011). This common association of UBQLN2 with inclusions indicates that it could have important roles in ALS and ALS/FTD caused by mutations in different genes.

1.4.2.2 *SQSTM1* mutations

Mutations in *SQSTM1*, encoding another ubiquitin-binding protein, p62, have been reported in fALS, sALS and FTD (Fecto *et al.* 2011, Rubino *et al.* 2012, Teyssou *et al.* 2013). P62 is a multifunctional protein with particularly important roles in proteasomal and autophagic protein degradation (Seibenhener *et al.* 2004, Bjorkoy *et al.* 2006). The involvement of p62 in neurodegeneration is becoming increasingly apparent, with p62-immunoreactive inclusions a common pathological feature in many neurodegenerative diseases including AD, PD, HD, FTD as well as in the motor neurons of ALS patients (Kuusisto *et al.* 2002, Zatloukal *et al.* 2002, Nakaso *et al.* 2004, Mizuno *et al.* 2006, Pikkarainen *et al.* 2008). It is often detected co-localised with TDP-43 and ubiquitin in the inclusions of ALS and FTD patients (Hiji *et al.* 2008, Deng *et al.* 2010, Keller *et al.* 2012, Teyssou *et al.* 2013).

The mutations that have been identified in ALS and FTD patients are distributed throughout the whole protein, but most affect amino acids that are highly conserved in mammals, and that are in different functional domains important for protein-protein interactions. For instance, several mutations have been found in its UBA domain, affecting the binding of p62 to ubiquitin and ubiquitylated proteins (Fecto *et al.* 2011, Teyssou *et al.* 2013). Both proteasomal and autophagic protein degradation may be severely impeded in such variants. Indeed, some mutations (e.g. K344E) have been detected in a region of the protein that interacts with LC3, a key autophagy-related protein, and are therefore likely to interfere with this interaction and thus

impede the autophagic pathway (Rubino *et al.* 2012). As well as a loss-of-function mechanism contributing to disease, mutations may lead to a toxic gain-of-function through dysregulation of the cell signalling pathways in which p62 has key roles. For example, several mutations affect the PEST (proline-, glutamic acid-, serine-, threonine-enriched) domain, which forms a signal peptide important for degradation of p62 and thus for regulating p62 protein levels (Fecto *et al.* 2011). Such altered levels of p62 may lead to both accumulation and aggregation of misfolded p62 and disturbance of the signalling pathways regulated by this protein. Given the common presence of p62 pathology in several neurodegenerative diseases, it is likely that it is fundamentally involved in the pathogenesis of these diseases, potentially through disruption of its functions in proteostasis.

1.4.2.3 *VCP* mutations

Mutations in *VCP* have been identified in patients suffering from a spectrum of neurodegenerative disorders including inclusion body myopathy with Paget disease of bone (PDB) and/or FTD (IBMPFD) (Weihl *et al.* 2009). An exome sequencing study revealed that *VCP* mutations were causal in a cohort of fALS cases, and that mutations in this gene may account for ~1-2% of fALS cases (Johnson *et al.* 2010). Mutations in *VCP* lead to TDP-43-immunoreactive, ubiquitylated cytoplasmic inclusions in muscle and frontal cortex neurons of patients (Watts *et al.* 2004, Weihl *et al.* 2008) and in transgenic mouse models harbouring the R155H and A232E mutations (Weihl *et al.* 2007, Badadani *et al.* 2010, Custer *et al.* 2010). A novel mutation in *VCP*, I114P, has also been detected in sALS (Koppers *et al.* 2012), though the pathogenicity of this variant is yet to be confirmed. This same study detected inclusions positive for p62, ubiquitin and TDP-43, and confirmed the *VCP*-ALS frequency of ~1-2% found in the exome sequencing study.

VCP is a highly conserved AAA+-ATPase, involved in the regulation of a variety of cellular functions. These include cell signalling, the cell cycle, organelle biogenesis, and in particular,

protein degradation via autophagy, the UPS, and the endoplasmic reticulum-associated degradation (ERAD) pathway; VCP provides mechanical force for extracting substrates from the ER membrane (Ye *et al.* 2001, Johnson *et al.* 2010, Meyer *et al.* 2012). In autophagy, VCP is essential for maturation of ubiquitin-containing autophagosomes. The *VCP* mutations identified in ALS and IBMPFD interestingly all occur in the N-terminal region of the protein, which functions in binding polyubiquitylated proteins (Watts *et al.* 2004, Johnson *et al.* 2010). Studies of mutant VCP using cell culture and transgenic mouse models has shown that loss of VCP activity impairs autophagy; specifically, autophagosomes fail to mature into autophagolysosomes, leading to the accumulation of non-degradative autophagosomes and aggregated proteins (Ju *et al.* 2009). Moreover, mutations in *VCP* have been found to lead to impaired proteasome activity, endoplasmic reticulum (ER) stress and activation of apoptosis signalling pathways (Gitcho *et al.* 2009). It is conceivable that the functions of VCP in protein degradation are disrupted in *VCP*-fALS, and that these disruptions lead to the accumulation and aggregation of ubiquitylated proteins in motor neurons.

1.4.2.4 *OPTN* mutations

Maruyama *et al.* (2010) reported the first findings of mutations in the *OPTN* gene in fALS patients, the product of which has been detected in inclusions within post-mortem spinal cord tissue from individuals with fALS and sALS, co-localised with ubiquitin, TDP-43, FUS and SOD1 in different cases (Maruyama *et al.* 2010, Ito and Suzuki 2011, Keller *et al.* 2012). OPTN is a multifunctional protein involved in maintenance of the Golgi apparatus and post-Golgi trafficking to the cell surface and to lysosomes through its interactions with huntingtin, Rab8 and myosin VI (Sahlender *et al.* 2005, del Toro *et al.* 2009). It may also have a role in regulating its own expression, as an inhibitor of the activation of nuclear factor kappa B (NF-κB), which mediates upregulation of OPTN (Zhu *et al.* 2007, Mrowka *et al.* 2008).

The co-localisation of OPTN in the SOD1-immunoreactive inclusions of *SOD1*-fALS patients,

as well as in other fALS variants, such as *C9ORF72* repeat expansion carriers and those with mutations in *TARDBP*, *FUS* and in individuals with sALS (Maruyama *et al.* 2010, Keller *et al.* 2012), indicates a broad role for OPTN in the pathogenic mechanisms of ALS. Moreover, OPTN has been detected in the inclusion bodies characteristic of a wide range of neurodegenerative diseases including AD, PD and Creutzfeldt-Jakob disease (CJD) (Osawa *et al.* 2011) and mutations have been implicated in primary open angle glaucoma (POAG), a neurodegenerative eye disease (Rezaie *et al.* 2002). This suggests that OPTN could contribute to neurodegeneration in these diseases via common pathogenic pathways. Two of the mutations in *OPTN*, a Q398X nonsense mutation and a homozygous deletion of exon 5 (Ex5del), result in a loss-of-function phenotype, disturbing Golgi organisation and regulation, and post-Golgi transport. Indeed, depletion of OPTN through RNA interference has been shown to result in Golgi disorganisation and reduced post-Golgi transport (Sahlender *et al.* 2005). As with *SQSTM1*-, *VCP*- and *UBQLN2*-fALS cases, mutations in *OPTN* potentially cause impairment of autophagy; mutations in *OPTN* and disruptions of its functions would lead to altered trafficking of lysosomal proteins from the Golgi, causing disruptions in lysosomal function.

The glutamic acid residue substituted in the E478G mutation is highly conserved among OPTN proteins of a wide range of species and occurs in the ubiquitin-binding domain of the protein that mediates its interaction with NF-κB (Maruyama *et al.* 2010). Consistent with the observation that OPTN-immunoreactivity in tissue from a patient with the E478G mutation is increased, the E478G mutation potentially causes upregulation of OPTN through overactive NF-κB activity. While the initial pathological mechanisms caused by these mutations differ, their downstream effects converge in disrupting proteostasis, through dysfunction of OPTN in protein degradation, or through increasing the levels of an aberrant mutant form of OPTN. It is also conceivable that aggregation of OPTN results in loss of soluble protein from the cell, and consequently causes further loss-of-function and disruption of its roles in proteostasis.

1.4.2.5 *VAPB* mutations

In 2004 a new chromosomal locus (20q13.3) was identified for an atypical form of ALS, ALS8 (Nishimura *et al.* 2004), and subsequently a novel missense mutation, P56S, was found in the gene encoding VAPB (Nishimura *et al.* 2004). VAPB belongs to a family of ubiquitously expressed, type II integral membrane VAP proteins that localise to the ER membrane and pre-Golgi intermediates (Skehel *et al.* 2000), and are involved in non-vesicular transfer of lipids, membrane trafficking, regulating ER-organelle and ER-cytoskeleton interactions, transport and secretion, as well as homeostatic and signalling functions at the neuromuscular junction (Soussan *et al.* 1999, Foster *et al.* 2000, Amarilio *et al.* 2005, Lev *et al.* 2008, De Vos *et al.* 2012, Han *et al.* 2012, Manford *et al.* 2012). The VAP protein family also target lipid-binding proteins carrying a short motif containing two phenylalanines in an acidic tract (FFAT motif). Recognising the FFAT motif, VAPs then recruit them to the cytosolic surface of ER membranes (Kaiser *et al.* 2005, Loewen and Levine 2005). Mammalian species have two VAP proteins; VAPA and VAPB (Nishimura *et al.* 1999).

Several mutations in *VAPB* have now been identified in people with ALS, however the P56S mutation is the only one currently known to co-segregate with ALS (Nishimura *et al.* 2004, Kabashi *et al.* 2013). *In vitro* and *in vivo* this mutation causes VAPB to oligomerise, aggregate and accumulate in inclusions (Nishimura *et al.* 2004, Teuling *et al.* 2007, Tudor *et al.* 2010, Kuijpers *et al.* 2013, Qiu *et al.* 2013). Interestingly, Teuling *et al.* (2007) found that mutant $VAPB^{P56S}$ aggregates are continuous with the ER, possibly through interactions between the transmembrane domains of the mutant VAPB proteins with $VAPB^{WT}$ still anchored to the ER membrane. Furthermore, by trapping endogenous $VAPB^{WT}$ in mutant aggregates and reducing cytosolic VAPB levels, this interaction impairs the normal function of VAPB. The hypothesis of a dominant-negative mechanism of action of mutant VAPB in disease is supported by other work carried out in yeast, mammalian cell culture, *Drosophila* and in transgenic mice

(Ratnaparkhi *et al.* 2008, Suzuki *et al.* 2009, Forrest *et al.* 2013, Kuijpers *et al.* 2013). Moreover, Teuling *et al.* (2007) reported that VAPA and VAPB levels are reduced in the spinal cord motor neurons of ALS patients, in contrast to the normally abundant levels of these proteins in the CNS of healthy individuals not affected by ALS, particularly in motor neurons. The relatively high lipid metabolism and lipid transport requirements of large, complex motor neurons makes them particularly vulnerable to reduced VAP function caused by mutation. Golgi disassembly has been shown to result from abnormal lipid metabolism (Fukunaga *et al.* 2000, Gonatas *et al.* 2006). The disruption of intracellular transport and membrane trafficking caused by reduced VAPB activity and abnormal lipid metabolism may additionally affect autophagy.

Strikingly, findings made in work by Kuijpers *et al.* (2013) suggest a novel mechanism in motor neurons that may enable them to cope with mutant VAPB levels that exceed the capacity of the normal quality control pathways. They reported on extensive data that support a hypothesis in which mutant VAPB inclusions represent a specialised ER-associated protein quality control compartment, reminiscent of aggresomes, that isolates misfolded and aggregated VAPB from the rest of the ER. Moreover, these researchers showed that mutant VAPB inclusions in $VAPB^{P56S}$ transgenic mice were reversible ER-associated structures that were enriched in factors that operate in the ERAD pathway (VCP, Derlin-1 and BAP31), the presence of which was not associated with signs of motor neuron degeneration (Kuijpers *et al.* 2013). The lack of neuronal pathology in these mice may be due to effective sequestration and clearance of mutant VAPB in this novel protective compartment, preventing its aberrant accumulation and interaction with $VAPB^{WT}$.

1.4.3 DNA/RNA-binding proteins in ALS

The role of aberrant RNA metabolism in ALS pathogenesis first came to light with the discovery that the D/RBP TDP-43 is one of the major protein constituents of ubiquitylated

inclusions in sALS, which comprises the majority (~90%) of all ALS cases (Neumann *et al.* 2006). It was also found to be the major constituent of inclusions in *MAPT*-negative FTD patients, providing the first biochemical evidence of a molecular link between ALS and FTD (Arai *et al.* 2006, Neumann *et al.* 2006). Subsequently, mutations were identified in a highly conserved region of the *TARDBP* gene in both fALS and sALS patients (Sreedharan *et al.* 2008), as well as ALS/FTD and FTD patients (Borroni *et al.* 2009, Gitcho *et al.* 2009, Andersen and Al-Chalabi 2011). Shortly following this, mutations in *FUS*, encoding another D/RBP, were detected in ~4-5% of fALS patients (Kwiatkowski *et al.* 2009, Vance *et al.* 2009). Mutations in *FUS* have also been identified in sALS and FTD patients (Belzil *et al.* 2009, Ticozzi *et al.* 2009, Blair *et al.* 2010, Corrado *et al.* 2010, DeJesus-Hernandez *et al.* 2010, Deng *et al.* 2010, Van Langenhove *et al.* 2010, Lai *et al.* 2011), and intraneuronal inclusions containing FUS are reported to occur in the brain and spinal cord of both familial and sporadic ALS and FTD patients (Kwiatkowski *et al.* 2009, Neumann *et al.* 2009, Neumann *et al.* 2009, Vance *et al.* 2009, Keller *et al.* 2012). Moreover, TDP-43 and FUS mislocalisation and pathology have been observed in several neurodegenerative disorders; both are implicated in polyglutamine disorders (Schwab *et al.* 2008, Doi *et al.* 2010), while TDP-43 pathology is also observed in AD and other forms of dementia, PD and various myopathies (Forman *et al.* 2007, Chen-Plotkin *et al.* 2010, Lagier-Tourenne *et al.* 2010).

TDP-43 and FUS are structurally and functionally related heterogeneous nuclear ribonucleoproteins (hnRNPs), both with roles in transcription regulation, pre-mRNA splicing, mRNA stabilisation and RNA transport (Buratti *et al.* 2001, Buratti *et al.* 2004, Mercado *et al.* 2005, Strong *et al.* 2007, Colombrita *et al.* 2009). Indeed, TDP-43 and FUS each have several thousand mRNA targets (Hoell *et al.* 2011, Polymenidou *et al.* 2011, Tollervey *et al.* 2011). Both proteins contain RNA recognition motifs (RRM), a nuclear localisation signal (NLS) and a glycine-rich region (GRR) that forms part of a yeast prion-like domain (Wang *et al.* 2004,

Buratti *et al.* 2005, Neumann *et al.* 2006, Lagier-Tourenne and Cleveland 2009, Cushman *et al.* 2010, Gitler and Shorter 2011, Udan and Baloh 2011). This functional and structural similarity led Couthouis *et al.* (2011) to screen for additional prion-like domain-containing D/RBPs that may contribute to ALS pathogenesis, through which they identified mutations in *TAF15* in fALS patients. A separate study also detected *TAF15* mutations in fALS patients (Ticozzi *et al.* 2011), and TAF15-positive intraneuronal inclusions are present within *TAF15*-fALS patients (Couthouis *et al.* 2011), findings that underscore a role for aberrant RNA metabolism in ALS.

Although predominantly localised to the nucleus, TDP-43 shuttles between the nucleus and cytoplasm in a transcription-dependent manner (Ayala *et al.* 2008). In the cytoplasm, TDP-43 has been found to have distinct functions, including mRNA stabilisation and translation (Wang *et al.* 2008) and the formation and regulation of stress granules (Colombrita *et al.* 2009, Liu-Yesucevitz *et al.* 2010, Dewey *et al.* 2011, McDonald *et al.* 2011, Bentmann *et al.* 2012). Stress granules (SGs) are punctate cytoplasmic foci, ranging in size from 0.1 to 2.0 μm, that sequester mRNA and ribosomal components to regulate translation and prioritise the synthesis of stress protective proteins in response to stressors, e.g. oxidative stress, heat shock, proteasome inhibition and other forms of cellular injury (Anderson and Kedersha 2009, Moisse *et al.* 2009, Moisse *et al.* 2009). SGs are transient structures; when the cellular stress has passed, SGs rapidly disaggregate, enabling their components to return to their normal localisation and function (Kedersha *et al.* 1999).

As with TDP-43, both FUS and TAF15 are predominantly nuclear proteins that have additional cytoplasmic functions, such as mRNA transport, local translation and RNA decay, and they incorporate into SGs (Fujii *et al.* 2005, Yoshimura *et al.* 2006, Andersson *et al.* 2008, Blechingberg *et al.* 2012). FUS and TAF15 are part of the FET (FUS, EWS, TAF15) family of structurally and functionally related D/RBPs (Tan and Manley 2009). These two proteins appear to associate with SGs via the same mechanisms, as the RNA-binding C-terminal

domains of both proteins, which contain RGG repeats and a zinc finger domain, mediate SG recruitment (Bentmann *et al.* 2012, Marko *et al.* 2012).

The key mechanisms by which these D/RBPs contribute to disease are not yet clear, although the fact that TDP-43 and FUS pathology occur in a wide variety of diseases is strong indication for an important pathogenic role of altered RNA metabolism. Nuclear import defects and cytoplasmic accumulation seem to be important events in both *FUS*- and *TARDBP*-linked ALS, and possibly in *TAF15*-linked disease. Most of the ALS-associated mutations in *FUS* are clustered within its C-terminal NLS, and multiple studies have shown a correlation between mutations that cause a severe cytoplasmic accumulation and a greater disease severity and progression rate (Kwiatkowski *et al.* 2009, Dormann *et al.* 2010, Gal *et al.* 2011, Niu *et al.* 2012). Mutations in the GRR of *TARDBP*, which constitute the majority of disease-linked mutations, have been shown to cause a progressive shift of TDP-43 localisation to the cytoplasm (Ayala *et al.* 2008, Johnson *et al.* 2009), and the cytoplasmic accumulation of TDP-43 has been shown to be toxic to neurons (Barmada *et al.* 2010). The GRR is also necessary for its association with SGs, and GRR mutations cause altered SG dynamics (Dewey *et al.* 2011).

Increased sequestration of TDP-43, FUS, TAF15 and other D/RBPs in cytoplasmic SGs interferes with their dynamic nucleus-cytoplasm shuttling, reducing levels of these proteins in the nucleus and their functional availability in the cytoplasm. Furthermore, the accumulation of TDP-43 into cytoplasmic inclusions that is characteristic of ALS, FTD, AD, PD and various myopathies (Forman *et al.* 2007, Schwab *et al.* 2008, Chen-Plotkin *et al*. 2010, Doi *et al.* 2010, Lagier-Tourenne *et al.* 2010) further depletes the functional pool of TDP-43 in neurons. The aggregation of TDP-43 into cytoplasmic inclusions in ALS may be triggered by cellular insult resulting from defective autophagic or UPS protein degradation, suggested by the recurrent finding that ubiquitin and p62 are co-localised in TDP-43-positive inclusions (Mizuno *et al.* 2006, Neumann *et al.* 2006, Deng *et al.* 2010, Keller *et al.* 2012). Moreover, in a *Drosophila*

model, disease-causing mutations in *VCP* were found to cause significant redistribution of TDP-43 to the cytoplasm, and this redistribution was sufficient to cause cytotoxicity (Ritson *et al.* 2010). It is entirely possible that the key roles of VCP in autophagy and ubiquitin-dependent segregation of substrates from multiprotein complexes, e.g. SGs, would be hindered in cases in which it is mutated, thus causing impaired recycling of TDP-43 from SGs back to the nucleus.

Many of the mRNA targets of TDP-43 and FUS are crucial for normal neuronal function (Polymenidou *et al.* 2011, Sephton *et al.* 2011, Tollervey *et al.* 2011, Colombrita *et al.* 2012, Dichmann and Harland 2012, Ishigaki *et al.* 2012, Lagier-Tourenne *et al.* 2012, Rogelj *et al.* 2012, Nakaya *et al.* 2013). Moreover, TDP-43 deficiency has been found to affect the levels of mRNAs encoding CHMP2B, FIG, OPTN, VAPB and VCP, all of which are implicated in ALS and have key roles in protein degradation pathways (Polymenidou *et al.* 2011). Another target of TDP-43 is the mRNA encoding ATG7, an autophagy-related protein (Bose *et al.* 2011). FUS has also been reported to bind to mRNAs encoding ALS-associated OPTN, VAPB, VCP and UBQLN2, as well as mRNAs encoding other proteins involved in the UPS (Hoell *et al.* 2011, Colombrita *et al.* 2012, Lagier-Tourenne *et al.* 2012). It is thus conceivable that abnormalities in mRNA splicing and processing resulting from dysregulation of TDP-43 and/or FUS lead to innumerable disturbances in neurons. Indeed, both deficiency *and* overexpression of WT and mutant forms of TDP-43 promote cytotoxicity, and it is intrinsically aggregation-prone in its WT form (Johnson *et al.* 2009, Laird *et al.* 2010, Liachko *et al.* 2010, Armakola *et al.* 2011, Huang *et al.* 2012, Uchida *et al.* 2012). Cytoplasmic accumulations of TDP-43, FUS or TAF15 may aberrantly sequester RNAs and/or other proteins (Voigt *et al.* 2010, Hoell *et al.* 2011), causing further dysfunction in cellular RNA metabolism and disruptions in the activities of the affected proteins.

The possible role of mutant TDP-43 in the disruption of proteostasis can also be extended to disturbance of the intracellular trafficking and secretory pathways in motor neurons. Fujita *et*

al. (2008) found that abnormal TDP-43 cytoplasmic immunoreactivity was associated with impaired functioning of the Golgi apparatus, leading to Golgi fragmentation. It is unknown whether errors in mRNA metabolism are responsible for this impairment. The Golgi apparatus has numerous important functions in maintaining proteostasis, including post-translational modification of proteins and protein trafficking.

1.5 ALS gene variants may converge in proteostasis dysfunction

Inclusion bodies containing visible accumulations of detergent-insoluble protein aggregates are a pathological hallmark of many neurodegenerative disorders including AD, PD, HD and CJD (Leigh *et al.* 1991, Chiti and Dobson 2006, Ticozzi *et al.* 2010), and ALS, in both sporadic and familial cases (Gurney *et al.* 1994, Wong *et al.* 1995, Bruijn *et al.* 1997, Bruijn *et al.* 1998, Watanabe *et al.* 2001, Boillee *et al.* 2006). Generally, specific aggregating proteins are implicated in each of these neurodegenerative diseases; α-synuclein in PD, huntingtin in HD, Aβ and tau in AD (Ilieva *et al.* 2009). In ALS, however, the situation appears to be more complex, with a multitude of different proteins being detected in the inclusion bodies inside affected motor neurons (Migheli *et al.* 1993, Okamoto *et al.* 1993, Buee-Scherrer *et al.* 1995, Wong *et al.* 2000, Arai *et al.* 2006, Mizuno *et al.* 2006, Neumann *et al.* 2006, Fujita *et al.* 2008, Maruyama *et al.* 2010, Deng *et al.* 2011). In fact, a number of morphologically different types of inclusions are found in ALS motor neurons, including: filamentous skeins, dense hyaline bodies, and round or conglomerate Lewy body-like forms (Leigh *et al.* 1991); Bunina bodies (Okamoto *et al.* 1993, Strong *et al.* 2005); basophilic inclusions (Nelson and Prensky 1972, Oda *et al.* 1978, Chou 1979); and spheroids (Leigh *et al.* 1991). Intra- and extraneuronal tau-immunoreactive aggregates have also been detected in a subgroup of ALS patients exhibiting features of FTD and cognitive decline (Yang *et al.* 2003), although the exact prevalence of these aggregates is yet to be determined.

Misfolded proteins aggregate and form inclusions when they accumulate to a concentration that

exceeds their solubility (Chiti and Dobson 2006). Yet proteins have co-evolved with their cellular environments to exist at optimal functional concentrations at which their solubility is near compromised (Tartaglia *et al.* 2007, Ciryam *et al.* 2013, Ciryam *et al.* 2015), seemingly making them vulnerable to precipitation in the face of changes to their environment. In order to prevent such changes to protein solubility, the cell must be able to actively maintain proteostasis, keeping cellular proteins in their correct conformation, concentration and location (Balch *et al.* 2008). Proteins can accumulate in the cell and form inclusions when these mechanisms maintaining proteostasis are compromised, or their capacity is exceeded (Yerbury and Kumita 2010, Gidalevitz *et al.* 2011, Yerbury *et al.* 2013). Conversely, as mentioned in section 1.2.2.1, aberrant protein species can be sequestered into inclusions that function as protein quality control compartments when proteostasis is compromised or capacity is exceeded, in a cellular response to protect against abnormal interactions of aberrant proteins with other molecules and macromolecular complexes within the cells (Johnston *et al.* 1998, Kopito 2000, Arrasate *et al.* 2004, Kaganovich *et al*. 2008, Treusch *et al*. 2009, Zhang and Qian 2011, Weisberg *et al.* 2012, Polling *et al.* 2014).

As cells age, the efficacy of proteostasis mechanisms declines (Balch *et al.* 2008, Ben-Zvi *et al.* 2009, Brehme *et al.* 2014). It is postulated that aging, proteostasis and neurodegenerative disease are closely linked (Morimoto 2008, Wyatt *et al.* 2013, Yerbury *et al.* 2016), explaining why most neurodegenerative diseases, including ALS, are late-onset, with most forms developing during middle-age and in later years (Derham and Harding 1997, Zhang *et al.* 2004, Erickson *et al.* 2006, Massey *et al.* 2006). Importantly, motor neurons have been shown to be particularly vulnerable to disruptions in proteostasis and to other stressful stimuli, including proteotoxic stress induced by aggregated proteins, even in comparison with other cells of the nervous system (Durham *et al.* 1997, Bruening *et al.* 1999, Batulan *et al.* 2003, Yerbury *et al.* 2019).

The common occurrence of ubiquitylated protein inclusions inside the diseased motor neurons of ALS patients harbouring a multitude of different genetic mutations leads to the hypothesis that altered proteostasis in motor neurons is a critical underlying cause of ALS (Figure 1.5). Investigating how mutations in the identified ALS-associated genes lead to dysfunction of proteostasis and the responses of motor neurons to these events will greatly increase our understanding of how neurodegeneration in ALS proceeds.

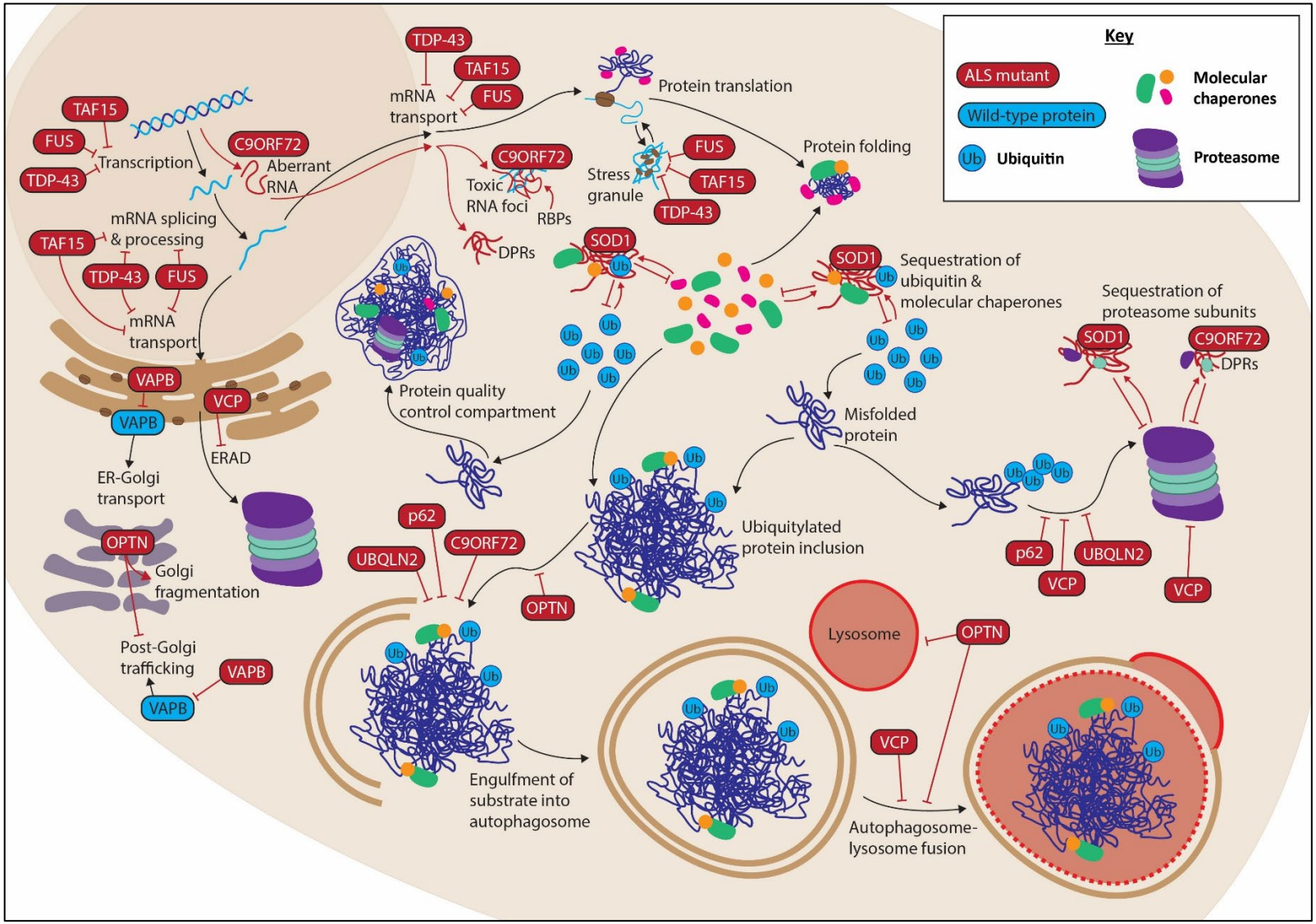
Key
ALS mutant
Wild-type protein
Ub Ubiquitin
Molecular chaperones
Proteasome
TAF15
FUS
TDP-43
Transcription
C9ORF72
Aberrant RNA
mRNA splicing & processing
mRNA transport
VAPB
VAPB
VCP
ERAD
ER-Golgi transport
OPTN
Golgi fragmentation
Post-Golgi trafficking
VAPB
VAPB
TDP-43
TAF15
FUS
mRNA transport
Protein translation
C9ORF72
Toxic RNA foci
RBPs
DPRs
Stress granule
FUS
TAF15
TDP-43
Protein folding
SOD1
Protein quality control compartment
SOD1
Sequestration of ubiquitin & molecular chaperones
Misfolded protein
Sequestration of proteasome subunits
SOD1
C9ORF72
DPRs
p62
C9ORF72
UBQLN2
OPTN
Ubiquitylated protein inclusion
p62
UBQLN2
VCP
VCP
Lysosome
OPTN
VCP
Engulfment of substrate into autophagosome
Autophagosome-lysosome fusion

Figure 1.5. Summary of potential mechanisms by which ALS-associated gene variants cause proteostasis dysfunction in motor neurons. Oligomeric or aggregated mutant SOD1 sequesters molecular chaperones, ubiquitin and proteasome subunits, interfering with chaperone activity and the UPS. Mutations in *C9ORF72* may lead to haploinsufficiency and thereby disruptions in C9ORF72 function in autophagy. *C9ORF72* mutations also result in the production of toxic RNA foci and dipeptide repeat proteins (DPRs). RNA foci sequester RNA-binding proteins (RBPs), disrupting their functions while DPRs may aberrantly interact with and sequester different cellular components, including proteasome subunits. Mutations in *UBQLN2* and *SQSTM1* (encoding p62) impair their functions in autophagy and in delivering ubiquitylated proteins to the proteasome for degradation. VCP is involved in protein degradation via autophagy, the UPS, and the endoplasmic reticulum-associated degradation (ERAD) pathway. Loss of VCP activity from ALS-associated mutations leads to impaired delivery of ubiquitylated proteins to the proteasome, disruptions in ERAD and failure of autophagosomes to mature into autophagolysosomes. Mutations in *OPTN* impair the functions of OPTN in Golgi organisation and post-Golgi transport, leading to Golgi disorganisation and fragmentation. Impaired OPTN activity potentially leads to altered delivery of ubiquitylated cargo to autophagosomes and disrupted trafficking of lysosomal proteins from the Golgi, causing disruptions in lysosomal function and autophagy. Mutations in *VAPB* are hypothesised to cause dominant-negative impairment of wild-type VAPB; aggregates formed by mutant VAPB interact aberrantly with and sequester wild-type VAPB. Consequently, impaired VAPB activity leads to disruptions in ER function, ER-Golgi transport and membrane trafficking. Mutations in the DNA/RNA-binding proteins *TARDBP* (encoding TDP-43)*, FUS* and *TAF15* cause disruptions in transcription, mRNA splicing and processing, mRNA transport and altered stress granule dynamics. Moreover, mutations in *TARDBP* and *FUS* lead to disruptions in the expression of the mRNA targets of TDP-43 and FUS. Figure adapted from Ciryam *et al.* 2017.

1.6 Studying dysregulation of proteostasis in ALS models: Summary and aims

Amongst the complexity and molecular heterogeneity of ALS, previous studies have identified disruptions in the proteostasis network that are associated with certain ALS gene variants. However, there remains a need to identify the exact proteostasis disruptions that are commonly associated with each of the ALS-causing genetic mutations, and those that are unique to each gene variant. It is hypothesised that dysfunction of the proteostasis network in motor neurons may be an underlying link between the different ALS-associated gene variants that contributes to motor neuron degeneration in ALS. As such, the overall objective of this PhD research was to develop and employ novel experimental strategies that enable investigation of the effects of different ALS-associated gene variants on common proteostasis components and processes. Such approaches may facilitate identification of the proteostasis components that have key roles in ALS pathogenesis, and thereby lead to the elucidation of potential therapeutic targets. To achieve this objective, the specific aims of this work were to:

1. Establish a high-throughput screening system using *Saccharomyces cerevisiae* to model pathological TDP-43 and FUS aggregation, and ALS-associated mutant SOD1.
2. Use this *S. cerevisiae* model to examine the effects of pathological TDP-43, FUS and SOD1 on common proteostasis components and processes.
3. Validate the relevance of key proteostasis components identified in the *S. cerevisiae* screens using neuronal cell culture models of ALS.
4. Establish a high-content screening (HCS) system that can be used to investigate proteostasis dysfunction in neuronal cell culture models of multiple different ALS-associated gene variants in parallel experiments.

Chapter 2: General materials and methods

This chapter outlines the general materials and methods used in the research detailed throughout this thesis. Additional materials and methods that pertain specifically to the work detailed in Chapters III – V are provided in the relevant chapters.

2.1 Materials and reagents

All media and buffers used in this research were prepared using Milli-Q water (Q-POD® Ultrapure Water Remote Dispenser, Millipore, Billerica, MA, USA). Ethylenediaminetetraacetic acid (EDTA) and tryptone were from Amresco (Solon, USA). HyperLadder™ I and HyperLadder™ II molecular weight markers were from Bioline (Alexandria, NSW, Australia). Mini-PROTEAN® TGX™ Precast Protein Gels, Precision Plus Protein™ Dual Color protein standards and sodium dodecyl sulphate (SDS) were from Bio-Rad (Hercules, CA, USA). Foetal Bovine Serum (heat-inactivated prior to use; FBS) was from Bovogen Biologicals (East Keilor, VIC, Australia). Sterile cell culture plates were from Greiner Bio-One (Frickenhausen, Germany). B-mercaptoethanol, bicinchoninic acid disodium salt hydrate (bicinchoninic acid, BCA), bovine serum albumin (BSA), Brilliant Blue R concentrate, copper sulphate pentahydrate ($CuSO_4.5H_2O$), dimethyl sulfoxide (DMSO), magnesium chloride ($MgCl_2$), methanol, paraformaldehyde (PFA), potassium chloride (KCl), sodium chloride (NaCl), Tris-hydrochloride (Tris-HCl), tris(hydroxymethyl)aminomethane, Triton X-100, Tween® 20 (polyethylene glycol sorbitan monolaurate) and yeast extract were from Sigma-Aldrich (St. Louis, MO, USA). Dulbecco's Modified Eagles Medium with nutrient mixture F-12 powder (DMEM/F-12) supplemented with 2.5 mM L-glutamine, DMEM/F-12 without phenol red supplemented with 2.5 mM L-glutamine, Halt™ Protease Inhibitor Cocktail (100X), Lipofectamine® 2000 and 3000, OptiMEM® I (1X) reduced serum medium, SuperSignal™ West Pico chemiluminescent substrate, 0.05% trypsin-EDTA were all obtained from Thermo Fisher Scientific (Waltham, MA, USA). All other reagents were from Amresco, Astral Scientific (Gymea, NSW, Australia) or Sigma-Aldrich and were endotoxin free.

2.2 Plasmids

The pEGFP-N1 expression vector containing human wild-type *SOD1* (SOD1^{WT}-EGFP) and *SOD1* altered by the disease-associated Ala4Val (A4V) mutation (SOD1^{A4V}-EGFP) were kindly provided by Assoc. Prof. Bradley Turner (The Florey Institute of Neuroscience & Mental Health, Victoria, Australia) and had been constructed as previously described (Turner *et al.* 2005). Both the SOD1-EGFP vectors and the pCMV6-AC-tGFP vector containing human wild-type *TARDBP* (TDP-43^{WT}-tGFP) and the disease-associated mutant M337V (TDP-43^{M337V}-tGFP) (OriGene, Maryland, USA) had previously been transformed into chemically competent *Escherichia coli (E. coli)* DH5-α cells and were stored in glycerol at -80 °C prior to plasmid DNA purification. The identity of these stocks had been confirmed by sequencing (Jake Matic, 2012, personal communication). Additional plasmids used in the research presented in Chapters III – V are detailed in the relevant chapters.

2.3 Transformation of *E. coli* and plasmid DNA purification

The subcloning procedures used throughout the research presented in Chapters III and V used the DH5-α *E. coli* strain. Chemically-competent DH5-α cells had kindly been previously prepared using calcium chloride-treatment by Dr. Luke McAlary (University of Wollongong, NSW, Australia). To transform cells using the heat-shock protocol, 100 µL of chemically-competent DH5-α cells were gently mixed with 10 ng of plasmid DNA and incubated on ice for 30 min. Cells were then heat-shocked at 42 °C for 45 sec and immediately transferred to ice to incubate for 5 min. Cells were then diluted with 500 µL of Super Optimal Broth with Catabolite repression (SOC; 0.5% (w/v) yeast extract, 2% (w/v) tryptone, 10 mM NaCl, 2.5 mM KCl, 10 mM $MgCl_2$, 10 mM $MgSO_4$, 20 mM glucose) and incubated for 1 h at 37 °C with agitation (190 rpm). Aliquots of 100 µL and 300 µL of transformation cultures were then plated onto pre-warmed sterile selective Luria-Bertani (LB)-agar plates (LB [1% (w/v) tryptone, 1% (w/v) NaCl, 0.5% (w/v) yeast extract], containing 15% (w/v) agar and the appropriate

antibiotic; either 100 µg/mL ampicillin, or 50 µg/mL kanamycin) and incubated overnight at 37 °C. Successfully transformed single bacterial colonies were selected and used to inoculate sterile selective LB broth containing the appropriate antibiotic, for plasmid purification using the CompactPrep Plasmid Maxi Kit (Qiagen, Hilden, Germany) as per the manufacturer's protocol. To confirm the purity of extracted plasmid DNA following the purification procedure and measure its concentration, the ratio of absorbance at 260 nm and 280 nm (A_{260}/A_{280} ratio) and concentration (A_{260}) were measured using a NanoDrop 2000c dual-mode UV-Vis Spectrophotometer (Thermo Fisher Scientific, Waltham, USA).

Samples of extracted plasmid DNA were examined using diagnostic restriction enzyme digestion with the appropriate restriction enzymes. Digested plasmid DNA samples were then prepared for agarose gel electrophoresis by mixing samples with DNA loading buffer (30% (v/v) glycerol, 0.25% (w/v) bromophenol blue) and resolved by electrophoresis on 1% (w/v) agarose gels in tris-acetate-EDTA (TAE) buffer (1 mM EDTA, 40 mM Tris and 20 mM acetic acid) alongside HyperLadder™ I (200 – 10037 bp) or HyperLadder™ II (50 – 2000 bp) molecular weight markers, as appropriate for each digested DNA sample. Following electrophoresis, agarose gels were stained with 0.005% (w/v) ethidium bromide solution for 20 min and destained in dH_2O for 20 min. The resulting stained DNA bands within the gels were visualised using UV light exposure in a Gel Logic 2200 Pro Imaging System (Carestream Health, Rochester, NY, USA).

2.4 Preparation of glycerol stocks of transformed *E. coli*

Glycerol stocks of successfully transformed DH5-α *E. coli* were prepared for the long-term storage of plasmid DNA at -80 °C. Selected single colonies of DH5-α *E. coli* transformed with each respective plasmid construct were used to inoculate 5 mL aliquots of LB broth supplemented with the appropriate antibiotic (either 100 µg/mL ampicillin, or 50 µg/mL kanamycin) and incubated overnight at 37 °C with agitation (190 rpm). The following day, 1

mL of each overnight culture was mixed with 1 mL of sterile glycerol in cryovials for storage at -80 °C.

2.5 Mammalian cell culture

The *M. musculus* neuroblastoma × spinal cord hybrid cell line (NSC-34) was supplied by Prof. Neil Cashman (University of British Columbia, Vancouver, Canada) (Cashman *et al.* 1992). NSC-34 cells were maintained in a routinely serviced 37 °C Heracell 150i incubator with humidified air containing 5% (v/v) carbon dioxide (CO_2). DMEM/F-12 supplemented with 10% (v/v) FBS (DMEM/F-12/FBS) was used for regular culturing of cells. Cells were passaged once they reached ~80% confluence, usually every 3 days. This involved rinsing the adherent cells with a small volume of serum-free DMEM/F-12 before incubating them with 0.05% trypsin-EDTA for 3 min at 37 °C. Cells were then collected by centrifugation at 1,500 rpm for 5 min at room temperature, followed by resuspension in DMEM/F-12/FBS and transfer of a suitable volume of resuspended cells to a sterile cell culture flask to achieve an appropriate dilution, usually a 1:6 dilution. Plasmid DNA transfections in NSC-34 cells performed in the experiments outlined in Chapters III and V are detailed in the relevant sections of each chapter.

2.6 Statistics

Results presented throughout Chapters III – V are the mean ± SEM of three independent experiments, unless otherwise indicated. To analyse and compare differences in means in experiments involving multiple treatments, one-way analysis of variance (ANOVA) tests were used, paired with post hoc testing using Tukey's multiple comparison test. Otherwise, Student's t tests were used to evaluate differences in means. Unless stated otherwise, statistical analyses were performed using GraphPad Prism® (Version 5.00, GraphPad Software, Inc., La Jolla, CA, USA). A significance level of $p < 0.05$ was used to define differences between means as significant for all statistical analyses.

Chapter 3: Yeast EGFP-fusion library screens reveal differential levels of ALS-associated proteins in yeast expressing TDP-43, FUS and SOD1

The research in this chapter was carried out in collaboration with Professor Stephen G. Oliver and Dr. Giorgio Favrin as part of a 12 month stay in the S. G. Oliver laboratory at the Department of Biochemistry, University of Cambridge, UK.

3.1 Introduction

The budding yeast *Saccharomyces cerevisiae* has become an established robust model for investigating mechanisms involved in several neurodegenerative diseases, including PD, HD, AD and ALS (Krobitsch and Lindquist 2000, Auluck *et al.* 2002, Outeiro and Lindquist 2003, Willingham *et al.* 2003, Cooper *et al.* 2006, Johnson *et al.* 2008, Gitler *et al.* 2009, Johnson *et al.* 2009, Elden *et al.* 2010, Sun *et al.* 2011, Treusch *et al.* 2011, Kim *et al.* 2014). The yeast genome is well characterised and many key molecular processes are conserved between yeast and higher eukaryotic organisms, including humans. Almost a third of yeast genes have a direct human orthologue (Botstein *et al.* 1997). Indeed, key pathways that are disrupted in neurodegenerative diseases, such as protein folding and other protein quality control mechanisms, are fundamental features of eukaryotic biology that are conserved across the spectrum of eukaryotic organisms. As such, yeast provide an ideal starting point to screen for genes and proteins that aberrantly or advantageously interact with neurodegenerative disease genes, with findings that can then be validated in neurologically relevant cellular and animal models (Elden *et al.* 2010, Couthouis *et al.* 2011, Sun *et al.* 2011, Kim *et al.* 2014). Methods to overexpress or knock out every yeast gene are well established. The development of Synthetic genetic array (SGA) methodology (Baryshnikova *et al.* 2010) has facilitated the study of genes and their associated pathways that are affected by or modify the effects of disease-associated genes (Yuen *et al.* 2007, Deshpande *et al.* 2013, van Pel *et al.* 2013, Bian *et al.* 2014). Such studies provide valuable insight into disease mechanisms at the genetic level. However, key post-transcriptional, translational and post-translational information can be missed without investigation at the protein level.

For the present study, a collection of yeast EGFP-fusion strains (Huh *et al.* 2003) was employed to develop a yeast screening system to explore proteins and molecular pathways that may be associated with the pathological effects of TDP-43, FUS and mutant SOD1 in ALS. This

collection was created by the integration of an EGFP at the C-terminus of the genomic locus of each yeast gene, preserving the natural promoter of each gene to facilitate minimal perturbation in the levels and activity of each encoded protein. Previously, most studies utilising this collection have investigated the localisation of proteins and their alterations under stress conditions using fluorescence microscopy (Huh *et al.* 2003, Breker *et al.* 2013, Breker *et al.* 2014). The use of a fluorescent plate reader to quantify the expression of the yeast EGFP-fusion proteins under different conditions has only recently emerged (Lichten *et al.* 2014). In the face of extrinsic or intrinsic stimuli that disturb cellular homeostasis, cells respond by up-regulating proteins that assist in maintaining a homeostatic state and down-regulating proteins that impair the cellular ability to appropriately respond to the disturbance (Beyer *et al.* 2004, Newman *et al.* 2006, Sigal *et al.* 2006, Erjavec *et al.* 2007, Sigal *et al.* 2007, Aragon *et al.* 2009, Frenkel-Morgenstern *et al.* 2010, Eden *et al.* 2011, Lee *et al.* 2011, Tkach *et al.* 2012, Breker *et al.* 2013). Consequently, the measurement of protein abundance changes in cells exposed to different stressors, such as the overexpression of disease-causing gene variants, can provide insight into the proteins and molecular processes involved in the cellular response to the specific stress. It was thus hypothesised that proteins found to have differential levels in yeast expressing human TDP-43, FUS and mutant SOD1 may be critically involved in the response of cells to these aberrant ALS-associated proteins.

There are no true homologues of TDP-43 and FUS in yeast (Johnson *et al.* 2008, Ju *et al.* 2011). In previously described yeast models, the expression of human TDP-43^{WT} and FUS^{WT} without the need for ALS specific mutation recapitulates key pathological features observed in human tissue, mammalian cell culture and animal models. These features include a shift from predominantly nuclear localisation to cytoplasmic sequestration and aggregation, and toxicity (Johnson *et al.* 2008, Johnson *et al.* 2009, Fushimi *et al.* 2011, Ju *et al.* 2011, Kryndushkin *et al.* 2011, Sun *et al.* 2011, Kim *et al.* 2014). Data gained from these and other yeast-based

studies of neurodegenerative disease mechanisms have gone on to be validated in neurologically relevant cellular and animal models, as well as in human tissue (Couthouis *et al.* 2011, Couthouis *et al.* 2012, Kim *et al.* 2014). For instance, findings from a yeast genome-wide screen were followed up using *Drosophila melanogaster* and mammalian cell culture models of ALS and led to the discovery that dysfunction in SG dynamics contributes significantly to toxicity caused by a pathological interaction between TDP-43 and ataxin-2 (Kim *et al.* 2014). Indeed, these findings from yeast led to the discovery of genetic association between ataxin-2 and ALS, clearly demonstrating the relevance of yeast as a model system. Furthermore, examining the findings from this yeast-based study in *D. melanogaster* led to the discovery of a protein that is critical for the pathological TDP-43-ataxin-2 interaction, polyadenylate-binding protein (PABP), and that this protein is present in cytoplasmic inclusions in post-mortem spinal cord tissue from individuals with ALS (Kim *et al.* 2014). Many of the early yeast-based studies into neurodegenerative disease mechanisms, and the correlation of the reported findings with those documented in mammalian cell culture and animal models, have been thoroughly reviewed elsewhere (Outeiro and Muchowski 2004).

As reviewed in Chapter I, while the mechanisms that have been postulated to contribute to ALS pathogenesis are diverse, many of them link either directly or indirectly to disruptions in the proteostasis network. There remains a need to further dissect these links to proteostasis dysfunction and to decipher precisely how this dysfunction proceeds with regard to the cellular response to ALS-causing pathological proteins. One way to gain such insight is to focus on the molecular processes that have been implicated in ALS pathogenesis, including molecular processes that are part of the proteostasis network, and examine whether any specific protein components of these processes are differentially regulated in cells expressing ALS-causing gene variants. Thus, to investigate the specific proteins that are involved in the cellular response to pathological TDP-43, FUS and mutant SOD1 expression in yeast, the aims of the work

described in this chapter were to:

(i) collate a list of proteins involved in molecular processes that have been previously implicated in ALS pathogenesis and

(ii) using the EGFP-fusion yeast library, determine whether the levels of these proteins are altered by the expression of the ALS-associated proteins TDP-43^{WT}, FUS^{WT}, SOD1^{WT} and mutant SOD1^{A4V}.

It was hypothesised that some of these proteostasis-associated proteins will have differential expression in the absence versus presence of TDP-43, FUS and mutant SOD1 and that these will represent proteins with key roles in the cellular response to ALS-linked pathology.

3.2 Materials and methods

3.2.1 Materials and reagents

Bacto™ agar, Bacto™ peptone, Bacto™ tryptone and Bacto™ yeast extract were from BD Biosciences (Becton, Dickinson and Co., San Jose, CA, USA). Sterile 384-well flat-bottom μclear microplates and sterile 96-well flat-bottom crystal-clear microplates were from Greiner Bio-One (Frickenhausen, Germany). Agarose (molecular biology grade, electrophoresis grade), glycine and tris(hydroxymethyl)aminomethane were from Melford (Suffolk, UK). The E.Z.N.A.® Plasmid DNA Mini Kit I was from Omega Bio-Tek, Inc. (Norcross, GA, USA). The QIAquick® Gel Extraction Kit was from Qiagen (Hilden, Germany). D-(+)-galactose, D-(+)-glucose, D-(+)-raffinose pentahydrate, glass beads (acid-washed), L-glutamic acid monosodium salt hydrate, L-leucine, uracil and yeast nitrogen base without amino acids (YNB) were from Sigma-Aldrich (St. Louis, MO, USA). Glycerol and sodium chloride (NaCl) were from Thermo Fisher Scientific (Waltham, MA, USA).

3.2.2 Advanced Gateway® Cloning, plasmids and yeast transformation

The human SOD1^{WT} and SOD1^{A4V} open reading frames (ORFs) in pEGFP-N1 were sub-cloned

into the pAG416GAL-ccdB-DsRed vector using the Advanced Gateway® BP and LR recombination reactions, as per the manufacturer's instructions (Figure 3.1, a). In order to carry out the BP recombination reaction, site-specific attachment (*att*B) sites were first added to the 5' and 3' ends of the ORFs of $SOD1^{WT}$ and $SOD1^{A4V}$ in pEGFP-N1. PCR primers were designed to add *att*B sites and isolate the $SOD1^{WT}$ and $SOD1^{A4V}$ ORFs from the backbone sequence (Table 3.1). Manufacturing of the primers was outsourced to Sigma-Aldrich (UK). The PCR procedure was carried out using VELOCITY DNA polymerase (Bioline, UK) as per the manufacturer's instructions. Following PCR, each reaction mixture was digested with 5 units of DpnI (New England BioLabs® Inc., MA, USA) at 37 °C for 1 h to remove any remnants of the original plasmids.

Table 3.1. PCR primer sequences used to add *att*B sites to $SOD1^{WT}$ and $SOD1^{A4V}$ in pEGFP-N1.

Gene/vector backbone	**Purpose**	**Primer sequence**
$SOD1^{WT}$ and $SOD1^{A4V}$ in pEGFP-N1.	To add *att*B1 and *att*B2 sites to the 5' and 3' ends of the SOD1 ORFs and isolate them from backbone sequence.	Forward: 5'-GGGGACAAGTTTGTACAAAAAAGCAGGCTCCATGGCGACGAAGGCCGTG-3'
		Reverse: 5'-GGGGACCACTTTGTACAAGAAAGCTGGGTGCAATTGGGCGATCCCAATTACAC-3'

To purify the PCR products from the reaction mixture, 50 µL of each reaction mixture was mixed with 10 µL of 6× DNA loading dye and subjected to agarose gel electrophoresis. DNA bands corresponding to human $SOD1^{WT}$ and $SOD1^{A4V}$ flanked with *att*B sites were then excised from the agarose gel and purified using the QIAquick® Gel Extraction Kit (Qiagen, Hilden, Germany). The purified *att*B-$SOD1^{WT}$ and *att*B-$SOD1^{A4V}$ PCR products were sub-cloned into the pDONR™221 vector using the Advanced Gateway® BP recombination reaction, as per the

manufacturer's instructions but with the following modifications to scale down volumes: 0.4 µL of 5× BP Clonase™, 0.4 µL of 5× BP Clonase™ Reaction Buffer, 30 ng of pDONR™221, 30 ng of either *att*B-SOD1^{WT}, *att*B-SOD1^{A4V} PCR product or pEXP7-tet (positive control) and TE buffer (pH 8.0) to a final volume of 2 µL, for a 1 h reaction at 25 °C. The reaction mixtures were then treated with 0.2 µL of Proteinase K. The resulting pDONR™221-SOD1^{WT}, pDONR™221-SOD1^{A4V} and positive control were then transformed into chemically-competent TOP10 *E. coli* using the heat-shock transformation protocol and incubated overnight at 37 °C on LB agar plates supplemented with 50 µg/mL kanamycin. The following day, 3 single colonies from each transformation plate were picked and streaked onto new LB agar-kanamycin plates followed by overnight incubation at 37 °C. Single colonies were isolated and used to inoculate 2.5 mL of LB broth containing 50 µg/mL kanamycin for overnight incubation at 37 °C with agitation.

Since the expression of human TDP-43^{WT} and FUS^{WT} in yeast recapitulates key pathological features observed in human tissue, mammalian cell culture and animal models, these were used to transform yeast rather than specific ALS-associated mutant isoforms of these genes. The expression of SOD1^{WT} in yeast, on the other hand, has no effect on the viability of yeast cells, and serves as a suitable control to yeast strains expressing ALS-associated *SOD1* mutations (e.g. A4V and G93A) (Gunther *et al.* 2004, Bastow *et al.* 2016). Human TDP-43^{WT} and FUS^{WT} in pDONR™221 (previously prepared by Dr. Daniel Bean, University of Cambridge, UK), and SOD1^{WT} and SOD1^{A4V} in pDONR™221 were sub-cloned into the pAG416GAL-ccdB-DsRed vector using the Advanced Gateway® LR recombination reaction, as per the manufacturer's instructions but with the following modifications to scale down volumes: 0.4 µL of 5× LR Clonase™ II, 30 ng of the Entry Clone (pDONR™221 containing TDP-43 or FUS) and of the Destination Vector (pAG416GAL-ccdB-DsRed), and TE buffer (pH 8.0) to a final volume of 2 µL, for a 1 hour reaction at 25 °C. The reaction mixture was then treated with 0.2 µL of

Proteinase K. The resulting pAG416GAL-TDP-43^{WT}-DsRed, pAG416GAL-FUS^{WT}-DsRed, pAG416GAL-SOD1^{WT}-DsRed and pAG416GAL-SOD1^{A4V}-DsRed expression clones were then transformed into chemically-competent TOP10 *E. coli* using the heat-shock transformation protocol. Plasmid DNA from successfully transformed single colonies was then extracted from bacterial cells using the E. Z. N. A. Plasmid DNA Mini Kit I (VWR International, Omega Bio-Tek, Inc., GA, USA) as per the manufacturer's instructions.

Extracted plasmid DNA was then subject to restriction enzyme digestion and agarose gel electrophoresis to verify that the recombinant plasmids had the correct backbone and insert size. Colonies identified to contain the correct plasmid DNA were then used to prepare glycerol stocks. Briefly, 2.5 mL aliquots of LB containing the appropriate antibiotic were inoculated with the selected colonies and incubated overnight at 37 °C with agitation. The following day these cultures were then diluted 1:1 with sterile 50% (v/v) glycerol solution and stored in sterile cryogenic tubes at -80 °C for long-term storage.

3.2.3 Yeast strains, transformation, media and culturing

Yeast were cultured at 30 °C unless otherwise indicated. The haploid *MATα* strain of *Saccharomyces cerevisiae,* Y7039 (*MATα can1Δ::STE2pr-LEU2 lyp1Δ his3Δ1 leu2Δ0 ura3Δ0 LYS2+),* was a gift from Prof. Charles Boone (University of Toronto, Canada). Y7039 cells were grown in rich media (yeast extract-peptone-dextrose; YPD; 1% (w/v) yeast extract, 2% (w/v) peptone, 2% (w/v) glucose) or in synthetic medium lacking leucine (0.67% (w/v) yeast nitrogen base without amino acids, 0.0109% (w/v) adenine, 0.00725% (w/v) uracil, 0.00725% (w/v) inositol, 0.000725% (w/v) para-aminobenzoic acid, 0.00725% (w/v) alanine, 0.00725% (w/v) arginine, 0.00725% (w/v) asparagine, 0.00725% (w/v) aspartic acid, 0.00725% (w/v) cysteine, 0.00725% (w/v) glutamic acid, 0.00725% (w/v) glutamine, 0.00725% (w/v) glycine, 0.00725% (w/v) histidine, 0.00725% (w/v) isoleucine, 0.00725% (w/v) lysine, 0.00725% (w/v) methionine, 0.00725% (w/v) phenylalanine, 0.00725% (w/v) proline, 0.00725% (w/v) serine,

0.00725% (w/v) threonine, 0.00725% (w/v) tryptophan, 0.00725% (w/v) tyrosine and 0.00725% (w/v) valine) containing 2% (w/v) glucose (SD/-Leu), 2% (w/v) raffinose (SRaf/-Leu), or 2% (w/v) galactose (SGal/-Leu).

Cultures of Y7039 were transformed with the pAG416GAL-TDP-43^{WT}-DsRed, pAG416GAL-FUS^{WT}-DsRed, pAG416GAL-SOD1^{WT}-DsRed, pAG416GAL-SOD1^{A4V}-DsRed and pAG416GAL-ccdB-DsRed constructs using the PEG/lithium acetate method to create four query strains and a control strain (Ito *et al.* 1983) (Figure 3.1, b). The pAG416GAL-ccdB-DsRed vector contains the URA3 selectable marker and enables growth of transformed cells on media lacking uracil. The Y7039 cultures transformed with pAG416GAL-TDP-43^{WT}-DsRed, pAG416GAL-FUS^{WT}-DsRed, pAG416GAL-SOD1^{WT}-DsRed, pAG416GAL-SOD1^{A4V}-DsRed or the pAG416GAL-ccdB-DsRed vector were grown in synthetic medium lacking leucine and uracil, supplemented with 2% (w/v) glucose (SD/-Leu/Ura), 2% (w/v) raffinose (SRaf/-Leu/Ura, or 2% (w/v) galactose (SGal/-Leu/Ura).

The yeast EGFP-fusion collection (Huh *et al.* 2003) was grown on solid synthetic medium lacking histidine (0.67% (w/v) yeast nitrogen base without amino acids, 0.0109% (w/v) adenine, 0.00725% (w/v) uracil, 0.00725% (w/v) inositol, 0.000725% (w/v) para-aminobenzoic acid, 0.00725% (w/v) alanine, 0.00725% (w/v) arginine, 0.00725% (w/v) asparagine, 0.00725% (w/v) aspartic acid, 0.00725% (w/v) cysteine, 0.00725% (w/v) glutamic acid, 0.00725% (w/v) glutamine, 0.00725% (w/v) glycine, 0.00725% (w/v) isoleucine, 0.036% (w/v) leucine, 0.00725% (w/v) lysine, 0.00725% (w/v) methionine, 0.00725% (w/v) phenylalanine, 0.00725% (w/v) proline, 0.00725% (w/v) serine, 0.00725% (w/v) threonine, 0.00725% (w/v) tryptophan, 0.00725% (w/v) tyrosine and 0.00725% (w/v) valine) containing 2% (w/v) glucose, 2% (w/v) agar and supplemented with 100 µg/mL ampicillin (SD/-His + Amp) in PlusPlates (Singer instruments, Somerset, UK). Single colonies from the 17× 384-colony-dense plates of the yeast EGFP-fusion collection were picked using the Stinger modular

extension of the ROTOR™ High-throughput Microbial Array Pinning Robot (Singer Instruments, Somerset, UK) and inoculated onto new PlusPlates to prepare 4× 96-colony-dense plates of customised arrays.

To prepare glycerol stocks of the full yeast EGFP-fusion collection and of the custom arrays, the ROTOR™ was used to pin colonies from agar plates to 96-well plates containing 140 µL/well of SD/-His broth. Plates were incubated overnight at 30 °C with agitation. The following day the cultures in each well were diluted with 60 µL of sterile 80% (v/v) glycerol solution. Wells were sealed using pre-cut sheets of sterile multi-well plate sealing film and stored at -80 °C for long-term storage.

3.2.4 Yeast mating procedure

The yeast mating procedure is illustrated schematically in Figure 3.1, c. Single colonies of Y7039 transformed with either pAG416GAL-TDP-43^{WT}-DsRed (^{GAL}TDP-43^{WT}-DsRed), pAG416GAL-FUS^{WT}-DsRed (^{GAL}FUS^{WT}-DsRed), pAG416GAL-SOD1^{WT}-DsRed (^{GAL}SOD1^{WT}-DsRed), pAG416GAL-SOD1^{A4V}-DsRed (^{GAL}SOD1^{A4V}-DsRed) or pAG416GAL-ccdB-DsRed (^{GAL}DsRed^{empty}; vector control) were inoculated into 10 mL of SD/-Leu/Ura and grown overnight at 30 °C with agitation. The following morning the overnight cultures were diluted into 30 mL of SD/-Leu/Ura and pinned in 96-colony density format to PlusPlates containing YPD using the ROTOR™, 4 plates per query strain. The pinned query strains were then grown for 48 h at 30 °C.

Each query strain and the control strain were crossed to an ordered 96-colony-dense array of a selection of 128 haploid *MAT*a strains from the EGFP-fusion collection of yeast strains. Each EGFP-fusion ORF in this collection is tagged with the *S. pombe* his5+ gene which allows growth on medium lacking histidine. The resulting heterozygous diploid strains were selected by growing the cells on solid (agar) synthetic medium lacking histidine and uracil,

supplemented with 2% (w/v) glucose (SD) – His/Ura), for 48 h at 30 °C (Figure 3.1, d).

Glycerol stocks of the diploid strains were prepared using the ROTOR™ to pin colonies from agar plates to 96-well plates containing 140 µL/well of SD/-His/Ura broth. Plates were incubated overnight at 30 °C with agitation. The following day the cultures in each well were diluted with 60 µL of sterile 80% (v/v) glycerol solution. Wells were sealed using pre-cut sheets of sterile multi-well plate sealing film and stored at -80 °C for long-term storage.

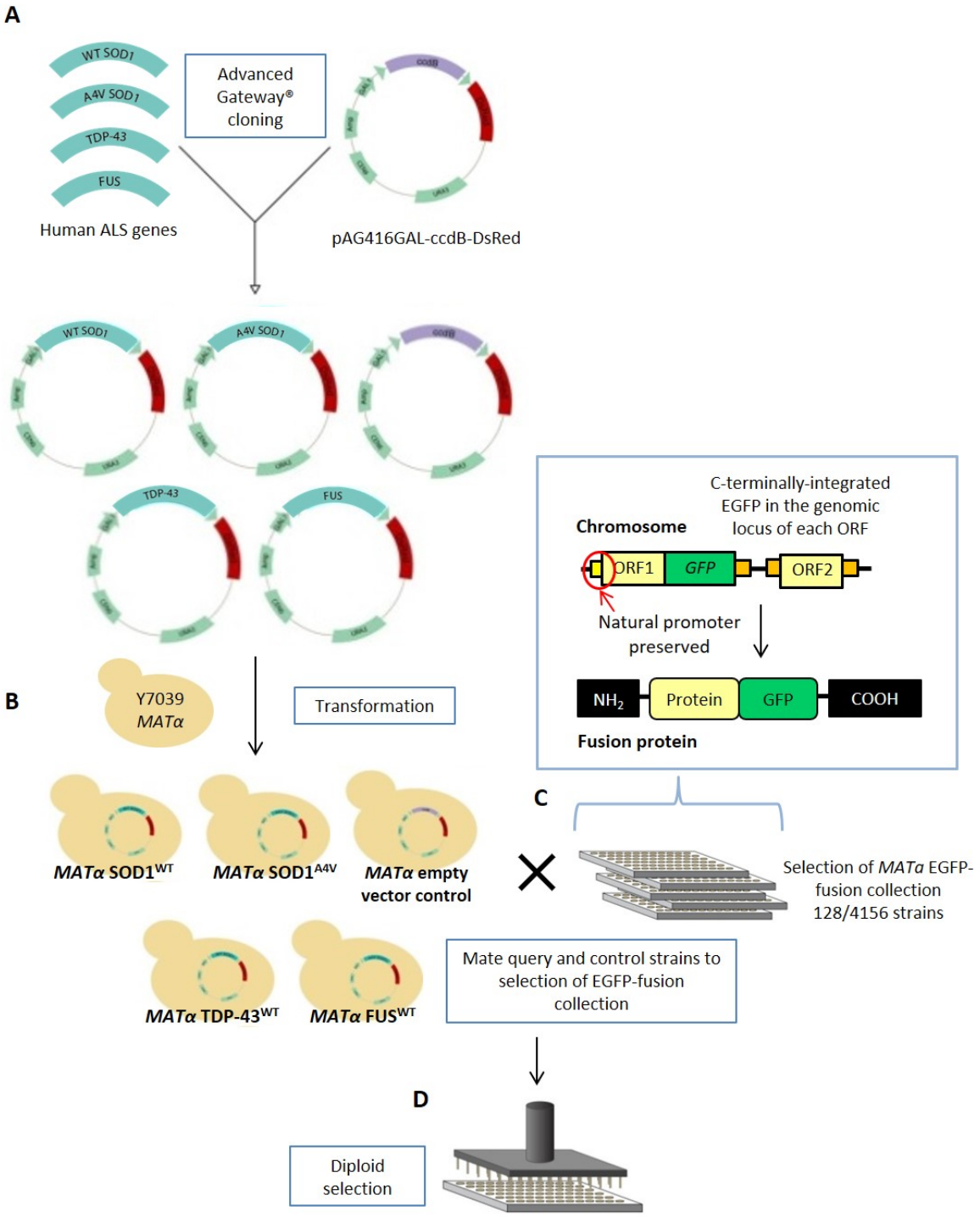
A
WT SOD1
A4V SOD1
TDP-43
FUS
Human ALS genes
Advanced Gateway® cloning
pAG416GAL-ccdB-DsRed
B
Y7039 MATα
Transformation
MATα SOD1WT
MATα SOD1A4V
MATα empty vector control
MATα TDP-43WT
MATα FUSWT
C
C-terminally-integrated EGFP in the genomic locus of each ORF
Chromosome
ORF1
GFP
ORF2
Natural promoter preserved
NH2
Protein
GFP
COOH
Fusion protein
Selection of MATα EGFP-fusion collection 128/4156 strains
Mate query and control strains to selection of EGFP-fusion collection
D
Diploid selection

Figure 3.1. Schematic representation of the generation of SOD1^{WT}-DsRed, SOD1^{A4V}-DsRed, TDP-43^{WT}-DsRed and FUS^{WT}-DsRed yeast query strains, mating with the yeast EGFP-fusion collection and diploid selection in preparation for screening experiments. (A) Human wild-type TDP-43 (TDP-43^{WT}), FUS^{WT}, SOD1^{WT} and SOD1^{A4V} were cloned from a mammalian expression vector into pAG416GAL-ccdB-DsRed using the Advanced Gateway® cloning system. (B) The resulting galactose-inducible pAG416GAL-TDP-43^{WT}-DsRed, pAG416GAL-FUS^{WT}-DsRed, pAG416GAL-SOD1^{WT}-DsRed, pAG416GAL-SOD1^{A4V}-DsRed and pAG416GAL-ccdB-DsRed (vector control) expression clones were transformed into the haploid *MATα* yeast strain Y7039 to create four query strains and a control strain. (C) Each query strain and the control strain were crossed to an ordered array of a selection of 128 haploid *MATa* strains from the EGFP-fusion collection of yeast strains (Huh *et al.* 2003). The EGFP-fusion strains were selected based on involvement in conserved proteostasis pathways, other pathways suspected to be involved in ALS pathogenesis as well as the yeast orthologues of human proteins that have been found colocalised in inclusions in ALS patients' motor neurons. Each EGFP-fusion ORF is tagged with the *S. pombe his5+* gene and allows growth on medium lacking histidine. (D) The resulting heterozygous diploid strains were selected by growing the cells on solid (agar) synthetic medium lacking histidine and uracil (synthetic dextrose (SD) – His/Ura).

3.2.5 Spotting assays

Single colonies of the haploid *MAT*α yeast query strains, generated through transformation of Y7039 with pAG416GAL-TDP-43^{WT}-DsRed (^{GAL}TDP-43^{WT}-DsRed), pAG416GAL-FUS^{WT}-DsRed (^{GAL}FUS^{WT}-DsRed), pAG416GAL-SOD1^{WT}-DsRed (^{GAL}SOD1^{WT}-DsRed), pAG416GAL-SOD1^{A4V}-DsRed (^{GAL}SOD1^{A4V}-DsRed) or pAG416GAL-ccdB-DsRed (^{GAL}DsRed^{empty}; vector control) and grown on SD/-Ura agar plates, were picked and used to inoculate 10 mL of SD/-Ura broth. Following overnight incubation at 30 °C with agitation, 125 µL of each culture was diluted into 2.5 mL of SRaf/-Ura broth and grown overnight at 30 °C with agitation. The following day this dilution procedure was repeated for a second night of growth in SRaf/-Ura broth. Cultures were then normalised for OD_{600}, serial diluted, spotted onto SD/-Ura or SGal/-Ura and incubated at 30 °C for 48 h. The incubated plates were then scanned using a standard HP® scanner, and the sizes of the resulting colonies were qualitatively examined for the diameter and density of yeast growth.

Spotting assays were also carried out following mating of haploid yeast query strains with haploid *MAT*a strains from the EGFP fusion collection of yeast strains, and consequent diploid selection. The resulting diploid strains were prepared for spotting assays using the procedure above, with the exception that SD/-His/Ura, SRaf/-His/Ura, and SGal/-His/Ura selective media were used to grow the cultures.

Query strains and diploid strains were grown in either galactose-supplemented media to induce expression of DsRed-tagged FUS^{WT}, TDP-43^{WT}, $SOD1^{WT}$, $SOD1^{A4V}$ or DsRed alone, or in glucose-supplemented media to control for differences in growth between strains that were not caused by expression of the DsRed-fusion genes.

3.2.6 DeltaVision OMX™ super resolution fluorescence microscopy

To characterise the localisation of TDP-43^{WT}-DsRed, FUS^{WT}-DsRed, $SOD1^{WT}$-DsRed and $SOD1^{A4V}$-DsRed and the EGFP fusion proteins in diploid strains, the fluorescent proteins were examined in cells using a DeltaVision OMX™ super resolution microscope (GE Healthcare Life Sciences, Marlborough, MA, USA). Super resolution microscopy was necessary for these experiments due to the size of the yeast cells; conventional microscopy would not provide the resolution needed to examine the intracellular localisation patterns of the EGFP-fusion proteins. To validate the use of diploid $^{GAL}DsRed^{empty}$ strains as control strains and to establish the baseline cellular levels of the EGFP-fusion proteins screened, it was crucial to ensure that the localisation of the EGFP-fusion proteins in the $^{GAL}DsRed^{empty}$ strains were comparable to the localisation patterns previously reported for growth in control conditions (Huh *et al.* 2003, Breker *et al.* 2013, Breker *et al.* 2014). Time limitations prevented the microscopic examination of all diploid strains used in the present work, thus only several strains were selected for microscopy. To microscopically examine a variety of localisation patterns, strains were selected to include EGFP-fusion proteins that have been reported to be localised to different macromolecular structures, organelles and to the cytosol. Slides were prepared for microscopy by placing flat agarose pads of 1 cm diameter, made of SGal/-His/Ura containing 1.5% (w/v) agarose, into the centre of each slide. To prepare diploid strains for microscopy, individual colonies on 96-colony-dense SD/-His/Ura plates were picked and used to inoculate 2.5 mL of SRaf/-His/Ura broth to grow overnight at 30 °C with agitation. The following day, 125 µL of each culture was diluted into 2.5 mL of SRaf/-His/Ura broth and grown overnight at 30 °C with

agitation. Following this second night of growth in SRaf/-His/Ura broth, 125 µL of each culture was diluted into 2.5 mL of SGal/-His/Ura broth and grown overnight at 30 °C with agitation to induce expression of ^{GAL}TDP-43^{WT}-DsRed, ^{GAL}FUS^{WT}-DsRed, ^{GAL}SOD1^{WT}-DsRed, ^{GAL}SOD1^{A4V}-DsRed or ^{GAL}DsRed^{empty}. In the later rounds of microscopy, in which diploid BMH1-EGFP, RPL40A-EGFP, RPN10-EGFP, TRS23-EGFP, MDJ1-EGFP, MGE1-EGFP, PUB1-EGFP, XRN1-EGFP and UFD4-EGFP strains were imaged, cells were counterstained with 0.8 µg/mL DAPI in PBS for 30 min at room temperature, followed by two washes in PBS (each wash involved centrifugation of cells at 1,000 × *g* followed by resuspension in 1 mL of PBS), centrifugation at 1,000 × *g* and resuspension in 1 mL of fresh SGal/-His/Ura broth. Resuspended cells from each culture (5 µL) was then pipetted onto SGal/-His/Ura agarose pads on prepared slides. Imaging was carried out using the 100× oil-immersion objective lens, with EGFP fluorescence excited at 488 nm and DsRed fluorescence excited at 568 nm using optically pumped, frequency-doubled vertical external cavity surface emitting lasers (VECSELs). The localisation of the EGFP-fusion yeast proteins observed through microscopy was compared with the localisation data documented on the Yeast GFP Fusion Localisation Database (YGFLD) [https://yeastgfp.yeastgenome.org/ - (Huh *et al.* 2003)], the LoQAtE database (Breker *et al.* 2013, Breker *et al.* 2014), the UniProt Database and the *Saccharomyces* Genome Database (SGD).

It should be noted that for diploid RPL40A-EGFP, RPN10-EGFP, TRS23-EGFP, MDJ1-EGFP, MGE1-EGFP, PUB1-EGFP, UFD4-EGFP and XRN1-EGFP strains, time restrictions prevented the microscopic examination of all five corresponding diploid strains (^{GAL}DsRed^{empty}, ^{GAL}TDP-43^{WT}-DsRed, ^{GAL}FUS^{WT}-DsRed, ^{GAL}SOD1^{WT}-DsRed and ^{GAL}SOD1^{A4V}-DsRed). However, the corresponding diploid EGFP-fusion/^{GAL}DsRed^{empty} strain was included as a control for microscopic examination of each diploid EGFP-fusion/^{GAL}TDP-43^{WT}-DsRed, EGFP-fusion/^{GAL}FUS^{WT}-DsRed, EGFP-fusion/^{GAL}SOD1^{WT}-DsRed and EGFP-

fusion/^{GAL}SOD1^{A4V}-DsRed strain, for comparisons of protein localisation patterns. Time limitations prevented the repetition of microscopy of each diploid strain, and thus the images presented and the observations described in the Results section are representative of n = 1 experiment.

3.2.7 Measurement of EGFP-fusion protein levels in diploid yeast strains

The methods used to measure levels of EGFP-fusion proteins in diploid strains is illustrated schematically in Figure 3.2. Each 96-colony-dense plate of diploid strains was pinned in quadruplicate to a 384-well microtitre plate containing 100 µL per well of SRaf/-His/Ura using the ROTOR™ and grown overnight at 30 °C with agitation (Figure 3.2, a). The following day the 100 µL overnight cultures were pinned to black-walled 384-well µclear plates containing 100 µL per well of SGal/-His/Ura to induce expression of ^{GAL}TDP-43^{WT}-DsRed, ^{GAL}FUS^{WT}-DsRed, ^{GAL}SOD1^{WT}-DsRed, ^{GAL}SOD1^{A4V}-DsRed or ^{GAL}DsRed^{empty}. The absorbance (optical density [OD] at 600 nm), EGFP (excitation 485/12 nm, emission collected at 510/20 nm) and DsRed (excitation 580/10 nm, emission collected at 612 nm) fluorescence were then measured in each plate of cells over 48 h using a FLUOstar® Optima plate reader (BMG LABTECH, Ortenberg, Germany) set to incubate plates at 30 °C (Figure 3.2, b).

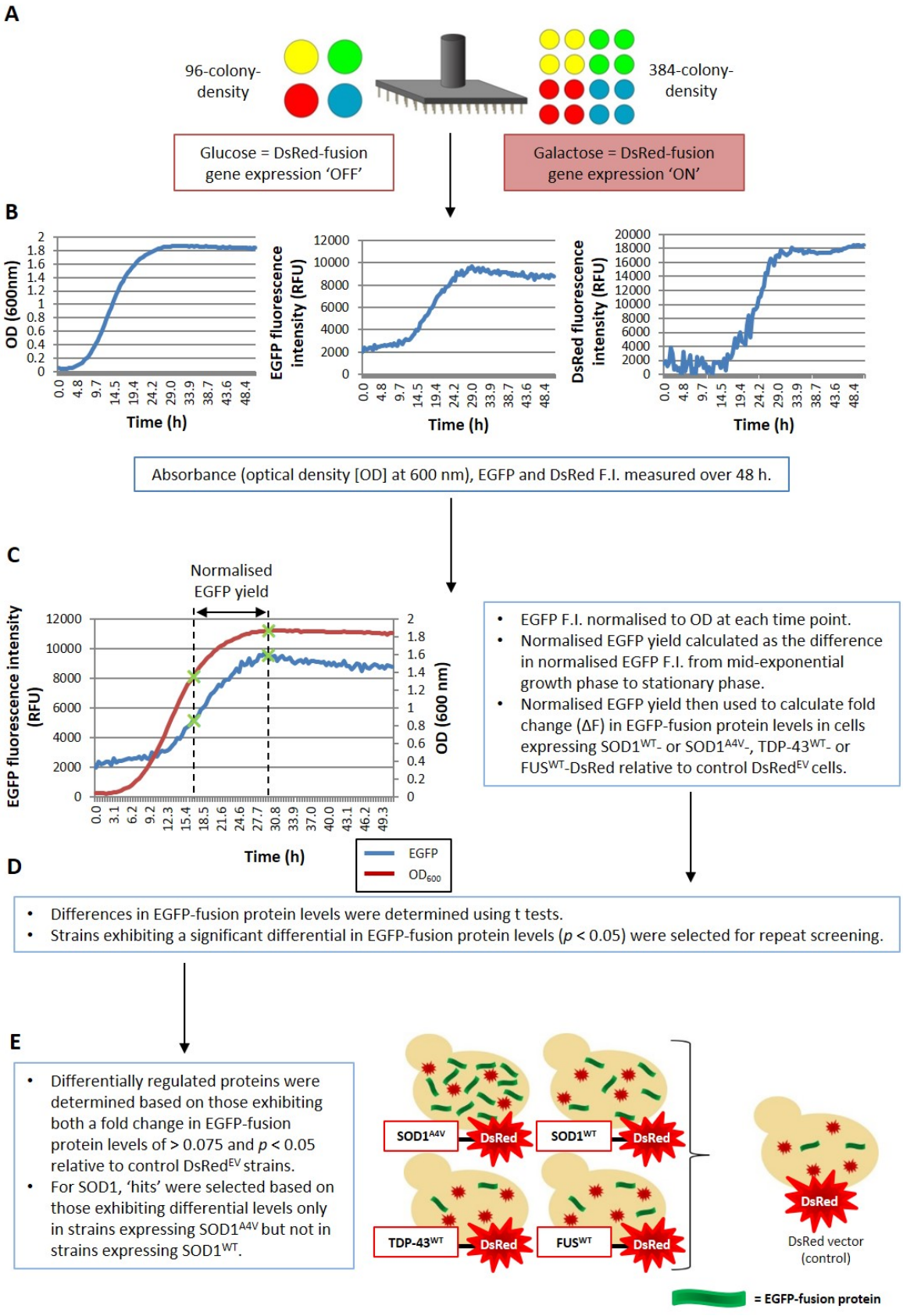
A
96-colony-density
384-colony-density
Glucose = DsRed-fusion gene expression 'OFF'
Galactose = DsRed-fusion gene expression 'ON'
B
OD (600nm)
EGFP fluorescence intensity (RFU)
DsRed fluorescence intensity (RFU)
Time (h)
Absorbance (optical density [OD] at 600 nm), EGFP and DsRed F.I. measured over 48 h.
C
Normalised EGFP yield
EGFP fluorescence intensity (RFU)
OD (600 nm)
Time (h)
EGFP
OD600
• EGFP F.I. normalised to OD at each time point.
• Normalised EGFP yield calculated as the difference in normalised EGFP F.I. from mid-exponential growth phase to stationary phase.
• Normalised EGFP yield then used to calculate fold change (ΔF) in EGFP-fusion protein levels in cells expressing SOD1WT- or SOD1A4V-, TDP-43WT- or FUSWT-DsRed relative to control DsRedEV cells.
D
• Differences in EGFP-fusion protein levels were determined using t tests.
• Strains exhibiting a significant differential in EGFP-fusion protein levels (p < 0.05) were selected for repeat screening.
E
• Differentially regulated proteins were determined based on those exhibiting both a fold change in EGFP-fusion protein levels of > 0.075 and p < 0.05 relative to control DsRedEV strains.
• For SOD1, 'hits' were selected based on those exhibiting differential levels only in strains expressing SOD1A4V but not in strains expressing SOD1WT.
SOD1A4V
DsRed
SOD1WT
DsRed
TDP-43WT
DsRed
FUSWT
DsRed
DsRed
DsRed vector (control)
= EGFP-fusion protein

Figure 3.2. Schematic representation of the analysis workflow used to identify yeast EGFP-fusion proteins with altered levels in yeast expressing human SOD1^{WT}-DsRed, SOD1^{A4V}-DsRed, TDP-43^{WT}-DsRed and FUS^{WT}-DsRed. (A) Each 96-colony-dense plate of diploid strains was pinned in quadruplicate to a 384-well microtitre plate containing SRaf/-His/Ura using the ROTOR™ and grown overnight at 30 °C with agitation. The following day the overnight cultures were pinned to black-walled 384-well µclear plates containing SGal/-His/Ura to induce expression of ^{GAL}TDP-43^{WT}-DsRed, ^{GAL}FUS^{WT}-DsRed, ^{GAL}SOD1^{WT}-DsRed, ^{GAL}SOD1^{A4V}-DsRed or ^{GAL}DsRed^{empty} (DsRed alone). (B) The absorbance (optical density [OD] at 600 nm), EGFP (excitation 485/12 nm, emission collected at 510/20 nm) and DsRed (excitation 580/10 nm, emission collected at 612 nm) fluorescence were then measured in each plate of cells over 48 h using a FLUOstar® Optima plate reader. (C) The EGFP fluorescence intensity (F.I.) measured at 485 nm in each well of cells was normalised to the absorbance at each time point to account for cell density in each well. The normalised EGFP values were used in subsequent analyses to calculate yield of EGFP-fusion protein levels in cells expressing ^{GAL}TDP-43^{WT}-DsRed, ^{GAL}FUS^{WT}-DsRed, ^{GAL}SOD1^{WT}-DsRed or ^{GAL}SOD1^{A4V}-DsRed relative to control cells expressing ^{GAL}DsRed^{empty}. Custom R scripts were used to analyse the normalised EGFP F.I. values over the 48 h assay period. Calculations of the yield of EGFP-fusion protein levels were based on the difference in normalised EGFP from mid-exponential growth phase to stationary phase (monitored by the OD at 600 nm), when EGFP F.I. reached a maximum. (D) T tests were carried out using a custom R script to determine the difference (fold change) in EGFP-fusion protein levels in strains expressing ^{GAL}TDP-43^{WT}-DsRed, ^{GAL}FUS^{WT}-DsRed, ^{GAL}SOD1^{WT}-DsRed or ^{GAL}SOD1^{A4V}-DsRed compared to strains expressing ^{GAL}DsRed^{empty}. (E) Strains exhibiting a significant differential in EGFP-fusion protein levels ($p < 0.05$) were selected for repeat screening. EGFP-fusion proteins were ranked as having differential levels in ^{GAL}TDP-43^{WT}-DsRed, ^{GAL}FUS^{WT}-DsRed, ^{GAL}SOD1^{WT}-DsRed or ^{GAL}SOD1^{A4V}-DsRed strains based on those exhibiting both a fold change in EGFP-fusion protein levels of > 0.075 (arbitrary cut-off value) and $p < 0.05$ relative to control ^{GAL}DsRed^{empty} strains. In the case of ^{GAL}SOD1^{A4V}-DsRed, 'hits' were selected based on those exhibiting differential protein levels only in strains expressing ^{GAL}SOD1^{A4V}-DsRed but not in strains expressing ^{GAL}SOD1^{WT}-DsRed.

3.2.8 Analysis of EGFP-fusion protein levels

Analyses of EGFP-fusion protein levels measured in each diploid strain are illustrated schematically in Figure 3.2, c, d and e. R statistical computing software, Microsoft® Office Excel and Graphpad Prism 5 (GraphPad Software Inc., La Jolla, CA, USA) were used for subsequent data analyses. The EGFP fluorescence intensity (F.I.) (excitation 485/12 nm, emission collected at 510/20 nm) measured in each well was normalised to the absorbance at 600 nm at each time point using Microsoft® Office Excel in order to account for cell density in each well. Normalisation involved dividing the EGFP F.I. value by the absorbance at each time point. The normalised EGFP values were used in subsequent analyses in R to calculate yield and fold change in EGFP-fusion protein levels in cells expressing ^{GAL}TDP-43^{WT}-DsRed, ^{GAL}FUS^{WT}-DsRed, ^{GAL}SOD1^{WT}-DsRed or ^{GAL}SOD1^{A4V}-DsRed relative to control cells expressing ^{GAL}DsRed^{empty} (DsRed alone). Custom R scripts (Appendix I) were originally written by Dr. Daniel Bean (University of Cambridge, UK) for analyses of yeast growth curves (absorbance) and modified in the present work for analyses of normalised EGFP F.I. values

over the 48 h assay period. Calculations of the yield of EGFP-fusion protein levels were based on the difference in normalised EGFP from mid-exponential growth phase to stationary phase, when EGFP F.I. reached a maximum. T tests were carried out using a custom R script (Appendix I) originally written by Ms Anastasiya Pachyna (University of Cambridge, UK) and modified in the present work to determine the difference (fold change; ΔF) in EGFP-fusion protein levels in strains expressing ^{GAL}TDP-43^{WT}-DsRed, ^{GAL}FUS^{WT}-DsRed, ^{GAL}SOD1^{WT}-DsRed or ^{GAL}SOD1^{A4V}-DsRed compared to strains expressing ^{GAL}DsRed^{empty} (DsRed alone), across two replicates per strain. Strains exhibiting a significant change in EGFP-fusion protein levels ($p < 0.05$) were selected for repeat screening (four replicates). EGFP-fusion proteins were ranked as having differential levels in ^{GAL}TDP-43^{WT}-DsRed, ^{GAL}FUS^{WT}-DsRed, ^{GAL}SOD1^{WT}-DsRed or ^{GAL}SOD1^{A4V}-DsRed strains based on those exhibiting both a fold change in EGFP-fusion protein levels of > 0.075 (arbitrary cut-off value) and $p < 0.05$ relative to control ^{GAL}DsRed^{empty} strains. In the case of ^{GAL}SOD1^{A4V}-DsRed, 'hits' were selected based on those exhibiting differential protein levels only in strains expressing ^{GAL}SOD1^{A4V}-DsRed but not in strains expressing ^{GAL}SOD1^{WT}-DsRed.

3.2.9 Analysis of protein-protein interaction networks

Interactions between yeast EGFP-fusion proteins that were identified to be present at altered levels in diploid ^{GAL}TDP-43^{WT}-DsRed, ^{GAL}FUS^{WT}-DsRed or ^{GAL}SOD1^{A4V}-DsRed strains relative to diploid control ^{GAL}DsRed^{empty} strains, 'hits', were analysed using the STRING database (Szklarczyk *et al.* 2015, Szklarczyk *et al.* 2017) and Cytoscape 3.7.1 (National Institute of General Medical Sciences (NIGMS) of the National Institutes of Health (NIH), USA). Each set of hits for ^{GAL}TDP-43^{WT}-DsRed, ^{GAL}FUS^{WT}-DsRed and ^{GAL}SOD1^{A4V}-DsRed was queried in STRING to identify interactions between the hits using co-expression, published experiments and databases as sources of interaction data. STRING computes confidence scores for all protein-protein interactions, and a high confidence cut-off (0.700) was used for the

present analyses. No more than ten secondary interacting genes/proteins of the hits were included in each interaction network. The resulting interaction network data was then imported into Cytoscape to format the network to distinguish between the primary hits for each of ^{GAL}TDP-43^{WT}-DsRed, ^{GAL}FUS^{WT}-DsRed and ^{GAL}SOD1^{A4V}-DsRed and the ten secondary interactors connecting the hits to each other.

Although these yeast EGFP-fusion protein collection screens were pathway-focused, in that only a selection of 128 strains from the full EGFP-fusion collection of strains were included, this selection nevertheless covered a spectrum of molecular functions. It was thus useful to examine the gene ontology (GO) functional enrichments of the hits for each of ^{GAL}TDP-43^{WT}-DsRed, ^{GAL}FUS^{WT}-DsRed and ^{GAL}SOD1^{A4V}-DsRed against the background pathway-focused selection of 128 EGFP-fusion proteins. GO analyses of each set of hits were carried out using PANTHER GO Enrichment Analysis (version 14) (Ashburner *et al.* 2000, Mi *et al.* 2019, The Gene Ontology Consortium 2019), with the pathway-focused selection of 128 EGFP-fusion proteins set as the background reference list.

3.2.10 Data quality control analyses

To ensure that growth and expression of ^{GAL}TDP-43^{WT}-DsRed, ^{GAL}FUS^{WT}-DsRed, ^{GAL}SOD1^{WT}-DsRed, ^{GAL}SOD1^{A4V}-DsRed and ^{GAL}DsRed^{empty} (DsRed alone) in diploid strains assayed on the FLUOstar® Optima plate reader were consistent between wells within each plate and between different plates in separate experiments, the raw absorbance (OD_{600}) and DsRed fluorescence data from each well were examined in GraphPad Prism. Specifically, growth between strains and between replicates was evaluated by examining the distribution of the OD_{600} yield (maximum OD_{600} – minimum OD_{600}) and the maximum exponential rate of change of OD_{600} (maximum growth rate; OD_{600}/h) between wells. The expression of ^{GAL}TDP-43^{WT}-DsRed, ^{GAL}FUS^{WT}-DsRed, ^{GAL}SOD1^{WT}-DsRed, ^{GAL}SOD1^{A4V}-DsRed or ^{GAL}DsRed^{empty} (DsRed alone) between wells was assessed by comparing the distribution of the maximum

DsRed F.I. (F_{max}; maximum DsRed F.I. – minimum DsRed F.I.; relative fluorescence units, RFU) and the maximum exponential rate of change of DsRed F.I. (maximum rate of DsRed F.I. increase; RFU/h).

3.3 Results

3.3.1 Collating the list of relevant EGFP-fusion yeast proteins to screen

The yeast EGFP-fusion collection comprises 4156 different strains (Huh *et al.* 2003). For the purposes of the work described in this chapter, it was pertinent to collate a focused selection of EGFP-fusion strains of relevance to human cellular biology in the context of ALS. Relevant proteins and the corresponding EGFP-fusion yeast strains were selected based on (i) involvement in conserved proteostasis pathways, (ii) other pathways suspected to be involved in ALS pathogenesis, or (iii) the yeast orthologues of human proteins that have been found colocalised in inclusions in ALS patients' motor neurons (Ciryam *et al.* 2017). Literature searches and online databases (Ensembl genome database, BioGRID, esyN, Kyoto Encyclopedia of Genes and Genomes (KEGG), PubMed, *Saccharomyces* genome database (SGD) and UniProt) were used to inform selection of the proteins of interest and to analyse their function, localisation, expression and interaction data. It was crucial that expression of the EGFP-fusion yeast genes could be reliably detected and measured using a fluorescent plate reader. Therefore, in most cases proteins with known abundance levels greater than 1,500 molecules per cell were included for analysis (Ghaemmaghami *et al.* 2003). However, some proteins (24) were included that had low cellular abundance (< 1,500 molecules/cell) (Ghaemmaghami *et al.* 2003) (Table S3.2, Appendix I) or did not have direct human orthologues (Table S3.3, Appendix I) because those proteins were particularly relevant to ALS pathogenesis. The final selection consisted of 128 EGFP-fusion yeast strains (Table S3.1, Appendix I). Of these, 19 have RNA metabolic functions, 13 have functions associated with ribosomes and protein translation, 21 are involved in ubiquitin homeostasis and/or the UPS, 2 are ubiquitin-like modifier proteins, 15 are molecular chaperones, 15 are involved in regulating ER proteostasis and/or responding to ER stress, 11 have functions in the endomembrane system, ER-Golgi transport and Golgi function, 2 are components of the cytoskeleton, 2 are

involved in autophagy, 1 is involved in aggresome function, 9 function in protein phosphorylation, trafficking and signal transduction, 15 are involved in mitochondrial homeostasis and antioxidant activity, 1 is a glutamine synthetase and 2 have functions in energy metabolism.

Following selection of EGFP-fusion strains to cross with the ^{GAL}TDP-43^{WT}-DsRed, ^{GAL}FUS^{WT}-DsRed, ^{GAL}SOD1^{WT}-DsRed and ^{GAL}SOD1^{A4V}-DsRed query strains and the ^{GAL}DsRed^{empty} (DsRed alone) control strain, it was found that 2 of the strains, UBP6-EGFP (YFR010W) and EIF2A-EGFP (YGR054W), were unable to grow properly, even in rich YPD media. These strains were thus excluded from the screens.

3.3.2 Characterisation of haploid query strains and diploid strains

To generate yeast models of SOD1, TDP-43 and FUS pathology, yeast centromeric galactose-inducible plasmids containing human SOD1^{WT}, SOD1^{A4V}, TDP-43^{WT} and FUS^{WT} with C-terminal DsRed tags were constructed and transformed into the haploid *MAT*α yeast strain Y7039. The resulting query strains along with a control strain transformed with the DsRed backbone vector were tested for toxicity caused by expression of the human genes using spotting assays (Figure 3.3). The untransformed Y7039 strain was included in the spotting assays to confirm that it had normal growth patterns (Figure 3.3, a, i and ii). To ensure that any differences in growth between strains were caused by expression of the DsRed-fusion human genes and not by unknown variables, the haploid query strains and the diploid strains were grown on glucose-supplemented plates (does not express DsRed-fusion human gene) in parallel to galactose-supplemented plates (expresses DsRed-fusion human gene). Comparison of the growth of each strain at each dilution on glucose-supplemented plates confirmed that without expression of the DsRed-tagged human genes, viability was similar between each haploid and diploid strain (Figure 3.3, b, ii and c, ii). Examining the growth of the haploid query strains on galactose-supplemented plates showed that expression of ^{GAL}TDP-43^{WT}-

DsRed strikingly reduced yeast viability, while ^{GAL}FUS^{WT}-DsRed, ^{GAL}SOD1^{WT}-DsRed and ^{GAL}SOD1^{A4V}-DsRed did not affect yeast viability relative to control yeast expressing ^{GAL}DsRed^{empty} (DsRed alone) (Figure 3.3, b, i). The toxicity of ^{GAL}TDP-43^{WT}-DsRed expression was also evident in diploid yeast, as represented in the PUB1-EGFP/^{GAL}TDP-43^{WT}-DsRed strain, while no reduction in growth was observed in the PUB1-EGFP/^{GAL}SOD1^{WT}-DsRed and PUB1-EGFP/^{GAL}SOD1^{A4V}-DsRed diploid strains relative to the diploid control strain PUB1-EGFP/^{GAL}DsRed^{empty} (Figure 3.3, c, i). Interestingly, while no reductions in cell viability were observed for the haploid ^{GAL}FUS^{WT}-DsRed strain, a slight decrease in viability was observed in diploid PUB1-EGFP/^{GAL}FUS^{WT}-DsRed yeast compared to the diploid PUB1-EGFP/^{GAL}DsRed^{empty} strain.

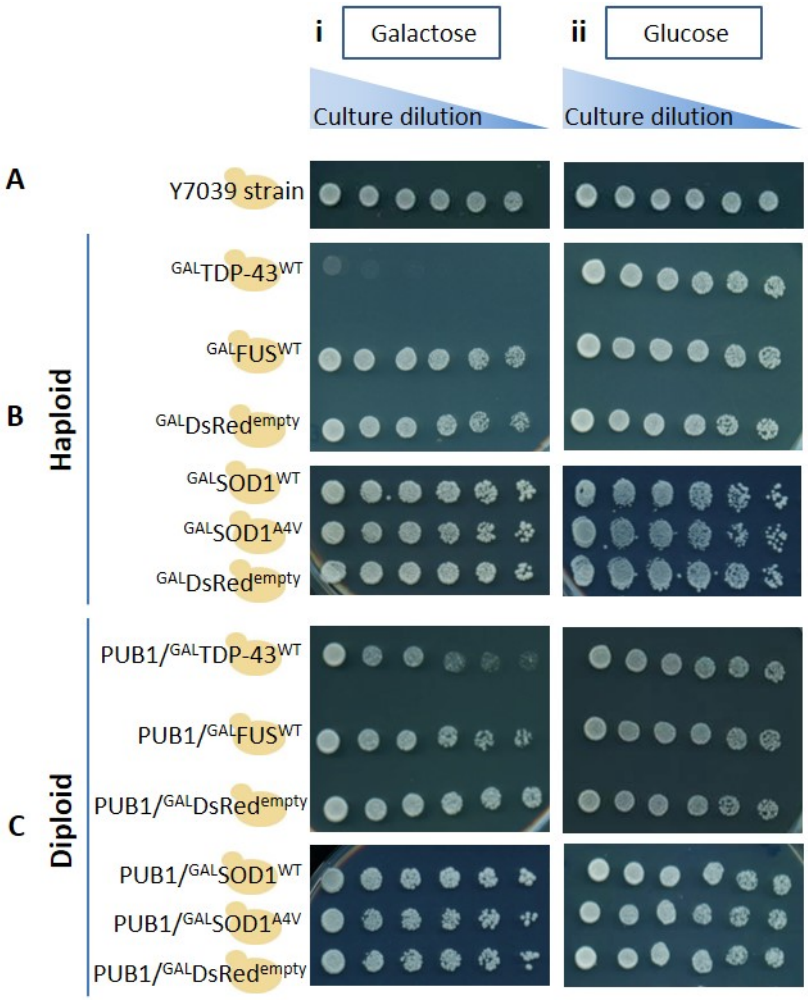

Figure 3.3. Viability of yeast expressing DsRed-tagged human SOD1^{WT}, SOD1^{A4V}, TDP-43^{WT}, or FUS^{WT} relative to yeast expressing DsRed alone. Spotting assays of (A) the haploid *MAT*α yeast strain, Y7039, (B) Y7039 transformed with pAG416GAL-TDP-43^{WT}-DsRed (^{GAL}TDP-43^{WT}), pAG416GAL-FUS^{WT}-DsRed (^{GAL}FUS^{WT}), pAG416GAL-SOD1^{WT}-DsRed (^{GAL}SOD1^{WT}), pAG416GAL-SOD1^{A4V}-DsRed (^{GAL}SOD1^{A4V}) or pAG416GAL-ccdB-DsRed (^{GAL}DsRed^{empty}; vector control (DsRed alone)) (haploid query strains) and (C) representative diploid strains created by mating each haploid query strain with the haploid PUB1-EGFP strain from the yeast EGFP fusion collection (Huh *et al.* 2003) and subsequent diploid selection. Yeast strains were grown overnight in (A) YPD, (B, i) SGal/-Ura or (B, ii) SD/-Ura, (C, i) SGal/-His/Ura or (C, ii) SD/-His/Ura broth at 30 °C with agitation. Cultures were then normalised for OD_{600}, serial diluted, spotted onto solid (A) YPD, (B, i) SGal/-Ura or (B, ii) SD/-Ura, (C, i) SGal/-His/Ura or (C, ii) SD/-His/Ura agar plates and incubated at 30 °C for 48 h. The incubated plates were then scanned using a standard HP® scanner, and the sizes of the resulting colonies were qualitatively examined for the diameter and density of yeast growth. Query strains and diploid strains were grown in either galactose-supplemented media to induce expression of DsRed-tagged ^{GAL}FUS^{WT}, ^{GAL}TDP-43^{WT}, ^{GAL}SOD1^{WT}, ^{GAL}SOD1^{A4V} or ^{GAL}DsRed^{empty} (DsRed alone), or in glucose-supplemented media to control for differences in growth between strains that were not caused by expression of the DsRed-tagged genes.

Prior to screening the levels of the EGFP-fusion proteins in each diploid strain using the fluorescent plate reader, it was imperative to microscopically examine the localisation patterns of both the DsRed-fusion proteins and a selection of the EGFP-fusion yeast proteins. This was important to ensure that the localisation of the EGFP-fusion proteins in control ^{GAL}DsRed^{empty}

strains did not deviate from those documented on the UniProt and SGD databases and as previously reported for the EGFP-fusion strains grown in control conditions (Breker *et al.* 2013, Breker *et al.* 2014), and thus that the ^{GAL}DsRed^{empty} strains could be used as valid controls. For this purpose, several strains were selected for microscopy to include EGFP-fusion proteins that have functions in different cellular compartments and thus diverse localisation patterns; CDC48, ERV25, ENO1, BMH1, RPL40A, RPN10, TRS23, MDJ1, MGE1/GRPE, PUB1, XRN1 and UFD4. The localisation patterns of TDP-43^{WT}-DsRed, FUS^{WT}-DsRed, SOD1^{WT}-DsRed and SOD1^{A4V}-DsRed were also assessed. While the spotting assays demonstrated that the expression of TDP-43^{WT}-DsRed and FUS^{WT}-DsRed was toxic in yeast, it was necessary to confirm that TDP-43^{WT}-DsRed and FUS^{WT}-DsRed shifted from a predominantly nuclear localisation to accumulate into cytoplasmic foci, and thus recapitulate the mislocalisation observed in human tissue, mammalian cell culture and animal models. The expression of SOD1^{A4V}-DsRed did not impair the viability of yeast, in contrast to the toxicity the SOD1^{A4V} mutant causes in neuronal cells (data presented in Chapter IV; Figure 4.1, a), in zebrafish, and the rapid disease progression in individuals with ALS who have this mutation (Cudkowicz *et al.* 1997, Juneja *et al.* 1997, Lemmens *et al.* 2007). Because SOD1-positive inclusions are a characteristic pathological feature observed in post-mortem spinal cord tissue samples from *SOD1*-fALS patients (Shibata *et al.* 1996, Kato *et al.* 2000) and mutant SOD1 transgenic mouse models (Bruijn *et al.* 1997, Johnston *et al*. 2000, Watanabe *et al*. 2001, Wang *et al.* 2002) it was of interest to examine whether SOD1^{A4V}-DsRed aggregated into inclusions in the diploid yeast strains.

Across all diploid strains examined, the expression of DsRed alone was observed to be relatively low (Figures S3.1 to S3.12, Appendix I). In cells in which its fluorescence was detectable, DsRed appeared to be localised to focal regions of the cell rather than more diffusely distributed throughout the cytoplasm, as is usually seen with expression of the pEGFP-N1

vector (EGFP alone) (data presented in Chapters IV and V). Both TDP-43^{WT}-DsRed and FUS^{WT}-DsRed were predominantly localised to small cytoplasmic foci in most cells. In contrast, SOD1^{WT}-DsRed and SOD1^{A4V}-DsRed exhibited a uniform distribution throughout the cytoplasm and nucleus of all cells. Interestingly, SOD1^{A4V}-DsRed was not observed to aggregate into inclusions but had a similar localisation pattern to that of SOD1^{WT}-DsRed.

The localisation patterns of the examined EGFP-fusion proteins (Figures S3.1 to S3.12, Appendix I) are summarised in Table 3.2. Importantly, examination of the EGFP-fusion proteins localisation patterns in diploid ^{GAL}DsRed^{empty} strains confirmed that there was no deviation from the localisation patterns that had previously been reported for the EGFP-fusion strains grown under control conditions (Breker *et al.* 2013, Breker *et al.* 2014) and as documented on the UniProt and SGD databases. Across the examined diploid strains expressing TDP-43^{WT}-DsRed, FUS^{WT}-DsRed, SOD1^{WT}-DsRed or SOD1^{A4V}-DsRed, several of the EGFP-fusion proteins exhibited differential localisation patterns. Although evaluation of the localisation patterns of the EGFP-fusion proteins across the different diploid strains was not a primary objective of the present study, and only a sub-selection of diploid strains were examined out of the full selection screened in the plate reader-based assays, it is worth noting the localisation changes that were observed in the microscopically examined diploid strains.

The localisation patterns of CDC48-EGFP, RPL40A-EGFP, RPN10-EGFP and PUB1-EGFP were observed to be altered in yeast expressing TDP-43^{WT}-DsRed compared to yeast expressing DsRed alone. The localisation patterns of RPN10-EGFP and PUB1-EGFP were also altered in yeast expressing FUS^{WT}-DsRed. In diploid CDC48-EGFP/^{GAL}TDP-43^{WT}-DsRed yeast, CDC48-EGFP appeared to colocalise to the cytoplasmic foci formed by TDP-43^{WT}-DsRed (Figure S3.1, Appendix I). In diploid RPL40A-EGFP/^{GAL}DsRed^{empty} and RPL40A-EGFP/^{GAL}SOD1^{A4V}-DsRed strains the EGFP-fusion protein was predominantly localised to cell nuclei, whereas in the diploid RPL40A-EGFP/^{GAL}TDP-43^{WT}-DsRed strain it was

distributed more evenly throughout the cytoplasm of cells (Figure S3.5, Appendix I). RPL40A is a fusion protein that is proteolytically cleaved to produce ubiquitin and the L40 ribosomal subunit protein (Finley *et al.* 1989). After cleavage, the L40 protein predominantly assembles into mature cytoplasmic pre-60 S ribosomal subunits (Fernández-Pevida *et al.* 2012). The cleaved ubiquitin forms a complex with ribosomal proteins and helps regulate translation (Kobayashi *et al.* 2016). The ribosomal subunit protein is in the C terminal region of RPL40A, to which EGFP is fused. It is unclear whether the pattern of EGFP fluorescence seen in cells may reflect the localisation of uncleaved RPL40A or cleaved L40 protein. For instance, the increased EGFP fluorescence intensity observed in the cytoplasm of RPL40A-EGFP/^{GAL}TDP-43^{WT}-DsRed cells could be due to increased association of L40 with cytoplasmic ribosomal subunits.

In diploid RPN10-EGFP/^{GAL}TDP-43^{WT}-EGFP and RPN10-EGFP/^{GAL}FUS^{WT}-EGFP yeast, cytoplasmic foci formed by TDP-43^{WT}-DsRed and FUS^{WT}-DsRed appeared to colocalise with areas of increased cytoplasmic RPN10-EGFP fluorescence intensity (Figure S3.6, Appendix I). RPN10 is one of the non-ATPase base subunits of the 19S regulatory particle of the proteasome (Glickman *et al.* 1998, Verma *et al.* 2004). The observed regions of increased RPN10-EGFP fluorescence intensity may indicate areas of higher concentration of assembled proteasomes. The localisation of TDP-43^{WT}-DsRed and FUS^{WT}-DsRed foci to these regions could be due to targeting of the foci for proteasomal degradation.

PUB1 is a poly (A)+ RBP involved in the regulation of translation and is an important component of SGs (reviewed in Buchan and Parker (2009)). In both PUB1-EGFP/^{GAL}TDP-43^{WT}-DsRed and PUB1-EGFP/^{GAL}FUS^{WT}-DsRed cells, a proportion of the cytosolic foci formed by TDP-43^{WT}-DsRed and FUS^{WT}-DsRed colocalised with foci formed by PUB1-EGFP (Figure S3.10, Appendix I). This is likely due to the association of these proteins in SGs. It is possible that cytosolic foci formed by TDP-43^{WT}-DsRed and FUS^{WT}-DsRed that were not

colocalised with PUB1-EGFP were cytosolic accumulations of the proteins into inclusions that were distinct from SGs.

TRS23 is one of the core subunits of transport protein particle (TRAPP) complexes I-III and is involved in ER-Golgi transport and autophagy (Sacher *et al.* 2001, Lynch-Day *et al.* 2010, Yip *et al.* 2010). As such, it localises to the ER and Golgi apparatus in the cytoplasm of cells. In diploid TRS23-EGFP/^{GAL}DsRed^{empty} and TRS23-EGFP/^{GAL}TDP-43^{WT}-DsRed cells, the fluorescence of TRS23-EGFP was diffuse throughout the cytoplasm of cells, excluded from cell nuclei and structures likely corresponding to vacuoles (Figure S3.7, Appendix I). There were also small regions of increased EGFP fluorescence intensity surrounding cell nuclei and the vacuoles. This was likely due to increased localisation of TRS23-EGFP to the ER, the Golgi apparatus and to vacuoles that may be involved in autophagy. Interestingly, the pattern of TRS23-EGFP fluorescence was strikingly different in TRS23-EGFP/^{GAL}SOD1^{A4V}-DsRed yeast. The overall fluorescence intensity of TRS23-EGFP was markedly reduced, there did not appear to be vacuole-like structures excluding TRS23-EGFP, and in some cells there were small EGFP fluorescent puncta.

In diploid UFD4-EGFP/^{GAL}FUS^{WT}-DsRed, UFD4-EGFP/^{GAL}SOD1^{A4V}-DsRed and UFD4-EGFP/^{GAL}DsRed^{empty} yeast cells, UFD4-EGFP was localised to distinct foci throughout the cytoplasm (Figure S3.12, Appendix I). In UFD4-EGFP/^{GAL}FUS^{WT}-DsRed yeast there were numerous larger UFD4-EGFP foci than were observed in UFD4-EGFP/^{GAL}SOD1^{A4V}-DsRed and UFD4-EGFP/^{GAL}DsRed^{empty} yeast cells, and these foci were colocalised with foci formed by FUS^{WT}-DsRed. UFD4 is an E3 ubiquitin ligase and has been reported to interact with subunits of the 19S regulatory particle of the proteasome (Xie and Varshavsky 2000). Proteins that have been conjugated to a few ubiquitin molecules by UFD4 are detected by the CDC48-UFD1-NPL4 complex, which subsequently recruits the ubiquitin chain elongation factor (E4), UFD2, to facilitate the extension of the polyubiquitin chain and direct substrate proteins to the

proteasome (Koegl *et al.* 1999). The UFD4-EGFP foci observed in diploid cells may be sites of ubiquitylation of proteins targeted for proteasomal degradation. This would suggest that colocalisation of FUS^{WT}-DsRed and UFD4-EGFP foci may be due to ubiquitylation and targeting of misfolded FUS^{WT}-DsRed to the proteasome for degradation.

Table 3.2. Localisation patterns of selected EGFP-fusion proteins as observed through super-resolution fluorescence microscopy. Diploid strains were grown for 2 nights in SRaf/-His/Ura broth before being diluted 20× into SGal/-His/Ura broth and grown overnight at 30 °C with agitation to induce expression of ^{GAL}TDP-43^{WT}-DsRed, ^{GAL}FUS^{WT}-DsRed, ^{GAL}SOD1^{WT}-DsRed, ^{GAL}SOD1^{A4V}-DsRed or ^{GAL}DsRed^{empty} (vector control; DsRed alone). The fluorescent proteins were examined in cells using the 100× oil-immersion objective lens of a DeltaVision OMX™ super resolution microscope. Localisation patterns were compared with those documented on the UniProt and SGD databases and as previously reported for the EGFP-fusion strains grown in control conditions (Breker *et al*. 2013, Breker *et al*. 2014).

Yeast Systematic Name	**Yeast Standard Name**	**Supp. figure no.**	**^{GAL}TDP-43^{WT}-DsRed**	**^{GAL}FUS^{WT}-DsRed**	**^{GAL}SOD1^{WT}-DsRed**	**^{GAL}SOD1^{A4V}-DsRed**	**^{GAL}DsRed^{empty}**	**Published localisation (Breker *et al.* 2013, Breker *et al.* 2014, Saccharomyces Genome Database; SGD, UniProt)**	**Description of yeast orthologue (*Saccharomyces* Genome Database; SGD, UniProt)**
YDL126C	CDC48	S3.1	Decreased diffuse cytosolic F.I.; colocalisation with TDP-43^{WT}-DsRed cytosolic foci	Cytosol and nucleus	Cytosol and nucleus	Cytosol and nucleus	Cytosol and nucleus	Cytosol	AAA ATPase; subunit of polyubiquitin-selective segregase complex involved in ERAD; subunit of complex involved in mitochondria-associated degradation, in macroautophagy, PMN, RAD, ribophagy (Ye *et al*. 2003, Heo *et al*. 2010).
YML012W	ERV25	S3.2	ER; reduced F.I.	ER	ER	ER	ER	ER	Transport between the ER and the Golgi apparatus as a component of COPII-coated ER-derived transport vesicles (Belden and Barlowe 1996).

YGR254W	ENO1	S3.3	Cytosol; excluded from vacuole-like structures	Cytosol; excluded from vacuole-like structures	Cytosol; excluded from vacuole-like structures	Cytosol; excluded from vacuole-like structures	Cytosol; excluded from vacuole-like structures	Cytosol	Phosphopyruvate hydratase; involved in glycolysis and gluconeogenesis (Cohen *et al*. 1987).
YER177W	BMH1	S3.4	Cytosol and nucleus; excluded from vacuole-like structures	Cytosol and nucleus; excluded from vacuole-like structures	Cytosol and nucleus; excluded from vacuole-like structures	Cytosol and nucleus; excluded from vacuole-like structures	Cytosol and nucleus; excluded from vacuole-like structures	Cytosol	14-3-3 protein; diverse functions including vesicle transport and aggresome formation (van Heusden *et al.* 1992, Xu *et al.* 2013).
YIL148W	RPL40A	S3.5	Nucleus and cytosol. Predominantly cytosolic	Not examined	Not examined	Nucleus and cytosol. Predominantly localised to cell nuclei	Nucleus and cytosol. Predominantly localised to cell nuclei	Nucleus and cytosol	Fusion protein that is proteolytically cleaved to produce ubiquitin and the L40 ribosomal subunit protein (Finley *et al.* 1989).
YHR200W	RPN10	S3.6	Cytosol and nucleus; colocalisation with TDP-43^{WT}-DsRed cytosolic foci	Cytosol and nucleus; colocalisation with FUS^{WT}-DsRed cytosolic foci	Not examined	Cytosol and nucleus; small defined regions of increased F.I. throughout cytosol	Cytosol and nucleus; small defined regions of increased F.I. throughout cytosol	Cytosol	Non-ATPase base subunit of the 19S regulatory particle of the proteasome (Glickman *et al.* 1998).
YDR246W	TRS23	S3.7	Cytosol; excluded from vacuole-like structures. Small regions of increased F.I. surrounding cell nuclei and vacuole-like structures	Not examined	Not examined	Reduced cytosolic F.I.; small cytosolic EGFP-fluorescent foci	Cytosol; excluded from vacuole-like structures. Small regions of increased F.I. surrounding cell nuclei and vacuole-like structures	Punctate in cytosol; ER, Golgi apparatus and pre-autophagosomal structures	Core subunit of transport protein particle (TRAPP) complexes I-III involved in ER-Golgi transport and autophagy (Sacher *et al.* 2001).

YFL016C	MDJ1	S3.8	Not examined	Mitochondria	Not examined	Mitochondria	Mitochondria	Mitochondria	HSP40 chaperone; involved in protein folding and refolding in the mitochondrial matrix (Rowley *et al*. 1994).
YOR232W	MGE1/ GRPE	S3.9	Not examined	Mitochondria and throughout cytosol; low F.I.	Not examined	Mitochondria and throughout cytosol	Mitochondria and throughout cytosol	Cytosol and mitochondria	Mitochondrial matrix cochaperone (Deloche *et al.* 1997).
YNL016W	PUB1	S3.10	Cytosol and nucleus; excluded from vacuole-like structures. Colocalisation with cytosolic TDP-43^{WT}-DsRed foci	Cytosol and nucleus; excluded from vacuole-like structures. Colocalisation with cytosolic FUS^{WT}-DsRed foci	Not examined	Not examined	Cytosol and nucleus; excluded from vacuole-like structures	Cytosol	Poly (A)+ RBP involved in translation regulation; key component of SGs (Matunis *et al*. 1993).
YGL173C	XRN1	S3.11	Cytosolic foci	Diffuse throughout cytosol, with cytosolic foci	Not examined	Not examined	Cytosolic foci	Cytosol and cytosolic foci (P-bodies)	5’ – 3’ exonuclease involved in mRNA decay (Larimer *et al*. 1992, Sheth and Parker 2003).
YKL010C	UFD4	S3.12	Not examined	Cytosolic foci colocalised with FUS^{WT}-DsRed foci	Not examined	Cytosolic foci	Cytosolic foci	Nucleus, cytosol and mitochondria	E3 ubiquitin ligase (Koegl *et al*. 1999).

As noted above, the main objective of the work presented in this chapter was to screen for alterations in the cellular levels of the ALS-relevant selection of 128 EGFP-fusion proteins, rather than to examine whether the localisation patterns of this set of proteins were altered in the presence of TDP-43, FUS and mutant SOD1. However, the documentation of the EGFP-fusion proteins observed here to have altered localisation in response to TDP-43, FUS or mutant SOD1 demonstrates that systematic evaluation of the localisation patterns of the full set of 128 EGFP-fusion proteins across strains expressing TDP-43^{WT}-DsRed, FUS^{WT}-DsRed and SOD1^{A4V}-DsRed could provide valuable information about the cellular responses to the expression of these ALS-linked genes.

3.3.3 Quality control analyses of FLUOstar® Optima plate reader data

There are various environmental and biological factors that can impact the growth of yeast strains and result in growth variation between individual cultures of the same strain. This is particularly important to consider for experiments involving the growth of yeast in 96- and 384-well microtitre plates, in which culture volumes are very small (< 200 µL). Variation in temperature and aeration between wells across each multi-well plate can significantly affect the activity and metabolism of yeast cells, as well as cause variation in rates of evaporation of culture medium, leading to differences in culture volumes and further impacting yeast growth. It was important to test that the expression of ^{GAL}TDP-43^{WT}-DsRed, ^{GAL}FUS^{WT}-DsRed, ^{GAL}SOD1^{WT}-DsRed, ^{GAL}SOD1^{A4V}-DsRed or ^{GAL}DsRed^{empty} (DsRed alone) in diploid strains, and that the growth of the strains, was consistent between wells within each plate and between different plates in separate experiments. This was done by examining the distribution of the raw absorbance (OD_{600}) and DsRed F.I. data from each well in all plates of yeast that were assayed for measurements of EGFP-fusion protein levels.

In diploid ^{GAL}TDP-43^{WT}-DsRed strains and the corresponding ^{GAL}DsRed^{empty} control strains, the OD_{600} yield was reasonably consistent between replicates of the same strains as well as

between the majority of the strains (Figure 3.4, a and b). A clear difference in the maximum exponential rate of change of OD_{600} (maximum growth rate) between diploid ^{GAL}TDP-43^{WT}-DsRed strains and the corresponding ^{GAL}DsRed^{empty} control strains was evident, with ^{GAL}TDP-43^{WT}-DsRed strains growing at a slower rate (Figure 3.4, c and d). This is consistent with the reduced growth of haploid and diploid ^{GAL}TDP-43^{WT}-DsRed strains observed in the spotting assays (Figure 3.3, section 3.3.2). Several strains exhibited lower OD_{600} yields and/or maximum growth rates than the majority of diploid ^{GAL}TDP-43^{WT}-DsRed and ^{GAL}DsRed^{empty} strains. Accordingly, the lower numbers of cells and slower growth rates of these strains corresponded with most of them exhibiting lower DsRed F_{max} and slower rates of exponential increase of DsRed F.I. (Figure 3.4, e, f, g and h). However, the DsRed F_{max} and rates of exponential increase of DsRed F.I. were also altered in individual replicates of several strains that did not display reduced growth.

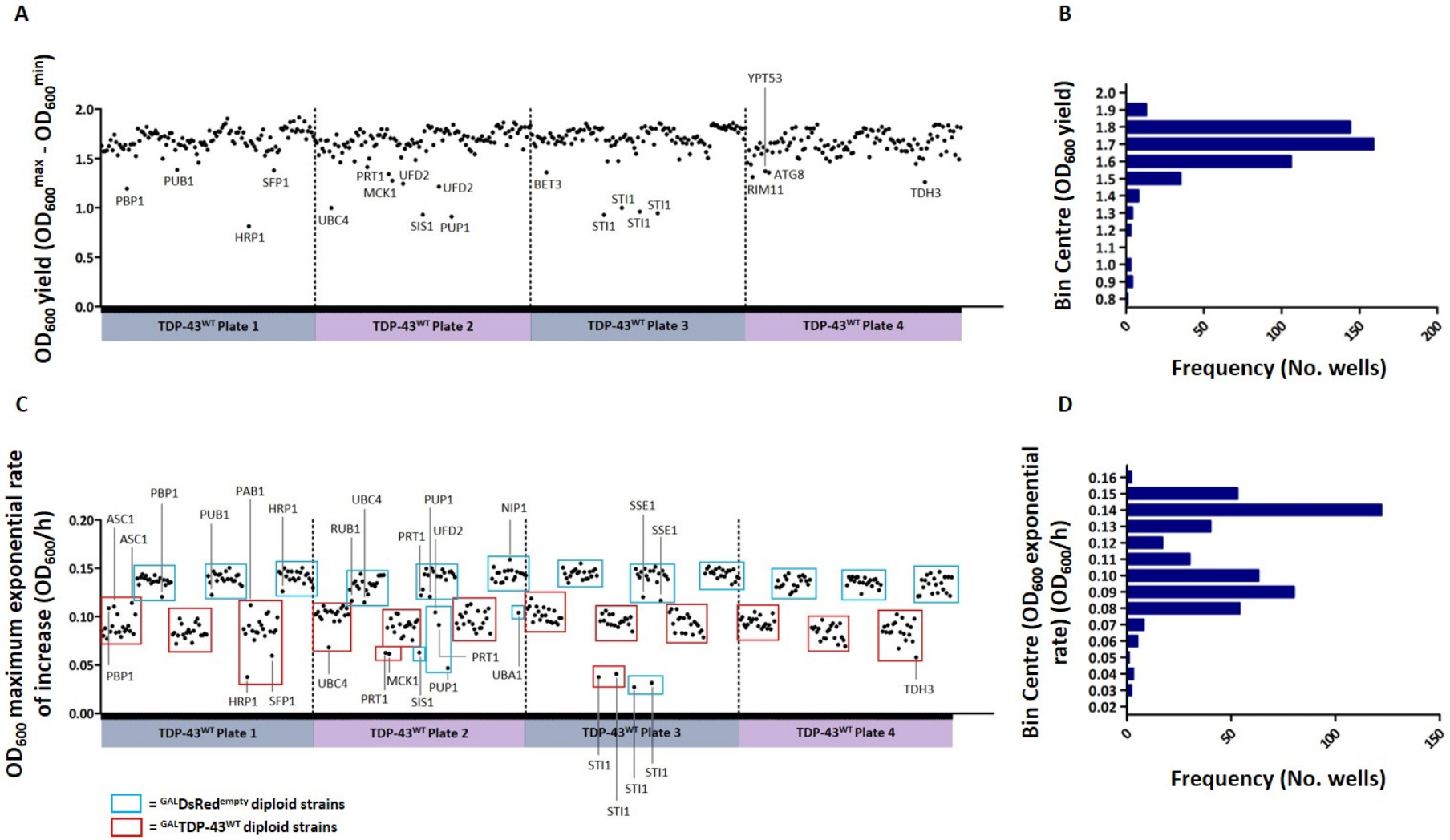
A
B
C
D
OD_{600} yield (OD_{600}^{max} - OD_{600}^{min})
Bin Centre (OD_{600} yield)
Frequency (No. wells)
OD_{600} maximum exponential rate of increase (OD_{600}/h)
Bin Centre (OD_{600} exponential rate) (OD_{600}/h)
TDP-43^{WT} Plate 1
TDP-43^{WT} Plate 2
TDP-43^{WT} Plate 3
TDP-43^{WT} Plate 4
= ^{GAL}DsRed^{empty} diploid strains
= ^{GAL}TDP-43^{WT} diploid strains

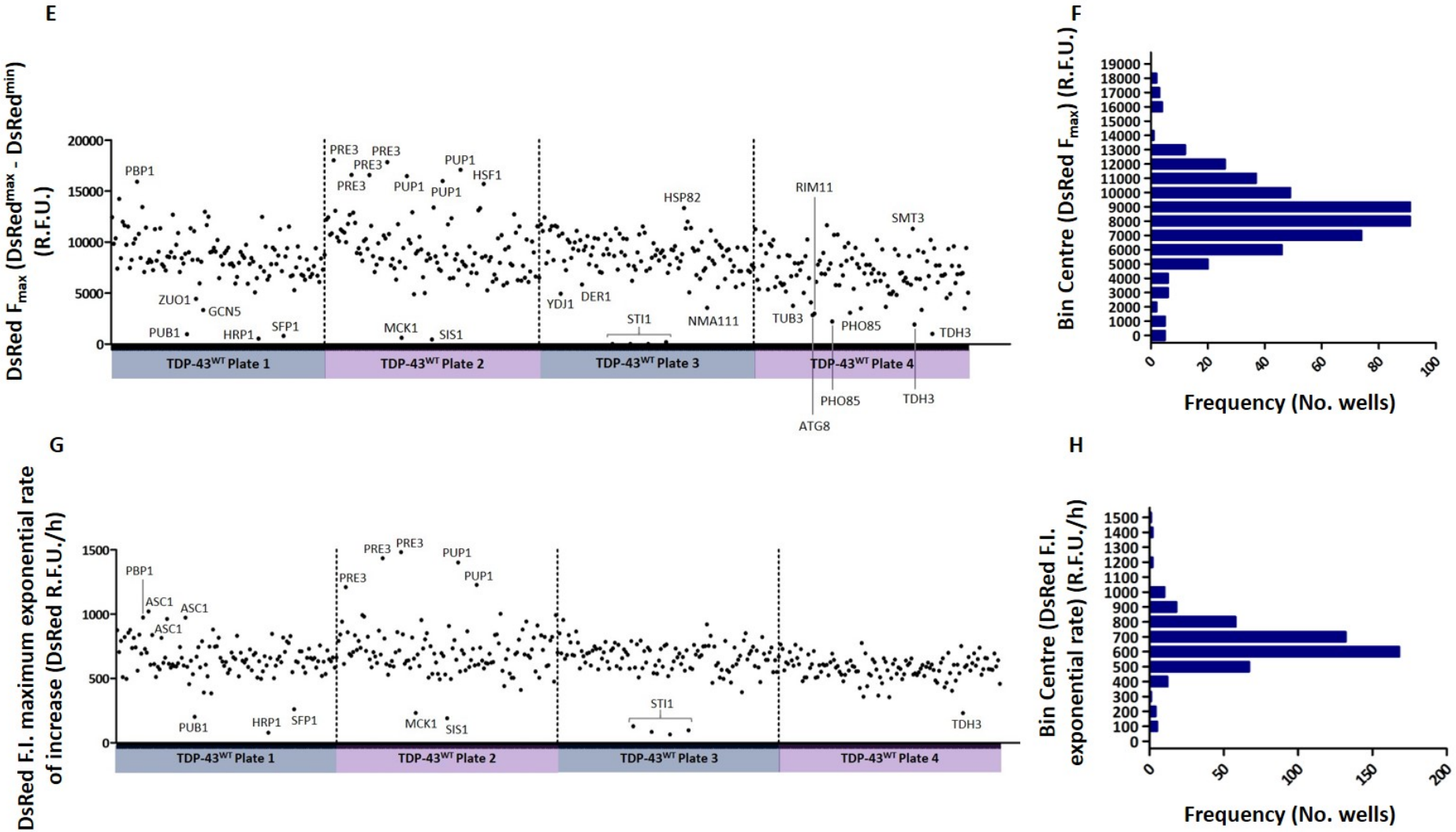
E
DsRed F_{max} (DsRed^{max} - DsRed^{min}) (R.F.U.)
PBP1
ZUO1
GCN5
PUB1
HRP1
SFP1
PRE3
PRE3
PRE3
PRE3
PUP1
PUP1
PUP1
HSF1
MCK1
SIS1
YDJ1
DER1
HSP82
STI1
NMA111
RIM11
TUB3
PHO85
SMT3
TDH3
ATG8
TDP-43^{WT} Plate 1
TDP-43^{WT} Plate 2
TDP-43^{WT} Plate 3
TDP-43^{WT} Plate 4
F
Bin Centre (DsRed F_{max}) (R.F.U.)
Frequency (No. wells)
G
DsRed F.I. maximum exponential rate of increase (DsRed R.F.U./h)
PBP1
ASC1
ASC1
ASC1
PUB1
HRP1
SFP1
PRE3
PRE3
PRE3
PUP1
PUP1
MCK1
SIS1
STI1
TDH3
TDP-43^{WT} Plate 1
TDP-43^{WT} Plate 2
TDP-43^{WT} Plate 3
TDP-43^{WT} Plate 4
H
Bin Centre (DsRed F.I. exponential rate) (R.F.U./h)
Frequency (No. wells)

Figure 3.4. Distribution of raw OD_{600} and DsRed fluorescence intensity data from FLUOstar® Optima plate reader assays of diploid yeast EGFP-fusion strains expressing DsRed-fusion human TDP-43^{WT} or DsRed alone. Diploid strains were created by mating haploid Y7039 transformed with pAG416GAL-TDP-43^{WT}-DsRed (^{GAL}TDP-43^{WT}) or pAG416GAL-ccdB-DsRed (^{GAL}DsRed^{empty}; vector control) with haploid strains from the yeast EGFP fusion collection (Huh *et al.* 2003). Duplicates of each diploid strain were grown in 384-well μclear plates containing 100 μL per well of SGal/-His/Ura to induce expression of ^{GAL}TDP-43^{WT} or ^{GAL}DsRed^{empty} in a FLUOstar® Optima plate reader. The absorbance (optical density [OD] at 600 nm), EGFP (excitation 485/12 nm, emission collected at 510/20 nm) and DsRed (excitation 580/10 nm, emission collected at 612 nm) fluorescence were measured over 48 h of yeast incubation at 30 °C. Raw data collected for each replicate were analysed to calculate the OD_{600} yield (maximum OD_{600} – minimum OD_{600}), the maximum exponential rate of change of OD_{600} (maximum growth rate; OD_{600}/h), the maximum DsRed fluorescence intensity (F_{max}) (maximum DsRed F.I. – minimum DsRed F.I.; relative fluorescence units, R.F.U.) and the maximum exponential rate of change of DsRed F.I. (maximum rate of DsRed F.I. increase; R.F.U./h). These data per replicate are presented as follows: (A) scatter plot and (B) histogram displaying the OD_{600} yield; (C) scatter plot and (D) histogram showing the maximum exponential rate of change of OD_{600} (maximum growth rate); (E) scatter plot and (F) histogram displaying the DsRed F_{max}; (G) scatter plot and (H) histogram displaying the maximum exponential rate of change of DsRed F.I. (maximum rate of DsRed F.I. increase; R.F.U./h).

In diploid ^{GAL}FUS^{WT}-DsRed strains and the corresponding ^{GAL}DsRed^{empty} control strains, the OD_{600} yield was reasonably consistent between replicates of the same strains as well as between the majority of strains (Figure 3.5, a and b). Unlike the diploid ^{GAL}TDP-43^{WT}-DsRed strains, there were no differences in the maximum exponential rate of change of OD_{600} (maximum growth rate) between diploid ^{GAL}FUS^{WT}-DsRed strains and the corresponding ^{GAL}DsRed^{empty} control strains (Figure 3.5, c and d). Several diploid strains were observed to have reduced growth compared to the majority of diploid strains. As was observed for the corresponding diploid STI1-EGFP/^{GAL}TDP-43^{WT}-DsRed strain, growth was much reduced in all replicates of STI1-EGFP/^{GAL}FUS^{WT}-DsRed and STI1-EGFP/^{GAL}DsRed^{empty}. The DsRed F_{max} and rate of exponential increase of DsRed F.I. were reduced in all replicates of STI1-EGFP/^{GAL}FUS^{WT}-DsRed and STI1-EGFP/^{GAL}DsRed^{empty}, and is in accordance with their reduced growth and lower culture density (Figure 3.5, e, f, g and h). Several other diploid strains exhibited markedly different DsRed F_{max} and/or rate of exponential increase of DsRed F.I. compared to the majority of diploid ^{GAL}FUS^{WT}-DsRed and ^{GAL}DsRed^{empty} strains. Notably, all replicates of the PRE3-EGFP/^{GAL}FUS^{WT}-DsRed and PRE3-EGFP/^{GAL}DsRed^{empty} strains exhibited greater DsRed F_{max} and rates of exponential increase of DsRed F.I., as was observed for all replicates of the corresponding PRE3-EGFP/^{GAL}TDP-43^{WT}-DsRed strain.

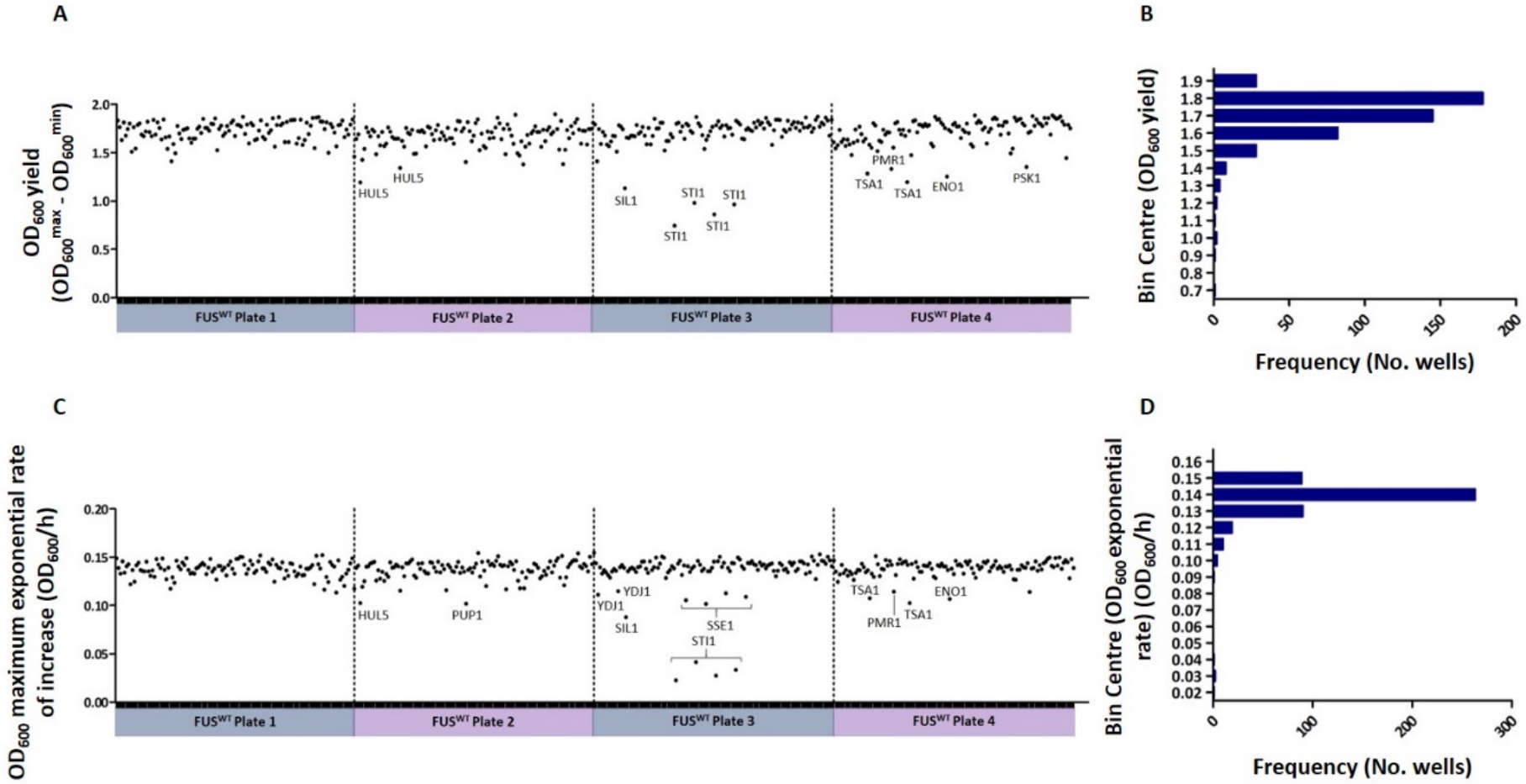
A
B
C
D
OD_{600} yield (OD_{600}^{max} - OD_{600}^{min})
Bin Centre (OD_{600} yield)
Frequency (No. wells)
OD_{600} maximum exponential rate of increase (OD_{600}/h)
Bin Centre (OD_{600} exponential rate) (OD_{600}/h)
Frequency (No. wells)
FUS^{WT} Plate 1
FUS^{WT} Plate 2
FUS^{WT} Plate 3
FUS^{WT} Plate 4
HUL5
SIL1
STI1
PMR1
TSA1
ENO1
PSK1
PUP1
YDJ1
SSE1

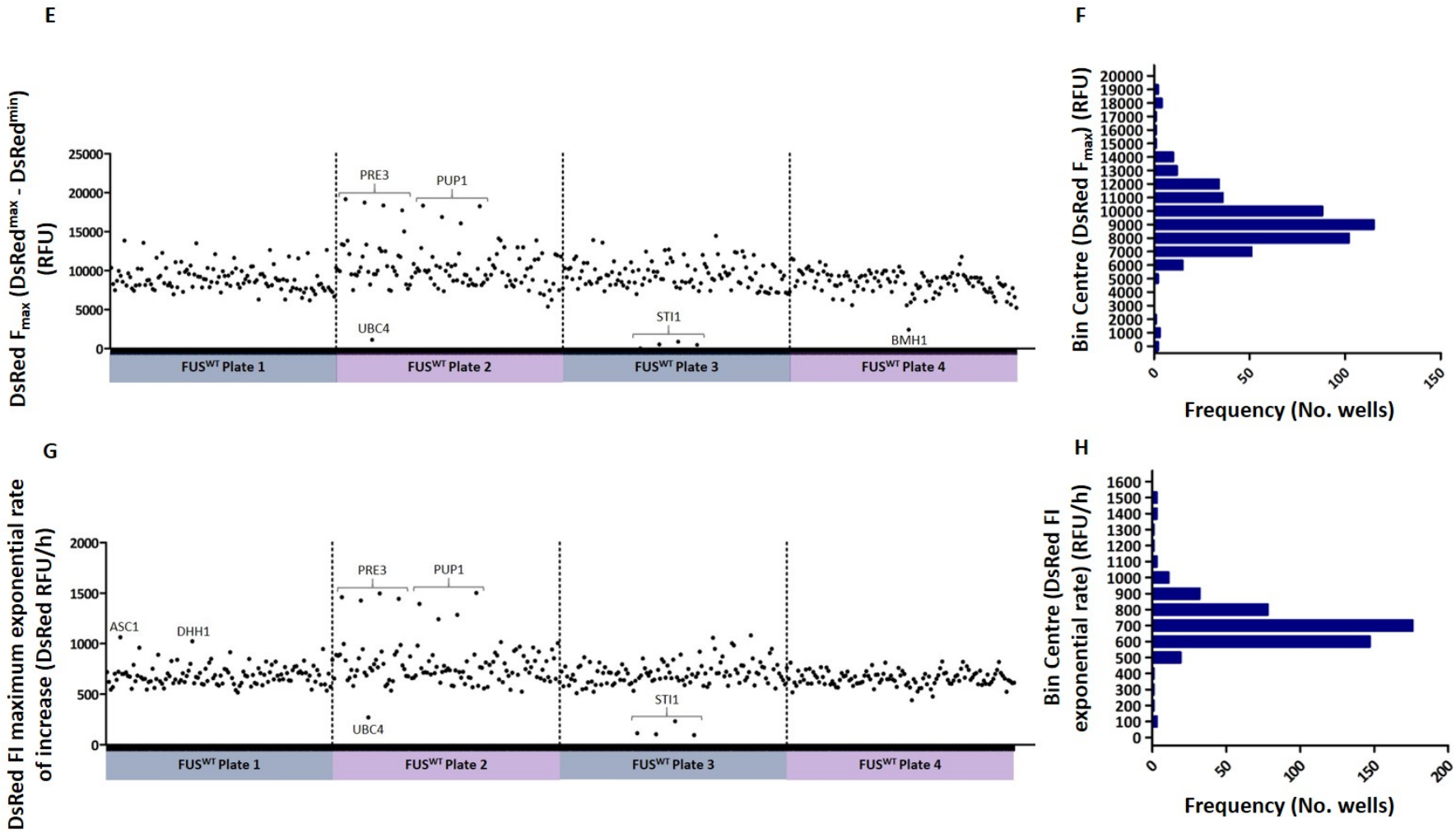
E
DsRed F_{max} ($DsRed^{max}$ - $DsRed^{min}$) (RFU)
25000
20000
15000
10000
5000
0
PRE3
PUP1
UBC4
STI1
BMH1
FUS^{WT} Plate 1
FUS^{WT} Plate 2
FUS^{WT} Plate 3
FUS^{WT} Plate 4
F
Bin Centre (DsRed F_{max}) (RFU)
20000
19000
18000
17000
16000
15000
14000
13000
12000
11000
10000
9000
8000
7000
6000
5000
4000
3000
2000
1000
0
0
50
100
150
Frequency (No. wells)
G
DsRed FI maximum exponential rate of increase (DsRed RFU/h)
2000
1500
1000
500
0
ASC1
DHH1
PRE3
PUP1
UBC4
STI1
FUS^{WT} Plate 1
FUS^{WT} Plate 2
FUS^{WT} Plate 3
FUS^{WT} Plate 4
H
Bin Centre (DsRed FI exponential rate) (RFU/h)
1600
1500
1400
1300
1200
1100
1000
900
800
700
600
500
400
300
200
100
0
0
50
100
150
200
Frequency (No. wells)

Figure 3.5. Distribution of raw OD_{600} and DsRed fluorescence intensity data from FLUOstar® Optima plate reader assays of diploid yeast EGFP-fusion strains expressing DsRed-fusion human FUS^{WT} or DsRed alone. Diploid strains were created by mating haploid Y7039 transformed with pAG416GAL-FUS^{WT}-DsRed ($^{GAL}FUS^{WT}$) or pAG416GAL-ccdB-DsRed ($^{GAL}DsRed^{empty}$; vector control) with haploid strains from the yeast EGFP fusion collection (Huh *et al.* 2003). Duplicates of each diploid strain were grown in 384-well μclear plates containing 100 μL per well of SGal/-His/Ura to induce expression of $^{GAL}FUS^{WT}$ or $^{GAL}DsRed^{empty}$ in a FLUOstar® Optima plate reader. The absorbance (optical density [OD] at 600 nm), EGFP (excitation 485/12 nm, emission collected at 510/20 nm) and DsRed (excitation 580/10 nm, emission collected at 612 nm) fluorescence were measured over 48 h of yeast incubation at 30 °C. Raw data collected for each replicate were analysed to calculate the OD_{600} yield (maximum OD_{600} – minimum OD_{600}), the maximum exponential rate of change of OD_{600} (maximum growth rate; OD_{600}/h), the maximum DsRed fluorescence intensity (F_{max}) (maximum DsRed F.I. – minimum DsRed F.I.; relative fluorescence units, R.F.U.) and the maximum exponential rate of change of DsRed F.I. (maximum rate of DsRed F.I. increase; R.F.U./h). These data per replicate are presented as follows: (A) scatter plot and (B) histogram displaying the OD_{600} yield; (C) scatter plot and (D) histogram showing the maximum exponential rate of change of OD_{600} (maximum growth rate); (E) scatter plot and (F) histogram displaying the DsRed F_{max}; (G) scatter plot and (H) histogram displaying the maximum exponential rate of change of DsRed F.I. (maximum rate of DsRed F.I. increase; R.F.U./h).

The OD_{600} yield and maximum exponential rate of change of OD_{600} were similar amongst replicates of diploid $^{GAL}SOD1^{WT}$-DsRed, $^{GAL}SOD1^{A4V}$-DsRed and the corresponding $^{GAL}DsRed^{empty}$ control strains (Figure 3.6, a, b, c and d). However, several diploid strains were observed to have variation in their growth relative to most of the diploid strains (Figure 3.6, a, b, c and d). Across the plate reader assays of diploid EGFP-fusion/$^{GAL}TDP\text{-}43^{WT}$-DsRed, /$^{GAL}FUS^{WT}$-DsRed, /$^{GAL}SOD1^{WT}$-DsRed, /$^{GAL}SOD1^{A4V}$-DsRed or /$^{GAL}DsRed^{empty}$, several EGFP-fusion strains were repeatedly observed to have variable growth amongst replicates; HRP1-EGFP, UBC4-EGFP, BET3-EGFP, STI1-EGFP, YDJ1-EGFP, PUP1-EGFP, HSP82-EGFP, ASC1-EGFP, SIL1-EGFP, HUL5-EGFP and TSA1-EGFP. Diploid $^{GAL}SOD1^{WT}$-DsRed and $^{GAL}SOD1^{A4V}$-DsRed strains exhibiting variable growth also, accordingly, exhibited variable DsRed F_{max} and differing rates of exponential increase of DsRed F.I. to the majority of diploid strains (Figure 3.6, e, f, g, h). However, the DsRed F_{max} and rate of exponential increase of DsRed F.I. measured in some strains did not correlate with the yield of their growth or with their growth rate, showing either increased or decreased DsRed F_{max} or rates of increase relative to the cell density of the culture.

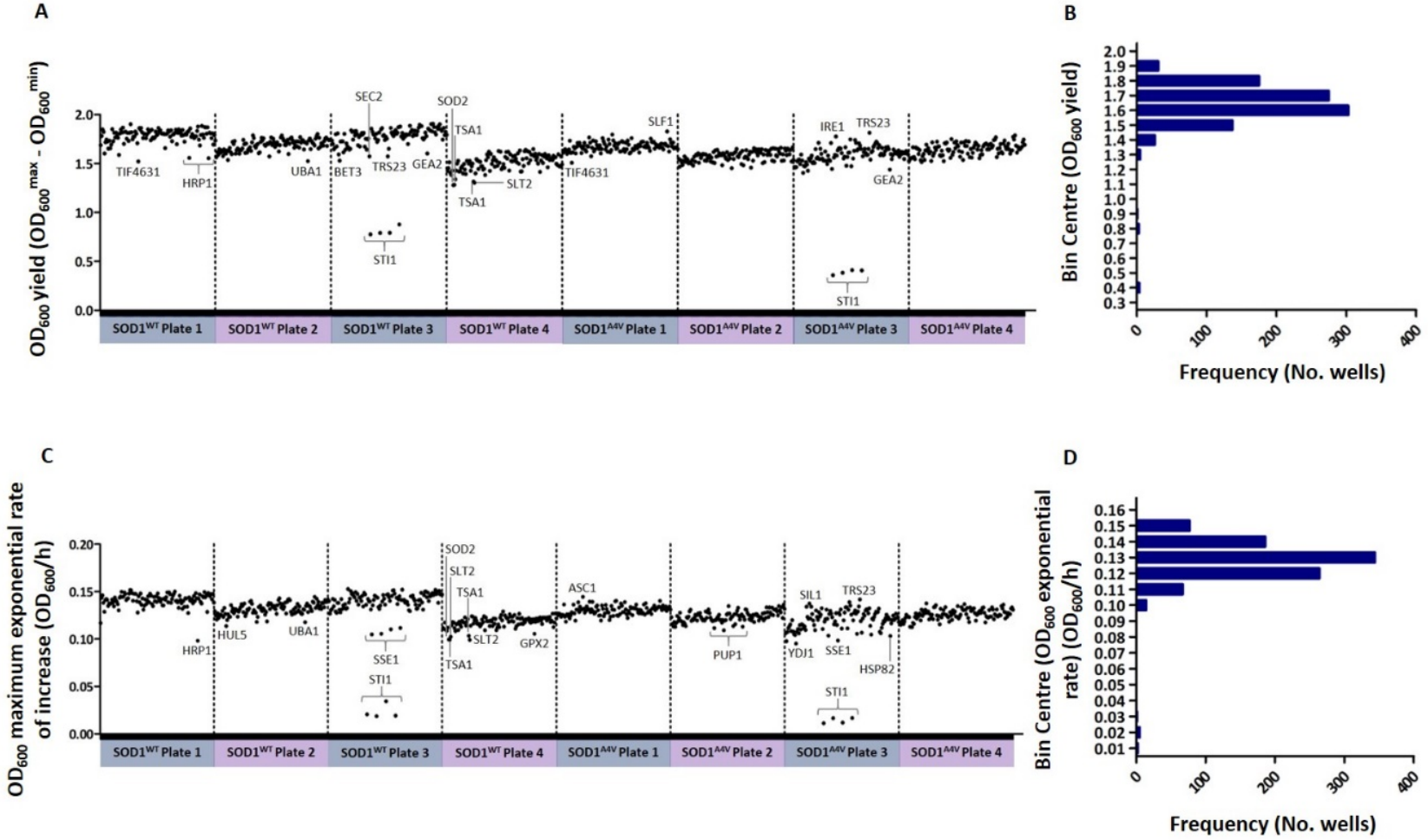
A
B
C
D
OD_{600} yield (OD_{600}^{max} - OD_{600}^{min})
Bin Centre (OD_{600} yield)
Frequency (No. wells)
OD_{600} maximum exponential rate of increase (OD_{600}/h)
Bin Centre (OD_{600} exponential rate) (OD_{600}/h)
Frequency (No. wells)
SOD1WT Plate 1
SOD1WT Plate 2
SOD1WT Plate 3
SOD1WT Plate 4
SOD1A4V Plate 1
SOD1A4V Plate 2
SOD1A4V Plate 3
SOD1A4V Plate 4
TIF4631
HRP1
UBA1
BET3
SEC2
TRS23
GEA2
SOD2
TSA1
SLT2
STI1
SLF1
IRE1
HUL5
SSE1
ASC1
SIL1
YDJ1
PUP1
GPX2
HSP82

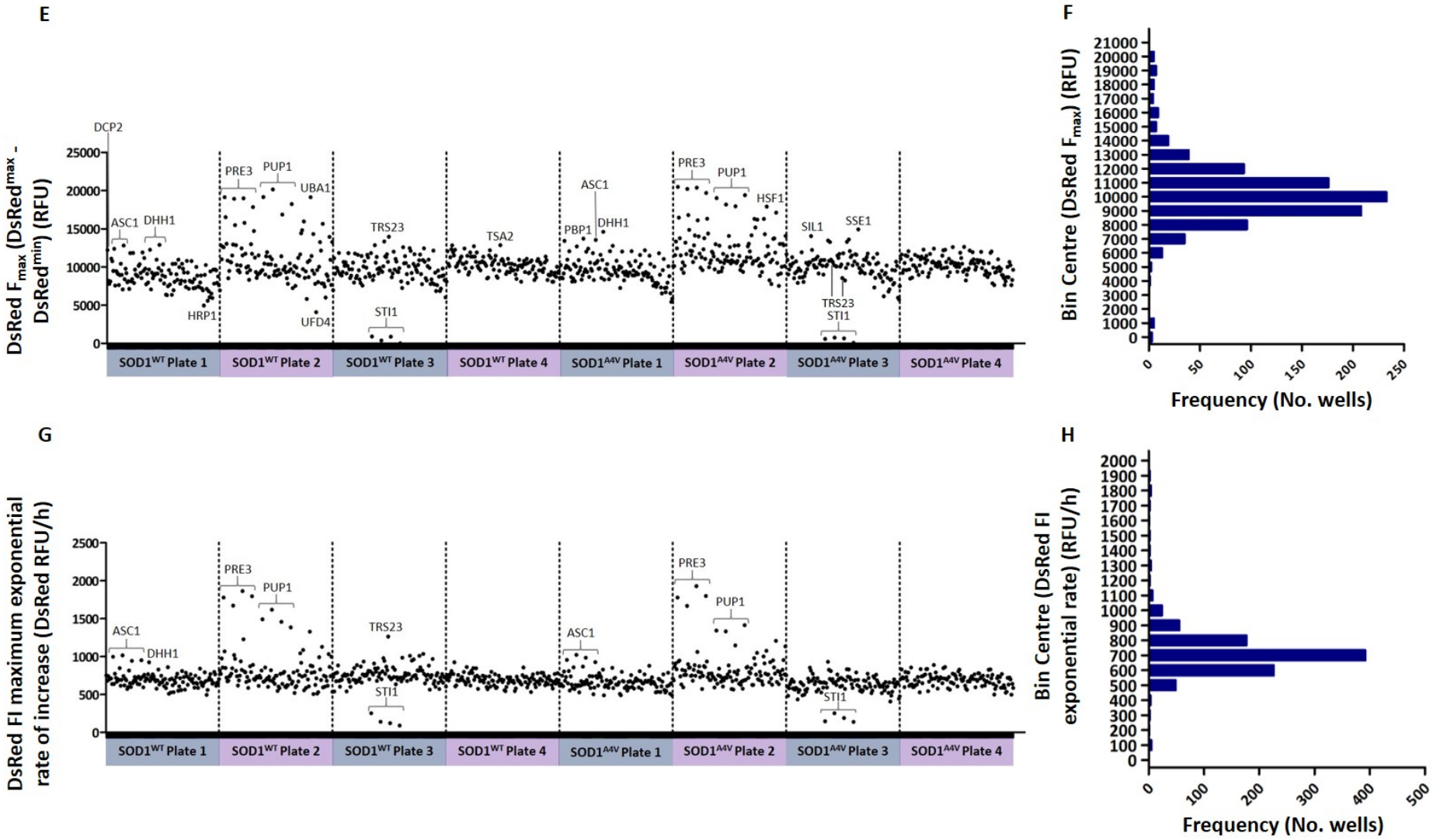
E
DsRed F_{max} (DsRed^{max} - DsRed^{min}) (RFU)
DCP2
ASC1
DHH1
HRP1
PRE3
PUP1
UBA1
UFD4
TRS23
STI1
TSA2
ASC1
PBP1
DHH1
PRE3
PUP1
HSF1
SIL1
SSE1
TRS23
STI1
SOD1WT Plate 1
SOD1WT Plate 2
SOD1WT Plate 3
SOD1WT Plate 4
SOD1A4V Plate 1
SOD1A4V Plate 2
SOD1A4V Plate 3
SOD1A4V Plate 4
F
Bin Centre (DsRed F_{max}) (RFU)
Frequency (No. wells)
G
DsRed FI maximum exponential rate of increase (DsRed RFU/h)
ASC1
DHH1
PRE3
PUP1
TRS23
STI1
ASC1
PRE3
PUP1
STI1
SOD1WT Plate 1
SOD1WT Plate 2
SOD1WT Plate 3
SOD1WT Plate 4
SOD1A4V Plate 1
SOD1A4V Plate 2
SOD1A4V Plate 3
SOD1A4V Plate 4
H
Bin Centre (DsRed FI exponential rate) (RFU/h)
Frequency (No. wells)

Figure 3.6. Distribution of raw OD_{600} and DsRed fluorescence intensity data from FLUOstar® Optima plate reader assays of diploid yeast EGFP-fusion strains expressing DsRed-fusion human $SOD1^{WT}$, $SOD1^{A4V}$ or DsRed alone. Diploid strains were created by mating haploid Y7039 transformed with pAG416GAL-$SOD1^{WT}$-DsRed ($^{GAL}SOD1^{WT}$), pAG416GAL-$SOD1^{A4V}$-DsRed ($^{GAL}SOD1^{A4V}$), or pAG416GAL-ccdB-DsRed ($^{GAL}DsRed^{empty}$; vector control) with haploid strains from the yeast EGFP fusion collection (Huh *et al.* 2003). Duplicates of each diploid strain were grown in 384-well µclear plates containing 100 µL per well of SGal/-His/Ura to induce expression of $^{GAL}SOD1^{WT}$, $^{GAL}SOD1^{A4V}$ or $^{GAL}DsRed^{empty}$ in a FLUOstar® Optima plate reader. The absorbance (optical density [OD] at 600 nm), EGFP (excitation 485/12 nm, emission collected at 510/20 nm) and DsRed (excitation 580/10 nm, emission collected at 612 nm) fluorescence were measured over 48 h of yeast incubation at 30 °C. Raw data collected for each replicate were analysed to calculate the OD_{600} yield (maximum OD_{600} – minimum OD_{600}), the maximum exponential rate of change of OD_{600} (maximum growth rate; OD_{600}/h), the maximum DsRed fluorescence intensity (F_{max}) (maximum DsRed F.I. – minimum DsRed F.I.; relative fluorescence units, R.F.U.) and the maximum exponential rate of change of DsRed F.I. (maximum rate of DsRed F.I. increase; R.F.U./h). These data per replicate are presented as follows: (A) scatter plot and (B) histogram displaying the OD_{600} yield; (C) scatter plot and (D) histogram showing the maximum exponential rate of change of OD_{600} (maximum growth rate); (E) scatter plot and (F) histogram displaying the DsRed F_{max}; (G) scatter plot and (H) histogram displaying the maximum exponential rate of change of DsRed F.I. (maximum rate of DsRed F.I. increase; R.F.U./h).

There are various factors that could have affected the expression of the galactose-inducible DsRed-fusion genes carried in the centromeric plasmids. For instance, the CEN/ARS elements in the plasmids may have interacted with DNA replication factors that were perhaps differentially active in the specific EGFP-fusion strains listed above. However, the combination of CEN and ARS sequences in yeast expression vectors are designed to provide greater stability of plasmid copy numbers in yeast cells (Duina *et al.* 2014). The varied levels of the DsRed-fusion proteins may also have been influenced by variation in the volume of growth media in the wells, differential rates of evaporation of the media, or slight variations in temperature across the 384-well plate. Each EGFP-fusion strain crossed with each different DsRed-fusion gene plasmid had the same position in each plate between replicates. Thus, there may have existed particular positions in the plates that resulted in a given well(s) being subject to conditions that varied from other wells in the plate. This may account for the repeated variability observed for some diploid strains.

Following analyses of EGFP-fusion protein levels and identification of EGFP-fusion proteins showing altered levels in diploid $^{GAL}TDP\text{-}43^{WT}$-DsRed, $^{GAL}FUS^{WT}$-DsRed, $^{GAL}SOD1^{WT}$-DsRed or $^{GAL}SOD1^{A4V}$-DsRed strains relative to control diploid $^{GAL}DsRed^{empty}$ strains (described in the following section 3.3.4), the corresponding diploid strains were analysed in

repeated assays to confirm the observed alterations in EGFP-fusion protein levels. In these repeated assays, the array of strains in each plate was changed to exclude strains that had not exhibited alterations in EGFP-fusion protein levels, and strains, including the diploid STI1-EGFP strains, that had consistently shown highly variable viability and growth. Each strain was arrayed in quadruplicate wells of 384-well plates and a total of 8 plates were arrayed and monitored using the FLUOstar® Optima. Examining the distribution of OD_{600} yield and the maximum exponential rate of change of OD_{600} (maximum growth rate) across the 8 plates, plate-to-plate variation in yeast growth was evident, including for the control $^{GAL}DsRed^{empty}$ strains (Figure S3.13, a, b, c and d, Appendix I). As was observed in the first round of assays of diploid $^{GAL}TDP\text{-}43^{WT}$ strains, there were clear differences in maximum growth rates between $^{GAL}TDP\text{-}43^{WT}$ strains and their corresponding $^{GAL}DsRed^{empty}$ strains, again highlighting the reduction in cell viability caused by expression of human TDP-43^{WT} observed in spotting assays (section 3.3.2.). In contrast, $^{GAL}FUS^{WT}$-DsRed, $^{GAL}SOD1^{WT}$-DsRed and $^{GAL}SOD1^{A4V}$-DsRed strains showed less deviation in growth relative to their corresponding $^{GAL}DsRed^{empty}$ strains. The DsRed F_{max} and the maximum exponential rate of change of DsRed F.I. (maximum rate of DsRed F.I. increase) measured in diploid $^{GAL}TDP\text{-}43^{WT}$ strains was greater than in the corresponding $^{GAL}DsRed^{empty}$ strains, despite the relatively greater growth of the $^{GAL}DsRed^{empty}$ strains (Figure S3.13, e, f, g and h, Appendix I). The DsRed F_{max} and the maximum rate of DsRed F.I. increase was also greater in diploid $^{GAL}SOD1^{A4V}$-DsRed strains relative to the corresponding $^{GAL}DsRed^{empty}$ strains. The expression of the $^{GAL}DsRed^{empty}$ plasmid (DsRed alone) resulted in a much lower DsRed F.I. than was seen in $^{GAL}TDP\text{-}43^{WT}$-DsRed, $^{GAL}FUS^{WT}$-DsRed, $^{GAL}SOD1^{WT}$-DsRed and $^{GAL}SOD1^{A4V}$-DsRed strains when viewed using a fluorescence microscope (section 3.3.2). Thus, the lower DsRed F.I. signal measured using the fluorescent plate reader is in accordance with the observations made by fluorescence microscopy.

In the following section 3.3.4, the analyses of EGFP-fusion protein levels amongst the diploid strains, it should be noted that any variation in growth between replicates of strains were accounted for by normalising the EGFP F.I. of the EGFP-fusion proteins to the OD_{600} at each measured time-point. Significant variations in normalised EGFP F.I. between replicates were accounted for in statistical analyses, ensuring that strains exhibiting variation between replicates would not be calculated to reach significance below the *p* value cut-off of 0.05.

3.3.4 Identification of yeast proteins with altered levels associated with the expression of human TDP-43^{WT}, FUS^{WT} and mutant SOD1^{A4V}

3.3.4.1 Expression of human TDP-43^{WT}-DsRed is associated with alterations in the levels of 24 yeast EGFP-fusion proteins

Out of the 128 diploid EGFP-fusion protein/^{GAL}TDP-43^{WT}-DsRed strains screened, differential levels of the EGFP-fusion proteins were observed in 24 strains (Figure 3.7 and Table 3.3). Of these, 20 proteins had decreased levels compared to control diploid ^{GAL}DsRed^{empty} strains while 4 proteins had increased levels.

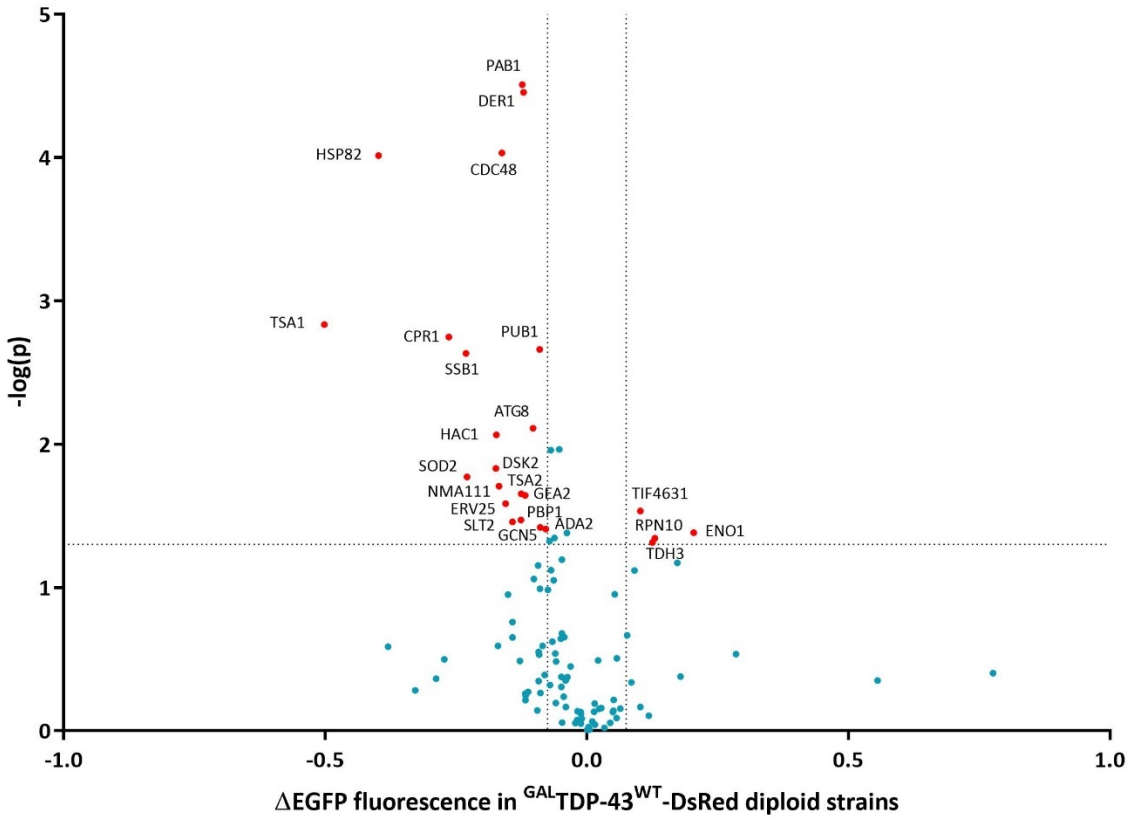

Figure 3.7. Expression of human TDP-43^{WT}-DsRed in yeast causes alterations in the levels of 24 yeast EGFP-fusion proteins. The absorbance and EGFP fluorescence of diploid EGFP-fusion protein/^{GAL}TDP-43^{WT}-DsRed strains grown in SGal/-His/Ura were measured over 48 h using a FLUOstar® Optima plate reader set to incubate plates at 30 °C. Alterations in EGFP-fusion protein levels in diploid EGFP-fusion protein/^{GAL}TDP-43^{WT}-DsRed strains were identified based on a fold change of > ±0.075 (arbitrary cut-off) and $p < 0.05$ from t tests comparing the mean normalised EGFP fluorescence intensity yield (yield from 0 to 48 h) relative to control diploid EGFP-fusion protein/^{GAL}DsRed^{empty} strains. These cut-offs are highlighted by dashed lines. Note that the *y* axis displays the -$\log_{10}$ of the *p* values. Data points represent the ΔEGFP fluorescence and -$\log_{10}$ of the *p* value from t tests comparing the differences in the means calculated from the average of quadruplicate samples. EGFP-fusion proteins exhibiting altered levels are displayed in red.

Table 3.3. Yeast EGFP-fusion proteins with altered levels in diploid strains expressing human TDP-43^{WT}-DsRed.

Major cellular function/s	Yeast orthologue	Human orthologue	Description of yeast orthologue (*Saccharomyces* Genome Database; SGD, UniProt)	ΔF	*p* value	Connection to ALS/Proteostasis function(s)/Interaction with relevant proteins (BioGRID)	Reference for gene/protein with direct connection to ALS
Increased							
Glycolysis and gluconeogenesis	ENO1	ENO1, ENO2, ENO3	Enolase I, a phosphopyruvate hydratase; catalyses conversion of 2-phosphoglycerate to phosphoenolpyruvate during glycolysis and the reverse reaction during gluconeogenesis.	0.204	0.0416	ENO2 has been detected in ubiquitin-immunoreactive inclusions in *SOD1*-linked fALS. Involved in glycolysis.	Kato *et al.* 1997
	TDH3	GAPDHS	Glyceraldehyde-3-phosphate dehydrogenase (GAPDH), isozyme 3; involved in glycolysis and gluconeogenesis; tetramer that catalyses the reaction of glyceraldehyde-3-phosphate to 1,3 bis-phosphoglycerate; detected in the cytoplasm and cell wall.	0.126	0.0486	Transcription, RNA transport, DNA replication, apoptosis. Modulates cytoskeleton organisation.	
Ubiquitin homeostasis, ubiquitin-proteasome system (UPS)	RPN10	PSMD4	Non-ATPase base subunit of the 19S regulatory particle of the 26S proteasome; N-terminus plays a role in maintaining the structural integrity of the regulatory particle; binds selectively to polyubiquitin chains.	0.13	0.0454	Proteasomal protein degradation; components of the 19S regulatory particle have been detected in nuclear inclusions in sALS.	Seilhean *et al.* 2004
Ribosomes and protein translation	TIF4631	EIF4G1	Translation initiation factor eIF4G; subunit of the mRNA cap-binding protein complex (eIF4F) that also contains eIF4E (CDC33); interacts with PAB1 and with eIF4A (TIF1); also has a role in biogenesis of the large ribosomal subunit. Interacts with CDC48.	0.102	0.0293	Present in ubiquitin-immunoreactive inclusions in *FUS*-linked fALS.	Dormann *et al.* 2010

Decreased							
mRNA splicing, transcription, RNA metabolism and stress granules.	ADA2	TADA2A/B	Transcription coactivator, component of the ADA and SAGA transcriptional adaptor/HAT (histone acetyltransferase) complexes.	-0.079	0.0392	Involved in chromatin remodelling, transcription and the UPR.	
	GCN5	BAZ1A/B, BAZ2A/B, KAT2A/B, CECR2, BPTF	Catalytic subunit of ADA and SAGA histone acetyltransferase complexes; modifies N-terminal lysines on histones H2B and H3; acetylates RSC4, a subunit of the RSC chromatin-remodelling complex, altering replication stress tolerance; relocalises to the cytosol in response to hypoxia.	-0.089	0.0382	Involved in chromatin remodelling, transcription and the UPR.	
	PBP1	ATXN2	Component of glucose deprivation induced stress granules; involved in P-body-dependent granule assembly; similar to human ataxin-2; interacts with PAB1 to regulate mRNA polyadenylation.	-0.126	0.0339	PBP1 enhances TDP-43 toxicity; ATXN2 is present in ubiquitin-immunoreactive inclusions in sALS and *FUS*-linked fALS.	Elden *et al.* 2010; Farg *et al.* 2013; Kim *et al.* 2014
	PAB1	RBMS2, RBMS3, PABPC1	Poly(A) binding protein; part of the 3'-end RNA-processing complex, mediates interactions between the 5' cap structure and the 3' mRNA poly(A) tail, involved in control of poly(A) tail length, interacts with translation factor eIF-4G.	-0.124	3.10E-05	PAB1 suppresses FUS toxicity; PABPC1 is present in basophilic ubiquitin-immunoreactive inclusions in sALS and *FUS*-linked fALS; PABP is required for TDP-43 toxicity in *Saccharomyces cerevisiae*; PABP mediates interaction between TDP-43 and ATXN2 in *Drosophila melanogaster.*	Sun *et al.* 2011; Kim *et al.* 2014

	PUB1	TIA-1	Poly (A)+ RNA-binding protein; abundant mRNP-component protein that binds mRNA and is required for stability of many mRNAs; component of glucose deprivation induced stress granules, involved in P-body-dependent granule assembly; implicated in regulation of translation; carries Q/N-rich domain at C- terminus, identified as candidate prion; human homologue TIA-1 is critical for normal synaptic plasticity.	-0.09	0.0022	Stress granule marker; colocalises with TDP-43 in stress granules.	Kim *et al.* 2014
Ribosomes and protein translation	SSB1	HSPA13	Cytoplasmic ATPase that is a ribosome-associated molecular chaperone; functions with J-protein partner ZUO1; may be involved in folding of newly-made polypeptide chains; member of the HSP70 family.	-0.231	0.0023	HSP70 molecular chaperone family.	Wolff, Weissman & Dillin, 2014 (review)
Ubiquitin homeostasis, ubiquitin-proteasome system (UPS)	DSK2	UBQLN2	Nuclear-enriched ubiquitin-like polyubiquitin-binding protein, required for spindle pole body (SPB) duplication and for transit through the G2/M phase of the cell cycle, involved in proteolysis, interacts with the proteasome.	-0.174	0.0148	Present in ubiquitin-immunoreactive inclusions in sALS and *SOD1-, TARDBP-, FUS-, OPTN-, UBQLN2-* and *C9ORF72*-linked fALS. Mutations in *UBQLN2* cause some forms of fALS.	Deng *et al.* 2011; Mori *et al.* 2013; May *et al.* 2014
Molecular chaperones, protein folding	CPR1	PPIE, PPIF	Cytoplasmic peptidyl-prolyl cis-trans isomerase (cyclophilin); catalyses the cis-trans isomerisation of peptide bonds N-terminal to proline residues.	-0.264	0.0018	Member of the peptidyl-prolyl cis-trans isomerase (PPIase; cyclophilin) family. PPIases have been detected in ubiquitin-immunoreactive inclusions in *SOD1*-linked fALS.	Basso *et al.* 2009
	HSP82	HSP90AA1, HSP90AB1	HSP90 chaperone; required for pheromone signalling, negative regulation of HSF1; docks with TOM70 for mitochondrial preprotein delivery; promotes telomerase DNA binding, nucleotide addition; contains two acid-rich unstructured regions that promote solubility of chaperone-substrate complexes.	-0.398	9.68E-05	Present in ubiquitin-immunoreactive inclusions in *SOD1*-linked fALS.	Basso *et al.* 2009

ER stress, UPR, ERAD	DER1	DERL1	ER membrane protein that promotes export of misfolded polypeptides; required for ERAD of misfolded or unassembled proteins; initiates export of aberrant polypeptides from ER lumen by threading them into ER membrane and routing them to HRD1 for ubiquitylation.	-0.121	3.51E-05	Involved in ERAD.	
	CDC48	VCP	AAA ATPase; subunit of polyubiquitin-selective segregase complex involved in ERAD, cell wall integrity during heat stress, mitotic spindle disassembly; subunit of complex involved in mitochondria-associated degradation; role in mobilising membrane bound transcription factors by regulated ubiquitin/proteasome-dependent processing, in macroautophagy, PMN, RAD, ribophagy, homotypic ER membrane fusion, disassembly of MET30 from SCF complex, functional orthologue of human p97/VCP.	-0.162	9.28E-05	*VCP* mutations cause some forms of ALS. VCP is present in ubiquitin-immunoreactive inclusions in *SOD1*-linked fALS.	Johnson *et al.* 2010; Abramzon *et al.* 2012; Weisberg *et al.* 2012
	HAC1	XBP1	Basic leucine zipper (bZIP) transcription factor (ATF/CREB1 homolog); regulates the UPR. ER stress-induced splicing pathway facilitates efficient HAC1 synthesis; translation initiation is repressed under non-stress conditions; protein abundance increases in response to DNA replication stress.	-0.173	0.0086	Involved in the UPR.	

	Nma111	HTRA2 (HtrA2/Omi)	Serine protease and general molecular chaperone; cleaves ROQ1, which modifies the substrate specificity of the UBR1 ubiquitin ligase, promoting the stress-induced homeostatically-regulated protein degradation (SHRED) of misfolded and native ER-membrane and cytosolic proteins; chaperone activity involved in the heat stress response; promotes apoptosis through proteolysis of BIR1; role in lipid homeostasis; mammalian Omi/HtrA2 serine protease family member.	-0.168	0.0197	Present in ubiquitin-immunoreactive inclusions in sALS and *SOD1*-linked fALS.	Kawamoto *et al.* 2010
Endomembrane system, ER-Golgi transport	ERV25	TMED10	Member of the p24 family involved in ER to Golgi transport; role in misfolded protein quality control.	-0.155	0.026	ER to Golgi transport; role in misfolded protein quality control.	
	GEA2	GBF1	Guanine nucleotide exchange factor for ADP ribosylation factors (ARFs); involved in vesicular transport between the Golgi and ER, Golgi organisation, and actin cytoskeleton organisation.	-0.118	0.0228	Vesicular transport between the Golgi and ER; Golgi organisation.	
Autophagy	ATG8	MAP1LC3 and GABARAP subfamilies	Component of autophagosomes and Cvt vesicles; regulator of ATG1, targets it to autophagosomes; binds the ATG1-ATG13 complex, triggering its vacuolar degradation; unique ubiquitin-like protein whose conjugation target is lipid phosphatidylethanolamine (PE); ATG8-PE is anchored to membranes, is involved in phagophore expansion, and may mediate membrane fusion during autophagosome formation; deconjugation of ATG8-PE is required for efficient autophagosome biogenesis.	-0.103	0.0078	Involved in autophagy.	

Protein phosphorylation, trafficking and signal transduction	SLT2	MAPK15	Serine/threonine MAP kinase; coordinates expression of all 19S regulatory particle assembly-chaperones (RACs) to control proteasome abundance; involved in regulating maintenance of cell wall integrity, cell cycle progression, nuclear mRNA retention in heat shock, septum assembly; required for mitophagy, pexophagy; affects recruitment of mitochondria to phagophore assembly site; regulated by the PKC1-mediated signalling pathway.	-0.142	0.0349	Regulates proteasome abundance. MAP kinases have been detected in ubiquitin-immunoreactive inclusions in *SOD1*-linked fALS and sALS.	Bendotti *et al.* 2004; Basso *et al.* 2009
Mitochondrial homeostasis and antioxidant activity	SOD2	SOD2	Mitochondrial manganese superoxide dismutase; protects cells against oxygen toxicity and oxidative stress; human mitochondrial SOD2 can complement a yeast null mutant and human cytoplasmic SOD1 can also complement when targeted to the mitochondrial matrix.	-0.229	0.0169	Mitochondrial manganese superoxide dismutase; involved in antioxidant activity.	
	TSA1	PRDX1, PRDX2, PRDX3, PRDX4	Thioredoxin peroxidase; acts as both ribosome-associated and free cytoplasmic antioxidant; self-associates to form high-molecular weight chaperone complex under oxidative stress; chaperone activity essential for growth in zinc deficiency; required for telomere length maintenance; binds and modulates CDC19 activity; protein abundance increases, forms cytoplasmic foci during DNA replication stress.	-0.502	0.0015	PRDX2 has been detected in ubiquitin-immunoreactive inclusions in *SOD1*-linked fALS. Involved in antioxidant activity.	Kato *et al.* 2004
	TSA2	PRDX2	Stress inducible cytoplasmic thioredoxin peroxidase; cooperates with TSA1 in the removal of reactive oxygen, nitrogen and sulphur species using thioredoxin as hydrogen donor.	-0.125	0.0223	Detected in ubiquitin-immunoreactive inclusions in *SOD1*-linked fALS. Involved in antioxidant activity.	Kato *et al.* 2004

STRING network analysis of protein-protein interactions amongst the hits identified several interactions (Figure 3.8). Noticeably, CDC48 was a hub for several interacting proteins; DER1, HSP82 and TIF4631 with its shared interactions with SSB1 and PAB1. Ten additional interacting proteins connected CDC48 indirectly with DSK2 and RPN10; PRE4, PRE5, PRE8, PRE9, RPT3, RPT4, RPT6, RPN5, RPN11 and RPN12.

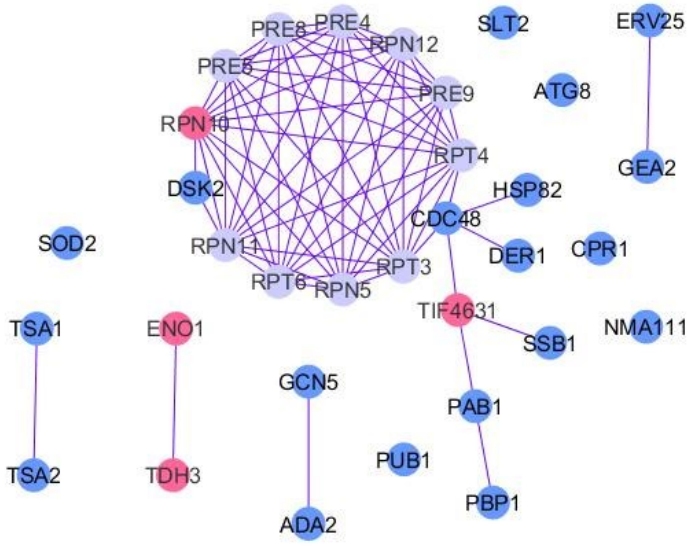

Figure 3.8. Protein-protein interaction network for EGFP-fusion protein/^{GAL}TDP-43^{WT}-DsRed screen hits. The twenty-four yeast EGFP-fusion proteins with altered levels in diploid EGFP-fusion protein/^{GAL}TDP-43^{WT}-DsRed strains were queried in the STRING protein-protein interaction database (Szklarczyk *et al.* 2015, Szklarczyk *et al.* 2017). Interactions between the hits were queried using co-expression, published experiments and databases as sources of interaction data, and only interactions scored with high confidence were included. It was selected that ten secondary interacting proteins would be included in the network analysis. The four up-regulated proteins are displayed as pink circles, while the twenty down-regulated proteins are displayed as blue circles. CDC48 is indirectly linked with DSK2 and RPN10 via a sub-network of ten secondary interactors, displayed as pale grey/purple circles.

Analysis of the 24 primary hits and the 10 secondary interactors was carried out to identify any GO term enrichment amongst the hits and interactors above the background pathway-focused selection of 128 EGFP-fusion proteins. The specific functions that have been documented for each of the 24 hits were additionally evaluated as collated in Table 3.3. GO term analysis identified that there was no enrichment in any one biological process amongst the hits out of the background set of 128 EGFP-fusion proteins. Nevertheless, the diverse functions that have

been reported for each of the 24 hits (Table 3.3) reveal specific molecular alterations caused by the expression of TDP-43^{WT}-DsRed.

TDH3 and ENO1, two of the four yeast EGFP-fusion proteins measured to have increased levels in diploid ^{GAL}TDP-43^{WT}-DsRed yeast, interact with each other and are both involved in glycolysis. Seven of the hits have functions that are involved in gene expression regulation; CPR1, ADA2, GCN5, PAB1, PBP1, PUB1 and TIF4631. With the exception of TIF4631, the levels of each of these proteins were found to be decreased in diploid ^{GAL}TDP-43^{WT}-DsRed yeast (Table 3.3). In a study identifying the composition of RNA-processing complexes in yeast, Krogan *et al.* (2004) detected an interaction between TIF4631 and CDC48. The levels of CDC48 were decreased in diploid ^{GAL}TDP-43^{WT}-DsRed yeast (p = 9.28E-05). CDC48 was indirectly linked with the hits DSK2 and RPN10 via ten additional interacting proteins. Each of these secondary interactors are subunits of the 26S proteasome. In total, 13 of the primary hits and all 10 secondary interactors have functions in misfolded protein quality control and protein degradation mechanisms in different cellular compartments (Table 3.3). CDC48 and DER1 are both required for the export of misfolded proteins from the ER for ERAD (Knop *et al.* 1996, Ye *et al.* 2001). ADA2 and GCN5 are catalytic subunits of the SAGA histone acetyltransferase complex that is involved in the transcriptional activation of ER-associated molecular chaperones in the IRE1-mediated UPR signalling pathway (Welihinda *et al.* 1997, Welihinda *et al.* 2000, Lew *et al.* 2015). HAC1 is essential in this pathway; the splicing of *HAC1* mRNA, mediated by IRE1 in response to an accumulation of unfolded or misfolded proteins in the ER lumen, is necessary for transcriptional activation of ER-associated molecular chaperones (Cox and Walter 1996, Mori *et al.* 1996, Ron and Walter 2007). SSB1, CPR1, HSP82 and NMA111 are molecular chaperones with diverse functions in protein folding and targeting substrate proteins for degradation (Borkovich *et al.* 1989, Haendler *et al.* 1989, Nelson *et al.* 1992, Hasumi and Nishikawa 1993, Nathan *et al.* 1997, Dolinski *et al.* 1998,

Lopez-Buesa *et al.* 1998, Pfund *et al.* 1998, Pfund *et al.* 2001, Gautschi *et al.* 2002, Picard 2002, Padmanabhan *et al.* 2009, Szoradi *et al.* 2018). SLT2, DSK2, RPN10, CDC48 and the 10 secondary interactors are required for functionality of the UPS (Funakoshi *et al.* 2002, Rao and Sastry 2002, Saeki *et al.* 2002, Carmody *et al.* 2010, Stolz *et al.* 2011, Rousseau and Bertolotti 2016). With the exception of RPN10, the levels of each of these proteins were found to be decreased in diploid TDP-43^{WT}-DsRed yeast. As well as their functions in proteasomal degradation, DSK2 and CDC48 are also important in the autophagy pathway, in which another hit, ATG8, has a key role (Kim and Klionsky 2000, Klionsky *et al.* 2003, Xie *et al.* 2008).

3.3.4.2 Alterations in the levels of 10 yeast EGFP-fusion proteins are associated with the expression of human FUS^{WT}-DsRed

In diploid EGFP-fusion protein/^{GAL}FUS^{WT}-DsRed strains, 10 yeast EGFP-fusion proteins had altered levels relative to their levels in control diploid EGFP-fusion protein/^{GAL}DsRed^{empty} strains (Figure 3.9 and Table 3.4). Of these, the levels of 9 proteins were increased, whilst 1 protein (MGE1) had decreased levels of expression.

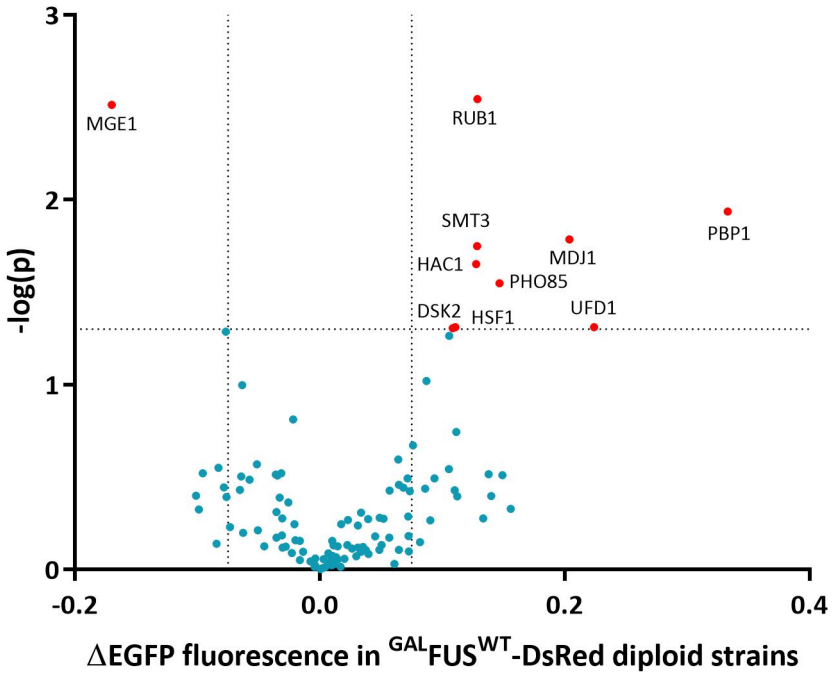

Figure 3.9. Expression of human FUS^{WT}-DsRed in yeast causes alterations in the levels of 10 yeast EGFP-fusion proteins. The absorbance and EGFP fluorescence of diploid EGFP-fusion protein/^{GAL}FUS^{WT}-DsRed strains grown in SGal/-His/Ura were measured over 48 h using a FLUOstar® Optima plate reader set to incubate plates at 30 °C. Alterations in EGFP-fusion protein levels in diploid EGFP-fusion protein/^{GAL}FUS^{WT}-DsRed strains were identified based on a fold change of > ±0.075 (arbitrary cut-off) and $p < 0.05$ from t tests comparing the mean normalised EGFP fluorescence intensity yield (yield from 0 to 48 h) relative to control diploid EGFP-fusion protein/^{GAL}DsRed^{empty} strains. These cut-offs are highlighted by dashed lines. Note that the *y* axis displays the -$\log_{10}$ of the *p* values. Data points represent the ΔEGFP fluorescence and -$\log_{10}$ of the *p* value from t tests comparing the differences in the means calculated from the average of quadruplicate samples. EGFP-fusion proteins exhibiting altered levels are displayed in red.

Table 3.4. Yeast EGFP-fusion proteins with altered levels in diploid strains expressing human FUS^{WT}-DsRed.

Major cellular function/s	Yeast orthologue	Human orthologue	Description of yeast orthologue (*Saccharomyces* Genome Database; SGD, UniProt)	ΔF	*p* value	Connection to ALS/Proteostasis function(s)/Interaction with relevant proteins (BioGRID)	Reference for gene/protein with direct connection to ALS
Increased							
mRNA splicing, transcription, RNA metabolism and stress granules.	PBP1	ATXN2	Component of glucose deprivation induced stress granules; involved in P-body-dependent granule assembly; similar to human ataxin-2; interacts with PAB1 to regulate mRNA polyadenylation.	0.3332407	0.0115777	PBP1 enhances TDP-43 toxicity; ATXN2 is present in ubiquitin-immunoreactive inclusions in sALS and *FUS*-linked fALS.	Elden *et al.* 2010; Farg *et al.* 2013; Kim *et al.* 2014
Ubiquitin homeostasis, ubiquitin-proteasome system (UPS)	DSK2	UBQLN2	Nuclear-enriched ubiquitin-like polyubiquitin-binding protein, required for spindle pole body (SPB) duplication and for transit through the G2/M phase of the cell cycle, involved in proteolysis, interacts with the proteasome.	0.1084386	0.0494203	Present in ubiquitin-immunoreactive inclusions in sALS and *SOD1-, TARDBP-*, *FUS-, OPTN-, UBQLN2-* and *C9ORF72*-linked fALS. Mutations in *UBQLN2* cause some forms of fALS.	Deng *et al.* 2011; Mori *et al.* 2013; May *et al.* 2014
Molecular chaperones, protein folding	HSF1	HSF1	Trimeric heat shock transcription factor; activates multiple genes in response to highly diverse stresses, including hyperthermia; recognises variable heat shock elements (HSEs); monitors translational status of cell at the ribosome through an RQC (Ribosomal Quality Control)-mediated translation-stress signal; involved in diauxic shift; posttranslationally regulated.	0.1105651	0.0489443	Heat shock response.	

ER stress, UPR, ERAD	UFD1	UFD1L	Substrate-recruiting cofactor of the CDC48-NPL4-UFD1 segregase; polyubiquitin binding protein that assists in the dislocation of misfolded, ERAD substrates that are subsequently delivered to the proteasome for degradation; involved in regulated destruction of ER membrane proteins such as HMG-CoA reductase (HMG1/2) and cytoplasmic proteins (FBP1); involved in mobilising membrane bound transcription factors by regulated Ub/proteasome-dependent processing.	0.2240214	0.0489068	ERAD pathway.	
	HAC1	XBP1	Basic leucine zipper (bZIP) transcription factor (ATF/CREB1 homologue); regulates the unfolded protein response, via UPRE binding, and membrane biogenesis; ER stress-induced splicing pathway facilitates efficient HAC1 synthesis; two functional forms of HAC1 are produced; translation initiation is repressed under non-stress conditions; protein abundance increases in response to DNA replication stress.	0.127716	0.0222142	UPR pathway.	
Protein phosphorylation, trafficking and signal transduction	PHO85	CDK5	Cyclin-dependent kinase; has ten cyclin partners; involved in regulating the cellular response to nutrient levels and environmental conditions and progression through the cell cycle; human lissencephaly-associated homologue CDK5 functionally complements null mutation.	0.1468222	0.0283158	Present in ubiquitin-immunoreactive inclusions in *SOD1*-linked fALS.	Nakamura *et al.* 1997
Mitochondrial homeostasis	MDJ1	DNAJA3	Co-chaperone that stimulates HSP70 protein SSC1 ATPase activity; involved in protein folding/refolding in the mitochondrial matrix; required for proteolysis of misfolded proteins; member of the HSP40 (DNAJ) family of chaperones.	0.2038949	0.0163733	Mitochondrial HSP40 chaperone.	
Miscellaneous	RUB1	NEDD8	Ubiquitin-like protein with similarity to mammalian NEDD8; conjugation (neddylation) substrates include the cullins CDC53, RTT101, and CUL3; activated by ULA1 and UBA3 (E1 enzyme pair); conjugation mediated by UBC12 (E2 enzyme).	0.1287392	0.0028463	Present in ubiquitin-immunoreactive inclusions in sALS and *SOD1*-linked fALS.	Tanji *et al.* 2007

	SMT3	SUMO1	Ubiquitin-like protein of the SUMO family; conjugated to lysine residues of target proteins; associates with transcriptionally active genes; regulates chromatid cohesion, chromosome segregation, APC-mediated proteolysis, DNA replication and septin ring dynamics; human homologue SUMO1 can complement yeast null mutant.	0.1283347	0.0177666	Sumoylation of Lys-75 in SOD1 modulates SOD1 aggregation; aggregates containing a spliced mutant of TDP-43 have been found to contain SUMO2/3; FUS can function as a SUMO E3 ligase, and can itself be sumoylated.	Fei *et al.* 2006; Oh *et al.* 2010; Seyfried *et al.* 2010
Decreased							
Mitochondrial homeostasis and antioxidant activity	MGE1/ GRPE	GRPEL1	Mitochondrial matrix cochaperone; nucleotide release factor for SSC1 in protein translocation and folding; also acts as cochaperone for SSQ1 in folding of Fe-S cluster proteins; acts as oxidative sensor to regulate mitochondrial SSC1; in presence of oxidative stress, dimeric MGE1 becomes a monomer and unable to regulate SSC1 function; homologue of *E. coli* GRPE and human MGE1 (GRPEL1), which also responds to oxidative stress.	-0.170056	0.0030688	Mitochondrial protein import; mitochondrial chaperone binding.	

GO term enrichment analysis of the hits against the background set of 128 EGFP-fusion proteins showed that there was no enrichment in any of the biological process terms annotated amongst the background set of proteins. However, evaluation of the specific functions reported for the hits, as collated in Table 3.4, was important to identify the molecular processes that were altered in cells expressing FUS^{WT}-DsRed. Moreover, STRING network analysis revealed interactions amongst the hits (Figure 3.10). Ten secondary interacting proteins link several of the hits with each other in sub-networks that highlight their shared molecular pathways. A sub-network linking HSF1, UFD1 and RUB1, each of which were up-regulated in diploid FUS^{WT}-DsRed yeast, included two secondary interactors; CDC48 and NPL4. CDC48, NPL4 and UFD1 form a polyubiquitin-selective segregase complex involved in ERAD (Ye *et al.* 2001). STRING analysis inferred a functional interaction between NPL4 and RUB1 from interactions that have been identified experimentally between their mammalian orthologues, rather than directly between these proteins in *Saccharomyces cerevisiae.* HSF1 linked into this sub-network via its interaction with CDC48. CDC48 has diverse functions in cells, one of which is in the ribosome quality control (RQC) complex (Brandman *et al.* 2012). In this complex, CDC48 signals to HSF1 under conditions of stress resulting from disruptions in protein translation to elicit transcriptional activation of the heat shock response (HSR), leading to the expression of diverse molecular chaperones. It is interesting to note that CDC48 was found to be down-regulated in diploid ^{GAL}TDP-43^{WT}-DsRed yeast (section 3.3.4.1).

A sub-network linked MDJ1 and MGE1 with 2 secondary interactors, SSC1 and TIM44. MDJ1 is a HSP40 co-chaperone that activates the HSP70 ATPase, SSC1, which is involved in protein folding and refolding in the mitochondrial matrix (Deloche *et al.* 1997, Kubo *et al.* 1999). MGE1 is another mitochondrial matrix co-chaperone that assists SSC1 in its protein translocation and folding functions. Interestingly, while the levels of MDJ1 were increased in yeast expressing FUS^{WT}-DsRed, the levels of MGE1 were decreased. Moreover, MGE1 was

the only protein measured to have decreased levels in diploid FUS^{WT}-DsRed yeast.

Three proteins that had been measured to have decreased levels in diploid $^{GAL}TDP\text{-}43^{WT}$-DsRed yeast, HAC1, PBP1 and DSK2, were observed to have increased levels in diploid $^{GAL}FUS^{WT}$-DsRed yeast. Through STRING analysis, no interactions were identified between these proteins and the other hits. The cyclin-dependent kinase, PHO85, and the ubiquitin-like protein, SMT3, were also not identified to share interactions with the other hits. However, they were connected to secondary interactors in their own distinct sub-networks.

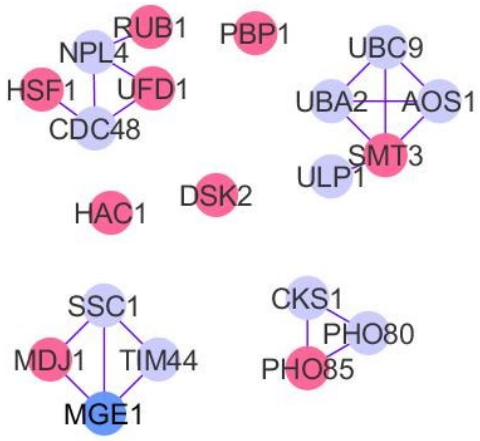

Figure 3.10. Protein-protein interaction network for EGFP-fusion protein/$^{GAL}FUS^{WT}$-DsRed screen hits. The ten yeast EGFP-fusion proteins with altered levels in diploid EGFP-fusion protein/$^{GAL}FUS^{WT}$-DsRed strains were queried in the STRING protein-protein interaction database (Szklarczyk *et al.* 2015, Szklarczyk *et al*. 2017). Interactions between the hits were queried using co-expression, published experiments and databases as sources of interaction data, and only interactions scored with high confidence were included. It was selected that ten secondary interacting proteins would be included in the network analysis. The nine up-regulated proteins are displayed as pink circles, while the one down-regulated protein is displayed as a blue circle. The ten secondary interacting proteins of the hits are displayed as pale grey/purple circles, showing sub-networks that link several of the hits with each other.

3.3.4.3 Expression of human SOD1^{A4V}-DsRed is associated with changes in the levels of 7 yeast EGFP-fusion proteins

In the set of 128 diploid EGFP-fusion protein/^{GAL}SOD1^{A4V}-DsRed yeast strains that were examined, altered levels of the EGFP-fusion proteins were measured in 7 strains (Figure 3.11 and Table 3.5). Out of these, the levels of 5 proteins were increased relative to the corresponding control diploid EGFP-fusion protein/^{GAL}DsRed^{empty} strains and EGFP-fusion protein/^{GAL}SOD1^{WT}-DsRed strains, whilst 2 proteins had decreased levels.

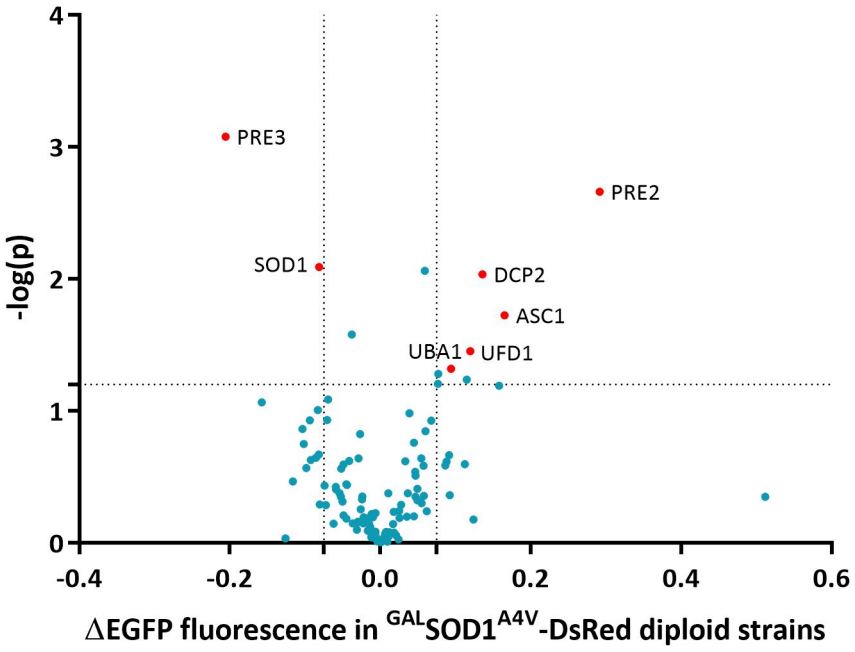

Figure 3.11. Expression of human SOD1^{A4V}-DsRed in yeast causes alterations in the levels of 7 yeast EGFP-fusion proteins. The absorbance and EGFP fluorescence of diploid EGFP-fusion protein/^{GAL}SOD1^{A4V}-DsRed strains grown in SGal/-His/Ura were measured over 48 h using a FLUOstar® Optima plate reader set to incubate plates at 30 °C. Alterations in EGFP-fusion protein levels in diploid EGFP-fusion protein/^{GAL}SOD1^{A4V}-DsRed strains were identified based on a fold change of > ±0.075 (arbitrary cut-off) and $p < 0.05$ from t tests comparing the mean normalised EGFP fluorescence intensity yield (yield from 0 to 48 h) relative to control diploid EGFP-fusion protein/^{GAL}DsRed^{empty} strains. These cut-offs are highlighted by dashed lines. Note that the *y* axis displays the -$\log_{10}$ of the *p* values. Data points represent the ΔEGFP fluorescence and -$\log_{10}$ of the *p* value from t tests comparing the differences in the means calculated from quadruplicate samples. Only EGFP-fusion proteins exhibiting altered levels in diploid EGFP-fusion protein/^{GAL}SOD1^{A4V}-DsRed strains but not in the corresponding diploid EGFP-fusion protein/^{GAL}SOD1^{WT}-DsRed strains were included in further analyses, and are displayed in red.

Table 3.5. Yeast EGFP-fusion proteins with altered levels in diploid strains expressing human SOD1^{A4V}-DsRed.

Major cellular function/s	Yeast orthologue	Human orthologue	Description of yeast orthologue (*Saccharomyces* Genome Database; SGD, UniProt)	ΔF	*p* value	Connection to ALS/Proteostasis function(s)/Interaction with relevant proteins (BioGRID)	Reference for gene/protein with direct connection to ALS
Increased							
mRNA splicing, transcription, RNA metabolism and stress granules.	DCP2	DCP2	Catalytic subunit of the DCP1-DCP2 decapping enzyme complex; removes the 5' cap structure from mRNAs prior to their degradation; also enters the nucleus and positively regulates transcription initiation; forms cytoplasmic foci upon DNA replication stress; human homologue DCP2 complements yeast DCP2 thermosensitive mutant.	0.135671	0.0092441	Reported to co-localise with FUS in stress granules. Native interactor of CDC48 (VCP). Involved in mRNA degradation.	Sun *et al.* 2011
Ribosomes and protein translation	ASC1	RACK1	An integral ribosomal protein; G-protein beta subunit and guanine dissociation inhibitor for GPA2; orthologue of RACK1 that inhibits translation; core component of the small (40S) ribosomal subunit; regulates P-body formation induced by replication stress.	0.1649825	0.0188575	Involved in protein quality control at ribosomes during translation.	Wolff, Weissman & Dillin, 2014 (review)
Ubiquitin homeostasis, ubiquitin-proteasome system (UPS)	PRE2	PSMB5, PSMB8, PSMB11	Beta 5 subunit of the 20S proteasome; responsible for the chymotryptic activity of the proteasome.	0.2916613	0.00218	Proteasomal protein degradation.	
	UBA1	UBA1	Ubiquitin activating enzyme (E1); catalyses the first step in ubiquitin conjugation to mark cellular proteins for degradation through the ubiquitin-proteasome system.	0.0941485	0.0479153	Ubiquitin homeostasis; ubiquitin-proteasome system (UPS).	

ER stress, UPR, ERAD	UFD1	UFD1L	Substrate-recruiting cofactor of the CDC48-NPL4-UFD1 segregase; polyubiquitin binding protein that assists in the dislocation of misfolded, ERAD substrates that are subsequently delivered to the proteasome for degradation; involved in regulated destruction of ER membrane proteins such as HMG-CoA reductase (HMG1/2) and cytoplasmic proteins (FBP1); involved in mobilising membrane bound transcription factors by regulated Ub/proteasome-dependent processing.	0.1193909	0.0352671	Endoplasmic reticulum-associated degradation (ERAD) pathway.	
Decreased							
Ubiquitin homeostasis, ubiquitin-proteasome system (UPS)	PRE3	PSMB6, PSMB9	Beta 1 subunit of the 20S proteasome; responsible for cleavage after acidic residues in peptides.	-0.205477	0.0008374	Proteasomal protein degradation.	
Mitochondrial homeostasis and antioxidant activity	SOD1	SOD1, SOD3, CCS	Cytosolic copper-zinc superoxide dismutase; detoxifies superoxide; stabilizes YCK1 and YCK2 kinases in glucose to repress respiration; phosphorylated by DUN1, enters nucleus under oxidative stress to promote transcription of stress response genes; human orthologue SOD1 implicated in ALS complements a null allele; localisation to mitochondrial intermembrane space is modulated by MICOS complex.	-0.081141	0.0081055	Mutations in *SOD1* cause ~20% of fALS cases. SOD1 is present in ubiquitin-immunoreactive inclusions in *SOD1*-linked fALS. Involved in antioxidant activity; scavenges free radicals in cells.	Shibata *et al.* 1994; Kato *et al.* 1997; Benatar *et al.* 2006

GO term enrichment analysis of the hits against the background set of 128 EGFP-fusion proteins showed that there was no enrichment in any biological process terms. STRING network analysis, however, identified that several of the hits were connected in interaction sub-networks, linked through ten secondary interacting proteins (Figure 3.12). This revealed that several of the hits and the majority of the secondary interactors shared a common interactor; RPS31. RPS31 and eight of the ten secondary interactors are ribosomal subunits (RPS12, RPS13, RPS15, RPS2, RPS20, RPS3, RPS31 and RPS5). RPS31 is one of two fusion proteins that are proteolytically cleaved to yield ubiquitin and the S31 ribosomal subunit (Finley *et al.* 1989, Oh *et al.* 2013). Of the primary hits, ASC1, PRE3, UBA1 and UFD1 directly interact with RPS31. ASC1 is a core component of the small (40S) ribosomal subunit. The levels of ASC1 were increased in diploid ^{GAL}SOD1^{A4V}-DsRed yeast (p = 0.0189). UFD1, which had increased levels in yeast expressing SOD1^{A4V}-DsRed (p = 0.0353), also had increased levels in yeast expressing FUS^{WT}-DsRed (see section 3.3.4.2). As described in section 3.3.4.2, UFD1 forms a polyubiquitin-selective segregase complex, together with NPL4 and CDC48, that is involved in ERAD (Ye *et al.* 2001). UBA1 is the primary E1 ubiquitin-activating enzyme in yeast, as is its orthologue in humans (Chiu *et al.* 2007, Jin *et al.* 2007, Pelzer *et al.* 2007). UBA1 levels were found to be increased in diploid ^{GAL}SOD1^{A4V}-DsRed yeast (p = 0.048). PRE3, the levels of which were decreased in yeast expressing SOD1^{A4V}-DsRed (p = 0.0008), is a β-subunit of the 20S proteasome that catalyses cleavage after acidic residues in peptides. PRE3 interacts with PRE2, another β-subunit of the 20S proteasome that is responsible for the chymotryptic activity of the proteasome. The secondary interactors of these two proteins, PRE7 and PUP1, are the β6 and β2 subunits of the 20S proteasome. Out of the 17 total primary hits and secondary interactors, 6 are involved in ubiquitin-dependent protein degradation (PRE2, PRE3, UBA1, UFD1, PRE7 and PUP1).

Two of the hits did not share interactions with the other hits or the secondary interactors; DCP2

and SOD1. Yeast SOD1 was found to be down-regulated in yeast expressing human SOD1^{A4V}-DsRed (p = 0.0081). The heterologous expression of human *SOD1* containing ALS-associated mutations (G93A, G85R and K100G) in yeast has been shown to complement a null yeast *SOD1* allele (Nishida *et al.* 1994). It is possible that the overexpression of human SOD1^{A4V}-DsRed was complementary to the activity of yeast SOD1, causing a decrease in the expression of yeast *SOD1*. DCP2, which had increased levels in diploid ^{GAL}SOD1^{A4V}-DsRed yeast (p = 0.0092), is a catalytic subunit of the DCP1-DCP2 decapping enzyme complex that removes the 5' cap from mRNAs before they are degraded (Dunckley and Parker 1999).

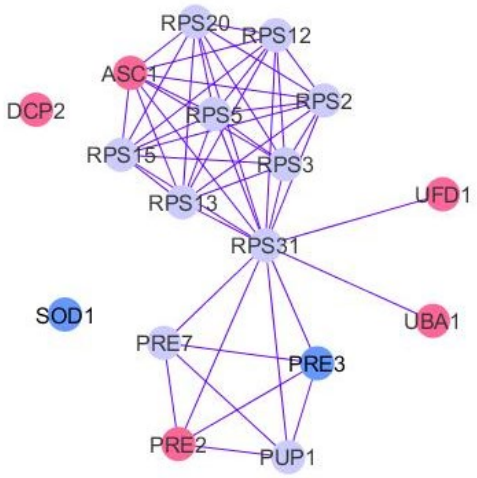

Figure 3.12. Protein-protein interaction network for EGFP-fusion protein/^{GAL}SOD1^{A4V}-DsRed screen hits. The seven yeast EGFP-fusion proteins with altered levels in diploid EGFP-fusion protein/^{GAL}SOD1^{A4V}-DsRed strains were queried in the STRING protein-protein interaction database (Szklarczyk *et al.* 2015, Szklarczyk *et al.* 2017). Interactions between the hits were queried using co-expression, published experiments and databases as sources of interaction data, and only interactions scored with high confidence were included. It was selected that ten secondary interacting proteins would be included in the network analysis. The five up-regulated proteins are displayed as pink circles, while the two down-regulated proteins are displayed as blue circles. The ten secondary interacting proteins of the hits are displayed as pale grey/purple circles, showing sub-networks that link several of the hits with each other.

3.3.4.4 Common hits and pathways differentially expressed in diploid EGFP-fusion strains expressing human TDP-43^{WT}, FUS^{WT} or SOD1^{A4V}

While there were no common hits between all three screens against TDP43, FUS and SOD1, three hits (PBP1, HAC1 and DSK2) were common between the TDP-43 and FUS screens and one hit (UFD1) was common between the FUS and SOD1 screens (Figure 3.13). The levels of UFD1 were found to be increased both in yeast expressing SOD1^{A4V}-DsRed and in yeast expressing FUS^{WT}-DsRed. As described in sections 3.3.4.2 and 3.3.4.3, UFD1 is one of the three proteins that form a polyubiquitin-selective segregase complex, together with NPL4 and CDC48, that is involved in ERAD (Ye *et al.* 2001). While the levels of HAC1, PBP1 and DSK2 were decreased in yeast expressing TDP-43^{WT}-DsRed, their levels were increased in yeast expressing FUS^{WT}-DsRed. These three proteins are not reported to directly interact with one another. DSK2 has several functions in proteolysis. It is a ubiquitin-like polyubiquitin-binding protein involved in the UPS, autophagy as well as in the ERAD pathway (Funakoshi *et al.* 2002, Saeki *et al.* 2002, Medicherla *et al.* 2004, Nolan *et al.* 2017). HAC1 is involved in the IRE1-mediated UPR signalling pathway. It is a transcription factor that promotes the expression of proteins important for ER quality control (Cox and Walter 1996, Mori *et al*. 1996, Ron and Walter 2007). PBP1 also has roles in regulating gene expression, however it is specifically involved in the maturation of pre-mRNAs for translation, mediating their polyadenylation (Mangus *et al.* 1998). PBP1 also regulates the assembly of SGs and P-bodies (Buchan *et al.* 2008).

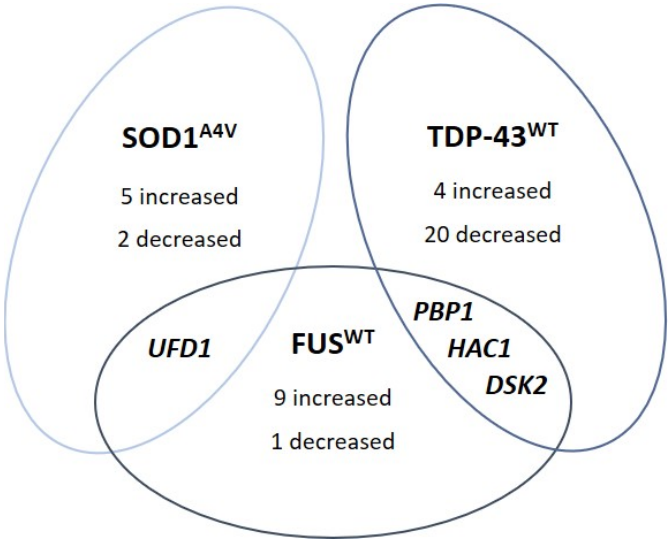

Figure 3.13. Venn diagram illustrating the yeast EGFP-fusion proteins that were commonly altered by the expression of human TDP-43^{WT}-DsRed, FUS^{WT}-DsRed and/or SOD1^{A4V}-DsRed in diploid yeast strains. Three proteins were altered both in yeast expressing TDP-43^{WT}-DsRed and in yeast expressing FUS^{WT}-DsRed; PBP1, HAC1 and DSK2. The levels of UFD1 were increased both in yeast expressing FUS^{WT}-DsRed and in yeast expressing SOD1^{A4V}-DsRed. PBP1 is involved in mRNA processing and stress granule dynamics and is the yeast orthologue of ATXN2, polyglutamine repeat expansions in which are a genetic risk factor for ALS (Elden *et al.* 2010, Farg *et al.* 2013, Tazen *et al.* 2013). HAC1 is the major regulator of the unfolded protein response. DSK2 is the yeast orthologue of UBQLN2, mutations in which are associated with ALS (Deng *et al.* 2011). UFD1 has crucial functions in the endoplasmic reticulum-associated degradation pathway.

GO term enrichment analysis for the primary hits identified in each screen against the background set of 128 EGFP-fusion proteins showed that there was no enrichment in any of the biological processes that have been annotated for the background set of proteins. However, several of the hits and secondary interactors identified in the screens of yeast expressing human TDP-43^{WT}-DsRed, FUS^{WT}-DsRed and SOD1^{A4V}-DsRed have functions in gene expression, SG assembly and dynamics, ERAD and the UPS (Table 3.6). In the screens of yeast expressing human TDP-43^{WT}-DsRed or FUS^{WT}-DsRed there were hits and interactors with molecular chaperone functions and involvement in autophagy.

Table 3.6. The common major categories of molecular processes that have been reported for the primary hits and secondary interactors identified in the screens of diploid yeast EGFP-fusion strains expressing human TDP-43^{WT}-DsRed, FUS^{WT}-DsRed or SOD1^{A4V}-DsRed.

Molecular process	TDP-43^{WT}-DsRed screen	FUS^{WT}-DsRed screen	SOD1^{A4V}-DsRed screen
Gene expression; transcription and translation	ADA2, GCN5, HAC1, PAB1, PBP1, PUB1, RPT3, RPT4, RPT6, SLT2, TIF4631	PBP1, CKS1, HAC1, HSF1, PHO80, PHO85	DCP2, RPS12, RPS13, RPS15, RPS2, RPS20, RPS3, RPS31, RPS5
Stress granules	PBP1, PUB1, TIF4631	PBP1	DCP2
Molecular chaperone activity	CPR1, HSP82, SSB1, TSA1, TSA2	MDJ1, MGE1, SSC1	
Transport between ER and Golgi	ATG8, ERV25, GEA2		
ER stress, UPR, ERAD	CDC48, DER1, DSK2, HAC1, RPT3, RPT4, RPT6, SLT2	CDC48, DSK2, HAC1, NPL4, UFD1	UFD1
Ubiquitin homeostasis, UPS	CDC48, HSP82, DSK2, PRE4, PRE9, RPN10, RPN11, RPN12, RPT3, RPT4, RPT6, PRE5, PRE8	CDC48, NPL4, UFD1, DSK2	PRE2, PRE3, PRE7, PUP1, UBA1, UFD1
Autophagy	ATG8, CDC48, DSK2, GEA2, SLT2	CDC48, DSK2, PHO80, PHO85	
Mitochondrion function		MDJ1, MGE1, SSC1, TIM44	
Antioxidant activity	SOD2, TSA1, TSA2		SOD1
Calcium-mediated signalling		PHO80, PHO85	

3.4 Discussion

Over the last two decades, the study of different neurodegenerative diseases, including PD, HD, AD and ALS, has benefited from the use of *Saccharomyces cerevisiae* as a model organism (Krobitsch and Lindquist 2000, Auluck *et al.* 2002, Outeiro and Lindquist 2003, Willingham *et al.* 2003, Cooper *et al.* 2006, Johnson *et al.* 2008, Gitler *et al.* 2009, Johnson *et al.* 2009, Elden *et al.* 2010, Sun *et al.* 2011, Treusch *et al.* 2011, Kim *et al.* 2014). Many conserved, fundamental biological processes that are affected by the expression of disease-causing genes in humans can be identified using yeast as a model system. In the present study, the effect of the heterologous expression of TDP-43^{WT}, FUS^{WT} and SOD1^{A4V} on the levels of a pathway-focused set of 128

different yeast proteins was investigated. It was hypothesised that any proteins in this selection that were found to have altered expression in the presence of TDP-43, FUS and mutant SOD1 may play a key role(s) in the cellular response to ALS-associated pathology. A comprehensive list of conserved yeast proteins to include for screening was compiled, including proteins involved in proteostasis mechanisms, other pathways suspected to be involved in ALS pathogenesis (e.g. mitochondrial dysfunction, disruptions in energy metabolism), and orthologues of human proteins that have been found colocalised in inclusions in post-mortem spinal cord tissue from ALS patients (Ciryam *et al.* 2017). The result of this yeast screen was the identification of 24, 10 and 7 yeast proteins found to have altered levels in yeast expressing TDP-43^{WT}-DsRed, FUS^{WT}-DsRed and SOD1^{A4V}-DsRed, respectively.

In future work it will be necessary to validate the hits from this yeast screen. The hits will first need to be validated biochemically through immunoblotting of lysates prepared from each diploid yeast strain. This could be done using an anti-EGFP antibody to probe for the EGFP-fusion yeast protein in each diploid strain, to then compare the levels of each EGFP-fusion protein between each diploid strain expressing the ALS gene relative to the corresponding control strain expressing DsRed alone. It will also be important to confirm that the changes in EGFP-fusion protein levels measured in the present study were of a magnitude that would have functional effects. There is no available method or formula to calibrate the measured changes in EGFP-fusion protein levels to an absolute quantity of the protein levels. This limits us from comparing the changes in EGFP-fusion protein levels that were observed with data published in the literature on protein expression level changes that would be sizeable enough to impact molecular and cellular function. One approach to investigate this experimentally would involve measuring the activity of molecular processes that are downstream from each hit, and comparing between each diploid yeast strain expressing the ALS gene and the corresponding control strain expressing DsRed alone. Differences in the activity of the targeted molecular

process in cells expressing the ALS gene relative to control cells expressing DsRed alone would provide evidence that the alterations in EGFP-fusion protein levels measured in the present study were of an amplitude great enough to have functional effects.

All biochemically confirmed hits would then need to be validated using mammalian cell culture models of SOD1, TDP-43 and FUS. Validation in these models would involve preparing cell lysates from each cell culture model and using these to immunoblot for the endogenous mammalian orthologue of each hit. As would be done for the yeast strains, the endogenous levels of the protein hit that was probed for would be compared between cells expressing the ALS gene mutant and corresponding control cells expressing GFP alone.

Beyond these proposed validation studies, it would be important to carry out knockdown studies using siRNA targeted to each hit. Conversely, it would also be important to carry out studies to examine the effects of overexpression of each hit. In these knockdown and overexpression studies, measurement of the effect on the activity of known downstream targets of the hit, cell viability, localisation of the ALS mutant and/or aggregation of the ALS mutant would provide valuable mechanistic information on the role that the hit may play in the cellular response to the expression of the ALS mutant.

3.4.1 Alterations in gene expression regulation may be common to ALS associated with SOD1, TDP-43 and FUS

In the past decade, studies to characterise alterations in protein levels resulting from factors that cause cellular stress have emerged as a way to gain insight into the molecular pathways involved in disease and in the cellular response to harmful stimuli (Breker *et al.* 2013, D'Souza *et al.* 2014, Fesenko *et al.* 2016, Tangsongcharoen *et al.* 2019). Between all three screens conducted as part of this work, the primary hits and secondary interactors identified have functions in several common molecular processes of the proteostasis network; gene expression, ERAD and the UPS. Of course, the set of 128 yeast EGFP-fusion strains included in the present study were

selected based on their relevance to the molecular mechanisms suspected to be involved in motor neuron dysfunction in ALS, particularly proteostasis. Thus, it is not surprising that processes related to proteostasis were identified to be affected; however, it is important to gain insight into commonly altered molecular processes in all three genetic screens, as well as any changes that are unique to each. For instance, gene expression alterations and changes in SG dynamics have been comprehensively investigated in the context of mutations in *TARDBP* and *FUS*, both of which are involved in RNA metabolism. Up until very recently, these molecular alterations had not received attention in relation to their association with mutations in *SOD1*. However, a 2016 study revealed an interaction between mutant SOD1 and G3BP1, a protein involved in SG dynamics (Gal *et al.* 2016). In the present work, the levels of the P-body and SG-associated protein, DCP2, were up-regulated in yeast expressing $SOD1^{A4V}$-DsRed. DCP2 is involved in gene expression through its function in mRNA degradation (Dunckley and Parker 1999). Some of the proteins identified in the $SOD1^{A4V}$ screen, ASC1 and its secondary interactors, are components of the small 40S ribosomal subunit and therefore essential for translation. One of these interactors, RPS31, was a central interactor linking ASC1 and the other primary hits UFD1, UBA1 and PRE3. The up-regulation of DCP2 and ASC1 and the connection between all seven primary hits of a ribosome subunit fusion protein, RPS31, suggest that there may have been an increased need for gene expression regulation in yeast expressing $SOD1^{A4V}$. Gene expression alterations may thus not only be associated with TDP-43 and FUS in ALS, but also altered in the presence of mutant SOD1.

Further to identifying that gene expression regulation, ERAD and the UPS were commonly affected molecular processes in yeast modelling TDP-43, FUS and SOD1 pathology, three specific proteins (PBP1, HAC1 and DSK2) were found to be commonly altered between the TDP-43 and FUS yeast screens, and one common hit (UFD1) was identified between the FUS and SOD1 yeast screens.

3.4.2 The expression of TDP-43^{WT} and FUS^{WT} cause alterations in the IRE1-mediated UPR signalling pathway in yeast

The expression of human TDP-43^{WT}-DsRed was clearly toxic in yeast, as demonstrated through spotting assays (see section 3.3.2), showing that critical processes were perturbed in these cells. Several proteins involved in ER protein quality control and the ER stress response were found to have decreased levels in yeast expressing TDP-43^{WT}-DsRed; ERV25 has functions in misfolded protein quality control in the ER (Copic *et al.* 2009), DER1 promotes the export of misfolded proteins from the ER for ERAD (Knop *et al.* 1996, Hitt and Wolf 2004), CDC48 is one of the three members of the polyubiquitin-selective segregase complex involved in ERAD (Ye *et al.* 2001, Ye *et al.* 2003), and NMA111 promotes stress-induced homeostatically-regulated protein degradation (SHRED) of misfolded and native ER-membrane proteins (Szoradi *et al.* 2018). Potentially, the presence of human TDP-43^{WT}-DsRed in yeast caused a widespread dysregulation of ER proteostasis. Reduction in the capacity of cells to ameliorate ER stress has previously been implicated to be involved in the pathogenic mechanisms of mutant TDP-43 (Walker *et al.* 2013, Wang *et al.* 2015). Compounding this, the decreased levels of HAC1 suggest that TDP-43^{WT}-DsRed further caused disruption of the pathway that regulates HAC1 translation, impairing the IRE1-mediated UPR signalling pathway that is triggered by ER stress (Cox and Walter 1996, Sidrauski and Walter 1997, Ron and Walter 2007).

The increased levels of HAC1 in yeast expressing FUS^{WT}-DsRed indicate that proteostasis in the ER of cells was compromised, causing ER stress, leading to increased splicing of *HAC1* mRNA and consequently up-regulation of HAC1. In line with this, there is evidence that the expression of mutant FUS in NSC-34 cells causes ER stress (Farg *et al.* 2012).

Importantly, these findings suggest that functionality of the IRE1-mediated UPR signalling pathway may be a key determinant of the cellular ability to respond to ER stress caused by mislocalised TDP-43 and FUS. Moreover, dysregulation of *HAC1* mRNA splicing may be a

key mechanism of TDP-43 toxicity, impairing cellular ability to restore ER proteostasis that is initially disrupted through the aberrant activity of mislocalised TDP-43.

3.4.3 Differential regulation of PBP1 reveals differences in the cellular response to mislocalised, toxic TDP-43^{WT} and FUS^{WT}

PBP1 is the yeast orthologue of ATXN2. Intermediate expansions of a CAG trinucleotide repeat in *ATXN2* are correlated with an increased risk for ALS (Elden *et al.* 2010, Tazen *et al.* 2013). ATXN2 has further been associated with ALS through discovery of its presence in ubiquitin-immunoreactive inclusions in tissue from patients with sALS and *FUS*-linked fALS (Farg *et al.* 2013, Tazen *et al.* 2013). In yeast expressing TDP-43^{WT}-DsRed it was found that PBP1 was down-regulated, whereas it was up-regulated in yeast expressing FUS^{WT}-DsRed. Findings from previous work investigating modifiers of TDP-43^{WT} toxicity indicated that increased levels of PBP1 enhance the toxicity caused by TDP-43^{WT} (Kim *et al.* 2014). It was further identified that polyadenylate-binding protein (PAB1) mediated interactions between TDP-43 and ATXN2/PBP1 that resulted in toxicity (Kim *et al.* 2014). In the present work, PAB1 was found to be down-regulated in yeast expressing TDP-43^{WT}-DsRed. The expression of human TDP-43^{WT}-DsRed caused striking toxicity in yeast. If, as reported by Kim *et al.* (2014), increased levels of PBP1 enhance the toxicity caused by TDP-43^{WT} in yeast, and PAB1 is involved in an aberrant interaction between PBP1 and TDP-43, then down-regulation of these proteins may improve the fitness of yeast expressing TDP-43^{WT}. The decreased levels of PBP1 and PAB1 in yeast expressing TDP-43^{WT} may thus be the result of selection for TDP-43^{WT}-DsRed-expressing cells that expressed lower levels of these proteins over successive cell divisions.

PBP1 is involved in diverse RNA processing pathways that control gene expression, including P-body-dependent SG assembly and the regulation of mRNA polyadenylation (Mangus *et al.* 1998, Buchan *et al.* 2008). The up-regulation of PBP1 in yeast expressing FUS^{WT}-DsRed may promote SG assembly and repression of translation as part of a cellular stress response to the

toxicity of mislocalised FUS^{WT}-DsRed. Indeed, as well as up-regulation of PBP1 in yeast expressing FUS^{WT}-DsRed, several other proteins with key functions in responding to proteotoxic stress were up-regulated, including HAC1 (as discussed above), DSK2, UFD1, SMT3, HSF1 and MDJ1.

3.4.4 Yeast differentially regulate DSK2 in response to proteotoxic stress caused by mislocalised TDP-43^{WT} and FUS^{WT}

The third common hit identified in the TDP-43^{WT}-DsRed and FUS^{WT}-DsRed screens, DSK2, is particularly interesting as it is the yeast orthologue of a protein that is closely associated with ALS; UBQLN2. Mutations in *UBQLN2* cause X-linked ALS and ALS/FTD (Deng *et al.* 2011, Teyssou *et al.* 2017). It is a commonly detected protein component of several different types of inclusions detected in ALS patients' motor neurons. It is detected in skein-like p62-, TDP-43-, FUS- and OPTN-positive inclusions in ALS patients with P497H or P506T mutations in *UBQLN2* and in patients with sALS and fALS patients with mutations in *SOD1, TARDBP* and *FUS* (Deng *et al.* 2011). It is also detected in TDP-43-negative, poly-(Gly-Ala), -(Gly-Pro), -(Gly-Arg) DPR-, p62- and ubiquitin-positive inclusions in patients with pathological hexanucleotide repeat expansions in *C9ORF72* (Mori *et al.* 2013, May *et al.* 2014). Both DSK2 and its mammalian orthologue have several functions in proteolysis. It is a ubiquitin-like polyubiquitin-binding protein involved in the UPS, autophagy and ERAD (Funakoshi *et al.* 2002, Saeki *et al.* 2002, Medicherla *et al.* 2004, Nolan *et al.* 2017). Interestingly, as was the case for the other two common hits, HAC1 and PBP1, DSK2 was down-regulated in yeast expressing TDP-43^{WT}-DsRed but up-regulated in yeast expressing FUS^{WT}-DsRed. Alterations in the levels of DSK2 indicate that downstream ubiquitin-dependent degradation pathways, namely the UPS, autophagy and ERAD, may be implicated in the cellular response to TDP-43^{WT}-DsRed and FUS^{WT}-DsRed. Indeed, as well as up-regulation of DSK2 in yeast expressing FUS^{WT}-DsRed, the other proteins found to be up-regulated have diverse functions that assist

cells in responding to proteotoxic stress. Apart from PBP1 (discussed above) the up-regulation of proteins involved in mitochondrial proteostasis (MDJ1), ERAD (DSK2, UFD1), the UPR (HAC1), the UPS and autophagy (DSK2) and, critically, the major regulator of the cellular response to proteotoxic stress (HSF1), indicate that the expression of FUS^{WT}-DsRed caused widespread proteostasis dysfunction in cells. Potentially, these proteins were up-regulated in an attempt by the cell to deal with proteostasis disruption caused by mislocalised FUS^{WT}-DsRed.

In yeast expressing TDP-43^{WT}-DsRed, as well as decreased levels of DSK2, the levels of ATG8, required for autophagosome membrane formation, and proteins involved in ERAD (CDC48, DER1, HAC1 and NMA111) were similarly decreased. Regarding the UPS, the primary proteasome-associated ubiquitin receptor, RPN10, was up-regulated in yeast expressing TDP-43^{WT}-DsRed. Moreover, the localisation of RPN10-EGFP was altered in yeast expressing TDP-43^{WT}-DsRed, observed to be colocalised with cytosolic TDP-43^{WT}-DsRed foci (Table 3.2, section 3.3.2 and Figure S3.6, Appendix I). RPN10 is an atypical component of the proteasome, as a large proportion of it exists in a proteasome-unassociated pool in which it functions, similarly to DSK2, as a ubiquitin/polyubiquitin shuttle factor (Fu *et al.* 1998). In a landmark study, Matiuhin *et al.* (2008) discovered a unique interaction between DSK2 and RPN10: through demonstrating that overexpression of *DSK2* was toxic in yeast, they unravelled a complex mechanism by which RPN10 competes with DSK2 for binding to the proteasome, and that RPN10 attenuates the toxicity associated with dysregulated DSK2. The toxicity mediated by dysregulated DSK2 results from its interference with the normal functioning of the UPS, altering the ratio of Lys48 to Lys63 polyubiquitin chains in the cellular ubiquitin pool (Matiuhin *et al.* 2008). The data reported by Matiuhin *et al.* (2008) suggests that the delivery of substrate polyubiquitylated proteins to the proteasome requires stringent regulation by the polyubiquitin shuttle proteins, particularly DSK2 and RPN10, for efficient proteolysis and prevention of proteasomal 'clogging'. In the present work, the down-regulation of DSK2 and up-regulation

of RPN10 may be due to an increased demand for RPN10 in shuttling proteasomal substrates for degradation. In this case, DSK2 may be down-regulated to prevent its interference with the ubiquitin/polyubiquitin shuttling activity of RPN10. Moreover, the colocalisation of RPN10 with cytosolic TDP-43^{WT}-DsRed foci may indicate an attempt to direct mislocalised, toxic TDP-43^{WT}-DsRed for proteasomal degradation. However, in the present work it was not investigated whether the cytosolic TDP-43^{WT}-DsRed foci were ubiquitylated. Microscopy of diploid RPN10-EGFP/TDP-43^{WT}-DsRed yeast immunostained for ubiquitin would be needed to examine whether the cytosolic RPN10-EGFP/TDP-43^{WT}-DsRed foci are ubiquitin-positive, and thus whether the colocalisation of RPN10-EGFP to these foci may be due to its ubiquitin/polyubiquitin shuttling activity.

3.4.5 UFD1 is up-regulated in the presence of mutant SOD1^{A4V} and mislocalised FUS^{WT} in yeast

In both yeast expressing FUS^{WT}-DsRed and yeast expressing SOD1^{A4V}-DsRed, the levels of UFD1 were found to be increased. UFD1 is a polyubiquitin binding protein that has a crucial role in ERAD, forming a segregase complex with CDC48 and NPL4 that extracts misfolded proteins from the ER and directs them to the proteasome for degradation (Ye *et al.* 2001). Three different ALS-causing mutations in *SOD1*, A4V, G85R and G93A, have been shown to cause disruptions in ER-Golgi trafficking and the secretory pathway, leading to ER stress (Atkin *et al.* 2014). The up-regulation of UFD1 in yeast expressing SOD1^{A4V}-DsRed may thus be due to augmentation of the ERAD pathway in an attempt to ameliorate ER stress caused by SOD1^{A4V}-DsRed-mediated disruption of ER proteostasis.

Interestingly, UFD1 and the CDC48-NPL4-UFD1 complex have been implicated in the DNA damage response (DDR) pathway. Nie *et al.* (2012) investigated SUMO-targeted ubiquitin ligases (STUbLs) and SUMOylation of target proteins in the context of toxicity caused by the accumulation of SUMOylated species in cells, and in the DDR pathway. SUMOylation and

ubiquitylation of target proteins are important modulators of the DDR pathway (reviewed in Jackson and Durocher (2013)). Using a proteomics approach Nie *et al.* (2012) discovered that the CDC48-NPL4-UFD1 complex was highly enriched among SUMO-binding proteins in the fission yeast *Schizosaccharomyces pombe*, revealing a role for the CDC48-NPL4-UFD1 complex as a STUbL cofactor which protects cells against SUMO chain-mediated toxicity. Furthermore, a combination of ubiquitin and SUMO recognition motifs within UFD1 appear to mediate the targeting of the CDC48-NPL4-UFD1 complex to SUMOylated and ubiquitylated substrates (Nie *et al.* 2012). Intriguingly, in the present work SMT3, a protein of the SUMO family, was also up-regulated in yeast expressing FUS^{WT}-DsRed. In another study, in cells in which the DDR pathway was activated, a mutation in *UFD1* lead to an accumulation of SUMOylated species in nuclear foci (Køhler *et al.* 2013). This supports a direct role for UFD1 in regulating SUMOylated species in the DDR pathway. The up-regulation of UFD1 and SMT3 in yeast expressing FUS^{WT}-DsRed observed here may be indicative of dysregulation of the DDR pathway. Indeed, several studies have demonstrated that FUS has important functions in the DDR pathway, and that mutations in the NLS of *FUS* result in impairment of this pathway (Wang *et al.* 2013, Higelin *et al.* 2016, Gong *et al.* 2017, Naumann *et al.* 2018). Further investigation of changes in the activity of UFD1 and its downstream effects in neuronal cell models of disease-associated *FUS* mutations may help elucidate a role for UFD1 in the DDR in the context of *FUS*-linked ALS.

3.4.6 Expression of TDP-43^{WT} in yeast is associated with decreased levels of two key autophagy proteins

CDC48 is a particularly intriguing hit from the TDP-43^{WT}-DsRed screen given that mutations in the human orthologue of *CDC48*, *VCP*, account for 1-2% of fALS and <1% of sALS cases (Johnson *et al.* 2010, Abramzon *et al.* 2012). Mutations in *VCP* also cause IBMPFD (Watts *et al.* 2004). TDP-43-positive inclusions are a hallmark pathological feature both in IBMPFD

patients' muscle and brain tissue (Watts *et al.* 2004, Kimonis *et al.* 2008) and in diseased motor neurons in ALS patients. It was previously hypothesised that SGs that persist abnormally in diseased cells seed the formation of inclusions, including TDP-43 inclusions (Dewey *et al.* 2012, Parker *et al.* 2012). More recent work has demonstrated that SGs do not seed the aggregation of TDP-43 into inclusions (Chen and Cohen 2019, Gasset-Rosa *et al.* 2019, Mann *et al.* 2019), however they may indirectly promote the pathological accumulation of TDP-43 into inclusions by interfering with the autophagic clearance of TDP-43 aggregates (Chen and Cohen 2019).

Importantly, CDC48/VCP has been reported to mediate the clearance of SGs through selective autophagy (Buchan *et al.* 2013). This provides a key link in diseases that are associated with *VCP* mutations between impaired VCP function and the occurrence of TDP-43-positive inclusions, with impairment in the autophagy pathway perhaps playing an important pathogenic role. Loss of VCP function may impair the autophagic clearance of TDP-43, and potentially further promote the accumulation of aggregated TDP-43 into inclusions due to impaired autophagic clearance of SGs. SGs that have escaped clearance may sequester proteins that have key functions in autophagy (Chen and Cohen 2019), further impairing the ability of cells to eliminate TDP-43 inclusions through autophagy. In the present work, the levels of CDC48 were reduced in yeast expressing TDP-43^{WT}-DsRed, as were the levels of the key autophagy-related protein ATG8. Through confocal microscopy, TDP-43^{WT}-DsRed was observed to form cytosolic foci in yeast cells, and there was minimal colocalisation with the SG protein PUB1, indicating that these TDP-43 foci likely represented pathological inclusions that were distinct from SGs (Table 3.2, section 3.3.2 and Figure S3.10, Appendix I). The localisation of CDC48-EGFP was unique in yeast expressing TDP-43^{WT}-DsRed compared to control diploid CDC48-EGFP/^{GAL}DsRed^{empty} yeast; it was observed to colocalise with cytosolic TDP-43^{WT}-DsRed foci. This apparent colocalisation may have been due to sequestration of CDC48-EGFP into TDP-

43 inclusions. Pathologically mislocalised, aggregated TDP-43^{WT}-DsRed may thus have impaired CDC48 function by depleting its functional levels in cells. Moreover, the decreased levels of CDC48 and ATG8 in yeast expressing TDP-43^{WT}-DsRed further suggest that pathological TDP-43^{WT}-DsRed may have aberrantly interacted with these proteins, consequently impairing their functions in autophagy. Potentially, TDP-43-mediated impairment of the functions of CDC48 and ATG8 in autophagy may have further enabled aggregated TDP-43^{WT}-DsRed to escape autophagic clearance and to accumulate in cells. To explore this hypothesis, immunocytochemistry to probe for ATG8 and other autophagy markers, including the yeast orthologue of beclin-1, VPS30, in CDC48-EGFP/^{GAL}TDP-43^{WT}-DsRed yeast at several time points is required in order to measure autophagic flux and determine if autophagy is impaired in yeast expressing TDP-43^{WT}-DsRed.

3.4.7 Up-regulation of key UPS proteins is associated with an absence of SOD1^{A4V} toxicity in yeast

An intriguing observation in the work presented in this chapter is that the expression of human *SOD1* containing the ALS-causing A4V mutation did not cause toxicity in yeast, whereas this mutation is associated with a rapidly progressive disease course in humans (Cudkowicz *et al.* 1997, Juneja *et al.* 1997). Coinciding with this distinct lack of toxicity in each of the diploid EGFP-fusion/^{GAL}SOD1^{A4V}-DsRed strains was up-regulation of three proteins with important roles in ubiquitin-dependent protein degradation; UBA1, PRE2 and UFD1. The secondary interactors of these proteins, PRE7 and PUP1, are β-subunits of the 20S proteasome complex, as is the primary hit PRE2. Interestingly, another β-subunit of the 20S proteasome complex, PRE3, was down-regulated in yeast expressing SOD1^{A4V}-DsRed.

The down-regulation of PRE3 is surprising given the up-regulation of UBA1, PRE2 and UFD1 as each of these proteins have functions in the UPS. Specifically, this raises the question as to why one key catalytic β-subunit of the proteasome was up-regulated (PRE2), while another key

catalytic β-subunit was down-regulated (PRE3). Differential regulation of proteasome subunits has been investigated in relation to the changes that occur throughout diverse processes including neonatal development, aging, cellular stress responses, cellular replicative senescence, and in response to targeted RNAi of specific proteasome subunits (Shibatani *et al.* 1996, Keller *et al.* 2000, Wójcik and DeMartino 2002, Chondrogianni *et al.* 2003, Claud *et al.* 2014). These findings demonstrate that differential regulation of specific proteasome subunits can enable cells to fine-tune their responses to changes in the intracellular environment, increasing their capacity to adapt. For instance, overexpression of catalytic β-subunits of the 20S proteasome complex can lead to augmentation of the specific catalytic activity of the overexpressed β-subunit (Gaczynska *et al.* 1994, Gaczynska *et al.* 1996). Overexpression of the β5 subunit in human fibroblasts has been reported to increase the replicative potential of cells (Chondrogianni *et al.* 2005). In the present work, the increased levels of PRE2, the β5 subunit of the 20S proteasome complex, in yeast expressing SOD1^{A4V}-DsRed may indicate that cells had an increased requirement for the catalytic chymotryptic activity of this subunit. Moreover, there may be decreased demand for the catalytic activity of the PRE3 β-subunit in these cells, and thus it was consequently down-regulated to further enable the up-regulation of PRE2. In this case, the cellular levels of PRE2 β5 subunits may even be a critical determinant of proteasome activity in cells expressing SOD1^{A4V}-DsRed. It has been hypothesised that reduced availability of β-subunits in cells is a rate-limiting factor in proteasome activity (Chondrogianni *et al.* 2005). In the present work, as yeast expressing SOD1^{A4V}-DsRed did not exhibit reduced cellular viability, down-regulation of PRE3 in the context of up-regulated PRE2 was not detrimental to the viability of yeast.

The up-regulation of UBA1, UFD1 and PRE2 suggest that UPS activity was increased in cells expressing SOD1^{A4V}-DsRed. Moreover, the common, central interactor of the primary hits and secondary interactors, RPS31, is one of the two ubiquitin-ribosomal subunit fusion proteins that

are conserved in eukaryotes (Finley *et al.* 1989, Oh *et al.* 2013). As such, it is one of four genes that encode ubiquitin in yeast, as is its mammalian orthologue. Common between these primary hits and secondary interactors (PRE7, PUP1 and RPS31) is that through their functions in cells they influence the distribution of ubiquitin in the cellular ubiquitin pools. In particular, UBA1 is a key enzyme that modulates the activated ubiquitin pool. It functions at the apex of the UPS, mediating ATP- and Mg^{2+}-dependent activation of ubiquitin before it is transferred to one of ~40 E2 enzymes which work in co-operation with one of > 600 E3 ligases to conjugate ubiquitin to target proteins (Ayusawa *et al.* 1992, Cook and Chock 1992, Clague *et al.* 2015). It is thus the key driver of the UPS. The increased levels of UBA1 and the other proteins of the UPS, and the lack of toxicity of $SOD1^{A4V}$-DsRed, suggest that yeast effected these changes in response to $SOD1^{A4V}$ and this protected against the toxicity of $SOD1^{A4V}$. Indeed, extensive evidence suggests that dysfunction of the UPS contributes to motor neuron degeneration in ALS. This includes, but is not limited to, the universal presence of ubiquitin and the frequent detection of proteasome subunits in inclusions in ALS patients' motor neurons (Leigh *et al.* 1991, Seilhean *et al.* 2004). It is thus warranted that the effect of increased levels and activity of key UPS proteins be investigated in neuronal cell culture models to gain an understanding as to whether increased UPS functionality can afford protection in neurons expressing ALS-causing mutations.

3.4.8 Concluding statements

The complexity of molecular mechanisms that underlie ALS and other neurodegenerative diseases make for an exceedingly challenging task in elucidating potential proteins and molecular processes that could be targeted for the development of a therapy. However, yeast represent a good model system to explore the fundamental molecular changes that are involved in neurodegenerative diseases. This is because many of the molecular disturbances involved in neurodegeneration occur in pathways of the proteostasis network that are well conserved

amongst eukaryotic organisms. In the work presented in this chapter, the heterologous expression of human TDP-43, FUS and SOD1^{A4V} in 128 yeast strains from the EGFP-fusion collection (Huh *et al.* 2003) led to the identification of processes that are potentially involved in cellular responses to the pathogenic mechanisms that underlie ALS. Moreover, each of these three ALS-associated proteins were found to have their own unique 'fingerprint' in terms of the specific cellular response they elicited. Indeed, the pathways by which these three ALS-associated proteins aggregate in cells are distinct to each (Farrawell *et al.* 2015). Validation of these findings in neuronal cell culture models will provide the basis for further studies into the specific roles of the differentially-regulated proteins, and the pathways in which they function, in ALS. Potentially, ALS linked to mutations in *TARDBP, FUS* and *SOD1* may benefit from, if not require, therapeutic targets that are specific to each.

Chapter 4: Increased levels of UBA1 protect against SOD1^{A4V} toxicity in NSC-34 cells

4.1 Introduction

Ubiquitin is essential for the regulation of many aspects of cell biology. In the neurodegeneration field, it is well known for its role in the degradation of misfolded proteins. However, beyond tagging proteins for degradation, ubiquitylation is one of the most abundant protein modifications in cellular signalling, controlling numerous cellular pathways such as transcription, translation, vesicle transport and apoptosis (Winston *et al.* 1999, Deng *et al.* 2000, Hoppe *et al.* 2000, Spence *et al.* 2000, Hoege *et al.* 2002, Haglund *et al.* 2003, Li *et al.* 2003, Margottin-Goguet *et al.* 2003, Wertz *et al.* 2004, Carter *et al.* 2007, Kravtsova-Ivantsiv *et al.* 2009, Raiborg and Stenmark 2009, Boname *et al.* 2010, Dynek *et al.* 2010, Goto *et al.* 2010, Ren and Hurley 2010, Gerlach *et al.* 2011, Ikeda *et al.* 2011). Ubiquitin labels substrate proteins via a highly ordered multi-step enzymatic cascade, with specific differences in the length and topology of poly-ubiquitin chains determining a range of signalling outcomes or proteolytic degradation via the proteasome. In the nervous system, the UPS contributes to the regulation of many aspects of neural function, such as neuronal growth and development, neuronal excitability, neurotransmission, long-term potentiation (LTP) and synapse formation and elimination (Mabb and Ehlers 2010, Kawabe and Brose 2011). Many factors can influence ubiquitin homeostasis, and accumulation of ubiquitin in large misfolded protein deposits found in ALS pathology may indirectly interfere with other essential ubiquitin-dependent cellular processes (Farrawell *et al.* 2018). Indeed, neurons are sensitive to ubiquitin dyshomeostasis, which if prolonged may lead to cell death (Tan *et al.* 2000, Tan *et al.* 2001). UPS function is therefore central to neuronal health and neurodegenerative disease, and ubiquitylation is emerging as a highly promising target for human therapy that remains to be fully exploited (Jankowska *et al.* 2013). However, ubiquitin-dependent cellular processes are highly interconnected, and there is a lack of systematic data on disease-related perturbations in these systems. Therefore, it is critical to gain comprehensive insight into the ubiquitylation machinery

in affected neurons and in response to therapeutic intervention.

Several of the genes implicated in fALS cohorts encode components and regulators of the UPS, including *VCP* (Johnson *et al.* 2010, Abramzon *et al.* 2012), *SQSTM1* (Fecto *et al.* 2011), *UBQLN2* (Deng *et al.* 2011, Teyssou *et al.* 2017), *OPTN* (Maruyama *et al.* 2010), *CCNF* (Williams *et al.* 2016) and *TBK1* (Cirulli *et al.* 2015). Defects in these genes are likely to lead to perturbations in ubiquitin homeostasis, but the precise effect of these mutations on the maintenance of ubiquitin homeostasis is currently unknown. Recent work using proteomics to map the ubiquitin-modified proteome in NSC-34 cells showed significant changes in the distribution of ubiquitin in mutant *SOD1*-expressing cells (Farrawell *et al.* 2018). Mutations in genes such as *TARDBP* also lead to disruption of ubiquitin homeostasis. For example, knockdown of the DUB, UBPY, exacerbated the toxicity of TDP-43 in *Drosophila melanogaster* (Hans *et al.* 2014).

Ubiquitin regulates cellular concentrations of TDP-43 and SOD1 (Miyazaki *et al.* 2004, Scotter *et al.* 2014) and their aberrant accumulation can be triggered by inhibition of the proteasome. In human skin fibroblasts, significantly higher accumulation of a UPS reporter was observed in ALS patient-derived cells compared to those from controls (Yang *et al.* 2015). Cell models of *CCNF*-linked fALS were also found to have higher levels of the reporter compared to controls (Williams *et al.* 2016), consistent with a compromised UPS in ALS. Similar reporters of UPS function demonstrated UPS dysfunction in cultures of NSC-34 cells expressing mutant *SOD1* (Crippa *et al.* 2010) and in the spinal motor neurons of mice with ALS caused by a *SOD1* mutation (Basso *et al.* 2009). Indeed, proteasomal clearance of mutant SOD1 was reported to be impaired uniquely in NSC-34 cells in contrast to muscle cells, which exhibited efficient degradation of mutant SOD1 (Onesto *et al.* 2011). Recent work has shown that *C9ORF72* poly-(Gly-Ala) aggregates sequester a large proportion of the cell's proteasomes and functionally impair them (Guo *et al.* 2018). Moreover, motor neuron-specific knockdown of proteasome

subunit RPT3 in the absence of an ALS genetic background can result in an ALS phenotype in mice, including locomotor dysfunction, progressive motor neuron loss and mislocalisation of TDP-43, FUS, UBQLN2, and OPTN (Tashiro *et al.* 2012). These data are consistent with a reduction in UPS capacity being sufficient to drive ALS pathology in mice. Indeed, not even overexpression of human mutant TDP-43 gives such an accurate reproduction of a human ALS-like phenotype in mice. The increased expression of components of the ubiquitin-dependent proteolysis machinery were identified as a significant distinguishing factor in the transcriptome of microdissected resistant oculomotor neurons compared to vulnerable motor neurons from the human spinal cord (Brockington *et al.* 2013), suggesting increased UPS capacity is protective in ALS.

In a screen for responses in the proteome to expression of $SOD1^{A4V}$ in yeast (Chapter III), the E1 ubiquitin-activating enzyme UBA1 was found to be up-regulated relative to control cells. The increased levels of UBA1 correlated with a distinct lack of $SOD1^{A4V}$ toxicity, which is in contrast to the toxicity this *SOD1* mutation causes in humans (Cudkowicz *et al.* 1997, Juneja *et al.* 1997). UBA1 is the primary initiator of the UPS cascade, mediating ATP- and Mg^{2+}-dependent activation of ubiquitin before it is transferred to one of ~40 E2 enzymes which work in co-operation with one of > 600 E3 ligases to conjugate ubiquitin to target proteins. UBA1 is fundamental to the UPS, and its downregulation attenuates UPS activity (Ciechanover *et al.* 1984, Ghaboosi and Deshaies 2007, Qin *et al.* 2016). It is known to be vital for motor neuron health as mutations in *UBA1* result in an infant onset motor neuron disease, X-linked spinal muscular atrophy (XL-SMA; (Ramser *et al.* 2008)). XL-SMA represents a rare form of SMA, however, notably, UBA1 is present at decreased levels in the majority of SMA cases caused by mutations in *SMN1* (Wishart *et al.* 2014, Powis *et al.* 2016). Increasing the levels of UBA1 restored motor performance and increased lifespan in mouse and zebrafish models of SMA (Powis *et al.* 2016). Hence, work presented in this chapter was aimed at investigating the

hypothesis that increased UBA1 expression is protective against cellular toxicity induced by $SOD1^{A4V}$. To investigate this hypothesis, the murine NSC-34 cell line was used as a mammalian neuronal cellular model of $SOD1^{A4V}$-ALS. The specific aims of the work presented in this chapter were to:

(i) compare the levels of endogenous UBA1 in mammalian neuronal cells overexpressing $SOD1^{A4V}$ with cells overexpressing $SOD1^{WT}$,

(ii) determine the effect of increased UBA1 expression on $SOD1^{A4V}$-induced toxicity in NSC-34 cells and

(iii) investigate the effect of increased UBA1 expression on $SOD1^{A4V}$ aggregation in cells.

4.2 Materials and methods

Saponin (Saponin from Quillaja bark, Cat. No. S4521-10G) was from Sigma-Aldrich (St. Louis, MO, USA).

4.2.1 Plasmid constructs for NSC-34 cells

The pEGFP-N1 vectors containing human $SOD1^{WT}$ ($SOD1^{WT}$-EGFP) and $SOD1^{A4V}$ ($SOD1^{A4V}$-EGFP) were described in Chapter II. The pEGFP-N1 vector, which encodes for EGFP alone, was used as a control for EGFP-tagged SOD1 expression. pCDNA3.1(+) constructs containing murine wild-type UBA1 ($UBA1^{WT}$) or a catalytically-inactive mutant C632S UBA1 ($UBA1^{C632S}$) isoform were generated by sub-cloning murine $UBA1^{WT}$ from pET28-mE1 (Addgene plasmid 32534, provided by Jorge Eduardo Azevedo (Carvalho *et al.* 2012)) into pCDNA3.1(+) and replacing Cys-632 with Ser, via GenScript's customised cloning and site-directed mutagenesis services. The pmCherry-C1 vector, which encodes mCherry alone, was used as a control in place of $UBA1^{WT}$ and $UBA1^{C632S}$ in co-transfections with $SOD1^{WT}$-EGFP or $SOD1^{A4V}$-EGFP. In these co-transfections the expression of mCherry alone was used to

measure co-transfection efficiency and to account for cell viability in the absence of $UBA1^{WT}$ and $UBA1^{C632S}$.

4.2.2 Mammalian cell culture and transfections

NSC-34 cells (neuroblastoma × spinal cord hybrid) were maintained as described in Chapter II. Cells were seeded at 1×10^5 cells/mL in DMEM/F-12/FBS into 6-well plates to prepare cell lysates for immunoblot analyses, 8-well µ-Slides (Ibidi, Planegg-Martinsried, Germany) for confocal microscopy, or 24-well plates for flow cytometry or IncuCyte® ZOOM imaging. Cells were transfected 24 h later using Lipofectamine® 3000 (Invitrogen, USA) according to the manufacturer's instructions, with 0.2 µg DNA per well for 8-well µ-Slides, 0.5 µg DNA per well for 24-well plates or 2.5 µg DNA per well for 6-well plates. For co-transfections the amount of DNA was divided equally between constructs. Non-transfected cells were included as controls in all experiments. For all experiments, a time-point of 48 h post-transfection was used for cell lysis or fixing for confocal microscopy.

4.2.3 IncuCyte® ZOOM live cell imaging

IncuCyte® ZOOM live cell imaging and analysis was used to carry out two different measures in NSC-34 cells transiently transfected with $SOD1^{WT}$-EGFP, $SOD1^{A4V}$-EGFP or EGFP alone, or co-transfected with these constructs together with either $UBA1^{WT}$, $UBA1^{C632S}$ or mCherry alone. One of the experiments involved monitoring the relative population growth of transfected cells (EGFP-positive cells) over 80 h. The net cell population growth (rate of cell division – rate of cell death) was used as a measure of cell viability, on the basis that toxicity caused by the overexpression of $SOD1^{A4V}$-EGFP would impair cellular ability to proliferate and/or result in the loss of cells relative to control cells overexpressing $SOD1^{WT}$-EGFP or EGFP alone. NSC-34 cells were transfected in 6-well plates and were re-plated at 24 h post-transfection at uniform cell density (5×10^4 cells/mL) in 200 µL/well DMEM/F-12/FBS into 96-well plates and imaged using the 10× objective lens of an IncuCyte® ZOOM over 70-90 h. To quantify the numbers of

viable transfected cells, a processing definition in the IncuCyte® ZOOM software was optimised to identify and count transfected cells based on a minimum level of EGFP fluorescence, and viable cells based on a minimum size. Non-transfected controls were used to account for and exclude background fluorescence and fluorescent artefacts, cell debris and dying cells.

The second experiment quantified cells containing inclusions using a modification of a saponin-permeabilisation protocol described by Pokrishevsky *et al.* (2018). Saponin is a mild, cholesterol-chelating detergent that creates pores in the plasma membrane of cells (Symons and Mitchison 1991). These pores allow soluble intracellular proteins to diffuse out of the cell, while trapping insoluble proteinaceous structures. NSC-34 cells were transfected with each expression construct in quadruplicate in 96-well plates, and after 48 h were imaged using an IncuCyte® ZOOM. These pre-permeabilisation images were used to measure the numbers of cells that were transfected (EGFP-positive) in each well. After imaging, cells were incubated with 0.03% (w/v) saponin in PBS for 10 min at RT to create pores in the cells' plasma membranes. Saponin-treated cells were then imaged again to measure the numbers of cells in which non-diffusable, insoluble EGFP-positive material remained following permeabilisation. The percentage of transfected cells containing insoluble EGFP-fusion proteins were then calculated using the following formula:

$$\%\ transfected\ cells\ containing\ insoluble\ EGFP\ fusion\ proteins = \left(\frac{Number\ of\ EGFP\ positive\ cells\ post\ permeabilisation}{Number\ of\ EGFP\ positive\ cells\ pre\ permeabilisation}\right) \times 100$$

Equation 4.1.

For all IncuCyte® experiments, the mean ± SEM was calculated across quadruplicate replicates, and used for statistical analyses.

4.2.4 Treatment with MG132

To test the susceptibility of cells to proteasome inhibition, NSC-34 cells transfected with each of $SOD1^{WT}$-EGFP, $SOD1^{A4V}$-EGFP or EGFP alone were first replated at 24 h post-transfection at uniform cell density and imaged in an IncuCyte® ZOOM. At 36 h post-transfection cells were treated with 0, 0.5, 1, 1.5, 2, 2.5, 3.5 or 5 μM of the proteasome inhibitor MG132 and imaging was continued for the next 50 h. Out of two independent experiments, for each concentration of MG132, the numbers of cells at 48 h post-transfection were quantified and the IC_{50} was calculated for cells transfected with $SOD1^{WT}$-EGFP, $SOD1^{A4V}$-EGFP or EGFP alone. To compare the IC_{50} for cells expressing $SOD1^{WT}$-EGFP, $SOD1^{A4V}$-EGFP or EGFP alone, the numbers of cells expressing $SOD1^{A4V}$-EGFP or EGFP alone were normalised to the numbers of cells expressing $SOD1^{WT}$-EGFP.

4.2.5 Cell lysis, protein extraction and quantification

NSC-34 cells transfected with $SOD1^{WT}$-EGFP, $SOD1^{A4V}$-EGFP or EGFP alone and grown in 6-well plates were harvested at 48 h post-transfection using 0.05% trypsin-EDTA. Cells were washed with PBS before being resuspended in RIPA buffer (50 mM Tris-HCl, pH 7.4 containing 0.5% (w/v) sodium deoxycholate, 150 mM NaCl, 1 mM EDTA, 1% (v/v) Triton X-100, 0.1% (w/v) SDS and Halt™ Protease Inhibitor Cocktail (Thermo Fisher Scientific, Sydney, Australia)) and incubated overnight at 4 °C to promote cell lysis. Using 23 G needles, each cell suspension was drawn up and down twelve times to ensure the nuclear membrane was broken and the chromosomal DNA sheared. An aliquot was taken for total protein quantitation by bicinchoninic acid (BCA) assay and the remainder of the samples stored at -80 °C.

4.2.6 Immunoblotting

The UBA1 antibody used in this study was a rabbit monoclonal to human UBA1, and had been commercially tested for reactivity with mouse, rat and human UBA1. As a monoclonal

antibody, it should have high specificity and minimal cross-reactivity, recognising a single epitope at the C-terminus of UBA1. As this epitope is at the C-terminus of UBA1, this antibody should react with both of the isoforms of UBA1 (UBA1a and UBA1b), which differ only at the N-terminus (there are an additional 40 amino acids at the N-terminus of UBA1a) (Stephen *et al.* 1997). For SDS-PAGE and immunoblotting, 100 µg of total cellular protein from NSC-34 lysates were prepared in appropriate volumes of 2× loading buffer (final concentrations: 2% (w/v) SDS, 0.5 M Tris-HCl, 25% (w/v) glycerol, 0.01% (w/v) bromophenol blue, 5% (v/v) β-mercaptoethanol). Samples were reduced and denatured by heating at 95 °C for 5 min before being electrophoresed on a Mini-PROTEAN TGX Stain-Free Gel (Bio-Rad, USA) for 1.5 h at 100 V. Prior to transfer, the total protein loaded per lane on each gel was imaged using a Criterion Stain-Free Imager (Bio-Rad, USA). Proteins were transferred onto a nitrocellulose membrane (Pall Corporation, USA) at 20 V overnight at 4 °C. The membrane was blocked in 5% (w/v) skim milk powder in Tris-buffered saline (TBS) supplemented with 0.05% (v/v) Tween-20 (TBS-T) overnight at 4 °C, followed by overnight incubation with rabbit monoclonal antibody to E1 ubiquitin activating enzyme (ab181225, Abcam) at 1:10,000 dilution in 5% (w/v) skim milk powder in TBS-T. The following day the membrane was washed three times with TBS-T over 30 min before being incubated overnight at 4 °C with horseradish peroxidise (HRP)-conjugated goat anti-rabbit antibody (A16104, Invitrogen) at 1:2,000 dilution in 5% skim milk powder in TBS-T. The membrane was then washed three times with TBS-T over 45 min and visualised with WesternBright™ Sirius chemiluminescent HRP substrate (Advansta) on an Amersham Imager 6600RGB. Four separate SDS-PAGE and immunoblotting experiments were carried out on cell lysates prepared in four separate transfection experiments. To measure the relative density of protein bands resolved in each immunoblotting experiment, the density of each band and of the total protein loaded in the respective lane of the gel were quantified using Image Studio™ software (LI-COR Biosciences, USA). The calculated density

of each band was then normalised to the calculated total protein density in the respective gel lane as is standard practice for immunoblots. The mean normalised relative band densities from the four biological repeats were compared using one-way ANOVA with Tukey's multiple comparisons post-hoc test.

4.2.7 Fixing, permeabilising, immunolabelling and confocal microscopy

At 48 h post-transfection, NSC-34 cells transfected with $SOD1^{WT}$-EGFP, $SOD1^{A4V}$-EGFP or EGFP alone, or co-transfected with these constructs as well as $UBA1^{WT}$, $UBA1^{C632S}$ or mCherry alone, were fixed in 4% (w/v) paraformaldehyde in PBS for 20 min at room temperature in monolayers in 8-well µ-Slides for confocal microscopy. Cells were then washed three times over 15 min with PBS (pH 7.4), and permeabilised with 1% (v/v) Triton X-100 in PBS for 30 min on crushed ice. Following permeabilisation, cells were washed twice over 10 min with PBS and blocked for 1 h at room temperature with 5% (v/v) FBS, 1% (w/v) bovine serum albumin, 0.3% (v/v) Triton X-100 in PBS. After blocking, cells were washed twice over 10 min with PBS and incubated for 16 h at 4 °C with rabbit monoclonal antibody to E1 ubiquitin activating enzyme (ab181225, Abcam) or rabbit IgG monoclonal isotype control (ab172730, Abcam) at 1:200 dilution. Primary antibodies were diluted in 1% (w/v) bovine serum albumin, 0.1% (v/v) Triton X-100 in PBS. The following day, cells were washed twice over 10 min with PBS and incubated for 5 h at room temperature with Alexa Fluor™ 647 goat anti-rabbit IgG (H+L) secondary antibody (ab150079, Abcam) at 1:500 dilution. Secondary antibodies were diluted in 1% (w/v) bovine serum albumin, 0.1% (v/v) Triton X-100 in PBS. Cells were then washed three times over 15 min in PBS.

Cells were imaged using a Leica TCS SP5 II confocal microscope with a 63× oil-immersion objective lens (Leica Microsystems, Wetzlar, Germany). EGFP fluorescence was excited at 488 nm by an argon laser; mCherry fluorescence was excited at 561 nm by a DPS 561 laser. Fluorescent emissions were acquired by sequential scanning using the Leica Application Suite

– Advanced Fluorescence (LAS-AF) software (version 3, Leica Microsystems, Wetzlar, Germany).

4.3 Results

4.3.1 Endogenous UBA1 levels are unaffected by overexpression of SOD1^{A4V}-EGFP in NSC-34 cells

The A4V mutation in *SOD1* causes one of the most aggressive forms of ALS (Cudkowicz *et al.* 1997, Juneja *et al.* 1997, Lemmens *et al.* 2007). In order to measure the effects of SOD1^{A4V}-EGFP overexpression on the viability of NSC-34 cells, live cell imaging on an IncuCyte® ZOOM was used to monitor cells over a 70 h time period. In this assay, reduced net population growth of cells overexpressing SOD1^{A4V}-EGFP relative to control cells overexpressing SOD1^{WT}-EGFP or EGFP alone was considered to be a toxic effect of SOD1^{A4V}-EGFP. Over the imaging period the numbers of cells expressing SOD1^{WT}-EGFP and EGFP alone steadily increased, while the numbers of cells expressing SOD1^{A4V}-EGFP increased at a slower rate (Figure 4.1, a). At 48 h post-replating there were significantly lower numbers of cells expressing SOD1^{A4V}-EGFP than cells expressing SOD1^{WT}-EGFP ($p = 0.0151$) or EGFP alone ($p = 0.0435$) (Figure 4.1, b). This indicates that the overexpression of SOD1^{A4V}-EGFP caused toxicity.

To characterise the appearance of transfected cells and the intracellular localisation of the EGFP-fusion proteins, cells were imaged 48 h post-transfection using confocal microscopy. While SOD1^{WT}-EGFP was observed to have a relatively even distribution throughout the cytoplasm and within nuclei, in a proportion of cells SOD1^{A4V}-EGFP formed multiple large inclusions in the cytoplasm (Figure 4.1, c).

Given that the heterologous expression of human SOD1^{A4V} in yeast did not cause toxicity, that there was an absence of SOD1^{A4V} aggregation in yeast cells, and that these observations coincided with increased levels of yeast UBA1 (Chapter III), the level of endogenous murine

UBA1 in NSC-34 cells expressing SOD1^{A4V}-EGFP, SOD1^{WT}-EGFP or EGFP alone was investigated. Immunoblot analysis showed that there were no differences in the levels of UBA1 (~118 kDa) between NSC-34 cells overexpressing SOD1^{A4V}-EGFP, SOD1^{WT}-EGFP and EGFP alone (Figure 4.1, d).

Considerable evidence supports impaired proteasome activity as one of the downstream toxic effects of mutant SOD1 expression in motor neurons (Urushitani *et al.* 2002, Allen *et al.* 2003, Kabashi *et al.* 2004, Cheroni *et al.* 2009, Crippa *et al.* 2010, Onesto *et al.* 2011). In yeast expressing human SOD1^{A4V} the levels of PRE2, a key proteasome subunit, and UFD1, a protein with important functions in ubiquitin-dependent protein degradation, were both increased (Chapter III). Given these data, the susceptibility of NSC-34 cells expressing SOD1^{A4V}-EGFP to proteasome inhibition were tested. Cells overexpressing SOD1^{A4V}-EGFP were more sensitive to proteasome inhibition by MG132 than cells overexpressing SOD1^{WT}-EGFP or EGFP alone. This was evident through the IC_{50} for cells overexpressing SOD1^{A4V}-EGFP being markedly lower than for cells overexpressing SOD1^{WT}-EGFP or EGFP alone (Figure 4.1, e).

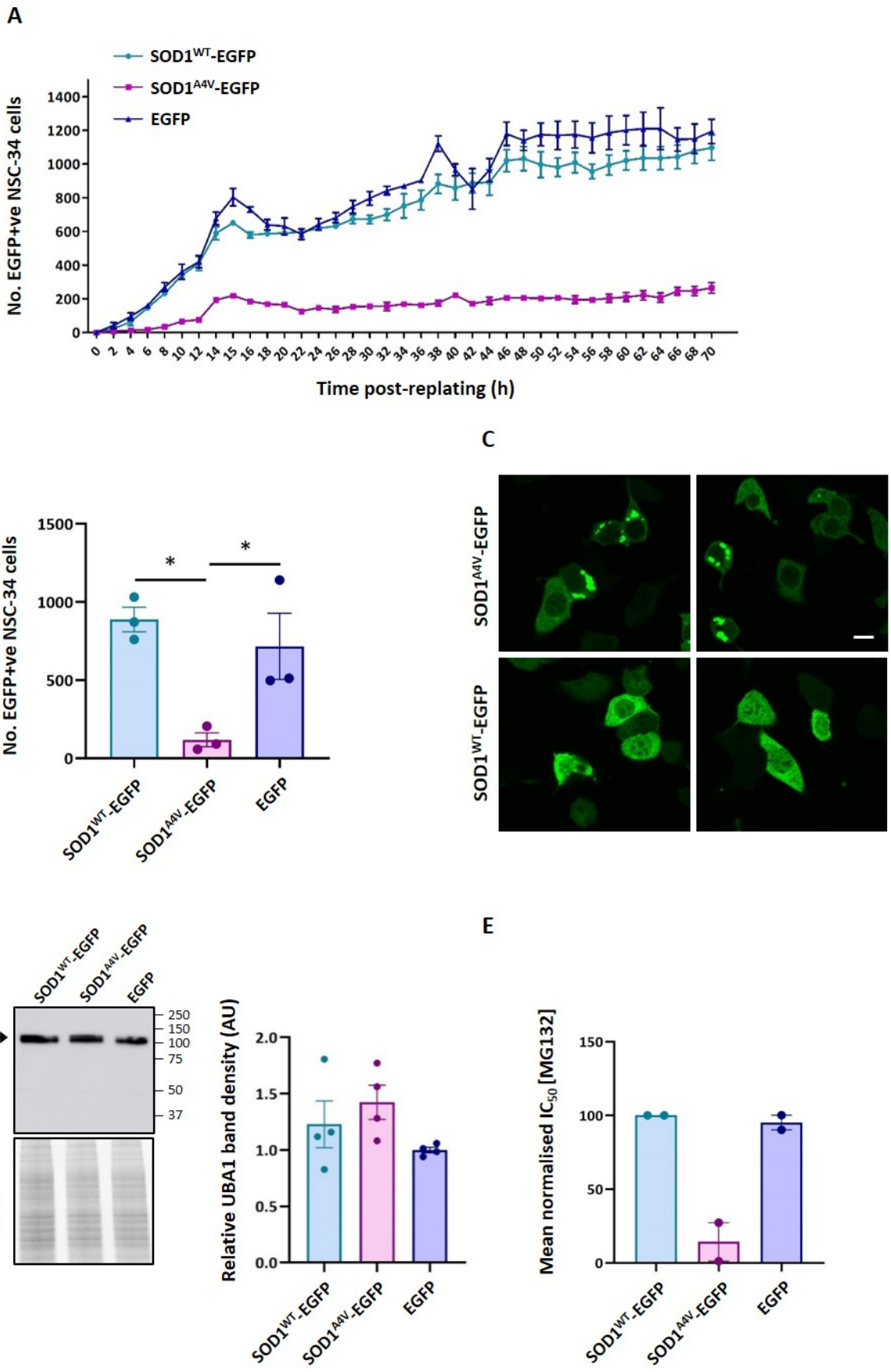
A
SOD1WT-EGFP
SOD1A4V-EGFP
EGFP
No. EGFP+ve NSC-34 cells
Time post-replating (h)
B
No. EGFP+ve NSC-34 cells
SOD1WT-EGFP
SOD1A4V-EGFP
EGFP
C
SOD1A4V-EGFP
SOD1WT-EGFP
D
UBA1
Total protein loading
Relative UBA1 band density (AU)
E
Mean normalised IC50 [MG132]

Figure 4.1. Endogenous UBA1 levels are unaffected by overexpression of SOD1^{A4V}-EGFP in NSC-34 cells. (A) Representative time-resolved plot from one of three experiments showing the numbers of NSC-34 cells transiently transfected with either SOD1^{WT}-EGFP, SOD1^{A4V}-EGFP or EGFP alone. Over time, cells overexpressing SOD1^{WT}-EGFP or EGFP alone continued to proliferate while the numbers of cells overexpressing SOD1^{A4V} steadily plateaued after the initial imaging period. Cells were replated at 24 h post-transfection at uniform cell density, before being imaged in an IncuCyte® ZOOM over 70 hours. (B) Comparison of the numbers of cells expressing SOD1^{WT}-EGFP, SOD1^{A4V}-EGFP or EGFP alone 48 h after replating and imaging in the IncuCyte® ZOOM. Graph represents the mean ± SEM from three independent experiments. Differences between the means were determined using a one-Way ANOVA followed by Tukey's multiple comparison test. * indicates $p < 0.05$. (C) SOD1^{A4V}-EGFP forms cytoplasmic aggregates in NSC-34 cells, while SOD1^{WT}-EGFP is diffusely distributed throughout the cell. Cells were imaged at 48 h post-transfection on a Leica TCS SP5 II confocal microscope. Scale bar represents 10 µm. (D) The levels of endogenous UBA1 in NSC-34 cells are not altered in cells overexpressing SOD1^{A4V}. NSC-34 cells overexpressing SOD1^{WT}-EGFP, SOD1^{A4V}-EGFP or EGFP alone were lysed at 48 h post-transfection. 100 µg total protein from each lysate were run on a SDS-PAGE gel and immunoblotted for UBA1. UBA1 band densities were normalised to total protein loaded in each gel lane. Total protein loading was assessed by imaging stain-free gels prior to transfer. Representative immunoblot showing bands corresponding to UBA1 (~118 kDa). Graph represents the mean ± SEM from four immunoblots of four independent transfection experiments. (E) NSC-34 cells overexpressing SOD1^{A4V}-EGFP are more susceptible to proteasome inhibition than cells overexpressing SOD1^{WT}-EGFP or EGFP alone. Cells were replated at 24 h post-transfection at uniform cell density, then treated with different concentrations (0, 0.5, 1, 1.5, 2, 2.5, 3.5 or 5 µM) of the proteasome inhibitor MG132 at 36 h post-transfection and imaged in an IncuCyte® ZOOM over 50 hours. 48 h after MG132 treatment, the concentration of MG132 required to cause half the number of cells overexpressing SOD1^{A4V}-EGFP to die (IC_{50}) was lower than that of cells overexpressing SOD1^{WT}-EGFP or EGFP alone. Graph represents the mean ± SEM from two independent experiments.

4.3.2 UBA1 expression is similar in NSC-34 cells transfected with either pcDNA3.1(+)-UBA1^{WT} or pcDNA3.1(+)-UBA1^{C632S} plasmids

To explore the effect of increasing the levels of UBA1 in NSC-34 cells overexpressing SOD1^{A4V}-EGFP, two plasmid constructs were generated; pcDNA3.1(+) containing murine UBA1^{WT} or UBA1^{C632S} (UBA1 with mutation of Cys-632, the residue responsible for its E1 catalytic activity) (Hatfield and Vierstra 1992, Forrester *et al.* 2011, Yang *et al.* 2012). To ensure that any effects observed in cells overexpressing UBA1^{WT} were due to the enzymatic capacity of UBA1 and not from differences in expression levels between pcDNA3.1(+)-UBA1^{WT} and pcDNA3.1(+)-UBA1^{C632S}, endogenous and overexpressed UBA1 levels were examined by immunocytochemistry and confocal microscopy. Visual inspection of the confocal images showed that the anti-UBA1 immunostaining was stronger in cells transfected with pcDNA3.1(+)-UBA1^{WT} or pcDNA3.1(+)-UBA1^{C632S} than in cells that were not transfected with these constructs (Figure 4.2, a). UBA1 appeared to be localised throughout the cytoplasm and within nuclei but staining was more intense in nuclei and in small foci throughout the

cytoplasm. This localisation pattern aligns with findings from other studies showing that UBA1 is present in nuclei and throughout the cytoplasm, including localising at high concentrations to several organelles (Schwartz *et al.* 1992, Moudry *et al.* 2012). Quantification of anti-UBA1 Alexa Fluor™ 647 fluorescence intensity confirmed that there were greater levels of UBA1 in cells transfected with either of the two UBA1 constructs than in non-transfected cells (pcDNA3.1(+)-UBA1^{WT}, $p = 0.0062$; pcDNA3.1(+)-UBA1^{C632S}, $p = 0.0036$) (Figure 4.2, b). Importantly, UBA1^{WT} and UBA1^{C632S} were expressed at comparable levels in transfected cells, with no significant differences calculated in the mean anti-UBA1 Alexa Fluor™ 647 fluorescence intensity between cells transfected with each of these two constructs.

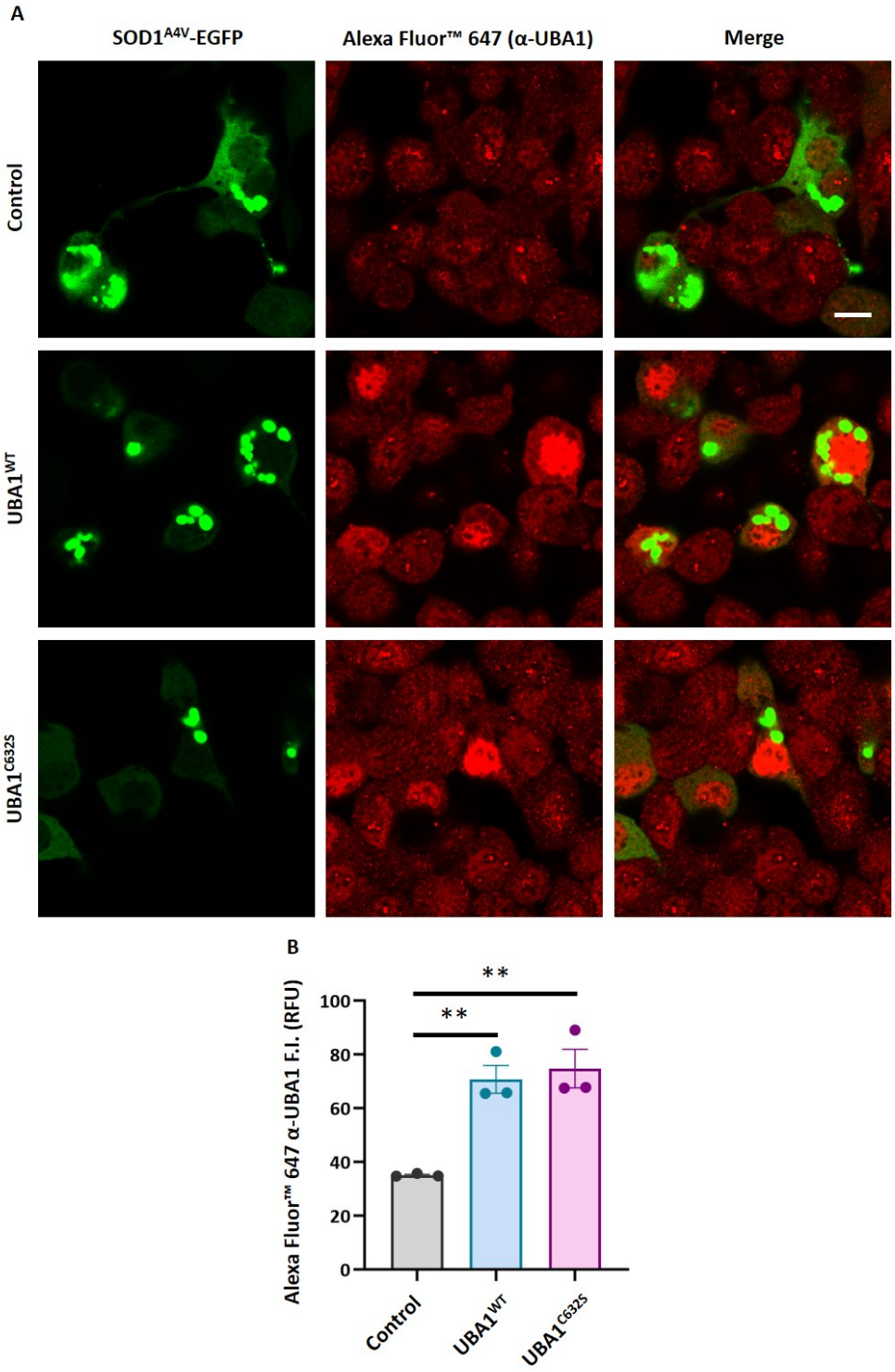

Figure 4.2. UBA1^{WT} and UBA1^{C632S} are expressed at the same levels in transfected NSC-34 cells. (A) Representative images showing immunostaining for UBA1 in NSC-34 cells transiently co-transfected with SOD1^{A4V}-EGFP and to express either mCherry alone ('control'), UBA1^{WT} or UBA1^{C632S}. Cells were fixed, permeabilised and stained for UBA1 (Alexa Fluor™ 647) 48 h post-transfection. Scale bar represents 10 µm. (B) Confocal images of the cells were analysed using a macro in Image J to quantify the fluorescence intensity (F.I.) of the Alexa Fluor™ 647 α-UBA1 staining. Graph represents the mean ± SEM from 3 wells of cells prepared in 3 separate transfection experiments. Means were compared using one-way ANOVA with Tukey's multiple comparisons test. ** indicates $p < 0.01$.

4.3.3 Overexpression of UBA1^{WT} reduces the toxicity of SOD1^{A4V}-EGFP in NSC-34 cells

To test the hypothesis that increased UBA1 expression protects the viability of cells overexpressing mutant SOD1, NSC-34 cells were co-transfected with SOD1^{WT}-EGFP, SOD1^{A4V}-EGFP or EGFP alone and either UBA1^{WT}, UBA1^{C632S} or mCherry alone, and the net population growth of EGFP-positive cells monitored over 90 h using an IncuCyte® ZOOM. As was observed for cells transfected with just SOD1^{WT}-EGFP or SOD1^{A4V}-EGFP (Figure 4.1, a), the numbers of cells overexpressing SOD1^{WT}-EGFP and either UBA1^{WT}, UBA1^{C632S} or mCherry alone continued to increase over the 90 h of imaging (Figure 4.3, a). Within the first ~32 h of imaging, the population growth rate of cells co-expressing SOD1^{A4V}-EGFP and UBA1^{WT} was greater than that of cells co-expressing SOD1^{A4V}-EGFP and UBA1^{C632S} or mCherry alone, such that, 48 h post-transfection, the numbers of cells co-expressing SOD1^{A4V}-EGFP and UBA1^{WT} were significantly greater than the numbers of cells co-expressing SOD1^{A4V}-EGFP and UBA1^{C632S} (p = 0.0020) or mCherry alone (p = 0.0003) (Figure 4.3, b). This suggests that the increased levels of catalytically active UBA1^{WT} buffered against the toxicity caused by SOD1^{A4V}-EGFP overexpression. The sudden decrease in cell numbers after the first 32 h of imaging may be due to a decrease in the availability of UBA1^{WT} in the cells over time, either due to dilution or degradation of the UBA1^{WT} plasmid DNA, or to functional saturation of the exogenous UBA1^{WT} molecules in activating ubiquitin and initiating the ubiquitylation cascade for target proteins.

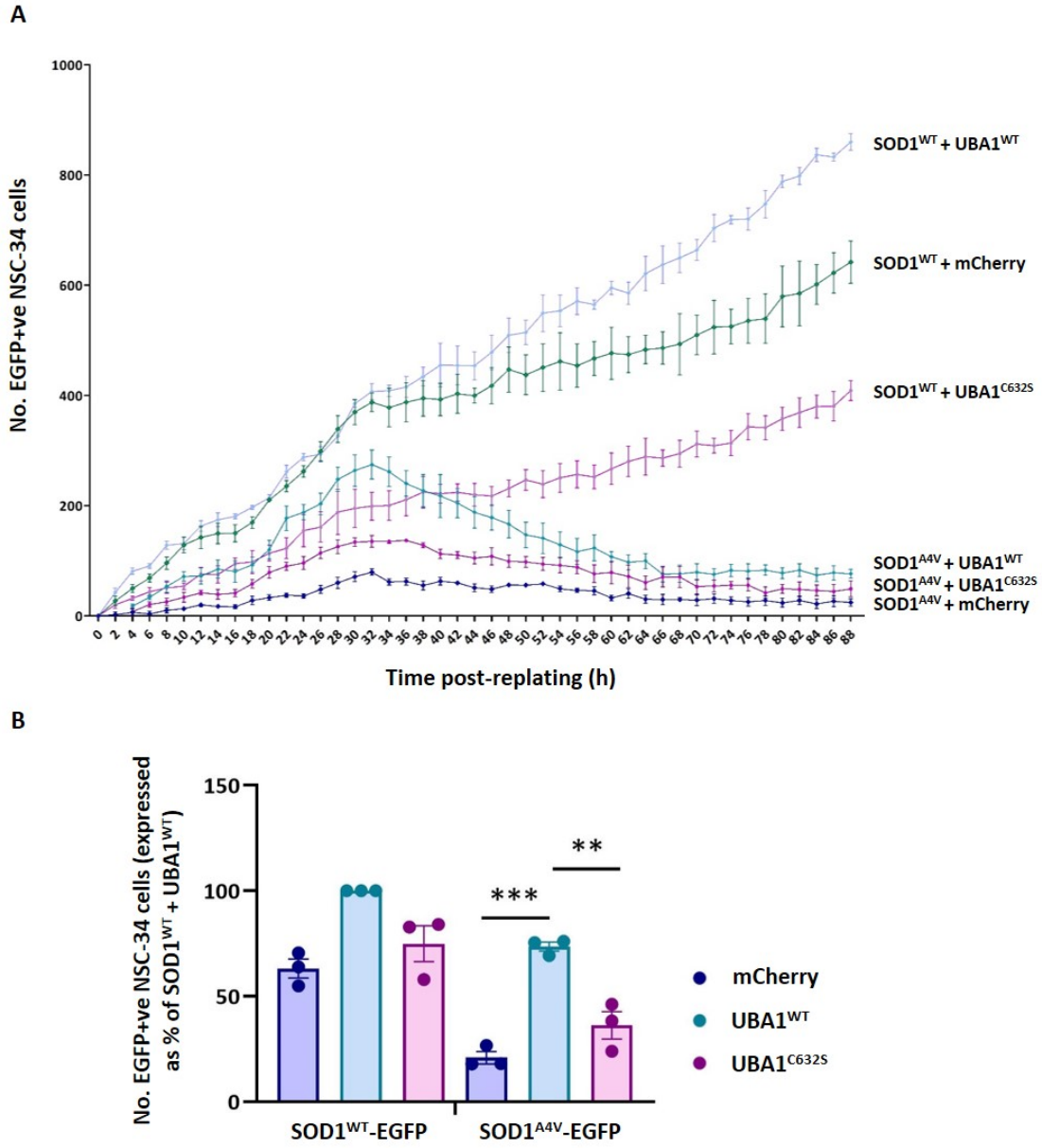

Figure 4.3. UBA1^{WT} overexpression increases viability of NSC-34 cells overexpressing SOD1^{A4V}-EGFP.(A) Representative graph showing numbers of NSC-34 cells transiently co-transfected to express either SOD1^{WT}-EGFP, SOD1^{A4V}-EGFP or EGFP and UBA1^{WT}, the catalytically inactive mutant UBA1^{C632S} or mCherry. Cells were replated at 24 h post-transfection at uniform cell density, before being imaged in an IncuCyte® ZOOM over 90 h. (B) Numbers of co-transfected NSC-34 cells at 48 h post-transfection, normalised to cells co-transfected with SOD1^{WT}-EGFP and UBA1^{WT}. Experiment was performed three times and the bar chart represents mean ± SEM. Differences between the means were determined using one-Way ANOVA followed by Tukey's multiple comparison test. ** indicates $p < 0.01$, *** indicates $p < 0.001$.

4.3.4 SOD1^{A4V}-EGFP aggregation is unaffected by UBA1^{WT} overexpression

After discovering that increased UBA1^{WT} expression protected against the toxicity caused by SOD1^{A4V}-EGFP in NSC-34 cells, it was next explored whether this effect may be mediated by inhibiting the accumulation of SOD1^{A4V}-EGFP aggregates. To quantify the numbers of transfected cells containing SOD1^{A4V}-EGFP aggregates, an assay was used in which the plasma membrane of transfected cells was permeabilised using saponin, allowing soluble intracellular proteins to diffuse out of the cell while trapping insoluble protein material. Cells were imaged pre- and post-permeabilisation with saponin, using an IncuCyte® ZOOM, to quantify numbers of transfected cells and numbers of cells containing insoluble EGFP-fusion proteins.

Saponin-permeabilisation and imaging of NSC-34 cells co-transfected with SOD1^{WT}-EGFP and either UBA1^{WT}, UBA1^{C632S} or mCherry alone showed that there was no fluorescent signal from cells overexpressing SOD1^{WT}-EGFP or EGFP alone following plasma membrane permeabilisation (Figure 4.4). In contrast, after permeabilisation, SOD1^{A4V}-EGFP protein remained in 8.82 ± 1.47%, 13.03 ± 2.31% and 14.3 ± 3.01% of SOD1^{A4V}-EGFP cells co-expressing mCherry alone, UBA1^{WT} and UBA1^{C632S}, respectively, indicating that similar amounts of insoluble, non-diffusable SOD1^{A4V}-EGFP were present in cells under each condition. These results indicate that increased levels of UBA1^{WT} had no impact on the overall numbers of SOD1^{A4V}-EGFP aggregates that formed in cells.

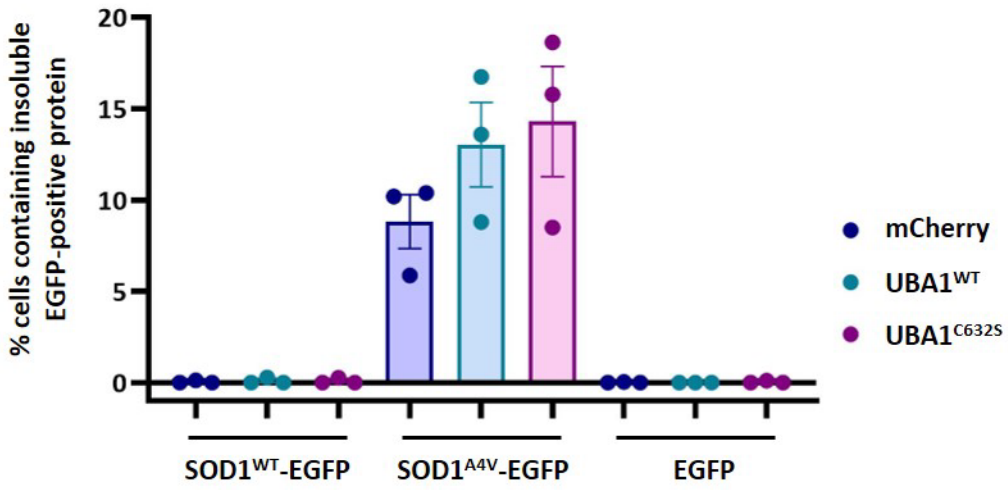

Figure 4.4. UBA1^{WT} overexpression does not affect SOD1^{A4V}-EGFP aggregation in NSC-34 cells. Percentages of transfected cells containing insoluble EGFP-positive inclusions. NSC-34 cells were transiently co-transfected to express either SOD1^{WT}-EGFP, SOD1^{A4V}-EGFP or EGFP alone and UBA1^{WT}, the catalytically inactive mutant UBA1^{C632S} or mCherry alone. After 48 h, cells were imaged on an IncuCyte® ZOOM, followed by incubation with 0.03% (w/v) saponin in PBS for 10 min at room temperature, before being imaged again. Cells were transfected in triplicate, and the experiment was performed three times. The data presented is the mean ± SEM of the percentage of transfected NSC-34 cells containing insoluble EGFP-positive protein following permeabilisation with saponin. The means were compared using one-Way ANOVA followed by Tukey's multiple comparison test.

As well as the toxicity associated with the aggregation of SOD1^{A4V} into insoluble inclusions, several studies have also reported that soluble oligomeric species formed by SOD1^{A4V} potently reduce cell viability (Redler *et al.* 2014, Proctor *et al.* 2016, Zhu *et al.* 2018). Thus, it was examined whether the protective effect of increased UBA1^{WT} expression against SOD1^{A4V}-EGFP toxicity was associated with it reducing the levels of SOD1^{A4V}-EGFP in cells. Comparison of the mean EGFP fluorescence intensity of cells co-expressing SOD1^{A4V}-EGFP and UBA1^{WT}, UBA1^{C632S} or mCherry alone prior to permeabilisation by saponin showed that there were no differences in SOD1^{A4V}-EGFP levels in cells co-expressing UBA1^{WT} relative to cells co-expressing UBA1^{C632S} or mCherry alone (Figure 4.5). Similarly, there were no differences in the levels of SOD1^{WT}-EGFP in cells co-expressing UBA1^{WT}, UBA1^{C632S} or mCherry alone. These data demonstrate that increased expression of UBA1^{WT} did not protect against SOD1^{A4V}-EGFP toxicity through reduction of the total levels of SOD1^{A4V}-EGFP in these cells.

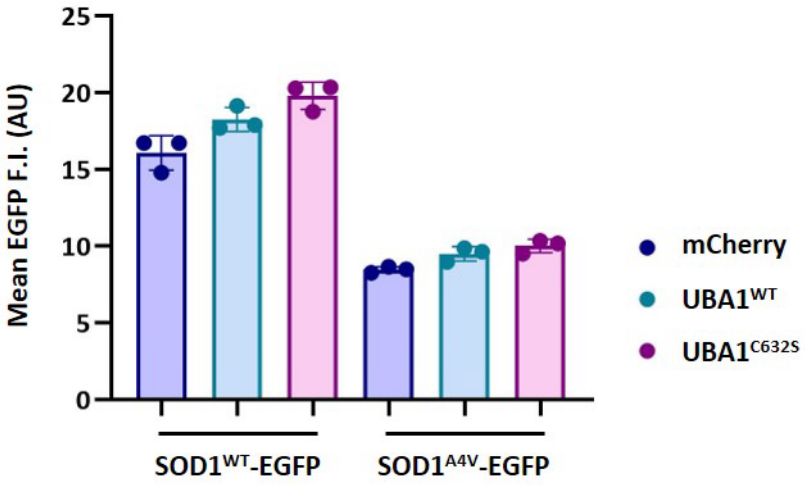

Figure 4.5. UBA1^{WT} overexpression has no effect on the total levels of SOD1^{A4V}-EGFP in NSC-34 cells. The mean EGFP F.I. of SOD1^{A4V}-EGFP and SOD1^{WT}-EGFP in NSC-34 cells co-expressing UBA1^{WT}, the catalytically inactive mutant UBA1^{C632S} or mCherry alone. NSC-34 cells were transiently co-transfected with either SOD1^{WT}-EGFP or SOD1^{A4V}-EGFP and UBA1^{WT}, UBA1^{C632S} or mCherry alone. After 48 h, cells were imaged on an IncuCyte® ZOOM, and the EGFP F.I. in cells was measured. Cells were transfected in triplicate, and the experiment was performed three times. The data presented are the mean ± SEM of the EGFP F.I. in transfected NSC-34 cells. The means were compared using one-Way ANOVA followed by Tukey's multiple comparison test.

4.4 Discussion

Extensive evidence implicates dysregulation of the UPS and ubiquitin homeostasis in the pathogenesis of ALS. One of the strongest connections is that the hallmark pathological feature of ALS-affected motor neurons is the presence of inclusions comprised of misfolded proteins and ubiquitin (Leigh *et al.* 1991). This sequestration of ubiquitin likely influences its distribution in the cellular pools in which it resides (Kaiser *et al.* 2011). In the pool comprised of polyubiquitin chains, the function of ubiquitin in tagging and directing target proteins for degradation through autophagy and through the UPS requires its activation by the E1 enzyme, UBA1 (Ayusawa *et al.* 1992, Cook and Chock 1992, Clague *et al.* 2015). In screening the levels of yeast proteins in response to the heterologous expression of human $SOD1^{A4V}$ (Chapter III), the levels of UBA1 were found to be increased, coinciding with a distinct lack of $SOD1^{A4V}$ toxicity. Because the A4V mutation in *SOD1* results in rapid motor neuron degeneration and ALS disease progression in humans (Cudkowicz *et al.* 1997, Juneja *et al.* 1997), it was hypothesised that the increased levels of UBA1 in yeast enabled cells to respond to the toxic mechanisms usually induced by the $SOD1^{A4V}$ protein, and thereby cell viability was not impaired. To test this hypothesis, in the present chapter the NSC-34 cell line was used to examine whether UBA1 was differentially regulated in NSC-34 cells overexpressing $SOD1^{A4V}$ or $SOD1^{WT}$, and to determine whether increased UBA1 expression was associated with modulation of $SOD1^{A4V}$ aggregation and toxicity.

4.4.1 Increased $UBA1^{WT}$ expression protects against $SOD1^{A4V}$ toxicity

In the work presented in this chapter it was found that $SOD1^{A4V}$-EGFP expression caused striking toxicity in NSC-34 cells, consistent with the toxicity the A4V *SOD1* mutation causes in human motor neurons (Cudkowicz *et al*. 1997, Juneja *et al*. 1997). Importantly, in contrast to yeast expressing $SOD1^{A4V}$, there were no differences in the levels of endogenous murine UBA1 in NSC-34 cells expressing $SOD1^{A4V}$-EGFP relative to NSC-34 cells expressing

SOD1^{WT}-EGFP or EGFP alone. It should be noted that the levels of UBA1 were not normalised to the transfection efficiency of SOD1, they were normalised to the total amount of protein loaded into each lane of the gel as is standard practice for immunoblots. The transfection efficiency of SOD1 was on average ~20%, thus, there would be a negligible effect on UBA1 levels as measured by immunoblot. Immunofluorescence, however, would be a suitable alternative technique to use as a read-out.

Through confocal microscopy it was observed that SOD1^{A4V}-EGFP formed multiple large aggregates in NSC-34 cells. Furthermore, NSC-34 cells expressing SOD1^{A4V}-EGFP were more vulnerable to proteasome inhibition using MG132 compared to cells expressing SOD1^{WT}-EGFP or EGFP alone, suggesting that there was disruption of normal UPS activity in cells expressing SOD1^{A4V}-EGFP before cells were exposed to MG132-mediated proteasome inhibition. Indeed, dysfunction of the UPS in motor neurons expressing mutant *SOD1* has been reported in several studies (Urushitani *et al.* 2002, Cheroni *et al.* 2009, Crippa *et al.* 2010, Onesto *et al.* 2011). Moreover, impaired proteasome activity in cultured cells expressing mutant SOD1 has been correlated with cellular toxicity (Matsumoto *et al.* 2005, Kitamura *et al.* 2014). Vulnerability to mutant SOD1-mediated UPS dysfunction is potentially greater in spinal cord motor neurons than in other cell types. Spinal cord motor neurons from mice have been found to be more vulnerable to proteasome inhibition than non-motor neurons (Urushitani *et al.* 2002). A transcriptomic study of populations of spinal motor neurons that succumb to degeneration in ALS compared to resistant oculomotor neurons discovered that UPS genes were downregulated in the spinal motor neurons (Brockington *et al.* 2013). Thus, it is logical to hypothesise that increasing UPS capacity in motor neurons expressing ALS-causing mutations in *SOD1* could provide cellular protection.

When the levels of UBA1^{WT} were increased through overexpression in NSC-34 cells expressing SOD1^{A4V}-EGFP, the toxicity caused by SOD1^{A4V}-EGFP was reduced. This was dependent on

the catalytic activity of UBA1, as the expression of UBA1^{C632S}, an isoform with a mutation of the catalytic cysteine residue, did not improve cell viability. UBA1 is the primary E1 ubiquitin-activating enzyme in mammalian cells (Schulman and Harper 2009, Ye and Rape 2009). It is crucial for proper UPS functioning in eukaryotes. Severe UPS inhibition has been reported in yeast cells harbouring a temperature-sensitive *UBA1* allele, causing depletion of ubiquitin conjugates (Ghaboosi and Deshaies 2007). Thus, in the present work, the increased levels of UBA1 in NSC-34 cells may have led to augmented UPS activity.

4.4.2 UBA1^{WT}-mediated protection against SOD1^{A4V} toxicity is not associated with suppression of SOD1^{A4V} aggregation

With the improved viability of NSC-34 cells expressing SOD1^{A4V}-EGFP resulting from UBA1^{WT} overexpression, it was hypothesised that this may have been mediated by improved UPS function and therefore suppression of SOD1^{A4V}-EGFP aggregation. It has long been debated whether the accumulation of misfolded, aggregated proteins into inclusions is a cause of cellular toxicity, a by-product of widespread proteostasis dysfunction in cells, or a protective mechanism used to sequester toxic intermediate oligomeric protein species into isolated compartments. Notably, mounting evidence shows that certain types of inclusions, such as the JUNQ compartment, can serve protective functions in the cell by sequestering toxic misfolded proteins, oligomeric species and aggregates (Kaganovich *et al.* 2008, Weisberg *et al.* 2012). Through a saponin-permeabilisation assay the results presented in the present work indicate that the overexpression of UBA1^{WT} did not lead to suppression of SOD1^{A4V}-EGFP aggregation. Moreover, the total cellular levels of SOD1^{A4V}-EGFP were not reduced in cells overexpressing UBA1^{WT}. Evidence from previous work has demonstrated that mutant SOD1^{G93A} aggregates can be toxic or nontoxic depending on whether they are localised to an active JUNQ (Weisberg *et al.* 2012). Weisberg *et al.* (2012) found that SOD1^{G93A} aggregates compartmentalised within the JUNQ were able to sequester the functional pool of HSP70 and other protein quality control

factors that reside inside the JUNQ. By sequestering and depleting the pool of chaperones, other quality control substrates that required degradation could not be delivered to JUNQ-localised proteasomes for degradation. Importantly, Weisberg *et al.* (2012) also showed that overexpression of HSP70 significantly reduced $SOD1^{G93A}$-mediated toxicity, thus demonstrating that up-regulation of quality control components that have been sequestered by aggregated $SOD1^{G93A}$ in the JUNQ can reverse this effect by increasing quality control capacity.

More recently it has been reported that aggregates formed by $SOD1^{A4V}$-EGFP in NSC-34 cells sequester free monomeric ubiquitin from the cytoplasm, depleting the free ubiquitin pool in cells (Farrawell *et al.* 2018). Moreover, when the ubiquitin-modified proteome (the 'ubiquitome') was analysed and compared between NSC-34 cells expressing $SOD1^{A4V}$-EGFP and those expressing $SOD1^{WT}$-EGFP, it was revealed that the expression of $SOD1^{A4V}$-EGFP caused widespread ubiquitin redistribution and consequent ubiquitin dyshomeostasis (Farrawell *et al.* 2018).

As the primary ubiquitin-activating enzyme, disruption of the normal activity of UBA1 results in ubiquitin dyshomeostasis in cells. In SMA linked to disruption of normal UBA1 activity, ubiquitin homeostasis disturbances have been well documented (Aghamaleky Sarvestany *et al.* 2014, Powis *et al.* 2014, Wishart *et al.* 2014). In a mouse model of SMA, increasing the levels of UBA1 through AAV9-mediated delivery led to increases in the levels of monoubiquitin and polyubiquitin, restoration of ubiquitin homeostasis and amelioration of impaired UPS activity (Powis *et al.* 2016). Moreover, AAV9-UBA1 treatment in these mice led to body weight stabilisation, improved motor performance and increased survival (Powis *et al.* 2016). The toxicity caused by $SOD1^{A4V}$-EGFP expression in NSC-34 cells observed in the present work may have been due, at least in part, to sequestration of free monomeric ubiquitin and depletion of the free ubiquitin pool in NSC-34 cells. This, in turn, may have contributed to dyshomeostasis of the cellular ubiquitin pools and disruption of downstream ubiquitin-

dependent molecular processes. Indeed, it was found that UPS activity was impaired in NSC-34 cells expressing SOD1^{A4V}-EGFP. Furthermore, if the SOD1^{A4V}-EGFP inclusions observed in NSC-34 cells represented localisation of SOD1^{A4V}-EGFP to JUNQ compartments, this may have disrupted the intra-JUNQ proteasomal degradation of ubiquitylated proteins. Thus, increasing the levels of UBA1^{WT} may have contributed to enhancement in the capacity of cells to ubiquitylate other proteins that critically need to be degraded by the proteasome. This hypothesised mechanistic pathway, however, remains to be explored through further investigation. This could be tested by measuring free ubiquitin levels as described in Farrawell *et al.* (2018).

Inhibiting UBA1 activity leads to interference of both excitatory and inhibitory synapses in hippocampal neurons (Rinetti and Schweizer 2010). Similarly, loss of UBA1 in *Drosophila melanogaster* causes defects in axon development (Watts *et al.* 2003). Additional work in *Drosophila melanogaster* has shown that mutations that cause modest impairment of UBA1 expression and function cause a neurodegeneration phenotype (Pfleger *et al.* 2007), while yet others have demonstrated that a *UBA1* mutation causing partial loss of function is associated with severe locomotion impairment and reduction in lifespan (Liu and Pfleger 2013). Of note, increased UBA1 levels have been implicated in the mechanism of action of the slow Wallerian degeneration mutation, which confers protection to synapses and axons in a range of traumatic and disease-related degeneration contexts (Wishart *et al.* 2007, Wishart *et al.* 2008).

4.4.3 Concluding statements

Importantly, the work presented in this chapter adds to previous efforts implicating the beneficial effects of increased UBA1 activity in neuronal cells. Moreover, the data from the present study extends on findings reported by others to demonstrate that augmented UBA1 activity may have the capacity to ameliorate ubiquitin dyshomeostasis and UPS dysfunction associated with SOD1^{A4V}-mediated toxicity. Taking these previously-reported findings

together with the work presented in this chapter, it is hypothesised that increasing the levels of UBA1 in motor neurons may be able to improve cell viability by restoring ubiquitin homeostasis. This may enable reestablishment of normal activity of the downstream ubiquitin-dependent molecular processes discussed above, including the UPS, that become dysfunctional in motor neurons as a result of the expression of ALS-causing mutations in *SOD1* and other genes implicated in ALS.

Chapter 5: A high-content screening system to evaluate protein aggregation and proteostasis capacity in cellular ALS models

5.1 Introduction

Post-mortem examination of spinal cord tissue from ALS patients consistently reveal the presence of TDP-43-, FUS- or SOD1- and ubiquitin-positive inclusions comprised of insoluble proteinaceous material. Extensive research suggests that misfolded proteins, as abnormal monomers and/or oligomeric precursors, possess cytotoxic properties (Bolognesi *et al.* 2010, Proctor *et al.* 2016, Zhu *et al.* 2018) and that their aggregation into certain kinds of inclusions may serve to protect cells and to assist in the clearance of these toxic species (Johnston *et al*. 1998, Kopito 2000, Kawaguchi *et al.* 2003, Arrasate *et al.* 2004, Kaganovich *et al.* 2008, Tan *et al*. 2008, Treusch *et al.* 2009, Zhang and Qian 2011, Weisberg *et al.* 2012, Polling *et al.* 2014). However, the formation of protein inclusions is also indicative of dysregulated proteostasis and the inability of the cell to properly monitor, refold or degrade non-native proteins. Further, it has been suggested that the progressive spread of pathology in patients could be due to the cell-to-cell propagation of protein misfolding and aggregation (Shaw 2002, Brettschneider *et al.* 2014). Indeed, the uptake of preformed SOD1 aggregates into neuronal cells from the surrounding cell culture media has been demonstrated in several studies (Munch *et al.* 2011, Sundaramoorthy *et al.* 2013, Grad *et al.* 2014, Zeineddine *et al.* 2015). Inclusions with distinct characteristics, and that have been formed through diverse pathways, are observed in cellular models of ALS and human post-mortem tissue from patients with ALS and other neurodegenerative disorders (Krobitsch and Lindquist 2000, Kamhi-Nesher *et al.* 2001, Huyer *et al.* 2004, Matsumoto *et al.* 2005, Matsumoto *et al.* 2006, Kaganovich *et al.* 2008, Farrawell *et al.* 2015); including aggresomes, JUNQ and IPOD inclusions. Aggresome-, JUNQ- and IPOD-like inclusions can be distinguished based on their mobility, microtubule-dependence and colocalisation with different components of protein quality control pathways, most notably ubiquitin, but also with 26S proteasomes, molecular chaperones, and markers of autophagy and ERAD (Taylor *et al.* 2003, Iwata *et al.* 2005, Kruse *et al.* 2006, Kaganovich *et al.* 2008). While

the majority of the inclusions examined in ALS patient tissue are ubiquitin-positive, additional types of inclusions that are ubiquitin-negative have also been reported (Forsberg *et al.* 2010). The ubiquitylation dynamics of misfolded proteins plays a key role in determining the type of inclusion they partition to (Kaganovich *et al.* 2008), however, the ubiquitylation dynamics of ALS-associated proteins have largely remained unclear. Also remaining to be characterised are the proteostasis disturbances that occur in motor neurons harbouring mutations in different ALS-associated genes.

There is a vital need for the development of effective diagnostic tools and therapeutic strategies for ALS. Given the heterogeneity of ALS, the ALS research field would benefit greatly from the development of assays that can measure multiple phenotypic features in cellular ALS models and extract rich, descriptive information of responses to candidate therapeutic compounds and modifiers of ALS gene toxicity. Assays that utilise the principles of high content screening (HCS) could help to address this investigative gap. In the past 20 years HCS approaches have evolved to emerge as attractive options for researchers interested in obtaining extensively descriptive phenotypic data through automated microscopy.

The overarching objective of the work presented in this chapter was to develop an experimental system with HCS capacity that could be used to extract multiplexed phenotypic data from cellular ALS models. The specific aims of this work were thus to:

(i) generate cellular models of SOD1-, TDP-43-, FUS-, CCNF-, VAPB-, VCP-, OPTN- and UBQLN2-associated ALS

(ii) develop a HCS method with the potential to examine pathological features in cellular ALS models

(iii) employ this system to examine proteostasis capacity in these ALS models.

5.2 Materials and methods

5.2.1 Plasmids

In addition to SOD1^{WT}-EGFP, SOD1^{A4V}-EGFP, TDP-43^{WT}-tGFP and TDP-43^{M337V}-tGFP (described in section 2.2, Chapter II), the plasmids used in the present work are detailed in Table 5.1. OPTN^{WT}-EGFP, OPTN^{Q398X}-EGFP and OPTN^{E478G}-EGFP had previously been transformed into chemically competent *E. coli* DH5-α cells, and were stored in glycerol at -80°C prior to plasmid DNA purification. Mammalian expression constructs comprised of the pCMV6-AC-tGFP vector containing human WT *FUS*, *VAPB*, *UBQLN2* and *VCP* were obtained from OriGene Technologies (MD, USA). To obtain constructs containing ALS-associated mutations in each gene, sequences were designed in-house according to mutant sequences described in the literature, and site-directed mutagenesis was outsourced to GenScript. Sequencing was carried out by GenScript as part of their service to confirm the correct full sequence of each construct.

The pCIneo mammalian expression construct containing sequences encoding C-terminally EGFP-tagged WT firefly luciferase (Fluc^{WT}-EGFP) and two conformationally destabilised mutants (containing a single mutation (SM), Fluc^{SM}-EGFP or two mutations (double mutant; DM), Fluc^{DM}-EGFP) were generously provided by Prof. Franz-Ulrich Hartl (Max Planck Institute of Biochemistry, Planegg, Germany). For detailed information on the design and construction of the destabilised Fluc-EGFP mutant plasmids see Gupta *et al.* (2011). Briefly, WT luciferase from the American firefly (*Photinus pyralis*) was mutationally optimised, PCR-amplified and sub-cloned into the pCIneo expression vector. Site-directed mutagenesis was used to introduce either a single mutation (R188Q) or two mutations (R188Q and R261Q) to generate increasingly destabilised forms of the protein. EGFP from pEGFP-N2 (Clontech) was inserted at the 3' end of luciferase in all three constructs to prepare EGFP-tagged versions.

Table 5.1. List of plasmids used in the present chapter. The backbone vector, insert gene, any custom modifications made, the in-text nomenclature used for each plasmid, the source of each plasmid and reference publications detailing the construction of certain plasmids are detailed.

Backbone vector	Insert	Custom modifications	In-text nomenclature	Source	Reference
pEGFP-C3	$OPTN^{WT}$		$OPTN^{WT}$-EGFP	Assoc. Prof. Julie Atkin, Macquarie University, NSW, Australia	
	$OPTN^{Q398X}$		$OPTN^{Q398X}$-EGFP		
	$OPTN^{E478G}$		$OPTN^{E478G}$-EGFP		
pCMV6-AC-tGFP	FUS^{WT}		FUS^{WT}-tGFP	Cat. No. RG201808, OriGene Technologies, MD, USA	
	FUS^{R495X}	Site-directed mutagenesis	FUS^{R495X}-tGFP	GenScript	
	FUS^{R521G}	Site-directed mutagenesis	FUS^{R521G}-tGFP	GenScript	
	$VAPB^{WT}$		$VAPB^{WT}$-tGFP	Cat. No. RG200517, OriGene Technologies, MD, USA	
	$VAPB^{P56S}$	Site-directed mutagenesis	$VAPB^{P56S}$-tGFP	GenScript	
	$UBQLN2^{WT}$		$UBQLN2^{WT}$-tGFP	Cat. No. RG209645, OriGene Technologies, MD, USA	
	$UBQLN2^{P497H}$	Site-directed mutagenesis	$UBQLN2^{P497H}$-tGFP	GenScript	
	$UBQLN2^{P525S}$	Site-directed mutagenesis	$UBQLN2^{P525S}$-tGFP	GenScript	
	VCP^{WT}		VCP^{WT}-tGFP	Cat. No. RG211130, OriGene Technologies, MD, USA	
	VCP^{R159H}	Site-directed mutagenesis	VCP^{R159H}-tGFP	GenScript	
	VCP^{R191Q}	Site-directed mutagenesis	VCP^{R191Q}-tGFP	GenScript	
pmCherry-C1	$CCNF^{WT}$		$CCNF^{WT}$-mCherry	Prof. Ian Blair, Macquarie University, NSW, Australia	
	$CCNF^{S621G}$		$CCNF^{S621G}$-mCherry		
pcDNA3.1(+)	$SOD1^{WT}$	C-terminal tdTomato tag	$SOD1^{WT}$-tdT	Custom cloned using GenScript	
	$SOD1^{A4V}$		$SOD1^{A4V}$-tdT		
pmRFP-ubiquitin (see reference)			^{mRFP}ubiquitin	Prof. Nico Dantuma, Karolinska Institute, Solna, Sweden (Addgene plasmid no. 11935)	Bergink *et al.* 2006

pmRFP-C1	LC3		^{mRFP}LC3	Prof. Tamotsu Yoshimori, Osaka University, Osaka, Japan (Addgene plasmid no. 21075)	Kimura *et al.* 2007
TDP-43^{WT}-tdTomato (see reference)			TDP-43^{WT}-tdT	Prof. Zuoshang Xu, University of Massachusetts, MA, USA (Addgene plasmid no. 28205)	Yang *et al.* 2010
pCIneo	WT firefly luciferase	C-terminal EGFP tag	Fluc^{WT}-EGFP	Prof. Franz-Ulrich Hartl, Max Planck Institute of Biochemistry, Planegg, Germany	Gupta *et al.* 2011
	Firefly luciferase containing a single mutation ('single mutant')		Fluc^{SM}-EGFP		
	Firefly luciferase containing two mutations ('double mutant')		Fluc^{DM}-EGFP		
pBOS-H2B-ECFP-N1 (see reference)				Prof. Angus Lamond, University of Dundee, UK	Leung *et al.* 2004

5.2.2 Transient transfections and treatment with proteasome inhibitor

NSC-34 cells were seeded at 100,000 cells/mL in 10% (v/v) FBS in DMEM/F-12 into either 8-well µ-Slides (Ibidi, Planegg-Martinsried, Germany) for confocal microscopy or 96-well plates (Greiner Bio-One, Frickenhausen, Germany) for imaging using the Thermo Scientific™ Cellomics® ArrayScan™ VTI High Content Screening microscope. After overnight incubation at 37 °C under 5% CO_2/95% air, cells were either single-transfected, dual-transfected or triple-transfected using Lipofectamine® 2000 (Invitrogen, Waltham, USA) according to manufacturer's instructions. Briefly, per well, 0.3 µL or 0.6 µL of Lipofectamine® 2000 and a total of 0.1 µg or 0.2 µg of plasmid DNA for the 96-well plate format or 8-well µ-Slide format, respectively, were used to transfect NSC-34 cells. For dual and triple transfections, plasmids were used at 1: 1 and 1: 1: 1 ratios, respectively. All transfection conditions were carried out in

quadruplicate. For confocal microscopy experiments, NSC-34 cells were single-transfected or dual-transfected. NSC-34 cells were single-transfected with SOD1^{WT}-EGFP, SOD1^{A4V}-EGFP, TDP-43^{WT}-tGFP, TDP-43^{M337V}-tGFP, FUS^{WT}-tGFP, FUS^{R495X}-tGFP, FUS^{R521G}-tGFP, CCNF^{WT}-mCherry, CCNF^{S621G}-mCherry, the pEGFP-N1 vector (EGFP alone) or the pmCherry-C1 vector (mCherry alone). NSC-34 cells were dual-transfected as detailed in Table 5.2. An additional dual transfection experiment was carried out with transfection of NSC-34 cells with (1) VCP^{WT}-tGFP, VCP^{R159H}-tGFP or VCP^{R191Q}-tGFP and (2) TDP-43^{WT}-tdTomato. For these dual transfection experiments, mCherry alone was used as a control for the expression of a RFP only, to ensure that the localisation patterns observed for ^{mRFP}LC3, ^{mRFP}ubiquitin and TDP-43^{WT}-tdT were not a result of the RFP tag itself.

Table 5.2. Plasmid combinations used in dual transfections. The localisation patterns of the EGFP-/tGFP proteins, ^{mRFP}LC3, ^{mRFP}ubiquitin and TDP-43^{WT}-tdT, encoded in the plasmids listed here, were examined in dual-transfected NSC-34 cells using confocal microscopy.

^{mRFP}LC3 localisation microscopy	
Plasmid 1	**Plasmid 2**
SOD1^{WT}-EGFP	^{mRFP}LC3
SOD1^{A4V}-EGFP	^{mRFP}LC3
TDP-43^{WT}-tGFP	^{mRFP}LC3
TDP-43^{M337V}-tGFP	^{mRFP}LC3
FUS^{WT}-tGFP	^{mRFP}LC3
FUS^{R495X}-tGFP	^{mRFP}LC3
FUS^{R521G}-tGFP	^{mRFP}LC3
EGFP alone	^{mRFP}LC3
^{mRFP}ubiquitin localisation microscopy	
Plasmid 1	**Plasmid 2**
VAPB^{WT}-tGFP	^{mRFP}ubiquitin
VAPB^{P56S}-tGFP	^{mRFP}ubiquitin
OPTN^{WT}-EGFP	^{mRFP}ubiquitin
OPTN^{E478G}-EGFP	^{mRFP}ubiquitin
UBQLN2^{WT}-tGFP	^{mRFP}ubiquitin
UBQLN2^{P497H}-tGFP	^{mRFP}ubiquitin
VCP^{WT}-tGFP	^{mRFP}ubiquitin
VCP^{R159H}-tGFP	^{mRFP}ubiquitin
VCP^{R191Q}-tGFP	^{mRFP}ubiquitin
EGFP alone	^{mRFP}ubiquitin
TDP-43^{WT}-tdT localisation	
Plasmid 1	**Plasmid 2**
VCP^{WT}-tGFP	TDP-43^{WT}-tdT
VCP^{R159H}-tGFP	TDP-43^{WT}-tdT
VCP^{R191Q}-tGFP	TDP-43^{WT}-tdT

For optimisation of the parameters used for automated imaging and image analysis using the Thermo Scientific™ Cellomics® ArrayScan™ VTI High Content Screening microscope, NSC-34 cells were triple-transfected as detailed in Table 5.3.

Table 5.3. Plasmid combinations used in triple transfections in preparation for HCS microscopy optimisation. Triple-transfected NSC-34 cells were used for preliminary experiments to optimise the parameters used for automated imaging and image analysis using a Cellomics® ArrayScan™ VTI HCS microscope.

Plasmid 1	Plasmid 2	Plasmid 3
H2B-ECFP	$SOD1^{WT}$-EGFP	mCherry alone
	$SOD1^{A4V}$-EGFP	
	TDP-43^{WT}-tGFP	
	TDP-43^{M337V}-tGFP	
	FUS^{WT}-tGFP	
	FUS^{R495X}-tGFP	
	FUS^{R521G}-tGFP	
	$VAPB^{WT}$-tGFP	
	$VAPB^{P56S}$-tGFP	
	$OPTN^{WT}$-EGFP	
	$OPTN^{E478G}$-EGFP	
	$UBQLN2^{WT}$-tGFP	
	$UBQLN2^{P497H}$-tGFP	
	VCP^{WT}-tGFP	
	VCP^{R159H}-tGFP	
	VCP^{R191Q}-tGFP	

Following optimisation of the parameters for automated imaging and image analysis, the Cellomics® ArrayScan™ VTI HCS platform was employed for an experiment using Fluc-EGFP variants as sensors of changes in cellular protein quality control network capacity in NSC-34 cells expressing mutant SOD1 or CCNF. For this experiment, NSC-34 cells were triple-transfected as detailed in Table 5.4. As a positive control for cells under proteome stress, quadruplicates of control cells expressing H2B-CFP, mCherry alone and the Fluc-EGFP variants were treated with MG132 to inhibit proteasomal activity. MG132 was solubilised in

DMSO at 20 mM and subsequently diluted to 5 µM in 10% (v/v) FBS in DMEM/F-12. The prepared solution was added to cells at 30 h post-transfection and incubated for 18 h. For mock treatment, 5 µM DMSO in 10% (v/v) FBS in DMEM/F-12 was instead added to cells. 48 h following triple-transfections with the Fluc-EGFP variants, cells were fixed in 4% (w/v) paraformaldehyde (PFA, pH 7.4) for 20 min at room temperature. Cells were then washed three times with PBS before the addition of 100 µL of PBS to prepare for imaging on the Cellomics® ArrayScan™ VTI High Content Screening microscope.

Table 5.4. Plasmid combinations used in triple transfections of NSC-34 cells in preparation for Fluc-EGFP experiments.

Plasmid 1	Plasmid 2	Plasmid 3	Additional treatment
H2B-ECFP	$SOD1^{WT}$-tdT	$Fluc^{WT}$-EGFP	No treatment
		$Fluc^{SM}$-EGFP	
		$Fluc^{DM}$-EGFP	
		EGFP alone	
H2B-ECFP	$SOD1^{A4V}$-tdT	$Fluc^{WT}$-EGFP	No treatment
		$Fluc^{SM}$-EGFP	
		$Fluc^{DM}$-EGFP	
		EGFP alone	
H2B-ECFP	$CCNF^{WT}$-mCherry	$Fluc^{WT}$-EGFP	No treatment
		$Fluc^{SM}$-EGFP	
		$Fluc^{DM}$-EGFP	
		EGFP alone	
H2B-ECFP	$CCNF^{S621G}$-mCherry	$Fluc^{WT}$-EGFP	No treatment
		$Fluc^{SM}$-EGFP	
		$Fluc^{DM}$-EGFP	
		EGFP alone	
H2B-ECFP	mCherry alone	$Fluc^{WT}$-EGFP	± MG132 treatment
		$Fluc^{SM}$-EGFP	
		$Fluc^{DM}$-EGFP	
		EGFP alone	

5.2.3 Confocal microscopy live cell imaging

Prior to setting up the Thermo Scientific™ Cellomics® ArrayScan™ VTI HCS platform, the localisation patterns of each EGFP- and mCherry-tagged WT and mutant ALS-associated protein in transfected NSC-34 cells were characterised by imaging using a Leica TCS SP5 II confocal microscope with a 63× oil-immersion objective lens (Leica Microsystems, Wetzlar, Germany). Imaging was carried out 48 h post-transfection for single transfections and dual transfections with ^{mRFP}LC3 and TDP-43^{WT}-tdT, or 24, 48 and 72 h post-transfection for dual transfections with ^{mRFP}ubiquitin. EGFP fluorescence was excited at 488 nm by an argon laser; RFP fluorescence was excited at 561 nm by a DPS 561 laser. Fluorescent emissions were acquired by sequential scanning using the Leica Application Suite – Advanced Fluorescence (LAS-AF) software (version 3, Leica Microsystems, Wetzlar, Germany). Across each set of quadruplicate wells of cells for each transfection treatment, a minimum of 100 transfected cells were imaged across 10-15 fields of view per replicate.

5.2.4 Confocal image analysis, inclusion characterisation and quantification

To characterise the localisation patterns of each EGFP-/tGFP- and mCherry-tagged ALS-associated protein in transfected NSC-34 cells and ensure that they corresponded with the patterns recorded in the literature, the images acquired by confocal microscopy were manually examined. To inform this characterisation, previous peer-reviewed studies revealing images of post-mortem spinal cord tissue from ALS patients were used to establish the morphology and size range of inclusions positive for mutant SOD1, TDP-43, FUS, VAPB, OPTN, UBQLN2 and VCP. This enabled a size minimum of 2 μm to be established for categorising fluorescent foci as inclusions as opposed to associations of the fluorescent ALS proteins with other cellular structures, granules (e.g stress or transport) or other irrelevant fluorescent debris and artefacts.

In order to quantify the percentage of VAPB^{WT}-tGFP, VAPB^{P56S}-tGFP, OPTN^{WT}-EGFP, OPTN^{E478G}-EGFP, UBQLN2^{WT}-tGFP, UBQLN2^{P497H}-tGFP, VCP^{WT}-tGFP, VCP^{R159H}-tGFP

and VCP^{R191Q}-tGFP inclusions that were positive for ^{mRFP}ubiquitin in each dual transfection treatment, the numbers of transfected cells and fluorescent protein-positive foci were manually counted in each image acquired at 24, 48 and 72 h post-transfection. First, the numbers of EGFP-positive transfected NSC-34 cells in each replicate across 10-15 fields of view were counted. The numbers of these containing EGFP-fluorescent foci larger than 2 μm were then recorded as inclusions positive for each EGFP-fusion ALS protein. RFP-fluorescent foci larger than 2 μm were then counted as inclusions positive for ^{mRFP}ubiquitin. The images collected in the green and red channels were then merged and the numbers of inclusions positive for EGFP and RFP fluorescence were counted as EGFP-fusion ALS protein inclusions positive for ^{mRFP}ubiquitin. Finally, the numbers of inclusions positive for EGFP and RFP fluorescence were divided by the numbers of inclusions positive for each respective EGFP-fusion ALS protein, and then multiplied by 100 to calculate the proportion of ALS protein inclusions that were ubiquitin-positive. It should be noted that due to time limitations, the localisation patterns of ^{mRFP}ubiquitin with mutant VAPB, OPTN and UBQLN2, of mutant VCP with TDP-43^{WT}-tdT and of mutant SOD1, TDP-43 and FUS with ^{mRFP}LC3 observed here are each from n = 1 experiment and furthermore were not confirmed through immunocytochemistry. Thus, these observations await confirmation by further experimentation.

5.2.5 IncuCyte® ZOOM live cell imaging and analysis

IncuCyte® ZOOM live cell imaging and analysis was used to carry out two different measures in NSC-34 cells transiently transfected with each of the EGFP- and mCherry-tagged WT and mutant ALS-associated proteins. Both experimental techniques are described in Chapter IV, section 4.2.3. Briefly, the first experimental technique was used as a measure of cell viability while the second technique was used to quantify numbers of transfected cells containing non-diffusable, insoluble EGFP- or mCherry-fusion proteins. For all IncuCyte® experiments, the mean ± SEM was calculated across quadruplicate samples and used for statistical analyses.

5.2.6 Developing a high content screening work flow for fluorescence-based analysis of cellular ALS models

Following characterisation of the localisation patterns, the solubility and the effect on cell viability of each EGFP-/tGFP-/mCherry-tagged WT and mutant ALS-associated gene in transfected NSC-34 cells, a Cellomics® ArrayScan™ VTI HCS platform was established with the overarching aim that it could be used for studies with each of these cellular ALS models. The Thermo Scientific™ HCS Studio™ software uses image analysis algorithms, termed BioApplications, designed to measure a range of different cellular features and biological processes. These BioApplications initially detect cells or cellular objects using the fluorescence in one channel, Channel 1/the primary channel, and then the fluorescence in up to another five channels. In the primary channel, cell nuclei or other cellular regions can be fluorescently labelled to serve as the primary object, defined by the algorithm using a mask for the first step of identifying and selecting cells. The regions of the cell detected in each of the remaining channels depend on the mask, or region, defined by the primary object. The masks in Channels 2-6 serve to enable measurement of different phenotypic features that report on cellular responses to different conditions.

By transfecting NSC-34 cells with histone H2B-ECFP, the nuclei of cells could be detected based on ECFP fluorescence in Channel 1 and served as the primary object in the analysis by the Spot Detector BioApplications (Figure 5.1, b). As will be outlined in Section 5.2.6.3.2, for each fluorescence channel imaged, the appropriate masks used by the Thermo Scientific™ HCS Studio™ software to identify and select cells were carefully optimised to ensure that only cells of interest were included for analysis. An NSC-34 cell line stably transfected with H2B-ECFP was generated for future experiments with the HCS platform, as a cell line with constant expression of a nuclear-localised ECFP-fusion protein that could be used for automated cell identification and analysis. The intention was that this would aid in the efficiency of the HCS

workflow. As time was limited for the development of this HCS platform, image processing and analysis parameters in the Thermo Scientific™ HCS Studio™ software were optimised concurrently with the generation of this stable cell line, which was instead frozen down as stocks to use in future experiments.

5.2.6.1 Generation of an NSC-34 cell line stably transfected with H2B-ECFP

The algorithms used for automated image analysis in the Thermo Scientific™ HCS Studio™ software can use two different methods for automated identification of cells in each image; one that is used for identifying bright objects/cells on a dark background (e.g. for a fluorescently labeled cell nucleus in an unlabeled cell), and one that detects dark objects/cells on a bright background (e.g. for an unlabeled cell nucleus in a labeled cytoplasm). For the present work it was of interest to generate an NSC-34 cell line stably expressing a nuclear-localised fluorescent protein-tagged protein that would enable automated identification of cells based on each cell having a bright, fluorescent nucleus. Histone H2B tagged with ECFP (H2B-ECFP) was selected for this purpose. H2B is a component of the histone protein core of nucleosomes and is thus localised to the nucleus. ECFP was used due to the good separation of its excitation and emission maxima from those of EGFP and RFP, enabling it to be used for co-expression with the EGFP and RFP-tagged ALS-associated proteins used in this study. The pBOS-H2B-ECFP-N1 construct contains the blasticidin antibiotic resistance gene. In order to generate an NSC-34 cell line stably transfected with pBOS-H2B-ECFP-N1, the optimal concentration of blasticidin for selecting transfected NSC-34 cells was established by generating a kill curve. NSC-34 cells were seeded at 100,000 cells/mL into 24-well plates in 10% (v/v) FBS in DMEM/F-12 containing blasticidin (CalBioChem, Cat. No. 203350) at the following concentrations: 0, 0.5, 1, 2, 4, 6, 8 and 10 µg/mL. Quadruplicate wells of cells were treated with each different blasticidin concentration. Cells were imaged every 4 h for 1 week using an IncuCyte® ZOOM, with the selective medium changed every 3 days. The numbers of cells grown at each blasticidin

concentration were plotted against time to establish a kill curve. From this, a blasticidin concentration of 6 µg/mL was established as the minimum concentration required to kill all non-transfected cells over 1 week.

Following determination of the optimal blasticidin concentration to use, NSC-34 cells were seeded at 100,000 cells/mL into two 100 mm × 20 mm (diameter × height) Corning® tissue culture treated culture dishes (Cat. No. CLS430167, Corning, USA) and one 6-well plate in 10% (v/v) FBS in DMEM/F-12. After 24 h, cells in the 100 mm × 20 mm dishes were transfected with 10 µg of pBOS-H2B-ECFP-N1 using 30 µL of Lipofectamine® 2000. Cells in the 6-well plate were used as non-transfected control cells throughout the blasticidin-selection process. At 48 h post-transfection, expression of H2B-ECFP in transfected cells was examined by imaging using a Leica DM500 fluorescent microscope. After confirming H2B-ECFP expression via nuclear-localised ECFP fluorescence, growth medium on cells in each dish and three wells of the 6-well plate was exchanged for 6 µg/mL blasticidin in 10% (v/v) FBS in DMEM/F-12. The remaining three wells of the 6-well plate were used as a no-antibiotic control. Every 2-3 days, cell growth was examined and selective medium was replaced with fresh selective medium. This continued until non-transfected control cells had been killed off, and small colonies of transfected cells began to form. Once colonies had expanded and cells had reached ~80% confluence, cells were passaged into two T-75 tissue culture flasks and grown to ~80% confluence. The generation of this polyclonal stable-transfected cell line was carried out simultaneously to the experiments outlined in section 5.2.6.2, and time limitations prevented the use of this cell line in any further experiments. Thus, stocks of the cell line were frozen down in liquid N_2 storage for use in future studies.

5.2.6.2 Imaging using a Cellomics® ArrayScan™ VTI High Content Screening microscope

NSC-34 cells that were triple-transfected were either live-imaged at 24 h, 48 h and 72 h post-

transfection, or for triple-transfections with the Fluc-EGFP variants, cells were fixed 48 h post-transfection before imaging using the 20× objective lens of a Cellomics® ArrayScan™ VTI High Content Screening microscope (Thermo Scientific, Waltham, USA). Fluorescence of ECFP-, EGFP- and tdT/mCherry-fusion proteins was imaged using excitation filters of 386 nm, 485 nm and 549 nm, respectively. Phase contrast and fluorescent images from 20 fields of view per well were acquired, with image analysis parameters optimised using the Spot Detector V4 BioApplication of the Thermo Scientific™ HCS Studio™ software, detailed in Section 5.2.6.3 and summarised in Figure 5.1. Modifications to this BioApplication were made for optimal detection of transfected cells and inclusions containing the EGFP- and tdT/mCherry-fusion proteins.

5.2.6.3 Optimisation of image processing and analysis parameters using the Cellomics® Spot Detector BioApplication

5.2.6.3.1 Image pre-processing

In the Thermo Scientific™ HCS Studio™ software, the first stage of automated image analysis is correction of background fluorescence in each image. A low pass filtration method was used to compute and subtract background fluorescence, in which the local background around each pixel is calculated, with the radius of the area sampled adjusted as determined by the user. The optimised parameter settings for image pre-processing are summarised in Figure 5.1, a. A radius value of 20 μm was found to adequately correct background fluorescence in the images of transfected NSC-34 cells. For all images analysed, it was selected that each BioApplication would reject any objects/cells lying on the image borders. The RejectBorderObjectsCh1 parameter controls this; a value of 1 sets the algorithm to exclude analysis of any objects/cells located on the border of each image, while a value of 0 results in the algorithm including all objects/cells in the image for analysis, including those on the image border. This parameter was set to a value of 1 to reject all cells located on the border of each image (Figure 5.1, a, ii).

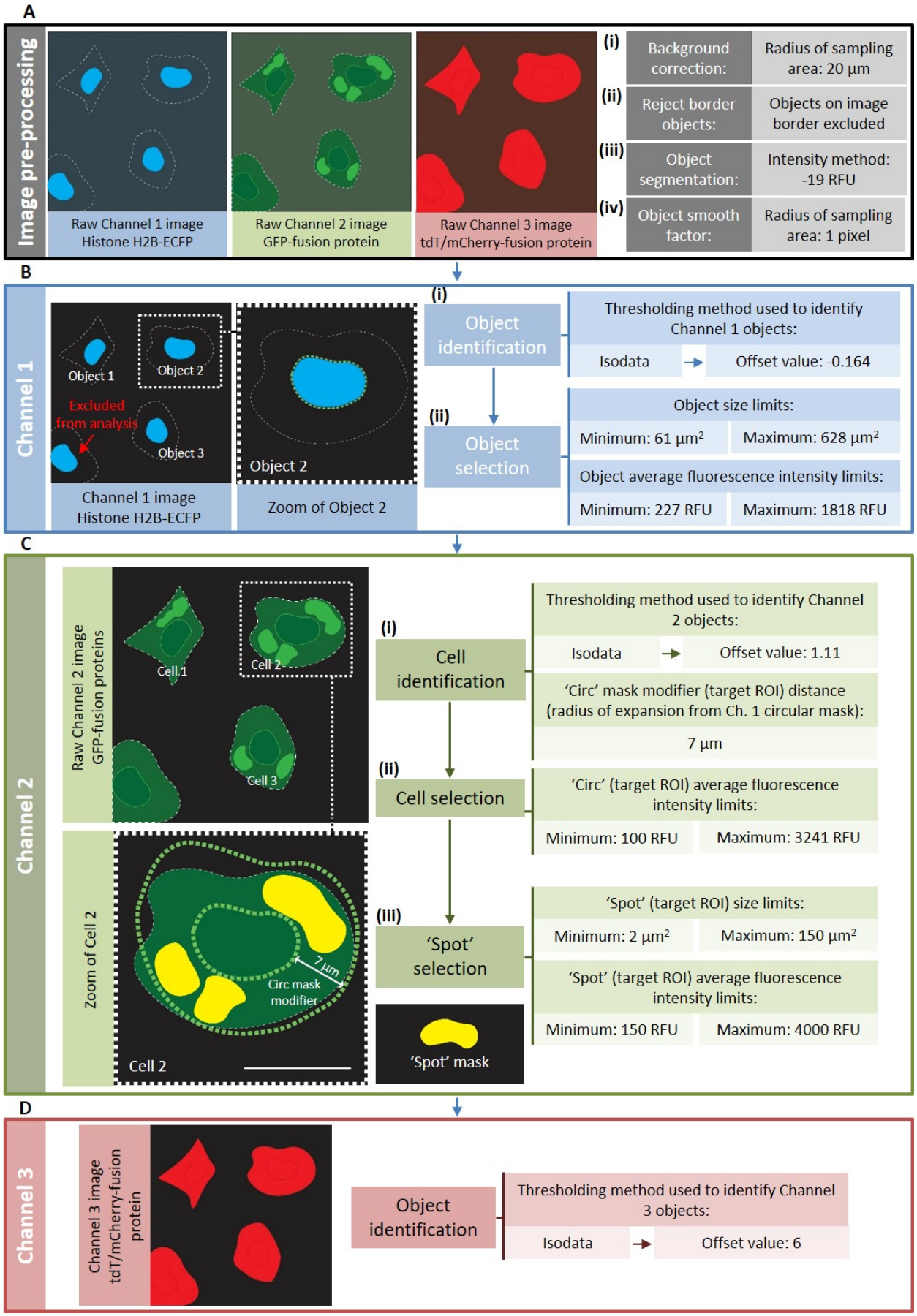
A
Image pre-processing
Raw Channel 1 image
Histone H2B-ECFP
Raw Channel 2 image
GFP-fusion protein
Raw Channel 3 image
tdT/mCherry-fusion protein
(i)
Background correction:
Radius of sampling area: 20 µm
(ii)
Reject border objects:
Objects on image border excluded
(iii)
Object segmentation:
Intensity method: -19 RFU
(iv)
Object smooth factor:
Radius of sampling area: 1 pixel
B
Channel 1
Object 1
Object 2
Excluded from analysis
Object 3
Channel 1 image
Histone H2B-ECFP
Object 2
Zoom of Object 2
(i)
Object identification
Thresholding method used to identify Channel 1 objects:
Isodata
Offset value: -0.164
(ii)
Object selection
Object size limits:
Minimum: 61 µm²
Maximum: 628 µm²
Object average fluorescence intensity limits:
Minimum: 227 RFU
Maximum: 1818 RFU
C
Channel 2
Raw Channel 2 image
GFP-fusion proteins
Cell 1
Cell 2
Cell 3
Zoom of Cell 2
7 µm
Circ mask modifier
Cell 2
(i)
Cell identification
Thresholding method used to identify Channel 2 objects:
Isodata
Offset value: 1.11
'Circ' mask modifier (target ROI) distance (radius of expansion from Ch. 1 circular mask):
7 µm
(ii)
Cell selection
'Circ' (target ROI) average fluorescence intensity limits:
Minimum: 100 RFU
Maximum: 3241 RFU
(iii)
'Spot' selection
'Spot' (target ROI) size limits:
Minimum: 2 µm²
Maximum: 150 µm²
'Spot' (target ROI) average fluorescence intensity limits:
Minimum: 150 RFU
Maximum: 4000 RFU
'Spot' mask
D
Channel 3
Channel 3 image
tdT/mCherry-fusion protein
Object identification
Thresholding method used to identify Channel 3 objects:
Isodata
Offset value: 6

Figure 5.1. Schematic of Cellomics® ArrayScan™ VTI High Content Screening (HCS) image processing and analysis optimisation using Thermo Scientific™ HCS Studio™ software. To analyse the fluorescence intensity of EGFP-/tGFP- and tdTomato (tdT)/mCherry-fusion proteins and quantify protein inclusions containing EGFP-/tGFP-fusion proteins in NSC-34 cells, an image analysis algorithm designed to analyse fluorescent foci in cells, termed the Cellomics® Spot Detector BioApplication, was optimised using the Thermo Scientific™ HCS Studio™ software. Optimisation was carried out using images of NSC-34 cells triple-transfected to express H2B-ECFP, either $SOD1^{WT}$-EGFP, $SOD1^{A4V}$-EGFP, TDP-43^{WT}-tGFP TDP-43^{M337V}-tGFP, FUS^{WT}-tGFP, FUS^{R495X}-tGFP, FUS^{R521G}-tGFP, $VAPB^{WT}$-tGFP, $VAPB^{P56S}$-tGFP, $OPTN^{WT}$-EGFP, $OPTN^{E478G}$-EGFP, $UBQLN2^{WT}$-tGFP, $UBQLN2^{P497H}$-tGFP, VCP^{WT}-tGFP, VCP^{R159H}-tGFP, VCP^{R191Q}-tGFP or EGFP alone and (3) mCherry alone. Cells were imaged at 48 h post-transfection using the 20× objective lens of a Cellomics® ArrayScan™ VTI HCS microscope. (A) Raw images from Channels 1 (H2B-ECFP), 2 (EGFP-/tGFP-fusion proteins) and 3 (tdTomato/mCherry-fusion proteins) were first pre-processed to (i) remove background fluorescence, (ii) exclude cells positioned on the border of each image from analysis and (iii) distinguish individual cells ('object' segmentation). (iv) Channel 1 images were additionally smoothed (blurred) to help reduce fluorescent noise that could lead to the false inclusion of image artefacts in subsequent analyses. (B) Biological 'objects', in this case cells, were identified using nuclear-localised H2B-ECFP fluorescence in Channel 1 images. (i) For detection of ECFP-fluorescent nuclei, a fluorescence intensity threshold was set using the Isodata method, which derives the threshold from the distribution of pixel intensities in each image. (ii) To select viable transfected cells for analysis and exclude image artefacts, dead cells and cell debris, cells were selected based on the size and fluorescence intensity of their ECFP-fluorescent nuclei. (C) The relevant measures for GFP fluorescence intensity and fluorescent foci were measured in Channel 2 (i) within a circular analysis mask that expanded the mask derived in Channel 1 by 7 μm. The green circular mask indicates cells selected for analysis, while yellow masks indicate fluorescent foci/'spots' selected for analysis. A fluorescence intensity threshold was set for Channel 2 using the Isodata method. An offset value of 1.11 enabled the image processing algorithm to correctly identify cells expressing the GFP-fusion proteins. (ii) To ensure that cells with particularly low expression of GFP-fusion genes were not included for analysis, GFP fluorescence intensity limits for CircAvgIntenCh2 were set to a minimum intensity of 100 RFU and a maximum intensity of 3241 RFU. (iii) To detect and analyse fluorescent foci corresponding to protein inclusions, upper and lower limits for size and fluorescence intensity were set. (D) Channel 3 objects were identified using the same mask as Channel 2, after establishing the fluorescence intensity threshold using the Isodata method with an offset value of 6.

To optimise the BioApplication's ability to resolve individual objects, an object segmentation method based on fluorescence intensity was used. This method separates objects/cells that are touching based on fluorescence intensity peaks of each pixel. Cells expressing H2B-ECFP in their nucleus exhibit a single, high intensity peak localised in the nucleus. Setting this parameter, ObjectSegmentationCh1, to a negative value sets the segmentation method to the Intensity method while a positive value sets it to the Geometric method based on the shape and size of objects, relying on indentations lying at object/cell boundaries. For the Intensity method, the absolute value selected governs the minimum relative height of the intensity peak to be used for segmentation. A value of -19 relative fluorescence units (RFU) was found to optimally separate touching fluorescent cells (Figure 5.1, a, iii). Object segmentation was further improved by additionally smoothing the Channel 1 image. Smoothing was also opted for as it helped to reduce noise that could lead to the false inclusion of image artefacts in subsequent

analyses. Smoothing involves sampling the region surrounding each pixel and then replacing the pixel using the average value of the pixels sampled. A SmoothFactorCh1 value of 1 pixel, specifying the radius sampled, was determined to optimally smooth each image (Figure 5.1, a, iv).

5.2.6.3.2 Identification and selection of cells for analysis

The optimised parameter settings for identification and selection of cells for analysis are summarised in Figure 5.1, b. To identify H2B-ECFP-expressing NSC-34 cells using Channel 1, a fluorescence intensity threshold was set using the Isodata method. In the Isodata method, the threshold is derived from the distribution of pixel intensities in each image and thus is dependent on each image. This method was chosen to ensure that image-to-image variations in H2B-ECFP intensity would not affect the analysis of cell features measured in the remaining channels. The Isodata thresholding method can be optimised by setting an offset value that alters the final threshold applied to each image. This user-defined offset alters the threshold that is computed automatically from the pixel intensities in the image to set a final optimised threshold that is then applied to each image. In the present work, an offset value of -0.164 was found to be optimal for altering the final threshold that was used to identify fluorescent cells as 'objects' (Figure 5.1, b, i). The 'objects' that were identified were then filtered to select only viable transfected cells for potential analysis in further image processing steps and exclude image artefacts, dead cells and cell debris. Cells were selected based on the size and fluorescence intensity of their ECFP-fluorescent nuclei. A nucleus size minimum of 61 μm^2 and maximum of 628 μm^2, and ECFP fluorescence intensity minimum of 227 RFU and maximum of 1818 RFU, were found to be appropriate for selecting nuclei of viable transfected cells (Figure 5.1, b, ii).

For Channel 2, the relevant measures for GFP fluorescence intensity and spots were measured within a circular mask ('Circ' mask) that expanded the primary object mask by 7 μm

(CircModifierCh2 = 7) (Figure 5.1, c, i). This setting ensured that data from the entire projected area of the cell would be collected. To ensure that the only cells included for analyses were those that were successfully transfected and expressing the GFP-fusion proteins in addition to H2B-ECFP, a fluorescence intensity threshold was set for Channel 2 using the Isodata method. An offset value of 1.11 enabled the image processing algorithm to correctly identify cells expressing the GFP-fusion proteins while excluding cells exhibiting autofluorescence. To ensure that cells with particularly low expression of EGFP-fusion genes were not included for analysis, GFP fluorescence intensity limits for CircAvgIntenCh2 were set to a minimum intensity of 100 RFU and a maximum intensity of 3241 RFU (Figure 5.1, c, ii).

5.2.6.3.3 Selection and analysis of intracellular fluorescent foci

To measure the presence of GFP-positive inclusions in cells, the Spot Detector BioApplication was optimised using Channel 2. To detect and measure fluorescent foci of sizes corresponding to protein inclusions, as established using confocal microscopy, a spot area minimum of 2 μm^2 and maximum of 150 μm^2 was set (Figure 5.1, c, iii). As inclusions are accumulations of high concentrations of proteins, the concentrated fluorescence of GFP-tagged proteins in inclusions allows them to be detected based on high fluorescence intensity. A spot average fluorescence intensity minimum of 150 RFU was found to detect appropriate foci corresponding to GFP-positive inclusions. tdTomato/mCherry-tagged proteins were imaged in Channel 3. For assays focused on examining the localisation patterns of GFP-tagged proteins and without in-depth analysis of tdTomato/mCherry-tagged proteins, Channel 3 objects were simply identified using the Isodata threshold method with an offset value of 6 (Figure 5.1, d).

5.3 Results

5.3.1 Characterisation of cellular models of SOD1-, TDP-43-, FUS-, CCNF- VAPB-, VCP-, OPTN-, and UBQLN2-associated ALS and optimisation of image analysis parameters

Given the extraordinary molecular heterogeneity of ALS, it was of interest to create ALS models that collectively would represent a diversity of fALS forms. Thus, models of SOD1-, TDP-43-, FUS-, CCNF-, VAPB-, VCP-, OPTN- and UBQLN2-associated ALS using the neuronal NSC-34 cell line and EGFP-/tGFP-/mCherry-fusion plasmids were generated. The genetic mutations in these models were selected after careful consideration of the mutations that segregate with ALS; *SOD1*^{A4V} (Deng *et al.* 1993), *TARDBP*^{M337V} (Tamaoka *et al.* 2010), *FUS*^{R495X}, *FUS*^{R521G} (Kwiatkowski *et al.* 2009, Vance *et al.* 2009), *CCNF*^{S621G} (Williams *et al.* 2016), *UBQLN2*^{P497H} (Deng *et al.* 2011), *OPTN*^{E478G} (Maruyama *et al.* 2010), *VAPB*^{P56S} (Nishimura *et al.* 2004), *VCP*^{R159H} and *VCP*^{R191Q} (Johnson *et al.* 2010, Abramzon *et al.* 2012, Koppers *et al.* 2012).

Prior to using these NSC-34 models with the HCS platform, the localisation patterns of each EGFP-/tGFP-/mCherry-fusion WT and mutant ALS-associated protein in transfected NSC-34 cells were characterised by imaging at 48 h post-transfection using confocal microscopy. As a measure of toxicity caused by the expression of each fusion gene, live cell fluorescent imaging was used to image and count the numbers of transfected cells (detected as EGFP-/tGFP- or mCherry-positive cells) over 80 h. The solubility of each protein in NSC-34 cells was examined using an assay to permeabilise the plasma membrane of transfected cells using saponin, allowing soluble intracellular proteins to diffuse out of the cell while trapping insoluble protein material. Cells were imaged pre- and post-permeabilisation with saponin to quantify numbers of transfected cells and numbers of cells containing insoluble EGFP-/tGFP- and mCherry-fusion proteins, respectively. To confirm that the fluorescent protein tags had little or no

aggregation propensity themselves, in each experiment NSC-34 cells were also transfected with empty vectors to express EGFP or mCherry alone. Confocal microscopy of cells transfected with EGFP or mCherry alone demonstrated that the EGFP and mCherry proteins are diffusely distributed throughout the cell and themselves do not aggregate (Figure 5.2, a, i and b, i). It was also confirmed that the expression of EGFP or mCherry alone had no effect on the viability of transfected cells. Numbers of cells expressing EGFP or mCherry alone steadily increased over the 80 h imaging period (Figure 5.2, a, ii and b, ii).

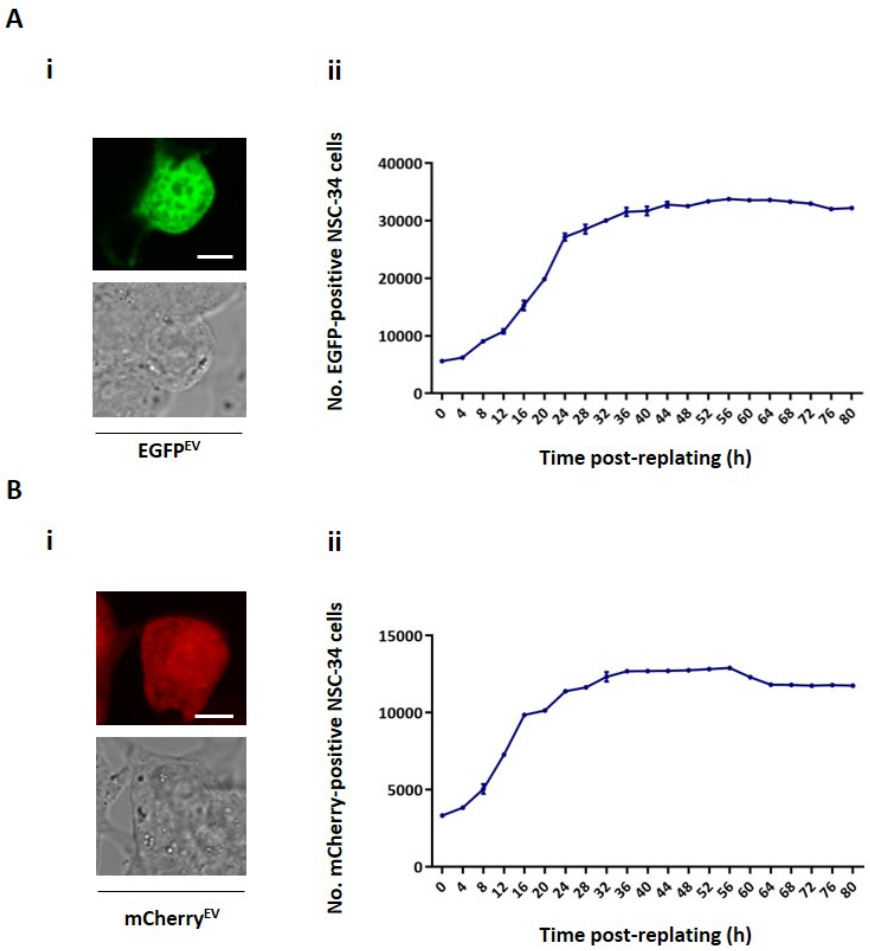

Figure 5.2. Localisation patterns of EGFP and mCherry alone, and cell population growth over time of NSC-34 cells expressing EGFP or mCherry alone. Live cell imaging of NSC-34 cells transiently transfected with (A) the pEGFP-N1 vector (EGFP alone) or (B) the pmCherry-C1 vector (mCherry alone). (A, i and B, i) Representative images of transfected cells taken using a Leica TCS SP5 II confocal microscope at 48 h post-transfection. Scale bars represent 10 µm. (A, ii and B, ii) To measure viability of NSC-34 cells transiently transfected to express EGFP or mCherry alone, cells were imaged in an IncuCyte® ZOOM and numbers of transfected cells (EGFP- or mCherry-positive cells) were monitored over 80 h. Graphs represent the mean ± SEM of the numbers of EGFP- or mCherry-positive transfected cells over 80 h.

5.3.1.1 Localisation patterns and aggregation of SOD1^{A4V}, TDP-43^{M337V}, FUS^{R495X}, FUS^{R521G} and CCNF^{S621G} in NSC-34 cells

It was important to be able to distinguish inclusions of the fusion proteins from the appearance of foci that could result from their normal colocalisation with other cellular structures and organelles; e.g. TDP-43 and FUS with SGs, OPTN with the Golgi apparatus (0.1-2 µm) (Guil *et al.* 2006, Maruyama *et al.* 2010). Inclusions of ALS-associated proteins are generally in the range 2-20 µm in diameter in human post-mortem tissue (Leigh *et al.* 1991, Shibata *et al.* 1994, Strong *et al.* 2005, Maruyama *et al.* 2010, Teyssou *et al.* 2013) and in cell culture models (Johnston 2000, Matsumoto *et al.* 2005, Matsumoto *et al.* 2006, Cozzolino 2008, Kuijpers *et al.* 2013, Zeineddine *et al.* 2015). A size minimum of 2 µm was thus established as suitable for categorising fluorescent foci as inclusions. The foci formed by SOD1^{A4V}-EGFP, TDP-43^{M337V}-tGFP, FUS^{R495X}-tGFP, FUS^{R521G}-tGFP and CCNF^{S621G}-mCherry were manually examined in images of cells and were consistently measured to be larger than 2 µm (Figures 5.3 and 5.4). The localisation patterns and solubility of SOD1^{A4V}-EGFP, and the toxicity caused by its expression in NSC-34 cells, was assayed and is presented in Ch. IV (Figures 4.1 and 4.4).

TDP-43, in addition to FUS, are predominantly nuclear-localised RBPs with additional cytoplasmic roles in the formation and dynamics of SGs. Imaging transfected NSC-34 cells using confocal microscopy, it was observed that the tGFP-tagged WT proteins remained localised to cell nuclei, while the TDP-43^{M337V}, FUS^{R521G} and FUS^{R495X} mutants mislocalised to the cytoplasm and formed large aggregates and smaller foci, as is observed in ALS patient tissue (Figure 5.3, a, i and b, i) (Kwiatkowski *et al.* 2009, Vance *et al.* 2009, Tamaoka *et al.* 2010). Although TDP-43^{WT}-tGFP was not observed to mislocalise and accumulate into cytoplasmic inclusions when transfected cells were examined using confocal microscopy, after permeabilising the plasma membrane of transfected cells and imaging using an IncuCyte TDP-43^{WT}-tGFP was found to remain inside 55% of transfected cells (Figure 5.3, a, ii). However, a

significantly greater percentage of cells expressing TDP-43^{M337V}-tGFP were tGFP-positive following saponin permeabilisation (79%) when compared to cells expressing TDP-43^{WT}-tGFP (p = 0.0035). The large proportion of TDP-43^{WT}-tGFP-expressing cells that remained tGFP-positive after saponin treatment may be due, in part, to the concentration of saponin solution used, and the length of time that cells were incubated in saponin solution being insufficient to permeabilise the nuclear membrane inside cells. Thus, TDP-43^{WT}-tGFP that was localised within nuclei may not have been released when cells were incubated with saponin solution. In this case, the saponin-permeabilisation assay may not be appropriate for assaying the formation of TDP-43 cytoplasmic inclusions, as it may not enable distinction between TDP-43 that is localised to nuclei and TDP-43 that has accumulated into insoluble cytoplasmic inclusions. Similarly, while FUS^{WT}-tGFP was not observed to mislocalise and accumulate into cytoplasmic inclusions when transfected cells were examined using confocal microscopy, the saponin-permeabilisation assay quantified that FUS^{WT}-tGFP remained in 22.7% of transfected cells following incubation with saponin solution (Figure, 5.3, b, ii). Moreover, the percentage of cells expressing FUS^{R495X}-tGFP that remained tGFP-positive following incubation with saponin solution (26.2%) was similar to that of cells expressing FUS^{WT}-tGFP. However, there was a significantly greater percentage of cells expressing FUS^{R521G}-tGFP that remained tGFP-positive following incubation with saponin solution (52.4%) compared to both cells expressing FUS^{WT}-tGFP and cells expressing FUS^{R495X}-tGFP (FUS^{WT}-tGFP, p = 0.0012; FUS^{R495X}-tGFP, p = 0.0023). As noted above, when cells expressing the FUS-tGFP constructs were examined using confocal microscopy, there was extensive formation of small foci (< 2 μm) and large aggregates by both FUS mutants (Figure 5.3, b, i). Thus, the similar percentages of cells expressing FUS^{WT}-tGFP and FUS^{R495X}-tGFP that remained tGFP-positive after saponin-permeabilisation compared to the marked differences in their localisation patterns indicates that the saponin-permeabilisation assay may not be appropriate for measuring the formation of insoluble

cytoplasmic mutant FUS-tGFP inclusions.

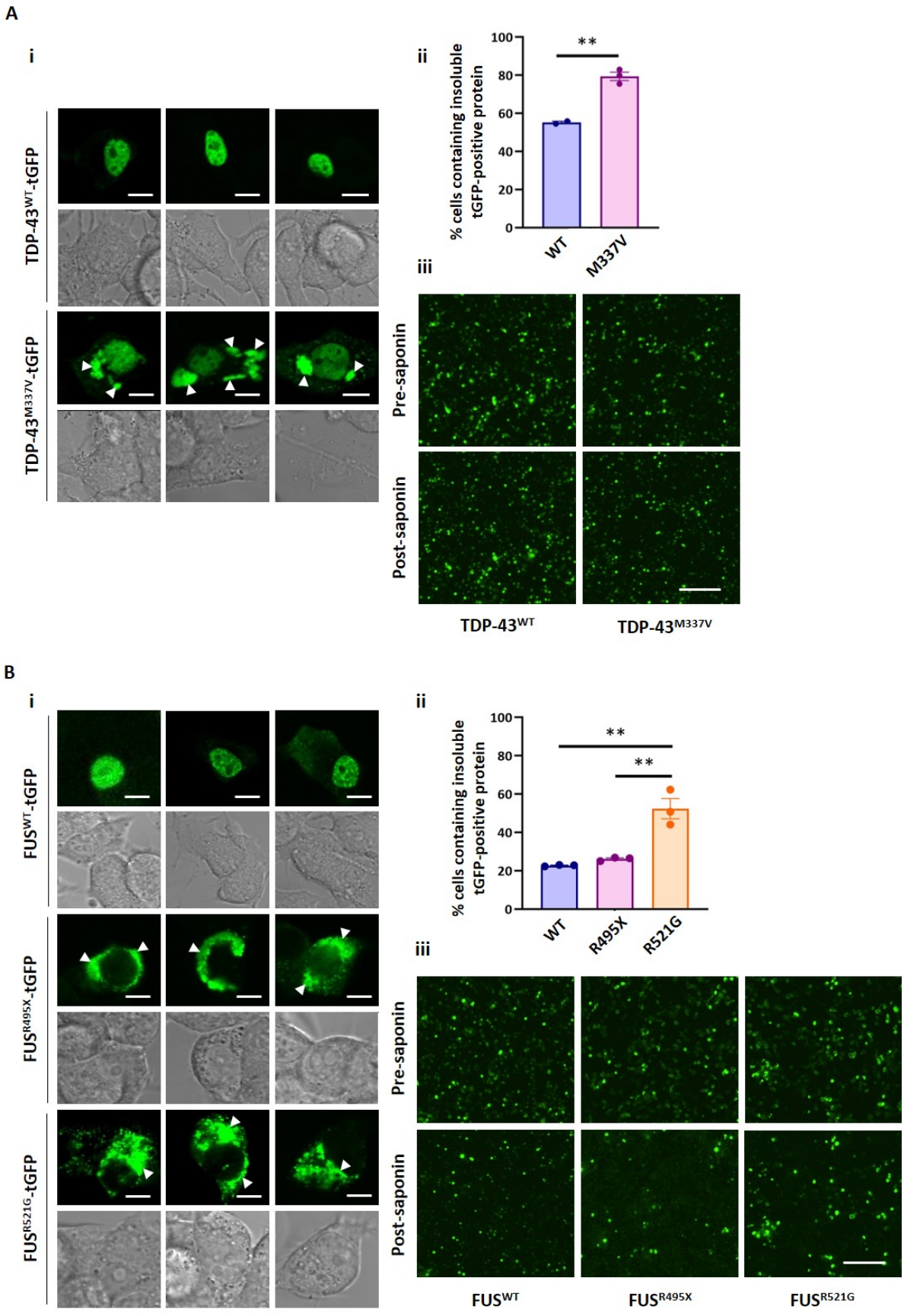
A
i
TDP-43WT-tGFP
TDP-43M337V-tGFP
ii
% cells containing insoluble tGFP-positive protein
100
80
60
40
20
0
**
WT
M337V
iii
Pre-saponin
Post-saponin
TDP-43WT
TDP-43M337V
B
i
FUSWT-tGFP
FUSR495X-tGFP
FUSR521G-tGFP
ii
% cells containing insoluble tGFP-positive protein
100
80
60
40
20
0
**
**
WT
R495X
R521G
iii
Pre-saponin
Post-saponin
FUSWT
FUSR495X
FUSR521G

Figure 5.3. Characterising the localisation patterns and intracellular solubility of ALS-associated TDP-43^{M337V}, FUS^{R495X} and FUS^{R521G}. NSC-34 cells were transiently transfected with (A) TDP-43^{WT}-tGFP or TDP-43^{M337V}-tGFP or (B) FUS^{WT}-tGFP, FUS^{R495X}-tGFP or FUS^{R521G}-tGFP. After 48 h, transfected cells were either (A, i and B, i) imaged using a Leica TCS SP5 II confocal microscope or (A, ii, iii and B, ii, iii) imaged on an IncuCyte® ZOOM, followed by incubation with 0.03% (w/v) saponin in PBS for 10 min at room temperature, before being imaged again on the IncuCyte. (A, i and B, i) Representative images from confocal microscopy, with white arrow heads indicating inclusions formed by the tGFP-fusion proteins. Scale bars represent 10 µm. (A, ii and B, ii) Cells were transfected in quadruplicate, and the data presented is the mean ± SEM of the percentage of transfected NSC-34 cells containing insoluble tGFP-positive protein following permeabilisation with saponin. Differences between the means were determined using Student's t test or one-Way ANOVA followed by Tukey's Multiple Comparison Test. ** indicates $p < 0.01$. (A, iii and B, iii) Representative IncuCyte images of NSC-34 cells prior to permeabilisation with saponin (pre-saponin) and immediately following permeabilisation with saponin (post-saponin), from which the graphs in A, ii and B, ii were derived. Scale bars represent 150 µm.

CCNF functions as a substrate recognition subunit of Skp1-Cul1-F-box (SCF) E3 ubiquitin ligase complexes that mediate the ubiquitylation and proteasomal degradation of target proteins (D'Angiolella *et al.* 2013). Since the identification of the S621G *CCNF* mutation in ALS and FTD patients (Williams *et al.* 2016), the localisation patterns of the CCNF^{S621G} mutant in motor neurons have not been investigated in detail. However, Lee *et al.* (2018) carried out immunofluorescence microscopy of CCNF^{S621G} in Neuro-2A cells, in which CCNF^{S621G} was localised to inclusion-like structures in a proportion of cells while CCNF^{WT} generally displayed diffuse distribution throughout the cells. In the present work, mCherry-tagged CCNF^{WT} fluorescence was observed to have a diffuse distribution throughout the nucleus and cytoplasm of all imaged cells (Figure 5.4, a). In contrast, CCNF^{S621G}-mCherry formed into particularly large amorphous aggregates ranging from 5 to > 10 µm. Interestingly, however, saponin-permeabilisation of the plasma membranes of cells expressing CCNF^{WT}-mCherry and CCNF^{S621G}-mCherry revealed that both proteins formed extensively into insoluble structures, with > 50% of both cells transfected with CCNF^{WT}-mCherry and cells transfected with CCNF^{S621G}-mCherry containing insoluble mCherry-positive protein following permeabilisation (Figure 5.4, b). Nevertheless, there were significantly more CCNF^{S621G}-mCherry-expressing cells containing insoluble mCherry-positive protein (67.8%) following permeabilisation than there were of CCNF^{WT}-mCherry cells (54.9%) ($p = 0.0085$).

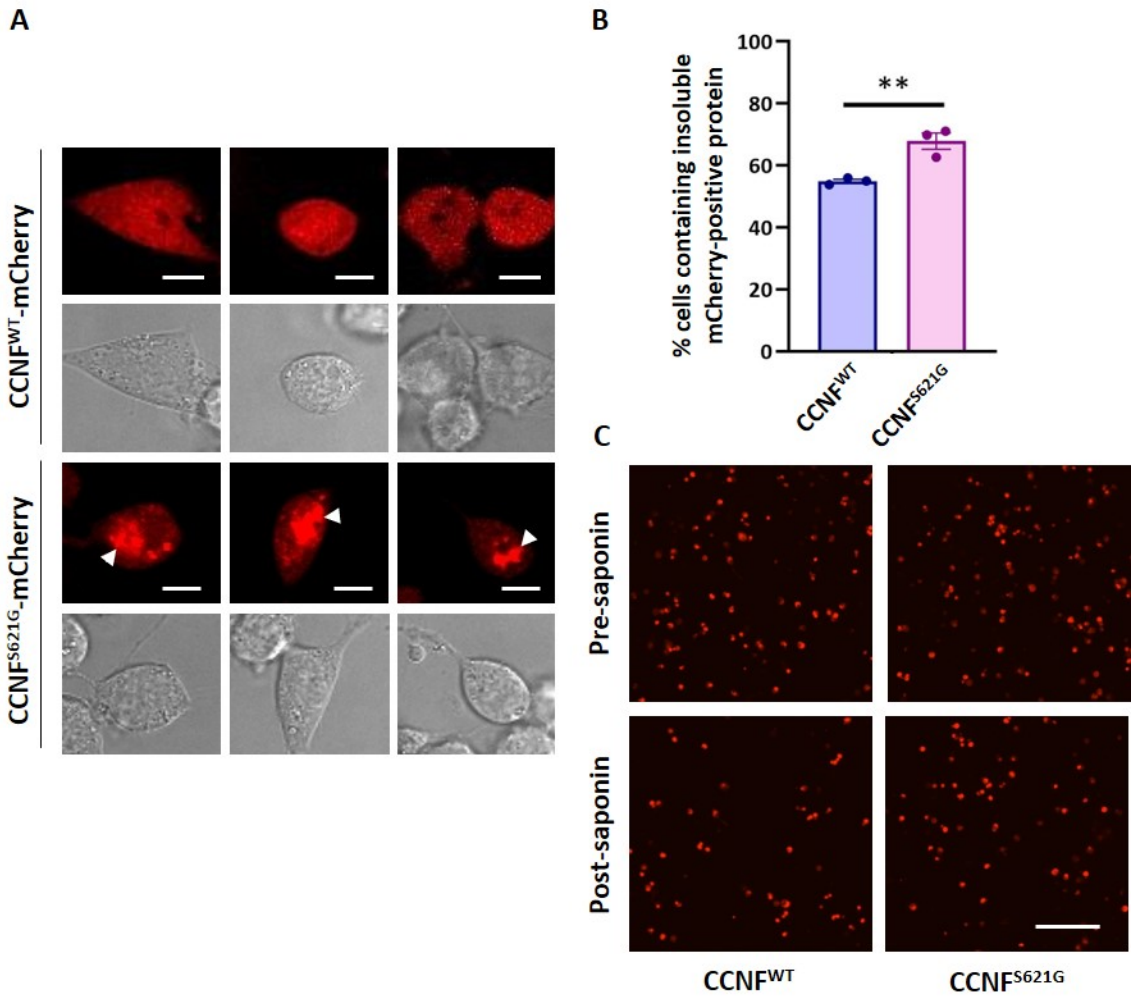

Figure 5.4. Characterising the localisation pattern and intracellular solubility of ALS-associated CCNF^{S621G}. NSC-34 cells were transiently transfected with CCNF^{WT}-mCherry or CCNF^{S621G}-mCherry. After 48 h, transfected cells were either (A) imaged using a Leica TCS SP5 II confocal microscope or (B and C) imaged on an IncuCyte® ZOOM, followed by incubation with 0.03% (w/v) saponin in PBS for 10 min at room temperature, before being imaged again on the IncuCyte. (A) Representative images from confocal microscopy, with white arrow heads indicating inclusions formed by CCNF^{S621G}-mCherry. Scale bars represent 10 µm. (B) Cells were transfected in quadruplicate, and the data presented is the mean ± SEM of the percentage of transfected NSC-34 cells containing insoluble mCherry-positive protein following permeabilisation with saponin. Differences between the means were determined using a Student's t test. ** indicates $p < 0.01$. (C) Representative IncuCyte images of NSC-34 cells prior to permeabilisation with saponin (pre-saponin) and immediately following permeabilisation with saponin (post-saponin), from which the graph in B was derived. Scale bar represents 150 µm.

5.3.1.2 The expression of SOD1^{A4V}, TDP-43^{M337V}, FUS^{R495X}, FUS^{R521G} and CCNF^{S621G} cause toxicity in NSC-34 cells

Live cell imaging of cells expressing TDP-43^{WT}-tGFP and TDP-43^{M337V}-tGFP to monitor cell population growth showed that the numbers of TDP-43^{M337V}-tGFP expressing cells had a significantly slower population growth rate compared to cells expressing TDP-43^{WT}-tGFP ($p <$

0.01) (Figure 5.5, a and b). The numbers of cells expressing TDP-43^{M337V}-tGFP began to plateau after ~48 h post-transfection (24 h post-replating) while the numbers of TDP-43^{WT}-tGFP expressing cells continued to increase steadily until ~72 h post-transfection (48 h post-replating). Comparison of the mean numbers of tGFP-positive transfected cells at 72 h post-transfection showed that there was a significantly greater number of cells expressing TDP-43^{WT}-tGFP than there was of cells expressing TDP-43^{M337V}-tGFP ($p < 0.001$) (Figure 5.5, c).

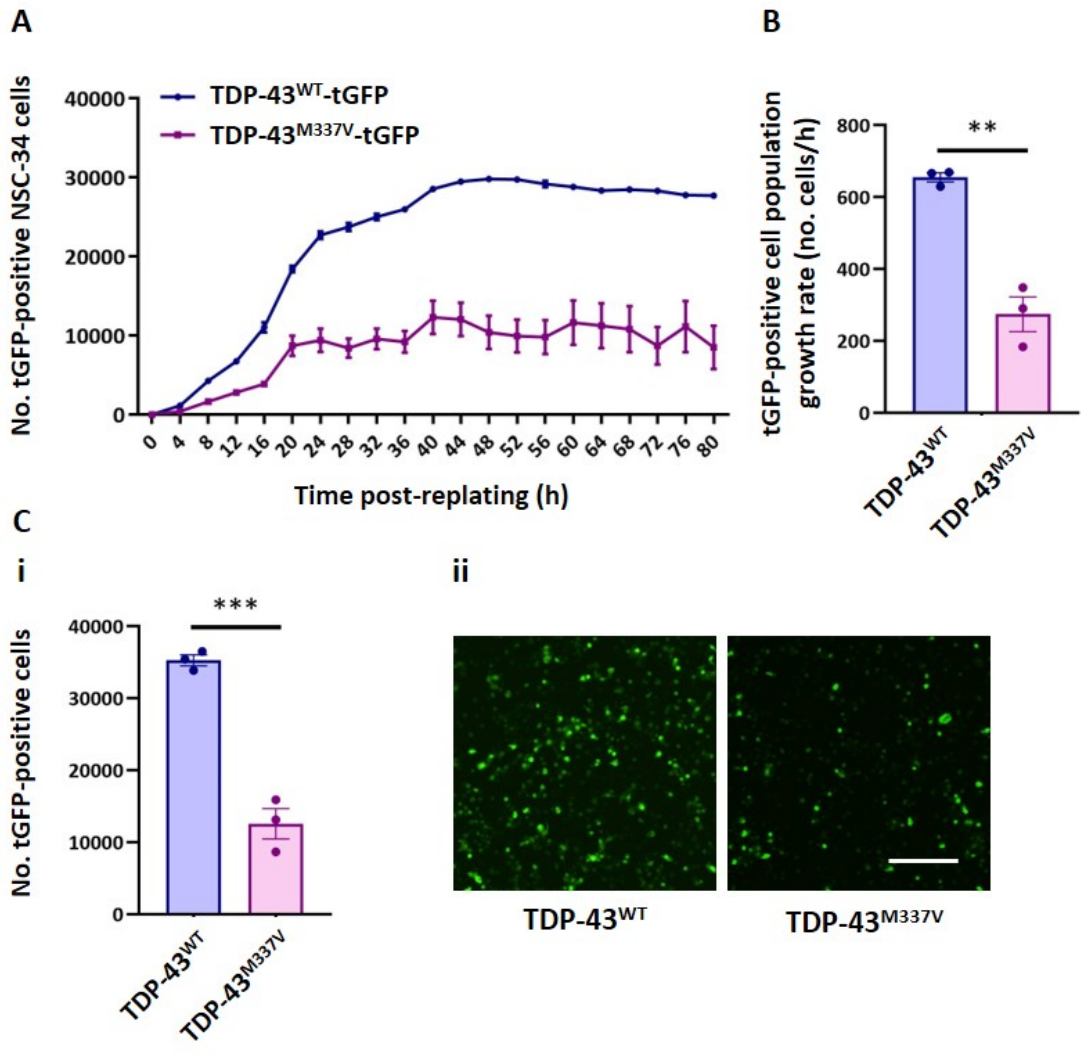

Figure 5.5. ALS-associated TDP-43^{M337V} causes toxicity in NSC-34 cells. NSC-34 cells were transiently transfected with TDP-43^{WT}-tGFP or TDP-43^{M337V}-tGFP and imaged in an IncuCyte® ZOOM over 80 h. Graphs represent the mean ± SEM of (A) numbers of tGFP-positive transfected cells over 80 h, (B) population growth rates of transfected cells and (C, i) numbers of transfected cells at 48 h post-replating, in triplicate wells of cells. (C, ii) Representative IncuCyte images of NSC-34 cells at 48 h post-replating, from which the graph in C, i, was derived. Scale bar represents 150 µm. Differences between the means were determined using Student's t tests. ** indicates $p < 0.01$, *** indicates $p < 0.001$.

The expression of FUS^{R495X}-tGFP and of FUS^{R521G}-tGFP was observed to cause reduced population growth of NSC-34 cells compared to FUS^{WT}-tGFP (Figure 5.6). While the numbers of cells expressing FUS^{WT}-tGFP continued to increase steadily over the 80 h imaging period, the numbers of both FUS^{R495X}-tGFP and FUS^{R521G}-tGFP cells began to plateau after ~40 h (Figure 5.6, a). There was no difference in population growth rate between the two FUS mutants, but both exhibited significantly reduced population growth compared to cells expressing FUS^{WT}-tGFP (FUS^{R495X}-tGFP, $p = 0.0019$; FUS^{R521G}-tGFP, $p = 0.0041$) (Figure 5.6, b). At 72 h post-transfection there were significantly greater numbers of cells expressing FUS^{WT}-tGFP than there were of cells expressing either of the two mutants (FUS^{R495X}-tGFP, $p = 0.0014$; FUS^{R521G}-tGFP, $p = 0.0023$) (Figure 5.6, c).

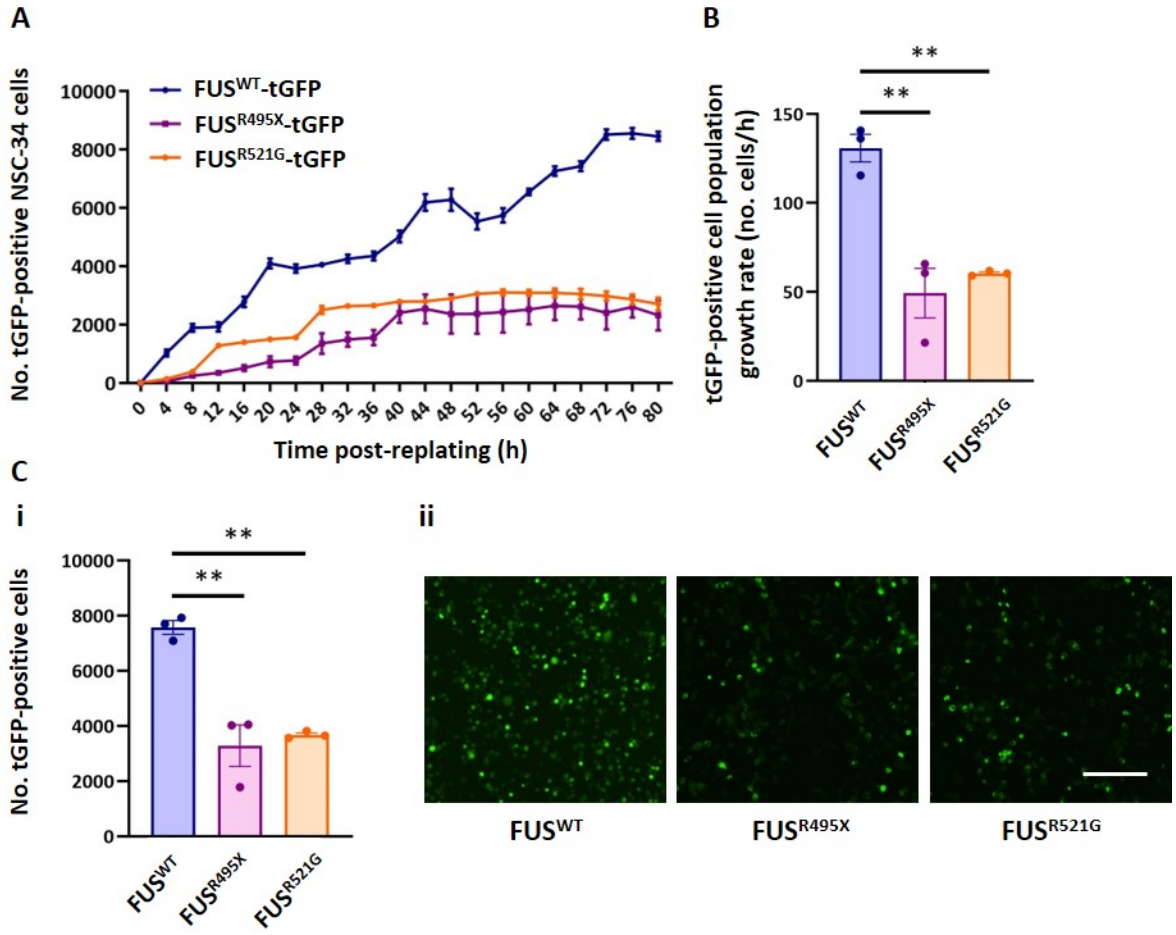

Figure 5.6. ALS-associated FUS^{R495X} and FUS^{R521G} cause toxicity in NSC-34 cells. NSC-34 cells were transiently transfected with FUS^{WT}-tGFP, FUS^{R495X}-tGFP or FUS^{R521G}-tGFP and imaged in an IncuCyte® ZOOM over 80 h. Graphs represent the mean ± SEM of (A) numbers of tGFP-positive transfected cells over 80 h, (B) population growth rates of transfected cells and (C, i) numbers of transfected cells at 48 h post-replating, in triplicate wells of cells. (C, ii) Representative IncuCyte images of NSC-34 cells at 48 h post-replating, from which the graph in C, i, was derived. Scale bar represents 150 µm. Differences between the means were determined using one-Way ANOVA followed by Tukey's Multiple Comparison Test. ** indicates $p < 0.01$.

CCNF^{S621G}-mCherry caused striking inhibition of cell population growth, with live cell imaging revealing that the numbers of CCNF^{S621G}-mCherry cells plateaued and dropped off steadily 28 h after replating (Figure 5.7, a). Analysis of the growth rates of the cell population expressing the CCNF-mCherry constructs showed that the rate of growth of CCNF^{S621G}-mCherry cells was markedly slower than that of CCNF^{WT}-mCherry cells ($p < 0.0001$) (Figure 5.7, b). At 72 h post-transfection the differences in growth between cells expressing CCNF^{WT}-mCherry and CCNF^{S621G}-mCherry was clearly evident in the significantly lower numbers of CCNF^{S621G}-

mCherry cells than CCNF^{WT}-mCherry cells ($p < 0.0001$) (Figure 5.7, c).

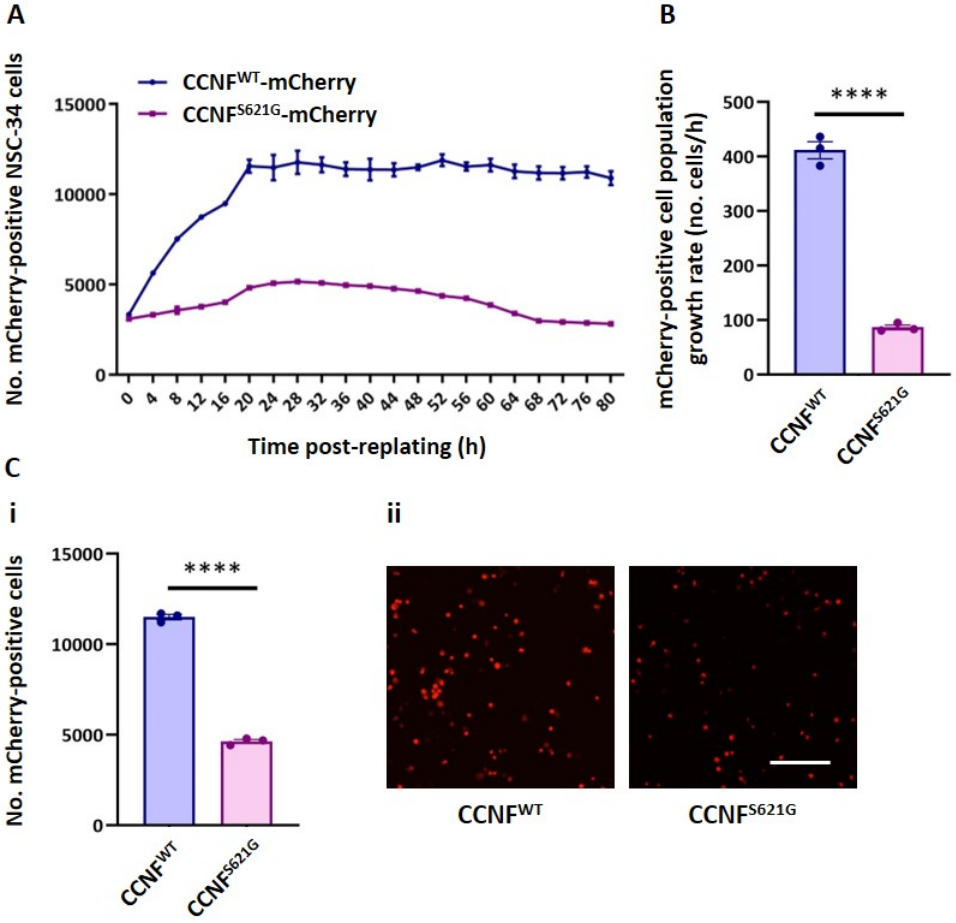

Figure 5.7. ALS-associated CCNF^{S621G} causes toxicity in NSC-34 cells. NSC-34 cells were transiently transfected with CCNF^{WT}-mCherry or CCNF^{S621G}-mCherry and imaged in an IncuCyte® ZOOM over 80 h. Graphs represent the mean ± SEM of (A) numbers of mCherry-positive transfected cells over 80 h, (B) population growth rates of transfected cells and (C, i) numbers of transfected cells at 48 h post-replating, in triplicate wells of cells. (C, ii) Representative IncuCyte images of NSC-34 cells at 48 h post-replating, from which the graph in C, i, was derived. Scale bar represents 150 µm. Differences between the means were determined using Student's t tests. **** indicates $p < 0.0001$.

5.3.1.3 The expression of UBQLN2^{P497H}, UBQLN2^{P525S}, OPTN^{E478G}, VAPB^{P56S}, VCP^{R159H} and VCP^{R191Q} cause toxicity in NSC-34 cells

Assaying cell population growth using live cell imaging over 80 h, expression of UBQLN2^{P497H}-tGFP and of UBQLN2^{P525S}-tGFP was found to cause reductions in cell population growth rates compared to the expression of UBQLN2^{WT}-tGFP (UBQLN2^{P497H}-tGFP, $p < 0.0001$; UBQLN2^{P525S}-tGFP, $p < 0.001$) (Figure 5.8, b). Interestingly, expression of

the UBQLN2^{P497H}-tGFP mutant was observed to cause greater inhibition of cell population growth compared to the UBQLN2^{P525S}-tGFP mutant, with UBQLN2^{P497H}-tGFP cells exhibiting slower population growth rates ($p = 0.0275$) and dropping down to significantly lower numbers by 72 h post-transfection ($p = 0.0264$) than UBQLN2^{P525S}-tGFP cells (Figure 5.8, c).

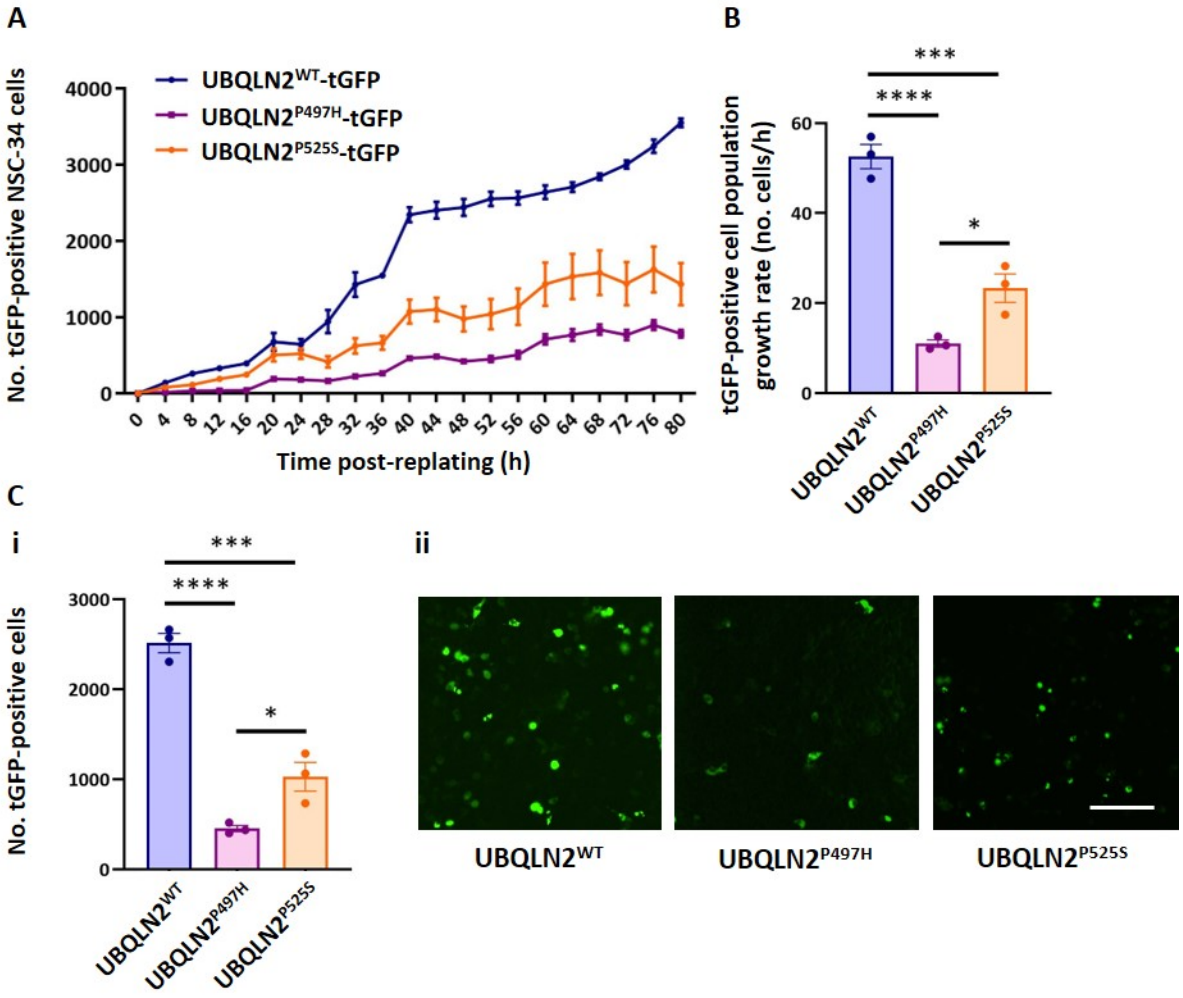

Figure 5.8. ALS-associated UBQLN2^{P497H} and UBQLN2^{P525S} cause toxicity in NSC-34 cells. NSC-34 cells were transiently transfected with UBQLN2^{WT}-tGFP, UBQLN2^{P497H}-tGFP or UBQLN2^{P525S}-tGFP and imaged in an IncuCyte® ZOOM over 80 h. Graphs represent the mean ± SEM of (A) numbers of tGFP-positive transfected cells over 80 h, (B) population growth rates of transfected cells and (C, i) numbers of transfected cells at 48 h post-replating, in triplicate wells of cells. (C, ii) Representative IncuCyte images of NSC-34 cells at 48 h post-replating, from which the graph in C, i, was derived. Scale bar represents 150 µm. Differences between the means were determined using one-Way ANOVA followed by Tukey's Multiple Comparison Test. * indicates $p < 0.05$, *** indicates $p < 0.001$, **** indicates $p < 0.0001$.

In NSC-34 cells expressing the VAPB-tGFP constructs, a clear reduction was observed in the population growth of cells expressing VAPB^{P56S}-tGFP compared to cells expressing VAPB^{WT}-tGFP (Figure 5.9). Although numbers of transfected cells were low due to low transfection efficiency, total cell density was high, increasing from ~70% to ~95% over the 80 h imaging period (data not shown). There was thus no potential effect of low total cell density on the proliferation or loss of the VAPB-tGFP-expressing cells. Comparison of the numbers of VAPB-tGFP cells in the first 20 h of imaging confirmed that VAPB^{P56S}-tGFP significantly reduced the population growth rate of cells ($p = 0.0203$) (Figure 5.9, b). The numbers of tGFP-positive cells expressing VAPB^{P56S}-tGFP at 48 h post-replating were significantly lower than cells expressing VAPB^{WT}-EGFP ($p < 0.0001$) (Figure 5.9, c), further highlighting the toxicity caused by expression of the P56S mutation.

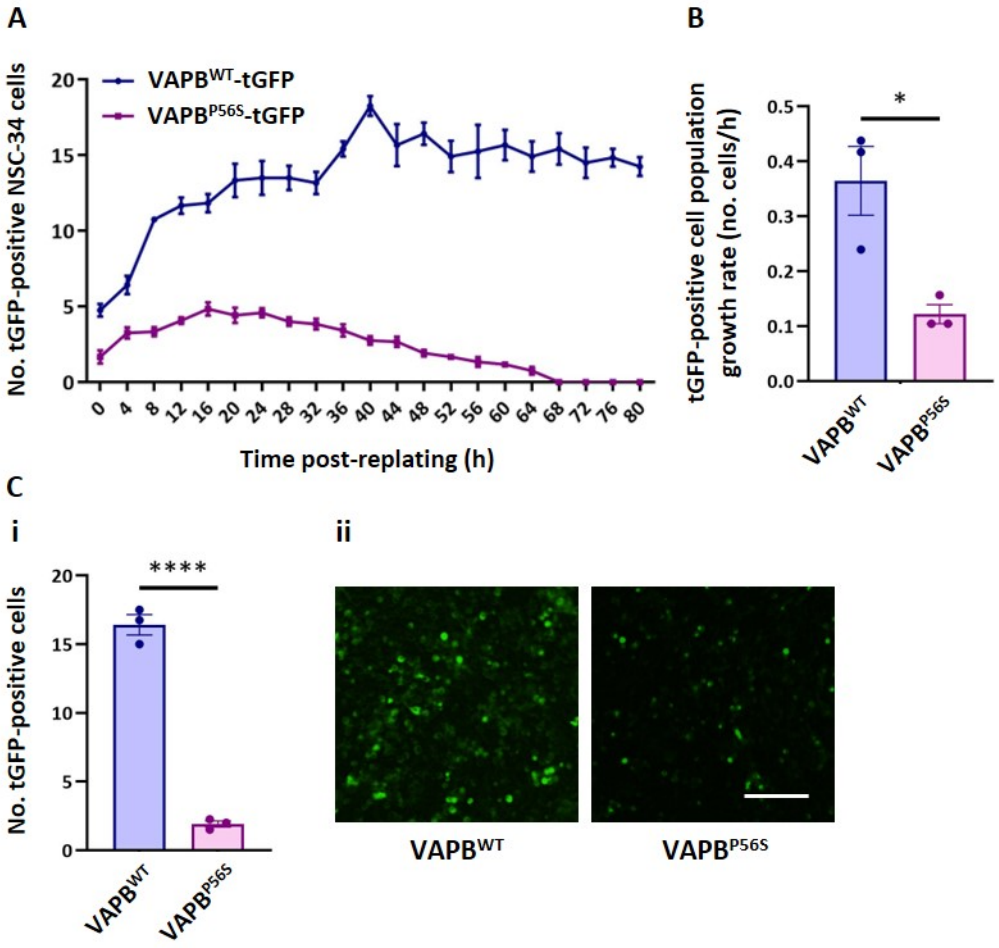

Figure 5.9. ALS-associated VAPB^{P56S} causes toxicity in NSC-34 cells. NSC-34 cells were transiently transfected with VAPB^{WT}-tGFP or VAPB^{P56S}-tGFP and imaged in an IncuCyte® ZOOM over 80 h. Graphs represent the mean ± SEM of (A) numbers of tGFP-positive transfected cells over 80 h, (B) population growth rates of transfected cells and (C, i) numbers of transfected cells at 48 h post-replating, in triplicate wells of cells. . (C, ii) Representative IncuCyte images of NSC-34 cells at 48 h post-replating, from which the graph in C, i, was derived. Scale bar represents 150 µm. Differences between the means were determined using Student's t tests. * indicates $p < 0.05$, **** indicates $p < 0.0001$.

The expression of OPTN^{E478G}-EGFP reduced the population growth rate of transfected cells compared to cells expressing OPTN^{WT}-EGFP (Figure 5.10). In the first 20 h of imaging, the population growth rate of OPTN^{E478G}-EGFP-expressing cells was significantly slower than that of OPTN^{WT}-EGFP expressing cells ($p = 0.0139$) (Figure 5.10, b). Comparison of the numbers of transfected cells at 48 h post-replating showed that there were significantly more viable OPTN^{WT}-EGFP-expressing cells than of OPTN^{E478G}-EGFP-expressing cells ($p < 0.001$) (Figure 5.10, c), demonstrating that overexpression of the E478G mutant caused considerable toxicity in NSC-34 cells.

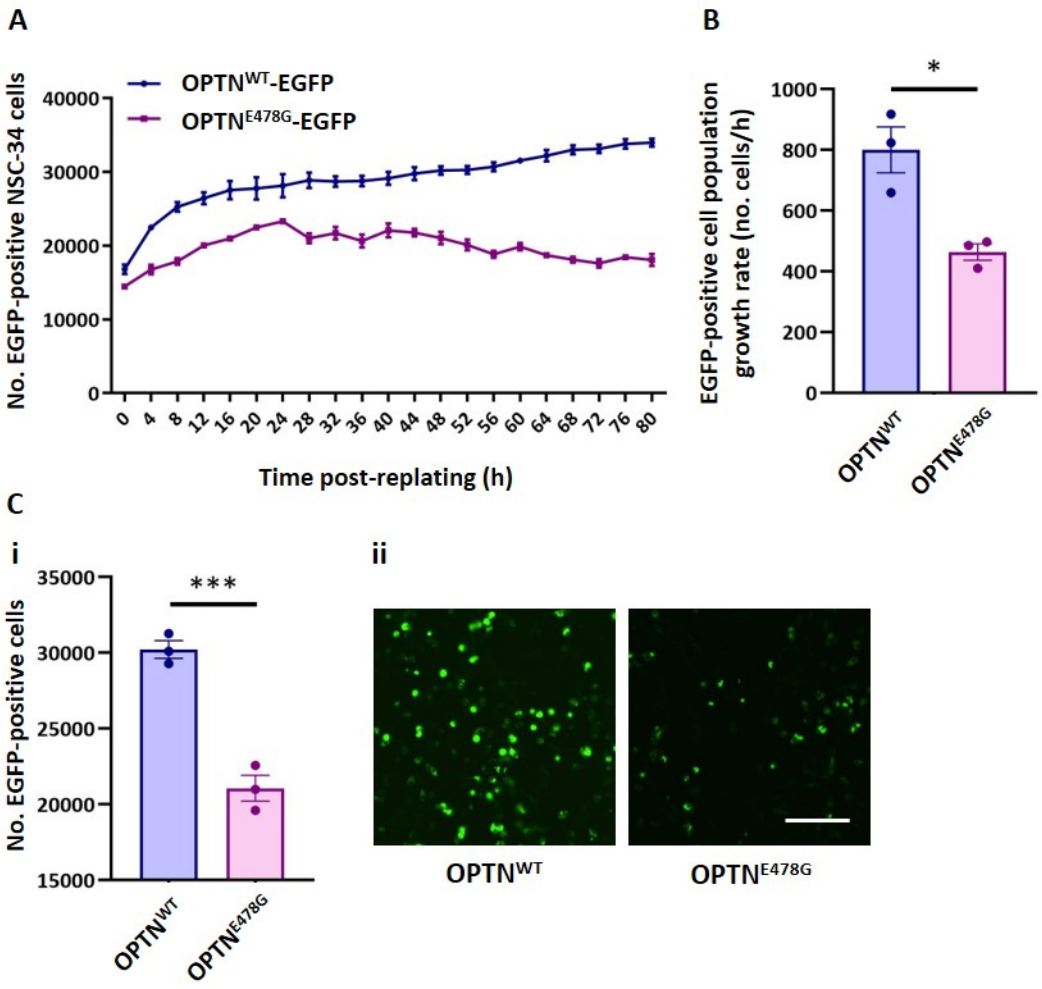

Figure 5.10. ALS-associated OPTN^{E478G} causes toxicity in NSC-34 cells. NSC-34 cells were transiently transfected with OPTN^{WT}-EGFP or OPTN^{E478G}-EGFP and imaged in an IncuCyte® ZOOM over 80 h. Graphs represent the mean ± SEM of (A) numbers of EGFP-positive transfected cells over 80 h, (B) population growth rates of transfected cells and (C, i) numbers of transfected cells at 48 h post-replating, in triplicate wells of cells. (C, ii) Representative IncuCyte images of NSC-34 cells at 48 h post-replating, from which the graph in C, i, was derived. Scale bar represents 150 µm. Differences between the means were determined using Student's t tests. * indicates $p < 0.05$, *** indicates $p < 0.001$.

Assaying the numbers of NSC-34 cells expressing the VCP-tGFP constructs over 80 h, it was observed that both mutants significantly reduced the population growth rate of transfected cells relative to VCP^{WT}-tGFP (Figure 5.11). The population growth rate of cells expressing VCP^{R191Q}-tGFP was notably slower than that of cells expressing VCP^{R159H}-tGFP ($p = 0.004$), and 48 h after replating cells the numbers of viable VCP^{R191Q}-tGFP-expressing cells were much lower than the numbers of VCP^{R159H}-tGFP cells ($p = 0.0012$) (Figure 5.11, b and c).

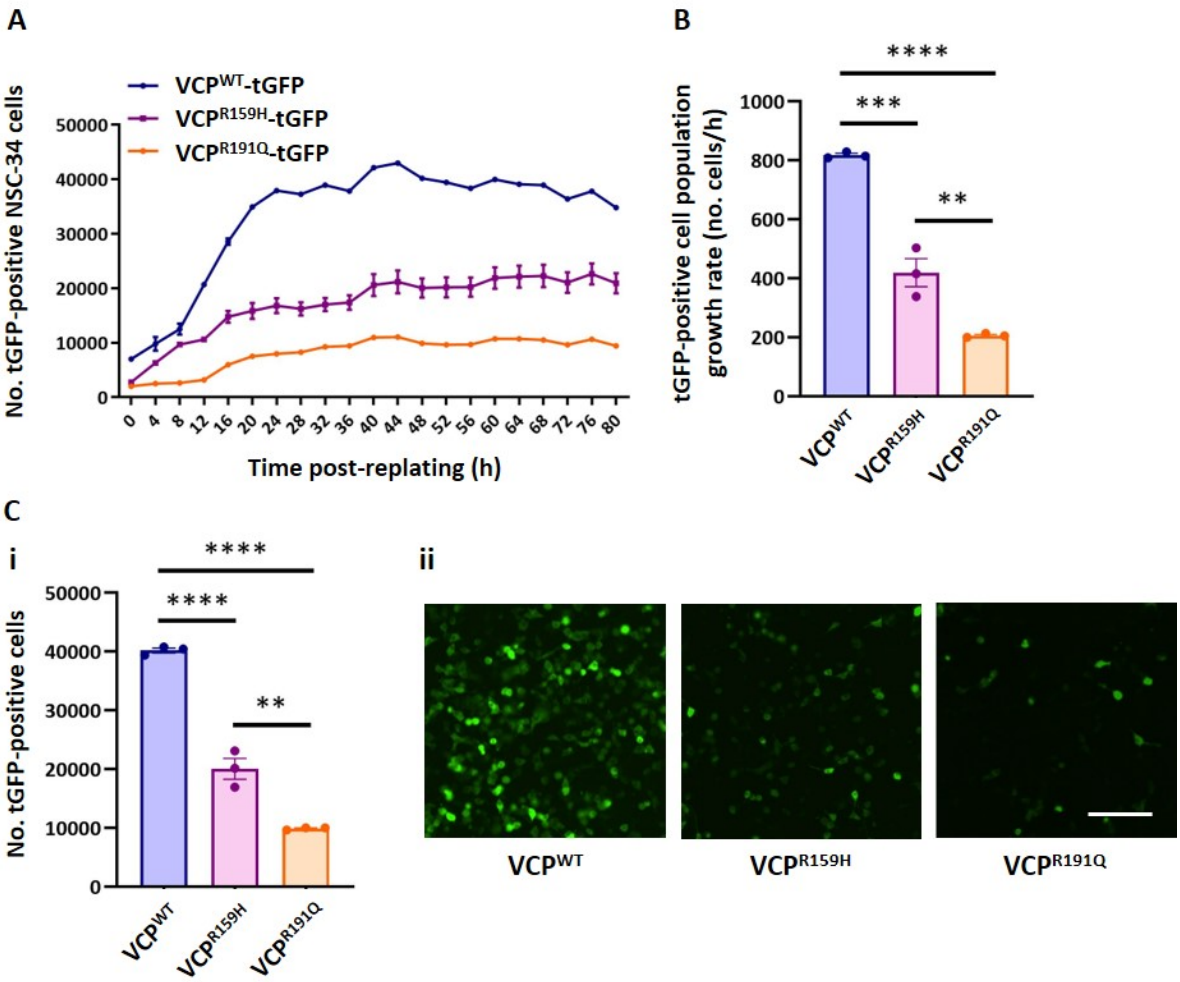

Figure 5.11. ALS-associated VCP^{R159H} and VCP^{R191Q} cause toxicity in NSC-34 cells. NSC-34 cells were transiently transfected with VCP^{WT}-tGFP, VCP^{R159H}-tGFP or VCP^{R191Q}-tGFP and imaged in an IncuCyte® ZOOM over 80 h. Graphs represent the mean ± SEM of (A) numbers of tGFP-positive transfected cells over 80 h, (B) population growth rates of transfected cells and (C, i) numbers of transfected cells at 48 h post-replating, in triplicate wells of cells. (C, ii) Representative IncuCyte images of NSC-34 cells at 48 h post-replating, from which the graph in C, i, was derived. Scale bar represents 150 µm. Differences between the means were determined using one-Way ANOVA followed by Tukey's Multiple Comparison Test. ** indicates $p < 0.01$, *** indicates $p < 0.001$ and **** indicates $p < 0.0001$.

5.3.1.4 Characterisation of mutant UBQLN2, OPTN, VAPB and VCP solubility, localisation and aggregation

The saponin-permeabilisation assay was next used to examine the mobility and solubility of UBQLN2^{P497H}-tGFP, UBQLN2^{P525S}-tGFP, OPTN^{E478G}-EGFP, VAPB^{P56S}-tGFP, VCP^{R159H}-tGFP and VCP^{R191Q}-tGFP in NSC-34 cells. In cells expressing the UBQLN2-tGFP constructs it was found that UBQLN2^{WT}-tGFP had a degree of immobility in cells, with 37% of transfected cells quantified to contain tGFP-positive protein following permeabilisation of their plasma

membranes (Figure 5.12, a). However, the two UBQLN2 mutants, UBQLN2^{P497H}-tGFP and UBQLN2^{P525S}-tGFP, remained inside significantly more cells following permeabilisation; 65.1% (p = 0.002) and 68.1% (p = 0.0012), respectively. Interestingly, the saponin-permeabilisation assay quantified that ~35% of both cells expressing OPTN^{WT}-EGFP and cells expressing OPTN^{E478G}-EGFP contained insoluble EGFP-positive protein following permeabilisation (Figure 5.12, b). As OPTN^{WT} can associate with proteins of the Golgi apparatus (Sahlender *et al.* 2005, Maruyama *et al.* 2010), a proportion of OPTN^{WT}-EGFP may have been bound to the Golgi and thus immobile and unable to diffuse out of cells following saponin treatment. Further experimentation is needed to determine the nature of this post-permeabilisation cell-bound OPTN^{WT}-EGFP. Through saponin permeabilisation of cells transfected with the VCP-tGFP constructs it was quantified that ~9.8% of cells transfected with VCP^{WT}-tGFP retained the tGFP-tagged protein following membrane permeabilisation (Figure 5.12, c). However, both VCP^{R191Q}-tGFP and VCP^{R159H}-tGFP remained cell-associated in significantly greater percentages of transfected cells (VCP^{R191Q}-tGFP, p = 0.0222; VCP^{R159H}-tGFP, p = 0.0111), indicating that both mutants were relatively less mobile and had reduced solubility compared to VCP^{WT}-tGFP.

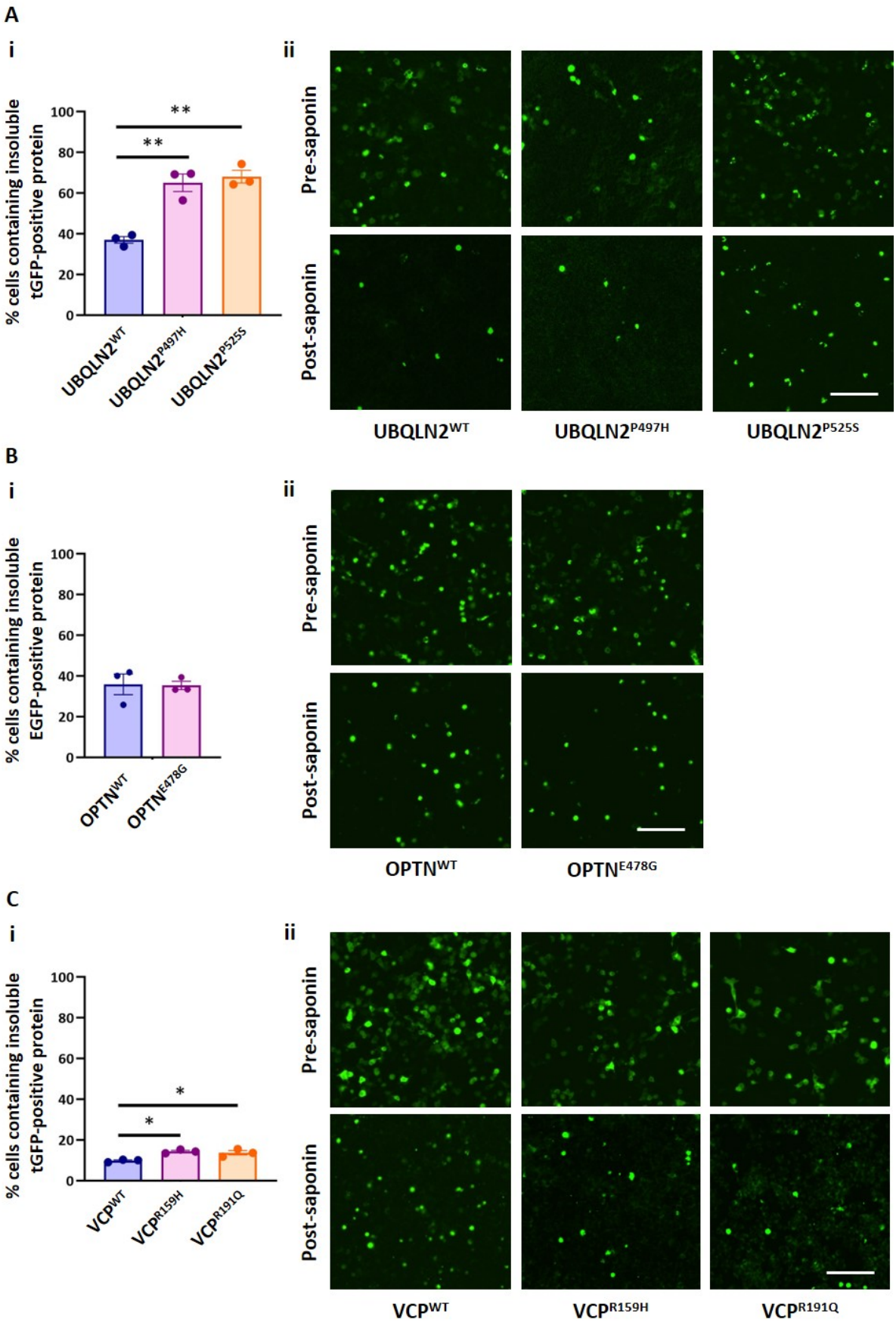
A
i
ii
% cells containing insoluble tGFP-positive protein
100
80
60
40
20
0
**
**
UBQLN2WT
UBQLN2P497H
UBQLN2P525S
Pre-saponin
Post-saponin
UBQLN2WT
UBQLN2P497H
UBQLN2P525S
B
i
ii
% cells containing insoluble EGFP-positive protein
100
80
60
40
20
0
OPTNWT
OPTNE478G
Pre-saponin
Post-saponin
OPTNWT
OPTNE478G
C
i
ii
% cells containing insoluble tGFP-positive protein
100
80
60
40
20
0
*
*
VCPWT
VCPR159H
VCPR191Q
Pre-saponin
Post-saponin
VCPWT
VCPR159H
VCPR191Q

Figure 5.12. Analysis of the release of EGFP-/tGFP-fusion mutant UBQLN2, OPTN and VCP from NSC-34 cells following saponin-permeabilisation. NSC-34 cells were transiently transfected with (A) UBQLN2^{WT}-tGFP, UBQLN2^{P497H}-tGFP or UBQLN2^{P525S}-tGFP, (B) OPTN^{WT}-EGFP or OPTN^{E478G}-EGFP or (C) VCP^{WT}-tGFP, VCP^{R159H}-tGFP or VCP^{R191Q}-tGFP. After 48 h, cells were imaged on an IncuCyte® ZOOM, followed by incubation with 0.03% (w/v) saponin in PBS for 10 min at room temperature, before being imaged again on the IncuCyte. (A, i, B, i and C, i) Cells were transfected in quadruplicate, and the data presented in each graph is the mean ± SEM of the percentage of transfected NSC-34 cells containing insoluble EGFP-/tGFP-positive protein following permeabilisation with saponin. Differences between the means were determined using either Student's t tests or one-Way ANOVA followed by Tukey's Multiple Comparison Test. * indicates $p < 0.05$, ** indicates $p < 0.01$. (A, ii, B, ii and C, ii) Representative IncuCyte images of NSC-34 cells prior to permeabilisation with saponin (pre-saponin) and immediately following permeabilisation with saponin (post-saponin), from which the graphs in A, i, B, i and C, i) were derived. Scale bars represent 150 µm.

Unfortunately, transfections with the VAPB-tGFP constructs for the IncuCyte-based assays resulted in considerably low transfection efficiencies, as can be seen in the low numbers of tGFP-positive transfected cells in Figure 5.9. The numbers of tGFP-positive cells at 48 h post-transfection detected pre- and post-permeabilisation with saponin for VAPB^{P56S}-tGFP were thus too low for analysis. This saponin-treatment experiment also may not have been appropriate for VAPB, as it is an integral membrane protein and thus in its native localisation in cells is immobile and unable to freely diffuse out of permeabilised cells.

The inclusion size cut-off of 2 µm established using confocal microscopy (section 5.3.1.1) was used to examine the association of ubiquitin with inclusions formed by VAPB^{P56S}-tGFP, VCP^{R191Q}-tGFP, VCP^{R159H}-tGFP, OPTN^{E478G}-EGFP and UBQLN2^{P497H}-tGFP. Based on previously published work showing that ubiquitylation of misfolded proteins can determine the type of inclusion into which they are compartmentalised (Kaganovich *et al.* 2008), it was hypothesised that the timing of ubiquitin association with inclusions may provide insight into the aggregation pathways of each ALS-associated protein. At the time of the present work, the dynamics of ubiquitin association with SOD1^{A4V}-EGFP, TDP-43^{M337V}-tGFP and FUS^{R495X}-tGFP inclusions were being characterised by Ms. N. Farrawell (University of Wollongong, NSW, Australia) and have since been published (Farrawell *et al.* 2015). Thus, for this study, the localisation patterns of ubiquitin and mutant VAPB, VCP, OPTN and UBQLN2 were examined in NSC-34 cells co-expressing VAPB^{P56S}-tGFP, VCP^{R191Q}-tGFP, VCP^{R159H}-tGFP,

OPTN^{E478G}-EGFP, or UBQLN2^{P497H}-tGFP and ^{mRFP}ubiquitin over 72 h. UBQLN2-positive inclusions in post-mortem spinal cord tissue from patients with ALS can have varying morphologies, including round and compact, skein-like and large, amorphous inclusions (Deng *et al.* 2011). In the present work, UBQLN2^{P497H}-tGFP formed large cytoplasmic inclusions with an amorphous appearance (Figure 5.13, b). UBQLN2^{P497H}-tGFP inclusions were consistently observed to colocalise with ubiquitin from 24 h through to 72 h post-transfection (Figure 5.13, a), which was also observed for SOD1^{A4V}-EGFP (Farrawell *et al.* 2015).

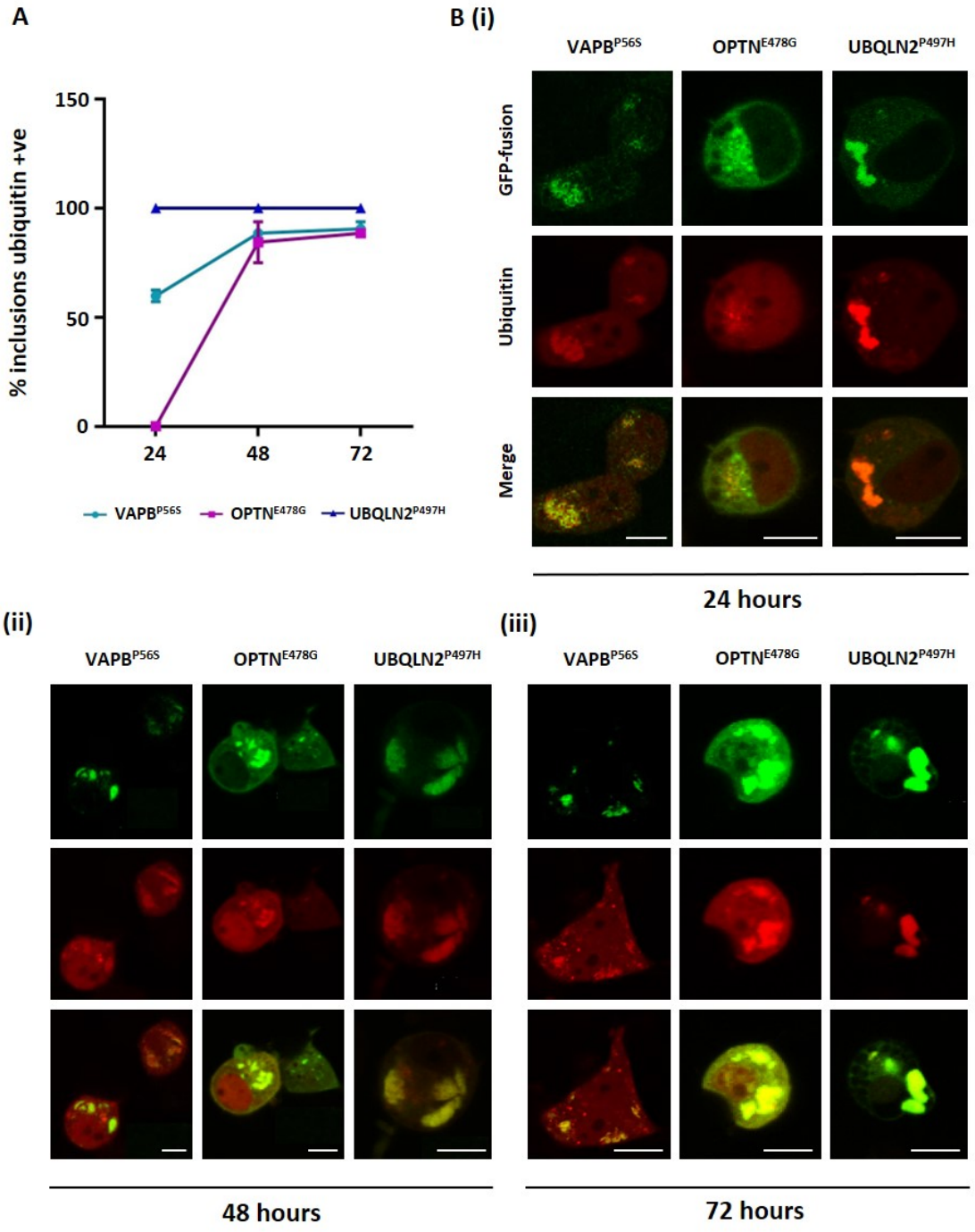

Figure 5.13. The timing of ubiquitin colocalisation to inclusions differs between inclusions formed by mutant VAPB, OPTN and UBQLN2. NSC-34 cells were transiently dual-transfected with VAPB^{P56S}-tGFP, OPTN^{E478G}-EGFP or UBQLN2^{P497H}-tGFP and ^{mRFP}ubiquitin, and imaged at 24 h, 48 h and 72 h post-transfection by confocal microscopy. (A) Percentages of inclusions containing the EGFP-/tGFP-fusion mutant proteins that were also positive for ^{mRFP}ubiquitin in dual-transfected NSC-34 cells at 24 h, 48 h and 72 h post-transfection. At each time point 10-15 fields of view were imaged, with a minimum of 10 dual-transfected cells counted per field. Percentages of EGFP-/tGFP-fusion mutant protein inclusions containing ^{mRFP}ubiquitin at each time point is the mean ± SEM from triplicate wells of dual-transfected cells, from n = 1 experiment. (B) Representative images of dual-transfected NSC-34 cells at (i) 24 h, (ii) 48 h and (iii) 72 h post-transfection. White arrow heads indicate inclusions containing both the EGFP-/tGFP-fusion mutant proteins and ^{mRFP}ubiquitin. Scale bars represent 10 µm.

VAPB is a small type IV membrane protein found in the ER, in intracellular vesicle membranes and in the plasma membrane (Soussan *et al.* 1999, Foster *et al.* 2000, Skehel *et al.* 2000, Amarilio *et al.* 2005, Manford *et al.* 2012). The P56S mutation in *VAPB* causes the protein to oligomerise and aggregate into distinct insoluble inclusions that have been ultrastructurally characterised to contain ER-derived membranous tubules (Nishimura *et al.* 2004, Teuling *et al.* 2007, Tsuda *et al.* 2008, Papiani *et al.* 2012, Kuijpers *et al.* 2013). In the present work, $VAPB^{P56S}$-tGFP inclusions did not always colocalise with ubiquitin, in contrast to mutant UBQLN2 inclusions, as was similarly the case for TDP-43^{M337V} and FUS^{R495X} inclusions (Farrawell *et al.* 2015). At 24 h post-transfection ~60% of $VAPB^{P56S}$-EGFP inclusions were colocalised with ubiquitin, increasing to ~91% after 72 h (Figure 5.13, a).

Imaging cells co-transfected with $OPTN^{WT}$-EGFP or $OPTN^{E478G}$-EGFP and ^{mRFP}ubiquitin using confocal microscopy, $OPTN^{E478G}$-EGFP cells were observed to contain small EGFP-positive foci (< 2 µm) at 24 h post-transfection. These foci were not scored as inclusions as they could not be distinguished from the potential association of OPTN with the Golgi apparatus and related vesicular structures (Ying *et al.* 2010, Ying and Yue 2012). The use of immunofluorescence staining for proteins of the Golgi apparatus and transport vesicles would have enabled characterisation of the nature of these observed foci at 24 h post-transfection. At 48 h post-transfection, $OPTN^{E478G}$-EGFP foci > 2 µm were observed, and were categorised as inclusions (Figure 5.13, a and b, I and ii). At this time point, ~84% of inclusions colocalised with ^{mRFP}ubiquitin, increasing to ~93% after 72 h (Figure 5.13, a and b, ii and iii).

Interestingly, mutant VCP did not form inclusions when co-expressed with ^{mRFP}ubiquitin, however ^{mRFP}ubiquitin inclusions were observed (Figure 5.14, a). As TDP-43-positive inclusions are one of the hallmark features of ALS, it was next examined whether or not the overexpression of WT or mutant VCP caused aggregation of TDP-43^{WT}. NSC-34 cells were co-transfected with VCP^{WT}-tGFP, VCP^{R191Q}-tGFP or VCP^{R159H}-tGFP and TDP-43^{WT}-tdT, a

construct previously generated and described by Yang *et al*. (2010), and imaged after 48 h of incubation. Both VCP-tGFP variants as well as VCP^{WT}-tGFP were observed to form inclusions that colocalised with TDP-43^{WT}-tdT in all cells that were imaged (Figure 5.14, b).

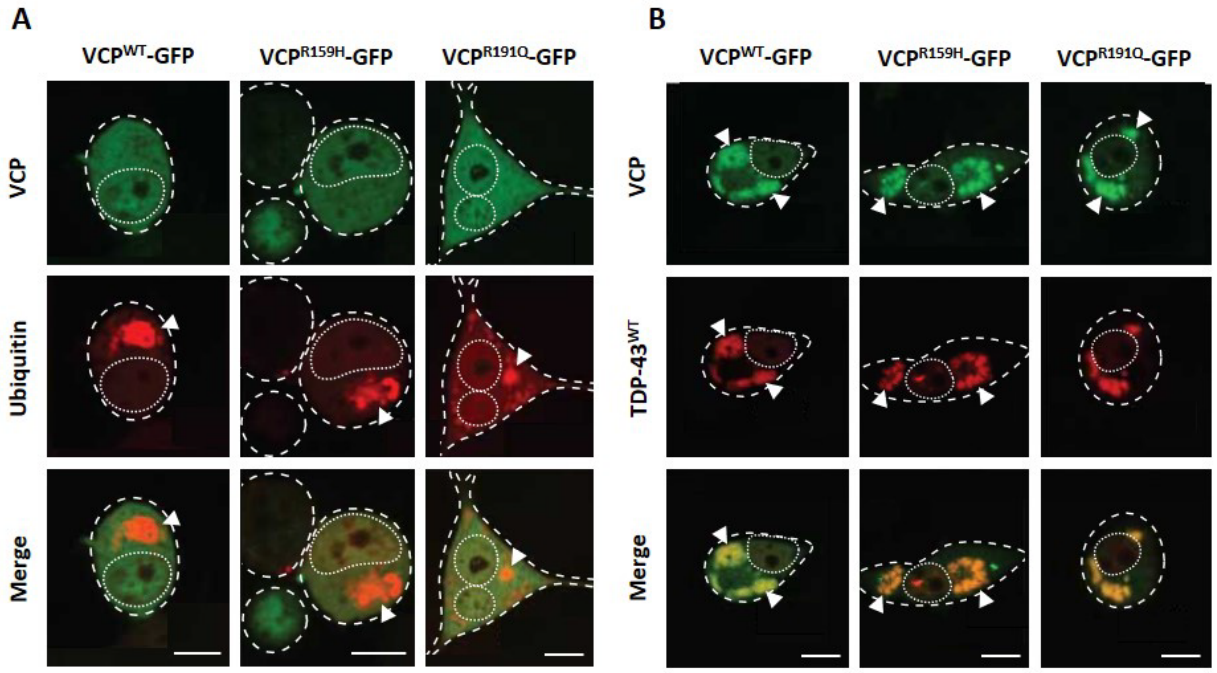

Figure 5.14. WT and mutant VCP do not aggregate into ubiquitylated inclusions, but are sequestered into inclusions when co-expressed with TDP-43^{WT}. NSC-34 cells were transiently dual-transfected with VCP^{WT}-tGFP, VCP^{R159H}-tGFP or VCP^{R191Q}-tGFP and (A) ^{mRFP}ubiquitin or (B) TDP-43^{WT}-tdTomato and imaged by confocal microscopy 48 h later. Images shown are representative of 10-15 fields of view per well, and each dual transfection was carried out in triplicate in n = 1 experiment. White arrow heads indicate inclusions formed by the tGFP-, mRFP- and tdTomato-fusion proteins. Scale bars indicate 10 µm.

Time limitations prevented further investigation into these findings observed for UBQLN2, VAPB, OPTN and VCP. Instead, the variable ubiquitin colocalisation timing found for $SOD1^{A4V}$, TDP-43^{M337V} and FUS^{R495X} inclusions obtained by Ms. N. Farrawell (University of Wollongong, NSW, Australia) and described in Farrawell *et al.* (2015) was prioritised for further investigation. It was tested whether inclusions negative for ubiquitin might colocalise with ^{mRFP}LC3, a marker of autophagy. No observable relationship was observed between $SOD1^{A4V}$-EGFP inclusions and ^{mRFP}LC3 (Figure 5.15). TDP-43^{M337V}-tGFP and FUS^{R495X}-tGFP inclusions, in contrast, were observed to be adjacent to ^{mRFP}LC3-positive foci, although they did not appear to be colocalised.

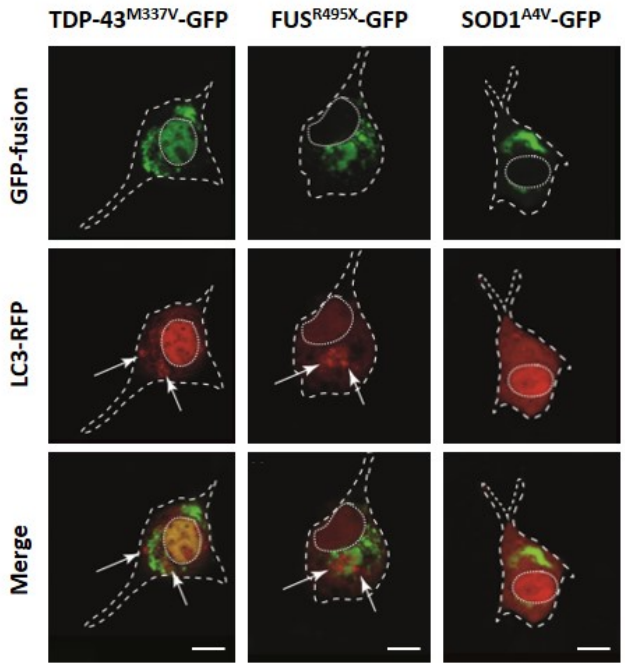

Figure 5.15. Mutant TDP-43^{M337V}-tGFP and FUS^{R495X}-tGFP inclusions are localised adjacent to ^{mRFP}LC3-positive foci. NSC-34 cells were transiently dual-transfected with TDP-43^{M337V}-tGFP, FUS^{R495X}-tGFP or SOD1^{A4V}-EGFP and ^{mRFP}LC3 and imaged 48 h later using confocal microscopy. Images shown are representative of 10-15 fields of view per well, and each dual transfection was carried out in triplicate in n = 1 experiment. White arrows indicate ^{mRFP}LC3 foci localised adjacent to TDP-43^{M337V}-tGFP and FUS^{R495X}-tGFP inclusions. Scale bars indicate 10 µm.

5.3.2 Firefly luciferase mutants report on proteostasis stress in NSC-34 cells expressing SOD1^{A4V} and CCNF^{S621G}

The optimised HCS Spot Detector assay was used for an assay comparing the effect of the overexpression of SOD1 and CCNF variants on the ability of the cellular protein quality control network to prevent the aggregation of conformationally destabilised, aggregation-prone mutants of firefly luciferase (Fluc). Fluc is a ~60 kDa multidomain protein that is known to be chaperone-dependent for folding and refolding (Nimmesgern and Hartl 1993, Schroder *et al.* 1993, Frydman *et al.* 1994, Thulasiraman and Matts 1996, Gupta *et al.* 2011). It was reasoned that reductions in the capacity of the protein quality control network would lead to increased aggregation of the EGFP-tagged Fluc mutants, as has been shown before (Gupta *et al.* 2011).

To ensure that the SpotDetector BioApplication was capable of identifying and analysing transfected cells and fluorescent foci reliably and accurately, images from each experimental condition were manually examined (Figure 5.16, a to d). While in some images transfected cells were occasionally not detected by the BioApplication, > 90% of ECFP- and EGFP-positive cells were detected (green circular masks). 'Spot' masks (yellow masks) were observed only on large foci with high fluorescence intensity, corresponding to the inclusion size and fluorescence intensity cut-offs established during assay optimisation.

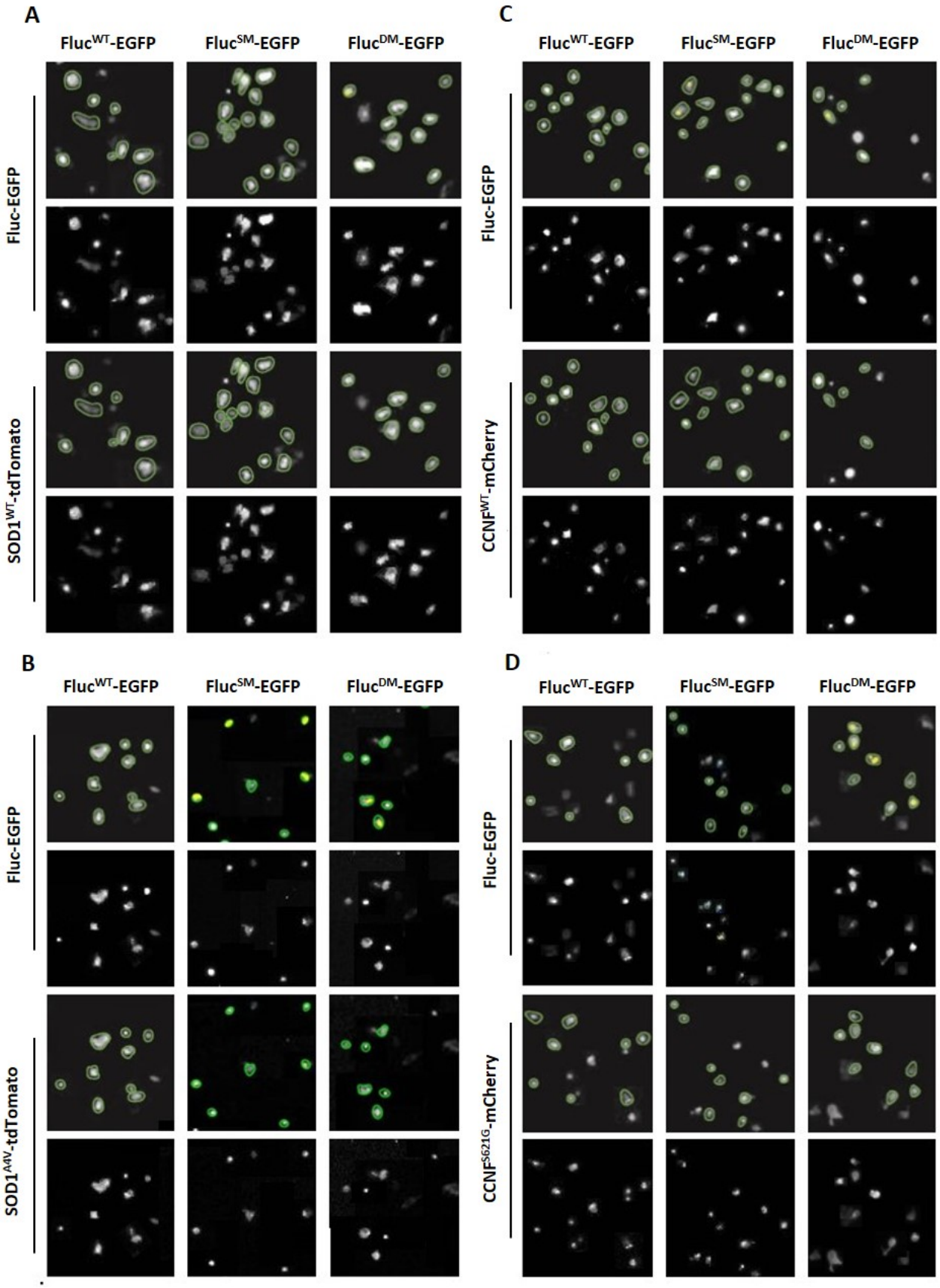
A
Fluc^WT-EGFP
Fluc^SM-EGFP
Fluc^DM-EGFP
Fluc-EGFP
SOD1^WT-tdTomato
C
Fluc^WT-EGFP
Fluc^SM-EGFP
Fluc^DM-EGFP
Fluc-EGFP
CCNF^WT-mCherry
B
Fluc^WT-EGFP
Fluc^SM-EGFP
Fluc^DM-EGFP
Fluc-EGFP
SOD1^A4V-tdTomato
D
Fluc^WT-EGFP
Fluc^SM-EGFP
Fluc^DM-EGFP
Fluc-EGFP
CCNF^S621G-mCherry

Figure 5.16. Optimised HCS SpotDetector BioApplication identifies and analyses transfected cells and Fluc-EGFP foci. Representative Cellomics® ArrayScan™ VTI images showing masks (first and third rows of each panel) used to identify and select NSC-34 cells co-transfected with either (A) $SOD1^{WT}$-tdTomato, (B) $SOD1^{A4V}$-tdTomato, (C) $CCNF^{WT}$-mCherry or (D) $CCNF^{S621G}$-mCherry and $Fluc^{WT}$-EGFP, $Fluc^{SM}$-EGFP or $Fluc^{DM}$-EGFP. Cells were imaged at 48 h post-transfection. Green circular masks indicate cells selected for analysis, yellow masks indicate 'spots' selected for analysis, representing aggregates. Images were acquired using a 20× objective lens.

Proteasome inhibition of cells expressing mCherry alone confirmed that increased proteome stress results in increased aggregation of the Fluc-EGFP isoforms. Cells expressing mCherry alone that were treated with MG132 developed significantly greater numbers of $Fluc^{WT}$-EGFP ($p < 0.0001$), $Fluc^{SM}$-EGFP ($p = 0.0001$) and $Fluc^{DM}$-EGFP ($p = 0.0021$) aggregates compared to untreated cells (Figure 5.17, a, i). MG132 treatment resulted in significantly higher numbers of $Fluc^{WT}$-EGFP aggregates than $Fluc^{DM}$-EGFP aggregates ($p = 0.0153$). $Fluc^{WT}$-EGFP aggregates were significantly smaller ($p = 0.002$) and more brightly fluorescent ($p < 0.0001$) than $Fluc^{DM}$-EGFP aggregates (Figure 5.17, b, i and c, i). Aggregates of the Fluc-EGFP isoforms were also detected in cells expressing SOD1-tdT, with a significant increase in the numbers of aggregates formed in cells expressing mutant $SOD1^{A4V}$-tdT compared to $SOD1^{WT}$-tdT ($Fluc^{WT}$-EGFP, $p = 0.0331$; $Fluc^{SM}$-EGFP, $p = 0.0061$; $Fluc^{DM}$-EGFP, $p = 0.0042$) (Figure 5.17, a, ii). There were also increases in the mean size of $Fluc^{DM}$-EGFP aggregates ($p = 0.0430$) and fluorescence intensity of aggregates of $Fluc^{WT}$-EGFP ($p < 0.0001$), $Fluc^{SM}$-EGFP ($p < 0.0001$) and $Fluc^{DM}$-EGFP ($p < 0.0001$) in cells expressing mutant $SOD1^{A4V}$-tdT compared to $SOD1^{WT}$-tdT (Figure 5.17, b, ii and c, ii). Interestingly, aggregation of $Fluc^{SM}$-EGFP and $Fluc^{DM}$-EGFP was as extensive in cells expressing $CCNF^{WT}$-mCherry as those expressing $CCNF^{S621G}$-mCherry (Figure 5.17, a, iii). Whilst aggregates of $Fluc^{WT}$-EGFP were also detected, there were significantly lower numbers of cells containing them compared to the numbers of cells containing aggregates of $Fluc^{SM}$-EGFP ($p < 0.001$) and $Fluc^{DM}$-EGFP ($p < 0.0001$), both in cells expressing $CCNF^{WT}$-mCherry and in cells expressing $CCNF^{S621G}$-mCherry. There was also the same trend in the size of aggregates of the Fluc-EGFP isoforms in cells expressing $CCNF^{WT}$-mCherry and those expressing $CCNF^{S621G}$-mCherry, with

significantly larger aggregates of $Fluc^{DM}$-EGFP formed than aggregates of $Fluc^{WT}$-EGFP ($CCNF^{WT}$-mCherry, $p = 0.0395$; $CCNF^{S621G}$-mCherry, $p = 0.0328$) (Figure 5.17, b, iii). There was no significant difference in the mean fluorescence intensity of the Fluc-EGFP aggregates of the Fluc-EGFP isoforms between cells expressing $CCNF^{WT}$-mCherry and cells expressing $CCNF^{S621G}$-mCherry (Figure 5.17, c, iii).

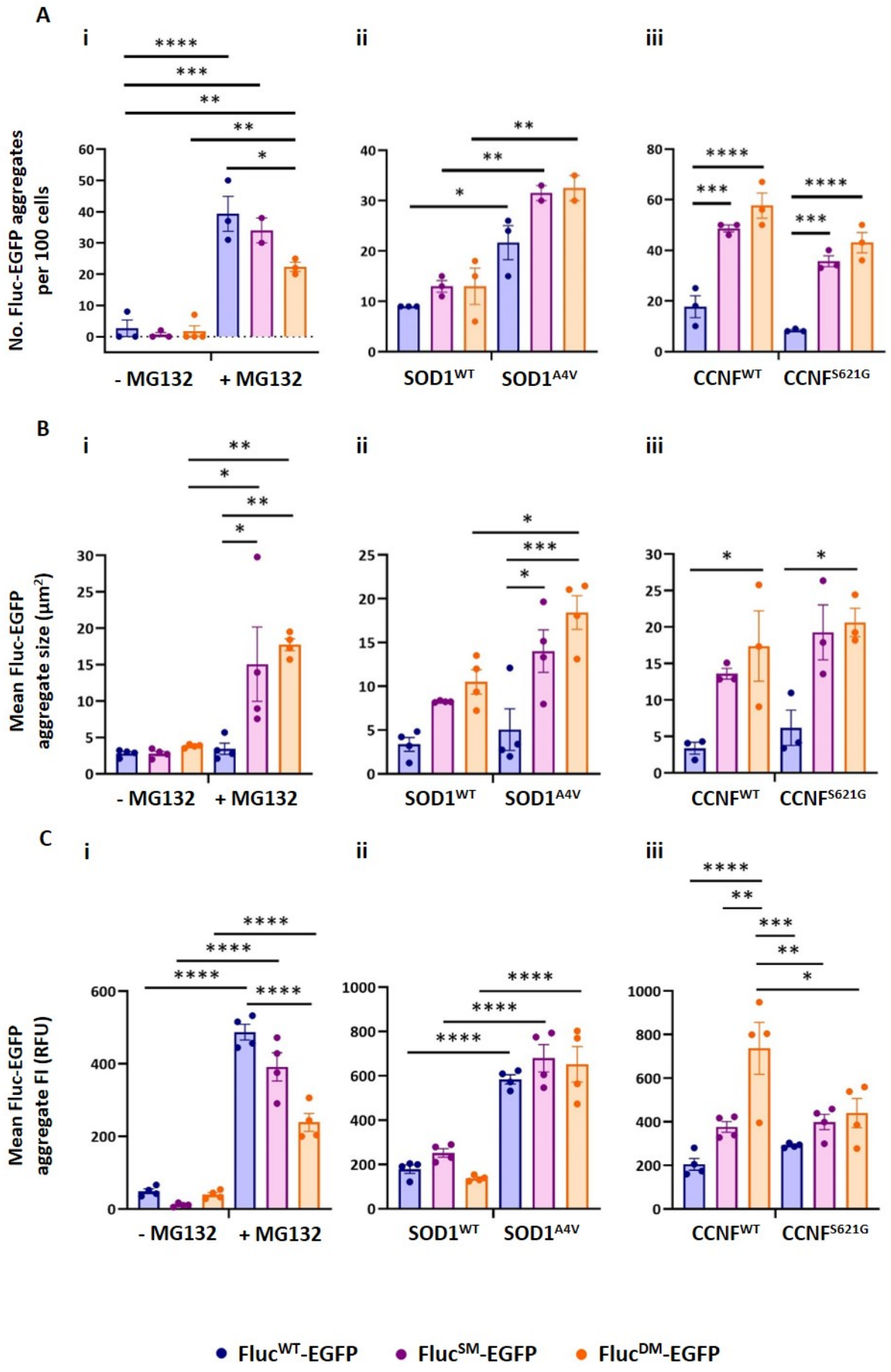
A
i
ii
iii
No. Fluc-EGFP aggregates per 100 cells
- MG132
+ MG132
SOD1WT
SOD1A4V
CCNFWT
CCNFS621G
B
Mean Fluc-EGFP aggregate size (µm²)
C
Mean Fluc-EGFP aggregate FI (RFU)
FlucWT-EGFP
FlucSM-EGFP
FlucDM-EGFP

Figure 5.17. Firefly luciferase mutants report on chaperone network activity in NSC-34 cells expressing SOD1 and CCNF. (A) Numbers of Fluc-EGFP aggregates per 100 transfected cells, (B) mean size of Fluc-EGFP aggregates (μm^2) and (C) mean fluorescence intensity (FI) of Fluc-EGFP aggregates imaged at 48 h post-transfection in NSC-34 cells expressing (i) mCherry alone ± treatment with 5 μM MG132, (ii) $SOD1^{WT}$-tdTomato or $SOD1^{A4V}$-tdTomato or (iii) $CCNF^{WT}$-mCherry or $CCNF^{S621G}$-mCherry. Treatment with MG132 was carried out at 30 h post-transfection. For mock treatment, 5 μM DMSO was instead added to cells. Graphs represent the mean ± SEM from quadruplicate wells of cells in n = 1 experiment. Differences between the means were determined using one-Way ANOVA followed by Tukey's Multiple Comparison Test. * indicates $p < 0.05$, ** indicates $p < 0.01$, *** indicates $p < 0.001$, **** indicates $p < 0.0001$.

5.4 Discussion

The heterogeneity of ALS distinguishes it from most other neurodegenerative diseases that can be linked to a single or a limited number of pathogenic mechanisms and phenotypes. The mechanisms underlying the degeneration of motor neurons in ALS vary with the genetic mutations involved and the various cellular insults and damage that accumulate in the CNS throughout an individual's lifetime. The ALS research field would benefit greatly from the use of experimental systems with HCS capacity to help navigate through this complexity. To address this, a project to develop a HCS methodology to use with cellular ALS models was undertaken. The overall objective of this work was to develop a system that could be used to collect descriptive phenotypic data from cellular ALS models that would enable (1) characterisation of the inclusion formation pathways of different ALS-associated proteins, and (2) the use of diverse markers of proteome stress and motor neuron dysfunction to assess potential therapeutic compounds and genetic modifiers of ALS gene disease mechanisms and toxicity.

5.4.1 Generation and characterisation of cellular models of SOD1-, TDP-43-, FUS-, CCNF-, VAPB-, VCP-, OPTN- and UBQLN2-associated ALS

Upon generating NSC-34 models of *SOD1-, TARDBP-, FUS-, CCNF-, VAPB-, VCP-, OPTN-* and *UBQLN2*-associated ALS, the localisation and aggregation patterns of each EGFP-/tGFP-/mCherry fusion WT and mutant protein were examined by confocal microscopy. The solubility and mobility of each protein in cells and the effect of each overexpressed protein on cell

viability were assessed using IncuCyte-based live cell imaging assays. As each of these are overexpression models, it was imperative to first confirm that the localisation patterns of each WT protein were not divergent from those of the endogenous WT proteins characterised in previous studies; SOD1 (Mackenzie *et al.* 2007, Tan *et al.* 2007), TDP-43 (Arai *et al.* 2006, Neumann *et al.* 2006, Mackenzie *et al.* 2007, Tan *et al.* 2007, Ayala *et al.* 2008, Winton *et al.* 2008, Pamphlett *et al.* 2009), FUS (Kwiatkowski *et al.* 2009, Vance *et al.* 2009, Mackenzie *et al.* 2011), UBQLN2 (Deng *et al.* 2011, Williams *et al.* 2012), OPTN (Maruyama *et al.* 2010), VAPB (Nishimura *et al.* 2004, Kanekura *et al.* 2006, Teuling *et al.* 2007, Chen *et al.* 2010) and VCP (Mizuno *et al.* 2003).

Although it was not tested in the present study, in any continued work utilising these NSC-34 cell models it would be valuable to compare the relative abundance of the exogenous ALS-associated mutants with the levels of the corresponding endogenous proteins. The vector backbone of each plasmid used in this study utilised a constitutive cytomegalovirus (CMV) promoter, a commonly used viral promoter for mammalian expression constructs. Incorporating the same promoter across all ALS-associated mutant (and corresponding wild-type) plasmids used in this study, in theory, enabled expression levels to be similar in each NSC-34 cell model. This was important for enabling comparison between the effects of expression of each mutant protein with the corresponding wild-type protein. The CMV promoter typically facilitates robust expression of the encoded gene following transfection, however, it is important to note that other molecular factors can affect the expression and turnover of exogenous proteins. This means that the abundance of the exogenous protein in each cellular model cannot be predicted with precision and requires measurement experimentally. This could be done through Western blotting and immunocytochemistry. As transfections were transient, not stable, transfection efficiency was variable. Thus, following transfection, cells would need to be sorted to isolate the population of transfected cells. Otherwise, the exogenous protein would be diluted

throughout the lysate of the whole cell population (i.e. all transfected and non-transfected cells). Following cell sorting, cells would be lysed and Western blotted for the ALS-associated protein, to then compare the relative abundance of the protein between transfected and non-transfected cell populations. Immunocytochemistry could be used to complement the Western blots. This would provide the added advantage of enabling examination and comparison of the localisation patterns of the exogenous and endogenous ALS-associated protein between transfected and non-transfected cells.

5.4.1.1 Localisation and aggregation patterns of SOD1, TDP-43 and FUS in NSC-34 cells

The localisation patterns of WT SOD1, TDP-43 and FUS and the ALS-associated $SOD1^{A4V}$, $TDP\text{-}43^{M337V}$, FUS^{R521G} and FUS^{R495X} mutants are well characterised. In human post-mortem tissue, mutant SOD1 is often detected in large perinuclear conglomerate inclusions (Chou *et al.* 1996). TDP-43 and FUS are predominantly nuclear-localised RBPs with additional cytoplasmic roles in the formation and dynamics of SGs and RNA transport granules (Colombrita *et al.* 2009, Liu-Yesucevitz *et al.* 2010, Dewey *et al.* 2011, McDonald *et al.* 2011, Bentmann *et al.* 2012, Colombrita *et al.* 2012, Sama *et al.* 2013, Alami *et al.* 2014). Mutant TDP-43 and FUS accumulate in cytoplasmic inclusions in patients with *TARDBP* or *FUS* mutations, respectively (Arai *et al.* 2006, Neumann *et al.* 2006, Mackenzie *et al.* 2007, Tan *et al.* 2007, Ayala *et al.* 2008, Winton *et al.* 2008, Kwiatkowski *et al.* 2009, Pamphlett *et al.* 2009, Vance *et al.* 2009, Mackenzie *et al.* 2011). These patterns were recapitulated in NSC-34 cells for each of the tGFP-tagged mutant TDP-43 and FUS proteins ($SOD1^{A4V}$-EGFP localisation, aggregation and solubility was examined and is detailed in Chapter IV). The $TDP\text{-}43^{M337V}$, FUS^{R521G} and FUS^{R495X} mutants mislocalised to the cytoplasm and formed into large aggregates and smaller foci. FUS^{R521G}-tGFP predominantly accumulated into large numbers of small foci. It was found that the saponin-permeabilisation assay was not suitable to compare the solubility and mobility

of FUS^{WT}-tGFP to the examined FUS-tGFP mutants, as it did not enable distinction between FUS-tGFP that is localised within nuclei and FUS-tGFP that has accumulated into insoluble cytoplasmic inclusions. However, using confocal microscopy it was observed that both FUS-tGFP mutants mislocalised from the nucleus and accumulated into cytoplasmic inclusions. Thus, the saponin-permeabilisation assay was useful to compare the solubility and mobility of cytoplasmic inclusions formed by FUS^{R495X}-tGFP and FUS^{R521G}-tGFP. A significant difference was found between the solubilities of the two FUS mutants. The data from the saponin-permeabilisation assay suggests that the aggregates formed by the two FUS mutants may have differing structural properties, with aggregates formed by the FUS^{R521G}-tGFP mutant largely becoming insoluble, while under these conditions the solubility of FUS^{R495X}-tGFP was indistinguishable from that of FUS^{WT}-tGFP. Both TDP-43 and FUS contain low sequence complexity prion-like domains that mediate their assembly into reversible, dynamic, non-membrane-bound hydrogel droplets that associate with RNA granule-like structures, as well as their assembly into irreversible fibrous prion-like aggregates (Han *et al.* 2012, Kato *et al.* 2012, King *et al.* 2012, Li *et al.* 2018). Whether or not the aggregates formed by FUS^{R495X}-tGFP observed in the present work develop into insoluble structures over a longer of period of time remains to be investigated.

5.4.1.2 Differential timing of ubiquitin association with $UBQLN2^{P497H}$, $OPTN^{E478G}$ and $VAPB^{P56S}$ inclusions

Ubiquitylation is a key factor governing the fate of misfolded proteins in cells (Kawaguchi *et al.* 2003, Tan *et al.* 2008, Kraft *et al.* 2010, Zhang and Qian 2011). Ubiquitylation is associated with the formation of certain types of inclusions, such as the JUNQ, that serve protein quality control functions in cells (Kaganovich *et al.* 2008, Weisberg *et al.* 2012). To gain an understanding of the aggregation pathways followed by mutant UBQLN2, OPTN, VAPB and VCP, their association with ubiquitin was examined by confocal microscopy using a mRFP-

tagged ubiquitin. Through this work, ^{mRFP}ubiquitin was observed to colocalise to inclusions containing UBQLN2^{P497H}-tGFP, OPTN^{E478G}-EGFP and VAPB^{P56S}-tGFP, with the timing of colocalisation differing for each mutant protein. In contrast, inclusions containing ^{mRFP}ubiquitin were observed at all time points in NSC-34 cells expressing VCP^{R191Q}-tGFP or VCP^{R159H}-tGFP, however there was no localisation of mutant VCP to these inclusions.

In cells expressing UBQLN2^{P497H}-tGFP, ^{mRFP}ubiquitin colocalisation to UBQLN2^{P497H}-tGFP inclusions was observed at all imaging time points. This is consistent with previous studies detecting UBQLN2 in the ubiquitylated inclusions in sALS and fALS patients with *UBQLN2* mutations as well as mutations in *SOD1, TARDBP, FUS* and hexanucleotide repeat expansions in *C9ORF72* (Deng *et al.* 2011, Brettschneider *et al.* 2012, Williams *et al.* 2012). UBQLN2 is a member of the ubiquilin family of ubiquitin-like proteins that function in both autophagy and the UPS (Kleijnen *et al.* 2000, Ko *et al.* 2004, N'Diaye *et al.* 2009). In the UPS, UBQLN2 delivers ubiquitylated proteins to the proteasome for degradation via its N-terminal UBL and C-terminal UBA domains (Kleijnen *et al.* 2000, Walters *et al.* 2002, Walters *et al.* 2004, Zhang *et al.* 2008). The presence of ^{mRFP}ubiquitin in all observed UBQLN2^{P497H}-tGFP inclusions from early on (24 h post-transfection) could be indicative of aberrant interactions between misfolded UBQLN2 and polyubiquitylated proteins. It may also suggest that UBQLN2^{P497H}-tGFP was sequestered into protein quality control compartments, for instance, in JUNQ inclusions, as a protective mechanism (Figure 5.18, a). Examining UBQLN2^{P497H}-tGFP inclusions for the presence of other quality control components such as 26S proteasomes and chaperones, using time-resolved imaging, would help in determining the formation pathway of these inclusions. For example, detection of quality control components in addition to the presence of ubiquitin in these inclusions may provide indication that UBQLN2^{P497H}-tGFP was directed to JUNQ-like inclusions. Both UBQLN2 mutants were observed to cause significant growth inhibition of NSC-34 cells, suggesting that they impaired cellular viability. Thus, sequestration of mutant

UBQLN2 in JUNQ inclusions could serve protective functions in cells. Indeed, evidence indicates that JUNQ inclusions function to sequester toxic misfolded protein species away from the cytosol, and that ubiquitylation is essential to maintain solubility of misfolded proteins for refolding or proteasomal degradation in the JUNQ (Kaganovich *et al.* 2008, Weisberg *et al.* 2012).

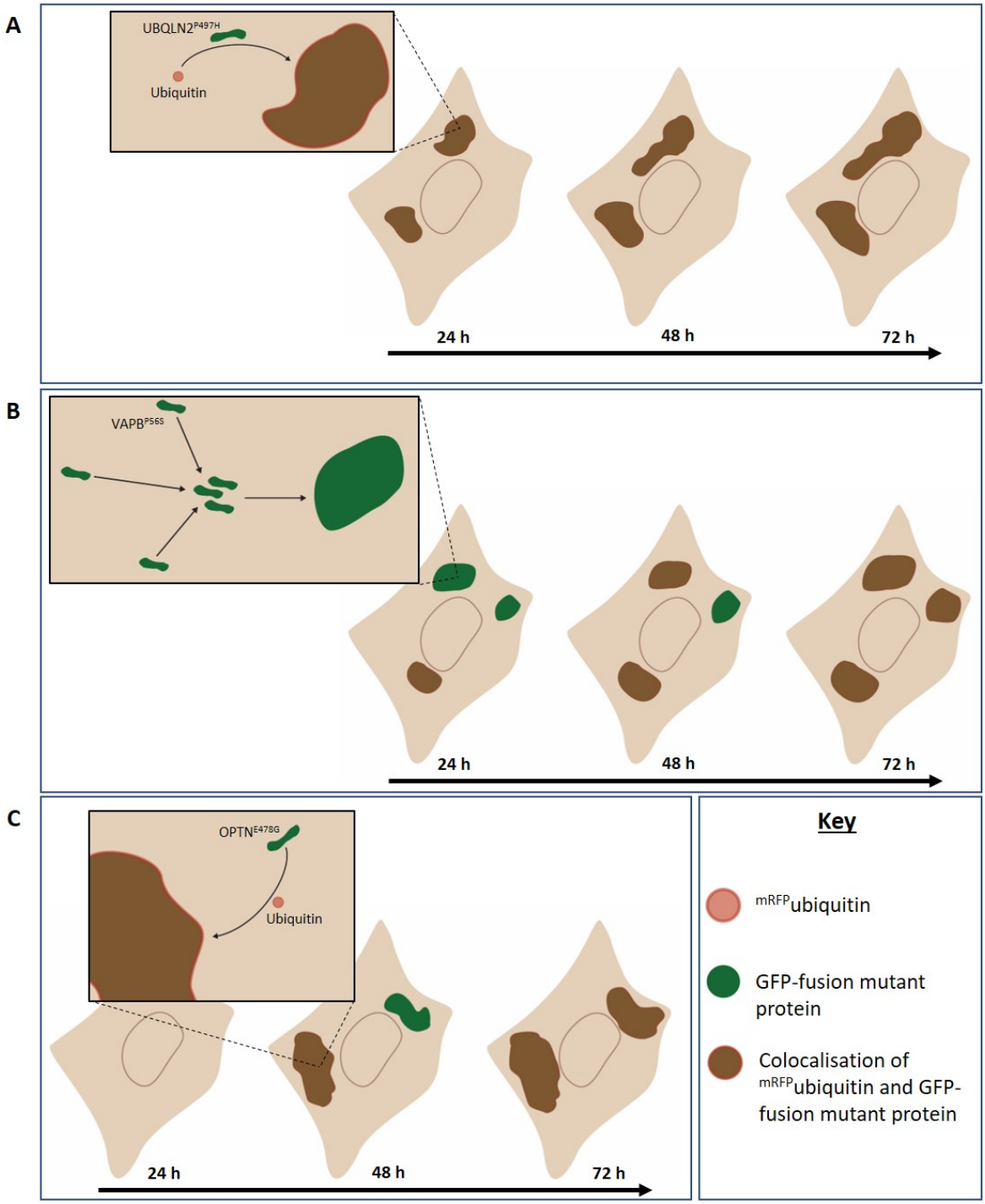

Figure 5.18. Summary of proposed dynamics of ubiquitin association with inclusions formed by UBQLN2^{P497H}, VAPB^{P56S} and OPTN^{E478G}. The localisation patterns of ^{mRFP}ubiquitin and (A) UBQLN2^{P497H}-tGFP, (B) VAPB^{P56S}-tGFP or (C) OPTN^{E478G}-EGFP in NSC-34 cells were tracked using live-cell imaging at 24 h, 48 h and 72 h post-transfection. (A) ^{mRFP}ubiquitin was observed to be associated with all UBQLN2^{P497H}-tGFP inclusions from early on (24 h post-transfection). Ubiquitin may have been involved in sequestration of UBQLN2^{P497H}-tGFP into protein quality control compartments, for instance, JUNQ inclusions, in a protective mechanism. (B) ^{mRFP}ubiquitin was not associated with all VAPB^{P56S}-tGFP inclusions at the earliest imaging time point, suggesting that a proportion of VAPB^{P56S}-tGFP inclusions did not represent quality control compartments. Rather, mutant VAPB molecules may have aggregated together to form inclusions. (C) Not all inclusions formed by OPTN^{E478G}-EGFP at an intermediate time point (48 h post-transfection) were associated with ^{mRFP}ubiquitin, indicating that their formation was not ubiquitin-dependent. Ubiquitin may have been aberrantly sequestered into inclusions formed by VAPB^{P56S}-tGFP and OPTN^{E478G}-EGFP over time.

In contrast to cells expressing UBQLN2^{P497H}-tGFP, ^{mRFP}ubiquitin did not colocalise with all observed VAPB^{P56S}-tGFP inclusions at an early stage (24 h post-transfection), but its association with the inclusions did increase over time. The association of ^{mRFP}ubiquitin with VAPB^{P56S}-tGFP inclusions is consistent with previous work in *Drosophila melanogaster*, transgenic mice and mammalian cell culture models of VAPB^{P56S}-ALS in which VAPB^{P56S} inclusions are ubiquitylated (Kanekura *et al.* 2006, Ratnaparkhi *et al.* 2008, Papiani *et al.* 2012, Kuijpers *et al.* 2013, Larroquette *et al.* 2015). There is evidence to suggest that VAPB inclusions are a unique type of ERAD quality control compartment. VAPB^{P56S} inclusions have been reported to contain ER tubules and proteins involved in ERAD, including VCP, Derlin-1 and BAP31 (Teuling *et al.* 2007, Kuijpers *et al.* 2013). Kuijpers *et al.* (2013) found that the presence of VAPB inclusions was not associated with neuronal toxicity in transgenic mice. In a separate study on VAPB^{P56S} transgenic mice by Qiu *et al.* (2013), they observed VAPB^{P56S} inclusions in the spinal cord of the mutant mice, but a distinct lack of neurodegeneration. Aliaga *et al.* (2013) interestingly documented that, while they observed VAPB^{P56S} inclusions in corticospinal and spinal motor neurons of transgenic mice, the effects of VAPB^{P56S} on these two populations of motor neurons differed. There was upregulation of the UPR and ER stress, and of pro-apoptotic factors in both populations of motor neurons, but there was only degeneration of the corticospinal motor neurons, not of the spinal motor neurons. The ability of cells to generate potential ERAD quality control compartments, and thus the toxicity of VAPB^{P56S} expression, appear to be variable between cell types and between different models. This could be due to differing expression levels of the mutant protein in different models. In the present work, the expression of VAPB^{P56S}-tGFP reduced the viability of transfected NSC-34 cells. If VAPB^{P56S} inclusions do represent an ERAD quality control compartment, the toxicity observed in transfected NSC-34 cells and in other cell culture and animal models in previous studies (Chen *et al.* 2010, Aliaga *et al.* 2013, Larroquette *et al.* 2015) may be the result of higher relative

expression levels. Higher expression levels could result in overloading of the cellular ability to sequester VAPB^{P56S} into potential ERAD quality control compartments, thus overwhelming this protective cellular strategy. Indeed, the observation in the present work that ubiquitin was not associated with all VAPB^{P56S}-tGFP inclusions at the earliest imaging time point suggests that at least a proportion of the observed inclusions did not represent quality control compartments (Figure 5.18, b).

Similarly to VAPB^{P56S}-tGFP, not all observed OPTN^{E478G}-EGFP inclusions were colocalised with ^{mRFP}ubiquitin at all imaging time points. OPTN^{E478G}-EGFP foci were not categorised as inclusions until 48 h post-transfection as they were consistently smaller than the inclusion size cut-off of 2 μm that had been established. OPTN is involved in vesicular trafficking, autophagosome maturation and it associates with proteins of the Golgi apparatus (Sahlender *et al.* 2005, del Toro *et al*. 2009), thus the small foci may have represented the localisation of OPTN to these structures. Indeed, OPTN^{WT} has been documented to form granular structures that are closely associated with the Golgi apparatus (Maruyama *et al.* 2010). OPTN^{WT} has also been detected on LC3-positive autophagosomes under basal autophagy conditions (Tumbarello *et al.* 2012). In the present work, the association of OPTN^{WT}-EGFP with these structures may also have reduced its mobility and solubility, thus rendering the saponin permeabilisation assay unsuitable for examining the mobility and solubility of mutant OPTN inclusions. Overexpression of OPTN^{WT} has been found to decrease the numbers of mutant huntingtin inclusions in Neuro2A cells through K63-linked polyubiquitin-mediated autophagy (Shen *et al.* 2015). The E478G mutation in OPTN alters its ubiquitin-binding domain. Shen *et al.* (2015) observed that OPTN^{E478G} retained an ability to bind to OPTN^{WT} and colocalised with polyubiquitylated mutant huntingtin inclusions, suggesting that its association with the polyubiquitylated inclusions occurred indirectly through its interaction with OPTN^{WT}. In the present work, examination of the large (> 2 μm) inclusions formed by OPTN^{E478G}-EGFP

showed that their association with ^{mRFP}ubiquitin increased from 48 h to 72 h post-transfection. The observation that not all of the inclusions formed by OPTN^{E478G}-EGFP at an intermediate time point (48 h post-transfection) were associated with ^{mRFP}ubiquitin suggests that their formation was not ubiquitin-dependent. Rather, over time ubiquitin may have been aberrantly sequestered into these inclusions from the cytoplasm (Figure 5.18, c). Moreover, the data reported by Shen *et al.* (2015) suggested that OPTN^{E478G} causes toxicity through a dominant-negative mechanism by binding to and inhibiting the activity of OPTN^{WT} in autophagosome maturation, thereby inhibiting the clearance of misfolded proteins and inclusions by autophagy. In the present work, the expression of OPTN^{E478G}-EGFP caused significant growth inhibition of NSC-34 cells, suggesting that cell viability was reduced. In these OPTN^{E478G}-EGFP-transfected NSC-34 cells, the potential of a dominant-negative mechanism of OPTN^{E478G} could be explored using various methods. For example, interaction between OPTN^{E478G} and OPTN^{WT} and alterations in autophagy could be examined by fluorescence microscopy of NSC-34 cells co-transfected with RFP-tagged OPTN^{WT} and EGFP-tagged OPTN^{E478G}, coupled with immunocytochemistry for autophagy markers such as LC3I and LC3II, p62, beclin-1 and Lamp2a. Alterations in autophagy could also be investigated by examination of autophagic flux using multiple complementary techniques in parallel studies (thorough review of methods for studying autophagy in Klionsky *et al.* (2016)). Notwithstanding, accumulating evidence indicates that OPTN^{WT} is broadly involved in ALS, with its detection in inclusions in spinal cord tissue of patients with non-*OPTN*-fALS and sALS in several studies (Maruyama *et al.* 2010, Deng *et al.* 2011, Osawa *et al.* 2011).

5.4.1.3 WT and mutant VCP associate with TDP-43^{WT} in cytoplasmic inclusions

It was interesting to observe that, when co-expressed with ^{mRFP}ubiquitin, neither VCP^{R191Q}-tGFP nor VCP^{R159H}-tGFP exhibited altered localisation patterns to that of VCP^{WT}-tGFP. Inclusions containing ^{mRFP}ubiquitin were present, however there was no colocalisation of the

tGFP-tagged VCP mutants or VCP^{WT} to these inclusions. The saponin permeabilisation assay showed that VCP^{WT}-tGFP was retained in about a tenth of transfected cells while both VCP-tGFP mutants were retained in significantly greater proportions of transfected cells. This retention of the tGFP-tagged proteins suggests that VCP^{WT} can be present in immobile and insoluble forms in cells. VCP is essential for various cellular processes, including Golgi apparatus and ER assembly, ERAD and autophagosome maturation (Song *et al.* 2003, Halawani and Latterich 2006, Ju *et al.* 2009, Tresse *et al.* 2010, Meyer *et al.* 2012). The mobility of VCP^{WT} would thus be reduced when it is associated with these membrane structures in cells. Moreover, VCP^{WT} has been observed to localise to aggresomes in viable, functional cells and to dynamically associate with other aggregated structures while mutant VCP persists in immobile forms in these structures (Ju *et al.* 2008). Additionally, VCP^{WT} has been reported to colocalise with insoluble inclusions containing different disease-associated mutant proteins in Machado-Joseph disease (MJD), HD and PD (Kawaguchi *et al.* 1994, Hirabayashi *et al.* 2001, Mizuno *et al.* 2003, Ishigaki *et al.* 2004).

As the presence of TDP-43 in inclusions is a typical feature of most non-*SOD1*- and non-*FUS*-related ALS cases, it was explored whether there was any association of VCP with $TDP\text{-}43^{WT}$ in transfected cells. When co-expressed with $TDP\text{-}43^{WT}$-tdT, VCP^{WT}-tGFP as well as both VCP mutants formed inclusions that colocalised with $TDP\text{-}43^{WT}$-tdT in all cells that were imaged. Unfortunately, time limitations prevented these observations being confirmed with repeat experiments. Nevertheless, the association between VCP and TDP-43 in neurodegenerative diseases has been investigated in several studies. As well as in ALS, mutations in VCP manifest as a plethora of different degenerative disorders, including hereditary spastic paraplegia (de Bot *et al.* 2012), parkinsonism (Kimonis *et al.* 2008), PD (Spina *et al.* 2013), Charcot-Marie-Tooth Type 2 (Gonzalez *et al.* 2014) and the multisystem degenerative disorder referred to as IBMPFD (Watts *et al.* 2004). In IBMPFD, the pathology is characterised by inclusions containing

ubiquitin and TDP-43, similarly to ALS pathology (Forman *et al.* 2006, Neumann *et al.* 2007). Notably, as mutant VCP is not detected in these inclusions, it has been suggested that alterations in VCP function lead to disrupted protein degradation pathways and impaired metabolism of TDP-43 (Forman *et al.* 2006, Neumann *et al.* 2007). Interestingly, ALS-associated mutations in VCP have been linked with impaired autophagic clearance of TDP-43-, FUS-, hnRNPA1- and hnRNPA2B1-positive SGs and pathogenic ribonucleoprotein (RNP) granules (Buchan *et al.* 2013). Given that TDP-43 has important roles in SG dynamics, this raises the possibility that one of the mechanisms by which VCP mutations lead to motor neuron dysfunction and degeneration is through disrupted clearance of SGs. In a study using a *Drosophila melanogaster* model of IBMPFD, disease-causing *VCP* mutations led to a genetic interaction between TDP-43 and VCP that enhanced degeneration (Ritson *et al.* 2010). TDP-43^{WT} redistribution to the cytoplasm was enough to cause degeneration in this model, and toxicity was further enhanced through overexpression of the ALS-causing *TARDBP*^{M337V} mutation with mutant *VCP*.

The mechanisms by which mutations in *VCP* lead to neurodegeneration are likely to be multifaceted, but the findings from these previous studies indicate that mutant *VCP* disease mechanisms involve, to some extent, alterations in the activity of TDP-43. These alterations in TDP-43 activity could result from loss of VCP functions in SG clearance and protein degradation via the UPS and autophagy (Kwon *et al.* 2007, Ju *et al.* 2008, Buchan *et al.* 2013). Although a preliminary finding from n = 1 experiment, the mutant *VCP* overexpression model used in this study recapitulates the hallmark accumulation of ubiquitin and TDP-43^{WT} in cytoplasmic inclusions observed in ALS patient tissue and diverse ALS models. Taken together, the reports from the literature discussed here and the preliminary finding of VCP colocalisation with TDP-43^{WT} in inclusions emphasise the importance of investigating the interactions between mutant VCP and TDP-43 that lead to neurodegeneration.

5.4.2 Development of an HCS assay to measure chaperone network activity in cellular ALS models

The NSC-34 models of ALS generated here were examined for the localisation patterns, the mobility and solubility of the EGFP-/tGFP- and mCherry-fusion proteins, and for toxicity caused by expression of the mutant proteins. The aim of these studies was to establish disease phenotypes that could be used in an experimental system with HCS capacity for further studies into disease mechanisms, and potentially for evaluation of candidate therapeutics. This experimental system was generated using the Cellomics® ArrayScan™ VTI HCS platform. Time limitations prevented multiple image analysis algorithms, BioApplications, from being optimised for studies that could utilise different markers of proteome stress and motor neuron dysfunction. Nevertheless, optimisation of the Spot Detector BioApplication was achieved for investigation into reductions in cellular protein folding/re-folding capacity caused by WT and mutant SOD1 and CCNF. Analysis of protein folding/re-folding capacity was facilitated by co-expression of conformationally destablised Fluc-EGFP mutants (Gupta *et al.* 2011) with WT and mutant SOD1 and CCNF. It was hypothesised that dysregulation of proteostasis mechanisms that may be exacerbated by ALS-associated mutations in SOD1 and CCNF would overload cellular proteostasis capacity, resulting in inability of the cellular pool of molecular chaperones to prevent aggregation of the Fluc-EGFP mutants. The optimised Spot Detector BioApplication enabled quantification of the numbers, the mean size and fluorescence intensity of aggregates formed by the Fluc-EGFP isoforms.

The ability of the Fluc-EGFP mutants to report on proteome stress was confirmed through proteasome inhibition of cells expressing mCherry alone with the Fluc-EGFP isoforms. As well as reduced stability of the single and double Fluc-EGFP mutants, increased proteome stress also results in reduced stability of $Fluc^{WT}$-EGFP (Gupta *et al.* 2011). In MG132-treated cells, $Fluc^{WT}$-EGFP aggregates that formed were smaller than the aggregates formed by $Fluc^{SM}$-

EGFP and Fluc^{DM}-EGFP, perhaps indicating that less of the WT protein misfolded and accumulated into the aggregates that did form. Without exogenous proteome stress induced by proteasome inhibition, there was negligible aggregation of the Fluc-EGFP isoforms, demonstrating that they were able to report on increased proteome stress.

The overexpression of SOD1^{A4V}-tdT resulted in increased numbers, size and fluorescence intensity of aggregates of the Fluc-EGFP isoforms compared to overexpression of SOD1^{WT}-tdT. The numbers and size of the analysed aggregates correlated with the instability of the Fluc-EGFP isoforms, with Fluc^{DM}-EGFP forming greater numbers of larger aggregates than Fluc^{SM}-EGFP, and more still than Fluc^{WT}-EGFP. Previous studies have reported evidence suggesting an association between the expression of mutant SOD1 and impaired chaperone activity (Bruening *et al.* 1999, Takeuchi *et al.* 2002, Tummala *et al.* 2005). The data from the present work demonstrates that the optimised HCS assay using the Fluc-EGFP isoforms is able to report on reduced activity of the cellular network of chaperones resulting from the expression of SOD1^{A4V}. The formation of Fluc-EGFP aggregates was similar between cells expressing CCNF^{WT}-mCherry and mutant CCNF^{S621G}-mCherry. As was observed in SOD1^{A4V}-tdT-expressing cells, a correlation was observed between relative stability of each Fluc-EGFP isoform and extent of aggregation. The overexpression of CCNF^{WT}-mCherry caused the same extent of Fluc-EGFP aggregation as CCNF^{S621G}-mCherry, indicating that mutant CCNF did not differentially affect the folding/re-folding activity of chaperones in cells compared to CCNF^{WT}. CCNF is an important protein in the UPS, as a mediator of protein ubiquitylation (D'Angiolella *et al.* 2013). Ubiquitylation of target proteins is altered in cells expressing mutant CCNF, causing aberrant accumulation of ubiquitylated proteins and consequent stress on the proteostasis network (Williams *et al.* 2016). The data obtained from the Fluc-EGFP HCS assay developed in the present work suggests that proteostasis disruption caused by mutant CCNF in cells does not involve impairment of the protein folding/re-folding activity of cellular

chaperones.

The Fluc-EGFP isoforms were designed to act as sensors of cellular protein folding/re-folding capacity that would themselves have minimal biological impact in most of the commonly used cellular and animal models (Gupta *et al.* 2011). In the present work it was demonstrated that they are suitable for use in a HCS assay format to report on disruptions in the activity of the cellular chaperone network. The extent of aggregation of the Fluc-EGFP isoforms can be easily measured using complementary readouts from a HCS microscope, including Fluc-EGFP aggregate size, density (fluorescence intensity) and overall numbers in cells. The ability to generate these HCS readouts enables higher resolution information to be obtained from the Fluc-EGFP isoforms about the extent of protein folding/re-folding impairment in cells. In future work it would be useful to optimise a HCS assay that utilises changes in luminescence activity of the Fluc-EGFP isoforms (Gupta *et al,* 2011) as an additional measure of protein folding/re-folding capacity in cells.

In addition to the use of this Fluc-EGFP HCS assay to examine cellular models of $SOD1^{A4V}$ and $CCNF^{S621G}$, it would be useful in future work to utilise this assay to examine protein folding/re-folding capacity in the cellular models of mutant TDP-43, FUS, UBQLN2, OPTN, VAPB and VCP generated in this work. Beyond establishing ALS-associated mutant proteins that impair the activity of the chaperone network in cells, this HCS assay could have potential for application in studies to screen for drugs that ameliorate chaperone activity impairment.

Chapter 6: Research significance and conclusions

6.1 Overview

Accumulating evidence from *in vitro* and *in vivo* models, and from post-mortem spinal cord tissue from ALS patients, suggests that alterations in the mechanisms that maintain proteostasis in motor neurons may be a common molecular feature of the different genetic forms of ALS. The overall objective of the work presented in this thesis was to investigate the role of proteostasis disruption in the pathogenesis of ALS caused by mutations in different ALS-associated genes. As the number of genes and molecular pathways implicated in ALS pathogenesis continues to grow, there may be value in identifying common mechanisms, and those distinct for each genetic mutation, that underlie the decline of motor neuron health and subsequent degeneration.

The exact processes that normally maintain proteostasis but that are uniquely disturbed in motor neurons expressing different genetic mutations, and the processes that are commonly disturbed amongst these diverse genetic contexts, remain to be established. Obtaining a better understanding of proteostasis disruption in association with different ALS-causing mutations may identify novel therapeutic targets and strategies for ALS patients. In this work, two main experimental approaches were developed to investigate proteostasis disturbances caused by the expression of several ALS-causing gene variants. A yeast genetic screen was developed to identify differentially regulated proteins and molecular pathways associated with SOD1, TDP-43 and FUS pathology. This approach was validated through confirmation of the relevance of one of the hits from the SOD1 yeast screen, UBA1, a protein that plays a critical role in maintaining ubiquitin homeostasis, by demonstrating that its overexpression can protect against $SOD1^{A4V}$-mediated toxicity in neuronal NSC-34 cells. A second experimental system was developed that exploited a HCS platform to examine dysregulated proteostasis in neuronal cell culture models of ALS-causing gene variants. In this chapter the key findings of this PhD

research are summarised, and the significance of these findings to the study and understanding of ALS pathogenesis is discussed.

6.2 A novel approach using *Saccharomyces cerevisiae* to identify proteostasis disturbances caused by ALS-associated proteins

The use of *Saccharomyces cerevisiae* to study complex neurodegenerative diseases is well established as many of the key molecular processes affected in these diseases are highly conserved and thus can be investigated in this simple eukaryote. Although many of these studies have provided significant insight into genes that interact with the examined disease genes, established high-throughput techniques have not previously been exploited to examine the pathological changes that occur at the protein level. Thus, to test the hypothesis that proteins found to have altered levels in the presence of pathological TDP-43, FUS or SOD1 are involved in the cellular response to these ALS genes, a fluorescent plate reader-based screening system using the yeast EGFP-fusion strain collection (Huh *et al.* 2003) was developed. By employing an established collection of yeast strains in which an EGFP had been integrated into the C-terminus of the genomic locus of each yeast gene, the natural promoter of each gene was preserved, enabling the examination of endogenous yeast proteins in a minimally perturbed biological system. This approach also bypassed the need to introduce extrachromosomal plasmid constructs containing yeast genes fused to fluorophores, and enabled the levels of endogenous yeast proteins to be quantified in high-throughput format using a fluorescent plate reader.

A subset of the yeast EGFP-fusion collection was selected to focus on proteins of relevance to pathological changes in proteostasis pathways that have previously been implicated in ALS (Figure 6.1, a). The collation of this subset of EGFP-fusion yeast proteins/strains is significant as they can now be employed in future investigations to examine proteostasis disruptions caused by other ALS-associated gene variants, for instance, *CCNF, UBQLN2, VAPB* and *VCP* variants.

Such efforts would be valuable to provide insight into the conserved proteins and molecular processes that are commonly and uniquely disrupted amongst different ALS-associated gene variants, beyond TDP-43, FUS and SOD1. However, a major caveat of screening only against this pathway-focused subset is the inherent bias of this approach. Albeit, the objective of this approach was to identify specific proteins within this subset that may be involved in the cellular response to mislocalised TDP-43, FUS and mutant SOD1. Yet there may be value in further screening the full collection of 4156 EGFP-fusion yeast strains to remove this bias to (1) identify other proteins that may be involved in the cellular response to different ALS gene variants and (2) examine if there is enrichment in any biological process GO terms that have not previously been associated with ALS gene variants.

The high-throughput plate reader-based approach used in the present study was appropriate for the purposes of this investigation as it enabled information on the mean response of populations of cells to the expression of each ALS gene mutant to be obtained. However, this approach was limited as information at the single-cell level on cell-to-cell variation in expression levels was lost. It would be interesting to follow up this screen with a microscopy approach in which single-cell information was obtained, to observe how variation in expression of TDP-43, FUS or mutant SOD1 between cells correlates with variation in the levels of the yeast EGFP-fusion proteins. It may also be beneficial to systematically examine the localisation patterns of the full collection of EGFP-fusion yeast proteins in cells expressing different ALS gene variants, using an automated microscopy approach similar to that described in Breker *et al.* (2013). Identification of proteins with altered localisation patterns could provide valuable information about the cellular response to each ALS gene variant. Such work may identify novel proteins and their associated molecular processes that could be targeted for the treatment of ALS.

6.2.1 Distinct disruptions in proteostasis caused by mutant SOD1 and mislocalised TDP-43 and FUS

Employing the pathway-focused selection of 128 EGFP-fusion yeast strains and measuring the levels of the EGFP-fusion proteins in yeast expressing TDP-43^{WT}, FUS^{WT} or SOD1^{A4V} enabled the identification of specific proteins that were involved in responses to the proteotoxic burden of these three ALS-linked proteins (Figure 6.1, b).

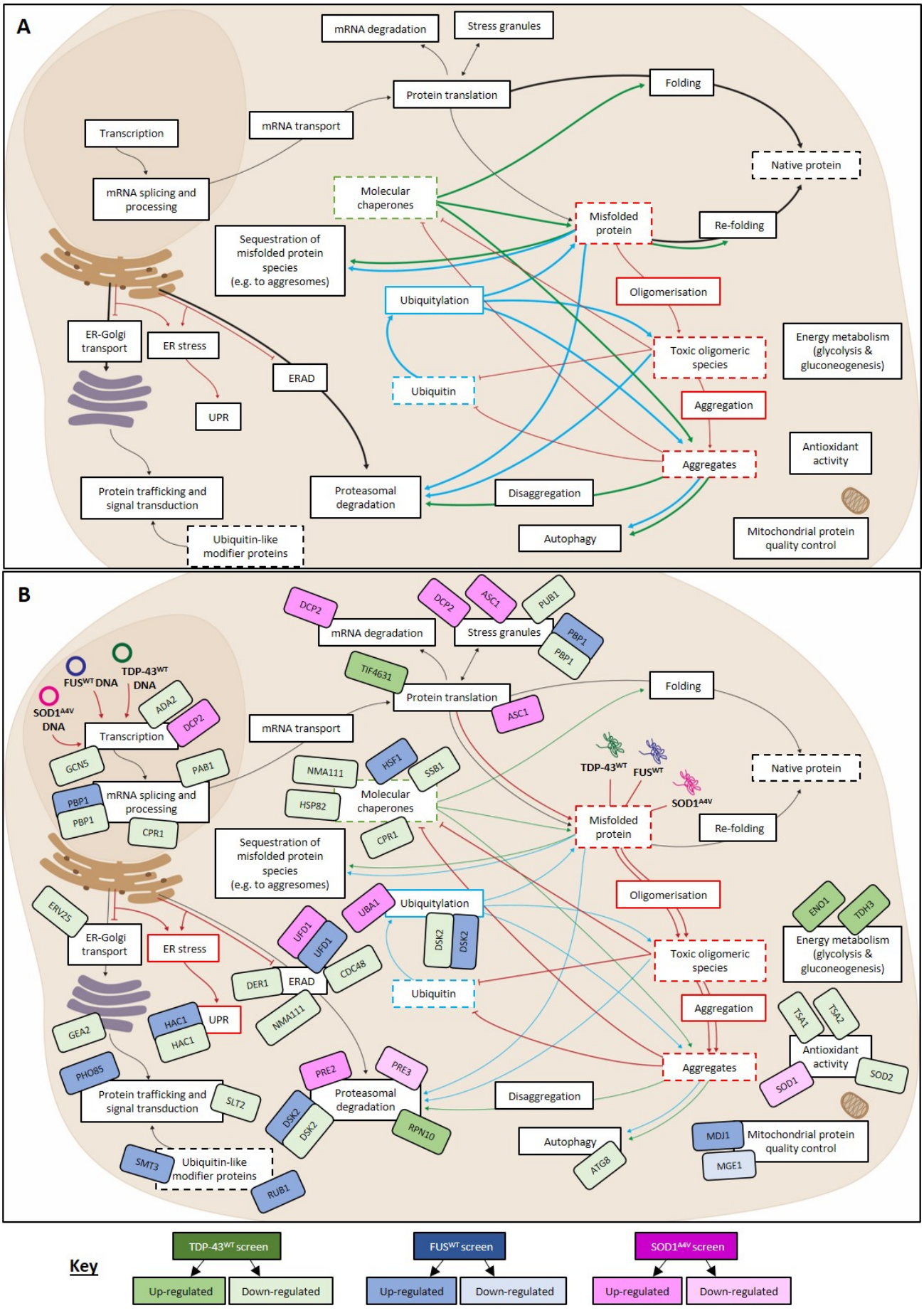
A
mRNA degradation
Stress granules
Protein translation
Folding
Transcription
mRNA transport
Native protein
mRNA splicing and processing
Molecular chaperones
Misfolded protein
Re-folding
Sequestration of misfolded protein species (e.g. to aggresomes)
Ubiquitylation
Oligomerisation
ER-Golgi transport
ER stress
Toxic oligomeric species
Energy metabolism (glycolysis & gluconeogenesis)
ERAD
Ubiquitin
Aggregation
UPR
Antioxidant activity
Aggregates
Protein trafficking and signal transduction
Proteasomal degradation
Disaggregation
Ubiquitin-like modifier proteins
Autophagy
Mitochondrial protein quality control
B
DCP2
mRNA degradation
DCP2
ASC1
PUB1
Stress granules
PBP1
PBP1
TIF4631
Protein translation
Folding
FUSWT DNA
TDP-43WT DNA
SOD1A4V DNA
ADA2
ASC1
Transcription
DCP2
mRNA transport
Native protein
GCN5
PAB1
NMA111
HSF1
SSB1
TDP-43WT
FUSWT
PBP1
PBP1
mRNA splicing and processing
HSP82
Molecular chaperones
SOD1A4V
Misfolded protein
Re-folding
CPR1
CPR1
Sequestration of misfolded protein species (e.g. to aggresomes)
ERV25
UBA1
Ubiquitylation
Oligomerisation
ENO1
TDH3
UFD1
UFD1
DSK2
DSK2
ER-Golgi transport
ER stress
Toxic oligomeric species
Energy metabolism (glycolysis & gluconeogenesis)
DER1
ERAD
CDC48
Ubiquitin
HAC1
UPR
NMA111
Aggregation
TSA1
TSA2
GEA2
HAC1
Antioxidant activity
PHO85
PRE2
PRE3
Aggregates
SOD1
SOD2
Protein trafficking and signal transduction
SLT2
Proteasomal degradation
Disaggregation
DSK2
DSK2
RPN10
Autophagy
MDJ1
Mitochondrial protein quality control
SMT3
Ubiquitin-like modifier proteins
ATG8
MGE1
RUB1
Key
TDP-43WT screen
Up-regulated
Down-regulated
FUSWT screen
Up-regulated
Down-regulated
SOD1A4V screen
Up-regulated
Down-regulated

Figure 6.1. Summary of the proteostasis components and processes found in this PhD research to be affected by expression of pathological TDP-43, FUS and SOD1. (A) The molecular processes that comprise the proteostasis network in eukaryotes (processes that regulate RNA metabolism, gene expression and protein quality control), and in which disruptions have previously been implicated in the pathogenesis of ALS. Errors in RNA metabolism, gene expression and protein quality control processes enable the production of misfolded proteins, which can subsequently oligomerise and aggregate. Misfolded, oligomeric and aggregated forms of proteins have all been shown to disrupt the protective actions of ubiquitin, molecular chaperones, and proteasomal and autophagic protein degradation. However, under normal physiological conditions cells are able to buffer against these aberrant protein forms through ubiquitylation and the action of different molecular chaperones. Misfolded proteins can be re-folded into their native conformations, toxic aggregates can be directed for autophagic degradation or disaggregated and degraded by the proteasome, or alternatively these aberrant protein forms can be sequestered into protein quality control compartments (e.g. aggresomes). (B) In yeast, the heterologous expression of human TDP-43^{WT}, FUS^{WT} or SOD1^{A4V} adds proteotoxic burden to the proteostasis network. Up-regulated proteins identified in yeast expressing TDP-43^{WT}, FUS^{WT} or SOD1^{A4V} may be involved in augmenting the degradation of these aberrant ALS-linked proteins and/or other compensatory processes to restore proteostasis. Down-regulated proteins may be involved in aberrant interactions with pathological TDP-43, FUS or SOD1. They may thus have been directly disrupted through these aberrant interactions. Figure adapted from Ciryam *et al.* 2017.

Gene expression alterations and changes in SG dynamics have been comprehensively investigated in relation to TDP-43 and FUS. Both proteins have functions in transcription regulation, pre-mRNA splicing, mRNA stabilisation and RNA transport (Buratti *et al.* 2001, Buratti *et al.* 2004, Mercado *et al.* 2005, Strong *et al.* 2007, Colombrita *et al.* 2009) and each have several thousand mRNA targets (Hoell *et al.* 2011, Polymenidou *et al.* 2011, Tollervey *et al.* 2011). Importantly, a key finding in this work was that alterations in processes that regulate gene expression were not only associated with TDP-43 and FUS, but were also altered in the presence of mutant SOD1. As the expression of SOD1^{A4V} in yeast did not impact cell viability, contrasting to the toxicity of SOD1^{A4V} expression in neuronal (NSC-34) cells, it is possible that the up-regulation of proteins involved in gene expression regulation (DCP2 and ASC1), along with proteins involved in the UPS and ERAD (UBA1, PRE2 and UFD1), provided cells with an enhanced capacity to manage the proteotoxic burden of mutant SOD1^{A4V}. Moreover, this suggests that dysregulation of RNA metabolism and alterations in gene expression regulation may be common molecular disturbances associated with mutant TDP-43, FUS and SOD1 in ALS (Figure 6.1, b).

The regulation of RNA metabolism and gene expression are necessary for maintenance of the proper levels of proteins in cells, and thus they form core processes of the proteostasis network.

Closely connected to these processes in the proteostasis network are the diverse mechanisms that manage protein quality control. These include mechanisms of protein folding, re-folding, the prevention of protein oligomerisation and aggregation, maintenance of mitochondrial proteostasis and ER proteostasis, protein ubiquitylation and the targeting of aberrant proteins for proteolytic degradation (Figure 6.1, a). The expression of TDP-43^{WT}, FUS^{WT} and SOD1^{A4V} in yeast were each a source of proteotoxic burden to cells, and cells enacted distinct responses by differentially regulating key proteins involved in protein quality control mechanisms (Figure 6.1, b). While the expression of SOD1^{A4V} in yeast did not impair cell viability, FUS^{WT} caused moderate growth inhibition and TDP-43^{WT} markedly reduced the growth of yeast, indicating reduced cell viability.

Most notable amongst the differentially-regulated proteins identified between the yeast screens was that up-regulation of UFD1, a key protein in maintaining ER proteostasis, correlated with suppression of SOD1^{A4V} toxicity and potentially increased cellular capacity to manage pathological FUS. Moreover, HAC1 (IRE1 UPR signalling pathway) (Ron and Walter 2007) and DSK2 (ubiquitin-dependent protein degradation, including ERAD, autophagy and the UPS) (Medicherla *et al.* 2004) abundance changes formed two of three key differentials (PBP1 being the third) between the TDP-43^{WT} and FUS^{WT} screens, with both HAC1 and DSK2 found to be down-regulated in TDP-43^{WT}-expressing yeast and up-regulated in FUS^{WT}-expressing yeast. The increased abundance of HAC1 in FUS^{WT}-expressing yeast, resulting from increased IRE1-mediated splicing of HAC1 mRNA, and the increased abundance and activity of DSK2, may have augmented cellular capacity to restore ER proteostasis. Importantly, abnormal ER morphology and ER stress have been frequently observed pathological features in studies of post-mortem spinal cord tissue from sALS patients and murine models of mutant *SOD1*^{G93A}-linked ALS (Dal Canto and Gurney 1995, Oyanagi *et al.* 2008, Sasaki 2010, Lautenschlaeger *et al.* 2012). Moreover, the IRE1 and ATF6 UPR signalling pathways have been reported to be

up-regulated in post-mortem spinal cord tissue from ALS patients (Montibeller and de Belleroche 2018). From these observations, it stands to reason that disruption of ER proteostasis and UPR signalling pathways are potentially key pathological processes that occur in the motor neurons of individuals with ALS. Hence, the findings made in Chapter III further suggest that disruptions in ER proteostasis and UPR signalling pathways could be common to different genetic forms of ALS. As prolonged UPR signalling can lead to induction of apoptosis (Schroder and Kaufman 2005), further studies into the mechanisms by which ALS proteins cause disruptions in ER proteostasis in neuronal cells are warranted.

DSK2 is the yeast orthologue of UBQLN2, a protein that is genetically implicated in ALS. UBQLN2 is a frequently detected component of inclusions in people with sALS, fALS linked to mutations in *SOD1, TARDBP, FUS* and *C9ORF72* and in fALS patients with *UBQLN2* mutations (Deng *et al.* 2011, Mori *et al.* 2013, May *et al.* 2014). The common theme of UBQLN2-positive inclusions in the motor neurons of people with diverse forms of fALS and sALS suggests that disruption of its functions in ubiquitin-dependent protein degradation, and the downstream consequences of this disruption, may be prominent features that lead to decline of motor neuron viability in ALS. Indeed, the decreased levels of DSK2 in yeast expressing TDP-43^{WT} (and decreased levels of several other proteins with key protective functions in cells), correlating with markedly reduced cellular viability, support the hypothesis that disruptions in DSK2/UBQLN2 and the conserved functions of these orthologues in conserved ubiquitin-dependent protein degradation are detrimental in the face of the proteotoxic burden of a pathological protein.

The research work of Chapter III demonstrates the utility of yeast as a simple eukaryote with the capacity to model the pathology caused by ALS-associated gene variants, and as a screen system. The key findings discussed here provide the foundation for continued investigation of the molecular pathways found to be commonly disturbed in the presence of ALS-associated

TDP-43, FUS and SOD1. Proteins were identified that were commonly affected by the expression of both TDP-43^{WT} and FUS^{WT} (PBP1, HAC1 and DSK2), and by FUS^{WT} and SOD1^{A4V} (UFD1). However, it will be necessary to confirm that the mammalian orthologues (XBP1, ATXN2, UBQLN2 and UFD1L) of these common protein hits are involved in the cellular response to mutant TDP-43, FUS and SOD1 in neuronal cells. Moreover, although proteins were identified that may be involved in the cellular response to mislocalised TDP-43, FUS and mutant SOD1, the mechanisms of their involvement were not examined. Hence, it will be important to determine the specific mechanisms by which these proteins are involved in the response to mutant TDP-43, FUS and SOD1 in neuronal cell culture models. This work could be carried out using the neuronal cell culture models of SOD1^{A4V}, TDP-43^{M337V} and FUS^{R495X}/FUS^{R521G} generated in Chapters IV and V. As numerous mutations in the genes encoding these proteins have been identified in people with ALS, in future mechanistic studies it would be beneficial to examine the common protein hits in motor neuron models generated from induced pluripotent stem cells (iPSCs) derived from ALS patients with different *TARDBP, FUS* and *SOD1* mutations.

6.3 Increased levels of UBA1 reduce SOD1^{A4V} toxicity but do not suppress SOD1^{A4V} aggregation

A particularly intriguing observation made in Chapter III was that the expression of human SOD1^{A4V} did not cause toxicity in yeast cells, which is in stark contrast to the severity of ALS in people carrying this mutation (Cudkowicz *et al.* 1997, Juneja *et al.* 1997). The distinct lack of SOD1^{A4V} toxicity in yeast coincided with up-regulation of UBA1, PRE2 and UFD1, proteins with key roles in the UPS, indicating that UPS activity was augmented in yeast expressing SOD1^{A4V}. UPS dysfunction is a critical occurrence that can lead to disastrous downstream disturbances in the cell (Yerbury *et al.* 2016). The UPS is responsible for the co-ordinated degradation of myriad regulatory short-lived proteins, and it heavily influences the distribution

of ubiquitin in the cellular ubiquitin pools. Ubiquitin also has the essential responsibility of modifying target proteins to control diverse pathways such as transcription, translation, vesicle transport and apoptosis (Carlson *et al.* 1987, Palombella *et al.* 1994, Mimnaugh *et al*. 1997, Ciechanover 1998, Terrell *et al.* 1998, Hoppe *et al.* 2000, Lucero *et al*. 2000, Nakatsu *et al*. 2000, Roth and Davis 2000, Katzmann *et al.* 2001, Muratani and Tansey 2003, de Napoles *et al*. 2004, Wang *et al*. 2004, Baarends *et al*. 2005, Ciechanover 2006, Ikeda *et al.* 2011). Thus, efficient UPS activity, and maintenance of ubiquitin homeostasis, is essential for normal cellular activity.

UBA1 functions at the apex of the ubiquitin-activation and conjugation cascade and thus has significant responsibility in modulating the cellular distribution of ubiquitin (Ayusawa *et al.* 1992, Cook and Chock 1992, Clague *et al.* 2015). Discovering that its levels were increased in yeast expressing $SOD1^{A4V}$ was an important finding in light of evidence from previous studies implicating its potentially protective role in another motor neuron disease, XL-SMA (Ramser *et al.* 2008, Wishart *et al.* 2014, Powis *et al.* 2016). Taking these findings together led to the hypothesis that the increased levels of UBA1 in $SOD1^{A4V}$ yeast formed part of a protective response against $SOD1^{A4V}$, which was then tested (Chapter IV) using the murine NSC-34 cell line as a mammalian neuronal cellular model of $SOD1^{A4V}$-ALS.

Work presented in Chapter IV confirmed that the expression of $SOD1^{A4V}$ in NSC-34 cells caused disruption of normal UPS activity (Figure 4.1, e, Chapter IV), and this correlated with cellular toxicity. $SOD1^{A4V}$ aggregation into large inclusions was a prominent feature in these cells (Figure 4.1, c, Chapter IV). Remarkably, increasing the levels of catalytically-active UBA1 (but not an inactive mutant) in these cells improved cell viability (Figure 4.3, Chapter IV). This is significant as it demonstrates that UBA1 has the capacity to confer a protective effect in neuronal cells beyond the genetic context of SMA. The protective mechanism of increased UBA1 activity did not involve suppression of $SOD1^{A4V}$ aggregation. It has previously

been shown that aggregates formed by SOD1 variants can promote cellular toxicity by sequestering ubiquitin and components of the protein quality control network, diminishing proteostasis capacity and causing ubiquitin dyshomeostasis (Weisberg *et al.* 2012, Farrawell *et al.* 2018). Hence, it is likely that increasing the levels of UBA1 in SOD1^{A4V}-EGFP-expressing NSC-34 cells helped to ameliorate SOD1^{A4V}-mediated deficiency of the activated ubiquitin pools (Figure 6.2). By increasing the capacity of the activated ubiquitin pools, augmented UBA1 activity may have therefore contributed to the restoration of downstream ubiquitin-dependent molecular processes, including the UPS, that become severely impaired in motor neurons as a result of the expression of ALS-causing mutations in *SOD1*. In this theoretical model, the improved viability of SOD1^{A4V}-EGFP-NSC-34 cells overexpressing UBA1 resulted from re-establishment of downstream ubiquitin-dependent molecular processes and efficient UPS activity, deficiencies in which lead to lethal impairment of normal cellular function.

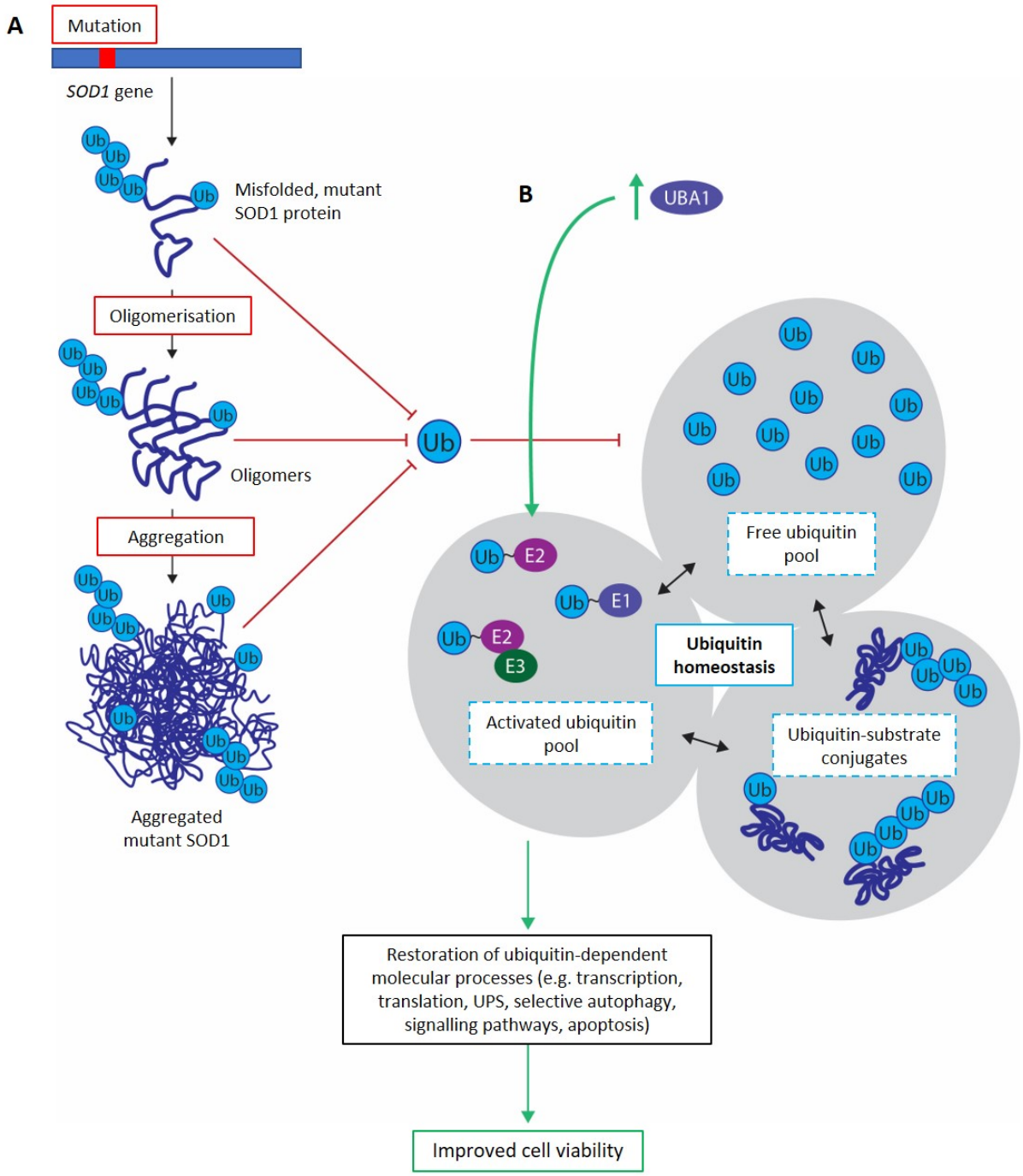

Figure 6.2. Proposed mechanism by which increased levels of UBA1 protect against SOD1^{A4V}-mediated toxicity. (A) Mutations in *SOD1* lead to the production of aberrant, misfolded SOD1 in cells. Mutant SOD1 oligomerises to form toxic oligomeric species, which are able to further aggregate. Misfolded, oligomeric and aggregated forms of SOD1 sequester ubiquitin, disrupting homeostasis of the cellular ubiquitin pools, including the activated ubiquitin pool. Dyshomeostasis of the cellular ubiquitin pools leads to impairment of downstream ubiquitin-dependent molecular processes, including the UPS, causing further disruption of normal cellular activity and eventually leading to loss of cell viability. (B) Increasing the levels of the major E1 ubiquitin-activating enzyme, UBA1, helps to restore SOD1^{A4V}-mediated deficiency of the activated ubiquitin pools and to re-establish ubiquitin homeostasis. By helping to restore ubiquitin homeostasis, increased UBA1 activity may therefore contribute to restoration of downstream ubiquitin-dependent molecular processes, thereby re-establishing normal cellular activity and improving cell viability.

As ubiquitin homeostasis may be disrupted in diverse forms of ALS due to the sequestration of ubiquitin into inclusions, increasing the levels of UBA1 may be beneficial in the context of other genetic mutations associated with ALS. Importantly, the present work adds to previous efforts investigating the role of UBA1 in SMA, demonstrating that modulating the expression or activity of this key enzyme may have therapeutic potential for motor neurons beyond SMA, specifically in the context of $SOD1^{A4V}$-associated ALS. Indeed, as post-mitotic, exceptionally large cells with long neurites, motor neurons have higher demands for stringent maintenance of proteostasis throughout the far reaches of the cytoplasm than most other cell types, including non-motor neurons (Urushitani *et al.* 2002, Onesto *et al.* 2011, Yerbury *et al.* 2016). Moreover, a unique subset of the motor neuron proteome encompasses metastable, aggregation-prone ('supersaturated') proteins, amounting to an exceptionally challenging environment for the proteostasis network (Ciryam *et al.* 2017).

In future research it will be important to examine whether UBA1 expression changes occur in the motor neurons of ALS patients carrying mutations in *SOD1* or other ALS-associated genes, which could be carried out using ALS patient-derived iPSC-motor neurons. It could further be tested if the protective effect of UBA1 observed in NSC-34 cells expressing $SOD1^{A4V}$ extends to iPSC-motor neuron models of different SOD1 mutants and other ALS-associated gene variants. To test this, human $UBA1^{WT}$ and $UBA1^{C632S}$ cloned into lentiviral vectors could be used to generate ALS patient-derived iPSC-motor neurons stably overexpressing $UBA1^{WT}$ and $UBA1^{C632S}$. It will be important to identify the mechanism of UBA1-mediated protection in $SOD1^{A4V}$-NSC-34 cells, or indeed in human iPSC-motor neurons from ALS patients. To evaluate the state of ubiquitin homeostasis after increasing UBA1 levels in these cellular models, orthogonal approaches should be employed. For example, ubiquitome analysis, first described in Nagarajan *et al.* (2017), has previously been used to show that the expression of $SOD1^{A4V}$ in NSC-34 cells causes widespread ubiquitin redistribution and dyshomeostasis

(Farrawell *et al.* 2018). In future work this technique could be used to compare the ubiquitomes of SOD1^{A4V}-NSC-34 cells overexpressing UBA1^{WT} or UBA1^{C632S}. This could be paired with experiments to compare the activated ubiquitin pools in these cells, using a technique described by Gavin *et al.* (2012). As the objective of these future studies would be to examine the potential of UBA1 as a target for gene therapy in ALS patients, there are important implications to consider. It would be crucial to examine potential side effects resulting from increased UBA1 activity in cells. In particular, dysregulated protein ubiquitylation and UPS activity are implicated in some cancers, e.g. multiple myeloma and mantle cell lymphoma (Popovic *et al.* 2014, Weathington and Mallampalli 2014). For instance, overactive ubiquitylation and degradation of the tumour suppressor, p53, may be implicated in the transformation of cells into a cancerous state (Scheffner *et al.* 1990, Michael and Oren 2003, Ciechanover and Schwartz 2004). Thus, analysis of the ubiquitylated state of p53 and other tumour suppressors could be used as a way to monitor if increased UBA1 expression causes off-target effects that promote oncogenesis in cell culture models. Beyond these potential studies in cell culture models, any significant findings would need to be examined and validated using animal models. For example, viral-delivery of UBA1 into transgenic mouse models of mutant SOD1 could be used to (1) confirm the protective effect of UBA1 against mutant SOD1 in the context of a functioning CNS and (2) examine potential off-target effects, including ubiquitylation of p53 and other markers of oncogenesis.

6.4 A high content imaging system to examine proteostasis capacity in neuronal cell culture models of ALS-causing gene variants

A HCS system was developed with the aim of examining proteostasis capacity in NSC-34 cell culture models of ALS-causing mutations in *TARDBP, FUS, CCNF, VAPB, VCP, OPTN* and *UBQLN2* in addition to the SOD1^{A4V} NSC-34 cell model used in Chapter IV. The NSC-34 cell models of *SOD1^{A4V}* and *CCNF^{S621G}* were further used in developing an assay to examine if the

expression of these mutations caused changes in the activity of the protein quality control network of chaperones.

As discussed in Chapter V, it was demonstrated that the Fluc-EGFP isoforms can be used in high-throughput format as a tool to measure cellular protein folding/re-folding capacity in cellular models of ALS-associated mutants. Applying this assay in high-throughput format provides the advantage of speed, combined with the capacity to gain single-cell resolution information about cellular phenotype using multiple readouts from the HCS platform. Although time did not permit the use of this novel HCS assay to examine whether there were alterations in the protein folding environment in the NSC-34 models of *TARDBP-, FUS-, VAPB-, VCP-, OPTN-* and *UBQLN2*-linked ALS, these experiments can now be readily carried out in a future research project. Furthermore, for ALS-associated mutant proteins that do cause reductions in the protein quality control capacity of neuronal cells, as is the case for $SOD1^{A4V}$, this HCS assay has the potential to be applied in drug and genetic screening studies to identify candidate compounds that are able to ameliorate this deficiency. Furthermore, in future work it would be beneficial to develop HCS assays that could be used to explore the findings made in Chapter III, using the generated NSC-34 cell culture models of ALS. Extension of this work may aid in elucidating the specific proteostasis disturbances caused by ALS-associated mutations in *SOD1, TARDBP, FUS, VAPB, VCP, OPTN* and *UBQLN2* in the context of neuronal cells. The HCS assays developed in this process could then be used to screen for candidate drugs that have the potential to target the identified proteostasis deficiencies.

6.5 Concluding statements

With the accelerating progression of ALS research since the first report of *SOD1* mutations in ALS patients (Rosen *et al.* 1993), there has been a steady increase in the number of genes and molecular processes associated with this devastating neurodegenerative disease. However, extensive evidence indicates that proteostasis dysfunction may underlie the dysfunction and

degeneration of motor neurons in ALS. Elucidating the proteostasis disturbances caused by different ALS-associated mutant proteins is therefore a necessary step towards understanding the pathogenic mechanisms that are unique to each gene variant and those that are common to all. While disturbances in the proteostasis network in ALS have been a major focus of research in the past two decades, there has been a lack of systematic approaches to examine multiple ALS-associated gene variants in parallel. This represents a significant disadvantage in the ALS research field since systematic, high-throughput approaches have the potential to fast-track the identification of therapeutic targets that are relevant to the diverse genetic contexts of people with ALS.

The work presented in this PhD thesis describes the development and use of two novel high-throughput methodologies to investigate proteostasis disturbances caused by diverse ALS-causing mutations. By using yeast as a model system amenable to high-throughput screens, common alterations in the proteostasis network caused by pathological TDP-43, FUS and SOD1 were identified, laying the groundwork for further research. Based on this screening approach, the therapeutic potential of UBA1 to suppress the toxicity associated with mutant SOD1 expression in neuronal cells was uncovered. Moreover, this work adds to previous efforts investigating the relevance of ubiquitin dyshomeostasis in *SOD1*-linked ALS. Finally, a HCS assay was developed to further investigate the protein quality control sub-network of the proteostasis network. This HCS assay furthermore has potential for drug screening applications. Continued development of HCS assays that can measure the identified deficiencies in the proteostasis network found through the yeast screens, utilising the neuronal cell culture models that were generated, will be valuable in the search for therapeutic targets. Overall, this work provides substantial foundation for further investigation into the specific proteostasis components that could be potent targets for therapeutic intervention in ALS.

Chapter 7: References

Abel, O., A. Shatunov, A. R. Jones, P. M. Andersen, J. F. Powell and A. Al-Chalabi (2013). "Development of a Smartphone App for a Genetics Website: The Amyotrophic Lateral Sclerosis Online Genetics Database (ALSoD)." JMIR Mhealth Uhealth **1**(2): e18.

Abramzon, Y., J. O. Johnson, S. W. Scholz, J. P. Taylor, M. Brunetti, A. Calvo, J. Mandrioli, M. Benatar, G. Mora, G. Restagno, A. Chio and B. J. Traynor (2012). "Valosin-containing protein (VCP) mutations in sporadic amyotrophic lateral sclerosis." Neurobiol Aging **33**(9): 2231.e2231-2231.e2236.

Aghamaleky Sarvestany, A., G. Hunter, A. Tavendale, D. J. Lamont, M. Llavero Hurtado, L. C. Graham, T. M. Wishart and T. H. Gillingwater (2014). "Label-Free Quantitative Proteomic Profiling Identifies Disruption of Ubiquitin Homeostasis As a Key Driver of Schwann Cell Defects in Spinal Muscular Atrophy." Journal of Proteome Research **13**(11): 4546-4557.

Akbari, M. and H. E. Krokan (2008). "Cytotoxicity and mutagenicity of endogenous DNA base lesions as potential cause of human aging." Mech Ageing Dev **129**(7-8): 353-365.

Al-Chalabi, A., F. Fang, M. F. Hanby, P. N. Leigh, C. E. Shaw, W. Ye, F. Rijsdijk (2010). “An estimate of amyotrophic lateral sclerosis heritability using twin data.” J Neurol Neurosurg Psychiatry; **81**(12):1324-6.

Al-Chalabi, A., P. M. Visscher (2014). “Motor neuron disease: Common genetic variants and the heritability of ALS.” Nat Rev Neurol.; **10**(10):549-50.

Alami, N. H., R. B. Smith, M. A. Carrasco, L. A. Williams, C. S. Winborn, S. S. W. Han, E. Kiskinis, B. Winborn, B. D. Freibaum, A. Kanagaraj, A. J. Clare, N. M. Badders, B. Bilican, E. Chaum, S. Chandran, C. E. Shaw, K. C. Eggan, T. Maniatis and J. P. Taylor (2014). "Axonal transport of TDP-43 mRNA granules is impaired by ALS-causing mutations." Neuron **81**(3): 536-543.

Aliaga, L., C. Lai, J. Yu, N. Chub, H. Shim, L. Sun, C. Xie, W.-J. Yang, X. Lin, M. J. O'Donovan and H. Cai (2013). "Amyotrophic lateral sclerosis-related VAPB P56S mutation

differentially affects the function and survival of corticospinal and spinal motor neurons." Human Molecular Genetics **22**(21): 4293-4305.

Allen, S., P. R. Heath, J. Kirby, S. B. Wharton, M. R. Cookson, F. M. Menzies, R. E. Banks and P. J. Shaw (2003). "Analysis of the cytosolic proteome in a cell culture model of familial amyotrophic lateral sclerosis reveals alterations to the proteasome, antioxidant defenses, and nitric oxide synthetic pathways." J Biol Chem **278**(8): 6371-6383.

Amarilio, R., S. Ramachandran, H. Sabanay and S. Lev (2005). "Differential regulation of endoplasmic reticulum structure through VAP-Nir protein interaction." J Biol Chem **280**(7): 5934-5944.

Anda, F. C., R. Madabhushi, D. Rei, J. Meng, J. Graff, O. Durak, K. Meletis, M. Richter, B. Schwanke, A. Mungenast and L. H. Tsai (2016). "Cortical neurons gradually attain a post-mitotic state." Cell Res **26**(9): 1033-1047.

Andersen, P. M. and A. Al-Chalabi (2011). "Clinical genetics of amyotrophic lateral sclerosis: what do we really know?" Nat Rev Neurol **7**(11): 603-615.

Anderson, J. S. and R. P. Parker (1998). "The 3' to 5' degradation of yeast mRNAs is a general mechanism for mRNA turnover that requires the SKI2 DEVH box protein and 3' to 5' exonucleases of the exosome complex." Embo j **17**(5): 1497-1506.

Anderson, P. and N. Kedersha (2009). "Stress granules." Curr Biol **19**(10): R397-398.

Andersson, M. K., A. Stahlberg, Y. Arvidsson, A. Olofsson, H. Semb, G. Stenman, O. Nilsson and P. Aman (2008). "The multifunctional FUS, EWS and TAF15 proto-oncoproteins show cell type-specific expression patterns and involvement in cell spreading and stress response." BMC Cell Biol **9**: 37.

Aragon, T., E. van Anken, D. Pincus, I. M. Serafimova, A. V. Korennykh, C. A. Rubio and P. Walter (2009). "Messenger RNA targeting to endoplasmic reticulum stress signalling sites." Nature **457**(7230): 736-740.

Arai, T., M. Hasegawa, H. Akiyama, K. Ikeda, T. Nonaka, H. Mori, D. Mann, K. Tsuchiya, M. Yoshida, Y. Hashizume and T. Oda (2006). "TDP-43 is a component of ubiquitin-positive tau-negative inclusions in frontotemporal lobar degeneration and amyotrophic lateral sclerosis." Biochem Biophys Res Commun **351**(3): 602-611.

Armakola, M., M. P. Hart and A. D. Gitler (2011). "TDP-43 toxicity in yeast." Methods **53**(3): 238-245.

Arndt, V., N. Dick, R. Tawo, M. Dreiseidler, D. Wenzel, M. Hesse, D. O. Furst, P. Saftig, R. Saint, B. K. Fleischmann, M. Hoch and J. Hohfeld (2010). "Chaperone-assisted selective autophagy is essential for muscle maintenance." Curr Biol **20**(2): 143-148.

Arndt, V., C. Rogon and J. Hohfeld (2007). "To be, or not to be--molecular chaperones in protein degradation." Cell Mol Life Sci **64**(19-20): 2525-2541.

Arnold, E. S., S. C. Ling, S. C. Huelga, C. Lagier-Tourenne, M. Polymenidou, D. Ditsworth, H. B. Kordasiewicz, M. McAlonis-Downes, O. Platoshyn, P. A. Parone, S. Da Cruz, K. M. Clutario, D. Swing, L. Tessarollo, M. Marsala, C. E. Shaw, G. W. Yeo and D. W. Cleveland (2013). "ALS-linked TDP-43 mutations produce aberrant RNA splicing and adult-onset motor neuron disease without aggregation or loss of nuclear TDP-43." Proc Natl Acad Sci U S A **110**(8): E736-745.

Arrasate, M., S. Mitra, E. S. Schweitzer, M. R. Segal and S. Finkbeiner (2004). "Inclusion body formation reduces levels of mutant huntingtin and the risk of neuronal death." Nature **431**(7010): 805-810.

Ash, P. E., K. F. Bieniek, T. F. Gendron, T. Caulfield, W. L. Lin, M. Dejesus-Hernandez, M. M. van Blitterswijk, K. Jansen-West, J. W. Paul, 3rd, R. Rademakers, K. B. Boylan, D. W.

Dickson and L. Petrucelli (2013). "Unconventional translation of C9ORF72 GGGGCC expansion generates insoluble polypeptides specific to c9FTD/ALS." Neuron **77**(4): 639-646.

Ashburner, M., C. A. Ball, J. A. Blake, D. Botstein, H. Butler, J. M. Cherry, A. P. Davis, K. Dolinski, S. S. Dwight, J. T. Eppig, M. A. Harris, D. P. Hill, L. Issel-Tarver, A. Kasarskis, S. Lewis, J. C. Matese, J. E. Richardson, M. Ringwald, G. M. Rubin and G. Sherlock (2000). "Gene ontology: tool for the unification of biology. The Gene Ontology Consortium." Nat Genet **25**(1): 25-29.

Atkin, J. D., M. A. Farg, K. Y. Soo, A. K. Walker, M. Halloran, B. J. Turner, P. Nagley and M. K. Horne (2014). "Mutant SOD1 inhibits ER-Golgi transport in amyotrophic lateral sclerosis." J Neurochem **129**(1): 190-204.

Auluck, P. K., H. Y. Chan, J. Q. Trojanowski, V. M. Lee and N. M. Bonini (2002). "Chaperone suppression of alpha-synuclein toxicity in a Drosophila model for Parkinson's disease." Science **295**(5556): 865-868.

Ayala, Y. M., P. Zago, A. D'Ambrogio, Y. F. Xu, L. Petrucelli, E. Buratti and F. E. Baralle (2008). "Structural determinants of the cellular localization and shuttling of TDP-43." J Cell Sci **121**(Pt 22): 3778-3785.

Ayusawa, D., S. Kaneda, Y. Itoh, H. Yasuda, Y. Murakami, K. Sugasawa, F. Hanaoka and T. Seno (1992). "Complementation by a cloned human ubiquitin-activating enzyme E1 of the S-phase-arrested mouse FM3A cell mutant with thermolabile E1." Cell Struct Funct **17**(2): 113-122.

Baarends, W. M., E. Wassenaar, R. van der Laan, J. Hoogerbrugge, E. Sleddens-Linkels, J. H. Hoeijmakers, P. de Boer and J. A. Grootegoed (2005). "Silencing of unpaired chromatin and histone H2A ubiquitination in mammalian meiosis." Mol Cell Biol **25**(3): 1041-1053.

Baboshina, O. V. and A. L. Haas (1996). "Novel multiubiquitin chain linkages catalyzed by the conjugating enzymes E2EPF and RAD6 are recognized by 26 S proteasome subunit 5." J Biol Chem **271**(5): 2823-2831.

Badadani, M., A. Nalbandian, G. D. Watts, J. Vesa, M. Kitazawa, H. Su, J. Tanaja, E. Dec, D. C. Wallace, J. Mukherjee, V. Caiozzo, M. Warman and V. E. Kimonis (2010). "VCP associated inclusion body myopathy and paget disease of bone knock-in mouse model exhibits tissue pathology typical of human disease." PLoS One **5**(10).

Balch, W. E., R. I. Morimoto, A. Dillin and J. W. Kelly (2008). "Adapting proteostasis for disease intervention." Science **319**(5865): 916-919.

Baltz, A. G., M. Munschauer, B. Schwanhausser, A. Vasile, Y. Murakawa, M. Schueler, N. Youngs, D. Penfold-Brown, K. Drew, M. Milek, E. Wyler, R. Bonneau, M. Selbach, C. Dieterich and M. Landthaler (2012). "The mRNA-bound proteome and its global occupancy profile on protein-coding transcripts." Mol Cell **46**(5): 674-690.

Barmada, S. J., G. Skibinski, E. Korb, E. J. Rao, J. Y. Wu and S. Finkbeiner (2010). "Cytoplasmic mislocalization of TDP-43 is toxic to neurons and enhanced by a mutation associated with familial amyotrophic lateral sclerosis." J Neurosci **30**(2): 639-649.

Baryshnikova, A., M. Costanzo, S. Dixon, F. J. Vizeacoumar, C. L. Myers, B. Andrews and C. Boone (2010). "Synthetic genetic array (SGA) analysis in Saccharomyces cerevisiae and Schizosaccharomyces pombe." Methods Enzymol **470**: 145-179.

Barzilai, A., S. Biton and Y. Shiloh (2008). "The role of the DNA damage response in neuronal development, organization and maintenance." DNA Repair (Amst) **7**(7): 1010-1027.

Basso, M., G. Samengo, G. Nardo, T. Massignan, G. D'Alessandro, S. Tartari, L. Cantoni, M. Marino, C. Cheroni, S. De Biasi, M. T. Giordana, M. J. Strong, A. G. Estevez, M. Salmona, C. Bendotti and V. Bonetto (2009). "Characterization of detergent-insoluble proteins in ALS

indicates a causal link between nitrative stress and aggregation in pathogenesis." PLoS One **4**(12): e8130.

Bastow, E. L., A. R. Peswani, D. S. J. Tarrant, D. R. Pentland, X. Chen, A. Morgan, G. L. Staniforth, J. M. Tullet, M. L. Rowe, M. J. Howard, M. F. Tuite and C. W. Gourlay (2016). "New links between SOD1 and metabolic dysfunction from a yeast model of amyotrophic lateral sclerosis." J Cell Sci. **129**(21): 4118-4129.

Batulan, Z., G. A. Shinder, S. Minotti, B. P. He, M. M. Doroudchi, J. Nalbantoglu, M. J. Strong and H. D. Durham (2003). "High Threshold for Induction of the Stress Response in Motor Neurons Is Associated with Failure to Activate HSF1." The Journal of Neuroscience **23**(13): 5789-5798.

Beck, J., M. Poulter, D. Hensman, J. D. Rohrer, C. J. Mahoney, G. Adamson, T. Campbell, J. Uphill, A. Borg, P. Fratta, R. W. Orrell, A. Malaspina, J. Rowe, J. Brown, J. Hodges, K. Sidle, J. M. Polke, H. Houlden, J. M. Schott, N. C. Fox, M. N. Rossor, S. J. Tabrizi, A. M. Isaacs, J. Hardy, J. D. Warren, J. Collinge and S. Mead (2013). "Large C9orf72 hexanucleotide repeat expansions are seen in multiple neurodegenerative syndromes and are more frequent than expected in the UK population." Am J Hum Genet **92**(3): 345-353.

Belden, W. J. and C. Barlowe (1996). "Erv25p, a component of COPII-coated vesicles, forms a complex with Emp24p that is required for efficient endoplasmic reticulum to Golgi transport." J Biol Chem **271**(43):26939-46.

Belzil, V. V., T. F. Gendron and L. Petrucelli (2013). "RNA-mediated toxicity in neurodegenerative disease." Mol Cell Neurosci **56**: 406-419.

Belzil, V. V., P. N. Valdmanis, P. A. Dion, H. Daoud, E. Kabashi, A. Noreau, J. Gauthier, P. Hince, A. Desjarlais, J. P. Bouchard, L. Lacomblez, F. Salachas, P. F. Pradat, W. Camu, V. Meininger, N. Dupre and G. A. Rouleau (2009). "Mutations in FUS cause FALS and SALS in French and French Canadian populations." Neurology **73**(15): 1176-1179.

Ben-Zvi, A., E. A. Miller and R. I. Morimoto (2009). "Collapse of proteostasis represents an early molecular event in Caenorhabditis elegans aging." Proc Natl Acad Sci U S A **106**(35): 14914-14919.

Bence, N. F., R. M. Sampat and R. R. Kopito (2001). "Impairment of the ubiquitin-proteasome system by protein aggregation." Science **292**(5521): 1552-1555.

Bennett, E. J., N. F. Bence, R. Jayakumar and R. R. Kopito (2005). "Global impairment of the ubiquitin-proteasome system by nuclear or cytoplasmic protein aggregates precedes inclusion body formation." Mol Cell **17**(3): 351-365.

Bentmann, E., M. Neumann, S. Tahirovic, R. Rodde, D. Dormann and C. Haass (2012). "Requirements for stress granule recruitment of fused in sarcoma (FUS) and TAR DNA-binding protein of 43 kDa (TDP-43)." J Biol Chem **287**(27): 23079-23094.

Bergeron, C., C. Petrunka and L. Weyer (1996). "Copper/zinc superoxide dismutase expression in the human central nervous system. Correlation with selective neuronal vulnerability." Am J Pathol **148**(1): 273-279.

Berndsen, C. E. and C. Wolberger (2014). "New insights into ubiquitin E3 ligase mechanism." Nat Struct Mol Biol **21**(4): 301-307.

Beyer, A., J. Hollunder, H. P. Nasheuer and T. Wilhelm (2004). "Post-transcriptional expression regulation in the yeast Saccharomyces cerevisiae on a genomic scale." Mol Cell Proteomics **3**(11): 1083-1092.

Bhattacharyya, S., H. Yu, C. Mim and A. Matouschek (2014). "Regulated protein turnover: snapshots of the proteasome in action." Nat Rev Mol Cell Biol **15**(2): 122-133.

Bian, Y., R. Kitagawa, P. K. Bansal, Y. Fujii, A. Stepanov and K. Kitagawa (2014). "Synthetic genetic array screen identifies PP2A as a therapeutic target in Mad2-overexpressing tumors." Proc Natl Acad Sci U S A **111**(4): 1628-1633.

Bjorkoy, G., T. Lamark and T. Johansen (2006). "p62/SQSTM1: a missing link between protein aggregates and the autophagy machinery." Autophagy **2**(2): 138-139.

Blair, I. P., K. L. Williams, S. T. Warraich, J. C. Durnall, A. D. Thoeng, J. Manavis, P. C. Blumbergs, S. Vucic, M. C. Kiernan and G. A. Nicholson (2010). "FUS mutations in amyotrophic lateral sclerosis: clinical, pathological, neurophysiological and genetic analysis." J Neurol Neurosurg Psychiatry **81**(6): 639-645.

Blechingberg, J., Y. Luo, L. Bolund, C. K. Damgaard and A. L. Nielsen (2012). "Gene expression responses to FUS, EWS, and TAF15 reduction and stress granule sequestration analyses identifies FET-protein non-redundant functions." PLoS One **7**(9): e46251.

Boeck, R., S. Tarun, Jr., M. Rieger, J. A. Deardorff, S. Muller-Auer and A. B. Sachs (1996). "The yeast Pan2 protein is required for poly(A)-binding protein-stimulated poly(A)-nuclease activity." J Biol Chem **271**(1): 432-438.

Boillee, S., C. Vande Velde and D. W. Cleveland (2006). "ALS: a disease of motor neurons and their nonneuronal neighbors." Neuron **52**(1): 39-59.

Bolognesi, B., J. R. Kumita, T. P. Barros, E. K. Esbjorner, L. M. Luheshi, D. C. Crowther, M. R. Wilson, C. M. Dobson, G. Favrin and J. J. Yerbury (2010). "ANS binding reveals common features of cytotoxic amyloid species." ACS Chem Biol **5**(8): 735-740.

Boname, J. M., M. Thomas, H. R. Stagg, P. Xu, J. Peng and P. J. Lehner (2010). "Efficient internalization of MHC I requires lysine-11 and lysine-63 mixed linkage polyubiquitin chains." Traffic **11**(2): 210-220.

Borkovich, K. A., F. W. Farrelly, D. B. Finkelstein, J. Taulien and S. Lindquist (1989). "hsp82 is an essential protein that is required in higher concentrations for growth of cells at higher temperatures." Mol Cell Biol **9**(9): 3919-3930.

Borroni, B., C. Bonvicini, A. Alberici, E. Buratti, C. Agosti, S. Archetti, A. Papetti, C. Stuani, M. Di Luca, M. Gennarelli and A. Padovani (2009). "Mutation within TARDBP leads to frontotemporal dementia without motor neuron disease." Hum Mutat **30**(11): E974-983.

Bosco, D. A., G. Morfini, N. M. Karabacak, Y. Song, F. Gros-Louis, P. Pasinelli, H. Goolsby, B. A. Fontaine, N. Lemay, D. McKenna-Yasek, M. P. Frosch, J. N. Agar, J. P. Julien, S. T. Brady and R. H. Brown, Jr. (2010). "Wild-type and mutant SOD1 share an aberrant conformation and a common pathogenic pathway in ALS." Nat Neurosci **13**(11): 1396-1403.

Bose, J. K., C. C. Huang and C. K. Shen (2011). "Regulation of autophagy by neuropathological protein TDP-43." J Biol Chem **286**(52): 44441-44448.

Botstein, D., S. A. Chervitz and J. M. Cherry (1997). "Yeast as a model organism." Science **277**(5330): 1259-1260.

Brandman, O., J. Stewart-Ornstein, D. Wong, A. Larson, C. C. Williams, G. W. Li, S. Zhou, D. King, P. S. Shen, J. Weibezahn, J. G. Dunn, S. Rouskin, T. Inada, A. Frost and J. S. Weissman (2012). "A ribosome-bound quality control complex triggers degradation of nascent peptides and signals translation stress." Cell **151**(5): 1042-1054.

Brehme, M., C. Voisine, T. Rolland, S. Wachi, J. H. Soper, Y. Zhu, K. Orton, A. Villella, D. Garza, M. Vidal, H. Ge and R. I. Morimoto (2014). "A chaperome subnetwork safeguards proteostasis in aging and neurodegenerative disease." Cell Rep **9**(3): 1135-1150.

Breker, M., M. Gymrek, O. Moldavski and M. Schuldiner (2014). "LoQAtE--Localization and Quantitation ATlas of the yeast proteomE. A new tool for multiparametric dissection of single-protein behavior in response to biological perturbations in yeast." Nucleic Acids Res **42**(Database issue): D726-730.

Breker, M., M. Gymrek and M. Schuldiner (2013). "A novel single-cell screening platform reveals proteome plasticity during yeast stress responses." J Cell Biol **200**(6): 839-850.

Brettschneider, J., K. Del Tredici, D. J. Irwin, M. Grossman, J. L. Robinson and L. Toledo (2014). "Sequential distribution of pTDP-43 pathology in behavioral variant frontotemporal dementia (bvFTD)." Acta Neuropathol **127**.

Brettschneider, J., V. M. Van Deerlin, J. L. Robinson, L. Kwong, E. B. Lee, Y. O. Ali, N. Safren, M. J. Monteiro, J. B. Toledo, L. Elman, L. McCluskey, D. J. Irwin, M. Grossman, L. Molina-Porcel, V. M. Lee and J. Q. Trojanowski (2012). "Pattern of ubiquilin pathology in ALS and FTLD indicates presence of C9ORF72 hexanucleotide expansion." Acta Neuropathol **123**(6): 825-839.

Brierley, E. J., M. A. Johnson, R. N. Lightowlers, O. F. James and D. M. Turnbull (1998). "Role of mitochondrial DNA mutations in human aging: implications for the central nervous system and muscle." Ann Neurol **43**(2): 217-223.

Brockington, A., K. Ning, P. R. Heath, E. Wood, J. Kirby, N. Fusi, N. Lawrence, S. B. Wharton, P. G. Ince and P. J. Shaw (2013). "Unravelling the enigma of selective vulnerability in neurodegeneration: motor neurons resistant to degeneration in ALS show distinct gene expression characteristics and decreased susceptibility to excitotoxicity." Acta Neuropathol **125**(1): 95-109.

Bruening, W., J. Roy, B. Giasson, D. A. Figlewicz, W. E. Mushynski and H. D. Durham (1999). "Up-regulation of protein chaperones preserves viability of cells expressing toxic Cu/Zn-superoxide dismutase mutants associated with amyotrophic lateral sclerosis." J Neurochem **72**(2): 693-699.

Bruijn, L. I., M. W. Becher, M. K. Lee, K. L. Anderson, N. A. Jenkins, N. G. Copeland, S. S. Sisodia, J. D. Rothstein, D. R. Borchelt, D. L. Price and D. W. Cleveland (1997). "ALS-linked SOD1 mutant G85R mediates damage to astrocytes and promotes rapidly progressive disease with SOD1-containing inclusions." Neuron **18**(2): 327-338.

Bruijn, L. I., M. K. Houseweart, S. Kato, K. L. Anderson, S. D. Anderson, E. Ohama, A. G. Reaume, R. W. Scott and D. W. Cleveland (1998). "Aggregation and motor neuron toxicity of

an ALS-linked SOD1 mutant independent from wild-type SOD1." Science **281**(5384): 1851-1854.

Bruijn, L. I., T. M. Miller and D. W. Cleveland (2004). "Unraveling the mechanisms involved in motor neuron degeneration in ALS." Annu Rev Neurosci **27**: 723-749.

Buchan, J. R., R.-M. Kolaitis, J. P. Taylor and R. Parker (2013). "Eukaryotic Stress Granules Are Cleared by Autophagy and Cdc48/VCP Function." Cell **153**(7): 1461-1474.

Buchan, J. R., D. Muhlrad and R. Parker (2008). "P bodies promote stress granule assembly in Saccharomyces cerevisiae." J Cell Biol **183**(3): 441-455.

Buchan, J. R. and R. Parker (2009). "Eukaryotic stress granules: the ins and outs of translation." Mol Cell **36**(6): 932-941.

Budhidarmo, R., Y. Nakatani and C. L. Day (2012). "RINGs hold the key to ubiquitin transfer." Trends Biochem Sci **37**(2): 58-65.

Buee-Scherrer, V., L. Buee, P. R. Hof, B. Leveugle, C. Gilles, A. J. Loerzel, D. P. Perl and A. Delacourte (1995). "Neurofibrillary degeneration in amyotrophic lateral sclerosis/parkinsonism-dementia complex of Guam. Immunochemical characterization of tau proteins." Am J Pathol **146**(4): 924-932.

Bukau, B., J. Weissman and A. Horwich (2006). "Molecular chaperones and protein quality control." Cell **125**(3): 443-451.

Buratti, E., A. Brindisi, M. Giombi, S. Tisminetzky, Y. M. Ayala and F. E. Baralle (2005). "TDP-43 Binds Heterogeneous Nuclear Ribonucleoprotein A/B through Its C-terminal Tail: AN IMPORTANT REGION FOR THE INHIBITION OF CYSTIC FIBROSIS TRANSMEMBRANE CONDUCTANCE REGULATOR EXON 9 SPLICING." Journal of Biological Chemistry **280**(45): 37572-37584.

Buratti, E., A. Brindisi, F. Pagani and F. E. Baralle (2004). "Nuclear factor TDP-43 binds to the polymorphic TG repeats in CFTR intron 8 and causes skipping of exon 9: a functional link with disease penetrance." Am J Hum Genet **74**(6): 1322-1325.

Buratti, E., T. Dork, E. Zuccato, F. Pagani, M. Romano and F. E. Baralle (2001). "Nuclear factor TDP-43 and SR proteins promote in vitro and in vivo CFTR exon 9 skipping." Embo j **20**(7): 1774-1784.

Carlson, N., S. Rogers and M. Rechsteiner (1987). "Microinjection of ubiquitin: changes in protein degradation in HeLa cells subjected to heat-shock." J Cell Biol **104**(3): 547-555.

Carmody, S. R., E. J. Tran, L. H. Apponi, A. H. Corbett and S. R. Wente (2010). "The mitogen-activated protein kinase Slt2 regulates nuclear retention of non-heat shock mRNAs during heat shock-induced stress." Mol Cell Biol **30**(21): 5168-5179.

Carrel, T. L., M. L. McWhorter, E. Workman, H. Zhang, E. C. Wolstencroft, C. Lorson, G. J. Bassell, A. H. Burghes and C. E. Beattie (2006). "Survival motor neuron function in motor axons is independent of functions required for small nuclear ribonucleoprotein biogenesis." J Neurosci **26**(43): 11014-11022.

Carter, S., O. Bischof, A. Dejean and K. H. Vousden (2007). "C-terminal modifications regulate MDM2 dissociation and nuclear export of p53." Nat Cell Biol **9**(4): 428-435.

Carulli, D., J. C. Kwok and T. Pizzorusso (2016). "Perineuronal Nets and CNS Plasticity and Repair." Neural Plast **2016**: 4327082.

Carvalho, A. F., M. P. Pinto, C. P. Grou, R. Vitorino, P. Domingues, F. Yamao, C. Sa-Miranda and J. E. Azevedo (2012). "High-yield expression in Escherichia coli and purification of mouse ubiquitin-activating enzyme E1." Mol Biotechnol **51**(3): 254-261.

Cashman, N. R., H. D. Durham, J. K. Blusztajn, K. Oda, T. Tabira and I. T. Shaw (1992). "Neuroblastoma x Spinal Cord (NSC) Hybrid Cell Lines Resemble Developing Motor Neurons." Dev Dynam **194**.

Castello, A., B. Fischer, K. Eichelbaum, R. Horos, B. M. Beckmann, C. Strein, N. E. Davey, D. T. Humphreys, T. Preiss, L. M. Steinmetz, J. Krijgsveld and M. W. Hentze (2012). "Insights into RNA biology from an atlas of mammalian mRNA-binding proteins." Cell **149**(6): 1393-1406.

Chau, V., J. W. Tobias, A. Bachmair, D. Marriott, D. J. Ecker, D. K. Gonda and A. Varshavsky (1989). "A multiubiquitin chain is confined to specific lysine in a targeted short-lived protein." Science **243**(4898): 1576-1583.

Chen-Plotkin, A. S., V. M. Lee and J. Q. Trojanowski (2010). "TAR DNA-binding protein 43 in neurodegenerative disease." Nat Rev Neurol **6**(4): 211-220.

Chen, H. J., G. Anagnostou, A. Chai, J. Withers, A. Morris, J. Adhikaree, G. Pennetta and J. S. de Belleroche (2010). "Characterization of the properties of a novel mutation in VAPB in familial amyotrophic lateral sclerosis." J Biol Chem **285**(51): 40266-40281.

Chen, S., P. Sayana, X. Zhang and W. Le (2013). "Genetics of amyotrophic lateral sclerosis: an update." Mol Neurodegener **8**: 28.

Chen, Y. and T. J. Cohen (2019). "Aggregation of the nucleic acid-binding protein TDP-43 occurs via distinct routes that are coordinated with stress granule formation." J Biol Chem **294**(10): 3696-3706.

Chen, Y. Z., C. L. Bennett, H. M. Huynh, I. P. Blair, I. Puls, J. Irobi, I. Dierick, A. Abel, M. L. Kennerson, B. A. Rabin, G. A. Nicholson, M. Auer-Grumbach, K. Wagner, P. De Jonghe, J. W. Griffin, K. H. Fischbeck, V. Timmerman, D. R. Cornblath and P. F. Chance (2004). "DNA/RNA helicase gene mutations in a form of juvenile amyotrophic lateral sclerosis (ALS4)." Am J Hum Genet **74**(6): 1128-1135.

Cheroni, C., M. Marino, M. Tortarolo, P. Veglianese, S. De Biasi, E. Fontana, L. V. Zuccarello, C. J. Maynard, N. P. Dantuma and C. Bendotti (2009). "Functional alterations of the ubiquitin-proteasome system in motor neurons of a mouse model of familial amyotrophic lateral sclerosis." Hum Mol Genet **18**(1): 82-96.

Cheroni, C., M. Peviani, P. Cascio, S. Debiasi, C. Monti and C. Bendotti (2005). "Accumulation of human SOD1 and ubiquitinated deposits in the spinal cord of SOD1G93A mice during motor neuron disease progression correlates with a decrease of proteasome." Neurobiol Dis **18**(3): 509-522.

Chiti, F. and C. M. Dobson (2006). "Protein misfolding, functional amyloid, and human disease." Annu Rev Biochem **75**.

Chitiprolu, M., C. Jagow, V. Tremblay, E. Bondy-Chorney, G. Paris, A. Savard, G. Palidwor, F. A. Barry, L. Zinman, J. Keith, E. Rogaeva, J. Robertson, M. Lavallée-Adam, J. Woulfe, J.-F. Couture, J. Côté and D. Gibbings (2018). "A complex of C9ORF72 and p62 uses arginine methylation to eliminate stress granules by autophagy." Nature Communications **9**(1): 2794.

Chiu, Y. H., Q. Sun and Z. J. Chen (2007). "E1-L2 activates both ubiquitin and FAT10." Mol Cell **27**(6): 1014-1023.

Chondrogianni, N., F. L. L. Stratford, I. P. Trougakos, B. Friguet, A. J. Rivett and E. S. Gonos (2003). "Central Role of the Proteasome in Senescence and Survival of Human Fibroblasts: INDUCTION OF A SENESCENCE-LIKE PHENOTYPE UPON ITS INHIBITION AND RESISTANCE TO STRESS UPON ITS ACTIVATION." Journal of Biological Chemistry **278**(30): 28026-28037.

Chondrogianni, N., C. Tzavelas, A. J. Pemberton, I. P. Nezis, A. J. Rivett and E. S. Gonos (2005). "Overexpression of Proteasome β5 Assembled Subunit Increases the Amount of Proteasome and Confers Ameliorated Response to Oxidative Stress and Higher Survival Rates." Journal of Biological Chemistry **280**(12): 11840-11850.

Chou, S. M. (1979). "Pathognomy of intraneuronal inclusions in ALS." Amyotrophic Lateral Sclerosis.: 135-176.

Chou, S. M., H. S. Wang and K. Komai (1996). "Colocalization of NOS and SOD1 in neurofilament accumulation within motor neurons of amyotrophic lateral sclerosis: an immunohistochemical study." J Chem Neuroanat **10**(3-4): 249-258.

Ciechanover, A. (1998). "The ubiquitin-proteasome pathway: on protein death and cell life." Embo j **17**(24): 7151-7160.

Ciechanover, A. (2006). "The ubiquitin proteolytic system: from a vague idea, through basic mechanisms, and onto human diseases and drug targeting." Neurology **66**(2 Suppl 1): S7-19.

Ciechanover, A., D. Finley and A. Varshavsky (1984). "The ubiquitin-mediated proteolytic pathway and mechanisms of energy-dependent intracellular protein degradation." J Cell Biochem **24**(1): 27-53.

Ciechanover, A. and A. L. Schwartz (2004). "The ubiquitin system: pathogenesis of human diseases and drug targeting." Biochimica et Biophysica Acta (BBA) - Molecular Cell Research **1695**(1): 3-17.

Ciechanover, A. and A. Stanhill (2014). "The complexity of recognition of ubiquitinated substrates by the 26S proteasome." Biochim Biophys Acta **1843**(1): 86-96.

Cirulli, E. T., B. N. Lasseigne, S. Petrovski, P. C. Sapp, P. A. Dion, C. S. Leblond, J. Couthouis, Y. F. Lu, Q. Wang, B. J. Krueger, Z. Ren, J. Keebler, Y. Han, S. E. Levy, B. E. Boone, J. R. Wimbish, L. L. Waite, A. L. Jones, J. P. Carulli, A. G. Day-Williams, J. F. Staropoli, W. W. Xin, A. Chesi, A. R. Raphael, D. McKenna-Yasek, J. Cady, J. M. Vianney de Jong, K. P. Kenna, B. N. Smith, S. Topp, J. Miller, A. Gkazi, F. S. Consortium, A. Al-Chalabi, L. H. van den Berg, J. Veldink, V. Silani, N. Ticozzi, C. E. Shaw, R. H. Baloh, S. Appel, E. Simpson, C. Lagier-Tourenne, S. M. Pulst, S. Gibson, J. Q. Trojanowski, L. Elman, L. McCluskey, M. Grossman, N. A. Shneider, W. K. Chung, J. M. Ravits, J. D. Glass, K. B. Sims, V. M. Van

Deerlin, T. Maniatis, S. D. Hayes, A. Ordureau, S. Swarup, J. Landers, F. Baas, A. S. Allen, R. S. Bedlack, J. W. Harper, A. D. Gitler, G. A. Rouleau, R. Brown, M. B. Harms, G. M. Cooper, T. Harris, R. M. Myers and D. B. Goldstein (2015). "Exome sequencing in amyotrophic lateral sclerosis identifies risk genes and pathways." Science.

Ciryam, P., R. Kundra, R. I. Morimoto, C. M. Dobson and M. Vendruscolo (2015). "Supersaturation is a major driving force for protein aggregation in neurodegenerative diseases." Trends Pharmacol Sci **36**(2): 72-77.

Ciryam, P., I. A. Lambert-Smith, D. M. Bean, R. Freer, F. Cid, G. G. Tartaglia, D. N. Saunders, M. R. Wilson, S. G. Oliver, R. I. Morimoto, C. M. Dobson, M. Vendruscolo, G. Favrin and J. J. Yerbury (2017). "Spinal motor neuron protein supersaturation patterns are associated with inclusion body formation in ALS." Proceedings of the National Academy of Sciences **114**(20): E3935-E3943.

Ciryam, P., G. G. Tartaglia, R. I. Morimoto, C. M. Dobson and M. Vendruscolo (2013). "Widespread aggregation and neurodegenerative diseases are associated with supersaturated proteins." Cell Rep **5**(3): 781-790.

Clague, M. J., C. Heride and S. Urbe (2015). "The demographics of the ubiquitin system." Trends Cell Biol **25**(7): 417-426.

Claud, E. C., J. A. McDonald, S. M. He, Y. Yu, L. Duong, J. Sun and E. O. Petrof (2014). "Differential expression of 26S proteasome subunits and functional activity during neonatal development." Biomolecules **4**(3): 812-826.

Cleveland, D. W. and J. D. Rothstein (2001). "From Charcot to Lou Gehrig: deciphering selective motor neuron death in ALS." Nat Rev Neurosci **2**(11): 806-819.

Cohen, R., T. Yokoi, J. P. Holland, A. E. Pepper, M. J. Holland (1987). “Transcription of the constitutively expressed yeast enolase gene ENO1 is mediated by positive and negative cis-acting regulatory sequences.” Mol Cell Biol **7**(8):2753-61.

Colombrita, C., E. Onesto, F. Megiorni, A. Pizzuti, F. E. Baralle, E. Buratti, V. Silani and A. Ratti (2012). "TDP-43 and FUS RNA-binding proteins bind distinct sets of cytoplasmic messenger RNAs and differently regulate their post-transcriptional fate in motoneuron-like cells." J Biol Chem **287**(19): 15635-15647.

Colombrita, C., E. Zennaro, C. Fallini, M. Weber, A. Sommacal, E. Buratti, V. Silani and A. Ratti (2009). "TDP-43 is recruited to stress granules in conditions of oxidative insult." J Neurochem **111**(4): 1051-1061.

Consortium, T. G. O. (2019). "The Gene Ontology Resource: 20 years and still GOing strong." Nucleic Acids Res **47**(D1): D330-d338.

Cook, J. C. and P. B. Chock (1992). "Isoforms of mammalian ubiquitin-activating enzyme." J Biol Chem **267**(34): 24315-24321.

Cooper, A. A., A. D. Gitler, A. Cashikar, C. M. Haynes, K. J. Hill, B. Bhullar, K. Liu, K. Xu, K. E. Strathearn, F. Liu, S. Cao, K. A. Caldwell, G. A. Caldwell, G. Marsischky, R. D. Kolodner, J. Labaer, J. C. Rochet, N. M. Bonini and S. Lindquist (2006). "Alpha-synuclein blocks ER-Golgi traffic and Rab1 rescues neuron loss in Parkinson's models." Science **313**(5785): 324-328.

Cooper, T. A., L. Wan and G. Dreyfuss (2009). "RNA and disease." Cell **136**(4): 777-793.

Copic, A., M. Dorrington, S. Pagant, J. Barry, M. C. Lee, I. Singh, J. L. t. Hartman and E. A. Miller (2009). "Genomewide analysis reveals novel pathways affecting endoplasmic reticulum homeostasis, protein modification and quality control." Genetics **182**(3): 757-769.

Corcia, P., W. Camu, J. M. Halimi, P. Vourc'h, C. Antar, S. Vedrine, B. Giraudeau, B. de Toffol and C. R. Andres (2006). "SMN1 gene, but not SMN2, is a risk factor for sporadic ALS." Neurology **67**(7): 1147-1150.

Corrado, L., R. Del Bo, B. Castellotti, A. Ratti, C. Cereda, S. Penco, G. Soraru, Y. Carlomagno, S. Ghezzi, V. Pensato, C. Colombrita, S. Gagliardi, L. Cozzi, V. Orsetti, M. Mancuso, G. Siciliano, L. Mazzini, G. P. Comi, C. Gellera, M. Ceroni, S. D'Alfonso and V. Silani (2010). "Mutations of FUS gene in sporadic amyotrophic lateral sclerosis." J Med Genet **47**(3): 190-194.

Corral-Debrinski, M., T. Horton, M. T. Lott, J. M. Shoffner, M. F. Beal and D. C. Wallace (1992). "Mitochondrial DNA deletions in human brain: regional variability and increase with advanced age." Nat Genet **2**(4): 324-329.

Corral-Debrinski, M., T. Horton, M. T. Lott, J. M. Shoffner, A. C. McKee, M. F. Beal, B. H. Graham and D. C. Wallace (1994). "Marked changes in mitochondrial DNA deletion levels in Alzheimer brains." Genomics **23**(2): 471-476.

Corral-Debrinski, M., J. M. Shoffner, M. T. Lott and D. C. Wallace (1992). "Association of mitochondrial DNA damage with aging and coronary atherosclerotic heart disease." Mutat Res **275**(3-6): 169-180.

Coskun, P. E., M. F. Beal and D. C. Wallace (2004). "Alzheimer's brains harbor somatic mtDNA control-region mutations that suppress mitochondrial transcription and replication." Proc Natl Acad Sci U S A **101**(29): 10726-10731.

Couthouis, J., M. P. Hart, R. Erion, O. D. King, Z. Diaz, T. Nakaya, F. Ibrahim, H. J. Kim, J. Mojsilovic-Petrovic, S. Panossian, C. E. Kim, E. C. Frackelton, J. A. Solski, K. L. Williams, D. Clay-Falcone, L. Elman, L. McCluskey, R. Greene, H. Hakonarson, R. G. Kalb, V. M. Lee, J. Q. Trojanowski, G. A. Nicholson, I. P. Blair, N. M. Bonini, V. M. Van Deerlin, Z. Mourelatos, J. Shorter and A. D. Gitler (2012). "Evaluating the role of the FUS/TLS-related gene EWSR1 in amyotrophic lateral sclerosis." Hum Mol Genet **21**(13): 2899-2911.

Couthouis, J., M. P. Hart, J. Shorter, M. DeJesus-Hernandez, R. Erion, R. Oristano, A. X. Liu, D. Ramos, N. Jethava, D. Hosangadi, J. Epstein, A. Chiang, Z. Diaz, T. Nakaya, F. Ibrahim, H. J. Kim, J. A. Solski, K. L. Williams, J. Mojsilovic-Petrovic, C. Ingre, K. Boylan, N. R. Graff-Radford, D. W. Dickson, D. Clay-Falcone, L. Elman, L. McCluskey, R. Greene, R. G.

Kalb, V. M. Lee, J. Q. Trojanowski, A. Ludolph, W. Robberecht, P. M. Andersen, G. A. Nicholson, I. P. Blair, O. D. King, N. M. Bonini, V. Van Deerlin, R. Rademakers, Z. Mourelatos and A. D. Gitler (2011). "A yeast functional screen predicts new candidate ALS disease genes." Proc Natl Acad Sci U S A **108**(52): 20881-20890.

Cox, J. S. and P. Walter (1996). "A novel mechanism for regulating activity of a transcription factor that controls the unfolded protein response." Cell **87**(3): 391-404.

Cozzolino, M. (2008). "Cysteine 111 Affects Aggregation and Cytotoxicity of Mutant Cu,Zn-superoxide Dismutase Associated with Familial Amyotrophic Lateral Sclerosis." **283**(2): 866-874.

Crapo, J. D., T. Oury, C. Rabouille, J. W. Slot and L. Y. Chang (1992). "Copper,zinc superoxide dismutase is primarily a cytosolic protein in human cells." Proc Natl Acad Sci U S A **89**(21): 10405-10409.

Crews, C. M. (2003). "Feeding the machine: mechanisms of proteasome-catalyzed degradation of ubiquitinated proteins." Curr Opin Chem Biol **7**(5): 534-539.

Crippa, V., D. Sau, P. Rusmini, A. Boncoraglio, E. Onesto, E. Bolzoni, M. Galbiati, E. Fontana, M. Marino, S. Carra, C. Bendotti, S. De Biasi and A. Poletti (2010). "The small heat shock protein B8 (HspB8) promotes autophagic removal of misfolded proteins involved in amyotrophic lateral sclerosis (ALS)." Hum Mol Genet **19**(17): 3440-3456.

Cudkowicz, M. E., D. McKenna-Yasek, P. E. Sapp, W. Chin, B. Geller, D. L. Hayden, D. A. Schoenfeld, B. A. Hosler, H. R. Horvitz and R. H. Brown (1997). "Epidemiology of mutations in superoxide dismutase in amyotrophic lateral sclerosis." Ann Neurol **41**(2): 210-221.

Cushman, M., B. S. Johnson, O. D. King, A. D. Gitler and J. Shorter (2010). "Prion-like disorders: blurring the divide between transmissibility and infectivity." J Cell Sci **123**(Pt 8): 1191-1201.

Custer, S. K., M. Neumann, H. Lu, A. C. Wright and J. P. Taylor (2010). "Transgenic mice expressing mutant forms VCP/p97 recapitulate the full spectrum of IBMPFD including degeneration in muscle, brain and bone." Hum Mol Genet **19**(9): 1741-1755.

D'Angiolella, V., M. Esencay and M. Pagano (2013). "A cyclin without cyclin-dependent kinases: cyclin F controls genome stability through ubiquitin-mediated proteolysis." Trends Cell Biol **23**(3): 135-140.

D'Souza, R. C., A. M. Knittle, N. Nagaraj, M. van Dinther, C. Choudhary, P. ten Dijke, M. Mann and K. Sharma (2014). "Time-resolved dissection of early phosphoproteome and ensuing proteome changes in response to TGF-beta." Sci Signal **7**(335): rs5.

Dal Canto, M. C. and M. E. Gurney (1995). "Neuropathological changes in two lines of mice carrying a transgene for mutant human Cu,Zn SOD, and in mice overexpressing wild type human SOD: a model of familial amyotrophic lateral sclerosis (FALS)." Brain Res **676**(1): 25-40.

Dammer, E. B., C. H. Na, P. Xu, N. T. Seyfried, D. M. Duong, D. Cheng, M. Gearing, H. Rees, J. J. Lah, A. I. Levey, J. Rush and J. Peng (2011). "Polyubiquitin linkage profiles in three models of proteolytic stress suggest the etiology of Alzheimer disease." J Biol Chem **286**(12): 10457-10465.

Dantuma, N. P., T. A. Groothuis, F. A. Salomons and J. Neefjes (2006). "A dynamic ubiquitin equilibrium couples proteasomal activity to chromatin remodeling." J Cell Biol **173**(1): 19-26.

de Bot, S. T., H. J. Schelhaas, E.-J. Kamsteeg and B. P. C. van de Warrenburg (2012). "Hereditary spastic paraplegia caused by a mutation in the VCP gene." Brain **135**(12): e223-e223.

de Napoles, M., J. E. Mermoud, R. Wakao, Y. A. Tang, M. Endoh, R. Appanah, T. B. Nesterova, J. Silva, A. P. Otte, M. Vidal, H. Koseki and N. Brockdorff (2004). "Polycomb

group proteins Ring1A/B link ubiquitylation of histone H2A to heritable gene silencing and X inactivation." Dev Cell **7**(5): 663-676.

De Vos, K. J., G. M. Morotz, R. Stoica, E. L. Tudor, K. F. Lau, S. Ackerley, A. Warley, C. E. Shaw and C. C. Miller (2012). "VAPB interacts with the mitochondrial protein PTPIP51 to regulate calcium homeostasis." Hum Mol Genet **21**(6): 1299-1311.

DeJesus-Hernandez, M., J. Kocerha, N. Finch, R. Crook, M. Baker, P. Desaro, A. Johnston, N. Rutherford, A. Wojtas, K. Kennelly, Z. K. Wszolek, N. Graff-Radford, K. Boylan and R. Rademakers (2010). "De novo truncating FUS gene mutation as a cause of sporadic amyotrophic lateral sclerosis." Hum Mutat **31**(5): E1377-1389.

DeJesus-Hernandez, M., Ian R. Mackenzie, Bradley F. Boeve, Adam L. Boxer, M. Baker, Nicola J. Rutherford, Alexandra M. Nicholson, NiCole A. Finch, H. Flynn, J. Adamson, N. Kouri, A. Wojtas, P. Sengdy, G.-Yuek R. Hsiung, A. Karydas, William W. Seeley, Keith A. Josephs, G. n. Coppola, Daniel H. Geschwind, Zbigniew K. Wszolek, H. Feldman, David S. Knopman, Ronald C. Petersen, Bruce L. Miller, Dennis W. Dickson, Kevin B. Boylan, Neill R. Graff-Radford and R. Rademakers (2011). "Expanded GGGGCC Hexanucleotide Repeat in Noncoding Region of C9ORF72 Causes Chromosome 9p-Linked FTD and ALS." Neuron **72**(2): 245-256.

del Toro, D., J. Alberch, F. Lazaro-Dieguez, R. Martin-Ibanez, X. Xifro, G. Egea and J. M. Canals (2009). "Mutant huntingtin impairs post-Golgi trafficking to lysosomes by delocalizing optineurin/Rab8 complex from the Golgi apparatus." Mol Biol Cell **20**(5): 1478-1492.

Deloche, O., W. L. Kelley and C. Georgopoulos (1997). "Structure-function analyses of the Ssc1p, Mdj1p, and Mge1p Saccharomyces cerevisiae mitochondrial proteins in Escherichia coli." J Bacteriol **179**(19): 6066-6075.

Deng, H. X., W. Chen, S. T. Hong, K. M. Boycott, G. H. Gorrie, N. Siddique, Y. Yang, F. Fecto, Y. Shi, H. Zhai, H. Jiang, M. Hirano, E. Rampersaud, G. H. Jansen, S. Donkervoort, E. H. Bigio, B. R. Brooks, K. Ajroud, R. L. Sufit, J. L. Haines, E. Mugnaini, M. A. Pericak-Vance

and T. Siddique (2011). "Mutations in UBQLN2 cause dominant X-linked juvenile and adult-onset ALS and ALS/dementia." Nature **477**(7363): 211-215.

Deng, H. X., A. Hentati, J. A. Tainer, Z. Iqbal, A. Cayabyab, W. Y. Hung, E. D. Getzoff, P. Hu, B. Herzfeldt, R. P. Roos and a. et (1993). "Amyotrophic lateral sclerosis and structural defects in Cu,Zn superoxide dismutase." Science **261**(5124): 1047.

Deng, H. X., Y. Shi, Y. Furukawa, H. Zhai, R. Fu and E. Liu (2006). "Conversion to the amyotrophic lateral sclerosis phenotype is associated with intermolecular linked insoluble aggregates of SOD1 in mitochondria." Proc Natl Acad Sci U S A **103**.

Deng, H. X., H. Zhai, E. H. Bigio, J. Yan, F. Fecto, K. Ajroud, M. Mishra, S. Ajroud-Driss, S. Heller, R. Sufit, N. Siddique, E. Mugnaini and T. Siddique (2010). "FUS-immunoreactive inclusions are a common feature in sporadic and non-SOD1 familial amyotrophic lateral sclerosis." Ann Neurol **67**(6): 739-748.

Deng, L., C. Wang, E. Spencer, L. Yang, A. Braun, J. You, C. Slaughter, C. Pickart and Z. J. Chen (2000). "Activation of the IkappaB kinase complex by TRAF6 requires a dimeric ubiquitin-conjugating enzyme complex and a unique polyubiquitin chain." Cell **103**(2): 351-361.

Derham, B. K. and J. J. Harding (1997). "Effect of aging on the chaperone-like function of human alpha-crystallin assessed by three methods." Biochem J **328 (Pt 3)**(Pt 3): 763-768.

Deshaies, R. J. and C. A. Joazeiro (2009). "RING domain E3 ubiquitin ligases." Annu Rev Biochem **78**: 399-434.

Deshpande, R., M. K. Asiedu, M. Klebig, S. Sutor, E. Kuzmin, J. Nelson, J. Piotrowski, S. H. Shin, M. Yoshida, M. Costanzo, C. Boone, D. A. Wigle and C. L. Myers (2013). "A comparative genomic approach for identifying synthetic lethal interactions in human cancer." Cancer Res **73**(20): 6128-6136.

Dewey, C. M., B. Cenik, C. F. Sephton, D. R. Dries, P. Mayer, 3rd, S. K. Good, B. A. Johnson, J. Herz and G. Yu (2011). "TDP-43 is directed to stress granules by sorbitol, a novel physiological osmotic and oxidative stressor." Mol Cell Biol **31**(5): 1098-1108.

Dewey, C. M., B. Cenik, C. F. Sephton, B. A. Johnson, J. Herz and G. Yu (2012). "TDP-43 aggregation in neurodegeneration: Are stress granules the key?" Brain Research **1462**: 16-25.

Dharmadasa, T., R. D. Henderson, P. S. Talman, R. A. Macdonell, S. Mathers, D. W. Schultz, M. Needham, M. Zoing, S. Vucic, M. C. Kiernan (2017). “Motor neurone disease: progress and challenges.” Med J Aust.; **206**(8):357-362.

Di Giovanni, S. (2009). "Molecular targets for axon regeneration: focus on the intrinsic pathways." Expert Opin Ther Targets **13**(12): 1387-1398.

Dichmann, D. S. and R. M. Harland (2012). "fus/TLS orchestrates splicing of developmental regulators during gastrulation." Genes Dev **26**(12): 1351-1363.

Ding, W. X. and X. M. Yin (2008). "Sorting, recognition and activation of the misfolded protein degradation pathways through macroautophagy and the proteasome." Autophagy **4**(2): 141-150.

Dobson-Stone, C., A. A. Luty, E. M. Thompson, P. Blumbergs, W. S. Brooks, C. L. Short, C. D. Field, P. K. Panegyres, J. Hecker, J. A. Solski, I. P. Blair, J. M. Fullerton, G. M. Halliday, P. R. Schofield and J. B. Kwok (2013). "Frontotemporal dementia-amyotrophic lateral sclerosis syndrome locus on chromosome 16p12.1-q12.2: genetic, clinical and neuropathological analysis." Acta Neuropathol **125**(4): 523-533.

Doi, H., S. Koyano, Y. Suzuki, N. Nukina and Y. Kuroiwa (2010). "The RNA-binding protein FUS/TLS is a common aggregate-interacting protein in polyglutamine diseases." Neurosci Res **66**(1): 131-133.

Dolinski, K. J., M. E. Cardenas and J. Heitman (1998). "CNS1 encodes an essential p60/Sti1 homolog in Saccharomyces cerevisiae that suppresses cyclophilin 40 mutations and interacts with Hsp90." Mol Cell Biol **18**(12): 7344-7352.

Dormann, D., R. Rodde, D. Edbauer, E. Bentmann, I. Fischer, A. Hruscha, M. E. Than, I. R. Mackenzie, A. Capell, B. Schmid, M. Neumann and C. Haass (2010). "ALS-associated fused in sarcoma (FUS) mutations disrupt Transportin-mediated nuclear import." Embo j **29**(16): 2841-2857.

Dou, C. L. and J. M. Levine (1994). "Inhibition of neurite growth by the NG2 chondroitin sulfate proteoglycan." J Neurosci **14**(12): 7616-7628.

Douglas, P. M. and A. Dillin (2010). "Protein homeostasis and aging in neurodegeneration." J Cell Biol **190**(5): 719-729.

Duina, A. A., M. E. Miller and J. B. Keeney (2014). "Budding yeast for budding geneticists: a primer on the Saccharomyces cerevisiae model system." Genetics **197**(1): 33-48.

Dunckley, T. and R. Parker (1999). "The DCP2 protein is required for mRNA decapping in Saccharomyces cerevisiae and contains a functional MutT motif." Embo j **18**(19): 5411-5422.

Durham, H. D., J. Roy, L. Dong and D. A. Figlewicz (1997). "Aggregation of mutant Cu/Zn superoxide dismutase proteins in a culture model of ALS." J Neuropathol Exp Neurol **56**(5): 523-530.

Dynek, J. N., T. Goncharov, E. C. Dueber, A. V. Fedorova, A. Izrael-Tomasevic, L. Phu, E. Helgason, W. J. Fairbrother, K. Deshayes, D. S. Kirkpatrick and D. Vucic (2010). "c-IAP1 and UbcH5 promote K11-linked polyubiquitination of RIP1 in TNF signalling." Embo j **29**(24): 4198-4209.

Eden, E., N. Geva-Zatorsky, I. Issaeva, A. Cohen, E. Dekel, T. Danon, L. Cohen, A. Mayo and U. Alon (2011). "Proteome half-life dynamics in living human cells." Science **331**(6018): 764-768.

Elden, A. C., H. J. Kim, M. P. Hart, A. S. Chen-Plotkin, B. S. Johnson, X. Fang, M. Armakola, F. Geser, R. Greene, M. M. Lu, A. Padmanabhan, D. Clay-Falcone, L. McCluskey, L. Elman, D. Juhr, P. J. Gruber, U. Rub, G. Auburger, J. Q. Trojanowski, V. M. Lee, V. M. Van Deerlin, N. M. Bonini and A. D. Gitler (2010). "Ataxin-2 intermediate-length polyglutamine expansions are associated with increased risk for ALS." Nature **466**(7310): 1069-1075.

Eletr, Z. M., D. T. Huang, D. M. Duda, B. A. Schulman and B. Kuhlman (2005). "E2 conjugating enzymes must disengage from their E1 enzymes before E3-dependent ubiquitin and ubiquitin-like transfer." Nat Struct Mol Biol **12**(10): 933-934.

Erickson, R. R., L. M. Dunning and J. L. Holtzman (2006). "The effect of aging on the chaperone concentrations in the hepatic, endoplasmic reticulum of male rats: the possible role of protein misfolding due to the loss of chaperones in the decline in physiological function seen with age." J Gerontol A Biol Sci Med Sci **61**(5): 435-443.

Erjavec, N., L. Larsson, J. Grantham and T. Nystrom (2007). "Accelerated aging and failure to segregate damaged proteins in Sir2 mutants can be suppressed by overproducing the protein aggregation-remodeling factor Hsp104p." Genes Dev **21**(19): 2410-2421.

Evans, M. D., M. Dizdaroglu and M. S. Cooke (2004). "Oxidative DNA damage and disease: induction, repair and significance." Mutat Res **567**(1): 1-61.

Farg, M. A., K. Y. Soo, A. K. Walker, H. Pham, J. Orian, M. K. Horne, S. T. Warraich, K. L. Williams, I. P. Blair and J. D. Atkin (2012). "Mutant FUS induces endoplasmic reticulum stress in amyotrophic lateral sclerosis and interacts with protein disulfide-isomerase." Neurobiol Aging **33**(12): 2855-2868.

Farg, M. A., K. Y. Soo, S. T. Warraich, V. Sundaramoorthy, I. P. Blair and J. D. Atkin (2013). "Ataxin-2 interacts with FUS and intermediate-length polyglutamine expansions enhance FUS-related pathology in amyotrophic lateral sclerosis." Hum Mol Genet **22**(4): 717-728.

Farrawell, N., I. A. Lambert-Smith, S. T. Warraich, I. P. Blair, D. N. Saunders, D. M. Hatters and J. J. Yerbury (2015). "Distinct partitioning of ALS associated TDP-43, FUS and SOD1 mutants into cellular inclusions " Scientific Reports **5**(13416): 1-14.

Farrawell, N. E., I. Lambert-Smith, K. Mitchell, J. McKenna, L. McAlary, P. Ciryam, K. L. Vine, D. N. Saunders and J. J. Yerbury (2018). "SOD1(A4V) aggregation alters ubiquitin homeostasis in a cell model of ALS." J Cell Sci.

Farrawell, N. E., I. A. Lambert-Smith, S. T. Warraich, I. P. Blair, D. N. Saunders, D. M. Hatters and J. J. Yerbury (2015). "Distinct partitioning of ALS associated TDP-43, FUS and SOD1 mutants into cellular inclusions." Scientific Reports **5**: 13416.

Fecto, F., Y. T. Esengul, H.-X. Deng and T. Siddique (2012). "Autophagy Is Impaired by UBQLN2 Mutations Linked to ALS/FTD (P05.164)." Neurology **78**(1 Supplement): P05.164-P105.164.

Fecto, F., J. Yan, S. P. Vemula, E. Liu, Y. Yang, W. Chen, J. G. Zheng, Y. Shi, N. Siddique, H. Arrat, S. Donkervoort, S. Ajroud-Driss, R. L. Sufit, S. L. Heller, H. X. Deng and T. Siddique (2011). "SQSTM1 mutations in familial and sporadic amyotrophic lateral sclerosis." Arch Neurol **68**(11): 1440-1446.

Fernández-Pevida, A., O. Rodríguez-Galán, A. Díaz-Quintana, D. Kressler and J. de la Cruz (2012). "Yeast ribosomal protein L40 assembles late into precursor 60 S ribosomes and is required for their cytoplasmic maturation." J Biol Chem **287**(45): 38390-38407.

Fesenko, I., A. Seredina, G. Arapidi, V. Ptushenko, A. Urban, I. Butenko, S. Kovalchuk, K. Babalyan, A. Knyazev, R. Khazigaleeva, E. Pushkova, N. Anikanov, V. Ivanov and V. M.

Govorun (2016). "The Physcomitrella patens Chloroplast Proteome Changes in Response to Protoplastation." Frontiers in Plant Science **7**(1661).

Finley, D., B. Bartel and A. Varshavsky (1989). "The tails of ubiquitin precursors are ribosomal proteins whose fusion to ubiquitin facilitates ribosome biogenesis." Nature **338**(6214): 394-401.

Forman, M. S., I. R. Mackenzie, N. J. Cairns, E. Swanson, P. J. Boyer, D. A. Drachman, B. S. Jhaveri, J. H. Karlawish, A. Pestronk, T. W. Smith, P. H. Tu, G. D. Watts, W. R. Markesbery, C. D. Smith and V. E. Kimonis (2006). "Novel ubiquitin neuropathology in frontotemporal dementia with valosin-containing protein gene mutations." J Neuropathol Exp Neurol **65**(6): 571-581.

Forman, M. S., J. Q. Trojanowski and V. M. Lee (2007). "TDP-43: a novel neurodegenerative proteinopathy." Curr Opin Neurobiol **17**(5): 548-555.

Forrest, S., A. Chai, M. Sanhueza, M. Marescotti, K. Parry, A. Georgiev, V. Sahota, R. Mendez-Castro and G. Pennetta (2013). "Increased levels of phosphoinositides cause neurodegeneration in a Drosophila model of amyotrophic lateral sclerosis." Hum Mol Genet **22**(13): 2689-2704.

Forrester, M. T., D. T. Hess, J. W. Thompson, R. Hultman, M. A. Moseley, J. S. Stamler and P. J. Casey (2011). "Site-specific analysis of protein S-acylation by resin-assisted capture." J Lipid Res **52**(2): 393-398.

Forsberg, K., P. A. Jonsson, P. M. Andersen, D. Bergemalm, K. S. Graffmo, M. Hultdin, J. Jacobsson, R. Rosquist, S. L. Marklund and T. Brännström (2010). "Novel Antibodies Reveal Inclusions Containing Non-Native SOD1 in Sporadic ALS Patients." PLOS ONE **5**(7): e11552.

Foster, L. J., M. L. Weir, D. Y. Lim, Z. Liu, W. S. Trimble and A. Klip (2000). "A functional role for VAP-33 in insulin-stimulated GLUT4 traffic." Traffic **1**(6): 512-521.

Frenkel-Morgenstern, M., A. A. Cohen, N. Geva-Zatorsky, E. Eden, J. Prilusky, I. Issaeva, A. Sigal, C. Cohen-Saidon, Y. Liron, L. Cohen, T. Danon, N. Perzov and U. Alon (2010). "Dynamic Proteomics: a database for dynamics and localizations of endogenous fluorescently-tagged proteins in living human cells." Nucleic Acids Res **38**(Database issue): D508-512.

Frydman, J., E. Nimmesgern, K. Ohtsuka and F. U. Hartl (1994). "Folding of nascent polypeptide chains in a high molecular mass assembly with molecular chaperones." Nature **370**(6485): 111-117.

Fu, H., S. Sadis, D. M. Rubin, M. Glickman, S. van Nocker, D. Finley and R. D. Vierstra (1998). "Multiubiquitin chain binding and protein degradation are mediated by distinct domains within the 26 S proteasome subunit Mcb1." J Biol Chem **273**(4): 1970-1981.

Fujii, R., S. Okabe, T. Urushido, K. Inoue, A. Yoshimura, T. Tachibana, T. Nishikawa, G. G. Hicks and T. Takumi (2005). "The RNA binding protein TLS is translocated to dendritic spines by mGluR5 activation and regulates spine morphology." Curr Biol **15**(6): 587-593.

Fujita, Y., Y. Mizuno, M. Takatama and K. Okamoto (2008). "Anterior horn cells with abnormal TDP-43 immunoreactivities show fragmentation of the Golgi apparatus in ALS." J Neurol Sci **269**(1-2): 30-34.

Fukunaga, T., M. Nagahama, K. Hatsuzawa, K. Tani, A. Yamamoto and M. Tagaya (2000). "Implication of sphingolipid metabolism in the stability of the Golgi apparatus." Journal of Cell Science **113**(18): 3299-3307.

Funakoshi, M., T. Sasaki, T. Nishimoto and H. Kobayashi (2002). "Budding yeast Dsk2p is a polyubiquitin-binding protein that can interact with the proteasome." Proc Natl Acad Sci U S A **99**(2): 745-750.

Fushimi, K., C. Long, N. Jayaram, X. Chen, L. Li and J. Y. Wu (2011). "Expression of human FUS/TLS in yeast leads to protein aggregation and cytotoxicity, recapitulating key features of FUS proteinopathy." Protein Cell **2**(2): 141-149.

Gaczynska, M., A. L. Goldberg, K. Tanaka, K. B. Hendil and K. L. Rock (1996). "Proteasome Subunits X and Y Alter Peptidase Activities in Opposite Ways to the Interferon-γ-induced Subunits LMP2 and LMP7." Journal of Biological Chemistry **271**(29): 17275-17280.

Gaczynska, M., K. L. Rock, T. Spies and A. L. Goldberg (1994). "Peptidase activities of proteasomes are differentially regulated by the major histocompatibility complex-encoded genes for LMP2 and LMP7." Proceedings of the National Academy of Sciences **91**(20): 9213-9217.

Gal, J., L. Kuang, K. R. Barnett, B. Z. Zhu, S. C. Shissler, K. V. Korotkov, L. J. Hayward, E. J. Kasarskis and H. Zhu (2016). "ALS mutant SOD1 interacts with G3BP1 and affects stress granule dynamics." Acta Neuropathol **132**(4): 563-576.

Gal, J., J. Zhang, D. M. Kwinter, J. Zhai, H. Jia, J. Jia and H. Zhu (2011). "Nuclear localization sequence of FUS and induction of stress granules by ALS mutants." Neurobiol Aging **32**(12): 2323.e2327-2340.

Gamerdinger, M., P. Hajieva, A. M. Kaya, U. Wolfrum, F. U. Hartl and C. Behl (2009). "Protein quality control during aging involves recruitment of the macroautophagy pathway by BAG3." Embo j **28**(7): 889-901.

Gasset-Rosa, F., S. Lu, H. Yu, C. Chen, Z. Melamed, L. Guo, J. Shorter, S. Da Cruz and D. W. Cleveland (2019). "Cytoplasmic TDP-43 De-mixing Independent of Stress Granules Drives Inhibition of Nuclear Import, Loss of Nuclear TDP-43, and Cell Death." Neuron **102**(2): 339-357.e337.

Gautschi, M., A. Mun, S. Ross and S. Rospert (2002). "A functional chaperone triad on the yeast ribosome." Proc Natl Acad Sci U S A **99**(7): 4209-4214.

Gavin, J. M., J. J. Chen, H. Liao, N. Rollins, X. Yang, Q. Xu, J. Ma, H. K. Loke, T. Lingaraj, J. E. Brownell, W. D. Mallender, A. E. Gould, B. S. Amidon and L. R. Dick (2012).

"Mechanistic studies on activation of ubiquitin and di-ubiquitin-like protein, FAT10, by ubiquitin-like modifier activating enzyme 6, Uba6." J Biol Chem **287**(19): 15512-15522.

Gendron, T. F., K. F. Bieniek, Y. J. Zhang, K. Jansen-West, P. E. Ash, T. Caulfield, L. Daughrity, J. H. Dunmore, M. Castanedes-Casey, J. Chew, D. M. Cosio, M. van Blitterswijk, W. C. Lee, R. Rademakers, K. B. Boylan, D. W. Dickson and L. Petrucelli (2013). "Antisense transcripts of the expanded C9ORF72 hexanucleotide repeat form nuclear RNA foci and undergo repeat-associated non-ATG translation in c9FTD/ALS." Acta Neuropathol **126**(6): 829-844.

Gerlach, B., S. M. Cordier, A. C. Schmukle, C. H. Emmerich, E. Rieser, T. L. Haas, A. I. Webb, J. A. Rickard, H. Anderton, W. W. Wong, U. Nachbur, L. Gangoda, U. Warnken, A. W. Purcell, J. Silke and H. Walczak (2011). "Linear ubiquitination prevents inflammation and regulates immune signalling." Nature **471**(7340): 591-596.

Ghaboosi, N. and R. J. Deshaies (2007). "A conditional yeast E1 mutant blocks the ubiquitin-proteasome pathway and reveals a role for ubiquitin conjugates in targeting Rad23 to the proteasome." Mol Biol Cell **18**(5): 1953-1963.

Ghaemmaghami, S., W. K. Huh, K. Bower, R. W. Howson, A. Belle, N. Dephoure, E. K. O'Shea and J. S. Weissman (2003). "Global analysis of protein expression in yeast." Nature **425**(6959): 737-741.

Gidalevitz, T., A. Ben-Zvi, K. H. Ho, H. R. Brignull and R. I. Morimoto (2006). "Progressive disruption of cellular protein folding in models of polyglutamine diseases." Science **311**(5766): 1471-1474.

Gidalevitz, T., V. Prahlad and R. I. Morimoto (2011). "The stress of protein misfolding: from single cells to multicellular organisms." Cold Spring Harb Perspect Biol **3**(6).

Gitcho, M. A., J. Strider, D. Carter, L. Taylor-Reinwald, M. S. Forman, A. M. Goate and N. J. Cairns (2009). "VCP Mutations Causing Frontotemporal Lobar Degeneration Disrupt

Localization of TDP-43 and Induce Cell Death." Journal of Biological Chemistry **284**(18): 12384-12398.

Gitler, A. D., A. Chesi, M. L. Geddie, K. E. Strathearn, S. Hamamichi, K. J. Hill, K. A. Caldwell, G. A. Caldwell, A. A. Cooper, J. C. Rochet and S. Lindquist (2009). "Alpha-synuclein is part of a diverse and highly conserved interaction network that includes PARK9 and manganese toxicity." Nat Genet **41**(3): 308-315.

Gitler, A. D. and J. Shorter (2011). "RNA-binding proteins with prion-like domains in ALS and FTLD-U." Prion **5**(3): 179-187.

Glickman, M. H., D. M. Rubin, O. Coux, I. Wefes, G. Pfeifer, Z. Cjeka, W. Baumeister, V. A. Fried and D. Finley (1998). "A subcomplex of the proteasome regulatory particle required for ubiquitin-conjugate degradation and related to the COP9-signalosome and eIF3." Cell **94**(5): 615-623.

Gonatas, N. K., A. Stieber and J. O. Gonatas (2006). "Fragmentation of the Golgi apparatus in neurodegenerative diseases and cell death." Journal of the Neurological Sciences **246**(1): 21-30.

Gong, J., M. Huang, F. Wang, X. Ma, H. Liu, Y. Tu, L. Xing, X. Zhu, H. Zheng, J. Fang, X. Li, Q. Wang, J. Wang, Z. Sun, X. Wang, Y. Wang, C. Guo and T. S. Tang (2017). "RBM45 competes with HDAC1 for binding to FUS in response to DNA damage." Nucleic Acids Res **45**(22): 12862-12876.

Gonzalez, M. A., S. M. Feely, F. Speziani, A. V. Strickland, M. Danzi, C. Bacon, Y. Lee, T. F. Chou, S. H. Blanton, C. C. Weihl, S. Zuchner and M. E. Shy (2014). "A novel mutation in VCP causes Charcot-Marie-Tooth Type 2 disease." Brain **137**(Pt 11): 2897-2902.

Goto, E., Y. Yamanaka, A. Ishikawa, M. Aoki-Kawasumi, M. Mito-Yoshida, M. Ohmura-Hoshino, Y. Matsuki, M. Kajikawa, H. Hirano and S. Ishido (2010). "Contribution of Lysine

11-linked Ubiquitination to MIR2-mediated Major Histocompatibility Complex Class I Internalization." Journal of Biological Chemistry **285**(46): 35311-35319.

Grad, L. I., J. J. Yerbury, B. J. Turner, W. C. Guest, E. Pokrishevsky and M. A. O'Neill (2014). "Intercellular propagated misfolding of wild-type Cu/Zn superoxide dismutase occurs via exosome-dependent and -independent mechanisms." Proc Natl Acad Sci U S A **111**.

Greenway, M. J., P. M. Andersen, C. Russ, S. Ennis, S. Cashman, C. Donaghy, V. Patterson, R. Swingler, D. Kieran, J. Prehn, K. E. Morrison, A. Green, K. R. Acharya, R. H. Brown, Jr. and O. Hardiman (2006). "ANG mutations segregate with familial and 'sporadic' amyotrophic lateral sclerosis." Nat Genet **38**(4): 411-413.

Groothuis, T. A., N. P. Dantuma, J. Neefjes and F. A. Salomons (2006). "Ubiquitin crosstalk connecting cellular processes." Cell Div **1**: 21.

Guil, S., J. C. Long and J. F. Cáceres (2006). "hnRNP A1 Relocalization to the Stress Granules Reflects a Role in the Stress Response." Molecular and Cellular Biology **26**(15): 5744-5758.

Gunther, M. R., R. Vangilder, J. Fang and D. S. Beattie (2004). "Expression of a Familial Amyotrophic Lateral Sclerosis-Associated Mutant Human Superoxide Dismutase in Yeast Leads to Decreased Mitochondrial Electron Transport." Arch Biochem Biophys. **431**(2): 207-214.

Guo, Q., C. Lehmer, A. Martinez-Sanchez, T. Rudack, F. Beck, H. Hartmann, M. Perez-Berlanga, F. Frottin, M. S. Hipp, F. U. Hartl, D. Edbauer, W. Baumeister and R. Fernandez-Busnadiego (2018). "In Situ Structure of Neuronal C9orf72 Poly-GA Aggregates Reveals Proteasome Recruitment." Cell **172**(4): 696-705.e612.

Guo, Y., T. Guettouche, M. Fenna, F. Boellmann, W. B. Pratt, D. O. Toft, D. F. Smith and R. Voellmy (2001). "Evidence for a mechanism of repression of heat shock factor 1 transcriptional activity by a multichaperone complex." J Biol Chem **276**(49): 45791-45799.

Gupta, R., P. Kasturi, A. Bracher, C. Loew, M. Zheng, A. Villella, D. Garza, F. U. Hartl and S. Raychaudhuri (2011). "Firefly luciferase mutants as sensors of proteome stress." Nat Methods **8**(10): 879-884.

Gurney, M. E., H. Pu, A. Y. Chiu, M. C. Dal Canto, C. Y. Polchow, D. D. Alexander, J. Caliendo, A. Hentati, Y. W. Kwon, H. X. Deng and et al. (1994). "Motor neuron degeneration in mice that express a human Cu,Zn superoxide dismutase mutation." Science **264**(5166): 1772-1775.

Haas, A. L. and I. A. Rose (1982). "The mechanism of ubiquitin activating enzyme. A kinetic and equilibrium analysis." J Biol Chem **257**(17): 10329-10337.

Haas, A. L., J. V. Warms, A. Hershko and I. A. Rose (1982). "Ubiquitin-activating enzyme. Mechanism and role in protein-ubiquitin conjugation." J Biol Chem **257**(5): 2543-2548.

Haendler, B., R. Keller, P. C. Hiestand, H. P. Kocher, G. Wegmann and N. R. Movva (1989). "Yeast cyclophilin: isolation and characterization of the protein, cDNA and gene." Gene **83**(1): 39-46.

Haeusler, A. R., C. J. Donnelly and J. D. Rothstein (2016). "The expanding biology of the C9orf72 nucleotide repeat expansion in neurodegenerative disease." Nat Rev Neurosci **17**(6): 383-395.

Haglund, K., S. Sigismund, S. Polo, I. Szymkiewicz, P. P. Di Fiore and I. Dikic (2003). "Multiple monoubiquitination of RTKs is sufficient for their endocytosis and degradation." Nat Cell Biol **5**(5): 461-466.

Halawani, D. and M. Latterich (2006). "p97: The cell's molecular purgatory?" Mol Cell **22**(6): 713-717.

Hall, C. N., M. C. Klein-Flugge, C. Howarth and D. Attwell (2012). "Oxidative phosphorylation, not glycolysis, powers presynaptic and postsynaptic mechanisms underlying brain information processing." J Neurosci **32**(26): 8940-8951.

Han, S. M., H. Tsuda, Y. Yang, J. Vibbert, P. Cottee, S. J. Lee, J. Winek, C. Haueter, H. J. Bellen and M. A. Miller (2012). "Secreted VAPB/ALS8 major sperm protein domains modulate mitochondrial localization and morphology via growth cone guidance receptors." Dev Cell **22**(2): 348-362.

Han, T. W., M. Kato, S. Xie, L. C. Wu, H. Mirzaei, J. Pei, M. Chen, Y. Xie, J. Allen, G. Xiao and S. L. McKnight (2012). "Cell-free formation of RNA granules: bound RNAs identify features and components of cellular assemblies." Cell **149**(4): 768-779.

Hans, F., F. C. Fiesel, J. C. Strong, S. Jackel, T. M. Rasse, S. Geisler, W. Springer, J. B. Schulz, A. Voigt and P. J. Kahle (2014). "UBE2E ubiquitin-conjugating enzymes and ubiquitin isopeptidase Y regulate TDP-43 protein ubiquitination." J Biol Chem **289**(27): 19164-19179.

Hartl, F. U., A. Bracher and M. Hayer-Hartl (2011). "Molecular chaperones in protein folding and proteostasis." Nature **475**(7356): 324-332.

Harty, R. N., M. E. Brown, G. Wang, J. Huibregtse and F. P. Hayes (2000). "A PPxY motif within the VP40 protein of Ebola virus interacts physically and functionally with a ubiquitin ligase: implications for filovirus budding." Proc Natl Acad Sci U S A **97**(25): 13871-13876.

Hasumi, H. and T. Nishikawa (1993). "Purification and properties of multiple molecular forms of yeast peptidyl prolyl cis-trans isomerase." Biochim Biophys Acta **1161**(2-3): 161-167.

Hatfield, P. M. and R. D. Vierstra (1992). "Multiple forms of ubiquitin-activating enzyme E1 from wheat. Identification of an essential cysteine by in vitro mutagenesis." J Biol Chem **267**(21): 14799-14803.

Henden, L., N. A. Twine, P. Szul, E. P. McCann, G. A. Nicholson, D. B. Rowe, M. C. Kiernan, D. C. Bauer, I. P. Blair, K. L. Williams (2019). “IBD analysis of Australian amyotrophic lateral sclerosis *SOD1*-mutation carriers identifies five founder events and links sporadic cases to existing ALS families.” BioRxiv 685925; doi: https://doi.org/10.1101/685925.

Heo, J. M., N. Livnat-Levanon, E.B. Taylor, K. T. Jones, N. Dephoure, J. Ring, J. Xie, J. L. Brodsky, F. Madeo, S. P. Gygi, K. Ashrafi, M. H. Glickman, J. Rutter (2010). “A stress-responsive system for mitochondrial protein degradation.” Mol Cell **40**(3):465-80.

Hernandez, F., J. J. Lucas and J. Avila (2013). "GSK3 and tau: two convergence points in Alzheimer's disease." J Alzheimers Dis **33 Suppl 1**: S141-144.

Herrup, K. (2013). "Post-mitotic role of the cell cycle machinery." Curr Opin Cell Biol **25**(6): 711-716.

Hershko, A. and A. Ciechanover (1998). "The ubiquitin system." Annu Rev Biochem **67**: 425-479.

Hershko, A., A. Ciechanover, H. Heller, A. L. Haas and I. A. Rose (1980). "Proposed role of ATP in protein breakdown: conjugation of protein with multiple chains of the polypeptide of ATP-dependent proteolysis." Proc Natl Acad Sci U S A **77**(4): 1783-1786.

Hershko, A., H. Heller, S. Elias and A. Ciechanover (1983). "Components of ubiquitin-protein ligase system. Resolution, affinity purification, and role in protein breakdown." J Biol Chem **258**(13): 8206-8214.

Higelin, J., M. Demestre, S. Putz, J. P. Delling, C. Jacob, A.-K. Lutz, J. Bausinger, A.-K. Huber, M. Klingenstein, G. Barbi, G. Speit, A. Huebers, J. H. Weishaupt, A. Hermann, S. Liebau, A. C. Ludolph and T. M. Boeckers (2016). "FUS Mislocalization and Vulnerability to DNA Damage in ALS Patients Derived hiPSCs and Aging Motoneurons." Frontiers in Cellular Neuroscience **10**(290).

Hiji, M., T. Takahashi, H. Fukuba, H. Yamashita, T. Kohriyama and M. Matsumoto (2008). "White matter lesions in the brain with frontotemporal lobar degeneration with motor neuron disease: TDP-43-immunopositive inclusions co-localize with p62, but not ubiquitin." Acta Neuropathol **116**(2): 183-191.

Hirabayashi, M., K. Inoue, K. Tanaka, K. Nakadate, Y. Ohsawa, Y. Kamei, A. H. Popiel, A. Sinohara, A. Iwamatsu, Y. Kimura, Y. Uchiyama, S. Hori and A. Kakizuka (2001). "VCP/p97 in abnormal protein aggregates, cytoplasmic vacuoles, and cell death, phenotypes relevant to neurodegeneration." Cell Death Differ **8**(10): 977-984.

Hitt, R. and D. H. Wolf (2004). "Der1p, a protein required for degradation of malfolded soluble proteins of the endoplasmic reticulum: topology and Der1-like proteins." FEMS Yeast Res **4**(7): 721-729.

Hoege, C., B. Pfander, G. L. Moldovan, G. Pyrowolakis and S. Jentsch (2002). "RAD6-dependent DNA repair is linked to modification of PCNA by ubiquitin and SUMO." Nature **419**(6903): 135-141.

Hoell, J. I., E. Larsson, S. Runge, J. D. Nusbaum, S. Duggimpudi, T. A. Farazi, M. Hafner, A. Borkhardt, C. Sander and T. Tuschl (2011). "RNA targets of wild-type and mutant FET family proteins." Nat Struct Mol Biol **18**(12): 1428-1431.

Holmberg, C. I., K. E. Staniszewski, K. N. Mensah, A. Matouschek and R. I. Morimoto (2004). "Inefficient degradation of truncated polyglutamine proteins by the proteasome." Embo j **23**(21): 4307-4318.

Hoppe, T., K. Matuschewski, M. Rape, S. Schlenker, H. D. Ulrich and S. Jentsch (2000). "Activation of a membrane-bound transcription factor by regulated ubiquitin/proteasome-dependent processing." Cell **102**(5): 577-586.

Howland, D. S., J. Liu, Y. She, B. Goad, N. J. Maragakis, B. Kim, J. Erickson, J. Kulik, L. DeVito, G. Psaltis, L. J. DeGennaro, D. W. Cleveland and J. D. Rothstein (2002). "Focal loss

of the glutamate transporter EAAT2 in a transgenic rat model of SOD1 mutant-mediated amyotrophic lateral sclerosis (ALS)." Proc Natl Acad Sci U S A **99**(3): 1604-1609.

Huang, C., J. Tong, F. Bi, H. Zhou and X. G. Xia (2012). "Mutant TDP-43 in motor neurons promotes the onset and progression of ALS in rats." J Clin Invest **122**(1): 107-118.

Huang, M., Q. Xu, K. Mitsui and Z. Xu (2014). "PSK1 regulates expression of SOD1 involved in oxidative stress tolerance in yeast." FEMS Microbiol Lett **350**(2): 154-160.

Hughes, T. and T. E. Rusten (2007). "Origin and evolution of self-consumption: autophagy." Adv Exp Med Biol **607**: 111-118.

Huh, W. K., J. V. Falvo, L. C. Gerke, A. S. Carroll, R. W. Howson, J. S. Weissman and E. K. O'Shea (2003). "Global analysis of protein localization in budding yeast." Nature **425**(6959): 686-691.

Huyer, G., G. L. Longsworth, D. L. Mason, M. P. Mallampalli, J. M. McCaffery, R. L. Wright and S. Michaelis (2004). "A Striking Quality Control Subcompartment in Saccharomyces cerevisiae: The Endoplasmic Reticulum-associated Compartment." Mol Biol Cell **15**(2): 908-921.

Ikeda, F., Y. L. Deribe, S. S. Skanland, B. Stieglitz, C. Grabbe, M. Franz-Wachtel, S. J. van Wijk, P. Goswami, V. Nagy, J. Terzic, F. Tokunaga, A. Androulidaki, T. Nakagawa, M. Pasparakis, K. Iwai, J. P. Sundberg, L. Schaefer, K. Rittinger, B. Macek and I. Dikic (2011). "SHARPIN forms a linear ubiquitin ligase complex regulating NF-kappaB activity and apoptosis." Nature **471**(7340): 637-641.

Ilieva, H., M. Polymenidou and D. W. Cleveland (2009). "Non-cell autonomous toxicity in neurodegenerative disorders: ALS and beyond." J Cell Biol **187**(6): 761-772.

Ishigaki, S., N. Hishikawa, J. Niwa, S. Iemura, T. Natsume, S. Hori, A. Kakizuka, K. Tanaka and G. Sobue (2004). "Physical and functional interaction between Dorfin and Valosin-

containing protein that are colocalized in ubiquitylated inclusions in neurodegenerative disorders." J Biol Chem **279**(49): 51376-51385.

Ishigaki, S., A. Masuda, Y. Fujioka, Y. Iguchi, M. Katsuno, A. Shibata, F. Urano, G. Sobue and K. Ohno (2012). "Position-dependent FUS-RNA interactions regulate alternative splicing events and transcriptions." Sci Rep **2**: 529.

Ito, D. and N. Suzuki (2011). "Conjoint pathologic cascades mediated by ALS/FTLD-U linked RNA-binding proteins TDP-43 and FUS." Neurology **77**(17): 1636.

Ito, H., Y. Fukuda, K. Murata and A. Kimura (1983). "Transformation of intact yeast cells treated with alkali cations." J Bacteriol **153**(1): 163-168.

Iwata, A., J. C. Christianson, M. Bucci, L. M. Ellerby, N. Nukina, L. S. Forno and R. R. Kopito (2005). "Increased susceptibility of cytoplasmic over nuclear polyglutamine aggregates to autophagic degradation." Proc Natl Acad Sci U S A **102**(37): 13135-13140.

Jaarsma, D., E. D. Haasdijk, J. A. Grashorn, R. Hawkins, W. van Duijn, H. W. Verspaget, J. London and J. C. Holstege (2000). "Human Cu/Zn superoxide dismutase (SOD1) overexpression in mice causes mitochondrial vacuolization, axonal degeneration, and premature motoneuron death and accelerates motoneuron disease in mice expressing a familial amyotrophic lateral sclerosis mutant SOD1." Neurobiol Dis **7**(6 Pt B): 623-643.

Jackson, S. P. and D. Durocher (2013). "Regulation of DNA damage responses by ubiquitin and SUMO." Mol Cell **49**(5): 795-807.

Jankowska, E., J. Stoj, P. Karpowicz, P. A. Osmulski and M. Gaczynska (2013). "The proteasome in health and disease." Curr Pharm Des **19**(6): 1010-1028.

Janssens, J. and C. Van Broeckhoven (2013). "Pathological mechanisms underlying TDP-43 driven neurodegeneration in FTLD-ALS spectrum disorders." Hum Mol Genet **22**(R1): R77-87.

Jin, J., X. Li, S. P. Gygi and J. W. Harper (2007). "Dual E1 activation systems for ubiquitin differentially regulate E2 enzyme charging." Nature **447**(7148): 1135-1138.

Jin, M., X. Liu and D. J. Klionsky (2013). "SnapShot: Selective autophagy." Cell **152**(1-2): 368-368.e362.

Johnson, B. S., J. M. McCaffery, S. Lindquist and A. D. Gitler (2008). "A yeast TDP-43 proteinopathy model: Exploring the molecular determinants of TDP-43 aggregation and cellular toxicity." Proc Natl Acad Sci U S A **105**(17): 6439-6444.

Johnson, B. S., D. Snead, J. J. Lee, J. M. McCaffery, J. Shorter and A. D. Gitler (2009). "TDP-43 is intrinsically aggregation-prone, and amyotrophic lateral sclerosis-linked mutations accelerate aggregation and increase toxicity." J Biol Chem **284**.

Johnson, E. S., P. C. Ma, I. M. Ota and A. Varshavsky (1995). "A proteolytic pathway that recognizes ubiquitin as a degradation signal." J Biol Chem **270**(29): 17442-17456.

Johnson, J. O., J. Mandrioli, M. Benatar, Y. Abramzon, V. M. Van Deerlin, J. Q. Trojanowski, J. R. Gibbs, M. Brunetti, S. Gronka, J. Wuu, J. Ding, L. McCluskey, M. Martinez-Lage, D. Falcone, D. G. Hernandez, S. Arepalli, S. Chong, J. C. Schymick, J. Rothstein, F. Landi, Y. D. Wang, A. Calvo, G. Mora, M. Sabatelli, M. R. Monsurro, S. Battistini, F. Salvi, R. Spataro, P. Sola, G. Borghero, G. Galassi, S. W. Scholz, J. P. Taylor, G. Restagno, A. Chio and B. J. Traynor (2010). "Exome sequencing reveals VCP mutations as a cause of familial ALS." Neuron **68**(5): 857-864.

Johnson, J. O., E. P. Pioro, A. Boehringer, R. Chia, H. Feit, A. E. Renton, H. A. Pliner, Y. Abramzon, G. Marangi, B. J. Winborn, J. R. Gibbs, M. A. Nalls, S. Morgan, M. Shoai, J. Hardy, A. Pittman, R. W. Orrell, A. Malaspina, K. C. Sidle, P. Fratta, M. B. Harms, R. H. Baloh, A. Pestronk, C. C. Weihl, E. Rogaeva, L. Zinman, V. E. Drory, G. Borghero, G. Mora, A. Calvo, J. D. Rothstein, C. Drepper, M. Sendtner, A. B. Singleton, J. P. Taylor, M. R. Cookson, G. Restagno, M. Sabatelli, R. Bowser, A. Chio and B. J. Traynor (2014). "Mutations in the Matrin 3 gene cause familial amyotrophic lateral sclerosis." Nat Neurosci **17**(5): 664-666.

Johnston, J. A. (2000). "Formation of high molecular weight complexes of mutant." **97**(23): 12571-12576.

Johnston, J. A., C. L. Ward and R. R. Kopito (1998). "Aggresomes: a cellular response to misfolded proteins." J Cell Biol **143**(7): 1883-1898.

Jonsson, P. A., K. Ernhill, P. M. Andersen, D. Bergemalm, T. Brannstrom, O. Gredal, P. Nilsson and S. L. Marklund (2004). "Minute quantities of misfolded mutant superoxide dismutase-1 cause amyotrophic lateral sclerosis." Brain **127**(Pt 1): 73-88.

Joo, H. Y., L. Zhai, C. Yang, S. Nie, H. Erdjument-Bromage, P. Tempst, C. Chang and H. Wang (2007). "Regulation of cell cycle progression and gene expression by H2A deubiquitination." Nature **449**(7165): 1068-1072.

Ju, J.-S., R. A. Fuentealba, S. E. Miller, E. Jackson, D. Piwnica-Worms, R. H. Baloh and C. C. Weihl (2009). "Valosin-containing protein (VCP) is required for autophagy and is disrupted in VCP disease." The Journal of Cell Biology **187**(6): 875.

Ju, J. S., S. E. Miller, P. I. Hanson and C. C. Weihl (2008). "Impaired protein aggregate handling and clearance underlie the pathogenesis of p97/VCP-associated disease." J Biol Chem **283**(44): 30289-30299.

Ju, S., D. F. Tardiff, H. Han, K. Divya, Q. Zhong, L. E. Maquat, D. A. Bosco, L. J. Hayward, R. H. Brown, Jr., S. Lindquist, D. Ringe and G. A. Petsko (2011). "A yeast model of FUS/TLS-dependent cytotoxicity." PLoS Biol **9**(4): e1001052.

Juneja, T., M. A. Pericak-Vance, N. G. Laing, S. Dave and T. Siddique (1997). "Prognosis in familial amyotrophic lateral sclerosis: progression and survival in patients with glu100gly and ala4val mutations in Cu,Zn superoxide dismutase." Neurology **48**(1): 55-57.

Kabashi, E., J. N. Agar, D. M. Taylor, S. Minotti and H. D. Durham (2004). "Focal dysfunction of the proteasome: a pathogenic factor in a mouse model of amyotrophic lateral sclerosis." J Neurochem **89**(6): 1325-1335.

Kabashi, E., H. El Oussini, V. Bercier, F. Gros-Louis, P. N. Valdmanis, J. McDearmid, I. A. Mejier, P. A. Dion, N. Dupre, D. Hollinger, J. Sinniger, S. Dirrig-Grosch, W. Camu, V. Meininger, J. P. Loeffler, F. Rene, P. Drapeau, G. A. Rouleau and L. Dupuis (2013). "Investigating the contribution of VAPB/ALS8 loss of function in amyotrophic lateral sclerosis." Hum Mol Genet **22**(12): 2350-2360.

Kaganovich, D., R. Kopito and J. Frydman (2008). "Misfolded proteins partition between two distinct quality control compartments." Nature **454**(7208): 1088-1095.

Kaiser, S. E., J. H. Brickner, A. R. Reilein, T. D. Fenn, P. Walter and A. T. Brunger (2005). "Structural basis of FFAT motif-mediated ER targeting." Structure **13**(7): 1035-1045.

Kaiser, S. E., B. E. Riley, T. A. Shaler, R. S. Trevino, C. H. Becker, H. Schulman and R. R. Kopito (2011). "Protein standard absolute quantification (PSAQ) method for the measurement of cellular ubiquitin pools." Nat Methods **8**(8): 691-696.

Kamhi-Nesher, S., M. Shenkman, S. Tolchinsky and S. V. Fromm (2001). "A Novel Quality Control Compartment Derived from the Endoplasmic." **12**(6): 1711-1723.

Kampinga, H. H. and E. A. Craig (2010). "The HSP70 chaperone machinery: J proteins as drivers of functional specificity." Nat Rev Mol Cell Biol **11**(8): 579-592.

Kaneko, M., I. Iwase, Y. Yamasaki, T. Takai, Y. Wu, S. Kanemoto, K. Matsuhisa, R. Asada, Y. Okuma, T. Watanabe, K. Imaizumi and Y. Nomura (2016). "Genome-wide identification and gene expression profiling of ubiquitin ligases for endoplasmic reticulum protein degradation." Sci Rep **6**: 30955.

Kanekura, K., I. Nishimoto, S. Aiso and M. Matsuoka (2006). "Characterization of amyotrophic lateral sclerosis-linked P56S mutation of vesicle-associated membrane protein-associated protein B (VAPB/ALS8)." J Biol Chem **281**(40): 30223-30233.

Kanning, K. C., A. Kaplan and C. E. Henderson (2010). "Motor neuron diversity in development and disease." Annu Rev Neurosci **33**: 409-440.

Kato, M., T. W. Han, S. Xie, K. Shi, X. Du, L. C. Wu, H. Mirzaei, E. J. Goldsmith, J. Longgood, J. Pei, N. V. Grishin, D. E. Frantz, J. W. Schneider, S. Chen, L. Li, M. R. Sawaya, D. Eisenberg, R. Tycko and S. L. McKnight (2012). "Cell-free formation of RNA granules: low complexity sequence domains form dynamic fibers within hydrogels." Cell **149**(4): 753-767.

Kato, S., M. Takikawa, K. Nakashima, A. Hirano, D. W. Cleveland, H. Kusaka, N. Shibata, M. Kato, I. Nakano and E. Ohama (2000). "New consensus research on neuropathological aspects of familial amyotrophic lateral sclerosis with superoxide dismutase 1 (SOD1) gene mutations: inclusions containing SOD1 in neurons and astrocytes." Amyotroph Lateral Scler Other Motor Neuron Disord **1**(3): 163-184.

Katzmann, D. J., M. Babst and S. D. Emr (2001). "Ubiquitin-dependent sorting into the multivesicular body pathway requires the function of a conserved endosomal protein sorting complex, ESCRT-I." Cell **106**(2): 145-155.

Kawabe, H. and N. Brose (2011). "The role of ubiquitylation in nerve cell development." Nat Rev Neurosci **12**(5): 251-268.

Kawaguchi, Y., J. J. Kovacs, A. McLaurin, J. M. Vance, A. Ito and T. P. Yao (2003). "The deacetylase HDAC6 regulates aggresome formation and cell viability in response to misfolded protein stress." Cell **115**(6): 727-738.

Kawaguchi, Y., T. Okamoto, M. Taniwaki, M. Aizawa, M. Inoue, S. Katayama, H. Kawakami, S. Nakamura, M. Nishimura, I. Akiguchi and et al. (1994). "CAG expansions in a novel gene for Machado-Joseph disease at chromosome 14q32.1." Nat Genet **8**(3): 221-228.

Kedersha, N. L., M. Gupta, W. Li, I. Miller and P. Anderson (1999). "RNA-binding proteins TIA-1 and TIAR link the phosphorylation of eIF-2 alpha to the assembly of mammalian stress granules." J Cell Biol **147**(7): 1431-1442.

Keller, B. A., K. Volkening, C. A. Droppelmann, L. C. Ang, R. Rademakers and M. J. Strong (2012). "Co-aggregation of RNA binding proteins in ALS spinal motor neurons: evidence of a common pathogenic mechanism." Acta Neuropathol **124**(5): 733-747.

Keller, J. N., F. F. Huang and W. R. Markesbery (2000). "Decreased levels of proteasome activity and proteasome expression in aging spinal cord." Neuroscience **98**(1): 149-156.

Kim, H. J., N. C. Kim, Y. D. Wang, E. A. Scarborough, J. Moore, Z. Diaz, K. S. MacLea, B. Freibaum, S. Li, A. Molliex, A. P. Kanagaraj, R. Carter, K. B. Boylan, A. M. Wojtas, R. Rademakers, J. L. Pinkus, S. A. Greenberg, J. Q. Trojanowski, B. J. Traynor, B. N. Smith, S. Topp, A. S. Gkazi, J. Miller, C. E. Shaw, M. Kottlors, J. Kirschner, A. Pestronk, Y. R. Li, A. F. Ford, A. D. Gitler, M. Benatar, O. D. King, V. E. Kimonis, E. D. Ross, C. C. Weihl, J. Shorter and J. P. Taylor (2013). "Mutations in prion-like domains in hnRNPA2B1 and hnRNPA1 cause multisystem proteinopathy and ALS." Nature **495**(7442): 467-473.

Kim, H. J., A. R. Raphael, E. S. LaDow, L. McGurk, R. A. Weber, J. Q. Trojanowski, V. M. Lee, S. Finkbeiner, A. D. Gitler and N. M. Bonini (2014). "Therapeutic modulation of eIF2alpha phosphorylation rescues TDP-43 toxicity in amyotrophic lateral sclerosis disease models." Nat Genet **46**(2): 152-160.

Kim, J. and D. J. Klionsky (2000). "Autophagy, cytoplasm-to-vacuole targeting pathway, and pexophagy in yeast and mammalian cells." Annu Rev Biochem **69**: 303-342.

Kim, S., E. A. Nollen, K. Kitagawa, V. P. Bindokas and R. I. Morimoto (2002). "Polyglutamine protein aggregates are dynamic." Nat Cell Biol **4**(10): 826-831.

Kim, W., E. J. Bennett, E. L. Huttlin, A. Guo, J. Li, A. Possemato, M. E. Sowa, R. Rad, J. Rush, M. J. Comb, J. W. Harper and S. P. Gygi (2011). "Systematic and quantitative assessment of the ubiquitin-modified proteome." Mol Cell **44**(2): 325-340.

Kimonis, V. E., E. Fulchiero, J. Vesa and G. Watts (2008). "VCP disease associated with myopathy, Paget disease of bone and frontotemporal dementia: review of a unique disorder." Biochim Biophys Acta **1782**(12): 744-748.

Kimonis, V. E., S. G. Mehta, E. C. Fulchiero, D. Thomasova, M. Pasquali, K. Boycott, E. G. Neilan, A. Kartashov, M. S. Forman, S. Tucker, K. Kimonis, S. Mumm, M. P. Whyte, C. D. Smith and G. D. Watts (2008). "Clinical studies in familial VCP myopathy associated with Paget disease of bone and frontotemporal dementia." Am J Med Genet A **146a**(6): 745-757.

King, O. D., A. D. Gitler and J. Shorter (2012). "The tip of the iceberg: RNA-binding proteins with prion-like domains in neurodegenerative disease." Brain Res **1462**: 61-80.

Kirkin, V., D. G. McEwan, I. Novak and I. Dikic (2009). "A role for ubiquitin in selective autophagy." Mol Cell **34**(3): 259-269.

Kitamura, A., N. Inada, H. Kubota, G. Matsumoto, M. Kinjo, R. I. Morimoto and K. Nagata (2014). "Dysregulation of the proteasome increases the toxicity of ALS-linked mutant SOD1." Genes Cells **19**(3): 209-224.

Kleiger, G. and T. Mayor (2014). "Perilous journey: a tour of the ubiquitin-proteasome system." Trends Cell Biol **24**(6): 352-359.

Kleijnen, M. F., A. H. Shih, P. Zhou, S. Kumar, R. E. Soccio, N. L. Kedersha, G. Gill and P. M. Howley (2000). "The hPLIC proteins may provide a link between the ubiquitination machinery and the proteasome." Mol Cell **6**(2): 409-419.

Klionsky, D. J., K. Abdelmohsen, A. Abe, M. J. Abedin, H. Abeliovich, A. Acevedo Arozena, H. Adachi, C. M. Adams, P. D. Adams, K. Adeli, P. J. Adhihetty, S. G. Adler, G. Agam, R.

Agarwal, M. K. Aghi, M. Agnello, P. Agostinis, P. V. Aguilar, J. Aguirre-Ghiso, E. M. Airoldi, S. Ait-Si-Ali, T. Akematsu, E. T. Akporiaye, M. Al-Rubeai, G. M. Albaiceta, C. Albanese, D. Albani, M. L. Albert, J. Aldudo, H. Algul, M. Alirezaei, I. Alloza, A. Almasan, M. Almonte-Beceril, E. S. Alnemri, C. Alonso, N. Altan-Bonnet, D. C. Altieri, S. Alvarez, L. Alvarez-Erviti, S. Alves, G. Amadoro, A. Amano, C. Amantini, S. Ambrosio, I. Amelio, A. O. Amer, M. Amessou, A. Amon, Z. An, F. A. Anania, S. U. Andersen, U. P. Andley, C. K. Andreadi, N. Andrieu-Abadie, A. Anel, D. K. Ann, S. Anoopkumar-Dukie, M. Antonioli, H. Aoki, N. Apostolova, S. Aquila, K. Aquilano, K. Araki, E. Arama, A. Aranda, J. Araya, A. Arcaro, E. Arias, H. Arimoto, A. R. Ariosa, J. L. Armstrong, T. Arnould, I. Arsov, K. Asanuma, V. Askanas, E. Asselin, R. Atarashi, S. S. Atherton, J. D. Atkin, L. D. Attardi, P. Auberger, G. Auburger, L. Aurelian, R. Autelli, L. Avagliano, M. L. Avantaggiati, L. Avrahami, S. Awale, N. Azad, T. Bachetti, J. M. Backer, D. H. Bae, J. S. Bae, O. N. Bae, S. H. Bae, E. H. Baehrecke, S. H. Baek, S. Baghdiguian, A. Bagniewska-Zadworna, H. Bai, J. Bai, X. Y. Bai, Y. Bailly, K. N. Balaji, W. Balduini, A. Ballabio, R. Balzan, R. Banerjee, G. Banhegyi, H. Bao, B. Barbeau, M. D. Barrachina, E. Barreiro, B. Bartel, A. Bartolome, D. C. Bassham, M. T. Bassi, R. C. Bast, Jr., A. Basu, M. T. Batista, H. Batoko, M. Battino, K. Bauckman, B. L. Baumgarner, K. U. Bayer, R. Beale, J. F. Beaulieu, G. R. Beck, Jr., C. Becker, J. D. Beckham, P. A. Bedard, P. J. Bednarski, T. J. Begley, C. Behl, C. Behrends, G. M. Behrens, K. E. Behrns, E. Bejarano, A. Belaid, F. Belleudi, G. Benard, G. Berchem, D. Bergamaschi, M. Bergami, B. Berkhout, L. Berliocchi, A. Bernard, M. Bernard, F. Bernassola, A. Bertolotti, A. S. Bess, S. Besteiro, S. Bettuzzi, S. Bhalla, S. Bhattacharyya, S. K. Bhutia, C. Biagosch, M. W. Bianchi, M. Biard-Piechaczyk, V. Billes, C. Bincoletto, B. Bingol, S. W. Bird, M. Bitoun, I. Bjedov, C. Blackstone, L. Blanc, G. A. Blanco, H. K. Blomhoff, E. Boada-Romero, S. Bockler, M. Boes, K. Boesze-Battaglia, L. H. Boise, A. Bolino, A. Boman, P. Bonaldo, M. Bordi, J. Bosch, L. M. Botana, J. Botti, G. Bou, M. Bouche, M. Bouchecareilh, M. J. Boucher, M. E. Boulton, S. G. Bouret, P. Boya, M. Boyer-Guittaut, P. V. Bozhkov, N. Brady, V. M. Braga, C. Brancolini, G. H. Braus, J. M. Bravo-San Pedro, L. A. Brennan, E. H. Bresnick, P. Brest, D. Bridges, M. A. Bringer, M. Brini, G. C. Brito, B. Brodin, P. S. Brookes, E. J. Brown, K. Brown, H. E. Broxmeyer, A. Bruhat, P. C. Brum, J. H. Brumell, N. Brunetti-Pierri, R. J. Bryson-Richardson, S. Buch, A. M. Buchan, H. Budak, D. V. Bulavin, S. J. Bultman, G. Bultynck, V. Bumbasirevic, Y. Burelle, R. E. Burke, M. Burmeister, P. Butikofer, L. Caberlotto, K. Cadwell, M. Cahova, D. Cai, J. Cai, Q. Cai, S. Calatayud, N. Camougrand, M. Campanella, G. R. Campbell, M. Campbell, S. Campello, R. Candau, I. Caniggia, L. Cantoni, L. Cao, A. B. Caplan, M. Caraglia, C. Cardinali, S. M. Cardoso, J. S. Carew, L. A. Carleton, C. R. Carlin, S. Carloni, S. R.

Carlsson, D. Carmona-Gutierrez, L. A. Carneiro, O. Carnevali, S. Carra, A. Carrier, B. Carroll, C. Casas, J. Casas, G. Cassinelli, P. Castets, S. Castro-Obregon, G. Cavallini, I. Ceccherini, F. Cecconi, A. I. Cederbaum, V. Cena, S. Cenci, C. Cerella, D. Cervia, S. Cetrullo, H. Chaachouay, H. J. Chae, A. S. Chagin, C. Y. Chai, G. Chakrabarti, G. Chamilos, E. Y. Chan, M. T. Chan, D. Chandra, P. Chandra, C. P. Chang, R. C. Chang, T. Y. Chang, J. C. Chatham, S. Chatterjee, S. Chauhan, Y. Che, M. E. Cheetham, R. Cheluvappa, C. J. Chen, G. Chen, G. C. Chen, G. Chen, H. Chen, J. W. Chen, J. K. Chen, M. Chen, M. Chen, P. Chen, Q. Chen, Q. Chen, S. D. Chen, S. Chen, S. S. Chen, W. Chen, W. J. Chen, W. Q. Chen, W. Chen, X. Chen, Y. H. Chen, Y. G. Chen, Y. Chen, Y. Chen, Y. Chen, Y. J. Chen, Y. Q. Chen, Y. Chen, Z. Chen, Z. Chen, A. Cheng, C. H. Cheng, H. Cheng, H. Cheong, S. Cherry, J. Chesney, C. H. Cheung, E. Chevet, H. C. Chi, S. G. Chi, F. Chiacchiera, H. L. Chiang, R. Chiarelli, M. Chiariello, M. Chieppa, L. S. Chin, M. Chiong, G. N. Chiu, D. H. Cho, S. G. Cho, W. C. Cho, Y. Y. Cho, Y. S. Cho, A. M. Choi, E. J. Choi, E. K. Choi, J. Choi, M. E. Choi, S. I. Choi, T. F. Chou, S. Chouaib, D. Choubey, V. Choubey, K. C. Chow, K. Chowdhury, C. T. Chu, T. H. Chuang, T. Chun, H. Chung, T. Chung, Y. L. Chung, Y. J. Chwae, V. Cianfanelli, R. Ciarcia, I. A. Ciechomska, M. R. Ciriolo, M. Cirone, S. Claerhout, M. J. Clague, J. Claria, P. G. Clarke, R. Clarke, E. Clementi, C. Cleyrat, M. Cnop, E. M. Coccia, T. Cocco, P. Codogno, J. Coers, E. E. Cohen, D. Colecchia, L. Coletto, N. S. Coll, E. Colucci-Guyon, S. Comincini, M. Condello, K. L. Cook, G. H. Coombs, C. D. Cooper, J. M. Cooper, I. Coppens, M. T. Corasaniti, M. Corazzari, R. Corbalan, E. Corcelle-Termeau, M. D. Cordero, C. Corral-Ramos, O. Corti, A. Cossarizza, P. Costelli, S. Costes, S. L. Cotman, A. Coto-Montes, S. Cottet, E. Couve, L. R. Covey, L. A. Cowart, J. S. Cox, F. P. Coxon, C. B. Coyne, M. S. Cragg, R. J. Craven, T. Crepaldi, J. L. Crespo, A. Criollo, V. Crippa, M. T. Cruz, A. M. Cuervo, J. M. Cuezva, T. Cui, P. R. Cutillas, M. J. Czaja, M. F. Czyzyk-Krzeska, R. K. Dagda, U. Dahmen, C. Dai, W. Dai, Y. Dai, K. N. Dalby, L. Dalla Valle, G. Dalmasso, M. D'Amelio, M. Damme, A. Darfeuille-Michaud, C. Dargemont, V. M. Darley-Usmar, S. Dasarathy, B. Dasgupta, S. Dash, C. R. Dass, H. M. Davey, L. M. Davids, D. Davila, R. J. Davis, T. M. Dawson, V. L. Dawson, P. Daza, J. de Belleroche, P. de Figueiredo, R. C. de Figueiredo, J. de la Fuente, L. De Martino, A. De Matteis, G. R. De Meyer, A. De Milito, M. De Santi, W. de Souza, V. De Tata, D. De Zio, J. Debnath, R. Dechant, J. P. Decuypere, S. Deegan, B. Dehay, B. Del Bello, D. P. Del Re, R. Delage-Mourroux, L. M. Delbridge, L. Deldicque, E. Delorme-Axford, Y. Deng, J. Dengjel, M. Denizot, P. Dent, C. J. Der, V. Deretic, B. Derrien, E. Deutsch, T. P. Devarenne, R. J. Devenish, S. Di Bartolomeo, N. Di Daniele, F. Di Domenico, A. Di Nardo, S. Di Paola, A. Di Pietro, L. Di Renzo, A. DiAntonio, G. Diaz-Araya, I. Diaz-Laviada, M. T.

Diaz-Meco, J. Diaz-Nido, C. A. Dickey, R. C. Dickson, M. Diederich, P. Digard, I. Dikic, S. P. Dinesh-Kumar, C. Ding, W. X. Ding, Z. Ding, L. Dini, J. H. Distler, A. Diwan, M. Djavaheri-Mergny, K. Dmytruk, R. C. Dobson, V. Doetsch, K. Dokladny, S. Dokudovskaya, M. Donadelli, X. C. Dong, X. Dong, Z. Dong, T. M. Donohue, Jr., K. S. Doran, G. D'Orazi, G. W. Dorn, 2nd, V. Dosenko, S. Dridi, L. Drucker, J. Du, L. L. Du, L. Du, A. du Toit, P. Dua, L. Duan, P. Duann, V. K. Dubey, M. R. Duchen, M. A. Duchosal, H. Duez, I. Dugail, V. I. Dumit, M. C. Duncan, E. A. Dunlop, W. A. Dunn, Jr., N. Dupont, L. Dupuis, R. V. Duran, T. M. Durcan, S. Duvezin-Caubet, U. Duvvuri, V. Eapen, D. Ebrahimi-Fakhari, A. Echard, L. Eckhart, C. L. Edelstein, A. L. Edinger, L. Eichinger, T. Eisenberg, A. Eisenberg-Lerner, N. T. Eissa, W. S. El-Deiry, V. El-Khoury, Z. Elazar, H. Eldar-Finkelman, C. J. Elliott, E. Emanuele, U. Emmenegger, N. Engedal, A. M. Engelbrecht, S. Engelender, J. M. Enserink, R. Erdmann, J. Erenpreisa, R. Eri, J. L. Eriksen, A. Erman, R. Escalante, E. L. Eskelinen, L. Espert, L. Esteban-Martinez, T. J. Evans, M. Fabri, G. Fabrias, C. Fabrizi, A. Facchiano, N. J. Faergeman, A. Faggioni, W. D. Fairlie, C. Fan, D. Fan, J. Fan, S. Fang, M. Fanto, A. Fanzani, T. Farkas, M. Faure, F. B. Favier, H. Fearnhead, M. Federici, E. Fei, T. C. Felizardo, H. Feng, Y. Feng, Y. Feng, T. A. Ferguson, A. F. Fernandez, M. G. Fernandez-Barrena, J. C. Fernandez-Checa, A. Fernandez-Lopez, M. E. Fernandez-Zapico, O. Feron, E. Ferraro, C. V. Ferreira-Halder, L. Fesus, R. Feuer, F. C. Fiesel, E. C. Filippi-Chiela, G. Filomeni, G. M. Fimia, J. H. Fingert, S. Finkbeiner, T. Finkel, F. Fiorito, P. B. Fisher, M. Flajolet, F. Flamigni, O. Florey, S. Florio, R. A. Floto, M. Folini, C. Follo, E. A. Fon, F. Fornai, F. Fortunato, A. Fraldi, R. Franco, A. Francois, A. Francois, L. B. Frankel, I. D. Fraser, N. Frey, D. G. Freyssenet, C. Frezza, S. L. Friedman, D. E. Frigo, D. Fu, J. M. Fuentes, J. Fueyo, Y. Fujitani, Y. Fujiwara, M. Fujiya, M. Fukuda, S. Fulda, C. Fusco, B. Gabryel, M. Gaestel, P. Gailly, M. Gajewska, S. Galadari, G. Galili, I. Galindo, M. F. Galindo, G. Galliciotti, L. Galluzzi, L. Galluzzi, V. Galy, N. Gammoh, S. Gandy, A. K. Ganesan, S. Ganesan, I. G. Ganley, M. Gannage, F. B. Gao, F. Gao, J. X. Gao, L. Garcia Nannig, E. Garcia Vescovi, M. Garcia-Macia, C. Garcia-Ruiz, A. D. Garg, P. K. Garg, R. Gargini, N. C. Gassen, D. Gatica, E. Gatti, J. Gavard, E. Gavathiotis, L. Ge, P. Ge, S. Ge, P. W. Gean, V. Gelmetti, A. A. Genazzani, J. Geng, P. Genschik, L. Gerner, J. E. Gestwicki, D. A. Gewirtz, S. Ghavami, E. Ghigo, D. Ghosh, A. M. Giammarioli, F. Giampieri, C. Giampietri, A. Giatromanolaki, D. J. Gibbings, L. Gibellini, S. B. Gibson, V. Ginet, A. Giordano, F. Giorgini, E. Giovannetti, S. E. Girardin, S. Gispert, S. Giuliano, C. L. Gladson, A. Glavic, M. Gleave, N. Godefroy, R. M. Gogal, Jr., K. Gokulan, G. H. Goldman, D. Goletti, M. S. Goligorsky, A. V. Gomes, L. C. Gomes, H. Gomez, C. Gomez-Manzano, R. Gomez-Sanchez, D. A. Goncalves, E. Goncu, Q. Gong, C. Gongora, C. B. Gonzalez, P.

Gonzalez-Alegre, P. Gonzalez-Cabo, R. A. Gonzalez-Polo, I. S. Goping, C. Gorbea, N. V. Gorbunov, D. R. Goring, A. M. Gorman, S. M. Gorski, S. Goruppi, S. Goto-Yamada, C. Gotor, R. A. Gottlieb, I. Gozes, D. Gozuacik, Y. Graba, M. Graef, G. E. Granato, G. D. Grant, S. Grant, G. L. Gravina, D. R. Green, A. Greenhough, M. T. Greenwood, B. Grimaldi, F. Gros, C. Grose, J. F. Groulx, F. Gruber, P. Grumati, T. Grune, J. L. Guan, K. L. Guan, B. Guerra, C. Guillen, K. Gulshan, J. Gunst, C. Guo, L. Guo, M. Guo, W. Guo, X. G. Guo, A. A. Gust, A. B. Gustafsson, E. Gutierrez, M. G. Gutierrez, H. S. Gwak, A. Haas, J. E. Haber, S. Hadano, M. Hagedorn, D. R. Hahn, A. J. Halayko, A. Hamacher-Brady, K. Hamada, A. Hamai, A. Hamann, M. Hamasaki, I. Hamer, Q. Hamid, E. M. Hammond, F. Han, W. Han, J. T. Handa, J. A. Hanover, M. Hansen, M. Harada, L. Harhaji-Trajkovic, J. W. Harper, A. H. Harrath, A. L. Harris, J. Harris, U. Hasler, P. Hasselblatt, K. Hasui, R. G. Hawley, T. S. Hawley, C. He, C. Y. He, F. He, G. He, R. R. He, X. H. He, Y. W. He, Y. Y. He, J. K. Heath, M. J. Hebert, R. A. Heinzen, G. V. Helgason, M. Hensel, E. P. Henske, C. Her, P. K. Herman, A. Hernandez, C. Hernandez, S. Hernandez-Tiedra, C. Hetz, P. R. Hiesinger, K. Higaki, S. Hilfiker, B. G. Hill, J. A. Hill, W. D. Hill, K. Hino, D. Hofius, P. Hofman, G. U. Hoglinger, J. Hohfeld, M. K. Holz, Y. Hong, D. A. Hood, J. J. Hoozemans, T. Hoppe, C. Hsu, C. Y. Hsu, L. C. Hsu, D. Hu, G. Hu, H. M. Hu, H. Hu, M. C. Hu, Y. C. Hu, Z. W. Hu, F. Hua, Y. Hua, C. Huang, H. L. Huang, K. H. Huang, K. Y. Huang, S. Huang, S. Huang, W. P. Huang, Y. R. Huang, Y. Huang, Y. Huang, T. B. Huber, P. Huebbe, W. K. Huh, J. J. Hulmi, G. M. Hur, J. H. Hurley, Z. Husak, S. N. Hussain, S. Hussain, J. J. Hwang, S. Hwang, T. I. Hwang, A. Ichihara, Y. Imai, C. Imbriano, M. Inomata, T. Into, V. Iovane, J. L. Iovanna, R. V. Iozzo, N. Y. Ip, J. E. Irazoqui, P. Iribarren, Y. Isaka, A. J. Isakovic, H. Ischiropoulos, J. S. Isenberg, M. Ishaq, H. Ishida, I. Ishii, J. E. Ishmael, C. Isidoro, K. Isobe, E. Isono, S. Issazadeh-Navikas, K. Itahana, E. Itakura, A. I. Ivanov, A. K. Iyer, J. M. Izquierdo, Y. Izumi, V. Izzo, M. Jaattela, N. Jaber, D. J. Jackson, W. T. Jackson, T. G. Jacob, T. S. Jacques, C. Jagannath, A. Jain, N. R. Jana, B. K. Jang, A. Jani, B. Janji, P. R. Jannig, P. J. Jansson, S. Jean, M. Jendrach, J. H. Jeon, N. Jessen, E. B. Jeung, K. Jia, L. Jia, H. Jiang, H. Jiang, L. Jiang, T. Jiang, X. Jiang, X. Jiang, X. Jiang, Y. Jiang, Y. Jiang, A. Jimenez, C. Jin, H. Jin, L. Jin, M. Jin, S. Jin, U. K. Jinwal, E. K. Jo, T. Johansen, D. E. Johnson, G. V. Johnson, J. D. Johnson, E. Jonasch, C. Jones, L. A. Joosten, J. Jordan, A. M. Joseph, B. Joseph, A. M. Joubert, D. Ju, J. Ju, H. F. Juan, K. Juenemann, G. Juhasz, H. S. Jung, J. U. Jung, Y. K. Jung, H. Jungbluth, M. J. Justice, B. Jutten, N. O. Kaakoush, K. Kaarniranta, A. Kaasik, T. Kabuta, B. Kaeffer, K. Kagedal, A. Kahana, S. Kajimura, O. Kakhlon, M. Kalia, D. V. Kalvakolanu, Y. Kamada, K. Kambas, V. O. Kaminskyy, H. H. Kampinga, M. Kandouz, C. Kang, R. Kang, T. C. Kang, T. Kanki, T. D. Kanneganti, H. Kanno, A. G. Kanthasamy, M.

Kantorow, M. Kaparakis-Liaskos, O. Kapuy, V. Karantza, M. R. Karim, P. Karmakar, A. Kaser, S. Kaushik, T. Kawula, A. M. Kaynar, P. Y. Ke, Z. J. Ke, J. H. Kehrl, K. E. Keller, J. K. Kemper, A. K. Kenworthy, O. Kepp, A. Kern, S. Kesari, D. Kessel, R. Ketteler, C. Kettelhut Ido, B. Khambu, M. M. Khan, V. K. Khandelwal, S. Khare, J. G. Kiang, A. A. Kiger, A. Kihara, A. L. Kim, C. H. Kim, D. R. Kim, D. H. Kim, E. K. Kim, H. Y. Kim, H. R. Kim, J. S. Kim, J. H. Kim, J. C. Kim, J. H. Kim, K. W. Kim, M. D. Kim, M. M. Kim, P. K. Kim, S. W. Kim, S. Y. Kim, Y. S. Kim, Y. Kim, A. Kimchi, A. C. Kimmelman, T. Kimura, J. S. King, K. Kirkegaard, V. Kirkin, L. A. Kirshenbaum, S. Kishi, Y. Kitajima, K. Kitamoto, Y. Kitaoka, K. Kitazato, R. A. Kley, W. T. Klimecki, M. Klinkenberg, J. Klucken, H. Knaevelsrud, E. Knecht, L. Knuppertz, J. L. Ko, S. Kobayashi, J. C. Koch, C. Koechlin-Ramonatxo, U. Koenig, Y. H. Koh, K. Kohler, S. D. Kohlwein, M. Koike, M. Komatsu, E. Kominami, D. Kong, H. J. Kong, E. G. Konstantakou, B. T. Kopp, T. Korcsmaros, L. Korhonen, V. I. Korolchuk, N. V. Koshkina, Y. Kou, M. I. Koukourakis, C. Koumenis, A. L. Kovacs, T. Kovacs, W. J. Kovacs, D. Koya, C. Kraft, D. Krainc, H. Kramer, T. Kravic-Stevovic, W. Krek, C. Kretz-Remy, R. Krick, M. Krishnamurthy, J. Kriston-Vizi, G. Kroemer, M. C. Kruer, R. Kruger, N. T. Ktistakis, K. Kuchitsu, C. Kuhn, A. P. Kumar, A. Kumar, A. Kumar, D. Kumar, D. Kumar, R. Kumar, S. Kumar, M. Kundu, H. J. Kung, A. Kuno, S. H. Kuo, J. Kuret, T. Kurz, T. Kwok, T. K. Kwon, Y. T. Kwon, I. Kyrmizi, A. R. La Spada, F. Lafont, T. Lahm, A. Lakkaraju, T. Lam, T. Lamark, S. Lancel, T. H. Landowski, D. J. Lane, J. D. Lane, C. Lanzi, P. Lapaquette, L. R. Lapierre, J. Laporte, J. Laukkarinen, G. W. Laurie, S. Lavandero, L. Lavie, M. J. LaVoie, B. Y. Law, H. K. Law, K. B. Law, R. Layfield, P. A. Lazo, L. Le Cam, K. G. Le Roch, H. Le Stunff, V. Leardkamolkarn, M. Lecuit, B. H. Lee, C. H. Lee, E. F. Lee, G. M. Lee, H. J. Lee, H. Lee, J. K. Lee, J. Lee, J. H. Lee, J. H. Lee, M. Lee, M. S. Lee, P. J. Lee, S. W. Lee, S. J. Lee, S. J. Lee, S. Y. Lee, S. H. Lee, S. S. Lee, S. J. Lee, S. Lee, Y. R. Lee, Y. J. Lee, Y. H. Lee, C. Leeuwenburgh, S. Lefort, R. Legouis, J. Lei, Q. Y. Lei, D. A. Leib, G. Leibowitz, I. Lekli, S. D. Lemaire, J. J. Lemasters, M. K. Lemberg, A. Lemoine, S. Leng, G. Lenz, P. Lenzi, L. O. Lerman, D. Lettieri Barbato, J. I. Leu, H. Y. Leung, B. Levine, P. A. Lewis, F. Lezoualc'h, C. Li, F. Li, F. J. Li, J. Li, K. Li, L. Li, M. Li, M. Li, Q. Li, R. Li, S. Li, W. Li, W. Li, X. Li, Y. Li, J. Lian, C. Liang, Q. Liang, Y. Liao, J. Liberal, P. P. Liberski, P. Lie, A. P. Lieberman, H. J. Lim, K. L. Lim, K. Lim, R. T. Lima, C. S. Lin, C. F. Lin, F. Lin, F. Lin, F. C. Lin, K. Lin, K. H. Lin, P. H. Lin, T. Lin, W. W. Lin, Y. S. Lin, Y. Lin, R. Linden, D. Lindholm, L. M. Lindqvist, P. Lingor, A. Linkermann, L. A. Liotta, M. M. Lipinski, V. A. Lira, M. P. Lisanti, P. B. Liton, B. Liu, C. Liu, C. F. Liu, F. Liu, H. J. Liu, J. Liu, J. J. Liu, J. L. Liu, K. Liu, L. Liu, L. Liu, Q. Liu, R. Y. Liu, S. Liu, S. Liu, W. Liu, X. D. Liu, X. Liu, X. H. Liu, X. Liu, X. Liu,

X. Liu, Y. Liu, Y. Liu, Z. Liu, Z. Liu, J. P. Liuzzi, G. Lizard, M. Ljujic, I. J. Lodhi, S. E. Logue, B. L. Lokeshwar, Y. C. Long, S. Lonial, B. Loos, C. Lopez-Otin, C. Lopez-Vicario, M. Lorente, P. L. Lorenzi, P. Lorincz, M. Los, M. T. Lotze, P. E. Lovat, B. Lu, B. Lu, J. Lu, Q. Lu, S. M. Lu, S. Lu, Y. Lu, F. Luciano, S. Luckhart, J. M. Lucocq, P. Ludovico, A. Lugea, N. W. Lukacs, J. J. Lum, A. H. Lund, H. Luo, J. Luo, S. Luo, C. Luparello, T. Lyons, J. Ma, Y. Ma, Y. Ma, Z. Ma, J. Machado, G. M. Machado-Santelli, F. Macian, G. C. MacIntosh, J. P. MacKeigan, K. F. Macleod, J. D. MacMicking, L. A. MacMillan-Crow, F. Madeo, M. Madesh, J. Madrigal-Matute, A. Maeda, T. Maeda, G. Maegawa, E. Maellaro, H. Maes, M. Magarinos, K. Maiese, T. K. Maiti, L. Maiuri, M. C. Maiuri, C. G. Maki, R. Malli, W. Malorni, A. Maloyan, F. Mami-Chouaib, N. Man, J. D. Mancias, E. M. Mandelkow, M. A. Mandell, A. A. Manfredi, S. N. Manie, C. Manzoni, K. Mao, Z. Mao, Z. W. Mao, P. Marambaud, A. M. Marconi, Z. Marelja, G. Marfe, M. Margeta, E. Margittai, M. Mari, F. V. Mariani, C. Marin, S. Marinelli, G. Marino, I. Markovic, R. Marquez, A. M. Martelli, S. Martens, K. R. Martin, S. J. Martin, S. Martin, M. A. Martin-Acebes, P. Martin-Sanz, C. Martinand-Mari, W. Martinet, J. Martinez, N. Martinez-Lopez, U. Martinez-Outschoorn, M. Martinez-Velazquez, M. Martinez-Vicente, W. K. Martins, H. Mashima, J. A. Mastrianni, G. Matarese, P. Matarrese, R. Mateo, S. Matoba, N. Matsumoto, T. Matsushita, A. Matsuura, T. Matsuzawa, M. P. Mattson, S. Matus, N. Maugeri, C. Mauvezin, A. Mayer, D. Maysinger, G. D. Mazzolini, M. K. McBrayer, K. McCall, C. McCormick, G. M. McInerney, S. C. McIver, S. McKenna, J. J. McMahon, I. A. McNeish, F. Mechta-Grigoriou, J. P. Medema, D. L. Medina, K. Megyeri, M. Mehrpour, J. L. Mehta, Y. Mei, U. C. Meier, A. J. Meijer, A. Melendez, G. Melino, S. Melino, E. J. de Melo, M. A. Mena, M. D. Meneghini, J. A. Menendez, R. Menezes, L. Meng, L. H. Meng, S. Meng, R. Menghini, A. S. Menko, R. F. Menna-Barreto, M. B. Menon, M. A. Meraz-Rios, G. Merla, L. Merlini, A. M. Merlot, A. Meryk, S. Meschini, J. N. Meyer, M. T. Mi, C. Y. Miao, L. Micale, S. Michaeli, C. Michiels, A. R. Migliaccio, A. S. Mihailidou, D. Mijaljica, K. Mikoshiba, E. Milan, L. Miller-Fleming, G. B. Mills, I. G. Mills, G. Minakaki, B. A. Minassian, X. F. Ming, F. Minibayeva, E. A. Minina, J. D. Mintern, S. Minucci, A. Miranda-Vizuete, C. H. Mitchell, S. Miyamoto, K. Miyazawa, N. Mizushima, K. Mnich, B. Mograbi, S. Mohseni, L. F. Moita, M. Molinari, M. Molinari, A. B. Moller, B. Mollereau, F. Mollinedo, M. Mongillo, M. M. Monick, S. Montagnaro, C. Montell, D. J. Moore, M. N. Moore, R. Mora-Rodriguez, P. I. Moreira, E. Morel, M. B. Morelli, S. Moreno, M. J. Morgan, A. Moris, Y. Moriyasu, J. L. Morrison, L. A. Morrison, E. Morselli, J. Moscat, P. L. Moseley, S. Mostowy, E. Motori, D. Mottet, J. C. Mottram, C. E. Moussa, V. E. Mpakou, H. Mukhtar, J. M. Mulcahy Levy, S. Muller, R. Munoz-Moreno, C. Munoz-Pinedo, C. Munz, M. E. Murphy, J. T. Murray,

A. Murthy, I. U. Mysorekar, I. R. Nabi, M. Nabissi, G. A. Nader, Y. Nagahara, Y. Nagai, K. Nagata, A. Nagelkerke, P. Nagy, S. R. Naidu, S. Nair, H. Nakano, H. Nakatogawa, M. Nanjundan, G. Napolitano, N. I. Naqvi, R. Nardacci, D. P. Narendra, M. Narita, A. C. Nascimbeni, R. Natarajan, L. C. Navegantes, S. T. Nawrocki, T. Y. Nazarko, V. Y. Nazarko, T. Neill, L. M. Neri, M. G. Netea, R. T. Netea-Maier, B. M. Neves, P. A. Ney, I. P. Nezis, H. T. Nguyen, H. P. Nguyen, A. S. Nicot, H. Nilsen, P. Nilsson, M. Nishimura, I. Nishino, M. Niso-Santano, H. Niu, R. A. Nixon, V. C. Njar, T. Noda, A. A. Noegel, E. M. Nolte, E. Norberg, K. K. Norga, S. K. Noureini, S. Notomi, L. Notterpek, K. Nowikovsky, N. Nukina, T. Nurnberger, V. B. O'Donnell, T. O'Donovan, P. J. O'Dwyer, I. Oehme, C. L. Oeste, M. Ogawa, B. Ogretmen, Y. Ogura, Y. J. Oh, M. Ohmuraya, T. Ohshima, R. Ojha, K. Okamoto, T. Okazaki, F. J. Oliver, K. Ollinger, S. Olsson, D. P. Orban, P. Ordonez, I. Orhon, L. Orosz, E. J. O'Rourke, H. Orozco, A. L. Ortega, E. Ortona, L. D. Osellame, J. Oshima, S. Oshima, H. D. Osiewacz, T. Otomo, K. Otsu, J. H. Ou, T. F. Outeiro, D. Y. Ouyang, H. Ouyang, M. Overholtzer, M. A. Ozbun, P. H. Ozdinler, B. Ozpolat, C. Pacelli, P. Paganetti, G. Page, G. Pages, U. Pagnini, B. Pajak, S. C. Pak, K. Pakos-Zebrucka, N. Pakpour, Z. Palkova, F. Palladino, K. Pallauf, N. Pallet, M. Palmieri, S. R. Paludan, C. Palumbo, S. Palumbo, O. Pampliega, H. Pan, W. Pan, T. Panaretakis, A. Pandey, A. Pantazopoulou, Z. Papackova, D. L. Papademetrio, I. Papassideri, A. Papini, N. Parajuli, J. Pardo, V. V. Parekh, G. Parenti, J. I. Park, J. Park, O. K. Park, R. Parker, R. Parlato, J. B. Parys, K. R. Parzych, J. M. Pasquet, B. Pasquier, K. B. Pasumarthi, D. Patschan, C. Patterson, S. Pattingre, S. Pattison, A. Pause, H. Pavenstadt, F. Pavone, Z. Pedrozo, F. J. Pena, M. A. Penalva, M. Pende, J. Peng, F. Penna, J. M. Penninger, A. Pensalfini, S. Pepe, G. J. Pereira, P. C. Pereira, V. Perez-de la Cruz, M. E. Perez-Perez, D. Perez-Rodriguez, D. Perez-Sala, C. Perier, A. Perl, D. H. Perlmutter, I. Perrotta, S. Pervaiz, M. Pesonen, J. E. Pessin, G. J. Peters, M. Petersen, I. Petrache, B. J. Petrof, G. Petrovski, J. M. Phang, M. Piacentini, M. Pierdominici, P. Pierre, V. Pierrefite-Carle, F. Pietrocola, F. X. Pimentel-Muinos, M. Pinar, B. Pineda, R. Pinkas-Kramarski, M. Pinti, P. Pinton, B. Piperdi, J. M. Piret, L. C. Platanias, H. W. Platta, E. D. Plowey, S. Poggeler, M. Poirot, P. Polcic, A. Poletti, A. H. Poon, H. Popelka, B. Popova, I. Poprawa, S. M. Poulose, J. Poulton, S. K. Powers, T. Powers, M. Pozuelo-Rubio, K. Prak, R. Prange, M. Prescott, M. Priault, S. Prince, R. L. Proia, T. Proikas-Cezanne, H. Prokisch, V. J. Promponas, K. Przyklenk, R. Puertollano, S. Pugazhenthi, L. Puglielli, A. Pujol, J. Puyal, D. Pyeon, X. Qi, W. B. Qian, Z. H. Qin, Y. Qiu, Z. Qu, J. Quadrilatero, F. Quinn, N. Raben, H. Rabinowich, F. Radogna, M. J. Ragusa, M. Rahmani, K. Raina, S. Ramanadham, R. Ramesh, A. Rami, S. Randall-Demllo, F. Randow, H. Rao, V. A. Rao, B. B. Rasmussen, T. M. Rasse, E. A. Ratovitski, P. E. Rautou,

S. K. Ray, B. Razani, B. H. Reed, F. Reggiori, M. Rehm, A. S. Reichert, T. Rein, D. J. Reiner, E. Reits, J. Ren, X. Ren, M. Renna, J. E. Reusch, J. L. Revuelta, L. Reyes, A. R. Rezaie, R. I. Richards, D. R. Richardson, C. Richetta, M. A. Riehle, B. H. Rihn, Y. Rikihisa, B. E. Riley, G. Rimbach, M. R. Rippo, K. Ritis, F. Rizzi, E. Rizzo, P. J. Roach, J. Robbins, M. Roberge, G. Roca, M. C. Roccheri, S. Rocha, C. M. Rodrigues, C. I. Rodriguez, S. R. de Cordoba, N. Rodriguez-Muela, J. Roelofs, V. V. Rogov, T. T. Rohn, B. Rohrer, D. Romanelli, L. Romani, P. S. Romano, M. I. Roncero, J. L. Rosa, A. Rosello, K. V. Rosen, P. Rosenstiel, M. Rost-Roszkowska, K. A. Roth, G. Roue, M. Rouis, K. M. Rouschop, D. T. Ruan, D. Ruano, D. C. Rubinsztein, E. B. Rucker, 3rd, A. Rudich, E. Rudolf, R. Rudolf, M. A. Ruegg, C. Ruiz-Roldan, A. A. Ruparelia, P. Rusmini, D. W. Russ, G. L. Russo, G. Russo, R. Russo, T. E. Rusten, V. Ryabovol, K. M. Ryan, S. W. Ryter, D. M. Sabatini, M. Sacher, C. Sachse, M. N. Sack, J. Sadoshima, P. Saftig, R. Sagi-Eisenberg, S. Sahni, P. Saikumar, T. Saito, T. Saitoh, K. Sakakura, M. Sakoh-Nakatogawa, Y. Sakuraba, M. Salazar-Roa, P. Salomoni, A. K. Saluja, P. M. Salvaterra, R. Salvioli, A. Samali, A. M. Sanchez, J. A. Sanchez-Alcazar, R. Sanchez-Prieto, M. Sandri, M. A. Sanjuan, S. Santaguida, L. Santambrogio, G. Santoni, C. N. Dos Santos, S. Saran, M. Sardiello, G. Sargent, P. Sarkar, S. Sarkar, M. R. Sarrias, M. M. Sarwal, C. Sasakawa, M. Sasaki, M. Sass, K. Sato, M. Sato, J. Satriano, N. Savaraj, S. Saveljeva, L. Schaefer, U. E. Schaible, M. Scharl, H. M. Schatzl, R. Schekman, W. Scheper, A. Schiavi, H. M. Schipper, H. Schmeisser, J. Schmidt, I. Schmitz, B. E. Schneider, E. M. Schneider, J. L. Schneider, E. A. Schon, M. J. Schonenberger, A. H. Schonthal, D. F. Schorderet, B. Schroder, S. Schuck, R. J. Schulze, M. Schwarten, T. L. Schwarz, S. Sciarretta, K. Scotto, A. I. Scovassi, R. A. Screaton, M. Screen, H. Seca, S. Sedej, L. Segatori, N. Segev, P. O. Seglen, J. M. Segui-Simarro, J. Segura-Aguilar, E. Seki, C. Sell, I. Seiliez, C. F. Semenkovich, G. L. Semenza, U. Sen, A. L. Serra, A. Serrano-Puebla, H. Sesaki, T. Setoguchi, C. Settembre, J. J. Shacka, A. N. Shajahan-Haq, I. M. Shapiro, S. Sharma, H. She, C. K. Shen, C. C. Shen, H. M. Shen, S. Shen, W. Shen, R. Sheng, X. Sheng, Z. H. Sheng, T. G. Shepherd, J. Shi, Q. Shi, Q. Shi, Y. Shi, S. Shibutani, K. Shibuya, Y. Shidoji, J. J. Shieh, C. M. Shih, Y. Shimada, S. Shimizu, D. W. Shin, M. L. Shinohara, M. Shintani, T. Shintani, T. Shioi, K. Shirabe, R. Shiri-Sverdlov, O. Shirihai, G. C. Shore, C. W. Shu, D. Shukla, A. A. Sibirny, V. Sica, C. J. Sigurdson, E. M. Sigurdsson, P. S. Sijwali, B. Sikorska, W. A. Silveira, S. Silvente-Poirot, G. A. Silverman, J. Simak, T. Simmet, A. K. Simon, H. U. Simon, C. Simone, M. Simons, A. Simonsen, R. Singh, S. V. Singh, S. K. Singh, D. Sinha, S. Sinha, F. A. Sinicrope, A. Sirko, K. Sirohi, B. J. Sishi, A. Sittler, P. M. Siu, E. Sivridis, A. Skwarska, R. Slack, I. Slaninova, N. Slavov, S. S. Smaili, K. S. Smalley, D. R. Smith, S. J. Soenen, S. A. Soleimanpour, A. Solhaug, K. Somasundaram, J.

H. Son, A. Sonawane, C. Song, F. Song, H. K. Song, J. X. Song, W. Song, K. Y. Soo, A. K. Sood, T. W. Soong, V. Soontornniyomkij, M. Sorice, F. Sotgia, D. R. Soto-Pantoja, A. Sotthibundhu, M. J. Sousa, H. P. Spaink, P. N. Span, A. Spang, J. D. Sparks, P. G. Speck, S. A. Spector, C. D. Spies, W. Springer, D. S. Clair, A. Stacchiotti, B. Staels, M. T. Stang, D. T. Starczynowski, P. Starokadomskyy, C. Steegborn, J. W. Steele, L. Stefanis, J. Steffan, C. M. Stellrecht, H. Stenmark, T. M. Stepkowski, S. T. Stern, C. Stevens, B. R. Stockwell, V. Stoka, Z. Storchova, B. Stork, V. Stratoulias, D. J. Stravopodis, P. Strnad, A. M. Strohecker, A. L. Strom, P. Stromhaug, J. Stulik, Y. X. Su, Z. Su, C. S. Subauste, S. Subramaniam, C. M. Sue, S. W. Suh, X. Sui, S. Sukseree, D. Sulzer, F. L. Sun, J. Sun, J. Sun, S. Y. Sun, Y. Sun, Y. Sun, Y. Sun, V. Sundaramoorthy, J. Sung, H. Suzuki, K. Suzuki, N. Suzuki, T. Suzuki, Y. J. Suzuki, M. S. Swanson, C. Swanton, K. Sward, G. Swarup, S. T. Sweeney, P. W. Sylvester, Z. Szatmari, E. Szegezdi, P. W. Szlosarek, H. Taegtmeyer, M. Tafani, E. Taillebourg, S. W. Tait, K. Takacs-Vellai, Y. Takahashi, S. Takats, G. Takemura, N. Takigawa, N. J. Talbot, E. Tamagno, J. Tamburini, C. P. Tan, L. Tan, M. L. Tan, M. Tan, Y. J. Tan, K. Tanaka, M. Tanaka, D. Tang, D. Tang, G. Tang, I. Tanida, K. Tanji, B. A. Tannous, J. A. Tapia, I. Tasset-Cuevas, M. Tatar, I. Tavassoly, N. Tavernarakis, A. Taylor, G. S. Taylor, G. A. Taylor, J. P. Taylor, M. J. Taylor, E. V. Tchetina, A. R. Tee, F. Teixeira-Clerc, S. Telang, T. Tencomnao, B. B. Teng, R. J. Teng, F. Terro, G. Tettamanti, A. L. Theiss, A. E. Theron, K. J. Thomas, M. P. Thome, P. G. Thomes, A. Thorburn, J. Thorner, T. Thum, M. Thumm, T. L. Thurston, L. Tian, A. Till, J. P. Ting, V. I. Titorenko, L. Toker, S. Toldo, S. A. Tooze, I. Topisirovic, M. L. Torgersen, L. Torosantucci, A. Torriglia, M. R. Torrisi, C. Tournier, R. Towns, V. Trajkovic, L. H. Travassos, G. Triola, D. N. Tripathi, D. Trisciuoglio, R. Troncoso, I. P. Trougakos, A. C. Truttmann, K. J. Tsai, M. P. Tschan, Y. H. Tseng, T. Tsukuba, A. Tsung, A. S. Tsvetkov, S. Tu, H. Y. Tuan, M. Tucci, D. A. Tumbarello, B. Turk, V. Turk, R. F. Turner, A. A. Tveita, S. C. Tyagi, M. Ubukata, Y. Uchiyama, A. Udelnow, T. Ueno, M. Umekawa, R. Umemiya-Shirafuji, B. R. Underwood, C. Ungermann, R. P. Ureshino, R. Ushioda, V. N. Uversky, N. L. Uzcategui, T. Vaccari, M. I. Vaccaro, L. Vachova, H. Vakifahmetoglu-Norberg, R. Valdor, E. M. Valente, F. Vallette, A. M. Valverde, G. Van den Berghe, L. Van Den Bosch, G. R. van den Brink, F. G. van der Goot, I. J. van der Klei, L. J. van der Laan, W. G. van Doorn, M. van Egmond, K. L. van Golen, L. Van Kaer, M. van Lookeren Campagne, P. Vandenabeele, W. Vandenberghe, I. Vanhorebeek, I. Varela-Nieto, M. H. Vasconcelos, R. Vasko, D. G. Vavvas, I. Vega-Naredo, G. Velasco, A. D. Velentzas, P. D. Velentzas, T. Vellai, E. Vellenga, M. H. Vendelbo, K. Venkatachalam, N. Ventura, S. Ventura, P. S. Veras, M. Verdier, B. G. Vertessy, A. Viale, M. Vidal, H. L. Vieira, R. D. Vierstra, N. Vigneswaran, N. Vij, M. Vila, M. Villar,

V. H. Villar, J. Villarroya, C. Vindis, G. Viola, M. T. Viscomi, G. Vitale, D. T. Vogl, O. V. Voitsekhovskaja, C. von Haefen, K. von Schwarzenberg, D. E. Voth, V. Vouret-Craviari, K. Vuori, J. M. Vyas, C. Waeber, C. L. Walker, M. J. Walker, J. Walter, L. Wan, X. Wan, B. Wang, C. Wang, C. Y. Wang, C. Wang, C. Wang, C. Wang, D. Wang, F. Wang, F. Wang, G. Wang, H. J. Wang, H. Wang, H. G. Wang, H. Wang, H. D. Wang, J. Wang, J. Wang, M. Wang, M. Q. Wang, P. Y. Wang, P. Wang, R. C. Wang, S. Wang, T. F. Wang, X. Wang, X. J. Wang, X. W. Wang, X. Wang, X. Wang, Y. Wang, Y. Wang, Y. Wang, Y. J. Wang, Y. Wang, Y. Wang, Y. T. Wang, Y. Wang, Z. N. Wang, P. Wappner, C. Ward, D. M. Ward, G. Warnes, H. Watada, Y. Watanabe, K. Watase, T. E. Weaver, C. D. Weekes, J. Wei, T. Weide, C. C. Weihl, G. Weindl, S. N. Weis, L. Wen, X. Wen, Y. Wen, B. Westermann, C. M. Weyand, A. R. White, E. White, J. L. Whitton, A. J. Whitworth, J. Wiels, F. Wild, M. E. Wildenberg, T. Wileman, D. S. Wilkinson, S. Wilkinson, D. Willbold, C. Williams, K. Williams, P. R. Williamson, K. F. Winklhofer, S. S. Witkin, S. E. Wohlgemuth, T. Wollert, E. J. Wolvetang, E. Wong, G. W. Wong, R. W. Wong, V. K. Wong, E. A. Woodcock, K. L. Wright, C. Wu, D. Wu, G. S. Wu, J. Wu, J. Wu, M. Wu, M. Wu, S. Wu, W. K. Wu, Y. Wu, Z. Wu, C. P. Xavier, R. J. Xavier, G. X. Xia, T. Xia, W. Xia, Y. Xia, H. Xiao, J. Xiao, S. Xiao, W. Xiao, C. M. Xie, Z. Xie, Z. Xie, M. Xilouri, Y. Xiong, C. Xu, C. Xu, F. Xu, H. Xu, H. Xu, J. Xu, J. Xu, J. Xu, L. Xu, X. Xu, Y. Xu, Y. Xu, Z. X. Xu, Z. Xu, Y. Xue, T. Yamada, A. Yamamoto, K. Yamanaka, S. Yamashina, S. Yamashiro, B. Yan, B. Yan, X. Yan, Z. Yan, Y. Yanagi, D. S. Yang, J. M. Yang, L. Yang, M. Yang, P. M. Yang, P. Yang, Q. Yang, W. Yang, W. Y. Yang, X. Yang, Y. Yang, Y. Yang, Z. Yang, Z. Yang, M. C. Yao, P. J. Yao, X. Yao, Z. Yao, Z. Yao, L. S. Yasui, M. Ye, B. Yedvobnick, B. Yeganeh, E. S. Yeh, P. L. Yeyati, F. Yi, L. Yi, X. M. Yin, C. K. Yip, Y. M. Yoo, Y. H. Yoo, S. Y. Yoon, K. Yoshida, T. Yoshimori, K. H. Young, H. Yu, J. J. Yu, J. T. Yu, J. Yu, L. Yu, W. H. Yu, X. F. Yu, Z. Yu, J. Yuan, Z. M. Yuan, B. Y. Yue, J. Yue, Z. Yue, D. N. Zacks, E. Zacksenhaus, N. Zaffaroni, T. Zaglia, Z. Zakeri, V. Zecchini, J. Zeng, M. Zeng, Q. Zeng, A. S. Zervos, D. D. Zhang, F. Zhang, G. Zhang, G. C. Zhang, H. Zhang, H. Zhang, H. Zhang, H. Zhang, J. Zhang, J. Zhang, J. Zhang, J. Zhang, J. P. Zhang, L. Zhang, L. Zhang, L. Zhang, L. Zhang, M. Y. Zhang, X. Zhang, X. D. Zhang, Y. Zhang, Y. Zhang, Y. Zhang, Y. Zhang, Y. Zhang, M. Zhao, W. L. Zhao, X. Zhao, Y. G. Zhao, Y. Zhao, Y. Zhao, Y. X. Zhao, Z. Zhao, Z. J. Zhao, D. Zheng, X. L. Zheng, X. Zheng, B. Zhivotovsky, Q. Zhong, G. Z. Zhou, G. Zhou, H. Zhou, S. F. Zhou, X. J. Zhou, H. Zhu, H. Zhu, W. G. Zhu, W. Zhu, X. F. Zhu, Y. Zhu, S. M. Zhuang, X. Zhuang, E. Ziparo, C. E. Zois, T. Zoladek, W. X. Zong, A. Zorzano and S. M. Zughaier (2016). "Guidelines for the use and interpretation of assays for monitoring autophagy (3rd edition)." Autophagy **12**(1): 1-222.

Klionsky, D. J., J. M. Cregg, W. A. Dunn, Jr., S. D. Emr, Y. Sakai, I. V. Sandoval, A. Sibirny, S. Subramani, M. Thumm, M. Veenhuis and Y. Ohsumi (2003). "A unified nomenclature for yeast autophagy-related genes." Dev Cell **5**(4): 539-545.

Knobel, K. M., W. S. Davis, E. M. Jorgensen and M. J. Bastiani (2001). "UNC-119 suppresses axon branching in C. elegans." Development **128**(20): 4079-4092.

Knop, M., A. Finger, T. Braun, K. Hellmuth and D. H. Wolf (1996). "Der1, a novel protein specifically required for endoplasmic reticulum degradation in yeast." Embo j **15**(4): 753-763.

Ko, H. S., T. Uehara, K. Tsuruma and Y. Nomura (2004). "Ubiquilin interacts with ubiquitylated proteins and proteasome through its ubiquitin-associated and ubiquitin-like domains." FEBS Lett **566**(1-3): 110-114.

Kobayashi, M., S. Oshima, C. Maeyashiki, Y. Nibe, K. Otsubo, Y. Matsuzawa, Y. Nemoto, T. Nagaishi, R. Okamoto, K. Tsuchiya, T. Nakamura and M. Watanabe (2016). "The ubiquitin hybrid gene UBA52 regulates ubiquitination of ribosome and sustains embryonic development." Scientific Reports **6**: 36780.

Koegl, M., T. Hoppe, S. Schlenker, H. D. Ulrich, T. U. Mayer and S. Jentsch (1999). "A novel ubiquitination factor, E4, is involved in multiubiquitin chain assembly." Cell **96**(5): 635-644.

Køhler, J. B., M. L. Jørgensen, G. Beinoraité, M. Thorsen and G. Thon (2013). "Concerted action of the ubiquitin-fusion degradation protein 1 (Ufd1) and Sumo-targeted ubiquitin ligases (STUbLs) in the DNA-damage response." PLoS One **8**(11): e80442.

Kopito, R. R. (2000). "Aggresomes, inclusion bodies and protein aggregation." Trends Cell Biol **10**(12): 524-530.

Koppers, M., M. M. van Blitterswijk, L. Vlam, P. A. Rowicka, P. W. J. van Vught, E. J. N. Groen, W. G. M. Spliet, J. Engelen-Lee, H. J. Schelhaas, M. de Visser, A. J. van der Kooi, W. L. van der Pol, R. J. Pasterkamp, J. H. Veldink and L. H. van den Berg (2012). "VCP mutations

in familial and sporadic amyotrophic lateral sclerosis." Neurobiology of Aging **33**(4): 837.e837-837.e813.

Körner, C. G., M. Wormington, M. Muckenthaler, S. Schneider, E. Dehlin and E. Wahle (1998). "The deadenylating nuclease (DAN) is involved in poly(A) tail removal during the meiotic maturation of Xenopus oocytes." Embo j **17**(18): 5427-5437.

Korolchuk, V. I., F. M. Menzies and D. C. Rubinsztein (2010). "Mechanisms of cross-talk between the ubiquitin-proteasome and autophagy-lysosome systems." FEBS Lett **584**(7): 1393-1398.

Kraft, C., M. Peter and K. Hofmann (2010). "Selective autophagy: ubiquitin-mediated recognition and beyond." Nat Cell Biol **12**(9): 836-841.

Kravtsova-Ivantsiv, Y., S. Cohen and A. Ciechanover (2009). "Modification by single ubiquitin moieties rather than polyubiquitination is sufficient for proteasomal processing of the p105 NF-kappaB precursor." Mol Cell **33**(4): 496-504.

Kraytsberg, Y., E. Kudryavtseva, A. C. McKee, C. Geula, N. W. Kowall and K. Khrapko (2006). "Mitochondrial DNA deletions are abundant and cause functional impairment in aged human substantia nigra neurons." Nat Genet **38**(5): 518-520.

Krobitsch, S. and S. Lindquist (2000). "Aggregation of huntingtin in yeast varies with the length of the polyglutamine expansion and the expression of chaperone proteins." Proc Natl Acad Sci U S A **97**(4): 1589-1594.

Krogan, N. J., W. T. Peng, G. Cagney, M. D. Robinson, R. Haw, G. Zhong, X. Guo, X. Zhang, V. Canadien, D. P. Richards, B. K. Beattie, A. Lalev, W. Zhang, A. P. Davierwala, S. Mnaimneh, A. Starostine, A. P. Tikuisis, J. Grigull, N. Datta, J. E. Bray, T. R. Hughes, A. Emili and J. F. Greenblatt (2004). "High-definition macromolecular composition of yeast RNA-processing complexes." Mol Cell **13**(2): 225-239.

Kruse, K. B., J. L. Brodsky and A. A. McCracken (2006). "Characterization of an ERAD gene as VPS30/ATG6 reveals two alternative and functionally distinct protein quality control pathways: one for soluble Z variant of human alpha-1 proteinase inhibitor (A1PiZ) and another for aggregates of A1PiZ." Mol Biol Cell **17**(1): 203-212.

Kryndushkin, D., R. B. Wickner and F. Shewmaker (2011). "FUS/TLS forms cytoplasmic aggregates, inhibits cell growth and interacts with TDP-43 in a yeast model of amyotrophic lateral sclerosis." Protein Cell **2**(3): 223-236.

Kubo, Y., T. Tsunehiro, S. Nishikawa, M. Nakai, E. Ikeda, A. Toh-e, N. Morishima, T. Shibata and T. Endo (1999). "Two distinct mechanisms operate in the reactivation of heat-denatured proteins by the mitochondrial Hsp70/Mdj1p/Yge1p chaperone system." J Mol Biol **286**(2): 447-464.

Kuijpers, M., V. van Dis, E. D. Haasdijk, M. Harterink, K. Vocking, J. A. Post, W. Scheper, C. C. Hoogenraad and D. Jaarsma (2013). "Amyotrophic lateral sclerosis (ALS)-associated VAPB-P56S inclusions represent an ER quality control compartment." Acta Neuropathol Commun **1**: 24.

Kujoth, G. C., A. Hiona, T. D. Pugh, S. Someya, K. Panzer, S. E. Wohlgemuth, T. Hofer, A. Y. Seo, R. Sullivan, W. A. Jobling, J. D. Morrow, H. Van Remmen, J. M. Sedivy, T. Yamasoba, M. Tanokura, R. Weindruch, C. Leeuwenburgh and T. A. Prolla (2005). "Mitochondrial DNA mutations, oxidative stress, and apoptosis in mammalian aging." Science **309**(5733): 481-484.

Kulak, N. A., G. Pichler, I. Paron, N. Nagaraj and M. Mann (2014). "Minimal, encapsulated proteomic-sample processing applied to copy-number estimation in eukaryotic cells." Nat Methods **11**(3): 319-324.

Kuusisto, E., A. Salminen and I. Alafuzoff (2002). "Early accumulation of p62 in neurofibrillary tangles in Alzheimer's disease: possible role in tangle formation." Neuropathol Appl Neurobiol **28**(3): 228-237.

Kwiatkowski, T. J., Jr., D. A. Bosco, A. L. Leclerc, E. Tamrazian, C. R. Vanderburg, C. Russ, A. Davis, J. Gilchrist, E. J. Kasarskis, T. Munsat, P. Valdmanis, G. A. Rouleau, B. A. Hosler, P. Cortelli, P. J. de Jong, Y. Yoshinaga, J. L. Haines, M. A. Pericak-Vance, J. Yan, N. Ticozzi, T. Siddique, D. McKenna-Yasek, P. C. Sapp, H. R. Horvitz, J. E. Landers and R. H. Brown, Jr. (2009). "Mutations in the FUS/TLS gene on chromosome 16 cause familial amyotrophic lateral sclerosis." Science **323**(5918): 1205-1208.

Kwok, J. B., M. Hallupp, C. T. Loy, D. K. Chan, J. Woo, G. D. Mellick, D. D. Buchanan, P. A. Silburn, G. M. Halliday and P. R. Schofield (2005). "GSK3B polymorphisms alter transcription and splicing in Parkinson's disease." Ann Neurol **58**(6): 829-839.

Kwon, S., Y. Zhang and P. Matthias (2007). "The deacetylase HDAC6 is a novel critical component of stress granules involved in the stress response." Genes Dev **21**(24): 3381-3394.

Lagier-Tourenne, C. and D. W. Cleveland (2009). "Rethinking ALS: the FUS about TDP-43." Cell **136**(6): 1001-1004.

Lagier-Tourenne, C., M. Polymenidou and D. W. Cleveland (2010). "TDP-43 and FUS/TLS: emerging roles in RNA processing and neurodegeneration." Hum Mol Genet **19**(R1): R46-64.

Lagier-Tourenne, C., M. Polymenidou, K. R. Hutt, A. Q. Vu, M. Baughn, S. C. Huelga, K. M. Clutario, S. C. Ling, T. Y. Liang, C. Mazur, E. Wancewicz, A. S. Kim, A. Watt, S. Freier, G. G. Hicks, J. P. Donohue, L. Shiue, C. F. Bennett, J. Ravits, D. W. Cleveland and G. W. Yeo (2012). "Divergent roles of ALS-linked proteins FUS/TLS and TDP-43 intersect in processing long pre-mRNAs." Nat Neurosci **15**(11): 1488-1497.

Lai, S. L., Y. Abramzon, J. C. Schymick, D. A. Stephan, T. Dunckley, A. Dillman, M. Cookson, A. Calvo, S. Battistini, F. Giannini, C. Caponnetto, G. L. Mancardi, R. Spataro, M. R. Monsurro, G. Tedeschi, K. Marinou, M. Sabatelli, A. Conte, J. Mandrioli, P. Sola, F. Salvi, I. Bartolomei, F. Lombardo, G. Mora, G. Restagno, A. Chio and B. J. Traynor (2011). "FUS mutations in sporadic amyotrophic lateral sclerosis." Neurobiol Aging **32**(3): 550.e551-554.

Laird, A. S., A. Van Hoecke, L. De Muynck, M. Timmers, L. Van den Bosch, P. Van Damme and W. Robberecht (2010). "Progranulin is neurotrophic in vivo and protects against a mutant TDP-43 induced axonopathy." PLoS One **5**(10): e13368.

Larimer, F. W., C. L. Hsu, M. K. Maupin and A. Stevens (1992). "Characterization of the XRN1 gene encoding a 5'-->3' exoribonuclease: sequence data and analysis of disparate protein and mRNA levels of gene-disrupted yeast cells." Gene **120**(1): 51-57.

Larroquette, F., L. Seto, P. L. Gaub, B. Kamal, D. Wallis, R. Larivière, J. Vallée, R. Robitaille and H. Tsuda (2015). "Vapb/Amyotrophic lateral sclerosis 8 knock-in mice display slowly progressive motor behavior defects accompanying ER stress and autophagic response." Human Molecular Genetics **24**(22): 6515-6529.

Lautenschlaeger, J., T. Prell and J. Grosskreutz (2012). "Endoplasmic reticulum stress and the ER mitochondrial calcium cycle in amyotrophic lateral sclerosis." Amyotroph Lateral Scler **13**(2): 166-177.

Leblond, C. S., Z. Gan-Or, D. Spiegelman, S. B. Laurent, A. Szuto, A. Hodgkinson, A. Dionne-Laporte, P. Provencher, M. de Carvalho, S. Orru, D. Brunet, J. P. Bouchard, P. Awadalla, N. Dupre, P. A. Dion and G. A. Rouleau (2016). "Replication study of MATR3 in familial and sporadic amyotrophic lateral sclerosis." Neurobiol Aging **37**: 209.e217-209.e221.

Lee, A., S. L. Rayner, S. S. L. Gwee, A. De Luca, H. Shahheydari, V. Sundaramoorthy, A. Ragagnin, M. Morsch, R. Radford, J. Galper, S. Freckleton, B. Shi, A. K. Walker, E. K. Don, N. J. Cole, S. Yang, K. L. Williams, J. J. Yerbury, I. P. Blair, J. D. Atkin, M. P. Molloy and R. S. Chung (2018). "Pathogenic mutation in the ALS/FTD gene, CCNF, causes elevated Lys48-linked ubiquitylation and defective autophagy." Cellular and Molecular Life Sciences **75**(2): 335-354.

Lee, M. V., S. E. Topper, S. L. Hubler, J. Hose, C. D. Wenger, J. J. Coon and A. P. Gasch (2011). "A dynamic model of proteome changes reveals new roles for transcript alteration in yeast." Mol Syst Biol **7**: 514.

Leigh, P. N., H. Whitwell, O. Garofalo, J. Buller, M. Swash, J. E. Martin, J. M. Gallo, R. O. Weller and B. H. Anderton (1991). "Ubiquitin-immunoreactive intraneuronal inclusions in amyotrophic lateral sclerosis. Morphology, distribution, and specificity." Brain **114 (Pt 2)**: 775-788.

Lemmens, R., A. Van Hoecke, N. Hersmus, V. Geelen, I. D'Hollander, V. Thijs, L. Van Den Bosch, P. Carmeliet and W. Robberecht (2007). "Overexpression of mutant superoxide dismutase 1 causes a motor axonopathy in the zebrafish." Hum Mol Genet **16**(19): 2359-2365.

Lev, S., D. Ben Halevy, D. Peretti and N. Dahan (2008). "The VAP protein family: from cellular functions to motor neuron disease." Trends Cell Biol **18**(6): 282-290.

Levine, T. P., R. D. Daniels, A. T. Gatta, L. H. Wong and M. J. Hayes (2013). "The product of C9orf72, a gene strongly implicated in neurodegeneration, is structurally related to DENN Rab-GEFs." Bioinformatics **29**(4): 499-503.

Lew, Q. J., K. L. Chu, Y. L. Chia, B. Soo, J. P. Ho, C. H. Ng, H. S. Kwok, C. M. Chiang, Y. Chang and S. H. Chao (2015). "GCN5 inhibits XBP-1S-mediated transcription by antagonizing PCAF action." Oncotarget **6**(1): 271-287.

Li, H.-R., W.-C. Chiang, P.-C. Chou, W.-J. Wang and J.-r. Huang (2018). "TAR DNA-binding protein 43 (TDP-43) liquid-liquid phase separation is mediated by just a few aromatic residues." Journal of Biological Chemistry.

Li, M., C. L. Brooks, F. Wu-Baer, D. Chen, R. Baer and W. Gu (2003). "Mono- versus polyubiquitination: differential control of p53 fate by Mdm2." Science **302**(5652): 1972-1975.

Liachko, N. F., C. R. Guthrie and B. C. Kraemer (2010). "Phosphorylation promotes neurotoxicity in a Caenorhabditis elegans model of TDP-43 proteinopathy." J Neurosci **30**(48): 16208-16219.

Lichten, C. A., R. White, I. B. Clark and P. S. Swain (2014). "Unmixing of fluorescence spectra to resolve quantitative time-series measurements of gene expression in plate readers." BMC Biotechnol **14**: 11.

Lin, K. P., P. C. Tsai, Y. C. Liao, W. T. Chen, C. P. Tsai, B. W. Soong and Y. C. Lee (2015). "Mutational analysis of MATR3 in Taiwanese patients with amyotrophic lateral sclerosis." Neurobiol Aging **36**(5): 2005.e2001-2004.

Lin, M. T., D. K. Simon, C. H. Ahn, L. M. Kim and M. F. Beal (2002). "High aggregate burden of somatic mtDNA point mutations in aging and Alzheimer's disease brain." Hum Mol Genet **11**(2): 133-145.

Linnane, A. W., S. Marzuki, T. Ozawa and M. Tanaka (1989). "Mitochondrial DNA mutations as an important contributor to ageing and degenerative diseases." Lancet **1**(8639): 642-645.

Liu-Yesucevitz, L., A. Bilgutay, Y. J. Zhang, T. Vanderweyde, A. Citro, T. Mehta, N. Zaarur, A. McKee, R. Bowser, M. Sherman, L. Petrucelli and B. Wolozin (2010). "Tar DNA binding protein-43 (TDP-43) associates with stress granules: analysis of cultured cells and pathological brain tissue." PLoS One **5**(10): e13250.

Liu, H.-Y. and C. M. Pfleger (2013). "Mutation in E1, the Ubiquitin Activating Enzyme, Reduces Drosophila Lifespan and Results in Motor Impairment." PLOS ONE **8**(1): e32835.

Liu, K., A. Tedeschi, K. K. Park and Z. He (2011). "Neuronal intrinsic mechanisms of axon regeneration." Annu Rev Neurosci **34**: 131-152.

Liu, Q., U. Fischer, F. Wang and G. Dreyfuss (1997). "The spinal muscular atrophy disease gene product, SMN, and its associated protein SIP1 are in a complex with spliceosomal snRNP proteins." Cell **90**(6): 1013-1021.

Liu, Y. C., P. M. Chiang and K. J. Tsai (2013). "Disease animal models of TDP-43 proteinopathy and their pre-clinical applications." Int J Mol Sci **14**(10): 20079-20111.

Llorens-Martín, M., J. Jurado, F. Hernández and J. Avila (2014). "GSK-3β, a pivotal kinase in Alzheimer disease." Front Mol Neurosci **7**: 46.

Loewen, C. J. and T. P. Levine (2005). "A highly conserved binding site in vesicle-associated membrane protein-associated protein (VAP) for the FFAT motif of lipid-binding proteins." J Biol Chem **280**(14): 14097-14104.

Lopez-Buesa, P., C. Pfund and E. A. Craig (1998). "The biochemical properties of the ATPase activity of a 70-kDa heat shock protein (Hsp70) are governed by the C-terminal domains." Proc Natl Acad Sci U S A **95**(26): 15253-15258.

Lucero, P., É. Peñalver, L. Vela and R. Lagunas (2000). "Monoubiquitination Is Sufficient To Signal Internalization of the Maltose Transporter in Saccharomyces cerevisiae." Journal of Bacteriology **182**(1): 241-243.

Lynch-Day, M. A., D. Bhandari, S. Menon, J. Huang, H. Cai, C. R. Bartholomew, J. H. Brumell, S. Ferro-Novick and D. J. Klionsky (2010). "Trs85 directs a Ypt1 GEF, TRAPPIII, to the phagophore to promote autophagy." Proc Natl Acad Sci U S A **107**(17): 7811-7816.

Mabb, A. M. and M. D. Ehlers (2010). "Ubiquitination in postsynaptic function and plasticity." Annu Rev Cell Dev Biol **26**: 179-210.

Mackenzie, I. R., O. Ansorge, M. Strong, J. Bilbao, L. Zinman, L. C. Ang, M. Baker, H. Stewart, A. Eisen, R. Rademakers and M. Neumann (2011). "Pathological heterogeneity in amyotrophic lateral sclerosis with FUS mutations: two distinct patterns correlating with disease severity and mutation." Acta Neuropathol **122**(1): 87-98.

Mackenzie, I. R., E. H. Bigio, P. G. Ince, F. Geser, M. Neumann, N. J. Cairns, L. K. Kwong, M. S. Forman, J. Ravits, H. Stewart, A. Eisen, L. McClusky, H. A. Kretzschmar, C. M. Monoranu, J. R. Highley, J. Kirby, T. Siddique, P. J. Shaw, V. M. Lee and J. Q. Trojanowski (2007). "Pathological TDP-43 distinguishes sporadic amyotrophic lateral sclerosis from amyotrophic lateral sclerosis with SOD1 mutations." Ann Neurol **61**(5): 427-434.

Mackenzie, I. R., A. M. Nicholson, M. Sarkar, J. Messing, M. D. Purice, C. Pottier, K. Annu, M. Baker, R. B. Perkerson, A. Kurti, B. J. Matchett, T. Mittag, J. Temirov, G. R. Hsiung, C. Krieger, M. E. Murray, M. Kato, J. D. Fryer, L. Petrucelli, L. Zinman, S. Weintraub, M. Mesulam, J. Keith, S. A. Zivkovic, V. Hirsch-Reinshagen, R. P. Roos, S. Zuchner, N. R. Graff-Radford, R. C. Petersen, R. J. Caselli, Z. K. Wszolek, E. Finger, C. Lippa, D. Lacomis, H. Stewart, D. W. Dickson, H. J. Kim, E. Rogaeva, E. Bigio, K. B. Boylan, J. P. Taylor and R. Rademakers (2017). "TIA1 Mutations in Amyotrophic Lateral Sclerosis and Frontotemporal Dementia Promote Phase Separation and Alter Stress Granule Dynamics." Neuron **95**(4): 808-816.e809.

Maduro, M. and D. Pilgrim (1995). "Identification and cloning of unc-119, a gene expressed in the Caenorhabditis elegans nervous system." Genetics **141**(3): 977-988.

Majounie, E., A. E. Renton, K. Mok, E. G. Dopper, A. Waite, S. Rollinson, A. Chio, G. Restagno, N. Nicolaou, J. Simon-Sanchez, J. C. van Swieten, Y. Abramzon, J. O. Johnson, M. Sendtner, R. Pamphlett, R. W. Orrell, S. Mead, K. C. Sidle, H. Houlden, J. D. Rohrer, K. E. Morrison, H. Pall, K. Talbot, O. Ansorge, D. G. Hernandez, S. Arepalli, M. Sabatelli, G. Mora, M. Corbo, F. Giannini, A. Calvo, E. Englund, G. Borghero, G. L. Floris, A. M. Remes, H. Laaksovirta, L. McCluskey, J. Q. Trojanowski, V. M. Van Deerlin, G. D. Schellenberg, M. A. Nalls, V. E. Drory, C. S. Lu, T. H. Yeh, H. Ishiura, Y. Takahashi, S. Tsuji, I. Le Ber, A. Brice, C. Drepper, N. Williams, J. Kirby, P. Shaw, J. Hardy, P. J. Tienari, P. Heutink, H. R. Morris, S. Pickering-Brown and B. J. Traynor (2012). "Frequency of the C9orf72 hexanucleotide repeat expansion in patients with amyotrophic lateral sclerosis and frontotemporal dementia: a cross-sectional study." Lancet Neurol **11**(4): 323-330.

Manford, A. G., C. J. Stefan, H. L. Yuan, J. A. Macgurn and S. D. Emr (2012). "ER-to-plasma membrane tethering proteins regulate cell signaling and ER morphology." Dev Cell **23**(6): 1129-1140.

Mangus, D. A., N. Amrani and A. Jacobson (1998). "Pbp1p, a factor interacting with Saccharomyces cerevisiae poly(A)-binding protein, regulates polyadenylation." Mol Cell Biol **18**(12): 7383-7396.

Mann, D. M., S. Rollinson, A. Robinson, J. Bennion Callister, J. C. Thompson, J. S. Snowden, T. Gendron, L. Petrucelli, M. Masuda-Suzukake, M. Hasegawa, Y. Davidson and S. Pickering-Brown (2013). "Dipeptide repeat proteins are present in the p62 positive inclusions in patients with frontotemporal lobar degeneration and motor neurone disease associated with expansions in C9ORF72." Acta Neuropathol Commun **1**: 68.

Mann, J. R., A. M. Gleixner, J. C. Mauna, E. Gomes, M. R. DeChellis-Marks, P. G. Needham, K. E. Copley, B. Hurtle, B. Portz, N. J. Pyles, L. Guo, C. B. Calder, Z. P. Wills, U. B. Pandey, J. K. Kofler, J. L. Brodsky, A. Thathiah, J. Shorter and C. J. Donnelly (2019). "RNA Binding Antagonizes Neurotoxic Phase Transitions of TDP-43." Neuron **102**(2): 321-338.e328.

Margottin-Goguet, F., J. Y. Hsu, A. Loktev, H. M. Hsieh, J. D. Reimann and P. K. Jackson (2003). "Prophase destruction of Emi1 by the SCF(betaTrCP/Slimb) ubiquitin ligase activates the anaphase promoting complex to allow progression beyond prometaphase." Dev Cell **4**(6): 813-826.

Marko, M., A. Vlassis, A. Guialis and M. Leichter (2012). "Domains involved in TAF15 subcellular localisation: dependence on cell type and ongoing transcription." Gene **506**(2): 331-338.

Martin, L. J. (2008). "DNA damage and repair: relevance to mechanisms of neurodegeneration." J Neuropathol Exp Neurol **67**(5): 377-387.

Maruyama, H., H. Morino, H. Ito, Y. Izumi, H. Kato, Y. Watanabe, Y. Kinoshita, M. Kamada, H. Nodera, H. Suzuki, O. Komure, S. Matsuura, K. Kobatake, N. Morimoto, K. Abe, N. Suzuki, M. Aoki, A. Kawata, T. Hirai, T. Kato, K. Ogasawara, A. Hirano, T. Takumi, H. Kusaka, K. Hagiwara, R. Kaji and H. Kawakami (2010). "Mutations of optineurin in amyotrophic lateral sclerosis." Nature **465**(7295): 223-226.

Massey, A. C., R. Kiffin and A. M. Cuervo (2006). "Autophagic defects in aging: looking for an "emergency exit"?" Cell Cycle **5**(12): 1292-1296.

Matiuhin, Y., D. S. Kirkpatrick, I. Ziv, W. Kim, A. Dakshinamurthy, O. Kleifeld, S. P. Gygi, N. Reis and M. H. Glickman (2008). "Extraproteasomal Rpn10 restricts access of the polyubiquitin-binding protein Dsk2 to proteasome." Mol Cell **32**(3): 415-425.

Matsumoto, G., S. Kim and R. I. Morimoto (2006). "Huntingtin and mutant SOD1 form aggregate structures with distinct molecular properties in human cells." J Biol Chem **281**(7): 4477-4485.

Matsumoto, G., A. Stojanovic, C. I. Holmberg, S. Kim and R. I. Morimoto (2005). "Structural properties and neuronal toxicity of amyotrophic lateral sclerosis–associated Cu/Zn superoxide dismutase 1 aggregates." J Cell Biol **171**(1): 75-85.

Matunis, M. J., E. L. Matunis, G. Dreyfuss (1993). “PUB1: a major yeast poly(A)+ RNA-binding protein.” Mol Cell Biol **13**(10):6114-23.

May, S., D. Hornburg, M. H. Schludi, T. Arzberger, K. Rentzsch, B. M. Schwenk, F. A. Grasser, K. Mori, E. Kremmer, J. Banzhaf-Strathmann, M. Mann, F. Meissner and D. Edbauer (2014). "C9orf72 FTLD/ALS-associated Gly-Ala dipeptide repeat proteins cause neuronal toxicity and Unc119 sequestration." Acta Neuropathol **128**(4): 485-503.

McAlary, L., J. A. Aquilina and J. J. Yerbury (2016). "Susceptibility of Mutant SOD1 to Form a Destabilized Monomer Predicts Cellular Aggregation and Toxicity but Not In vitro Aggregation Propensity." Frontiers in Neuroscience **10**(499).

McCord, J. M. and I. Fridovich (1969). "Superoxide dismutase. An enzymic function for erythrocuprein (hemocuprein)." J Biol Chem **244**(22): 6049-6055.

McDonald, K. K., A. Aulas, L. Destroismaisons, S. Pickles, E. Beleac, W. Camu, G. A. Rouleau and C. Vande Velde (2011). "TAR DNA-binding protein 43 (TDP-43) regulates stress granule dynamics via differential regulation of G3BP and TIA-1." Hum Mol Genet **20**(7): 1400-1410.

McKinnon, P. J. (2009). "DNA repair deficiency and neurological disease." Nat Rev Neurosci **10**(2): 100-112.

Medicherla, B., Z. Kostova, A. Schaefer and D. H. Wolf (2004). "A genomic screen identifies Dsk2p and Rad23p as essential components of ER-associated degradation." EMBO Rep **5**(7): 692-697.

Mercado, P. A., Y. M. Ayala, M. Romano, E. Buratti and F. E. Baralle (2005). "Depletion of TDP 43 overrides the need for exonic and intronic splicing enhancers in the human apoA-II gene." Nucleic Acids Research **33**(18): 6000-6010.

Meyer, H., M. Bug and S. Bremer (2012). "Emerging functions of the VCP/p97 AAA-ATPase in the ubiquitin system." Nature Cell Biology **14**: 117.

Mi, H., A. Muruganujan, D. Ebert, X. Huang and P. D. Thomas (2019). "PANTHER version 14: more genomes, a new PANTHER GO-slim and improvements in enrichment analysis tools." Nucleic Acids Res **47**(D1): D419-d426.

Michael, D. and M. Oren (2003). "The p53–Mdm2 module and the ubiquitin system." Seminars in Cancer Biology **13**(1): 49-58.

Michikawa, Y., F. Mazzucchelli, N. Bresolin, G. Scarlato and G. Attardi (1999). "Aging-dependent large accumulation of point mutations in the human mtDNA control region for replication." Science **286**(5440): 774-779.

Migheli, A., T. Pezzulo, A. Attanasio and D. Schiffer (1993). "Peripherin immunoreactive structures in amyotrophic lateral sclerosis." Lab Invest **68**(2): 185-191.

Mimnaugh, E. G., H. Y. Chen, J. R. Davie, J. E. Celis and L. Neckers (1997). "Rapid deubiquitination of nucleosomal histones in human tumor cells caused by proteasome inhibitors and stress response inducers: effects on replication, transcription, translation, and the cellular stress response." Biochemistry **36**(47): 14418-14429.

Miyazaki, K., T. Fujita, T. Ozaki, C. Kato, Y. Kurose, M. Sakamoto, S. Kato, T. Goto, Y. Itoyama, M. Aoki and A. Nakagawara (2004). "NEDL1, a novel ubiquitin-protein isopeptide ligase for dishevelled-1, targets mutant superoxide dismutase-1." J Biol Chem **279**(12): 11327-11335.

Mizuno, Y., M. Amari, M. Takatama, H. Aizawa, B. Mihara and K. Okamoto (2006). "Immunoreactivities of p62, an ubiqutin-binding protein, in the spinal anterior horn cells of patients with amyotrophic lateral sclerosis." J Neurol Sci **249**(1): 13-18.

Mizuno, Y., S. Hori, A. Kakizuka and K. Okamoto (2003). "Vacuole-creating protein in neurodegenerative diseases in humans." Neurosci Lett **343**(2): 77-80.

Moisse, K., J. Mepham, K. Volkening, I. Welch, T. Hill and M. J. Strong (2009). "Cytosolic TDP-43 expression following axotomy is associated with caspase 3 activation in NFL-/- mice: support for a role for TDP-43 in the physiological response to neuronal injury." Brain Res **1296**: 176-186.

Moisse, K., K. Volkening, C. Leystra-Lantz, I. Welch, T. Hill and M. J. Strong (2009). "Divergent patterns of cytosolic TDP-43 and neuronal progranulin expression following axotomy: implications for TDP-43 in the physiological response to neuronal injury." Brain Res **1249**: 202-211.

Monia, B. P., D. J. Ecker, S. Jonnalagadda, J. Marsh, L. Gotlib, T. R. Butt and S. T. Crooke (1989). "Gene synthesis, expression, and processing of human ubiquitin carboxyl extension proteins." J Biol Chem **264**(7): 4093-4103.

Montibeller, L. and J. de Belleroche (2018). "Amyotrophic lateral sclerosis (ALS) and Alzheimer's disease (AD) are characterised by differential activation of ER stress pathways: focus on UPR target genes." Cell Stress Chaperones **23**(5): 897-912.

Mori, K., T. Arzberger, F. A. Grasser, I. Gijselinck, S. May, K. Rentzsch, S. M. Weng, M. H. Schludi, J. van der Zee, M. Cruts, C. Van Broeckhoven, E. Kremmer, H. A. Kretzschmar, C.

Haass and D. Edbauer (2013). "Bidirectional transcripts of the expanded C9orf72 hexanucleotide repeat are translated into aggregating dipeptide repeat proteins." Acta Neuropathol **126**(6): 881-893.

Mori, K., T. Kawahara, H. Yoshida, H. Yanagi and T. Yura (1996). "Signalling from endoplasmic reticulum to nucleus: transcription factor with a basic-leucine zipper motif is required for the unfolded protein-response pathway." Genes to Cells **1**(9): 803-817.

Mori, K., S. M. Weng, T. Arzberger, S. May, K. Rentzsch, E. Kremmer, B. Schmid, H. A. Kretzschmar, M. Cruts, C. Van Broeckhoven, C. Haass and D. Edbauer (2013). "The C9orf72 GGGGCC repeat is translated into aggregating dipeptide-repeat proteins in FTLD/ALS." Science **339**(6125): 1335-1338.

Morimoto, R. I. (2008). "Proteotoxic stress and inducible chaperone networks in neurodegenerative disease and aging." Genes Dev **22**(11): 1427-1438.

Moudry, P., C. Lukas, L. Macurek, H. Hanzlikova, Z. Hodny, J. Lukas and J. Bartek (2012). "Ubiquitin-activating enzyme UBA1 is required for cellular response to DNA damage." Cell Cycle **11**(8): 1573-1582.

Mrowka, R., N. Bluthgen and M. Fahling (2008). "Seed-based systematic discovery of specific transcription factor target genes." Febs j **275**(12): 3178-3192.

Mukherjee, D., M. Gao, J. P. O'Connor, R. Raijmakers, G. Pruijn, C. S. Lutz and J. Wilusz (2002). "The mammalian exosome mediates the efficient degradation of mRNAs that contain AU-rich elements." Embo j **21**(1-2): 165-174.

Munch, C., J. O'Brien and A. Bertolotti (2011). "Prion-like propagation of mutant superoxide dismutase-1 misfolding in neuronal cells." Proc Natl Acad Sci U S A **108**.

Muratani, M. and W. P. Tansey (2003). "How the ubiquitin-proteasome system controls transcription." Nat Rev Mol Cell Biol **4**(3): 192-201.

N'Diaye, E. N., J. Debnath and E. J. Brown (2009). "Ubiquilins accelerate autophagosome maturation and promote cell survival during nutrient starvation." Autophagy **5**(4): 573-575.

Nagai, M., M. Aoki, I. Miyoshi, M. Kato, P. Pasinelli, N. Kasai, R. H. Brown, Jr. and Y. Itoyama (2001). "Rats expressing human cytosolic copper-zinc superoxide dismutase transgenes with amyotrophic lateral sclerosis: associated mutations develop motor neuron disease." J Neurosci **21**(23): 9246-9254.

Nagarajan, S. R., A. E. Brandon, J. A. McKenna, H. C. Shtein, T. Q. Nguyen, E. Suryana, P. Poronnik, G. J. Cooney, D. N. Saunders and A. J. Hoy (2017). "Insulin and diet-induced changes in the ubiquitin-modified proteome of rat liver." PLoS One **12**(3): e0174431.

Nakaso, K., Y. Yoshimoto, T. Nakano, T. Takeshima, Y. Fukuhara, K. Yasui, S. Araga, T. Yanagawa, T. Ishii and K. Nakashima (2004). "Transcriptional activation of p62/A170/ZIP during the formation of the aggregates: possible mechanisms and the role in Lewy body formation in Parkinson's disease." Brain Res **1012**(1-2): 42-51.

Nakatsu, F., M. Sakuma, Y. Matsuo, H. Arase, S. Yamasaki, N. Nakamura, T. Saito and H. Ohno (2000). "A Di-leucine signal in the ubiquitin moiety. Possible involvement in ubiquitination-mediated endocytosis." J Biol Chem **275**(34): 26213-26219.

Nakaya, T., P. Alexiou, M. Maragkakis, A. Chang and Z. Mourelatos (2013). "FUS regulates genes coding for RNA-binding proteins in neurons by binding to their highly conserved introns." Rna **19**(4): 498-509.

Nathan, D. F., M. H. Vos and S. Lindquist (1997). "In vivo functions of the Saccharomyces cerevisiae Hsp90 chaperone." Proc Natl Acad Sci U S A **94**(24): 12949-12956.

Naumann, M., A. Pal, A. Goswami, X. Lojewski, J. Japtok, A. Vehlow, M. Naujock, R. Gunther, M. Jin, N. Stanslowsky, P. Reinhardt, J. Sterneckert, M. Frickenhaus, F. Pan-Montojo, E. Storkebaum, I. Poser, A. Freischmidt, J. H. Weishaupt, K. Holzmann, D. Troost, A. C. Ludolph, T. M. Boeckers, S. Liebau, S. Petri, N. Cordes, A. A. Hyman, F. Wegner, S.

W. Grill, J. Weis, A. Storch and A. Hermann (2018). "Impaired DNA damage response signaling by FUS-NLS mutations leads to neurodegeneration and FUS aggregate formation." Nat Commun **9**(1): 335.

Nelson, J. S. and A. L. Prensky (1972). "Sporadic juvenile amyotrophic lateral sclerosis. A clinicopathological study of a case with neuronal cytoplasmic inclusions containing RNA." Arch Neurol **27**(4): 300-306.

Nelson, R. J., T. Ziegelhoffer, C. Nicolet, M. Werner-Washburne and E. A. Craig (1992). "The translation machinery and 70 kd heat shock protein cooperate in protein synthesis." Cell **71**(1): 97-105.

Neumann, M., L. K. Kwong, E. B. Lee, E. Kremmer, A. Flatley, Y. Xu, M. S. Forman, D. Troost, H. A. Kretzschmar, J. Q. Trojanowski and V. M. Lee (2009). "Phosphorylation of S409/410 of TDP-43 is a consistent feature in all sporadic and familial forms of TDP-43 proteinopathies." Acta Neuropathol **117**(2): 137-149.

Neumann, M., I. R. Mackenzie, N. J. Cairns, P. J. Boyer, W. R. Markesbery, C. D. Smith, J. P. Taylor, H. A. Kretzschmar, V. E. Kimonis and M. S. Forman (2007). "TDP-43 in the ubiquitin pathology of frontotemporal dementia with VCP gene mutations." J Neuropathol Exp Neurol **66**(2): 152-157.

Neumann, M., R. Rademakers, S. Roeber, M. Baker, H. A. Kretzschmar and I. R. Mackenzie (2009). "A new subtype of frontotemporal lobar degeneration with FUS pathology." Brain **132**(Pt 11): 2922-2931.

Neumann, M., D. M. Sampathu, L. K. Kwong, A. C. Truax, M. C. Micsenyi, T. T. Chou, J. Bruce, T. Schuck, M. Grossman, C. M. Clark, L. F. McCluskey, B. L. Miller, E. Masliah, I. R. Mackenzie, H. Feldman, W. Feiden, H. A. Kretzschmar, J. Q. Trojanowski and V. M. Lee (2006). "Ubiquitinated TDP-43 in frontotemporal lobar degeneration and amyotrophic lateral sclerosis." Science **314**(5796): 130-133.

Newman, J. R., S. Ghaemmaghami, J. Ihmels, D. K. Breslow, M. Noble, J. L. DeRisi and J. S. Weissman (2006). "Single-cell proteomic analysis of S. cerevisiae reveals the architecture of biological noise." Nature **441**(7095): 840-846.

Nguyen, H. P., C. Van Broeckhoven, J. Van der Zee (2018). "ALS Genes in the Genomic Era and their Implications for FTD." Trends Genet. **34**(6):404-423.

Nie, M., A. Aslanian, J. Prudden, J. Heideker, A. A. Vashisht, J. A. Wohlschlegel, J. R. Yates, 3rd and M. N. Boddy (2012). "Dual recruitment of Cdc48 (p97)-Ufd1-Npl4 ubiquitin-selective segregase by small ubiquitin-like modifier protein (SUMO) and ubiquitin in SUMO-targeted ubiquitin ligase-mediated genome stability functions." J Biol Chem **287**(35): 29610-29619.

Nijman, S. M., M. P. Luna-Vargas, A. Velds, T. R. Brummelkamp, A. M. Dirac, T. K. Sixma and R. Bernards (2005). "A genomic and functional inventory of deubiquitinating enzymes." Cell **123**(5): 773-786.

Nimmesgern, E. and F. U. Hartl (1993). "ATP-dependent protein refolding activity in reticulocyte lysate. Evidence for the participation of different chaperone components." FEBS Lett **331**(1-2): 25-30.

Nishida, C. R., E. B. Gralla and J. S. Valentine (1994). "Characterization of three yeast copper-zinc superoxide dismutase mutants analogous to those coded for in familial amyotrophic lateral sclerosis." Proc Natl Acad Sci U S A **91**(21): 9906-9910.

Nishimura, A. L., M. Mitne-Neto, H. C. A. Silva, J. R. M. Oliveira, M. Vainzof and M. Zatz (2004). "A novel locus for late onset amyotrophic lateral sclerosis/motor neurone disease variant at 20q13." Journal of Medical Genetics **41**(4): 315-320.

Nishimura, A. L., M. Mitne-Neto, H. C. A. Silva, A. Richieri-Costa, S. Middleton, D. Cascio, F. Kok, J. R. M. Oliveira, T. Gillingwater, J. Webb, P. Skehel and M. Zatz (2004). "A Mutation in the Vesicle-Trafficking Protein VAPB Causes Late-Onset Spinal Muscular Atrophy and Amyotrophic Lateral Sclerosis." American Journal of Human Genetics **75**(5): 822-831.

Nishimura, Y., M. Hayashi, H. Inada and T. Tanaka (1999). "Molecular cloning and characterization of mammalian homologues of vesicle-associated membrane protein-associated (VAMP-associated) proteins." Biochem Biophys Res Commun **254**(1): 21-26.

Niu, C., J. Zhang, F. Gao, L. Yang, M. Jia, H. Zhu and W. Gong (2012). "FUS-NLS/Transportin 1 complex structure provides insights into the nuclear targeting mechanism of FUS and the implications in ALS." PLoS One **7**(10): e47056.

Nolan, T. M., B. Brennan, M. Yang, J. Chen, M. Zhang, Z. Li, X. Wang, D. C. Bassham, J. Walley and Y. Yin (2017). "Selective Autophagy of BES1 Mediated by DSK2 Balances Plant Growth and Survival." Dev Cell **41**(1): 33-46.e37.

Oda, M., N. Akagawa, Y. Tabuchi and H. Tanabe (1978). "A sporadic juvenile case of the amyotrophic lateral sclerosis with neuronal intracytoplasmic inclusions." Acta Neuropathol **44**(3): 211-216.

Oh, C., S. Park, E. K. Lee and Y. J. Yoo (2013). "Downregulation of ubiquitin level via knockdown of polyubiquitin gene Ubb as potential cancer therapeutic intervention." Sci Rep **3**: 2623.

Okamoto, K., S. Hirai, M. Amari, M. Watanabe and A. Sakurai (1993). "Bunina bodies in amyotrophic lateral sclerosis immunostained with rabbit anti-cystatin C serum." Neurosci Lett **162**(1-2): 125-128.

Onesto, E., P. Rusmini, V. Crippa, N. Ferri, A. Zito, M. Galbiati and A. Poletti (2011). "Muscle cells and motoneurons differentially remove mutant SOD1 causing familial amyotrophic lateral sclerosis." Journal of Neurochemistry **118**(2): 266-280.

Osawa, T., Y. Mizuno, Y. Fujita, M. Takatama, Y. Nakazato and K. Okamoto (2011). "Optineurin in neurodegenerative diseases." Neuropathology **31**(6): 569-574.

Ott, D. E., L. V. Coren, T. D. Copeland, B. P. Kane, D. G. Johnson, R. C. Sowder, 2nd, Y. Yoshinaka, S. Oroszlan, L. O. Arthur and L. E. Henderson (1998). "Ubiquitin is covalently attached to the p6Gag proteins of human immunodeficiency virus type 1 and simian immunodeficiency virus and to the p12Gag protein of Moloney murine leukemia virus." J Virol **72**(4): 2962-2968.

Outeiro, T. F. and S. Lindquist (2003). "Yeast cells provide insight into alpha-synuclein biology and pathobiology." Science **302**(5651): 1772-1775.

Outeiro, T. F. and P. J. Muchowski (2004). "Molecular genetics approaches in yeast to study amyloid diseases." J Mol Neurosci **23**(1-2): 49-60.

Oyanagi, K., M. Yamazaki, H. Takahashi, K. Watabe, M. Wada, T. Komori, T. Morita and T. Mizutani (2008). "Spinal anterior horn cells in sporadic amyotrophic lateral sclerosis show ribosomal detachment from, and cisternal distention of the rough endoplasmic reticulum." Neuropathol Appl Neurobiol **34**(6): 650-658.

Padmanabhan, N., L. Fichtner, A. Dickmanns, R. Ficner, J. B. Schulz and G. H. Braus (2009). "The yeast HtrA orthologue Ynm3 is a protease with chaperone activity that aids survival under heat stress." Mol Biol Cell **20**(1): 68-77.

Palombella, V. J., O. J. Rando, A. L. Goldberg and T. Maniatis (1994). "The ubiquitin-proteasome pathway is required for processing the NF-kappa B1 precursor protein and the activation of NF-kappa B." Cell **78**(5): 773-785.

Pamphlett, R., N. Luquin, C. McLean, S. K. Jew and L. Adams (2009). "TDP-43 neuropathology is similar in sporadic amyotrophic lateral sclerosis with or without TDP-43 mutations." Neuropathol Appl Neurobiol **35**(2): 222-225.

Papiani, G., A. Ruggiano, M. Fossati, A. Raimondi, G. Bertoni, M. Francolini, R. Benfante, F. Navone and N. Borgese (2012). "Restructured endoplasmic reticulum generated by mutant

amyotrophic lateral sclerosis-linked VAPB is cleared by the proteasome." J Cell Sci **125**(Pt 15): 3601-3611.

Parker, R. and H. Song (2004). "The enzymes and control of eukaryotic mRNA turnover." Nat Struct Mol Biol **11**(2): 121-127.

Parker, S. J., J. Meyerowitz, J. L. James, J. R. Liddell, P. J. Crouch, K. M. Kanninen and A. R. White (2012). "Endogenous TDP-43 localized to stress granules can subsequently form protein aggregates." Neurochem Int **60**(4): 415-424.

Pasinelli, P. and R. H. Brown (2006). "Molecular biology of amyotrophic lateral sclerosis: insights from genetics." Nat Rev Neurosci **7**.

Patnaik, A., V. Chau and J. W. Wills (2000). "Ubiquitin is part of the retrovirus budding machinery." Proc Natl Acad Sci U S A **97**(24): 13069-13074.

Pellizzoni, L., N. Kataoka, B. Charroux and G. Dreyfuss (1998). "A novel function for SMN, the spinal muscular atrophy disease gene product, in pre-mRNA splicing." Cell **95**(5): 615-624.

Pelzer, C., I. Kassner, K. Matentzoglu, R. K. Singh, H. P. Wollscheid, M. Scheffner, G. Schmidtke and M. Groettrup (2007). "UBE1L2, a novel E1 enzyme specific for ubiquitin." J Biol Chem **282**(32): 23010-23014.

Peng, J., D. Schwartz, J. E. Elias, C. C. Thoreen, D. Cheng, G. Marsischky, J. Roelofs, D. Finley and S. P. Gygi (2003). "A proteomics approach to understanding protein ubiquitination." Nat Biotechnol **21**(8): 921-926.

Peters, O. M., G. T. Cabrera, H. Tran, T. F. Gendron, J. E. McKeon, J. Metterville, A. Weiss, N. Wightman, J. Salameh, J. Kim, H. Sun, K. B. Boylan, D. Dickson, Z. Kennedy, Z. Lin, Y. J. Zhang, L. Daughrity, C. Jung, F. B. Gao, P. C. Sapp, H. R. Horvitz, D. A. Bosco, S. P. Brown, P. de Jong, L. Petrucelli, C. Mueller and R. H. Brown, Jr. (2015). "Human C9ORF72

Hexanucleotide Expansion Reproduces RNA Foci and Dipeptide Repeat Proteins but Not Neurodegeneration in BAC Transgenic Mice." Neuron **88**(5): 902-909.

Pfleger, C. M., K. F. Harvey, H. Yan and I. K. Hariharan (2007). "Mutation of the gene encoding the ubiquitin activating enzyme ubal causes tissue overgrowth in Drosophila." Fly (Austin) **1**(2): 95-105.

Pfund, C., P. Huang, N. Lopez-Hoyo and E. A. Craig (2001). "Divergent functional properties of the ribosome-associated molecular chaperone Ssb compared with other Hsp70s." Mol Biol Cell **12**(12): 3773-3782.

Pfund, C., N. Lopez-Hoyo, T. Ziegelhoffer, B. A. Schilke, P. Lopez-Buesa, W. A. Walter, M. Wiedmann and E. A. Craig (1998). "The molecular chaperone Ssb from Saccharomyces cerevisiae is a component of the ribosome-nascent chain complex." Embo j **17**(14): 3981-3989.

Picard, D. (2002). "Heat-shock protein 90, a chaperone for folding and regulation." Cell Mol Life Sci **59**(10): 1640-1648.

Picher-Martel, V., P. N. Valdmanis, P. V. Gould, J. P. Julien and N. Dupre (2016). "From animal models to human disease: a genetic approach for personalized medicine in ALS." Acta Neuropathol Commun **4**(1): 70.

Pickart, C. M. and I. A. Rose (1985). "Functional heterogeneity of ubiquitin carrier proteins." J Biol Chem **260**(3): 1573-1581.

Pikkarainen, M., P. Hartikainen and I. Alafuzoff (2008). "Neuropathologic features of frontotemporal lobar degeneration with ubiquitin-positive inclusions visualized with ubiquitin-binding protein p62 immunohistochemistry." J Neuropathol Exp Neurol **67**(4): 280-298.

Pokrishevsky, E., L. I. Grad, M. Yousefi, J. Wang, I. R. Mackenzie and N. R. Cashman (2012). "Aberrant localization of FUS and TDP43 is associated with misfolding of SOD1 in amyotrophic lateral sclerosis." PLoS One **7**(4): e35050.

Pokrishevsky, E., L. McAlary, N. E. Farrawell, B. Zhao, M. Sher, J. J. Yerbury and N. R. Cashman (2018). "Tryptophan 32-mediated SOD1 aggregation is attenuated by pyrimidine-like compounds in living cells." Scientific Reports **8**(1): 15590.

Polling, S., Y. F. Mok, Y. M. Ramdzan, B. J. Turner, J. J. Yerbury, A. F. Hill and D. M. Hatters (2014). "Misfolded polyglutamine, polyalanine, and superoxide dismutase 1 aggregate via distinct pathways in the cell." J Biol Chem **289**(10): 6669-6680.

Polymenidou, M., C. Lagier-Tourenne, K. R. Hutt, S. C. Huelga, J. Moran, T. Y. Liang, S. C. Ling, E. Sun, E. Wancewicz, C. Mazur, H. Kordasiewicz, Y. Sedaghat, J. P. Donohue, L. Shiue, C. F. Bennett, G. W. Yeo and D. W. Cleveland (2011). "Long pre-mRNA depletion and RNA missplicing contribute to neuronal vulnerability from loss of TDP-43." Nat Neurosci **14**(4): 459-468.

Popovic, D., D. Vucic and I. Dikic (2014). "Ubiquitination in disease pathogenesis and treatment." Nat Med **20**(11): 1242-1253.

Powis, R. A., E. Karyka, P. Boyd, J. Côme, R. A. Jones, Y. Zheng, E. Szunyogova, E. J. N. Groen, G. Hunter, D. Thomson, T. M. Wishart, C. G. Becker, S. H. Parson, C. Martinat, M. Azzouz and T. H. Gillingwater (2016). "Systemic restoration of UBA1 ameliorates disease in spinal muscular atrophy." JCI Insight **1**(11).

Powis, R. A., C. A. Mutsaers, T. M. Wishart, G. Hunter, B. Wirth and T. H. Gillingwater (2014). "Increased levels of UCHL1 are a compensatory response to disrupted ubiquitin homeostasis in spinal muscular atrophy and do not represent a viable therapeutic target." Neuropathology and Applied Neurobiology **40**(7): 873-887.

Primorac, I. and A. Musacchio (2013). "Panta rhei: the APC/C at steady state." J Cell Biol **201**(2): 177-189.

Proctor, E. A., L. Fee, Y. Tao, R. L. Redler, J. M. Fay, Y. Zhang, Z. Lv, I. P. Mercer, M. Deshmukh, Y. L. Lyubchenko and N. V. Dokholyan (2016). "Nonnative SOD1 trimer is toxic

to motor neurons in a model of amyotrophic lateral sclerosis." Proc Natl Acad Sci U S A **113**(3): 614-619.

Qin, Z., B. Cui, J. Jin, M. Song, B. Zhou, H. Guo, D. Qian, Y. He and L. Huang (2016). "The ubiquitin-activating enzyme E1 as a novel therapeutic target for the treatment of restenosis." Atherosclerosis **247**: 142-153.

Qiu, L., T. Qiao, M. Beers, W. Tan, H. Wang, B. Yang and Z. Xu (2013). "Widespread aggregation of mutant VAPB associated with ALS does not cause motor neuron degeneration or modulate mutant SOD1 aggregation and toxicity in mice." Mol Neurodegener **8**: 1.

Raiborg, C. and H. Stenmark (2009). "The ESCRT machinery in endosomal sorting of ubiquitylated membrane proteins." Nature **458**(7237): 445-452.

Ramser, J., M. E. Ahearn, C. Lenski, K. O. Yariz, H. Hellebrand, M. von Rhein, R. D. Clark, R. K. Schmutzler, P. Lichtner, E. P. Hoffman, A. Meindl and L. Baumbach-Reardon (2008). "Rare Missense and Synonymous Variants in UBE1 Are Associated with X-Linked Infantile Spinal Muscular Atrophy." American Journal of Human Genetics **82**(1): 188-193.

Rao, H. and A. Sastry (2002). "Recognition of specific ubiquitin conjugates is important for the proteolytic functions of the ubiquitin-associated domain proteins Dsk2 and Rad23." J Biol Chem **277**(14): 11691-11695.

Ratnaparkhi, A., G. M. Lawless, F. E. Schweizer, P. Golshani and G. R. Jackson (2008). "A Drosophila model of ALS: human ALS-associated mutation in VAP33A suggests a dominant negative mechanism." PLoS One **3**(6): e2334.

Ravid, T. and M. Hochstrasser (2008). "Diversity of degradation signals in the ubiquitin-proteasome system." Nat Rev Mol Cell Biol **9**(9): 679-690.

Reaume, A. G., J. L. Elliott, E. K. Hoffman, N. W. Kowall, R. J. Ferrante, D. F. Siwek, H. M. Wilcox, D. G. Flood, M. F. Beal, R. H. Brown, Jr., R. W. Scott and W. D. Snider (1996).

"Motor neurons in Cu/Zn superoxide dismutase-deficient mice develop normally but exhibit enhanced cell death after axonal injury." Nat Genet **13**(1): 43-47.

Redler, R. L., L. Fee, J. M. Fay, M. Caplow and N. V. Dokholyan (2014). "Non-native soluble oligomers of Cu/Zn superoxide dismutase (SOD1) contain a conformational epitope linked to cytotoxicity in amyotrophic lateral sclerosis (ALS)." Biochemistry **53**(14): 2423-2432.

Ren, X. and J. H. Hurley (2010). "VHS domains of ESCRT-0 cooperate in high-avidity binding to polyubiquitinated cargo." Embo j **29**(6): 1045-1054.

Renton, Alan E., E. Majounie, A. Waite, J. Simón-Sánchez, S. Rollinson, J R. Gibbs, Jennifer C. Schymick, H. Laaksovirta, John C. van Swieten, L. Myllykangas, H. Kalimo, A. Paetau, Y. Abramzon, Anne M. Remes, A. Kaganovich, Sonja W. Scholz, J. Duckworth, J. Ding, Daniel W. Harmer, Dena G. Hernandez, Janel O. Johnson, K. Mok, M. Ryten, D. Trabzuni, Rita J. Guerreiro, Richard W. Orrell, J. Neal, A. Murray, J. Pearson, Iris E. Jansen, D. Sondervan, H. Seelaar, D. Blake, K. Young, N. Halliwell, Janis B. Callister, G. Toulson, A. Richardson, A. Gerhard, J. Snowden, D. Mann, D. Neary, Michael A. Nalls, T. Peuralinna, L. Jansson, V.-M. Isoviita, A.-L. Kaivorinne, M. Hölttä-Vuori, E. Ikonen, R. Sulkava, M. Benatar, J. Wuu, A. Chiò, G. Restagno, G. Borghero, M. Sabatelli, D. Heckerman, E. Rogaeva, L. Zinman, Jeffrey D. Rothstein, M. Sendtner, C. Drepper, E. E. Eichler, C. Alkan, Z. Abdullaev, Svetlana D. Pack, A. Dutra, E. Pak, J. Hardy, A. Singleton, Nigel M. Williams, P. Heutink, S. Pickering-Brown, Huw R. Morris, Pentti J. Tienari and Bryan J. Traynor (2011). "A Hexanucleotide Repeat Expansion inC9ORF72Is the Cause of Chromosome 9p21-Linked ALS-FTD." Neuron **72**(2): 257-268.

Renton, A. E., A. Chiò, B. J. Traynor (2014). “State of play in amyotrophic lateral sclerosis genetics.” Nat Neurosci.; **17**(1):17-23.

Rezaie, T., A. Child, R. Hitchings, G. Brice, L. Miller, M. Coca-Prados, E. Heon, T. Krupin, R. Ritch, D. Kreutzer, R. P. Crick and M. Sarfarazi (2002). "Adult-onset primary open-angle glaucoma caused by mutations in optineurin." Science **295**(5557): 1077-1079.

Rinetti, G. V. and F. E. Schweizer (2010). "Ubiquitination acutely regulates presynaptic neurotransmitter release in mammalian neurons." J Neurosci **30**(9): 3157-3166.

Ripps, M. E., G. W. Huntley, P. R. Hof, J. H. Morrison and J. W. Gordon (1995). "Transgenic mice expressing an altered murine superoxide dismutase gene provide an animal model of amyotrophic lateral sclerosis." Proc Natl Acad Sci U S A **92**(3): 689-693.

Ritson, G. P., S. K. Custer, B. D. Freibaum, J. B. Guinto, D. Geffel, J. Moore, W. Tang, M. J. Winton, M. Neumann, J. Q. Trojanowski, V. M. Lee, M. S. Forman and J. P. Taylor (2010). "TDP-43 mediates degeneration in a novel Drosophila model of disease caused by mutations in VCP/p97." J Neurosci **30**(22): 7729-7739.

Robberecht, W. and T. Philips (2013). "The changing scene of amyotrophic lateral sclerosis." Nat Rev Neurosci **14**(4): 248-264.

Rogelj, B., L. E. Easton, G. K. Bogu, L. W. Stanton, G. Rot, T. Curk, B. Zupan, Y. Sugimoto, M. Modic, N. Haberman, J. Tollervey, R. Fujii, T. Takumi, C. E. Shaw and J. Ule (2012). "Widespread binding of FUS along nascent RNA regulates alternative splicing in the brain." Sci Rep **2**: 603.

Ron, D. and P. Walter (2007). "Signal integration in the endoplasmic reticulum unfolded protein response." Nat Rev Mol Cell Biol **8**(7): 519-529.

Rosen, D. R., T. Siddique, D. Patterson, D. A. Figlewicz, P. Sapp, A. Hentati, D. Donaldson, J. Goto, J. P. O'Regan, H.-X. Deng, Z. Rahmani, A. Krizus, D. McKenna-Yasek, A. Cayabyab, S. M. Gaston, R. Berger, R. E. Tanzi, J. J. Halperin, B. Herzfeldt, R. Van den Bergh, W.-Y. Hung, T. Bird, G. Deng, D. W. Mulder, C. Smyth, N. G. Laing, E. Soriano, M. A. Pericak-Vance, J. Haines, G. A. Rouleau, J. S. Gusella, H. R. Horvitz and R. H. Brown (1993). "Mutations in Cu/Zn superoxide dismutase gene are associated with familial amyotrophic lateral sclerosis." Nature **362**(6415): 59-62.

Rossoll, W., S. Jablonka, C. Andreassi, A. K. Kroning, K. Karle, U. R. Monani and M. Sendtner (2003). "Smn, the spinal muscular atrophy-determining gene product, modulates axon growth and localization of beta-actin mRNA in growth cones of motoneurons." J Cell Biol **163**(4): 801-812.

Roth, A. F. and N. G. Davis (2000). "Ubiquitination of the PEST-like Endocytosis Signal of the Yeast a-Factor Receptor." Journal of Biological Chemistry **275**(11): 8143-8153.

Rothenberg, C., D. Srinivasan, L. Mah, S. Kaushik, C. M. Peterhoff, J. Ugolino, S. Fang, A. M. Cuervo, R. A. Nixon and M. J. Monteiro (2010). "Ubiquilin functions in autophagy and is degraded by chaperone-mediated autophagy." Hum Mol Genet **19**(16): 3219-3232.

Rotin, D. and S. Kumar (2009). "Physiological functions of the HECT family of ubiquitin ligases." Nat Rev Mol Cell Biol **10**(6): 398-409.

Rousseau, A. and A. Bertolotti (2016). "An evolutionarily conserved pathway controls proteasome homeostasis." Nature **536**(7615): 184-189.

Rowley, N., C. Prip-Buus, B. Westermann, C. Brown, E. Schwarz, B. Barrell, W. Neupert (1994). "Mdj1p, a novel chaperone of the DnaJ family, is involved in mitochondrial biogenesis and protein folding." Cell **77**(2):249-59.

Rubino, E., I. Rainero, A. Chio, E. Rogaeva, D. Galimberti, P. Fenoglio, Y. Grinberg, G. Isaia, A. Calvo, S. Gentile, A. C. Bruni, P. H. St George-Hyslop, E. Scarpini, S. Gallone and L. Pinessi (2012). "SQSTM1 mutations in frontotemporal lobar degeneration and amyotrophic lateral sclerosis." Neurology **79**(15): 1556-1562.

Sacher, M., J. Barrowman, W. Wang, J. Horecka, Y. Zhang, M. Pypaert and S. Ferro-Novick (2001). "TRAPP I implicated in the specificity of tethering in ER-to-Golgi transport." Mol Cell **7**(2): 433-442.

Saeki, Y., A. Saitoh, A. Toh-e and H. Yokosawa (2002). "Ubiquitin-like proteins and Rpn10 play cooperative roles in ubiquitin-dependent proteolysis." Biochem Biophys Res Commun **293**(3): 986-992.

Sahlender, D. A., R. C. Roberts, S. D. Arden, G. Spudich, M. J. Taylor, J. P. Luzio, J. Kendrick-Jones and F. Buss (2005). "Optineurin links myosin VI to the Golgi complex and is involved in Golgi organization and exocytosis." J Cell Biol **169**(2): 285-295.

Sama, R. R., C. L. Ward, L. J. Kaushansky, N. Lemay, S. Ishigaki, F. Urano and D. A. Bosco (2013). "FUS/TLS assembles into stress granules and is a prosurvival factor during hyperosmolar stress." J Cell Physiol **228**(11): 2222-2231.

Sasaki, S. (2010). "Endoplasmic reticulum stress in motor neurons of the spinal cord in sporadic amyotrophic lateral sclerosis." J Neuropathol Exp Neurol **69**(4): 346-355.

Scheffner, M., B. A. Werness, J. M. Huibregtse, A. J. Levine and P. M. Howley (1990). "The E6 oncoprotein encoded by human papillomavirus types 16 and 18 promotes the degradation of p53." Cell **63**(6): 1129-1136.

Schroder, H., T. Langer, F. U. Hartl and B. Bukau (1993). "DnaK, DnaJ and GrpE form a cellular chaperone machinery capable of repairing heat-induced protein damage." Embo j **12**(11): 4137-4144.

Schroder, M. and R. J. Kaufman (2005). "The mammalian unfolded protein response." Annu Rev Biochem **74**: 739-789.

Schulman, B. A. and J. W. Harper (2009). "Ubiquitin-like protein activation by E1 enzymes: the apex for downstream signalling pathways." Nat Rev Mol Cell Biol **10**(5): 319-331.

Schwab, C., T. Arai, M. Hasegawa, S. Yu and P. L. McGeer (2008). "Colocalization of transactivation-responsive DNA-binding protein 43 and huntingtin in inclusions of Huntington disease." J Neuropathol Exp Neurol **67**(12): 1159-1165.

Schwab, M. E. and S. M. Strittmatter (2014). "Nogo limits neural plasticity and recovery from injury." Curr Opin Neurobiol **27**: 53-60.

Schwartz, A. L., J. S. Trausch, A. Ciechanover, J. W. Slot and H. Geuze (1992). "Immunoelectron microscopic localization of the ubiquitin-activating enzyme E1 in HepG2 cells." Proc Natl Acad Sci U S A **89**(12): 5542-5546.

Scotter, E. L., C. Vance, A. L. Nishimura, Y. B. Lee, H. J. Chen, H. Urwin, V. Sardone, J. C. Mitchell, B. Rogelj, D. C. Rubinsztein and C. E. Shaw (2014). "Differential roles of the ubiquitin proteasome system and autophagy in the clearance of soluble and aggregated TDP-43 species." J Cell Sci **127**(Pt 6): 1263-1278.

Seibenhener, M. L., J. R. Babu, T. Geetha, H. C. Wong, N. R. Krishna and M. W. Wooten (2004). "Sequestosome 1/p62 is a polyubiquitin chain binding protein involved in ubiquitin proteasome degradation." Mol Cell Biol **24**(18): 8055-8068.

Seilhean, D., J. Takahashi, K. H. El Hachimi, H. Fujigasaki, A. S. Lebre, V. Biancalana, A. Durr, F. Salachas, J. Hogenhuis, H. de The, J. J. Hauw, V. Meininger, A. Brice and C. Duyckaerts (2004). "Amyotrophic lateral sclerosis with neuronal intranuclear protein inclusions." Acta Neuropathol **108**(1): 81-87.

Sephton, C. F., C. Cenik, A. Kucukural, E. B. Dammer, B. Cenik, Y. Han, C. M. Dewey, F. P. Roth, J. Herz, J. Peng, M. J. Moore and G. Yu (2011). "Identification of neuronal RNA targets of TDP-43-containing ribonucleoprotein complexes." J Biol Chem **286**(2): 1204-1215.

Shatunov, A., K. Mok, S. Newhouse, M. E. Weale, B. Smith, C. Vance, L. Johnson, J. H. Veldink, M. A. van Es, L. H. van den Berg, W. Robberecht, P. Van Damme, O. Hardiman, A. E. Farmer, C. M. Lewis, A. W. Butler, O. Abel, P. M. Andersen, I. Fogh, V. Silani, A. Chio, B. J. Traynor, J. Melki, V. Meininger, J. E. Landers, P. McGuffin, J. D. Glass, H. Pall, P. N. Leigh, J. Hardy, R. H. Brown, Jr., J. F. Powell, R. W. Orrell, K. E. Morrison, P. J. Shaw, C. E. Shaw and A. Al-Chalabi (2010). "Chromosome 9p21 in sporadic amyotrophic lateral sclerosis in the UK and seven other countries: a genome-wide association study." Lancet Neurol **9**(10): 986-994.

Shaw, P. J. (2002). "Toxicity of CSF in motor neurone disease: a potential route to neuroprotection." Brain **125**.

Shen, W.-C., H.-Y. Li, G.-C. Chen, Y. Chern and P.-h. Tu (2015). "Mutations in the ubiquitin-binding domain of OPTN/optineurin interfere with autophagy-mediated degradation of misfolded proteins by a dominant-negative mechanism." Autophagy **11**(4): 685-700.

Sherman, M. Y. and A. L. Goldberg (2001). "Cellular defenses against unfolded proteins: a cell biologist thinks about neurodegenerative diseases." Neuron **29**(1): 15-32.

Sheth, U. and R. Parker (2003). "Decapping and decay of messenger RNA occur in cytoplasmic processing bodies." Science **300**(5620):805-8.

Shibata, N., A. Hirano, M. Kobayashi, S. Sasaki, T. Kato, S. Matsumoto, Z. Shiozawa, T. Komori, A. Ikemoto, T. Umahara and et al. (1994). "Cu/Zn superoxide dismutase-like immunoreactivity in Lewy body-like inclusions of sporadic amyotrophic lateral sclerosis." Neurosci Lett **179**(1-2): 149-152.

Shibata, N., A. Hirano, M. Kobayashi, T. Siddique, H. X. Deng, W. Y. Hung, T. Kato and K. Asayama (1996). "Intense superoxide dismutase-1 immunoreactivity in intracytoplasmic hyaline inclusions of familial amyotrophic lateral sclerosis with posterior column involvement." J Neuropathol Exp Neurol **55**(4): 481-490.

Shibatani, T., M. Nazir and W. F. Ward (1996). "Alteration of rat liver 20S proteasome activities by age and food restriction." J Gerontol A Biol Sci Med Sci **51**(5): B316-322.

Sidrauski, C. and P. Walter (1997). "The transmembrane kinase Ire1p is a site-specific endonuclease that initiates mRNA splicing in the unfolded protein response." Cell **90**(6): 1031-1039.

Sigal, A., T. Danon, A. Cohen, R. Milo, N. Geva-Zatorsky, G. Lustig, Y. Liron, U. Alon and N. Perzov (2007). "Generation of a fluorescently labeled endogenous protein library in living human cells." Nat Protoc **2**(6): 1515-1527.

Sigal, A., R. Milo, A. Cohen, N. Geva-Zatorsky, Y. Klein, I. Alaluf, N. Swerdlin, N. Perzov, T. Danon, Y. Liron, T. Raveh, A. E. Carpenter, G. Lahav and U. Alon (2006). "Dynamic proteomics in individual human cells uncovers widespread cell-cycle dependence of nuclear proteins." Nat Methods **3**(7): 525-531.

Skehel, P. A., R. Fabian-Fine and E. R. Kandel (2000). "Mouse VAP33 is associated with the endoplasmic reticulum and microtubules." Proc Natl Acad Sci U S A **97**(3): 1101-1106.

Smit, J. J. and T. K. Sixma (2014). "RBR E3-ligases at work." EMBO Rep **15**(2): 142-154.

Song, C., Q. Wang and C.-C. H. Li (2003). "ATPase Activity of p97-Valosin-containing Protein (VCP): D2 MEDIATES THE MAJOR ENZYME ACTIVITY, AND D1 CONTRIBUTES TO THE HEAT-INDUCED ACTIVITY." Journal of Biological Chemistry **278**(6): 3648-3655.

Soussan, L., D. Burakov, M. P. Daniels, M. Toister-Achituv, A. Porat, Y. Yarden and Z. Elazar (1999). "ERG30, a VAP-33-related protein, functions in protein transport mediated by COPI vesicles." J Cell Biol **146**(2): 301-311.

Spence, J., R. R. Gali, G. Dittmar, F. Sherman, M. Karin and D. Finley (2000). "Cell cycle-regulated modification of the ribosome by a variant multiubiquitin chain." Cell **102**(1): 67-76.

Spina, S., A. D. Van Laar, J. R. Murrell, R. L. Hamilton, J. K. Kofler, F. Epperson, M. R. Farlow, O. L. Lopez, J. Quinlan, S. T. DeKosky and B. Ghetti (2013). "Phenotypic variability in three families with valosin-containing protein mutation." Eur J Neurol **20**(2): 251-258.

Spratt, D. E., H. Walden and G. S. Shaw (2014). "RBR E3 ubiquitin ligases: new structures, new insights, new questions." Biochem J **458**(3): 421-437.

Sreedharan, J., I. P. Blair, V. B. Tripathi, X. Hu, C. Vance, B. Rogelj, S. Ackerley, J. C. Durnall, K. L. Williams, E. Buratti, F. Baralle, J. de Belleroche, J. D. Mitchell, P. N. Leigh, A. Al-Chalabi, C. C. Miller, G. Nicholson and C. E. Shaw (2008). "TDP-43 mutations in familial and sporadic amyotrophic lateral sclerosis." Science **319**(5870): 1668-1672.

Steiger, M., A. Carr-Schmid, D. C. Schwartz, M. Kiledjian and R. Parker (2003). "Analysis of recombinant yeast decapping enzyme." Rna **9**(2): 231-238.

Stephen, A. G., J. S. Trausch-Azar, P. M. Handley-Gearhart, A. Ciechanover and A. L. Schwartz (1997). "Identification of a Region within the Ubiquitin-activating Enzyme Required for Nuclear Targeting and Phosphorylation." Journal of Biological Chemistry **272**(16): 10895-10903.

Stolz, A., W. Hilt, A. Buchberger and D. H. Wolf (2011). "Cdc48: a power machine in protein degradation." Trends Biochem Sci **36**(10): 515-523.

Strack, B., A. Calistri, M. A. Accola, G. Palu and H. G. Gottlinger (2000). "A role for ubiquitin ligase recruitment in retrovirus release." Proc Natl Acad Sci U S A **97**(24): 13063-13068.

Strong, M. J., S. Kesavapany and H. C. Pant (2005). "The pathobiology of amyotrophic lateral sclerosis: a proteinopathy?" J Neuropathol Exp Neurol **64**(8): 649-664.

Strong, M. J., K. Volkening, R. Hammond, W. Yang, W. Strong, C. Leystra-Lantz and C. Shoesmith (2007). "TDP43 is a human low molecular weight neurofilament (hNFL) mRNA-binding protein." Mol Cell Neurosci **35**(2): 320-327.

Sun, Z., Z. Diaz, X. Fang, M. P. Hart, A. Chesi, J. Shorter and A. D. Gitler (2011). "Molecular determinants and genetic modifiers of aggregation and toxicity for the ALS disease protein FUS/TLS." PLoS Biol **9**(4): e1000614.

Sundaramoorthy, V., A. K. Walker, J. Yerbury, K. Y. Soo, M. A. Farg and V. Hoang (2013). "Extracellular wildtype and mutant SOD1 induces ER-Golgi pathology characteristic of amyotrophic lateral sclerosis in neuronal cells." Cell Mol Life Sci **70**.

Suzuki, H., K. Kanekura, T. P. Levine, K. Kohno, V. M. Olkkonen, S. Aiso and M. Matsuoka (2009). "ALS-linked P56S-VAPB, an aggregated loss-of-function mutant of VAPB, predisposes motor neurons to ER stress-related death by inducing aggregation of co-expressed wild-type VAPB." J Neurochem **108**(4): 973-985.

Symons, M. H. and T. J. Mitchison (1991). "Control of actin polymerization in live and permeabilized fibroblasts." J Cell Biol **114**(3): 503-513.

Szklarczyk, D., A. Franceschini, S. Wyder, K. Forslund, D. Heller, J. Huerta-Cepas, M. Simonovic, A. Roth, A. Santos, K. P. Tsafou, M. Kuhn, P. Bork, L. J. Jensen and C. von Mering (2015). "STRING v10: protein-protein interaction networks, integrated over the tree of life." Nucleic Acids Res **43**(Database issue): D447-452.

Szklarczyk, D., J. H. Morris, H. Cook, M. Kuhn, S. Wyder, M. Simonovic, A. Santos, N. T. Doncheva, A. Roth, P. Bork, L. J. Jensen and C. von Mering (2017). "The STRING database in 2017: quality-controlled protein-protein association networks, made broadly accessible." Nucleic Acids Res **45**(D1): D362-d368.

Szoradi, T., K. Schaeff, E. M. Garcia-Rivera, D. N. Itzhak, R. M. Schmidt, P. W. Bircham, K. Leiss, J. Diaz-Miyar, V. K. Chen, D. Muzzey, G. H. H. Borner and S. Schuck (2018). "SHRED Is a Regulatory Cascade that Reprograms Ubr1 Substrate Specificity for Enhanced Protein Quality Control during Stress." Mol Cell **70**(6): 1025-1037.e1025.

Takeuchi, H., Y. Kobayashi, T. Yoshihara, J. Niwa, M. Doyu, K. Ohtsuka and G. Sobue (2002). "Hsp70 and Hsp40 improve neurite outgrowth and suppress intracytoplasmic aggregate formation in cultured neuronal cells expressing mutant SOD1." Brain Res **949**(1-2): 11-22.

Tamaoka, A., M. Arai, M. Itokawa, T. Arai, M. Hasegawa, K. Tsuchiya, H. Takuma, H. Tsuji, A. Ishii, M. Watanabe, Y. Takahashi, J. Goto, S. Tsuji and H. Akiyama (2010). "TDP-43 M337V mutation in familial amyotrophic lateral sclerosis in Japan." Intern Med **49**(4): 331-334.

Tan, A. Y. and J. L. Manley (2009). "The TET family of proteins: functions and roles in disease." J Mol Cell Biol **1**(2): 82-92.

Tan, C. F., H. Eguchi, A. Tagawa, O. Onodera, T. Iwasaki, A. Tsujino, M. Nishizawa, A. Kakita and H. Takahashi (2007). "TDP-43 immunoreactivity in neuronal inclusions in familial amyotrophic lateral sclerosis with or without SOD1 gene mutation." Acta Neuropathol **113**(5): 535-542.

Tan, J. M., E. S. Wong, D. S. Kirkpatrick, O. Pletnikova, H. S. Ko, S. P. Tay, M. W. Ho, J. Troncoso, S. P. Gygi, M. K. Lee, V. L. Dawson, T. M. Dawson and K. L. Lim (2008). "Lysine 63-linked ubiquitination promotes the formation and autophagic clearance of protein inclusions associated with neurodegenerative diseases." Hum Mol Genet **17**(3): 431-439.

Tan, Z., W. Qu, W. Tu, W. Liu, M. Baudry and S. S. Schreiber (2000). "p53 accumulation due to down-regulation of ubiquitin: relevance for neuronal apoptosis." Cell Death Differ **7**(7): 675-681.

Tan, Z., W. Tu and S. S. Schreiber (2001). "Downregulation of free ubiquitin: a novel mechanism of p53 stabilization and neuronal cell death." Brain Res Mol Brain Res **91**(1-2): 179-188.

Tangsongcharoen, C., S. Roytrakul and D. R. Smith (2019). "Analysis of cellular proteome changes in response to ZIKV NS2B-NS3 protease expression." Biochim Biophys Acta Proteins Proteom **1867**(2): 89-97.

Tanji, K., F. Mori, A. Kakita, H. Zhang, K. Kito, T. Kamitani, H. Takahashi and K. Wakabayashi (2007). "Immunohistochemical localization of NUB1, a synphilin-1-binding protein, in neurodegenerative disorders." Acta Neuropathol **114**(4): 365-371.

Tartaglia, G. G., S. Pechmann, C. M. Dobson and M. Vendruscolo (2007). "Life on the edge: a link between gene expression levels and aggregation rates of human proteins." Trends Biochem Sci **32**(5): 204-206.

Tashiro, Y., M. Urushitani, H. Inoue, M. Koike, Y. Uchiyama, M. Komatsu, K. Tanaka, M. Yamazaki, M. Abe, H. Misawa, K. Sakimura, H. Ito and R. Takahashi (2012). "Motor neuron-specific disruption of proteasomes, but not autophagy, replicates amyotrophic lateral sclerosis." J Biol Chem **287**(51): 42984-42994.

Taylor, J. P., F. Tanaka, J. Robitschek, C. M. Sandoval, A. Taye, S. Markovic-Plese and K. H. Fischbeck (2003). "Aggresomes protect cells by enhancing the degradation of toxic polyglutamine-containing protein." Hum Mol Genet **12**(7): 749-757.

Tazen, S., K. Figueroa, J. Y. Kwan, J. Goldman, A. Hunt, J. Sampson, L. Gutmann, S. M. Pulst, H. Mitsumoto and S. H. Kuo (2013). "Amyotrophic lateral sclerosis and spinocerebellar ataxia type 2 in a family with full CAG repeat expansions of ATXN2." JAMA Neurol **70**(10): 1302-1304.

Tedeschi, A. and F. Bradke (2017). "Spatial and temporal arrangement of neuronal intrinsic and extrinsic mechanisms controlling axon regeneration." Curr Opin Neurobiol **42**: 118-127.

Terrell, J., S. Shih, R. Dunn and L. Hicke (1998). "A function for monoubiquitination in the internalization of a G protein-coupled receptor." Mol Cell **1**(2): 193-202.

Teuling, E., S. Ahmed, E. Haasdijk, J. Demmers, M. O. Steinmetz, A. Akhmanova, D. Jaarsma and C. C. Hoogenraad (2007). "Motor neuron disease-associated mutant vesicle-associated membrane protein-associated protein (VAP) B recruits wild-type VAPs into endoplasmic reticulum-derived tubular aggregates." J Neurosci **27**(36): 9801-9815.

Teyssou, E., L. Chartier, M. D. Amador, R. Lam, G. Lautrette, M. Nicol, S. Machat, S. Da Barroca, C. Moigneu, M. Mairey, T. Larmonier, S. Saker, C. Dussert, S. Forlani, B. Fontaine, D. Seilhean, D. Bohl, S. Boillee, V. Meininger, P. Couratier, F. Salachas, G. Stevanin and S. Millecamps (2017). "Novel UBQLN2 mutations linked to amyotrophic lateral sclerosis and atypical hereditary spastic paraplegia phenotype through defective HSP70-mediated proteolysis." Neurobiol Aging **58**: 239.e211-239.e220.

Teyssou, E., T. Takeda, V. Lebon, S. Boillee, B. Doukoure, G. Bataillon, V. Sazdovitch, C. Cazeneuve, V. Meininger, E. LeGuern, F. Salachas, D. Seilhean and S. Millecamps (2013). "Mutations in SQSTM1 encoding p62 in amyotrophic lateral sclerosis: genetics and neuropathology." Acta Neuropathol **125**(4): 511-522.

Thrower, J. S., L. Hoffman, M. Rechsteiner and C. M. Pickart (2000). "Recognition of the polyubiquitin proteolytic signal." Embo j **19**(1): 94-102.

Thulasiraman, V. and R. L. Matts (1996). "Effect of geldanamycin on the kinetics of chaperone-mediated renaturation of firefly luciferase in rabbit reticulocyte lysate." Biochemistry **35**(41): 13443-13450.

Ticozzi, N., A. Ratti and V. Silani (2010). "Protein aggregation and defective RNA metabolism as mechanisms for motor neuron damage." CNS Neurol Disord Drug Targets **9**(3): 285-296.

Ticozzi, N., V. Silani, A. L. LeClerc, P. Keagle, C. Gellera, A. Ratti, F. Taroni, T. J. Kwiatkowski, Jr., D. M. McKenna-Yasek, P. C. Sapp, R. H. Brown, Jr. and J. E. Landers (2009). "Analysis of FUS gene mutation in familial amyotrophic lateral sclerosis within an Italian cohort." Neurology **73**(15): 1180-1185.

Ticozzi, N., C. Vance, A. L. Leclerc, P. Keagle, J. D. Glass, D. McKenna-Yasek, P. C. Sapp, V. Silani, D. A. Bosco, C. E. Shaw, R. H. Brown, Jr. and J. E. Landers (2011). "Mutational analysis reveals the FUS homolog TAF15 as a candidate gene for familial amyotrophic lateral sclerosis." Am J Med Genet B Neuropsychiatr Genet **156b**(3): 285-290.

Tkach, J. M., A. Yimit, A. Y. Lee, M. Riffle, M. Costanzo, D. Jaschob, J. A. Hendry, J. Ou, J. Moffat, C. Boone, T. N. Davis, C. Nislow and G. W. Brown (2012). "Dissecting DNA damage response pathways by analysing protein localization and abundance changes during DNA replication stress." Nat Cell Biol **14**(9): 966-976.

Todd, P. K. and H. L. Paulson (2010). "RNA-mediated neurodegeneration in repeat expansion disorders." Ann Neurol **67**(3): 291-300.

Tollervey, J. R., T. Curk, B. Rogelj, M. Briese, M. Cereda, M. Kayikci, J. Konig, T. Hortobagyi, A. L. Nishimura, V. Zupunski, R. Patani, S. Chandran, G. Rot, B. Zupan, C. E. Shaw and J. Ule (2011). "Characterizing the RNA targets and position-dependent splicing regulation by TDP-43." Nat Neurosci **14**(4): 452-458.

Topp, J. D., N. W. Gray, R. D. Gerard and B. F. Horazdovsky (2004). "Alsin is a Rab5 and Rac1 guanine nucleotide exchange factor." J Biol Chem **279**(23): 24612-24623.

Tresse, E., F. A. Salomons, J. Vesa, L. C. Bott, V. Kimonis, T. P. Yao, N. P. Dantuma and J. P. Taylor (2010). "VCP/p97 is essential for maturation of ubiquitin-containing autophagosomes and this function is impaired by mutations that cause IBMPFD." Autophagy **6**(2): 217-227.

Treusch, S., D. M. Cyr and S. Lindquist (2009). "Amyloid deposits: protection against toxic protein species?" Cell Cycle **8**(11): 1668-1674.

Treusch, S., S. Hamamichi, J. L. Goodman, K. E. Matlack, C. Y. Chung, V. Baru, J. M. Shulman, A. Parrado, B. J. Bevis, J. S. Valastyan, H. Han, M. Lindhagen-Persson, E. M. Reiman, D. A. Evans, D. A. Bennett, A. Olofsson, P. L. DeJager, R. E. Tanzi, K. A. Caldwell, G. A. Caldwell and S. Lindquist (2011). "Functional links between Abeta toxicity, endocytic trafficking, and Alzheimer's disease risk factors in yeast." Science **334**(6060): 1241-1245.

Tsuda, H., S. M. Han, Y. Yang, C. Tong, Y. Q. Lin, K. Mohan, C. Haueter, A. Zoghbi, Y. Harati, J. Kwan, M. A. Miller and H. J. Bellen (2008). "The amyotrophic lateral sclerosis 8

protein VAPB is cleaved, secreted, and acts as a ligand for Eph receptors." Cell **133**(6): 963-977.

Tucker, M., M. A. Valencia-Sanchez, R. R. Staples, J. Chen, C. L. Denis and R. Parker (2001). "The transcription factor associated Ccr4 and Caf1 proteins are components of the major cytoplasmic mRNA deadenylase in Saccharomyces cerevisiae." Cell **104**(3): 377-386.

Tudor, E. L., C. M. Galtrey, M. S. Perkinton, K. F. Lau, K. J. De Vos, J. C. Mitchell, S. Ackerley, T. Hortobagyi, E. Vamos, P. N. Leigh, C. Klasen, D. M. McLoughlin, C. E. Shaw and C. C. Miller (2010). "Amyotrophic lateral sclerosis mutant vesicle-associated membrane protein-associated protein-B transgenic mice develop TAR-DNA-binding protein-43 pathology." Neuroscience **167**(3): 774-785.

Tumbarello, D. A., B. J. Waxse, S. D. Arden, N. A. Bright, J. Kendrick-Jones and F. Buss (2012). "Autophagy receptors link myosin VI to autophagosomes to mediate Tom1-dependent autophagosome maturation and fusion with the lysosome." Nat Cell Biol **14**(10): 1024-1035.

Tummala, H., C. Jung, A. Tiwari, C. M. Higgins, L. J. Hayward and Z. Xu (2005). "Inhibition of chaperone activity is a shared property of several Cu,Zn-superoxide dismutase mutants that cause amyotrophic lateral sclerosis." J Biol Chem **280**(18): 17725-17731.

Turner, B. J., J. D. Atkin, M. A. Farg, D. W. Zang, A. Rembach and E. C. Lopes (2005). "Impaired extracellular secretion of mutant superoxide dismutase 1 associates with neurotoxicity in familial amyotrophic lateral sclerosis." J Neurosci **25**.

Twine, N. A., P. Szul, L. Henden, E. P. McCann, I. P. Blair, K. L. Williams, D. C. Bauer (2019). “TRIBES: A user-friendly pipeline for relatedness detection and disease gene discovery.” BioRxiv 686253; doi: https://doi.org/10.1101/686253

Tyson, J. R. and C. J. Stirling (2000). "LHS1 and SIL1 provide a lumenal function that is essential for protein translocation into the endoplasmic reticulum." Embo j **19**(23): 6440-6452.

Uchida, A., H. Sasaguri, N. Kimura, M. Tajiri, T. Ohkubo, F. Ono, F. Sakaue, K. Kanai, T. Hirai, T. Sano, K. Shibuya, M. Kobayashi, M. Yamamoto, S. Yokota, T. Kubodera, M. Tomori, K. Sakaki, M. Enomoto, Y. Hirai, J. Kumagai, Y. Yasutomi, H. Mochizuki, S. Kuwabara, T. Uchihara, H. Mizusawa and T. Yokota (2012). "Non-human primate model of amyotrophic lateral sclerosis with cytoplasmic mislocalization of TDP-43." Brain **135**(Pt 3): 833-846.

Udan, M. and R. H. Baloh (2011). "Implications of the prion-related Q/N domains in TDP-43 and FUS." Prion **5**(1): 1-5.

Urushitani, M., J. Kurisu, K. Tsukita and R. Takahashi (2002). "Proteasomal inhibition by misfolded mutant superoxide dismutase 1 induces selective motor neuron death in familial amyotrophic lateral sclerosis." J Neurochem **83**(5): 1030-1042.

van Blitterswijk, M., P. W. van Vught, M. A. van Es, H. J. Schelhaas, A. J. van der Kooi, M. de Visser, J. H. Veldink and L. H. van den Berg (2012). "Novel optineurin mutations in sporadic amyotrophic lateral sclerosis patients." Neurobiol Aging **33**(5): 1016.e1011-1017.

van der Zee, J., I. Gijselinck, L. Dillen, T. Van Langenhove, J. Theuns, S. Engelborghs, S. Philtjens, M. Vandenbulcke, K. Sleegers, A. Sieben, V. Baumer, G. Maes, E. Corsmit, B. Borroni, A. Padovani, S. Archetti, R. Perneczky, J. Diehl-Schmid, A. de Mendonca, G. Miltenberger-Miltenyi, S. Pereira, J. Pimentel, B. Nacmias, S. Bagnoli, S. Sorbi, C. Graff, H. H. Chiang, M. Westerlund, R. Sanchez-Valle, A. Llado, E. Gelpi, I. Santana, M. R. Almeida, B. Santiago, G. Frisoni, O. Zanetti, C. Bonvicini, M. Synofzik, W. Maetzler, J. M. Vom Hagen, L. Schols, M. T. Heneka, F. Jessen, R. Matej, E. Parobkova, G. G. Kovacs, T. Strobel, S. Sarafov, I. Tournev, A. Jordanova, A. Danek, T. Arzberger, G. M. Fabrizi, S. Testi, E. Salmon, P. Santens, J. J. Martin, P. Cras, R. Vandenberghe, P. P. De Deyn, M. Cruts, C. Van Broeckhoven, J. van der Zee, I. Gijselinck, L. Dillen, T. Van Langenhove, J. Theuns, S. Philtjens, K. Sleegers, V. Baumer, G. Maes, E. Corsmit, M. Cruts, C. Van Broeckhoven, J. van der Zee, I. Gijselinck, L. Dillen, T. Van Langenhove, S. Philtjens, J. Theuns, K. Sleegers, V. Baumer, G. Maes, M. Cruts, C. Van Broeckhoven, S. Engelborghs, P. P. De Deyn, P. Cras, S. Engelborghs, P. P. De Deyn, M. Vandenbulcke, M. Vandenbulcke, B. Borroni, A. Padovani, S. Archetti, R. Perneczky, J. Diehl-Schmid, M. Synofzik, W. Maetzler, J. Muller Vom Hagen, L. Schols, M. Synofzik, W. Maetzler, J. Muller Vom Hagen, L. Schols, M. T. Heneka, F.

Jessen, A. Ramirez, D. Kurzwelly, C. Sachtleben, W. Mairer, A. de Mendonca, G. Miltenberger-Miltenyi, S. Pereira, C. Firmo, J. Pimentel, R. Sanchez-Valle, A. Llado, A. Antonell, J. Molinuevo, E. Gelpi, C. Graff, H. H. Chiang, M. Westerlund, C. Graff, A. Kinhult Stahlbom, H. Thonberg, I. Nennesmo, A. Borjesson-Hanson, B. Nacmias, S. Bagnoli, S. Sorbi, V. Bessi, I. Piaceri, I. Santana, B. Santiago, I. Santana, M. Helena Ribeiro, M. Rosario Almeida, C. Oliveira, J. Massano, C. Garret, P. Pires, G. Frisoni, O. Zanetti, C. Bonvicini, S. Sarafov, I. Tournev, A. Jordanova, I. Tournev, G. G. Kovacs, T. Strobel, M. T. Heneka, F. Jessen, A. Ramirez, D. Kurzwelly, C. Sachtleben, W. Mairer, F. Jessen, R. Matej, E. Parobkova, A. Danel, T. Arzberger, G. Maria Fabrizi, S. Testi, S. Ferrari, T. Cavallaro, E. Salmon, P. Santens and P. Cras (2013). "A pan-European study of the C9orf72 repeat associated with FTLD: geographic prevalence, genomic instability, and intermediate repeats." Hum Mutat **34**(2): 363-373.

van Heusden, G. P., T. J. Wenzel, E. L. Lagendijk, H. Y. de Steensma, J. A. van den Berg (1992). “Characterization of the yeast BMH1 gene encoding a putative protein homologous to mammalian protein kinase II activators and protein kinase C inhibitors.” FEBS Lett **302**(2):145-50.

Van Langenhove, T., J. van der Zee, K. Sleegers, S. Engelborghs, R. Vandenberghe, I. Gijselinck, M. Van den Broeck, M. Mattheijssens, K. Peeters, P. P. De Deyn, M. Cruts and C. Van Broeckhoven (2010). "Genetic contribution of FUS to frontotemporal lobar degeneration." Neurology **74**(5): 366-371.

van Pel, D. M., P. C. Stirling, S. W. Minaker, P. Sipahimalani and P. Hieter (2013). "Saccharomyces cerevisiae genetics predicts candidate therapeutic genetic interactions at the mammalian replication fork." G3 (Bethesda) **3**(2): 273-282.

Vance, C., B. Rogelj, T. Hortobagyi, K. J. De Vos, A. L. Nishimura, J. Sreedharan, X. Hu, B. Smith, D. Ruddy, P. Wright, J. Ganesalingam, K. L. Williams, V. Tripathi, S. Al-Saraj, A. Al-Chalabi, P. N. Leigh, I. P. Blair, G. Nicholson, J. de Belleroche, J. M. Gallo, C. C. Miller and C. E. Shaw (2009). "Mutations in FUS, an RNA processing protein, cause familial amyotrophic lateral sclerosis type 6." Science **323**(5918): 1208-1211.

Veldink, J. H., S. Kalmijn, A. H. Van der Hout, H. H. Lemmink, G. J. Groeneveld, C. Lummen, H. Scheffer, J. H. Wokke and L. H. Van den Berg (2005). "SMN genotypes producing less SMN protein increase susceptibility to and severity of sporadic ALS." Neurology **65**(6): 820-825.

Verma, R., L. Aravind, R. Oania, W. H. McDonald, J. R. Yates, 3rd, E. V. Koonin and R. J. Deshaies (2002). "Role of Rpn11 metalloprotease in deubiquitination and degradation by the 26S proteasome." Science **298**(5593): 611-615.

Verma, R., R. Oania, J. Graumann and R. J. Deshaies (2004). "Multiubiquitin chain receptors define a layer of substrate selectivity in the ubiquitin-proteasome system." Cell **118**(1): 99-110.

Vittal, V., M. D. Stewart, P. S. Brzovic and R. E. Klevit (2015). "Regulating the Regulators: Recent Revelations in the Control of E3 Ubiquitin Ligases." J Biol Chem **290**(35): 21244-21251.

Voigt, A., D. Herholz, F. C. Fiesel, K. Kaur, D. Muller, P. Karsten, S. S. Weber, P. J. Kahle, T. Marquardt and J. B. Schulz (2010). "TDP-43-mediated neuron loss in vivo requires RNA-binding activity." PLoS One **5**(8): e12247.

Voisine, C., J. S. Pedersen and R. I. Morimoto (2010). "Chaperone networks: tipping the balance in protein folding diseases." Neurobiol Dis **40**(1): 12-20.

Walczak, H., K. Iwai and I. Dikic (2012). "Generation and physiological roles of linear ubiquitin chains." BMC Biology **10**(1): 23.

Walker, A. K., K. Y. Soo, V. Sundaramoorthy, S. Parakh, Y. Ma, M. A. Farg, R. H. Wallace, P. J. Crouch, B. J. Turner, M. K. Horne and J. D. Atkin (2013). "ALS-associated TDP-43 induces endoplasmic reticulum stress, which drives cytoplasmic TDP-43 accumulation and stress granule formation." PLoS One **8**(11): e81170.

Walters, K. J., A. M. Goh, Q. Wang, G. Wagner and P. M. Howley (2004). "Ubiquitin family proteins and their relationship to the proteasome: a structural perspective." Biochim Biophys Acta **1695**(1-3): 73-87.

Walters, K. J., M. F. Kleijnen, A. M. Goh, G. Wagner and P. M. Howley (2002). "Structural studies of the interaction between ubiquitin family proteins and proteasome subunit S5a." Biochemistry **41**(6): 1767-1777.

Wan, L., D. J. Battle, J. Yong, A. K. Gubitz, S. J. Kolb, J. Wang and G. Dreyfuss (2005). "The survival of motor neurons protein determines the capacity for snRNP assembly: biochemical deficiency in spinal muscular atrophy." Mol Cell Biol **25**(13): 5543-5551.

Wang, H., L. Wang, H. Erdjument-Bromage, M. Vidal, P. Tempst, R. S. Jones and Y. Zhang (2004). "Role of histone H2A ubiquitination in Polycomb silencing." Nature **431**(7010): 873-878.

Wang, H. Y., I. F. Wang, J. Bose and C. K. Shen (2004). "Structural diversity and functional implications of the eukaryotic TDP gene family." Genomics **83**(1): 130-139.

Wang, I. F., L. S. Wu, H. Y. Chang and C. K. Shen (2008). "TDP-43, the signature protein of FTLD-U, is a neuronal activity-responsive factor." J Neurochem **105**(3): 797-806.

Wang, J., H. Slunt, V. Gonzales, D. Fromholt, M. Coonfield, N. G. Copeland, N. A. Jenkins and D. R. Borchelt (2003). "Copper-binding-site-null SOD1 causes ALS in transgenic mice: aggregates of non-native SOD1 delineate a common feature." Hum Mol Genet **12**(21): 2753-2764.

Wang, Q., J. L. Johnson, N. Y. Agar and J. N. Agar (2008). "Protein aggregation and protein instability govern familial amyotrophic lateral sclerosis patient survival." PLoS Biol **6**(7): e170.

Wang, W. Y., L. Pan, S. C. Su, E. J. Quinn, M. Sasaki, J. C. Jimenez, I. R. Mackenzie, E. J. Huang and L. H. Tsai (2013). "Interaction of FUS and HDAC1 regulates DNA damage response and repair in neurons." Nat Neurosci **16**(10): 1383-1391.

Wang, X., M. A. Khaleque, M. J. Zhao, R. Zhong, M. Gaestel and S. K. Calderwood (2006). "Phosphorylation of HSF1 by MAPK-activated protein kinase 2 on serine 121, inhibits transcriptional activity and promotes HSP90 binding." J Biol Chem **281**(2): 782-791.

Wang, X., S. Zhou, X. Ding, M. Ma, J. Zhang, Y. Zhou, E. Wu and J. Teng (2015). "Activation of ER Stress and Autophagy Induced by TDP-43 A315T as Pathogenic Mechanism and the Corresponding Histological Changes in Skin as Potential Biomarker for ALS with the Mutation." Int J Biol Sci **11**(10): 1140-1149.

Wang, Y., C. L. Liu, J. D. Storey, R. J. Tibshirani, D. Herschlag and P. O. Brown (2002). "Precision and functional specificity in mRNA decay." Proceedings of the National Academy of Sciences **99**(9): 5860-5865.

Wang, Z., X. Jiao, A. Carr-Schmid and M. Kiledjian (2002). "The hDcp2 protein is a mammalian mRNA decapping enzyme." Proc Natl Acad Sci U S A **99**(20): 12663-12668.

Watanabe, M., M. Dykes-Hoberg, V. C. Culotta, D. L. Price, P. C. Wong and J. D. Rothstein (2001). "Histological evidence of protein aggregation in mutant SOD1 transgenic mice and in amyotrophic lateral sclerosis neural tissues." Neurobiol Dis **8**(6): 933-941.

Watts, G. D., J. Wymer, M. J. Kovach, S. G. Mehta, S. Mumm, D. Darvish, A. Pestronk, M. P. Whyte and V. E. Kimonis (2004). "Inclusion body myopathy associated with Paget disease of bone and frontotemporal dementia is caused by mutant valosin-containing protein." Nat Genet **36**(4): 377-381.

Watts, G. D. J., J. Wymer, M. J. Kovach, S. G. Mehta, S. Mumm, D. Darvish, A. Pestronk, M. P. Whyte and V. E. Kimonis (2004). "Inclusion body myopathy associated with Paget disease

of bone and frontotemporal dementia is caused by mutant valosin-containing protein." Nature Genetics **36**: 377.

Watts, R. J., E. D. Hoopfer and L. Luo (2003). "Axon pruning during Drosophila metamorphosis: evidence for local degeneration and requirement of the ubiquitin-proteasome system." Neuron **38**(6): 871-885.

Weathington, N. M. and R. K. Mallampalli (2014). "Emerging therapies targeting the ubiquitin proteasome system in cancer." J Clin Invest **124**(1): 6-12.

Webster, C. P., E. F. Smith, C. S. Bauer, A. Moller, G. M. Hautbergue, L. Ferraiuolo, M. A. Myszczynska, A. Higginbottom, M. J. Walsh, A. J. Whitworth, B. K. Kaspar, K. Meyer, P. J. Shaw, A. J. Grierson and K. J. De Vos (2016). "The C9orf72 protein interacts with Rab1a and the ULK1 complex to regulate initiation of autophagy." Embo j **35**(15): 1656-1676.

Weihl, C. C., S. E. Miller, P. I. Hanson and A. Pestronk (2007). "Transgenic expression of inclusion body myopathy associated mutant p97/VCP causes weakness and ubiquitinated protein inclusions in mice." Hum Mol Genet **16**(8): 919-928.

Weihl, C. C., A. Pestronk and V. E. Kimonis (2009). "Valosin-containing protein disease: inclusion body myopathy with Paget's disease of the bone and fronto-temporal dementia." Neuromuscul Disord **19**(5): 308-315.

Weihl, C. C., P. Temiz, S. E. Miller, G. Watts, C. Smith, M. Forman, P. I. Hanson, V. Kimonis and A. Pestronk (2008). "TDP-43 accumulation in inclusion body myopathy muscle suggests a common pathogenic mechanism with frontotemporal dementia." J Neurol Neurosurg Psychiatry **79**(10): 1186-1189.

Weisberg, S. J., R. Lyakhovetsky, A. C. Werdiger, A. D. Gitler, Y. Soen and D. Kaganovich (2012). "Compartmentalization of superoxide dismutase 1 (SOD1G93A) aggregates determines their toxicity." Proc Natl Acad Sci U S A **109**(39): 15811-15816.

Welihinda, A. A., W. Tirasophon, S. R. Green and R. J. Kaufman (1997). "Gene induction in response to unfolded protein in the endoplasmic reticulum is mediated through Ire1p kinase interaction with a transcriptional coactivator complex containing Ada5p." Proc Natl Acad Sci U S A **94**(9): 4289-4294.

Welihinda, A. A., W. Tirasophon and R. J. Kaufman (2000). "The transcriptional co-activator ADA5 is required for HAC1 mRNA processing in vivo." J Biol Chem **275**(5): 3377-3381.

Wertz, I. E., K. M. O'Rourke, H. Zhou, M. Eby, L. Aravind, S. Seshagiri, P. Wu, C. Wiesmann, R. Baker, D. L. Boone, A. Ma, E. V. Koonin and V. M. Dixit (2004). "De-ubiquitination and ubiquitin ligase domains of A20 downregulate NF-kappaB signalling." Nature **430**(7000): 694-699.

Wiborg, O., M. S. Pedersen, A. Wind, L. E. Berglund, K. A. Marcker and J. Vuust (1985). "The human ubiquitin multigene family: some genes contain multiple directly repeated ubiquitin coding sequences." Embo j **4**(3): 755-759.

Wilkinson, K. D., V. L. Tashayev, L. B. O'Connor, C. N. Larsen, E. Kasperek and C. M. Pickart (1995). "Metabolism of the polyubiquitin degradation signal: structure, mechanism, and role of isopeptidase T." Biochemistry **34**(44): 14535-14546.

Williams, K. L., S. Topp, S. Yang, B. Smith, J. A. Fifita, S. T. Warraich, K. Y. Zhang, N. Farrawell, C. Vance, X. Hu, A. Chesi, C. S. Leblond, A. Lee, S. L. Rayner, V. Sundaramoorthy, C. Dobson-Stone, M. P. Molloy, M. van Blitterswijk, D. W. Dickson, R. C. Petersen, N. R. Graff-Radford, B. F. Boeve, M. E. Murray, C. Pottier, E. Don, C. Winnick, E. P. McCann, A. Hogan, H. Daoud, A. Levert, P. A. Dion, J. Mitsui, H. Ishiura, Y. Takahashi, J. Goto, J. Kost, C. Gellera, A. S. Gkazi, J. Miller, J. Stockton, W. S. Brooks, K. Boundy, M. Polak, J. L. Munoz-Blanco, J. Esteban-Perez, A. Rabano, O. Hardiman, K. E. Morrison, N. Ticozzi, V. Silani, J. de Belleroche, J. D. Glass, J. B. Kwok, G. J. Guillemin, R. S. Chung, S. Tsuji, R. H. Brown, Jr., A. Garcia-Redondo, R. Rademakers, J. E. Landers, A. D. Gitler, G. A. Rouleau, N. J. Cole, J. J. Yerbury, J. D. Atkin, C. E. Shaw, G. A. Nicholson and I. P. Blair (2016). "CCNF mutations in amyotrophic lateral sclerosis and frontotemporal dementia." Nat Commun **7**: 11253.

Williams, K. L., S. T. Warraich, S. Yang, J. A. Solski, R. Fernando, G. A. Rouleau, G. A. Nicholson and I. P. Blair (2012). "UBQLN2/ubiquilin 2 mutation and pathology in familial amyotrophic lateral sclerosis." Neurobiology of Aging **33**(10): 2527.e2523-2527.e2510.

Willingham, S., T. F. Outeiro, M. J. DeVit, S. L. Lindquist and P. J. Muchowski (2003). "Yeast genes that enhance the toxicity of a mutant huntingtin fragment or alpha-synuclein." Science **302**(5651): 1769-1772.

Winkler, C., C. Eggert, D. Gradl, G. Meister, M. Giegerich, D. Wedlich, B. Laggerbauer and U. Fischer (2005). "Reduced U snRNP assembly causes motor axon degeneration in an animal model for spinal muscular atrophy." Genes Dev **19**(19): 2320-2330.

Winston, J. T., P. Strack, P. Beer-Romero, C. Y. Chu, S. J. Elledge and J. W. Harper (1999). "The SCFbeta-TRCP-ubiquitin ligase complex associates specifically with phosphorylated destruction motifs in IkappaBalpha and beta-catenin and stimulates IkappaBalpha ubiquitination in vitro." Genes Dev **13**(3): 270-283.

Winton, M. J., L. M. Igaz, M. M. Wong, L. K. Kwong, J. Q. Trojanowski and V. M. Lee (2008). "Disturbance of nuclear and cytoplasmic TAR DNA-binding protein (TDP-43) induces disease-like redistribution, sequestration, and aggregate formation." J Biol Chem **283**(19): 13302-13309.

Wishart, T. M., C. A. Mutsaers, M. Riessland, M. M. Reimer, G. Hunter, M. L. Hannam, S. L. Eaton, H. R. Fuller, S. L. Roche, E. Somers, R. Morse, P. J. Young, D. J. Lamont, M. Hammerschmidt, A. Joshi, P. Hohenstein, G. E. Morris, S. H. Parson, P. A. Skehel, T. Becker, I. M. Robinson, C. G. Becker, B. Wirth and T. H. Gillingwater (2014). "Dysregulation of ubiquitin homeostasis and beta-catenin signaling promote spinal muscular atrophy." J Clin Invest **124**(4): 1821-1834.

Wishart, T. M., J. M. Paterson, D. M. Short, S. Meredith, K. A. Robertson, C. Sutherland, M. A. Cousin, M. B. Dutia and T. H. Gillingwater (2007). "Differential proteomics analysis of synaptic proteins identifies potential cellular targets and protein mediators of synaptic

neuroprotection conferred by the slow Wallerian degeneration (Wlds) gene." Mol Cell Proteomics **6**(8): 1318-1330.

Wishart, T. M., H. N. Pemberton, S. R. James, C. J. McCabe and T. H. Gillingwater (2008). "Modified cell cycle status in a mouse model of altered neuronal vulnerability (slow Wallerian degeneration; Wlds)." Genome Biol **9**(6): R101.

Wojciechowska, M. and W. J. Krzyzosiak (2011). "Cellular toxicity of expanded RNA repeats: focus on RNA foci." Hum Mol Genet **20**(19): 3811-3821.

Wójcik, C. and G. N. DeMartino (2002). "Analysis of Drosophila 26 S Proteasome Using RNA Interference." Journal of Biological Chemistry **277**(8): 6188-6197.

Wong, N. K., B. P. He and M. J. Strong (2000). "Characterization of neuronal intermediate filament protein expression in cervical spinal motor neurons in sporadic amyotrophic lateral sclerosis (ALS)." J Neuropathol Exp Neurol **59**(11): 972-982.

Wong, P. C., C. A. Pardo, D. R. Borchelt, M. K. Lee, N. G. Copeland, N. A. Jenkins, S. S. Sisodia, D. W. Cleveland and D. L. Price (1995). "An adverse property of a familial ALS-linked SOD1 mutation causes motor neuron disease characterized by vacuolar degeneration of mitochondria." Neuron **14**(6): 1105-1116.

Wu, C. H., C. Fallini, N. Ticozzi, P. J. Keagle, P. C. Sapp, K. Piotrowska, P. Lowe, M. Koppers, D. McKenna-Yasek, D. M. Baron, J. E. Kost, P. Gonzalez-Perez, A. D. Fox, J. Adams, F. Taroni, C. Tiloca, A. L. Leclerc, S. C. Chafe, D. Mangroo, M. J. Moore, J. A. Zitzewitz, Z. S. Xu, L. H. van den Berg, J. D. Glass, G. Siciliano, E. T. Cirulli, D. B. Goldstein, F. Salachas, V. Meininger, W. Rossoll, A. Ratti, C. Gellera, D. A. Bosco, G. J. Bassell, V. Silani, V. E. Drory, R. H. Brown, Jr. and J. E. Landers (2012). "Mutations in the profilin 1 gene cause familial amyotrophic lateral sclerosis." Nature **488**(7412): 499-503.

Wyatt, A. R., J. J. Yerbury, H. Ecroyd and M. R. Wilson (2013). "Extracellular chaperones and proteostasis." Annu Rev Biochem **82**: 295-322.

Xie, Y. and A. Varshavsky (2000). "Physical association of ubiquitin ligases and the 26S proteasome." Proc Natl Acad Sci U S A **97**(6): 2497-2502.

Xie, Z., U. Nair and D. J. Klionsky (2008). "Atg8 controls phagophore expansion during autophagosome formation." Mol Biol Cell **19**(8): 3290-3298.

Xu, P., D. M. Duong, N. T. Seyfried, D. Cheng, Y. Xie, J. Robert, J. Rush, M. Hochstrasser, D. Finley and J. Peng (2009). "Quantitative proteomics reveals the function of unconventional ubiquitin chains in proteasomal degradation." Cell **137**(1): 133-145.

Xu, Z., K. Graham, M. Foote, F. Liang, R. Rizkallah, M. Hurt, Y. Wang, Y. Wu, Y. Zhou (2013). "14-3-3 protein targets misfolded chaperone-associated proteins to aggresomes." J Cell Sci **126**(Pt 18):4173-86.

Yang, C., W. Tan, C. Whittle, L. Qiu, L. Cao, S. Akbarian and Z. Xu (2010). "The C-terminal TDP-43 fragments have a high aggregation propensity and harm neurons by a dominant-negative mechanism." PLoS One **5**(12): e15878.

Yang, E., E. van Nimwegen, M. Zavolan, N. Rajewsky, M. Schroeder, M. Magnasco and J. E. Darnell (2003). "Decay Rates of Human mRNAs: Correlation With Functional Characteristics and Sequence Attributes." Genome Research **13**(8): 1863-1872.

Yang, S., K. Y. Zhang, R. Kariawasam, M. Bax, J. A. Fifita, L. Ooi, J. J. Yerbury, G. A. Nicholson and I. P. Blair (2015). "Evaluation of Skin Fibroblasts from Amyotrophic Lateral Sclerosis Patients for the Rapid Study of Pathological Features." Neurotox Res **28**(2): 138-146.

Yang, U., H. Y. Yang, J. S. Kim and T. H. Lee (2012). "The functional role of UBA1 cysteine-278 in ubiquitination." Biochem Biophys Res Commun **427**(3): 587-592.

Yao, T. and R. E. Cohen (2002). "A cryptic protease couples deubiquitination and degradation by the proteasome." Nature **419**(6905): 403-407.

Ye, Y., H. H. Meyer and T. A. Rapoport (2001). "The AAA ATPase Cdc48/p97 and its partners transport proteins from the ER into the cytosol." Nature **414**(6864): 652-656.

Ye, Y., H. H. Meyer and T. A. Rapoport (2003). "Function of the p97-Ufd1-Npl4 complex in retrotranslocation from the ER to the cytosol: dual recognition of nonubiquitinated polypeptide segments and polyubiquitin chains." J Cell Biol **162**(1): 71-84.

Ye, Y. and M. Rape (2009). "Building ubiquitin chains: E2 enzymes at work." Nat Rev Mol Cell Biol **10**(11): 755-764.

Yerbury, J. and J. Kumita (2010). "Protein Chemistry of Amyloid Fibrils and Chaperones: Implications for Amyloid Formation and Disease." Current Chemical Biology **4**(2): 89-98.

Yerbury, J. J., D. Gower, L. Vanags, K. Roberts, J. A. Lee and H. Ecroyd (2013). "The small heat shock proteins alphaB-crystallin and Hsp27 suppress SOD1 aggregation in vitro." Cell Stress Chaperones **18**.

Yerbury, J. J., L. Ooi, I. P. Blair, P. Ciryam, C. M. Dobson and M. Vendruscolo (2019). "The metastability of the proteome of spinal motor neurons underlies their selective vulnerability in ALS." Neurosci Lett **704**: 89-94.

Yerbury, J. J., L. Ooi, A. Dillin, D. N. Saunders, D. M. Hatters, P. M. Beart, N. R. Cashman, M. R. Wilson and H. Ecroyd (2016). "Walking the tightrope: proteostasis and neurodegenerative disease." J Neurochem **137**(4): 489-505.

Ying, H., X. Shen, B. Park and B. Y. Yue (2010). "Posttranslational modifications, localization, and protein interactions of optineurin, the product of a glaucoma gene." PLoS One **5**(2): e9168.

Ying, H. and B. Y. J. T. Yue (2012). "Cellular and molecular biology of optineurin." International review of cell and molecular biology **294**: 223-258.

Yip, C. K., J. Berscheminski and T. Walz (2010). "Molecular architecture of the TRAPPII complex and implications for vesicle tethering." Nat Struct Mol Biol **17**(11): 1298-1304.

Yoshimura, A., R. Fujii, Y. Watanabe, S. Okabe, K. Fukui and T. Takumi (2006). "Myosin-Va facilitates the accumulation of mRNA/protein complex in dendritic spines." Curr Biol **16**(23): 2345-2351.

Yuen, K. W. Y., C. D. Warren, O. Chen, T. Kwok, P. Hieter and F. A. Spencer (2007). "Systematic genome instability screens in yeast and their potential relevance to cancer." Proceedings of the National Academy of Sciences of the United States of America **104**(10): 3925-3930.

Zatloukal, K., C. Stumptner, A. Fuchsbichler, H. Heid, M. Schnoelzer, L. Kenner, R. Kleinert, M. Prinz, A. Aguzzi and H. Denk (2002). "p62 Is a common component of cytoplasmic inclusions in protein aggregation diseases." Am J Pathol **160**(1): 255-263.

Zeineddine, R., J. F. Pundavela, L. Corcoran, E. M. Stewart, D. Do-Ha, M. Bax, G. Guillemin, K. L. Vine, D. M. Hatters, H. Ecroyd, C. M. Dobson, B. J. Turner, L. Ooi, M. R. Wilson, N. R. Cashman and J. J. Yerbury (2015). "SOD1 protein aggregates stimulate macropinocytosis in neurons to facilitate their propagation." Molecular Neurodegeneration **10**(1): 57.

Zhang, D., L. M. Iyer, F. He and L. Aravind (2012). "Discovery of Novel DENN Proteins: Implications for the Evolution of Eukaryotic Intracellular Membrane Structures and Human Disease." Front Genet **3**: 283.

Zhang, D., S. Raasi and D. Fushman (2008). "Affinity makes the difference: nonselective interaction of the UBA domain of Ubiquilin-1 with monomeric ubiquitin and polyubiquitin chains." J Mol Biol **377**(1): 162-180.

Zhang, H., L. Xing, W. Rossoll, H. Wichterle, R. H. Singer and G. J. Bassell (2006). "Multiprotein Complexes of the Survival of Motor Neuron Protein SMN with Gemins Traffic

to Neuronal Processes and Growth Cones of Motor Neurons." The Journal of Neuroscience **26**(33): 8622-8632.

Zhang, H. L., F. Pan, D. Hong, S. M. Shenoy, R. H. Singer and G. J. Bassell (2003). "Active Transport of the Survival Motor Neuron Protein and the Role of Exon-7 in Cytoplasmic Localization." The Journal of Neuroscience **23**(16): 6627-6637.

Zhang, Q., E. T. Powers, J. Nieva, M. E. Huff, M. A. Dendle, J. Bieschke, C. G. Glabe, A. Eschenmoser, P. Wentworth, Jr., R. A. Lerner and J. W. Kelly (2004). "Metabolite-initiated protein misfolding may trigger Alzheimer's disease." Proc Natl Acad Sci U S A **101**(14): 4752-4757.

Zhang, X. and S. B. Qian (2011). "Chaperone-mediated hierarchical control in targeting misfolded proteins to aggresomes." Mol Biol Cell **22**(18): 3277-3288.

Zhang, Z., F. Lotti, K. Dittmar, I. Younis, L. Wan, M. Kasim and G. Dreyfuss (2008). "SMN deficiency causes tissue-specific perturbations in the repertoire of snRNAs and widespread defects in splicing." Cell **133**(4): 585-600.

Zhu, C., M. V. Beck, J. D. Griffith, M. Deshmukh and N. V. Dokholyan (2018). "Large SOD1 aggregates, unlike trimeric SOD1, do not impact cell viability in a model of amyotrophic lateral sclerosis." Proc Natl Acad Sci U S A **115**(18): 4661-4665.

Zhu, G., C. J. Wu, Y. Zhao and J. D. Ashwell (2007). "Optineurin negatively regulates TNFalpha- induced NF-kappaB activation by competing with NEMO for ubiquitinated RIP." Curr Biol **17**(16): 1438-1443.

Zimmerman, E. S., B. A. Schulman and N. Zheng (2010). "Structural assembly of cullin-RING ubiquitin ligase complexes." Curr Opin Struct Biol **20**(6): 714-721.

Zou, J., Y. Guo, T. Guettouche, D. F. Smith and R. Voellmy (1998). "Repression of heat shock transcription factor HSF1 activation by HSP90 (HSP90 complex) that forms a stress-sensitive complex with HSF1." Cell **94**(4): 471-480.

Zu, T., Y. Liu, M. Banez-Coronel, T. Reid, O. Pletnikova, J. Lewis, T. M. Miller, M. B. Harms, A. E. Falchook, S. H. Subramony, L. W. Ostrow, J. D. Rothstein, J. C. Troncoso and L. P. Ranum (2013). "RAN proteins and RNA foci from antisense transcripts in C9ORF72 ALS and frontotemporal dementia." Proc Natl Acad Sci U S A **110**(51): E4968-4977.

Chapter 8: Appendix

R scripts

R script to fit plate reader absorbance (optical density), EGFP and DsRed fluorescence data:

```
###
# Plate reader curve fitting and plotting
# Function to fit fluorescence and absorbance data
###

localMaxima <- function(x) {
  # Use -Inf instead if x is numeric (non-integer)
  y <- diff(c(-.Machine$integer.max, x)) > 0L
  rle(y)$lengths

  y <- cumsum(rle(y)$lengths)
  y <- y[seq.int(1L, length(y), 2L)]
  if (x[[1]] == x[[2]]) {
    y <- y[-1]
  }
  y
}

localMinima <- function(x) {
  # Use -Inf instead if x is numeric (non-integer)
  y <- diff(c(.Machine$integer.max, x)) > 0L
  rle(y)$lengths
  y <- cumsum(rle(y)$lengths)
  y <- y[seq.int(1L, length(y), 2L)]
  if (x[[1]] == x[[2]]) {
    y <- y[-1]
  }
  y
}

#fits a single curve i.e. a vector
robustfit <- function(data, time, name="NA", smoothing=0.7, upto=65 ){
  #set up output
  out <- list(min.fit.x = NA, min.fit.y = NA, max.fit.x = NA, max.fit.y = NA, exp.rate = NA,
lag = NA, max.before.chosen.time = NA, rate.before.chosen.time = NA)

  #time must be a numeric vector
  time <- as.numeric(time)

  #fit
  y.spl <- smooth.spline(x = time, y= as.numeric(data), spar = smoothing)
  xrange<-c(min(c(min(time),min(y.spl$x))), max(c(max(time),max(y.spl$x))))
  yrange<-c(min(c(min(data),min(y.spl$y))), max(c(max(data),max(y.spl$y))))
  plot(xrange,yrange,type='n', main=name)
  lines(y.spl$x, y.spl$y,type="l", col="red")
  points(time,as.numeric(data))
```

```
  #get the gradient through each point
  dydt.spl <- predict(y.spl, time, deriv = 1) #using predict.smooth.spline
  index <- which.max(dydt.spl$y)
  t.max <- dydt.spl$x[index]
  dydt.max <- max(dydt.spl$y)
  y.max <- y.spl$y[index]
  mu.spl <- dydt.max
  b.spl <- y.max - dydt.max * t.max
  lambda.spl <- -b.spl/mu.spl #this is the old method

  #calculate lambda
  #if it grew exponentially from the start, what time would it have reached y.max
  #use the first 10 timepoints to establish a baseline
  t.st <- (y.max-mean(as.numeric(data[c(1:10)])))/dydt.max
  t.lam <- t.max - t.st
  abline(v=t.lam, col="brown")
  #intercept baseline and exp.slope
  bl = mean(as.numeric(data[c(1:10)])) #we use the mean of the first 10 timepoints as a
baseline
  const = y.max - (dydt.max * t.max)
  t.int = (bl-const)/dydt.max
  abline(v=t.int, col="green")
  if(t.int < 0){
    cat("Warning: improved lag negative for: ",name,"\n")
  }

  #save
  #positive.y <- y.spl$y[y.spl$y >= 0]
  y.above.t.int <- y.spl$y[which(y.spl$x > t.int)]
  positive.y <- ifelse(sum(y.above.t.int > 0) == 0, y.above.t.int[y.above.t.int < 0],
y.above.t.int[y.above.t.int > 0])

  out$min.fit.y <- positive.y[which.min(positive.y)]
  out$min.fit.x <- y.spl$x[which(out$min.fit.y == y.spl$y)]

  out$max.fit.x <- y.spl$x[which.max(y.spl$y)]
  out$max.fit.y <- y.spl$y[which(out$max.fit.x == y.spl$x)]

  out$exp.rate <- mu.spl
  out$lag <- t.int

  local_maximas = y.spl$y[localMaxima(y.spl$y)]
  out$second.max.y = ifelse(length(local_maximas) >=2, local_maximas[2],
local_maximas[1])
  out$second.max.x = y.spl$x[which(out$second.max.y == y.spl$y)]

  points(out$max.fit.x, out$max.fit.y, col="grey", pch=19)
  points(out$second.max.x, out$second.max.y, col="purple", pch=19)
```

```
  local_minimas = y.spl$y[localMinima(y.spl$y)]
  out$second.min.y = ifelse(length(local_minimas) >=2, local_minimas[2], local_minimas[1])
  out$second.min.x = y.spl$x[which(out$second.min.y == y.spl$y)]

  points(out$min.fit.x, out$min.fit.y, col="blue", pch=19)
  points(out$second.min.x, out$second.min.y, col="pink", pch=19)

  #add parameter A to plot
  abline(h=out$max.fit.y, col='orange')

  #add the maximum exponential rate to plot
  mu <- mu.spl
  lambda <- lambda.spl
  bla <- y.spl$x * mu
  bla <- bla + (-mu * lambda)
  lines(y.spl$x, bla, lw = 2, lty = 2, col="blue")

  ########## get max and rate up to the given timepoint
  out$max.before.chosen.time <- max(y.spl$y[c(1:upto)])
  out$rate.before.chosen.time <- max(dydt.spl$y[c(1:upto)])
  abline(h=out$max.before.chosen.time, col='orange',lty=2)

  return(out)

}

#wraps robustfit to call it on every row of a matrix
#this is just for convenience
#returns a list of fit results, one entry per row in the same order as the input
#name is a vector of strings
RFall <- function(data, time, name="NA", smoothing=0.7, upto=65){
  #set up output
  out <- NULL
  for(i in 1:dim(data)[1]){
    n <- name[i] #otherwise all plots get all the names, even if you subset in the function call
    cat(n, '\n')
    out[[i]] <- robustfit(data[i,], time, n, smoothing, upto)
  }

  return(out)
}

#overview plot
#use sample positions to interpret layout in the plate
#positions are the row and column
#all wells are plotted on the same scale
plot96 <- function(data, times, positions){
  #save original settings
  mar <- par()$mar
  mfrow <- par()$mfrow
```

```
  par(mfrow=c(8,12))
  par(mar=c(0,0,0,0))

  xrange <- range(times)
  yrange <- range(data)

  column <- 1 #the current column in the plate
  rows <- c("A", "B", "C", "D", "E", "F", "G", "H") #use to convert between out numeric
index and the alphabetical one used on the plates
  row <- 1
  i <- 1 #the plot we're currently working on
  plotnumber <- 0

  while(plotnumber < 96){
    plot(xrange, yrange, type="n", xaxt="n", yaxt="n")
    if(i < dim(data)[1]){
      if(positions[i,1] == column && positions[i,2] == rows[row]){
        #plot data
        lines(times, data[i,])
        i <- i+1
        column <- column + 1
      } else {
        #move on to the next column
        column <- column + 1
      }
    } else {
      #all the rest of the columns will be blank from this point, there are no rows left in the
input data
      #move on to the next column
      column <- column + 1
    }

    plotnumber <- plotnumber + 1
    if(column == 13){
      column <- 1 #we reached the end of a row, go back to the start
      row <- row + 1 #row only ever increases
    }
  }

  #reset plot parameters
  par(mfrow=mfrow)
  par(mar=mar)
}

#overview plot for any number of channels
#data must be a list of arrays with samples in rows
#use sample positions to interpret layout in the plate
#positions are the row and column
#if scale == TRUE, all wells are plotted on the same scale, otherwise the axes are rescaled for
every list element - i.e. every dataset has it's own scale but within datasets the scale is the
```

```
same
plot96_all <- function(data, times, positions, scale, colours = 'auto'){
  #save original settings
  mar <- par()$mar
  mfrow <- par()$mfrow
  par(mfrow=c(8,12))
  par(mar=c(0,0,0,0))

  xrange <- range(times)
  yranges <- NULL
  if(scale == TRUE){
    #set the y range using ALL of the input data, so the scale is the same for all datasets
    for(i in 1:length(data)){
      yranges[[i]] <- range(data)
    }
  } else {
    #set the y range once per dataset
    for(i in 1:length(data)){
      yranges[[i]] <- range(data[[i]])
    }
  }

  #colours
  if(colours == 'auto'){
    colours <- rainbow(length(data))
  }

  column <- 1 #the current column in the plate
  rows <- c("A", "B", "C", "D", "E", "F", "G", "H") #use to convert between out numeric
index and the alphabetical one used on the plates
  row <- 1
  i <- 1 #the plot we're currently working on
  plotnumber <- 0

  while(plotnumber < 96){

    if(i < dim(data[[1]])[1]){
      if(positions[i,1] == column && positions[i,2] == rows[row]){
        #plot data
        for(j in range(1:length(data))){
          plot(xrange, yranges[[j]], type="n", xaxt="n", yaxt="n")
          lines(times, data[[j]][i,], col = colours[j])
          if(j != length(data)){
            par(new=TRUE) #to put different axes on one plot. Don't want to set this the last
time.
          }
        }
        i <- i+1
        column <- column + 1
      } else {
```

```
      #move on to the next column
      column <- column + 1
      plot(xrange, yranges[[1]], type="n", xaxt="n", yaxt="n")
    }
  } else {
    #all the rest of the columns will be blank from this point, there are no rows left in the
input data
    #move on to the next column
    column <- column + 1
    plot(xrange, yranges[[1]], type="n", xaxt="n", yaxt="n")
  }

  plotnumber <- plotnumber + 1
  if(column == 13){
    column <- 1 #we reached the end of a row, go back to the start
    row <- row + 1 #row only ever increases
  }
 }

 #reset plot parameters
 par(mfrow=mfrow)
 par(mar=mar)
}
```

R script to run t tests to:

Calculate difference, between diploid EGFP-fusion/^{GAL}TDP-43^{WT}-DsRed, EGFP-fusion/^{GAL}FUS^{WT}-DsRed, EGFP-fusion/^{GAL}SOD1^{WT}-DsRed, EGFP-fusion/^{GAL}SOD1^{A4V}-DsRed and the corresponding control EGFP-fusion/^{GAL}DsRed^{empty} strains, of the yield of normalised EGFP fluorescence intensity from mid-exponential to stationary growth phase:

```
setwd("insert directory location of data file")
fitsn <- read.delim("output_A_GFP.csv", sep=",", header=T, stringsAsFactors=F)
fitsn <- fitsn[,-1]
rate <- as.numeric(fitsn[5, ])
lag <- as.numeric(fitsn[6, ])
max2 <- as.numeric(fitsn[9, ])
yield <- as.numeric(fitsn[15, ])#yield_to_use (DEFAULT min.fit.y to second.max.y)
#minfitmax2_yield <- as.numeric(fitsn [17, ])#second.max_norm.GFP_yield (min.fit.y &
second.max.y)
#min2max2_yield <- as.numeric(fitsn [18, ]) #second.min.2ndmax.norm.GFP_yield
#min2maxfit_yield <- as.numeric(fitsn[19, ]) #second.min.max.fit.norm.GFP_yield
#mid_yield <- as.numeric(fitsn [21, ])

p <- c()
p_yield <- c()
t_yield <- c()
p_max2 <- c()
t_max2 <- c()
#estimate_yield <- c()
#conf.int_yield <- c()
#p_minfitmax2_yield <- c()
#p_min2max2_yield <- c()
#p_min2maxfit_yield <- c()
p_rate <- c()
p_lag <- c()
growth_dif <- c()
#p_mid_yield <- c()

#These sequences combined run t tests of ONLY galactose-grown samples (for GLUC: (i in
seq(1+k,20+k,2)))
for (k in seq(1, 161, 80)) {

  for (i in seq(0+k,19+k,2)) {
    t_yield[i] = t.test(c(yield[i],yield[i+1],yield[i+20],yield[i+21]), c(yield[i+40], yield[i+41],
yield[i+60], yield[i+61]))$statistic
    p_yield[i] = t.test(c(yield[i],yield[i+1],yield[i+20],yield[i+21]), c(yield[i+40], yield[i+41],
yield[i+60], yield[i+61]))$p.value
    t_max2[i] = t.test(c(max2[i],max2[i+1],max2[i+20],max2[i+21]), c(max2[i+40],
max2[i+41], max2[i+60], max2[i+61]))$statistic
```

```
   p_max2[i] = t.test(c(max2[i],max2[i+1],max2[i+20],max2[i+21]), c(max2[i+40],
max2[i+41], max2[i+60], max2[i+61]))$p.value
   p_rate[i] = t.test(c(rate[i], rate[i+1], rate[i+20], rate[i+21]), c(rate[i+40], rate[i+41],
rate[i+60], rate[i+61]))$p.value
   p_lag[i] = t.test(c(lag[i], lag[i+1], lag[i+20], lag[i+21]), c(lag[i+40], lag[i+41], lag[i+60],
lag[i+61]))$p.value
   #p_mid_yield[i] = t.test(c(mid_yield[i],mid_yield[i+20]), c(mid_yield[i+40],
mid_yield[i+60]))$p.value

   #growth_dif[i] = log(mean(c(yield[i],yield[i+20]))/mean(c(yield[i+40], yield[i+60])))
  }
}

#Trying to figure out sequences for the for loop:
#a.vector <- c(1:240)
#a.element <- c()
#for (k in seq(1, 161, 80)) {

#  for (i in seq(0+k,19+k,2)) {
#    a.element[i] <- a.vector[i]
#  }
#}

#tidy up
keep = !is.na(p_yield)
p_yield = p_yield[keep]
t_yield = t_yield[keep]
p_max2 = p_max2[keep]
t_max2 = t_max2[keep]
p_rate = p_rate[keep]
p_lag = p_lag[keep]

layout.GFP <- read.delim("NAMES_REP_8_t tests.csv",sep=",",header=F,stringsAsFactors
= F)

#calculate combined score for p-values of mid.point yield and total yield
#X <- c()
#p_combined <- c()
#for (i in c(1:60)) {
#  X[i] <- -2*(log(p_mid_yield[i])+log(p_yield[i]))
#  p_combined[i] <- pchisq(X[i],df=4,lower.tail=FALSE)
#}
p_values_revised = cbind(c(t(layout.GFP)), t_max2, p_max2, t_yield,p_yield,p_rate, p_lag)
write.table(p_values_revised,"p_values_revised.txt",sep="\t",quote=F, row.names = FALSE)
write.csv(p_values_revised,file="p_values_revised.csv")

significant_yield_0.05 <- p_values_1[which(p_yield < 0.05)]

#significant_minfitmax2_yield_0.05 <- p_values_1[which(p_minfitmax2_yield < 0.05)]
#significant_min2max2_yield_0.05 <- p_values_1[which(p_min2max2_yield < 0.05)]
```

```
#significant_min2maxfit_yield_0.05 <- p_values_1[which(p_min2maxfit_yield < 0.05)]
#significant_rate_dif_0.05 <- layout2[which(p_rate < 0.05)]
#significant_lag_dif_0.05 <- layout2[which(p_lag < 0.05)]
```

Supplementary data from Deltavision OMX™ super resolution microscopy of diploid strains

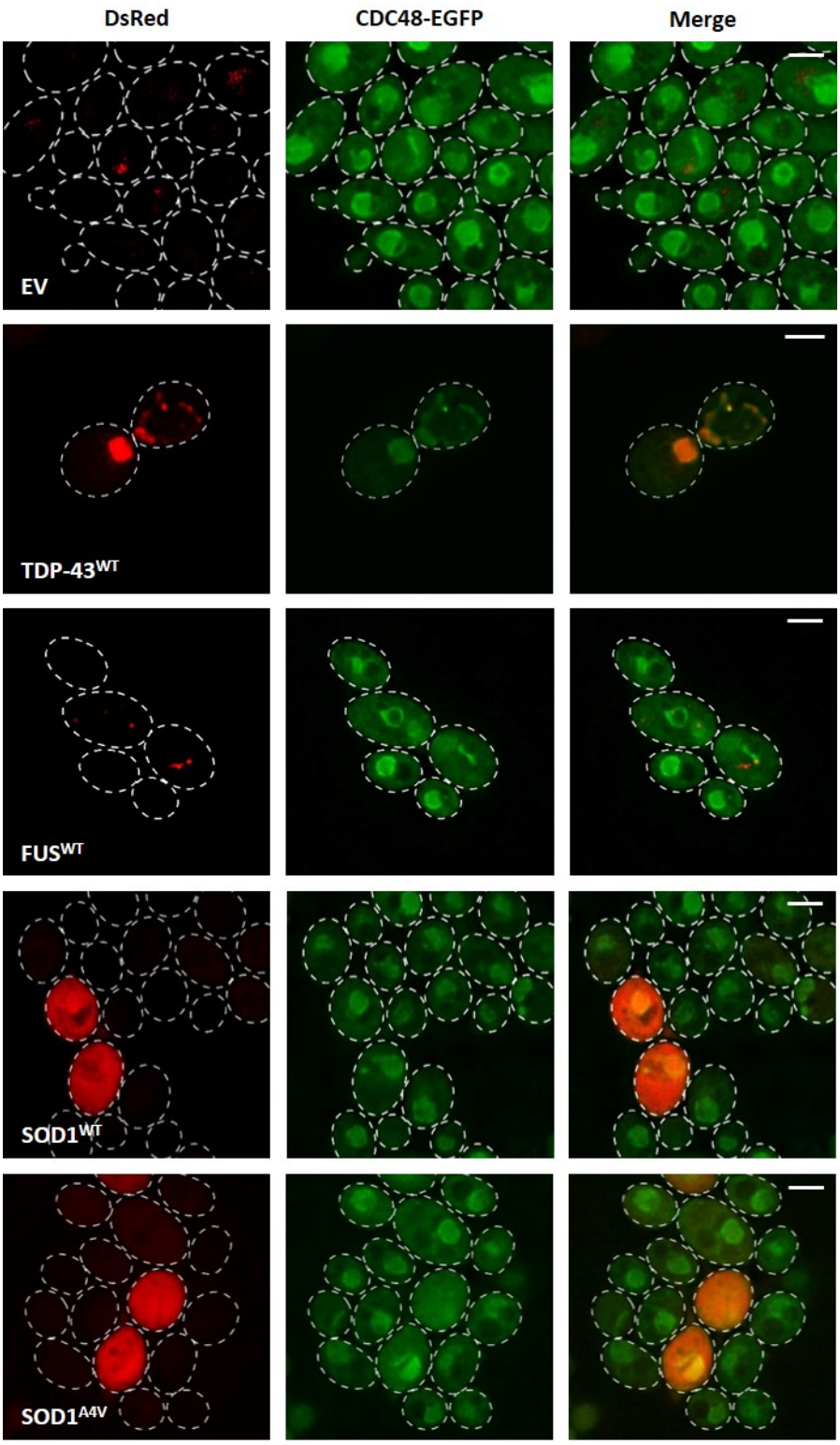

Figure S3.1. Characterising the localisation of yeast CDC48-EGFP and DsRed-tagged human TDP-43^{WT}, FUS^{WT}, SOD1^{WT} and SOD1^{A4V} in diploid strains. Representative images showing the localisation of each DsRed-fusion protein and CDC48-EGFP in the respective diploid strains. Diploid strains were grown for 2 nights in SRaf/-His/Ura broth before being diluted 20× into SGal/-His/Ura broth and grown overnight at 30 °C with agitation to induce expression of ^{GAL}TDP-43^{WT}-DsRed, ^{GAL}FUS^{WT}-DsRed, ^{GAL}SOD1^{WT}-DsRed, ^{GAL}SOD1^{A4V}-DsRed or ^{GAL}DsRed^{empty} ('empty' vector control (DsRed alone); EV). The fluorescent proteins were examined in cells using the 100× oil-immersion objective lens of a DeltaVision OMX™ super resolution microscope. Outlines of cells are indicated by white dashed lines. Scale bars represent 5 µm.

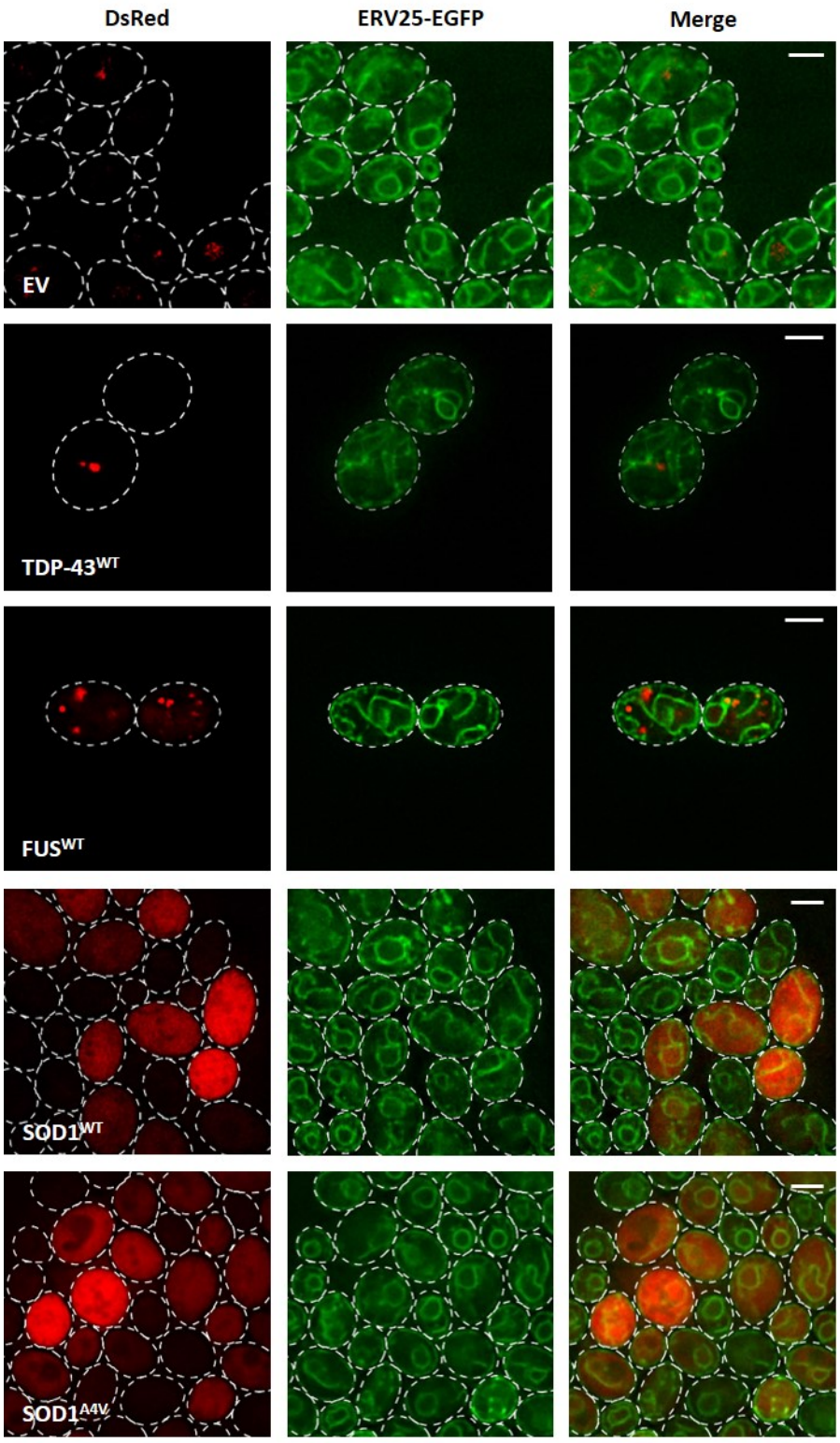

Figure S3.2. Characterising the localisation of yeast ERV25-EGFP and DsRed-tagged human TDP-43^{WT}, FUS^{WT}, SOD1^{WT} and SOD1^{A4V} in diploid strains. Representative images showing the localisation of each DsRed-fusion protein and ERV25-EGFP in the respective diploid strains. Diploid strains were grown for 2 nights in SRaf/-His/Ura broth before being diluted 20× into SGal/-His/Ura broth and grown overnight at 30 °C with agitation to induce expression of ^{GAL}TDP-43^{WT}-DsRed, ^{GAL}FUS^{WT}-DsRed, ^{GAL}SOD1^{WT}-DsRed, ^{GAL}SOD1^{A4V}-DsRed or ^{GAL}DsRed^{empty} ('empty' vector control (DsRed alone); EV). The fluorescent proteins were examined in cells using the 100× oil-immersion objective lens of a DeltaVision OMX™ super resolution microscope. Outlines of cells are indicated by white dashed lines. Scale bars represent 5 µm.

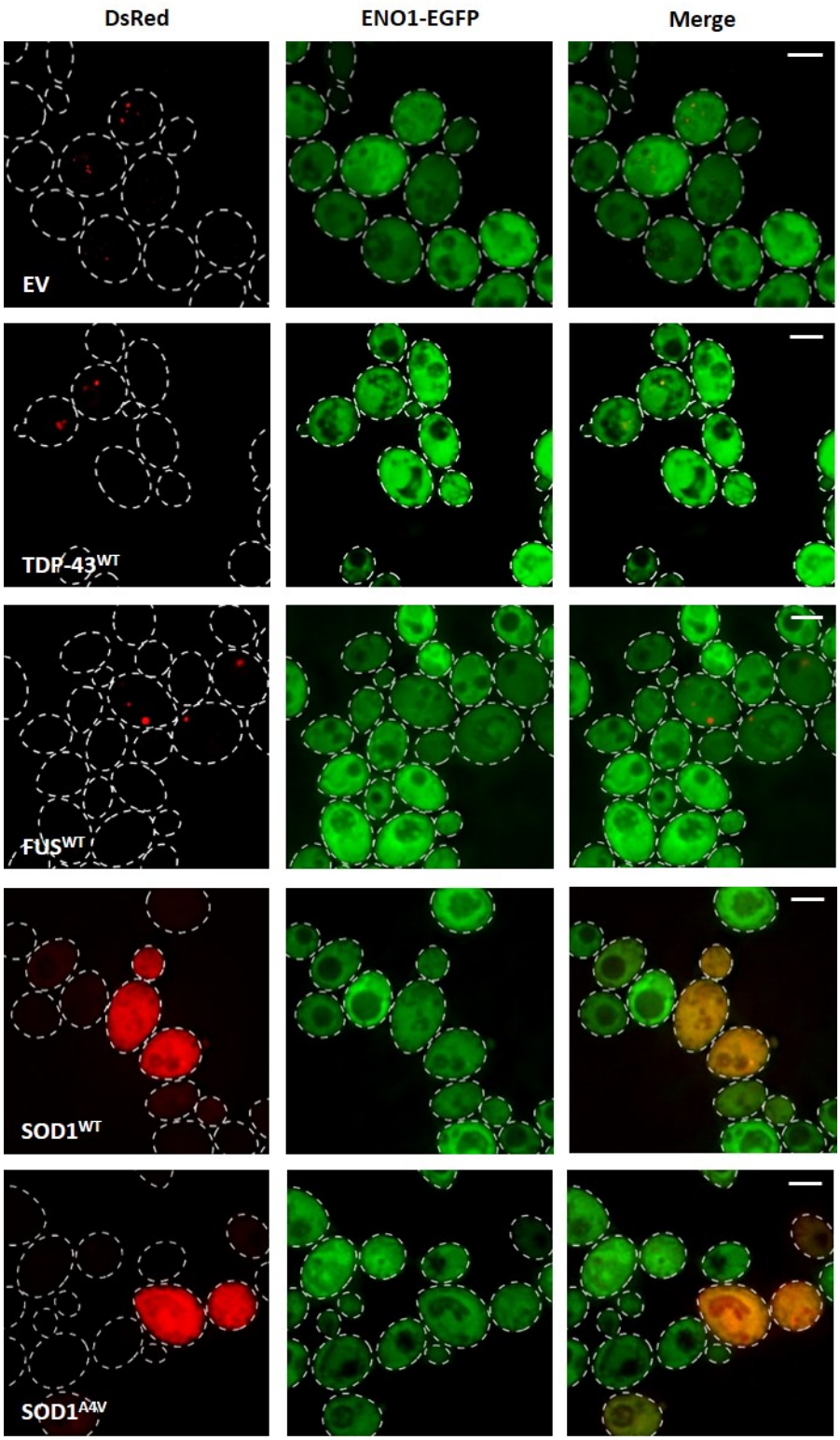

Figure S3.3. Characterising the localisation of yeast ENO1-EGFP and DsRed-tagged human TDP-43^{WT}, FUS^{WT}, SOD1^{WT} and SOD1^{A4V} in diploid strains. Representative images showing the localisation of each DsRed-fusion protein and ENO1-EGFP in the respective diploid strains. Diploid strains were grown for 2 nights in SRaf/-His/Ura broth before being diluted 20× into SGal/-His/Ura broth and grown overnight at 30 °C with agitation to induce expression of ^{GAL}TDP-43^{WT}-DsRed, ^{GAL}FUS^{WT}-DsRed, ^{GAL}SOD1^{WT}-DsRed, ^{GAL}SOD1^{A4V}-DsRed or ^{GAL}DsRed^{empty} ('empty' vector control (DsRed alone); EV). The fluorescent proteins were examined in cells using the 100× oil-immersion objective lens of a DeltaVision OMX™ super resolution microscope. Outlines of cells are indicated by white dashed lines. Scale bars represent 5 μm.

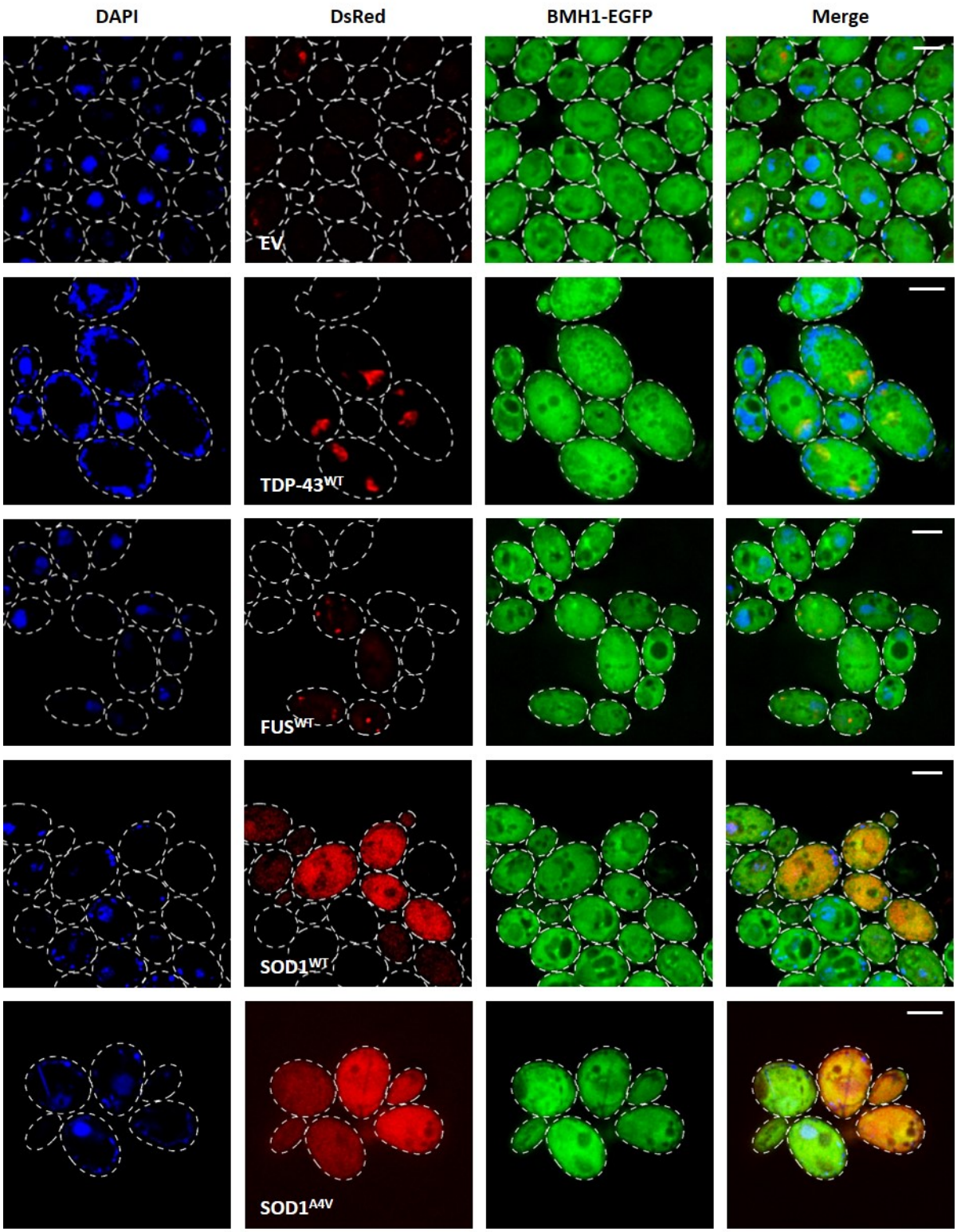

Figure S3.4. Characterising the localisation of yeast BMH1-EGFP and DsRed-tagged human TDP-43^{WT}, FUS^{WT}, SOD1^{WT} and SOD1^{A4V} in diploid strains. Representative images showing the localisation of each DsRed-fusion protein and BMH1-EGFP in the respective diploid strains. Diploid strains were grown for 2 nights in SRaf/-His/Ura broth before being diluted 20× into SGal/-His/Ura broth and grown overnight at 30 °C with agitation to induce expression of ^{GAL}TDP-43^{WT}-DsRed, ^{GAL}FUS^{WT}-DsRed, ^{GAL}SOD1^{WT}-DsRed, ^{GAL}SOD1^{A4V}-DsRed or ^{GAL}DsRed^{empty} ('empty' vector control (DsRed alone); EV). The fluorescent proteins were examined in cells using the 100× oil-immersion objective lens of a DeltaVision OMX™ super resolution microscope. Outlines of cells are indicated by white dashed lines. Scale bars represent 5 µm.

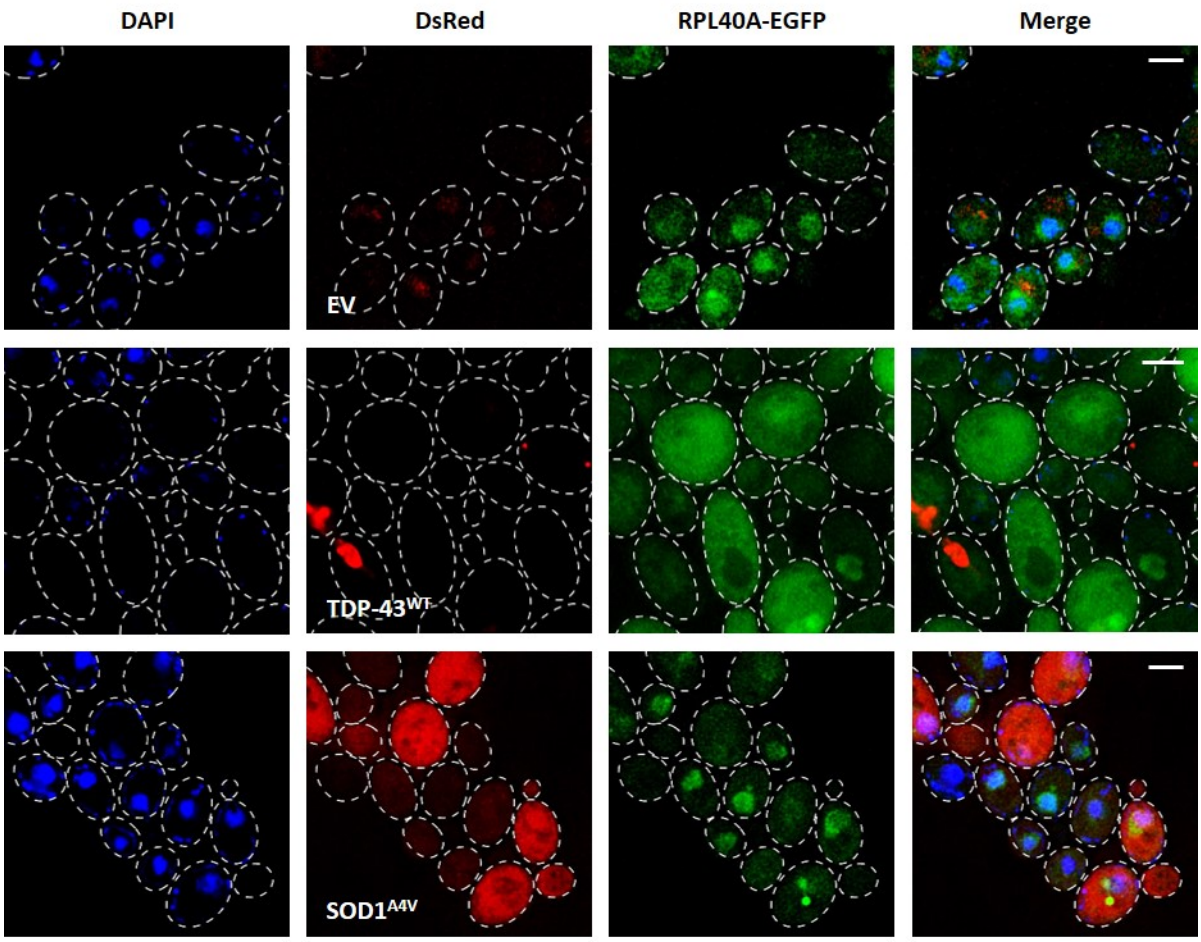

Figure S3.5. Characterising the localisation of yeast RPL40A-EGFP and DsRed-tagged human TDP-43^{WT} and SOD1^{A4V} in diploid strains. Representative images showing the localisation of each DsRed-fusion protein and RPL40A-EGFP in the respective diploid strains. Diploid strains were grown for 2 nights in SRaf/-His/Ura broth before being diluted 20× into SGal/-His/Ura broth and grown overnight at 30 °C with agitation to induce expression of ^{GAL}TDP-43^{WT}-DsRed, ^{GAL}SOD1^{A4V}-DsRed or ^{GAL}DsRed^{empty} ('empty' vector control (DsRed alone); EV). The fluorescent proteins were examined in cells using the 100× oil-immersion objective lens of a DeltaVision OMX™ super resolution microscope. Outlines of cells are indicated by white dashed lines. Scale bars represent 5 μm.

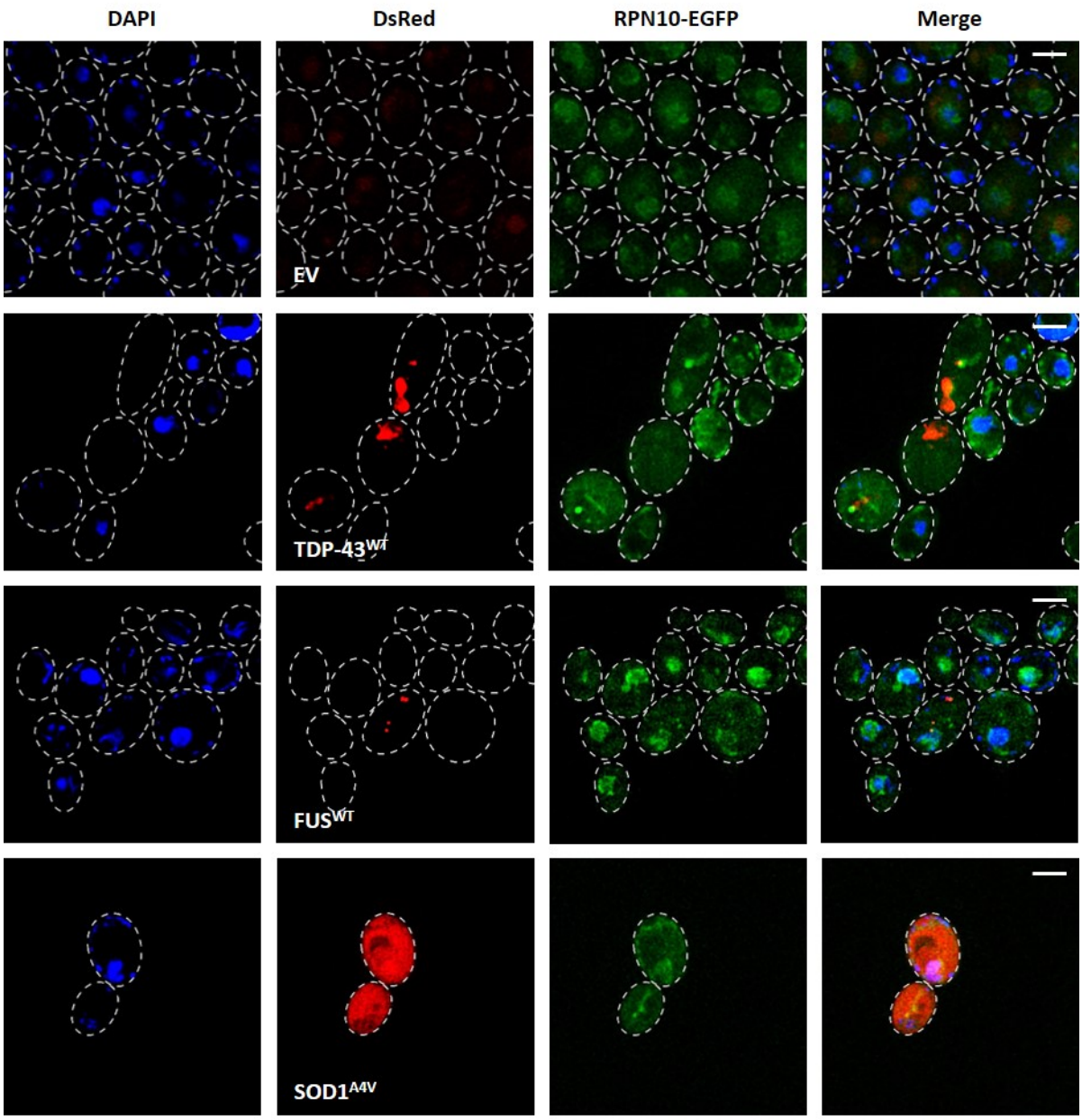

Figure S3.6. Characterising the localisation of yeast RPN10-EGFP and DsRed-tagged human TDP-43^{WT}, FUS^{WT} and SOD1^{A4V} in diploid strains. Representative images showing the localisation of each DsRed-fusion protein and RPN10-EGFP in the respective diploid strains. Diploid strains were grown for 2 nights in SRaf/-His/Ura broth before being diluted 20× into SGal/-His/Ura broth and grown overnight at 30 °C with agitation to induce expression of ^{GAL}TDP-43^{WT}-DsRed, ^{GAL}FUS^{WT}-DsRed, ^{GAL}SOD1^{A4V}-DsRed or ^{GAL}DsRed^{empty} ('empty' vector control (DsRed alone); EV). The fluorescent proteins were examined in cells using the 100× oil-immersion objective lens of a DeltaVision OMX™ super resolution microscope. Outlines of cells are indicated by white dashed lines. Scale bars represent 5 μm.

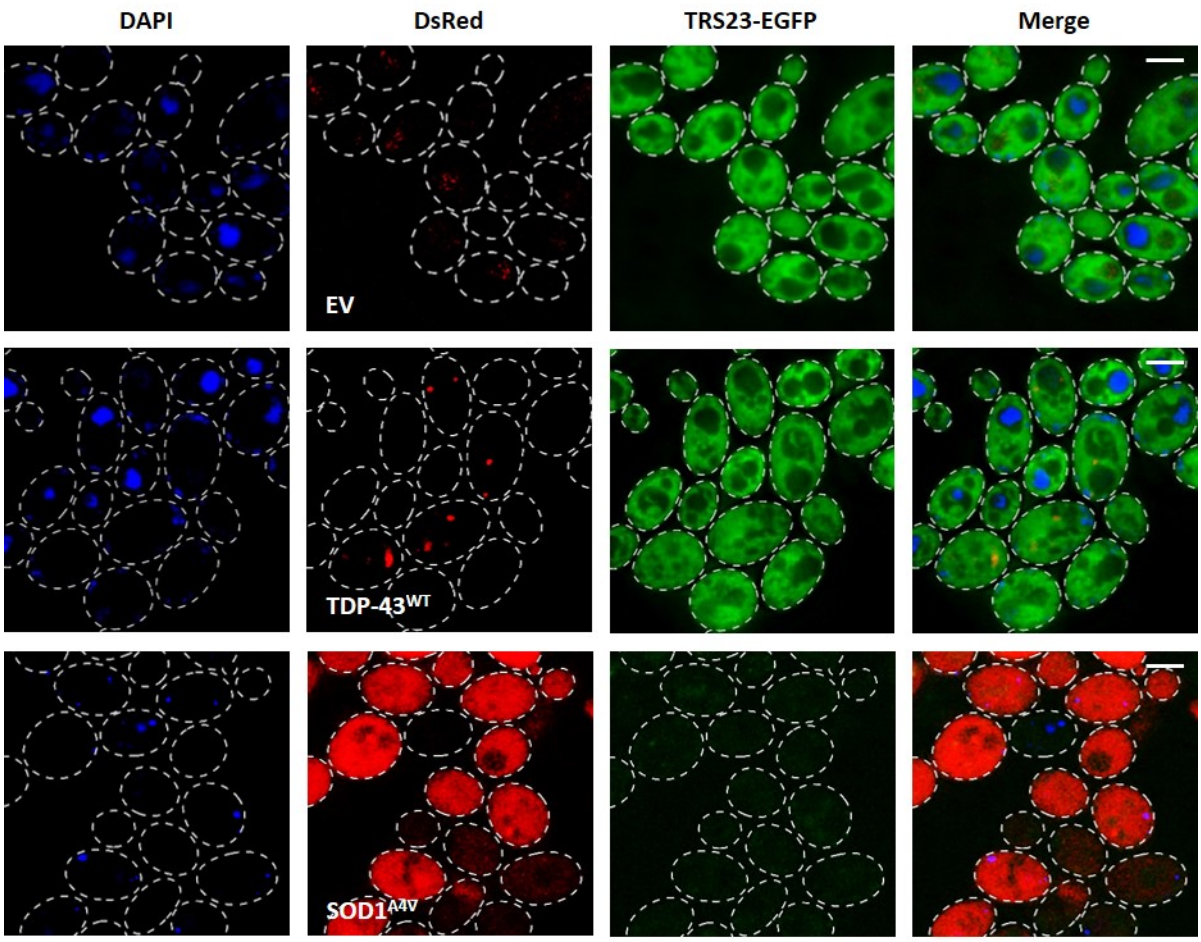

Figure S3.7. Characterising the localisation of yeast TRS23-EGFP and DsRed-tagged human TDP-43^{WT} and SOD1^{A4V} in diploid strains. Representative images showing the localisation of each DsRed-fusion protein and TRS23-EGFP in the respective diploid strains. Diploid strains were grown for 2 nights in SRaf/-His/Ura broth before being diluted 20× into SGal/-His/Ura broth and grown overnight at 30 °C with agitation to induce expression of ^{GAL}TDP-43^{WT}-DsRed, ^{GAL}SOD1^{A4V}-DsRed or ^{GAL}DsRed^{empty} ('empty' vector control (DsRed alone); EV). The fluorescent proteins were examined in cells using the 100× oil-immersion objective lens of a DeltaVision OMX™ super resolution microscope. Outlines of cells are indicated by white dashed lines. Scale bars represent 5 μm.

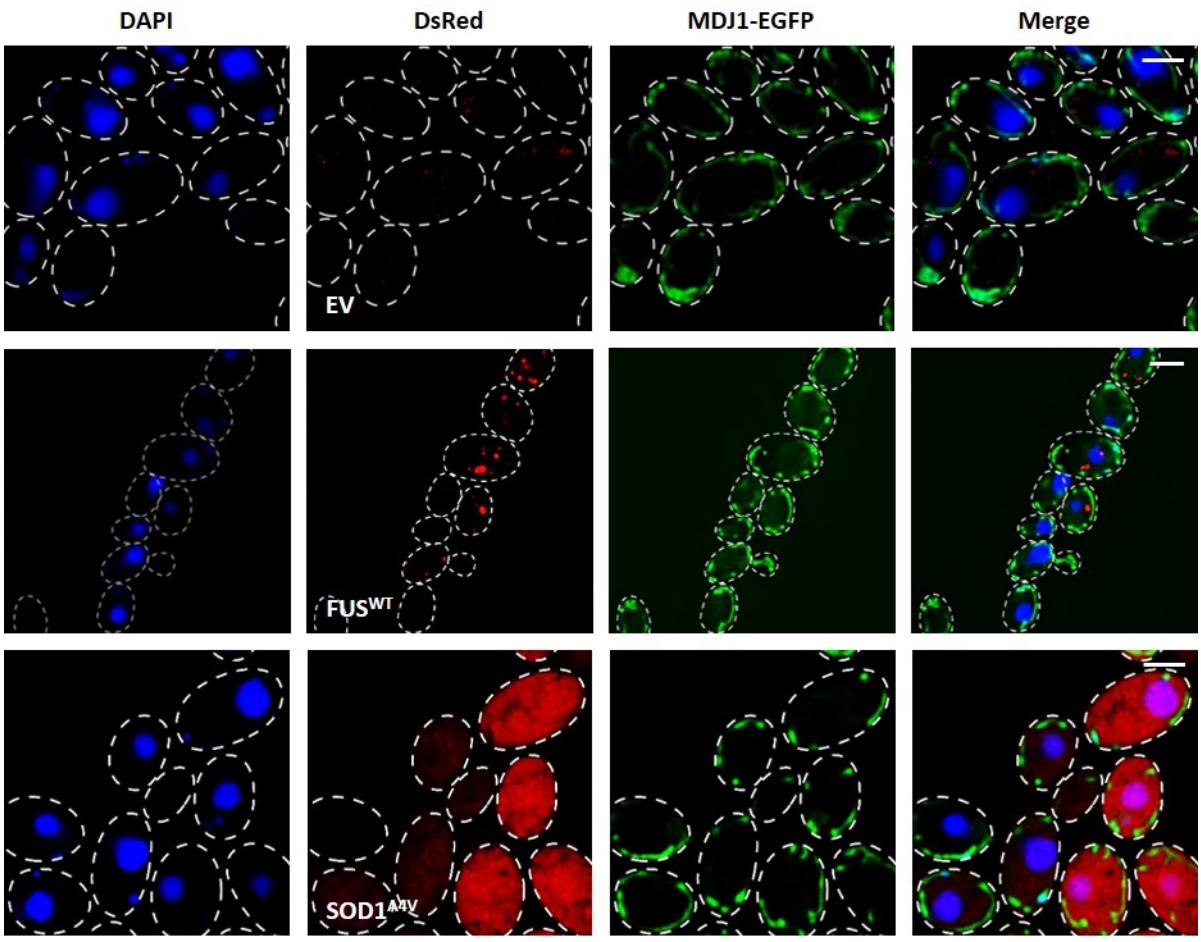

Figure S3.8. Characterising the localisation of yeast MDJ1-EGFP and DsRed-tagged human FUS^{WT} and SOD1^{A4V} in diploid strains. Representative images showing the localisation of each DsRed-fusion protein and MDJ1-EGFP in the respective diploid strains. Diploid strains were grown for 2 nights in SRaf/-His/Ura broth before being diluted 20× into SGal/-His/Ura broth and grown overnight at 30 °C with agitation to induce expression of ^{GAL}FUS^{WT}-DsRed, ^{GAL}SOD1^{A4V}-DsRed or ^{GAL}DsRed^{empty} ('empty' vector control (DsRed alone); EV). The fluorescent proteins were examined in cells using the 100× oil-immersion objective lens of a DeltaVision OMX™ super resolution microscope. Outlines of cells are indicated by white dashed lines. Scale bars represent 5 μm.

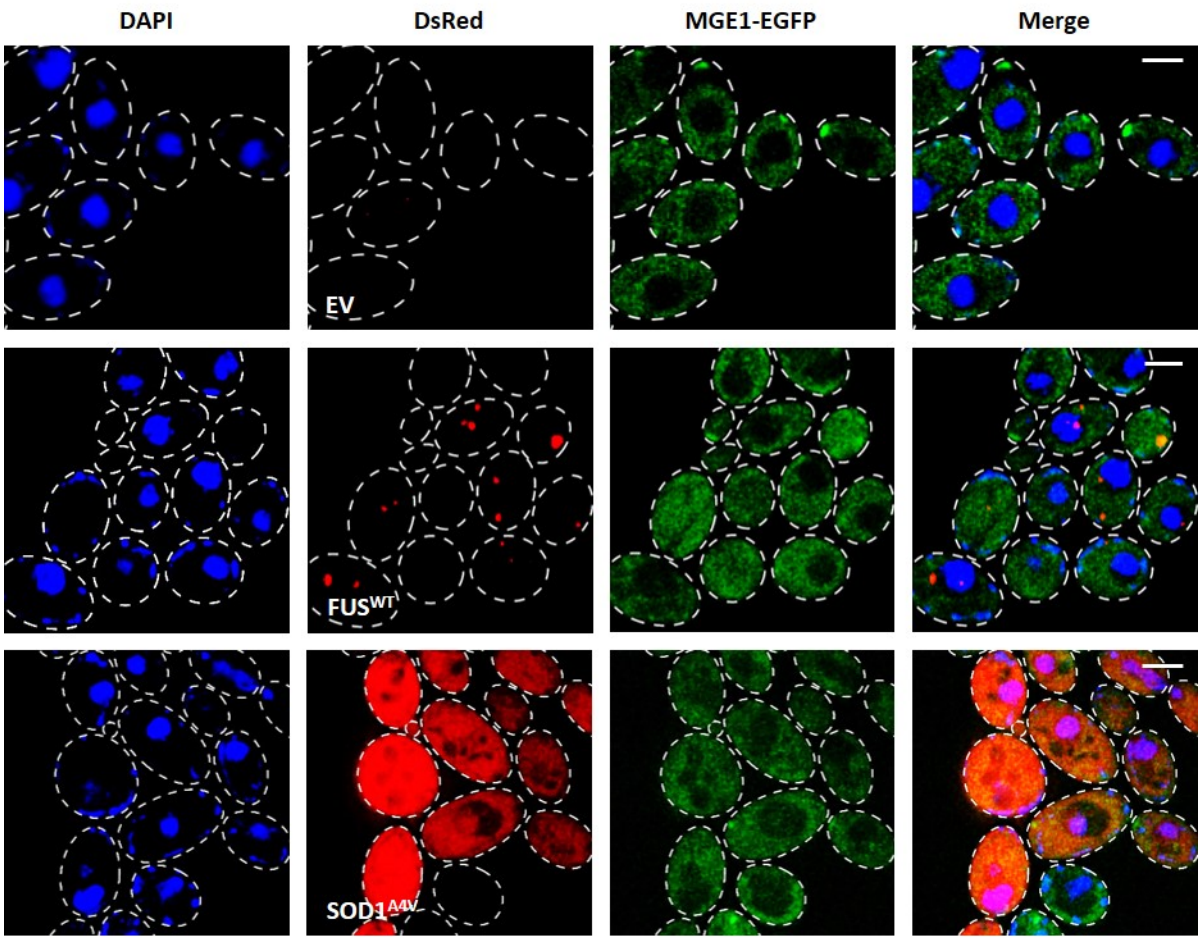

Figure S3.9. Characterising the localisation of yeast MGE1-EGFP and DsRed-tagged human FUS^{WT} and $SOD1^{A4V}$ in diploid strains. Representative images showing the localisation of each DsRed-fusion protein and MGE1-EGFP in the respective diploid strains. Diploid strains were grown for 2 nights in SRaf/-His/Ura broth before being diluted 20× into SGal/-His/Ura broth and grown overnight at 30 °C with agitation to induce expression of $^{GAL}FUS^{WT}$-DsRed, $^{GAL}SOD1^{A4V}$-DsRed or $^{GAL}DsRed^{empty}$ ('empty' vector control (DsRed alone); EV). The fluorescent proteins were examined in cells using the 100× oil-immersion objective lens of a DeltaVision OMX™ super resolution microscope. Outlines of cells are indicated by white dashed lines. Scale bars represent 5 μm.

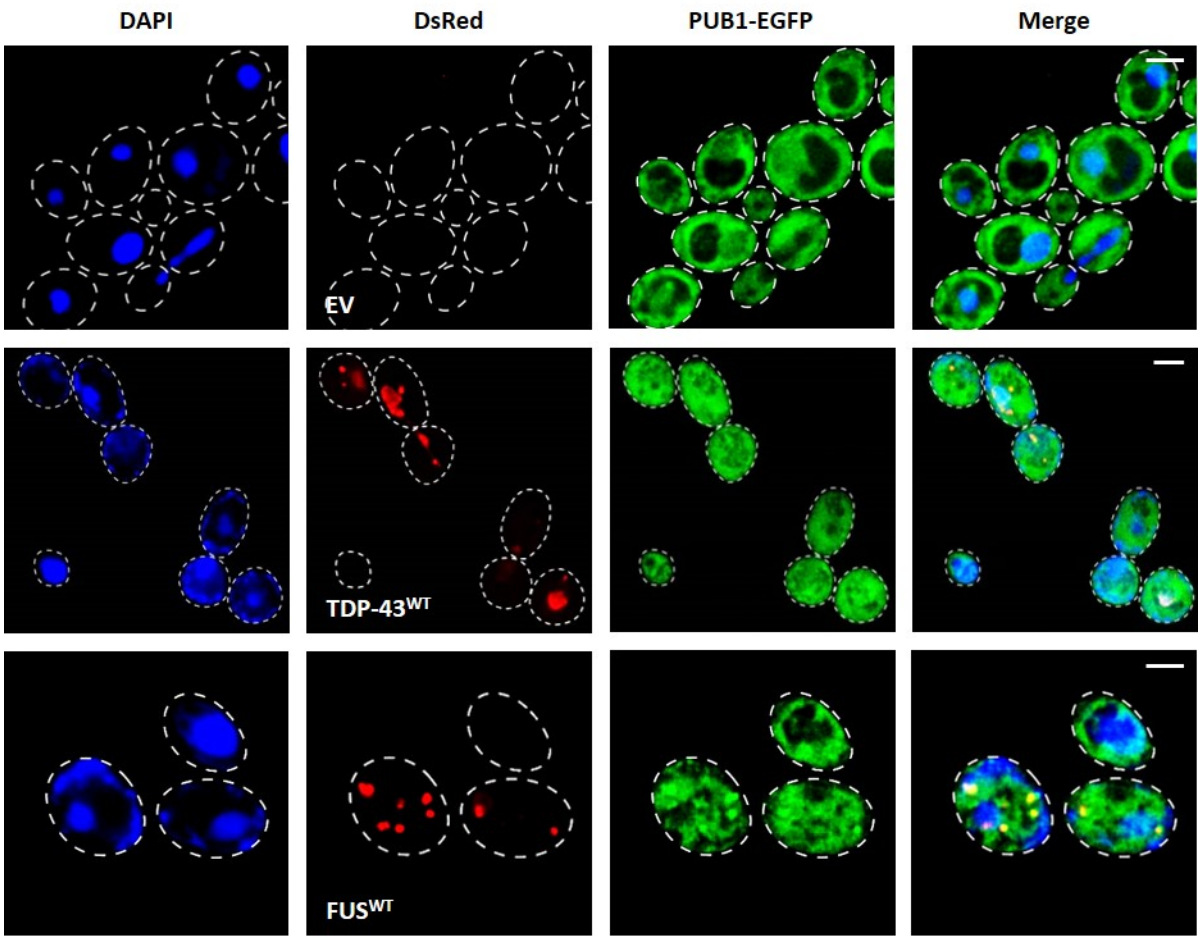

Figure S3.10. Characterising the localisation of yeast PUB1-EGFP and DsRed-tagged human TDP-43^{WT} and FUS^{WT} in diploid strains. Representative images showing the localisation of each DsRed-fusion protein and PUB1-EGFP in the respective diploid strains. Diploid strains were grown for 2 nights in SRaf/-His/Ura broth before being diluted 20× into SGal/-His/Ura broth and grown overnight at 30 °C with agitation to induce expression of ^{GAL}TDP-43^{WT}-DsRed, ^{GAL}FUS^{WT}-DsRed or ^{GAL}DsRed^{empty} ('empty' vector control (DsRed alone); EV). The fluorescent proteins were examined in cells using the 100× oil-immersion objective lens of a DeltaVision OMX™ super resolution microscope. Outlines of cells are indicated by white dashed lines. Scale bars represent 5 μm.

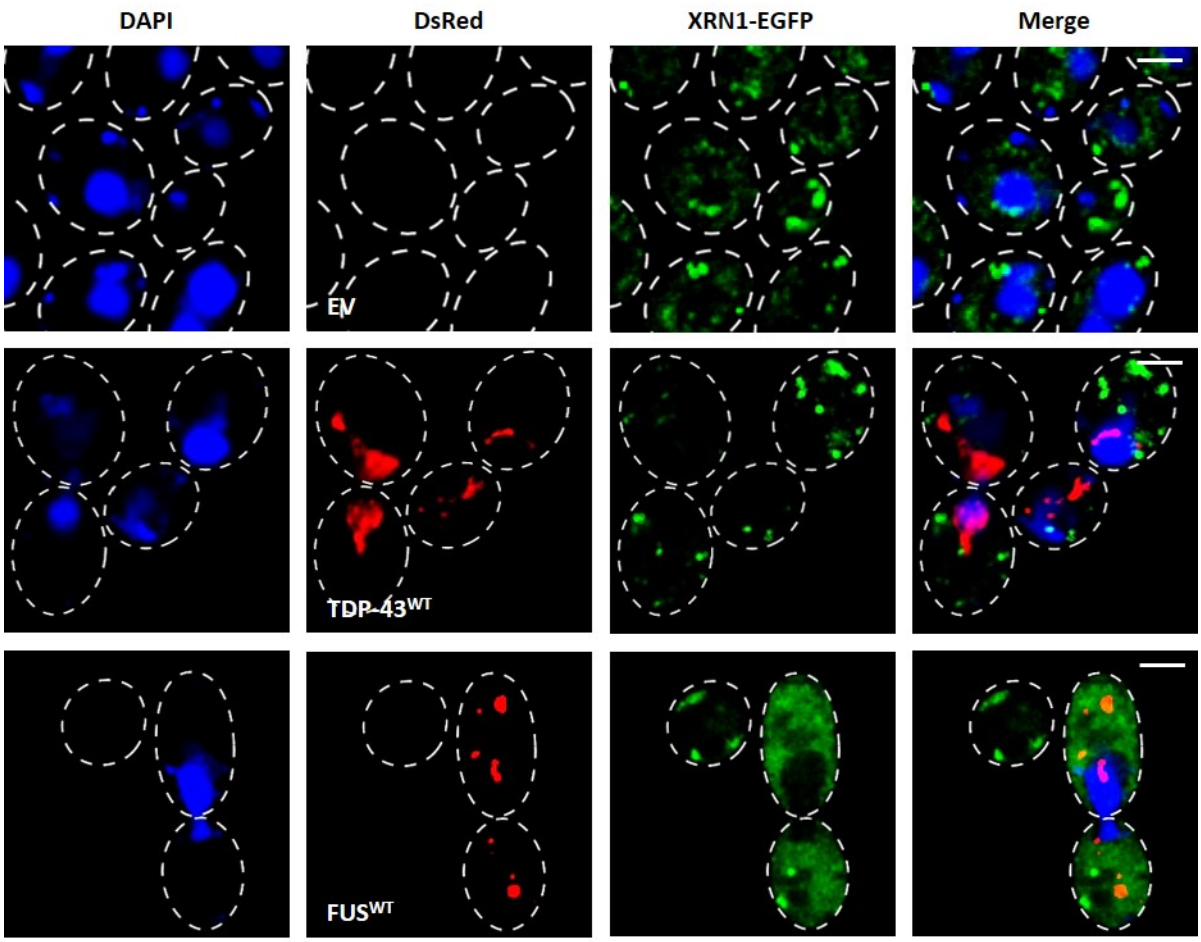

Figure S3.11. Characterising the localisation of yeast XRN1-EGFP and DsRed-tagged human TDP-43^{WT} and FUS^{WT} in diploid strains. Representative images showing the localisation of each DsRed-fusion protein and XRN1-EGFP in the respective diploid strains. Diploid strains were grown for 2 nights in SRaf/-His/Ura broth before being diluted 20× into SGal/-His/Ura broth and grown overnight at 30 °C with agitation to induce expression of ^{GAL}TDP-43^{WT}-DsRed, ^{GAL}FUS^{WT}-DsRed or ^{GAL}DsRed^{empty} ('empty' vector control (DsRed alone); EV). The fluorescent proteins were examined in cells using the 100× oil-immersion objective lens of a DeltaVision OMX™ super resolution microscope. Outlines of cells are indicated by white dashed lines. Scale bars represent 5 μm.

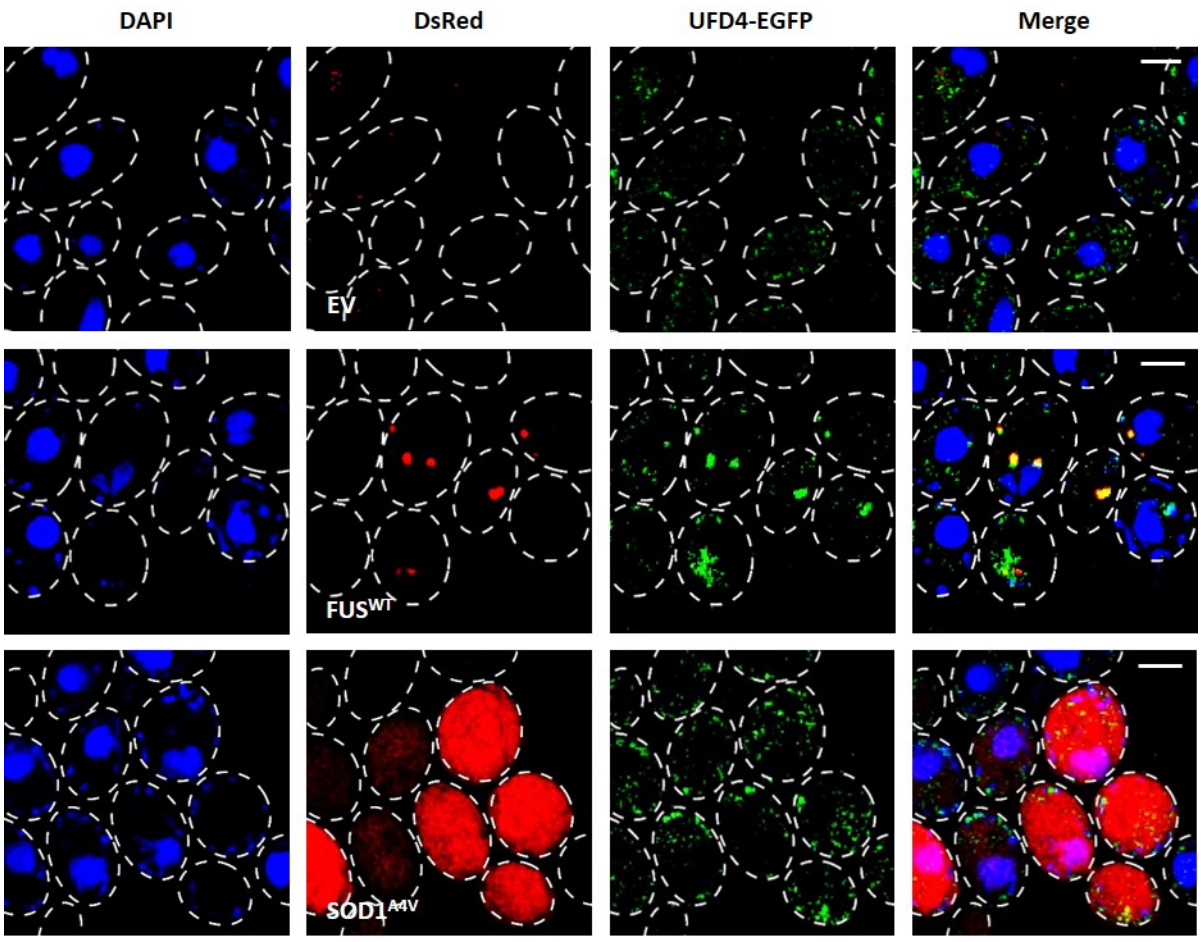

Figure S3.12. Characterising the localisation of yeast UFD4-EGFP and DsRed-tagged human FUS^{WT} and SOD1^{A4V} in diploid strains. Representative images showing the localisation of each DsRed-fusion protein and UFD4-EGFP in the respective diploid strains. Diploid strains were grown for 2 nights in SRaf/-His/Ura broth before being diluted 20× into SGal/-His/Ura broth and grown overnight at 30 °C with agitation to induce expression of ^{GAL}FUS^{WT}-DsRed, ^{GAL}SOD1^{A4V}-DsRed or ^{GAL}DsRed^{empty} ('empty' vector control (DsRed alone); EV). The fluorescent proteins were examined in cells using the 100× oil-immersion objective lens of a DeltaVision OMX™ super resolution microscope. Outlines of cells are indicated by white dashed lines. Scale bars represent 5 μm.

Supplementary data from quality control analyses of FLUOstar® Optima plate reader data

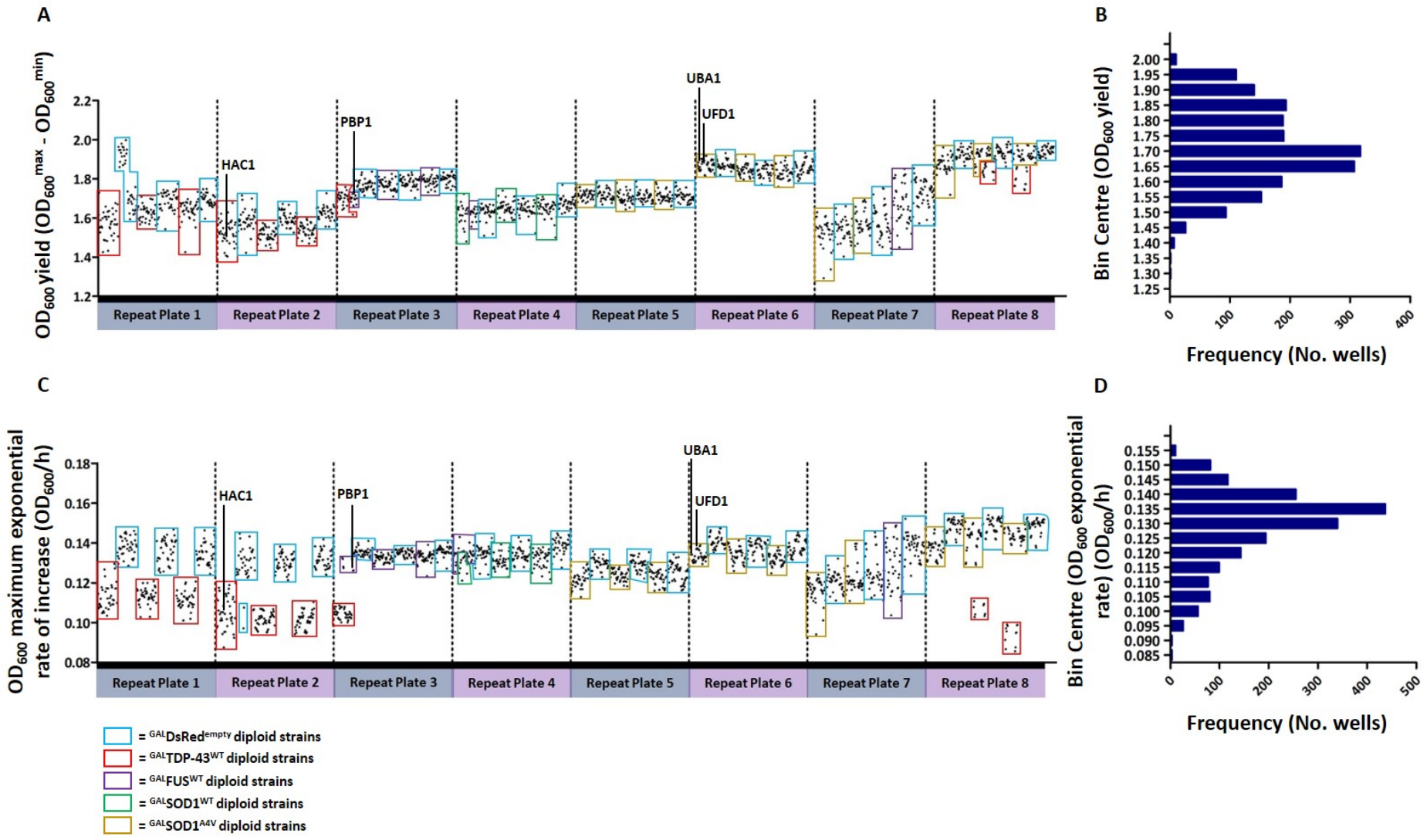
A
B
C
D
HAC1
PBP1
UBA1
UFD1
Repeat Plate 1
Repeat Plate 2
Repeat Plate 3
Repeat Plate 4
Repeat Plate 5
Repeat Plate 6
Repeat Plate 7
Repeat Plate 8
OD600 yield (OD600max - OD600min)
Bin Centre (OD600 yield)
Frequency (No. wells)
OD600 maximum exponential rate of increase (OD600/h)
Bin Centre (OD600 exponential rate) (OD600/h)
= GALDsRedempty diploid strains
= GALTDP-43WT diploid strains
= GALFUSWT diploid strains
= GALSOD1WT diploid strains
= GALSOD1A4V diploid strains

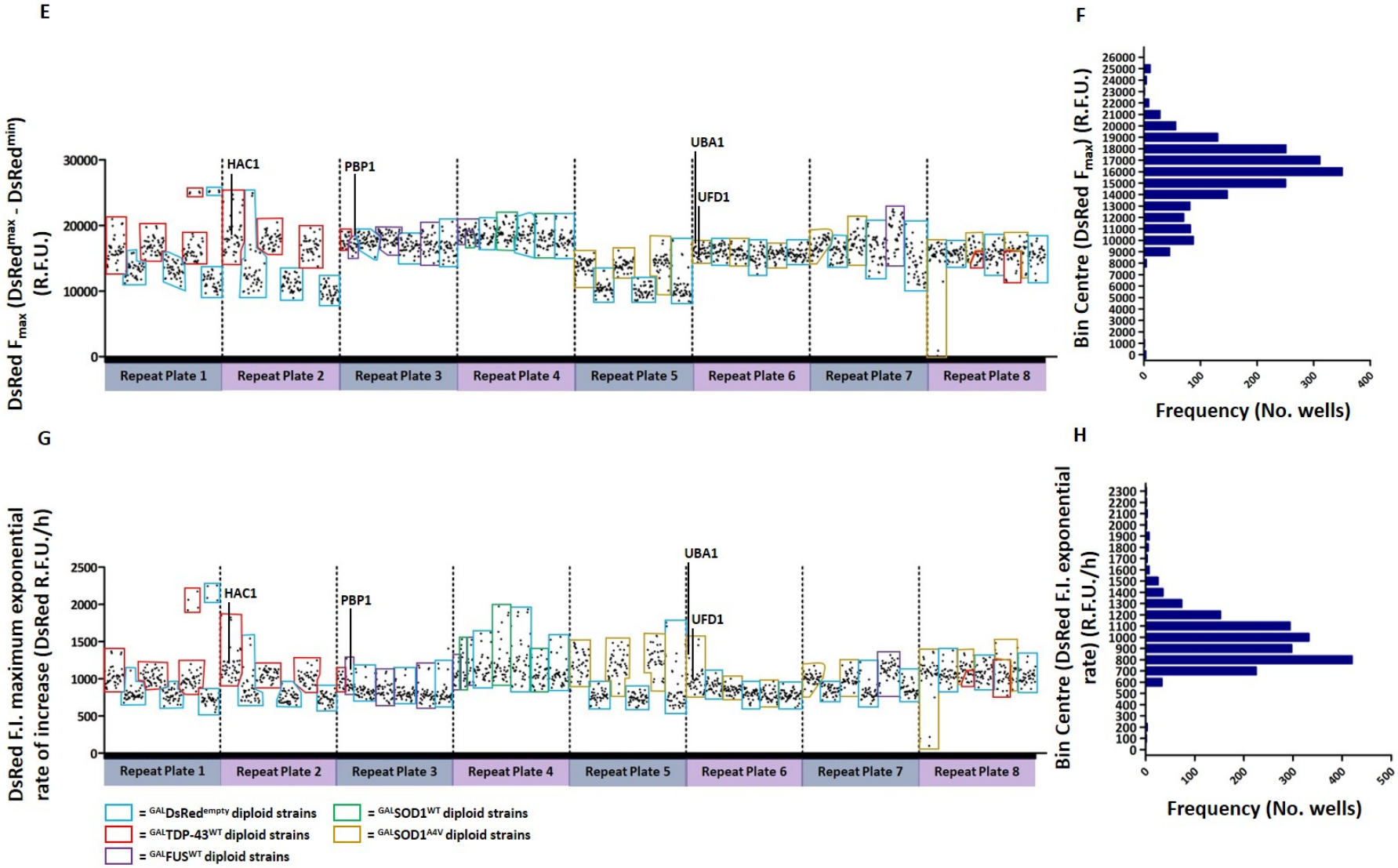
E
F
G
H
DsRed F_{max} (DsRed^{max} - DsRed^{min}) (R.F.U.)
Bin Centre (DsRed F_{max}) (R.F.U.)
Frequency (No. wells)
DsRed F.I. maximum exponential rate of increase (DsRed R.F.U./h)
Bin Centre (DsRed F.I. exponential rate) (R.F.U./h)
HAC1
PBP1
UBA1
UFD1
Repeat Plate 1
Repeat Plate 2
Repeat Plate 3
Repeat Plate 4
Repeat Plate 5
Repeat Plate 6
Repeat Plate 7
Repeat Plate 8
= GALDsRedempty diploid strains
= GALTDP-43WT diploid strains
= GALFUSWT diploid strains
= GALSOD1WT diploid strains
= GALSOD1A4V diploid strains

Figure S3.13. Distribution of raw OD_{600} and DsRed fluorescence intensity data from repeats of the FLUOstar® Optima plate reader assays of diploid yeast EGFP-fusion strains expressing DsRed-fusion human TDP-43^{WT}, FUS^{WT}, SOD1^{WT}, SOD1^{A4V} or DsRed alone. Diploid strains were created by mating haploid Y7039 transformed with pAG416GAL-TDP-43^{WT}-DsRed (^{GAL}TDP-43^{WT}), pAG416GAL-FUS^{WT}-DsRed (^{GAL}FUS^{WT}), pAG416GAL-SOD1^{WT}-DsRed (^{GAL}SOD1^{WT}), pAG416GAL-SOD1^{A4V}-DsRed (^{GAL}SOD1^{A4V}), or pAG416GAL-ccdB-DsRed (^{GAL}DsRed^{empty}; vector control) with haploid strains from the yeast EGFP fusion collection (Huh *et al.* 2003). After first screening 128 different strains from the yeast EGFP fusion collection, EGFP-fusion proteins exhibiting altered levels in ^{GAL}TDP-43^{WT}, ^{GAL}FUS^{WT}, ^{GAL}SOD1^{WT} or ^{GAL}SOD1^{A4V} relative to ^{GAL}DsRed^{empty} strains were re-assayed to confirm the altered levels. Quadruplicates of each diploid strain were grown in 384-well μclear plates containing 100 μL per well of SGal/-His/Ura to induce expression of ^{GAL}TDP-43^{WT}, ^{GAL}FUS^{WT}, ^{GAL}SOD1^{WT}, ^{GAL}SOD1^{A4V} or ^{GAL}DsRed^{empty} in a FLUOstar® Optima plate reader. The absorbance (optical density [OD] at 600 nm), EGFP (excitation 485/12 nm, emission collected at 510/20 nm) and DsRed (excitation 580/10 nm, emission collected at 612 nm) fluorescence were measured over 48 h of yeast incubation at 30 °C. Raw data collected for each replicate were analysed to calculate the OD_{600} yield (maximum OD_{600} – minimum OD_{600}), the maximum exponential rate of change of OD_{600} (maximum growth rate; OD_{600}/h), the maximum DsRed fluorescence intensity (F_{max}) (maximum DsRed F.I. – minimum DsRed F.I.; relative fluorescence units, R.F.U.) and the maximum exponential rate of change of DsRed F.I. (maximum rate of DsRed F.I. increase; R.F.U./h). These data per replicate are presented as follows: (A) scatter plot and (B) histogram displaying the OD_{600} yield; (C) scatter plot and (D) histogram showing the maximum exponential rate of change of OD_{600} (maximum growth rate); (E) scatter plot and (F) histogram displaying the DsRed F_{max}; (G) scatter plot and (H) histogram displaying the maximum exponential rate of change of DsRed F.I. (maximum rate of DsRed F.I. increase; R.F.U./h).